UNCLASSIFIED

AD NUMBER

ADB952222

NEW LIMITATION CHANGE

TO

Approved for public release, distribution unlimited

FROM

Distribution authorized to U.S. Gov't. agencies only; Test and Evaluation; 09 OCT 1959. Other requests shall be referred to Defense Threat Reduction Agency, Fort Belvoir, VA 22060-6201.

AUTHORITY

DNA ltr, 2 Oct 1981

THIS PAGE IS UNCLASSIFIED

THIS REPORT HAS BEEN DELIMITED
AND CLEARED FOR PUBLIC RELEASE
UNDER DOD DIRECTIVE 5200.20 AND
NO RESTRICTIONS ARE IMPOSED UPON
ITS USE AND DISCLOSURE.

DISTRIBUTION STATEMENT A

APPROVED FOR PUBLIC RELEASE;
DISTRIBUTION UNLIMITED.

UNCLASSIFIED

AD B952222

AUTHORITY: DNA

ltr, 2 OCT 81

UNCLASSIFIED

PHOTOGRAPH THIS SHEET

UNANNOUNCED

LEVEL

INVENTORY

AD B952222

DTIC ACCESSION NUMBER

REC

WT-366

DOCUMENT IDENTIFICATION

Jun. '52

Distribution limited to U.S. Gov't. agencies only; Test and Evaluation; 9 Oct. '59 . Other requests for this document must be referred to Director, Defense Nuclear Agency, Washington, DC 20305.

DISTRIBUTION STATEMENT

| ACCESSION FOR | | |
|---|---|---|
| NTIS | GRA&I | ☐ |
| DTIC | TAB | ☐ |
| UNANNOUNCED | | ☒ |
| JUSTIFICATION | | |
| | | |
| | | |
| BY Per Ltr. on file | | |
| DISTRIBUTION / | | |
| AVAILABILITY CODES | | |
| DIST | AVAIL AND/OR SPECIAL | |
| B | | |

DISTRIBUTION STAMP

DTIC
ELECTE
S FEB 3 1981 D
D

DATE ACCESSIONED

80 8 28 052

DATE RECEIVED IN DTIC

PHOTOGRAPH THIS SHEET AND RETURN TO DTIC-DDA-2

DTIC FORM OCT 79 70A

DOCUMENT PROCESSING SHEET

CONFIDENTIAL

W1 – 366
Copy

Defense Info

UNCLASSIFIED

Operation

"NATIONAL SECURITY INFORMATION"
"Unauthorized Disclosure Subject to Criminal Sanctions."

# JANGLE

## NEVADA PROVING GROUNDS
## OCTOBER-NOVEMBER 1951

BLAST AND SHOCK MEASUREMENTS I

~~EXCLUDED FROM GENERAL DECLASSIFICATION SCHEDULE DOD 5200.1-R ISPR JULY 1972, 4-501~~

Classification canceled (or changed to unclassified) by authority of TID-CC-WER-9072 + GDS
Name and number of [illegible]
Dorothy Wagner GS-C
Name & Grade of officer making change

[redacted]

ARMED FORCES SPECIAL WEAPONS PROJECT
WASHINGTON, D.C.

AD B952222

Best Available Copy

UNCLASSIFIED

[redacted]

I-9453-52/1

UNCLASSIFIED

[redacted]

SECURITY INFORMATION

[redacted]

Defense Info

RESTRICTED DATA

This document [redacted] as defined in the Atomic [redacted] 1946. Its transmittal [redacted] disclosure of its [redacted] in any [redacted] to an unauthorized person is prohibited.

This document contains information affecting the national defense of the United States within the meaning of the Espionage Laws, Title 18 U. S. C. Sections 793 and 794. The transmission or the revelation of its contents in any manner to an unauthorized person is prohibited by law.

Classification canceled ~~(or~~ changed to Cat D1 )
by authority of TID 90.72 Jun 60 by
Name and Grade of Officer authorizing change
E B Monroe 24 Jan 61
Name & Grade of Officer making change Date

[redacted]

[redacted]

UNCLASSIFIED

Defense Info

[redacted] UNCLASSIFIED

WT-366

This document consists of 413 plus 4 pages (counting all preliminary pages in all reports and all unnumbered blanks)

Copy [illegible] of 243 copies, Series B

[redacted]

# OPERATION JANGLE

## BLAST AND SHOCK MEASUREMENTS I.

Project 1.1 Ground Acceleration Measurement (WT-388)

Project 1.2a-1 Peak Air Blast Pressures Along the Ground from Shock Velocity Measurements (WT-323)

Project 1.2a-2 Transient Ground Mechanical Effects from HE and Nuclear Explosions (WT-385)

[redacted] [redacted]

ATOMIC ENERGY ACT 1946

Reproduced Direct from Manuscript Copy by
AEC Technical Information Service
Oak Ridge, Tennessee

UNCLASSIFIED

[redacted]

OPERATION JANGLE

Project 1.1

# GROUND ACCELERATION MEASUREMENTS

By

W. E. Morris

and

Staff

June 1952

Naval Ordnance Laboratory
White Oak
Silver Spring 19, Maryland

UNCLASSIFIED

[redacted]

# PREFACE

The purpose of this report is to describe the ground acceleration measurements for the surface and underground shots of operation JANGLE. For a survey of the procedure and results, without going into instrumentation and operational details, it is suggested that Chapter 3, Plan of the Experiment, Chapter 7, Results and Discussion, and Chapter 8, Conclusions and Recommendations, be read in that order.

When separated from this report, Chapter 4, Sections 4.1 and 4.2 on Accelerometer Development and Calibration may be treated as unclassified. At a later date the sections of the report dealing with accelerometer development and calibration as well as the recording and playback sections will be published as unclassified Navords.

## ACKNOWLEDGEMENTS

The Ground Shock Program was planned with the assistance of Dr. G. K. Hartmann of the Naval Ordnance Laboratory and Dr. C. W. Lampson of the Ballistics Research Laboratories, Aberdeen Proving Grounds. The Aberdeen Proving Grounds provided valuable test facilities for pre-operation tests to check procedures and equipment. The Vitro Corporation (formerly the Kellex Corporation), through a Bureau of Ordnance contract, supplemented the engineering and supply staff of NOL and provided much able assistance in design, field engineering and procurement. The Schaevitz Engineering Company, Merchantville, New Jersey, undertook the development and manufacture of accelerometers on a very stringent time schedule and with a flexible working agreement. The fact that a new instrument was developed and two hundred and sixty units produced in about three and one-half months reflects the spirit and technical competence with which the company performed the job.

The Naval Ordnance Laboratory is indebted to the eight military officers and one civilian who were assigned to the project by the Armed Forces Special Weapons Project. This group, which comprised over one third of the total personnel, contributed in great measure to the success of the project.

The project group is indebted to LCDR D. C. Campbell, Director, Program 1, for his forthright support throughout the planning and execution of the operation.

Appreciation is expressed to Mary M. Case and Rita B. Granet who typed and assembled this report.

[redacted]

PROJECT 1.1

CONTENTS


PREFACE . . . . . iii

ACKNOWLEDGEMENTS . . . . . v

LIST OF AUTHORS . . . . . xix

ABSTRACT . . . . . xxi

CHAPTER 1 INTRODUCTION . . . . . 1

1.1 Objective . . . . . 1
1.2 History and Chronology . . . . . 1
1.2.1 Assignment of Tasks . . . . . 1
1.2.2 Operational Changes . . . . . 2
1.2.3 Preparatory Work at NOL . . . . . 3
1.2.4 Field Tests . . . . . 4
1.2.5 Preparations for the Nuclear Shot . . . 4
1.2.6 Chronology of Events. . . . . 4

CHAPTER 2 THEORY AND PREDICTIONS . . . . . 6

2.1 The Lampson Theory . . . . . 6
2.2 Predictions for the Nuclear Tests from the Lampson Theory . . . . . 7
2.3 Dugway Results . . . . . 7
2.3.1 Effect of Dugway Results in the Nuclear Predictions . . . . . 8
2.4 Underground Test at Yucca Flats . . . . . 8
2.5 Nuclear Predictions for Results of the Yucca Flats Tests . . . . . 8
2.5.1 Underground Shot . . . . . 8
2.5.2 Surface Shot . . . . . 9
2.6 Summary Reports of Seismic Waves . . . . . 9
2.7 Predictions of Frequencies for the Nuclear Underground Test . . . . . 10
2.8 Correlation of Acceleration with Damage to Structures . . . . . 10
2.8.1 Range of Acceleration to be Measured... 11

CHAPTER 3 PLAN OF THE EXPERIMENT . . . . . 14

3.1 The Plan for Amchitka Island . . . . . 14
3.2 The Revised Plan . . . . . 15
3.2.1 Effects of the Change in Site . . . . . 15
3.2.2 Effects of Results from HE Firings . . 15
3.2.3 The Final Plan . . . . . 15




[redacted]

3.2.4 Gage Distribution . . . . . 16
3.2.5 Gage Installation . . . . . 16
3.2.6 Instrumentation System . . . . . 16

CHAPTER 4 ACCELEROMETER DEVELOPMENT, CALIBRATION AND INSTALLATION . . . . . 21

4.1 Accelerometer Development . . . . . 21
4.1.1 Introductory Remarks . . . . . 21
4.1.2 Design Specifications . . . . . 22
4.1.3 Description of Gage . . . . . 23
4.1.4 Spring-Mass System . . . . . 23
4.1.5 Magnetic Circuit . . . . . 24
4.1.6 Calibration Techniques . . . . . 25
4.1.7 Damping . . . . . 28
4.1.8 Resonant Frequency . . . . . 29
4.1.9 Transfer Characteristics . . . . . 30
4.1.10 Selectivity Factor . . . . . 32
4.1.11 Temperature Dependence . . . . . 32
4.1.12 Accuracy . . . . . 33
4.1.13 Recommendations for Further Development . 33
4.2 Calibration and Oil Filling Technique of Accelerometers . . . . . 35
4.2.1 Purpose of Field Calibration . . . . . 35
4.2.2 Field Calibration Procedure . . . . . 36
4.2.3 Technique for Filling Gages with Damping Fluid . . . . . 36
4.2.4 Advisability of Use of Normalized Calibration Curves . . . . . 37
4.2.5 Establishment of Normalized Calibration Curves . . . . . 37
4.2.6 Calibration Techniques . . . . . 39
4.2.7 Electronic Equipment Used . . . . . 41
4.2.8 Calibration Procedure . . . . . 41
4.3 The Gage Capsule . . . . . 42
4.3.1 The Gage Mounting Block . . . . . 43
4.3.2 The Stem and Top Cap . . . . . 43
4.3.3 The Sleeve . . . . . 43
4.3.4 The Nose Cap . . . . . 43
4.3.5 Assembly of Capsule . . . . . 44
4.4 Gage Mounting, Capsule Assembly and Waterproofing Procedure . . . . . 44
4.4.1 Procedure for Mounting Gages in Capsule . 44
4.4.2 Assembly of Capsule . . . . . 45
4.4.3 Tuning Oscillator for Center Frequencies. 45
4.4.4 Waterproofing of Capsule and Connectors . 46

4.5 Capsule Placement . . . . . 47
4.5.1 The Placement Gear . . . . . 47
4.5.2 The Problem of Alignment . . . . . 47
4.5.3 Alignment and Placement Procedure . . . 48
4.6 Recovery of Capsules . . . . . 50
4.6.1 Desirability of Recovery . . . . . 50
4.6.2 Procedure for Recovery . . . . . 50

CHAPTER 5 RECORDING AND PLAYBACK . . . . . 75

5.1 Design Considerations . . . . . 75
5.2 Design Features . . . . . 76
5.3 Performance Characteristics . . . . . 78
5.4 [illegible]d Units . . . . . 78
5.4.1 Gage . . . . . 78
5.4.2 Gage Cable . . . . . 78
5.4.3 Oscillator-Amplifier . . . . . 79
5.4.4 Transmission Cable . . . . . 80
5.5 Instrumentation Trailer Units . . . . . 81
5.5.1 Auxiliary Signal Units . . . . . 81
5.5.2 Magnetic Tape Recorder . . . . . 82
5.5.3 Auxiliary Units . . . . . 83
5.5.4 Primary Power . . . . . 87
5.5.5 Instrumentation Trailer . . . . . 88
5.6 Record Reduction . . . . . 88
5.6.1 Reproducer . . . . . 88
5.6.2 Discriminator . . . . . 89
5.6.3 String Galvanometer Oscillograph . . . . 90
5.6.4 Calibration Oscillator . . . . . 91
5.6.5 Sequencing Unit . . . . . 92
5.6.6 Photographic Technique . . . . . 93
5.7 Performance and Recommendations . . . . . 93

CHAPTER 6 FIELD CONSTRUCTION . . . . . 137

6.1 Trailer Revetments . . . . . 137
6.2 Gage Holes . . . . . 138
6.2.1 Hole Requirements . . . . . 138
6.2.2 Drilling Operation . . . . . 139
6.2.3 Composition of Overburden . . . . . 139
6.3 Cable Trenches . . . . . 139
6.4 Roads . . . . . 142
6.5 General Conditions in Area . . . . . 142

CHAPTER 7 RESULTS AND DISCUSSION . . . . . 150

7.1 Success of the Tests . . . . . 150
7.2 Arrangement of the Accelerometers . . . . . 150

[redacted]

PROJECT 1.1


7.3 Presentation of the Data . . . . . 150
7.4 Ground Shock Phenomena Deduced from Inspection of the Acceleration Records . . . . . 151
7.4.1 Appearance of Acceleration Records . . 151
7.4.2 Ground Shock Induced by Air Blast . . . 151
7.4.3 Reflected and Refracted Ground Shock. . 152
7.4.4 Recapitulation of the Origins of Ground Shock . . . . . 153
7.4.5 Superposition of Fundamental Acceleration and Air Blast Acceleration . . . . 153
7.5 Ground Shock Propagation . . . . . 154
7.5.1 Surface Shot . . . . . 154
7.5.2 Underground Shot . . . . . 155
7.6 Analysis of Acceleration as a Function of Distance . . . . . 155
7.6.1 Reasons for the Form of the Analysis. . 155
7.6.2 Surface Shot Analysis . . . . . 157
7.6.3 Underground shot Analysis . . . . . 159
7.6.4 Comparison of Acceleration from the Surface Shot with Acceleration from the Underground Shot . . . . . 161
7.6.5 Attenuation of Air Blast Acceleration . 163
7.7 Study of Acceleration as a Function of Depth . 164
7.7.1 Surface Shot. . . . . 164
7.7.2 Underground Shot . . . . . 164
7.7.3 Summary of Depth Studies for the Surface and Underground Shots . . . . . 165
7.8 Ground Shock Frequencies . . . . . 165
7.8.1 General Comments on Acceleration Record Frequencies . . . . . 165
7.8.2 Comparison of Surface Shot and Underground Shot Frequencies . . . . . 165
7.8.3 Implications of the Frequency Analysis. 173
7.9 Gage Frequencies and their Influence on the Recording of Acceleration . . . . . 173
7.10 Scaling of HE and Nuclear Charges . . . . . 175
7.10.1 General Difficulties in Scaling . . . . 175
7.10.2 Scaling for the Underground Shot . . . 176
7.10.3 Scaling for the Surface Shot . . . . . 178
7.10.4 General Observations Concerning Scaling . . . . . 178
7.11 Accuracy of the Measurements . . . . . 179
7.11.1 Accuracy of the Accelerometers . . . . 179
7.11.2 Effect of the Ratio of Signal to Gage Frequency on the Accuracy . . . . . 179
7.11.3 Accuracy of the Recording System . . . 180
7.11.4 Apparent Inaccuracies . . . . . 180


[redacted]



[redacted]

CHAPTER 8 CONCLUSIONS AND RECOMMENDATIONS . . . . . 226

8.1 Conclusions . . . . . 226
8.2 Recommendations . . . . . 228

CHAPTER 9 ADMINISTRATIVE ARRANGEMENTS . . . . . 231

9.1 Arrangements with the Ballistic Research Laboratories . . . . . 231
9.2 Field Group Organization . . . . . 231
9.3 Supply Arrangements at the Naval Ordnance Laboratory . . . . . 232
9.4 Shipping . . . . . 233
9.5 Amount of Shipping . . . . . 234
9.6 Return Shipping . . . . . 235

APPENDIX A Results of Acceleration Measurements from the 40,000 lb. HE Shot at Yucca Flats . . . . . 236

APPENDIX B Copies of Acceleration Records for the Surface and Underground Nuclear Shots . . . . . 249

[redacted]

PROJECT 1.1

ILLUSTRATIONS


CHAPTER 2 THEORY AND PREDICTIONS

2.1 Ground Acceleration from the Dugway Underground Tests . . . . . 12
2.2 Prediction of Horizontal and Vertical Ground Acceleration Based on Scaling of NOL Results from the 40,000 lb HE Shot at Yucca Flats . . . . . 13

CHAPTER 3 PLAN OF THE EXPERIMENT

3.1 Layout of Blast Lines . . . . . 19
3.2 Typical Blast Line Layout . . . . . 20

CHAPTER 4 ACCELEROMETER DEVELOPMENT, CALIBRATION AND INSTALLATION

4.1 Sectional Diagram of Gage Construction . . . . . 52
4.2 Schaevitz Type B Accelerometer . . . . . 53
4.3 Inductance of Coil vs Gap Spacing . . . . . 54
4.4 Q of Coil vs Gap Spacing . . . . . 55
4.5 Variation of Inductance Due to Lateral Displacement of Pad Along Line of Pole Faces . . . 56
4.6 Variation of Inductance Due to Lateral Displacement of Pad in a Direction Normal to the Line of Pole Faces . . . . . 57
4.7 Variation of Inductance Due to Rotation of Mu-metal Pad . . . . . 58
4.8 NOL Spin Table Used for Static Calibrations . . . . 59
4.9 Tilt Table Used for Static Calibrations . . . . . 60
4.10 MB Shake Table Used for Dynamic Calibrations . . . 61
4.11 Frequency Response to Sinusoidal Excitation . . . . 62
4.12 Study of Damping Properties by Drop Tests . . . . . 63
4.13 Normalized Variation of Damping Factor with Temperature . . . . . 64
4.14 Natural Frequency vs Gage Rating . . . . . 65
4.15 Gage Transfer Characteristic . . . . . 66
4.16 Peak to Peak Response to Sinusoidal Excitation . . 67
4.17 Capsule Assembly - Gage Mounting Block . . . . . 68
4.18 Capsule Assembly - Stem and Top Cap . . . . . 68
4.19 Capsule Assembly - Sleeve . . . . . 68
4.20 Capsule Assembly - Nose Cap . . . . . 68
4.21 Components of Capsule Assembly . . . . . 69
[redacted]age Capsule . . . . . 69


[redacted]



[redacted]

4.23 Gages Installed on Mounting Block . . . . . 70
4.24 Capsule on Calibration Tripod . . . . . 70
4.25 Field Calibration Console . . . . . 71
4.26 End View of Waterproofed Capsule . . . . . 71
4.27 Assembled and Waterproofed Capsule . . . . . 72
4.28 Placement Gear Assembly . . . . . 73
4.29 Pouring Cal-Seal . . . . . 72
4.30 Lowering Capsule into Gage Hole . . . . . 74
4.31 Friction Block Arrangement for Lowering Gage Capsule . . . . . 74

CHAPTER 5 RECORDING AND PLAYBACK

5.1 Typical Station Installation . . . . . 96
5.2 Signal Distribution for Typical Bank . . . . . 97
5.3 Power Distribution for Typical Bank . . . . . 98
5.4 Over-all Recording System . . . . . 99
5.5 Oscillator - Amplifier . . . . . 100
5.6 Bridge Circuit for Combined Output . . . . . 101
5.7 Signal Attenuation in MCOS-6 Cable . . . . . 102
5.8 Cable Laying . . . . . 103
5.9 Cable Connection . . . . . 103
5.10 Inter-Cabinet Layout . . . . . 104
5.11 Distribution Panel . . . . . 105
5.12 D.C. Power Supply Panel . . . . . 106
5.13 Dynamotor Circuit . . . . . 107
5.14 Filament Supply Panel . . . . . 108
5.15 Ampex Magnetic Tape Recorder . . . . . 109
5.16 Seven Channel Record Amplifier . . . . . 110
5.17 Record Amplifier Power Supply and Bias Oscillator . 111
5.18 Power Amplifier for Capstan Motor Supply . . . . . 112
5.19 Timing Oscillator . . . . . 113
5.20 Reference Oscillator . . . . . 114
5.21 Reference Oscillator Power Supply . . . . . 115
5.22 Filter Scope . . . . . 116
5.23 Field Cable Tester . . . . . 117
5.24 Blue Box . . . . . 118
5.25 Battery Banks in Trailer . . . . . 119
5.26 Motor Generators in Trailer . . . . . 119
5.27 Power Control for Typical Bank . . . . . 120
5.28 Timing Relays . . . . . 121
5.29 Instrumentation Trailer . . . . . 122
5.30 Instrumentation Trailer-Inside-Towards Rear . . . . 122

5.31 Instrumentation Trailer-Inside-Right Side . . . . 123
5.32 Instrumentation Trailer-Inside-Left Side . . . . 123
5.33 Instrumentation Trailer - Layout . . . . . 124
5.34 Instrumentation Trailer - Battery Chargers . . . 125
5.35 Playback System . . . . . 126
5.36 Ampex Magnetic Tape Reproducer . . . . . 127
5.37 Playback Amplifier . . . . . 128
5.38 69 Cycle Capstan Motor Amplifier . . . . . 129
5.39 Tape Speed Controller . . . . . 130
5.40 Discriminator . . . . . 131
5.41 String Galvanometer Oscillograph . . . . . 132
5.42 Calibration Oscillator . . . . . 133
5.43 Calibration Oscillator Power Supply . . . . . 134
5.44 Sequencing Unit . . . . . 135
5.45 Developing Tanks. . . . . 136
5.46 Print Dryer . . . . . 136

CHAPTER 6 FIELD CONSTRUCTION

6.1 Details of Trailer Shelter . . . . . 143
6.2 Trailer Shelter Construction . . . . . 144
6.3 Trailer Shelter and Trailer . . . . . 144
6.4 Rotary Drill Rig Showing Bucket Type Bit . . . . 145
6.5 Rotary Drill Rig and Crew . . . . . 145
6.6 Geophysical Drill Rig and Crew . . . . . 146
6.7 Gage Holes Drilled in Bottom of Lateral Cable Trench . . . . . 146
6.8 General View of Blast Line Showing Main and Lateral Cable Trenches . . . . . 147
6.9 Gage Holes Drilled at Sides of Lateral Cable Trench . . . . . 147
6.10 Details of a Typical Station on NOL - BRL Blast Line . . . . . 148
6.11 View Along Blast Line . . . . . 149
6.12 Working Conditions in the Dust Along the Blast Line . . . . . 149

CHAPTER 7 RESULTS AND DISCUSSION

7.1 Surface Shot - Arrival Times of Air and Ground Shock . . . . . 181
7.2 Surface Shot - Velocity of Initial Ground Shock . . . . . 182
7.3 Surface Shot - First Outward Horizontal Acceleration (Excluding Air Blast Effect) . . . . 183

[redacted]

PROJECT 1.1


7.4 Surface Shot - Maximum Inward Horizontal Acceleration . . . . . 184
7.5 Surface Shot - Maximum Outward Horizontal Acceleration (Excluding Air Blast) . . . . . 185
7.6 Surface Shot - Maximum Upward Vertical Acceleration (Excluding Air Blast Effect) . . . . . 186
7.7 Surface Shot - Maximum Downward Vertical Acceleration (Excluding Air Blast Effect) . . . . . 187
7.8 Surface Shot - Maximum Inward Horizontal Acceleration (Including Air Blast Effect) . . . . . 188
7.9 Surface Shot - Maximum Outward Horizontal Acceleration (Including Air Blast Effect) . . . . . 189
7.10 Surface Shot - Maximum Upward Vertical Acceleration (Including Air Blast Effect) . . . . . 190
7.11 Surface Shot - Maximum Downward Vertical Acceleration (Including Air Blast Effect) . . . . . 191
7.12 Surface Shot - Maximum Transverse Acceleration (Including Air Blast Effect) . . . . . 192
7.13 Surface Shot - Composite of All Maximum Acceleration Plots which Exclude Air Blast Effect (Figs. 7.4 to 7.7) . . . . . 193
7.14 Surface Shot - Composite of All Maximum Acceleration Plots that Include Air Blast Effect (Figs. 7.8 to 7.12) . . . . . 194
7.15 Surface Shot - Composite Plot of Overall Maximum Horizontal, Vertical, and Transverse Acceleration (Including and Excluding Air Blast Effect) . . . . 195
7.16 Surface Shot - Maximum Horizontal Acceleration vs Depth (Excluding Air Blast Effect) . . . . . 196
7.17 Surface Shot - Maximum Vertical Acceleration vs Depth (Excluding Air Blast Effect) . . . . . 197
7.18 Surface Shot - Maximum Horizontal Acceleration vs Depth (Including Air Blast Effect) . . . . . 198
7.19 Surface Shot - Maximum Vertical Acceleration vs Depth (Including Air Blast Effect) . . . . . 199
7.20 Surface Shot - Arrival Times of Corresponding Peaks . . . . . 200
7.21 Underground Shot - Arrival Times of Air and Ground Shock . . . . . 201
7.22 Underground Shot - Velocity of Initial Ground Shock . . . . . 202
7.23 Underground Shot - First Outward Horizontal Acceleration (Excluding Air Blast Effect) . . . . . 203
7.24 Underground Shot - Maximum Inward Horizontal Acceleration (Excluding Air Blast Effect) . . . . . 204


[redacted]



[redacted]

7.25 Underground Shot - Maximum Outward Horizontal Acceleration (Excluding Air Blast Effect) . . . . 205
7.26 Underground Shot - Maximum Upward Vertical Acceleration (Excluding Air Blast Effect) . . . . 206
7.27 Underground Shot - Maximum Downward Vertical Acceleration (Excluding Air Blast Effect) . . . . 207
7.28 Underground Shot - Maximum Inward Horizontal Acceleration (Including Air Blast Effect) . . . . 208
7.29 Underground Shot - Maximum Outward Horizontal Acceleration (Including Air Blast Effect) . . . . 209
7.30 Underground Shot - Maximum Upward Vertical Acceleration (Including Air Blast Effect) . . . . 210
7.31 Underground Shot - Maximum Downward Vertical Acceleration (Including Air Blast Effect) . . . . 211
7.32 Underground Shot - Maximum Transverse Acceleration (Including Air Blast Effect) . . . . 212
7.33 Underground Shot - Composite of All Maximum Acceleration Plots Which Exclude Air Blast Effect (Figs. 7.24 to 7.27) . . . . . 213
7.34 Underground Shot - Composite of All Maximum Acceleration Plots Which Include Air Blast Effect (Figs. 7.28 to 7.32) . . . . . 214
7.35 Underground Shot - Composite Plot of Overall Maximum Horizontal, Vertical, and Transverse Acceleration (Including and Excluding Air Blast Effect) . . . . . 215
7.36 Underground Shot - Maximum Horizontal Acceleration vs Depth (Excluding Air Blast Effect) . . . . . 216
7.37 Underground Shot - Maximum Vertical Acceleration vs Depth (Excluding Air Blast Effect) . . . . . 217
7.38 Underground Shot - Maximum Horizontal Acceleration vs Depth (Including Air Blast Effect) . . . . . 218
7.39 Underground Shot - Maximum Vertical Acceleration vs Depth (Including Air Blast Effect) . . . . . 219
7.40 Underground Shot - Arrival Times of Corresponding Peaks . . . . . 220
7.41 Surface and Underground Shot - Composite Plot of Overall Maximum Horizontal Acceleration . . . 221
7.42 Surface and Underground Shot - Composite Plot of Overall Maximum Vertical Acceleration . . . . 222

[redacted]



7.43 Surface and Underground Shot - Composite Plot of Overall Maximum Horizontal, Vertical, and Transverse Acceleration . . . . . 223
7.44 Typical Response Characteristics of Accelerometers to Sinusoidal Acceleration . . . . . 224
7.45 Typical Response Characteristics of Accelerometers to Transient Accelerations . . . . . 225

APPENDIX A RESULTS OF ACCELERATION MEASUREMENTS FROM THE 40,000 lb HE SHOT AT YUCCA FLATS

A.1 40,000 lb Shot - Prediction of Maximum Acceleration from Lampson's Theory and Comparison With the Test Result . . . . . 238
A.2 40,000 lb Shot - Arrival Time of Initial Ground Acceleration . . . . . 239
A.3 40,000 lb Shot - Velocity of Initial Ground Shock . 240
A.4 40,000 lb Shot - First Horizontal Acceleration Outward (Including Air Blast) . . . . . 241
A.5 40,000 lb Shot - Maximum Horizontal Acceleration (Including Air Blast) . . . . . 242
A.6 40,000 lb Shot - First Vertical Acceleration Upward (Excluding Air Blast) . . . . . 243
A.7 40,000 lb Shot - Maximum Vertical Acceleration (Including Air Blast) . . . . . 244
A.8 40,000 lb Shot - Maximum Downward Acceleration Due to Air Blast Alone . . . . . 245
A.9 NOL Acceleration Records from HE-2 (40,000 lb) . . 247

APPENDIX B COPIES OF ACCELERATION RECORDS FOR THE SURFACE AND UNDERGROUND NUCLEAR SHOTS

B.1 Horizontal Accelerations from Surface Shot . . . . 251
B.2 Vertical Accelerations from Surface Shot . . . . . 252
B.3 Transverse Accelerations from Surface Shot . . . . 253
B.4 Horizontal Accelerations from Primary and Back-up Gages on Surface Shot . . . . . 253
B.5 Vertical Accelerations from Primary and Back-up Gages on Surface Shot . . . . . 253
B.6 Horizontal Accelerations from Surface Shot for 10, 20, 30 ft Depths . . . . . 254
B.7 Vertical Accelerations from Surface Shot for 10, 20, 30 ft Depths . . . . . 255
B.8 Horizontal Accelerations from Underground Shot . . 256
B.9 Vertical Acceleration from Underground Shot . . . 257

[redacted]



[redacted]

[redacted]



B.10 Transverse Accelerations from Underground shot . . 258
B.11 Horizontal Acceleration from Primary and Back-up Gages on Underground Shot . . . . . 258
B.12 Vertical Acceleration from Primary and Back-up Gages on Underground Shot . . . . . 258
B.13 Horizontal Accelerations from Underground Shot for 10, 20, 30 ft Depths . . . . . 259
B.14 Vertical Accelerations from Underground Shot for 10, 20, 30 ft Depths . . . . . 260
B.15 Samples of Original Records Showing High and Low Signal to Noise Ratio . . . . . 261

TABLES

CHAPTER 3 PLAN OF THE EXPERIMENT

3.1 Accelerometer Placement Data . . . . . 17

CHAPTER 5 RECORDING AND PLAYBACK

5.1 Station Distribution to Instrumentation Banks . . 77

CHAPTER 6 FIELD CONSTRUCTION

6.1 Composition of Overburden Along Instrument Lines . . . . . 140

CHAPTER 7 RESULTS AND DISCUSSION

7.1 Compilation of the Magnitudes of Acceleration Components at Several Distances for the Surface and Underground Shots . . . . . 162

7.2 Comparison of Air Blast and Air Blast Acceleration for the Surface and Underground Shots . . . . 163

7.3 Tabulation of Surface Shot Frequencies and Associated Accelerometer Characteristics . . . . . 166

7.4 Tabulation of Underground Shot Frequencies and Associated Accelerometer Characteristics . . . 169

[redacted]



[redacted]

[redacted]

PROJECT 1.1

## LIST OF AUTHORS


CHAPTER 1 Introduction
by - W. E. Morris and F. E. Somers

CHAPTER 2 Theory and Predictions
by - W. E. Morris

CHAPTER 3 Plan of the Experiment
by - F. E. Somers and W. E. Morris

CHAPTER 4 Accelerometer Development, Calibration and Installation
by - B. Sussholz, assisted by P. W. Aronson, F. E. Somers, V. E. Denning, W. H. Fleming, Jr., B. M. Loring, R. G. Quick, E. J. Culling, J. F. Vogl, J. W. Kee, R. E. Frederick, S. F. Brigham, and J. I. Mather

CHAPTER 5 Recording and Playback
by - J. Petes, assisted by P. W. Shadle, F. H. Brannin, Jr., L. B. Browder, B. B. Fannin, J. W. Kee, S. F. Brigham, J. I. Mather, and on drawings by G. W. Robinson and H. A. Milloit

CHAPTER 6 Field Construction
by - F. E. Somers

CHAPTER 7 Results
by - W. E. Morris with the assistance of B. Sussholz, P. W. Aronson, W. H. Fleming, Jr., and V. E. Denning in data reduction

CHAPTER 8 Conclusions and Recommendations
by - W. E. Morris

CHAPTER 9 Administrative
by - F. E. Somers


[redacted]



[redacted]

PROJECT 1.1

## ABSTRACT

Ground acceleration from 1 kt nuclear weapons detonated on the surface and at a depth of 17 ft in the ground were measured in the vertical, radial, and transverse directions at various distances.

A new inductance type accelerometer and the recording system are described. The ground shock intelligence received by the accelerometer was multiplexed and transmitted by cable as an FM signal and recorded on magnetic tape.

Excellent acceleration records were obtained from the 76 and 80 channels employed on the surface and underground shots respectively.

Important contributions to the acceleration pattern are made by ground shock transmitted directly from the charge, ground shock reflected and refracted from underlying bedrock, and from ground shock induced by the air blast.

The propagation, effect of depth, frequency characteristics, and attenuation of the ground acceleration are discussed. The air blast induced acceleration attenuates like the air blast, and is different from the so-called fundamental acceleration (air blast effect excluded) which attenuates at about the 1.6 power of the reduced distance, $\lambda$.

The effectiveness of the surface and underground shots is discussed from the standpoint of magnitude and frequency. When the high frequency transient air blast acceleration is considered, the surface shot is more effective; when the air blast effect is excluded and only the fundamental type acceleration, which has much lower frequencies, is considered, the underground shot is more effective.

Scaling is discussed and the results indicate that when the air blast acceleration is separated out, the acceleration from the underground shot scales reasonably well with the 40,000 lb TNT charge detonated at the site.

[redacted]

# CHAPTER 1

# INTRODUCTION

## 1.1 OBJECTIVES

The principle objectives of Project 1.1, Ground Acceleration Measurements, were as follows:

1. To measure the radial, vertical, and transverse components of ground acceleration as a function of time, distance, and depth from nuclear weapons detonated on the ground surface and in the ground.

2. To compare the effectiveness of a surface nuclear explosion with an underground nuclear explosion.

3. To investigate scaling of nuclear explosions with TNT explosions.

4. To obtain information from surface and underground nuclear explosions on the propagation, attentuation, wave form, and frequency characteristics of ground acceleration.

5. In cooperation with other projects, to correlate medium effects such as acceleration, pressure, and displacement with damage to structures.

## 1.2 HISTORY AND CHRONOLOGY

### 1.2.1 Assignment of Tasks

The task of making ground shock and air blast measurements was assigned jointly to the Naval Ordnance Laboratory and the Ballistics Research Laboratories through conferences and official correspondence in the Fall of 1950. The responsibilities for the assignments to these laboratories under Projects 1.1 and 1.2 were divided as follows:

Ballistics Research Laboratories

1. Air blast measurements along the ground (peak pressure by velocity method)

2. Ground pressure measurements in free earth



[redacted]

3. Back-up measurements for ground accelerations (ERA gages)

Naval Ordnance Laboratory

1. Ground acceleration measurements

2. FM recording system and power supply for acceleration and pressure measurements using inductance gages

3. Analysis of base surge (Photography by Sandia)

4. Analysis of transient ground displacements (Photography by Sandia)

5. Measurement of Free Air peak pressure by smoke rocket photography method

6. Procurement and shipping of major items of equipment.

1.2.2 Operational Changes

Originally the operation bore the name of WINDSTORM and was scheduled to occur on Amchitka Island in September 1951. The Amchitka site appeared suitable as determined from a seismic and geological survey conducted in June of 1950; bedrock was at a 400 foot depth or greater, the water table was low, and the area was sufficiently level to permit measurements. A later survey indicated that no area on the Island was suitable and that the most acceptable location could not be used because of the lack of roads. The alternate area which was selected had a conglomerate soil consisting of boulders, rock strata, geological faults and dykes, a shallow water table, and bedrock depths varying from zero to eighty feet. The conduct of the test in this area was strongly opposed by the Naval Ordnance Laboratory because of the impossibility of reliable predictions and the questionable meaning of any results which would be obtained. The operational site was changed to Nevada in May 1951; the operation was renamed JANGLE and was finally scheduled for the month of November 1951. The size of the weapon to be used for the test was changed from twenty-five KT to one KT. These changes necessitated many alterations in the operational and instrumentation plans. The change in weapon yield required that the instrument lines be shortened and that the instrumentation system be correspondingly modified. Some accelerometers were shipped back to the manufacturer for modifications to their ratings and related changes made in other elements of the instrumentation system.

[redacted]



[redacted]

1.2.3 Preparatory Work at NOL

Project work at the Laboratory commenced on a limited scale in December 1950, and got into full swing in January upon the arrival of most of the personnel who were to be associated with the field group. Weekly meetings were held with Vitro Corporation representatives and certain phases of the program were delegated to that group for design, development, and production. Some of the most important items so delegated were the field oscillators, distribution panels, field test equipment, and the capsule placement gear.

Because of the short time schedule of the project it was decided to use an inductance type gage, if possible, and to adopt the FM magnetic tape recording system used on GREENHOUSE. The recorders required some modifications of design to permit multiplexing but their procurement presented no serious threat to the time schedule as did the accelerometers.

Research into the gage and oscillator design proceeded at an accelerated pace, along with considerations of expected effects. It became apparent rather early that the type of instrument required was not manufactured commercially in the required quantity. This predicated a decision to design and develop a new gage in conjunction with the Schaevitz Engineering Company, Merchantville, New Jersey. The design of the gage was discussed formally with Schaevitz during the last week of February, and a preliminary model was delivered to the laboratory about three weeks later. By cooperative and concentrated effort, the many problems normal to gage development were successfully solved as materials were being procured and standard components manufactured. Production, research, and calibration ran almost concurrently, with the net result that three and one-half months after the design conference over two hundred and fifty of the accelerometers had been delivered. It is believed to be worthy to note at this point that one hundred and fifty two of these gages were placed in the ground in the middle of September, and all except one functioned during the shots in the latter part of November.

Some thought and effort was devoted to the procurement of velocity and displacement gages, but instruments which suited the situation and the recording system were not available. A project to develop a displacement gage and a velocity gage was abandoned after preliminary sketches and models indicated that such gages could not be developed and produced in the limited time available.

The procurement of general supplies and materials was accomplished by the NOL Supply Department and the Vitro Corporation. In general, large items such as cable and oscillators were procured

by the Vitro Corporation while the larger number of smaller items were purchased through the Navy supply sources.

### 1.2.4 Field Tests

During the last two weeks in May the NOL and Vitro Corporation field groups conducted a series of tests at the Aberdeen Proving Grounds to check out the instrumentation system. Two 500 pound HE underground shots and a 1,000 pound HE surface shot were successfully instrumented and information was obtained as to the relative magnitude of effects from a surface shot as compared to an underground shot.

In general, equipment and procedures proved satisfactory and the minor difficulties noted were easily adjusted during the next few weeks.

The entire field group proceeded to the Nevada Test Site during the latter part of August 1951, and instrumented the 40.000 pound HE shot (HE-2) on September 3, 1951. This participation in HE-2 was extremely valuable in giving experience to the field group and in providing information from which the predicted results from the nuclear shots were revised. Favorable comparison of NOL and SRI instrumentation was also obtained. Records and results of this test are contained in Appendix A.

### 1.2.5 Preparations for the Nuclear Shot

After analysis of the results from HE-2 shot and consideration of other firings in the area, the planned layout of gages for the nuclear shots was modified. A final plan was drawn up and work commenced on installing the gages in the ground. The installations for both the surface and underground instrument lines were completed in the latter part of September. After the two systems had been checked out using the power supply and recorders that were to be used for the tests, the main field parties returned to their laboratories, leaving only test personnel at the site. The complete field parties returned to the Site on November 1, 1951 to complete preparations. On the basis of a revised prediction of the crater sizes an additional station was installed nearer the zero point on the underground instrument line. The installation of timing signals and final adjustments were completed well ahead of the scheduled time for the surface shot.

### 1.2.6 Chronology of Events

A chronology of a few of the most important events are listed below to give an indication of the time schedule of the project:

## CHRONOLOGY

| | |
|---|---|
| June 1950 | Preliminary discussions and correspondence |
| November 1950 | First planning conferences |
| November 15, 1950 | First funds received at NOL |
| November 30, 1950 | Contract let to Kellex Corporation |
| | Approval of operation by RDB |
| January 1951 | Recording system instrumentation decided upon |
| March 1, 1951 | Gage design decided upon |
| May 9, 1951 | Site changed from Amchitka Island to Nevada Test Site |
| May 15 to June 1951 | Field test at Aberdeen Proving Grounds |
| July 1, 1951 | Recording trailers purchased |
| July 1951 | Packing started at NOL |
| August 29, 1951 | Field party arrived Nevada Test Site |
| September 3, 1951 | Participation in HE-2 at Nevada Test Site (40,000 pound HE) |
| September 29, 1951 | Principal preparations for nuclear shots completed - main party returned to NOL |
| November 1, 1951 | Main party returned to site and completed preparations |
| November 19, 1951 | Surface shot |
| November 29, 1951 | Underground shot |
| December 1, 1951 | Main party returned to NOL |
| December 19, 1951 | Preliminary report delivered to AFSWP |

[redacted]

CHAPTER 2

## THEORY AND PREDICTIONS

### 2.1 THE LAMPSON THEORY

The only theory on the effects of underground explosions is that of C. W. Lampson[1] who derived empirical formulae for ground acceleration, velocity, displacement, cratering, and damage to structures from experiments conducted at Princeton, Camp Gruber in Oklahoma, and other places. Lampson's formula for peak acceleration takes the form:

$$A = \frac{Fk\,10^{-5}}{\rho\, W^{1/3}} \left(120\,\lambda^{-4} + 0.3\,\lambda^{-2} + .04\,\lambda^{-1}\right) \qquad (2.1)$$

Where A = horizontal or vertical acceleration in units of gravity

W = weight of TNT (lbs)

$\rho$ = soil density $\left(\frac{\text{lbs}}{384\ \text{in}^3}\right)$

k = soil constant; is equal to $\frac{1}{25}\rho v^2$ where $\rho$ is the density as above and v is the velocity (in/sec)

F = coupling factor determined by the depth of burial of the charge

F = 0.21 for charge on the surface

F = 0.32 for $\lambda_c = 0.135$, where $\lambda_c$ is equal to the depth of burial of the charge divided by $W^{1/3}$. This is the $\lambda_c$ value for a 1 KT bomb at a depth of 17 ft.

$\lambda = r/W^{1/3}$ where r is the distance from the center of the charge (ft).

The factors influencing the transmission of acceleration, velocity, pressure, etc. through the ground are discussed in detail in reference 1.

---

[1] C. W. Lampson, Effects of Underground Explosions
Vol. I Subsurface and Target Phenomena
Vol. II Subsurface and Surface Phenomena
Vol. III Resulting Damage to Structures
Vol. I, II, III: Interim Report No. 26 to the Chief of Engineers U.S. Army by the Committee on Fortification Design, National Research Council
Vol. IV Influence of Variations of Soil Type and Depths of Charge and Gauge, NDRC Report No. A-359, OSRD Report No. 6304.
Final Report on Effects of Underground Explosions, NRDC Report A-479, OSRD Report No. 6645.

[redacted]



[redacted]

The acceleration is very dependent on the type of soil, as is evident from the fact that the soil constant, k, may vary by a factor of as much as 100 for different soils. To a less degree the acceleration is dependent on F, the coupling factor related to the depth of burial of the charge. This factor may vary by a factor of 5 when the charge depth varies from the surface to an optimum depth of 2 $W^{1/3}$.

It should be borne in mind that most of these early experiments were carried out at charge depths and gage depths of 2 $W^{1/3}$ ($\lambda_c = 2$). This depth differs considerably from the HE and nuclear tests conducted at a $\lambda_c$ of 0.135. It may also be mentioned that most of the acceleration records were derived from velocity records, where the first significant velocity peak was the only one analysed. It is true that usually this first peak was the maximum.

## 2.2 PREDICTIONS FOR THE NUCLEAR TESTS FROM THE LAMPSON THEORY

As is evident in equation 2.1, the underground tests on different size charges showed that acceleration scaled in accordance with the $W^{1/3}$ scaling law. Our predictions also assumed the validity of the scaling law and were based on this equation. Great extrapolation was necessary from several thousand pounds to 40,000,000 lbs, later reduced to 2,000,000 lbs. Also it was necessary to assume that a nuclear underground explosion scaled the same as HE.

Values of the seismic velocity used to compute the soil constant were not available for purposes of preliminary planning at both the Amchitka site and the Nevada site. Consequently, early predicted results were based on an estimated k upon which little reliability could be placed. The ranges of the instruments of necessity were based on these early predictions. Later, when reliable seismic velocity and soil density information became available, the value for k had to be revised by a factor of 4 or more, and this necessitated several revisions of the blast line layout and the changing of some gage ranges.

## 2.3 DUGWAY RESULTS

In July, 1951, preliminary results from the 320,000 lb shot and smaller shots at the Dugway Proving Grounds became available from Engineering Research Associates and the Stanford Research Institute. The results were compared to the Lampson formula, and are illustrated in Fig. 2.1, which is a composite plot of the data. In this comparison a "best guess" of 7,000 was selected for k. For the 2,560 lb and 40,000 lb shot, the slope of the SRI curve and the Lampson curve agrees, and if the soil constant were adjusted, the theoretical and

experimental values would be in substantial agreement. The existence of a plateau for the 40,000 lb shot was ascribed to reflection and refraction from some underlying layer or from the water table. This, then, would be a local condition and would not apply at a different location.

Considerable confusion resulted from the results of the 320,000 lb shot. The ERA data initially appeared to follow the Lampson curve, while the SRI data was at considerable variance with the Lampson curve. The SRI curve gave a slope of about 1.5 instead of an initial slope of 4 required by the Lampson formula. This raised the question as to whether the Lampson formula would scale for very large charges.

### 2.3.1 Effect of Dugway Results in the Nuclear Predictions

The net result of the Dugway Results was that they gave some assurance that our predictions were of the right order of magnitude, since the full scale Dugway shot was 0.54 scale for a 1 KT charge. However, due to these inconclusive Dugway results, the Lampson equation was used for predictions at the Nevada site.

## 2.4 UNDERGROUND TEST AT YUCCA FLATS

The Naval Ordnance Laboratory participated in the 40,000 lb (HE-2) shot at Yucca Flats in September, 1951. On the basis of seismic information, a k of 8,000 was suggested for a distance from zero up to 400 ft., and a k of 18,000 was suggested for distances beyond 400 ft. The results are summarized in Appendix A, and show that the Lampson theory did not agree with the results, either in first acceleration peaks ( Fig. A.4 and Fig. A.6) or in maximum acceleration (Fig. A.5 and Fig. A.7). The curves have a slope of around 1.6 instead of a slope of 4 as predicted by the Lampson equation. Figure A.1 shows the difference between the predicted and actual results for the 40,000 lb shot. It is observed that for a soil constant of 8,000 and at a $\lambda$ of 2 the maximum acceleration is 8.2 g as against the predicted value of 35.4 g, which is a factor of 4.4 less than that predicted. For a soil constant of 18,000 and at a $\lambda$ of 20, the maximum acceleration is 0.2 g instead of the predicted .036 g, which is a factor of 5.6 larger than predicted. The cross over point for the two curves is at a $\lambda$ of 3.6. These figures give an indication of the magnitude of the differences between the results and the predictions from the Lampson formula.

## 2.5 NUCLEAR PREDICTIONS FROM RESULTS OF THE YUCCA FLATS TESTS

### 2.5.1 Underground Shot

As a result of the HE tests at Yucca Flats, it was apparent that the Lampson formula did not apply for this site.

Accordingly, it was decided to scale the HE curve for maximum acceleration up to the nuclear charge weight. The RC yield of the nuclear weapon was predicted to be 1.25 KT. Not knowing the fraction of energy available for ground shock, it was agreed to assume a nominal value of 1 KT. This scaling is accomplished by dividing the HE acceleration at a given $\lambda$ by the scale factor $\left(\frac{2,000,000}{40,000}\right)^{1/3} = 3.68$. The HE horizontal and vertical values for acceleration differed by about 25%; however, due to the uncertainty involved, a single curve averaging the curves of Fig . A.5 and Fig. A.7 was used for predicting both the horizontal and vertical acceleration for the nuclear underground shot. Figure 2.2 shows the predicted acceleration for the underground and surface nuclear shots.

### 2.5.2 Surface Shot

No data existed on the acceleration to be expected from a surface shot at the time the instrumentation was installed for the nuclear test, as the 2,500 lb surface shot data (HE-4) was not yet available. Several months previous, NOL and BRL had conducted an instrument check out test at Aberdeen, wherein charges were detonated when resting on the surface and when just buried. These charges were not at scale depth, and the water table was about 5 ft below the ground surface, so the conditions of this test were not at all similar to the Nevada tests. The results indicated that the surface shot, in this case, produced about 1/2 the acceleration that was produced by the shallow underground shot.

The coupling factor, F, in equation 2.1 decreases from 0.3 to 0.2 for a charge at a depth of $\lambda_c = 0.135$ and a charge with its center of gravity at the surface respectively. Thus for a charge resting on the ground it would seem reasonable to assume that the surface shot would produce accelerations somewhat less than 2/3 that of the underground shot.

Considering all these factors, it was decided that the surface shot prediction would be 1/2 that of the underground shot; accordingly, 1/2 of the expected acceleration for the underground shot was taken as the prediction for the surface shot.

## 2.6 SUMMARY REPORTS OF SEISMIC WAVES

In the early stages of planning and preparation time was at a premium and much information was needed. In order to assist NOL and BRL in their preliminary planning, Dr. Henry J. Birkenhauer, S.J., from the Seismological Observatory of John Carroll University prepared

two reports[2,3] summarizing the literature and current knowledge on the subject of the nature and effects of seismic waves from earthquakes and underground explosions. These reports contain a good bibliography and furnish valuable resumes on the subject of the nature of propagation, magnitude, and periods of seismic waves from earthquakes and underground explosions. Structural response to seismic waves, design criteria, and damage criteria are also discussed.

## 2.7 PREDICTION OF FREQUENCIES FOR THE NUCLEAR UNDERGROUND TEST

In designing instruments to measure a particular phenomenon, it is important to know the frequencies involved. In an accelerometer of the type described in Chap. 4, the frequency of the phenomenon being measured should be low compared to the natural frequency of the gage, for as the frequency being measured approaches the natural frequency of the gage the error in the measured acceleration increases. In addition to the gage, the recording system places limitations on the frequencies that can be measured.

Due to the importance of knowing the frequencies to be measured an effort was made to estimate the frequencies to be expected from an underground atomic explosion. Various sources such as the Princeton and Camp Gruber data of Lampson, underground measurements of the TRINITY and GREENHOUSE tests, records of various earthquakes, the summary of various earthquake and quarry blasting data[2,3], and the Dugway results were all examined. The frequencies reported covered ranges from 0.1 to over 20 cps. For a 20 KT bomb, the best guess indicated that the main frequency would be about 1 cps, with higher secondary frequencies up to 20 or 30 cycles being very probable. This estimate was based in part on assuming that the frequency would decrease as the charge weight increased, though examination of the available HE data did not reveal any consistent correlation between frequency and charge weight. When the yield of the bomb was changed to 1 KT, it was assumed that the frequency would increase to perhaps 3 or 4 cps. Needless to say, considerable uncertainty existed regarding the frequencies that would result.

## 2.8 CORRELATION OF ACCELERATION WITH DAMAGE TO STRUCTURES

Another consideration of importance was the correlation of acceleration to damage. This was important in the placing of structures and in

---

[2] Henry J. Birkenhauer, The Prevention of Destruction from Seismic Waves

[3] Henry J. Birkenhauer, Propagation of Seismic Waves at Short Distances

determining the extent of the blast line. Birkenhauer[2] reviews various criteria such as acceleration, displacement, and energy which have been used to correlate damage to structures. Using falling plaster as an index of beginning damage, the conclusions from all three of the above criteria indicate that within frequency limits damage will occur when the acceleration exceeds 1 g, with the threshold being in the neighborhood of 0.1 g. For military structures the acceleration necessary to produce damage is much greater than 1 g. For example, analysis of the Lampson reports[1] on damage to structures indicated that an acceleration of 5 g was necessary to produce light damage (1/8 in. crack width) and an acceleration of 25 g to produce moderate damage (1 in. crack width) in a reinforced concrete wall 5 ft thick.

### 2.8.1 Range of Accelerations to be Measured

On the basis of these considerations of damage it was decided that measurements should cover the acceleration range from below 0.1 g to as high a g as possible (as close to zero as practicable).

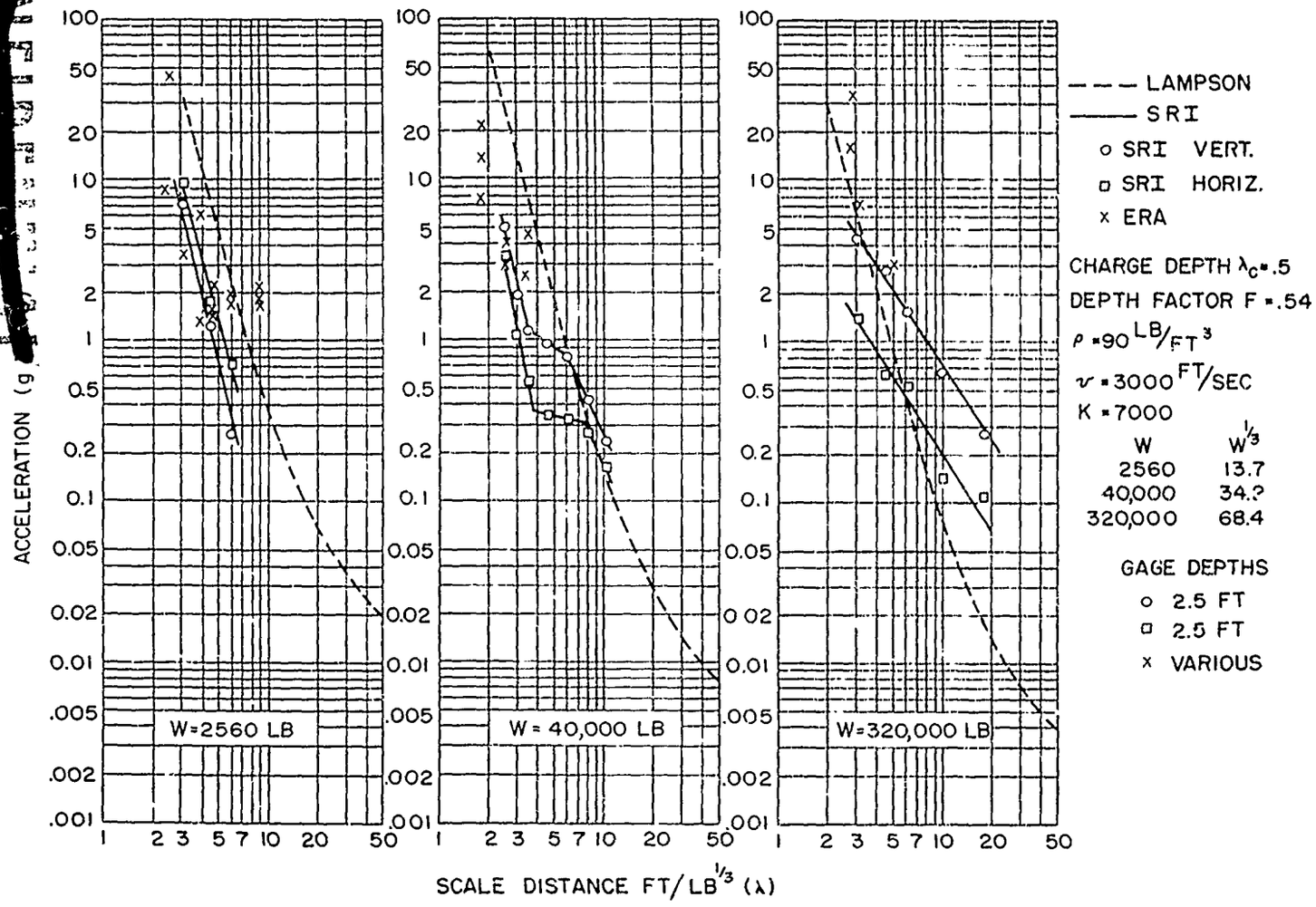


Fig. 2.1 Ground Acceleration from the Dugway Underground Tests



PROJECT 1.1

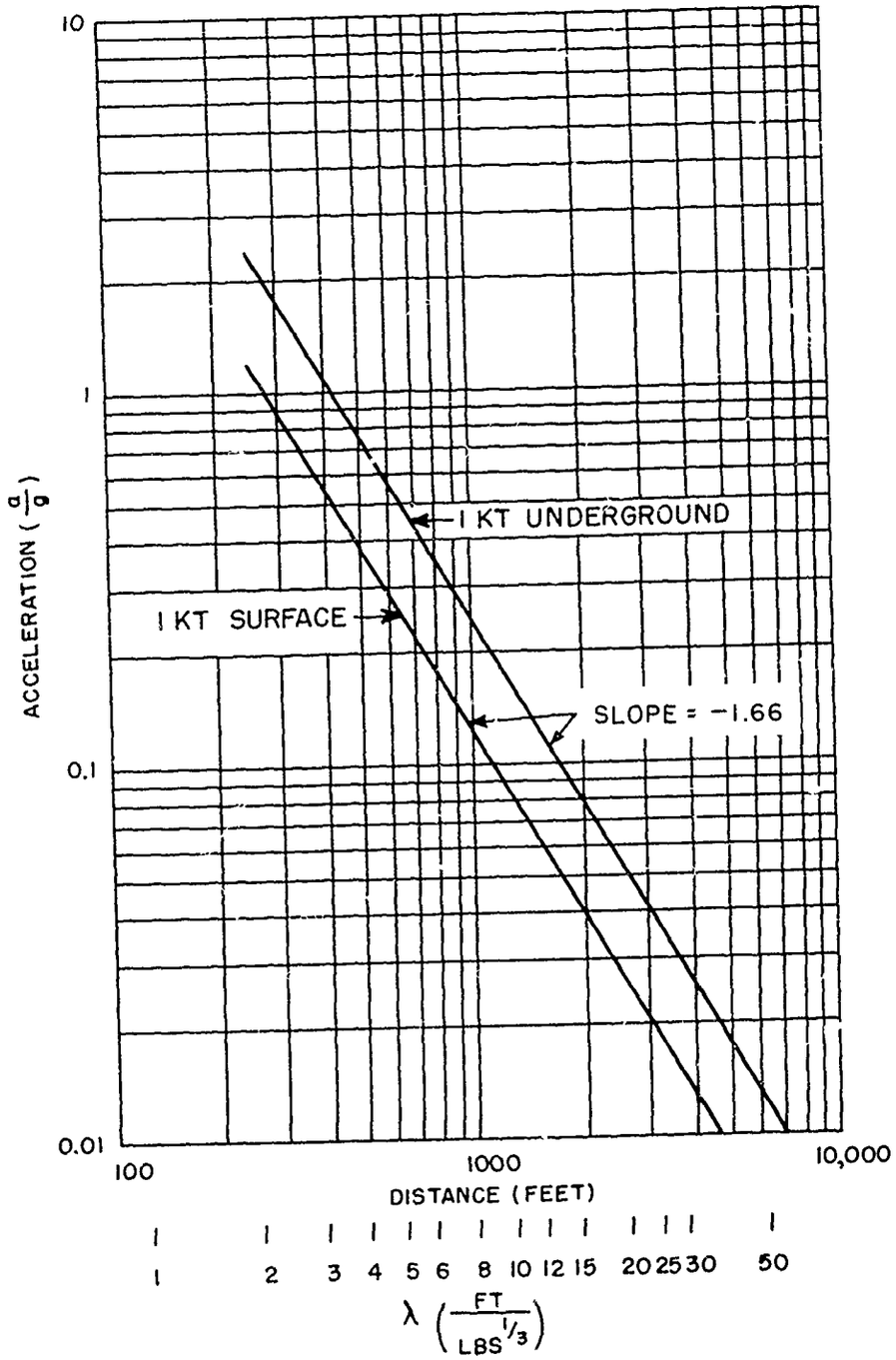


Fig. 2.2 Prediction of Horizontal and Vertical Ground Acceleration Based on Scaling of NOL Results from the 40,000 lb HE Shot at Yucca Flats

CHAPTER 3

## PLAN OF THE EXPERIMENT

This chapter contains an account of the planning phases of the project. A general description of the methods employed for obtaining the data is also included to give the reader a brief account of the measuring technique used. For a more technical account of these techniques and a detailed description of the equipment the reader is referred to Chapters Four and Five.

The plans for instrumenting the ground accelerations underwent many variations in following the course of operational changes. The absence of abundant data, as are available for measurements in air, the lack of desired instruments, and the nature of the medium, also contributed uncertainties to the decisive problems of planning.

### 3.1 THE PLAN FOR AMCHITKA ISLAND

As a basis for expected effects on Amchitka Island from a 20 KT weapon, the best geophysical data available for that island was substituted into the Lampson Formulae and curves drawn up for acceleration, displacement, pressure and impulse. A few of the values taken from these curves are listed below to give an indication of the order of results expected at the time preliminary plans and gage development were in progress:

Diameter of Crater - 1,000 ft
Diameter of Lip - 2,000 ft

| Distance from zero (ft) | 1,000 | 1,500 | 2,500 | 5,000 |
|---|---|---|---|---|
| Acceleration (g units) | 3.4 | .7 | .1 | .013 |
| Hor. Displacement (ft) | 37 | 11 | 2.5 | .3 |
| Ground pressure (psi) | 200 | 38 | 5 | .3 |

Noting the large expected displacements at distances closer than 1,000 ft from zero and considering the lack of gages with which to measure less than 0.1 g, an instrument line was decided upon to extend from 1,000 ft to 6,500 ft from zero. Considering the depths of the structure foundations and the practical problems of gage placement, depth stations at 10, 20, and 30 ft depths were planned. For protection against air blast, missiles and contamination it was planned to locate the recording units at two miles from the zero points. To provide for back-up and as protection against the expected losses of recording

channels on such an operation a total of twelve stations were provided, four of which were to measure the effects at three depths. The order of events to carry out the many details of the above plan in the climate and geology of Amchitka presented many difficult problems.

## 3.2 THE REVISED PLAN

### 3.2.1 Effects of the Change in Site

While the change in the operational site to Nevada decreased many of the uncertainties of the problem, it necessitated many detailed alterations to the plan. The principal changes were occasioned by the change in weapon yield from 20 KT to 1 KT. As soon as geophysical data for the new area became available it was used for revising the estimates of predicted effects. The smaller charge and smaller soil constant lowered the values of expected effects considerably. These expected effects were again computed by Lampson Theory, and as the predictions followed an emperical law, the layout of gages along the instrument lines were planned at logarithmic distances along a radial line from the zero point. This resulted in a concentration of gage stations near zero and a scarcity at the greater distances. The closest station was positioned at 275 ft from zero and the most distant at 3,000 ft from zero for both the surface and underground shots. It was felt safe to reduce the distance of the recording units to 8,000 ft from zero.

### 3.2.2 Effects of Results from HE Firings

Early in September the project group installed ten stations for instrumentation of the effects from a 40,000 pound HE shot in Yucca Flats. The results obtained from this test differed considerably from the Lampson theory predictions; therefore, the emperical results obtained from this test were scaled up to 1 KT and the nuclear instrumentation layout was revised and based on these revised predictions.

### 3.2.3 The Final Plan

The relative locations of the two nuclear instrument lines on the HE area are shown in Fig. 3.1. It will be noted that the HE area lies midway between the surface shot and the underground shot locations. This plan proved to be of immense value in belaying doubts as to the geophysical characteristics of the area. Such a plan is highly recommended for future operations.

The gage stations on the two nuclear instrument lines were at similar distances from zero, the exception being one station at 200 ft from zero on the underground shot instrument line which was

installed late in the preparatory period on the basis of revised estimates. A sketch of a typical gage station layout, along with descriptive data, is shown on Fig. 3.2. A detailed table of the gage distribution is given in Table 3.1. In summary, the plans of gage placement along the two lines provided for the measurement of radial, vertical and transverse accelerations at twelve separate distances from 275 to 3,000 ft from zero and at 10, 20, and 30 ft depths. Throughout the report the radial component is that which is measured in the horizontal plane and is referred to as the horizontal component, designated as (H); the vertical component is designated as (V); the transverse component perpendicular to both horizontal and vertical, is designated as (T).

### 3.2.4 Gage Distribution

Each gage station normally had four accelerometers and one BRL pressure gage. Two accelerometers of different ranges at any one station for measuring the same component of acceleration were provided to increase the dynamic range of the system and to provide back-up. This back-up was considered advisable because of the uncertainty as to the magnitude and natural frequency of the effects to be measured. The two gages of any one type (H, V, or T) at each station were selected so that their full scale ranges were twelve times and four times the value of expected accelerations. Inasmuch as the recording system was capable of resolving any signal down to four per cent of the gage rating the dynamic range of the component system extended from 12 to .04 times the expected effects.

As the transverse acceleration component was expected to be small, the main emphasis was placed on the radial and vertical measurements. As shown in Table 3.1 transverse gages were placed only at stations 2, 5, 8, 10, and 12.

### 3.2.5 Gage Installation

Accurate alignment of the accelerometers vertically and in azimuth was necessary. To accomplish this the gage capsule was attached to a sectional metal conduit and lowered into the ground to the 10, 20 or 30 ft level. The rod and capsule acted as a pendulum when suspended from a tripod placed over the gage hole and with the aid of levels, proper alignment was obtained. The capsule was coupled to the earth by Calseal, a quick setting cement, which had been poured into the hole to a depth sufficient to cover the top of the capsule.

### 3.2.6 Instrumentation System

The accelerometers were developed by the Naval Ordnance Laboratory and the Schaevitz Engineering Company, Merchantville, N. J.

Table 3.1

Accelerometer Placement Data  Project 1.1 (NOL)

| NOL Station Number | Distance From Zero | | "S" Shot | | | | | | "U" Shot | | | | | |
|---|---|---|---|---|---|---|---|---|---|---|---|---|---|---|
| | | | Expected Max a/g (H & V) | Gage Ranges - a/g | | | | | Expected Max a/g (H & V) | Gage Ranges - a/g | | | | |
| | (Ft) | (λ) | | H | H' | V | V' | T | | H | H' | V | V' | T |
| 1-10[1] | 275 | 2.18 | 1.0 | 20.0 | 3.0 | 20.0 | 3.0 | --- | 2.0 | 38.0 | 10.0 | 38.0 | 10.0 | --- |
| 2-10 | 340 | 2.70 | 0.75 | 20.0 | 3.0 | 10.0 | --- | 0.5 | 1.5 | 20.0 | 10.0 | 20.0 | ---- | 1.0 |
| 2-20 | 340 | 2.70 | 0.75 | 10.0 | # | 20.0 | 3.0 | --- | 1.5 | 20.0 | ---- | 20.0 | 10.0 | --- |
| 2-30 | 340 | 2.70 | 0.75 | 10.0 | 3.0 | 10.0 | 3.0 | --- | 1.5 | 10.0 | 3.0 | 10.0 | 3.0 | --- |
| 3-10 | 420 | 3.34 | 0.5 | 10.0 | 1.0 | 10.0 | 1.0 | --- | 1.0 | 10.0 | 3.0 | 10.0 | 3.0 | --- |
| 4-10 | 520 | 4.14 | 0.35 | 3.0 | 1.0 | 3.0 | 1.0 | --- | 0.70 | 10.0 | 3.0 | 10.0 | 3.0 | --- |
| 5-10 | 642 | 5.10 | 0.25 | 3.0 | # | 3.0 | 1.0 | 0.1 | 0.50 | 3.0 | ---- | 3.0 | 1.0 | 0.5 |
| 5-20 | 642 | 5.10 | 0.25 | 3.0 | 1.0 | 3.0 | 1.0 | --- | 0.50 | 10.0 | 3.0 | 10.0 | 3.0 | --- |
| 5-30 | 642 | 5.10 | 0.25 | 3.0 | 1.0 | 3.0 | # | --- | 0.50 | 10.0 | 3.0 | 10.0 | ---- | --- |
| 6-10 | 794 | 6.30 | 0.17 | 3.0 | 0.5 | 3.0 | 0.5 | --- | 0.34 | 3.0 | 1.0 | 3.0 | 1.0 | --- |
| 7-10 | 982 | 7.79 | 0.125 | 1.0 | 0.5 | 1.0 | 0.5 | --- | 0.25 | 3.0 | 0.5 | 3.0 | 0.5 | --- |
| 8-10 | 1213 | 9.62 | 0.09 | 1.0 | 0.5 | 1.0 | --- | 0.1 | 0.18 | 1.0 | 0.5 | 1.0 | ---- | 0.1 |
| 8-20 | 1213 | 9.62 | 0.09 | 1.0 | # | 1.0 | 0.5 | --- | 0.18 | 1.0 | ---- | 1.0 | 0.5 | --- |
| 8-30 | 1213 | 9.62 | 0.09 | 1.0 | 0.5 | 1.0 | 0.5 | --- | 0.18 | 1.0 | 0.5 | 1.0 | 0.5 | --- |
| 9-10 | 1500 | 11.9 | 0.063 | 0.5 | 0.1 | 0.5 | 0.1 | --- | 0.126 | 1.0 | 0.5 | 1.0 | 0.5 | --- |
| 10-10 | 1890 | 15.0 | 0.042 | 0.5 | --- | 0.5 | 0.1 | 0.1 | 0.084 | 1.0 | ---- | 1.0 | 0.5 | 0.1 |
| 10-20 | 1890 | 15.0 | 0.042 | 0.5 | 0.1 | 0.5 | 0.1 | --- | 0.084 | 1.0 | 0.5 | 1.0 | 0.5 | --- |
| 10-30 | 1890 | 15.0 | 0.042 | 0.5 | 0.1 | 0.5 | # | --- | 0.084 | 1.0 | 0.5 | 1.0 | ---- | --- |
| 11-10 | 2331 | 18.5 | 0.031 | 0.5 | 0.1 | 0.5 | 0.1 | --- | 0.062 | 0.5 | 0.1 | 0.5 | 0.1 | --- |
| 12-10 | 3000 | 23.8 | 0.02 | 0.5 | 0.1 | 0.5 | --- | 0.1 | 0.04 | 0.5 | 0.1 | 0.5 | ---- | 0.1 |
| A-10[2] | 200 | 1.59 | ----- | ---- | --- | ---- | --- | --- | 3.3 | 38.0 | 10.0 | 38.0 | 10.0 | --- |

H - Horizontal Accelerometer  H' - Backup "H" Accelerometer  V - Vertical Accelerometer
V' - Backup "V" Accelerometer  T - Transverse Accelerometer  # - Channel for Backup Pressure Gage

1. 1-10 means station 1 at a 10 foot depth
2. This station was added just prior to the underground shot

These gages, with ranges from 0.1g to 38.0g, operated on a variable inductance principle. When a mass unit suspended by a double cantilever spring was accelerated, it displaced an attached mu-metal pad relative to an E-coil. The resulting change in the reluctance of the magnetic circuit produced an inductance change in the E-coil which comprised the inductance element in the tank circuit in an FM oscillator. Thus an acceleration appeared as a frequency modulation on an FM carrier signal. At every station, individual cables from the four accelerometers and one pressure gage were connected to five oscillators which were enclosed in a single unit in a water-tight section of pipe which was buried between the accelerometer and pressure gage holes at a depth of three ft. The five oscillators at a given station were of the Hartley type and operated on center frequencies of 3.9, 5.4, 7.35, 10.5, and 14.5 kc. The outputs of these five oscillators were combined and transmitted over a single cable to one recording channel of a multi-channel Ampex magnetic tape recorder. Each Ampex unit consisted of seven recorder heads recording on one-half inch tape. Five of the heads recorded the gage intelligence and the remaining two heads were used for calibration and timing. Thus with multi-plexing, twenty-five signals were recorded on a single tape recorder.

The recorders were mounted in trailers which were located 8,000 ft from the zero points. Four recorders were required to record the one hundred signals from each shot. Four additional recorders obtained from Operation GREENHOUSE were used for back-up recording. This back-up was considered advisable because of the large amount of data entrusted to a single tape.

The primary power supply was also located in the trailers and consisted of motor-generator sets run from storage batteries. All power was supplied from this source. Power to the oscillators was piped down separate leads of the same cable that carried the signal from the gages to the recorder.

In playback, the five combined signals were separated by filters, then fed to five discriminators and the five outputs individually recorded by a string oscillograph on photographic paper. In the process of data reduction the photographic records from the oscillograph were used for measurements. These original records were traced by hand for quantitative comparison and are contained in Appendix B of this report.

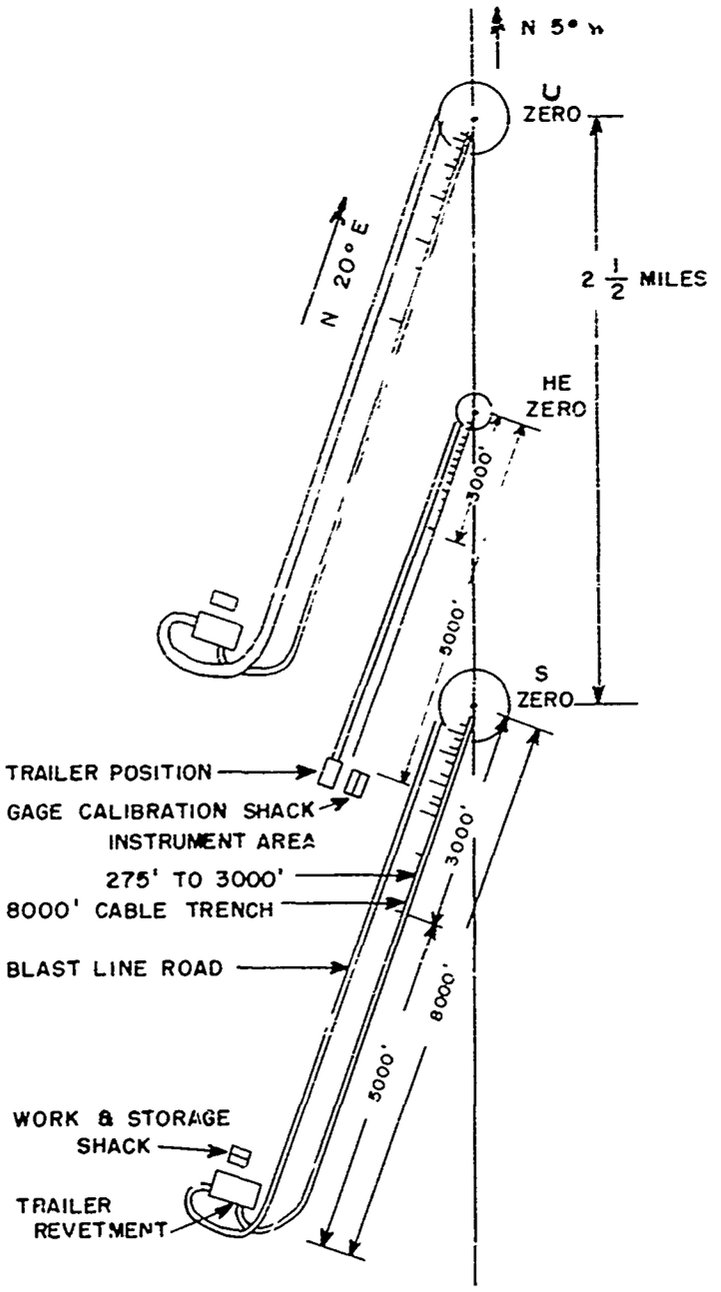


Fig. 3.1 Layout of Blast Lines

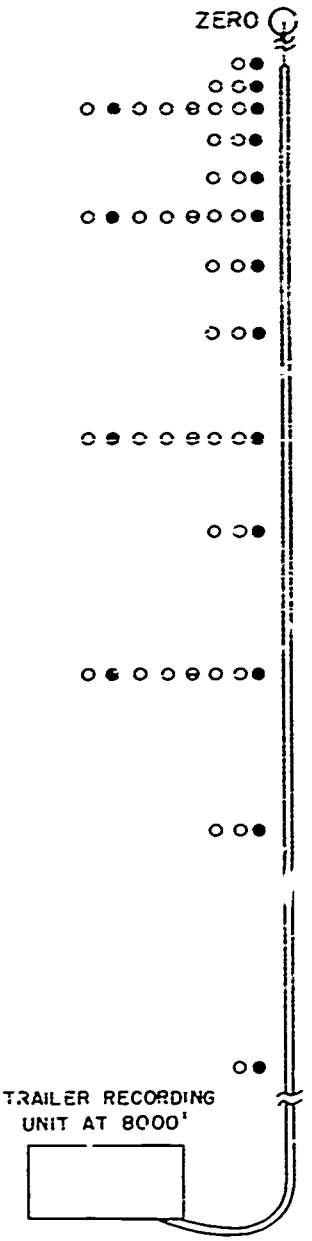


| STA. NO. | DISTANCE FROM ZERO FT | λ | EXPECTED $\frac{a}{g}$ S | U |
|---|---|---|---|---|
| A | 200 | 1.6 | — | 3.4 |
| 1 | 275 | 2.2 | 1.0 | 2.0 |
| 2 | 340 | 2.7 | 0.8 | 1.5 |
| 3 | 420 | 3.3 | 0.6 | 1.1 |
| 4 | 520 | 4.1 | 0.37 | 0.73 |
| 5 | 642 | 5.1 | 0.3 | 0.51 |
| 6 | 794 | 6.3 | 0.18 | 2.36 |
| 7 | 982 | 7.8 | 0.13 | 0.25 |
| 8 | 1213 | 9.6 | 0.09 | 0.18 |
| 9 | 1500 | 11.9 | 0.07 | 0.13 |
| 10 | 1890 | 15.0 | 0.04 | 1.025 |
| 11 | 2331 | 18.9 | 0.03 | 0.06 |
| 12 | 3000 | 23.9 | 0.02 | 0.04 |

● ACCELEROMETER AT 10' DEPTH
⊖ " " 20' "
● " " 30' "
○ PRESSURE GAGES OR ERA ACCELEROMETERS

Fig. 3.2 Typical Blast Line Layout

[redacted]

# CHAPTER 4

## ACCELEROMETER DEVELOPMENT, CALIBRATION AND INSTALLATION

### 4.1 ACCELEROMETER DEVELOPMENT

#### 4.1.1 Introductory Remarks

In the early stages of planning for the test, it was established that accelerometer records were to be obtained by recording FM signals on magnetic tape. The gages were to be coupled to field oscillators located at the respective test stations and FM signals from the oscillators transmitted directly by cable to the recording units.

In determining the type of the accelerometers to be used, it was considered advisable to require a unit operating on a variable inductance or variable capacitance principle. Other types of accelerometers would have required a relatively complex oscillator design which had as yet been undeveloped. Time limitations were such as not to allow for such development work to be undertaken. A further consideration was the possibility that increased complexity of the oscillator circuit would result in reduced reliability.

An extensive survey was made through various commercial and government agencies of the availability of an accelerometer with suitable electrical and mechanical properties. Units with the frequency and high sensitivity characteristics required for a large number of gage stations could not be located. Further, those commercial units which would have been satisfactory for some of the stations could not be obtained in the time required.

An experimental and theoretical research program was therefore established at the Naval Ordnance Laboratory (NOL) which resulted in the development of the accelerometers used on the test. The final design was completed in cooperation with Schaevitz Engineering of Camden, N.J., where all of the units required for the test were manufactured. The instrument is now available commercially as the Schaevitz Accelerometer, Type B.

A comprehensive study of the general properties of the gage was conducted at NOL. A summary of the research and testing program is presented in the following section of this report. Individual topics are generally unrelated; however, an attempt has been made to offer some degree of continuity in the order of presentation.



[redacted]

### 8.1.2 Design Specifications

All efforts were directed toward producing an accelerometer operating on a variable inductance principle and capable of measuring linear accelerations.

The desired mechanical properties were:

(a) Vibratory system to have one degree of freedom with linear response characteristics

(b) Full-scale sensitivities from ± 0.1 g to ± 38 g for both vertical and horizontal units

(c) Resonant frequency as high as possible

(d) Damping between 0.5 and 0.7 of critical

(e) Variation of sensitivity due to temperature changes less that 2% between 32°F and 78°F

(f) Accuracy within 5% over the gage range

(g) Accelerations normal to the gage axis to introduce negligible effects

(h) Over-all dimensions not to exceed 3 in. in any direction.

The necessary electrical properties as governed by the characteristics of the recording system were:

(a) Initial inductance approximately 130 mh at 4 kc to 10 kc

(b) Q of the coil greater than 10 at 4 kc to 10 kc

(c) Inductance variations of about 15% corresponding to full-scale accelerations

(d) Double stops to limit frequency range to a maximum of ± 10% of the center frequency.

### 4.1.3 Description of Gage

Based on the foregoing requirements, the accelerometer design evolved by NOL and Schaevitz Engineering had the basic features outlined schematically in Fig. 4.1. The instrument consists of a metal housing within which are mounted an inductor and two cantilever beams. The beams are located directly above one another with a mass centrally supported between them at their free ends. Fixed rigidly to one end of the mass is a Mu-metal pad having a high permeability. A sensitive magnetic circuit is formed by locating the Mu-metal pad in close proximity to the inductor. Alignment of the various elements of the instrument is such as to afford a single axis of sensitivity.

When subjected to an acceleration, the movable mass and Mu-metal pad undergo an excursion controlled by the bending of the cantilevers. The motion of the Mu-metal pad changes the gap spacing in the magnetic circuit, resulting in a change of magnetic reluctance. A measure of the reluctance change is the corresponding inductance variation of inductor E-coil. The gage is coupled to an inductance controlled oscillator whose frequency of oscillation is a function of the displacement of the Mu-metal pad from equilibrium.

To provide necessary damping, the instrument is filled with a non-corrosive damping oil. A neoprene gasket separating the fluid from a vented recess in the cover plate permits expansion and contraction of the fluid.

A double stop is provided limiting the frequency range as required to $\pm$ 10% of the center frequency. The purpose of the stop mechanism is essentially to prevent damage to mechanical parts due to excessive accelerations and to prevent the subcarrier frequency from going out of its band and interfering with other channels.

The final model weighs approximately 0.7 lbs, and has overall dimensions of 2.1 x 1.5 x 2 inches. A photograph of the instrument is shown in Fig. 4.2.

### 4.1.4 Spring-Mass System

Extensive information can be found in the literature[1-4] on

---

[1] P.M. Morse, "Vibration and Sound", McGraw-Hill Book Co.

[2] S. Timoshenko, "Vibration problems in Engineering", D. Van Nostrand Co.

[3] R. J. Roark, "Formulas for Stress and Strain", McGraw-Hill Book Co.

[4] Gross & Lehr, "Die Federn", VDI Berlin.

the deflection and vibration properties of cantilever springs, generally classified as fixed-free beams. The response of a double cantilever system with simple mass load at the free ends, as used in the gage, closely resembles that of a single cantilever with both axial and lateral loads. The coupling of the free ends by the terminal mass restricts the freedom of rotation by introducing an axial force which is a function of the deflection of the springs and the relative spacing between them.

A double cantilever system was chosen because of its stability against torsional and rotational effects. This feature was highly desirable in order to minimize potential extraneous signals when the instrument is subjected to accelerations in random directions.

The various parameters of the spring-mass system were determined empirically. In general, it was necessary to vary only the spring thickness for different gage ratings. Because of its low temperature coefficient, Ni Span-C was used for the spring material. To insure uniform electrical sensitivity for various gage ranges, the displacement of the mass under peak rated accelerations was designed to be the same in each case, within reasonable tolerances. All displacements of the mass under operating conditions were small so that the linear stress-strain limits of the springs were not exceeded.

### 4.1.5 Magnetic Circuit

The inductor of the gage consists of an E-coil mounted in a metal housing and cemented in position by a potting compound. The E-coil is composed of a series of E-shaped Mu-metal laminations bound together by an electrical coil wound around the center arms.

To insure the required high permeability of the Mu-metal pad, a hydrofining process was necessary. The pads were heated in a furnace box to about 2,100°F. While the temperature was steadily increasing a stream of specially dried hydrogen was introduced. The units were then kept at 2,100°F for a period of 5 hours. Following this soaking treatment, the parts were then cooled in a similar stream of hydrogen. This entire process increased the permeability of the Mu-metal chiefly by removing impurities (mostly carbon) from the alloy.

The E-coil and Mu-metal pad of the gage comprise a magnetic circuit whose reluctance varies with gap spacing. A corresponding variation results in the inductance of the E-coil. Shown in Fig. 4.3 is a typical example of the relation between inductance L and gap spacing d. Fig. 4.4 shows how the Q of the gage coil varies with gap spacing, where Q is a measure of the energy loss in the magnetic circuit per cycle of AC current through the E-coil.

An experimental study was made of the sensitivity of inductance to transverse and rotational motions of the Mu-metal pad. The results of this study are summarized by the series of contours in Figs. 4.5, 4.6, and 4.7. On the basis of these results and other auxiliary tests, a gap spacing of 15 mils was chosen as most practical for the gage design, with the pad deflection to be 5 mils at an acceleration equal to the gage rating.

For the gage oscillator, a shunt-feed Hartley circuit was used to minimize any magnetic attractions that would result from DC current passing through the E-coil. In the case of the 0.1 g gage the magnetic effect proved to be serious when a series-feed circuit was first used.

### 4.1.6 Calibration techniques

Of the various methods available for calibration of accelerometers[5-7], three were applied in the present case. A spin table and tilt table permitted independent static calibrations and a shake table offered a means for dynamic calibration.

Due to the unavailability of a commercial unit within the required time limit, a spin table was designed and built at NOL. The unit was highly stable, well balanced and easily transportable for field use. Incorporated in the design was the use of a positive speed control which minimized drift and hunt and allowed for quick adjustments to exact speeds. A report[8] now in preparation describes in detail the construction and operation of the spin table. A photograph of the unit is shown in Fig. 4.8. In principle, an accelerometer is mounted on an arm which is pivoted at its center and rotated in a horizontal plane at a constant angular velocity. The acceleration applied to the gage

---

5 Armour Research Foundation, "Study of Methods of Calibration of Accelerometer, Velocimeters and Displacement Gages", Proj. 90-534, Oct. 1947.

6 S. Levy, A. E. McPherson & E. V. Hobbs, "Calibration of Accelerometers", BuStds Res. Paper 1930, Vol. 41, Nov. 1948.

7 Statham Laboratories, "Calibration and Test of Accelerometers", Instrument Notes No. 6, Dec. 1948.

8 R. G. Quick, "Spin Table for Calibrating Accelerometers", NavOrd Rpt. 2301.

is $a = r\omega^2$, where r is the distance of the instrument from the center of the arm and $\omega$ is $2\pi$ times the frequency of rotation. By means of a tachometer generator geared to the drive shaft of the arm, an accurate measure of the speed of rotation of the arm was available. Balancing of the arm was accomplished by an adjustable counterweight. Accelerometers could be mounted at a distance of either 9 in. or 11 in. from the center of the arm. The speed limits were 17 to 430 rpm, so that the over-all acceleration range was about 0.08 g to 55 g.

The tilt table used was a standard universal dividing head with sensitive leveling adjustment and a vernier scale for reading angle of rotation. Accelerometers were mounted on the flat plate of the head and rotated to an angle such that a fractional component of the earth's gravitational field acted along the sensitive axis of the gage. (See Fig. 4.9). Because of its range limitations, the tilt table was used for gages with ratings of 1.0 g or lower. Excellent resolution was available for calibrating 0.1 g gages.

The auxiliary electronic equipment required for static calibration consisted of the gage oscillator, an oscilloscope, and a variable reference oscillator. The gage oscillator was coupled to one set of plates of the oscilloscope and the reference oscillator to the other set. By means of Lissajous patterns, the frequency changes of the gage circuit were easily determined. A similar technique was used to determine the speed of rotation of the spin table, where the output of the tachometer generator replaced that of the gage oscillator.

The accelerometers were calibrated dynamically using an MB Model C31 Shake Table (see Fig. 4.10). Rigidly fixed to the table head, the gage was subjected to a forced sinusoidal motion of various amplitudes and frequencies. Automatic control of this motion was possible such that the acceleration was constant over a continuum of frequencies. A measure of the excitation of the gage was gained by means of a velocity meter which formed an integral part of the vibratory system of the table. The gage oscillator was coupled to an FM discriminator whose output voltage signals were used for analysis of the gage characteristics.

PROJECT 1.1

In the early use of the shake table, a problem of correct interpretation of the output data developed because of the non-linear transfer characteristics of the gage. However, further investigation showed that the peak to peak output signal of the gage was linearly proportional to the input acceleration within 2 to 3% over an entire gage range. Thereafter, a vacuum tube voltmeter reading peak to peak voltages was used for recording gage output signals. All frequency response studies were based on this peak to peak data.

A typical normalized response curve is shown in Fig. 4.11 for a 10 g gage subjected to a uniform 10 g input acceleration over a range of applied frequencies. The same response curve was found for constant inputs of 5 g to 7.5 g. For comparison, a theoretical curve is shown in Fig. 4.11 by the solid line, corresponding to the response of a one-degree-of-freedom system with pure viscous damping. The theoretical curve was calculated to coincide with the experimental curve at $\omega/\omega_0 = 1$. The good agreement between the two curves indicates that the gage response to sinusoidal excitation may be analyzed by simple linear theory.

In the design of the accelerometer, it was necessary that the damping factor $\beta$ be limited to values of between 0.5 and 0.7 of critical. On the basis of the foregoing agreement between theory and experiment, the $\beta$ for any particular gage could be evaluated by determining the ratio between the gage output signals at $\omega/\omega_0 = 1$ and $\omega/\omega_0 \ll 1$. According to theory, this ratio is equal to $1/2\beta$. In general, good results were obtained by this method. However, some problems were encountered at low frequencies because of distortion in the vibration of the shake table.

A phase comparison for determining $\beta$ was devised which gave good agreement with the foregoing method. After the natural frequency was found, this technique permitted all measurements to be made at a single excitation frequency chosen in a range outside of any singular difficulties associated with the shake table. A report[9] on

[9] E. J. Culling, "A Phase Comparison Technique for Determining Damping Coefficients of Accelerometers", NavOrd Rpt. 2342.

this method is now in preparation. The method in essence may be described as follows. Considering peak to peak output, the accelerometer responds like a system of one degree of freedom with pure viscous damping. An electrical equivalent of the accelerometer by means of a passive L, C, R circuit can easily be devised. It has been shown in the literature[10] that for minimum-phase networks, one of which is the equivalent accelerometer circuit, there is only one possible phase vs frequency function for a specific amplitude vs frequency dependence. This leads to the possibility of comparing the accelerometer phase with the phase of an equivalent electrical simulating circuit. In this respect, the non-linear transfer characteristics of the gage do not influence its phase response and therefore a direct comparison may be made between the gage and simulating circuit. Common reference for the comparison was the signal from the velocity meter of the shake table. A nul technique by means of Lissajous patterns was applied to find the required simulating circuit having the same phase relation to the velocity signal as the gage output. A simple relation between the L, C, R parameters of the equivalent circuit determined the desired damping factor of the gage.

### 4.1.7 Damping

Early models of the accelerometer showed evidence of non-linear damping properties. It appeared that the damping factor $\zeta$ was a function of both the initial gap spacing in the magnetic circuit and the amplitude of displacement of the pad under motion. A study of the problem indicated that this effect could be eliminated by having the pole faces of the E-coil extend 50 mils above the level of the potting compound. Records for a series of free-fall drop tests taken with an early and final model of the gage are shown in Fig. 4.12, indicating the results of this change in the design of the E-coil. The patterns yielded by the final model are independent of the gap spacing. It might be noted that there is an excessive curvature in the respective signals. This was due to a characteristic angular motion of the recording pen over its range of motion.

The damping fluid used in all of the studies and final design was Dow Corning DC-200 Silicone Oil. Extensive measurements were

---

10 H. W. Bode, "Network Analysis and Feedback Amplifier Design", Bell Telephone Laboratories.

made to determine the proper viscosity required for each individual gage range. A group of similar gages, with the same viscosity fluid, was found to have a variation in $\beta$ of about 20%. These differences are possibly due to tolerances in the clearance between the mass and its channel of travel.

The variation of $\beta$ with temperature was investigated to obtain information for expected field test conditions. For pure viscous damping, $\beta$ is linearly proportional to the viscosity of the damping fluid. Therefore the temperature variation of viscosity for DC-200 fluids given in commercial literature also determines the corresponding variation of $\beta$. A study of viscosities from 20 to 1000 centistokes indicated that a single normalized curve $\eta/\eta_o$ vs T could represent the entire group over a temperature range of about 7°C to 50°C, with a maximum error of only 5%. The normalization factor $\eta_o$ is the rated viscosity at 25°C. A plot of this curve, designated as $\beta/\beta_o$ vs T because of the linear relation, is shown in Fig. 4.13. With the aid of this plot, estimates of $\beta$ expected under operating conditions are easily found from values of $\beta$ measured accurately at convenient laboratory temperatures.

Oil leakage from a gage may at times be serious, depending on where resulting air bubbles become trapped. An experiment with one unit indicated there was little effect even when 25% of the damping fluid was lacking. (The total volume of fluid contained in a gage is 15 cc). This test consisted of determining a frequency response curve and a characteristic damping coefficient as compared to the data acquired when the unit was full. In general, even though possible effects may be small, extreme precautions were taken in the oil filling technique to eliminate any air bubbles, and the body of the gage was coated externally with a clear lacquer to minimize potential oil leakage.

### 4.1.8 Resonant Frequency

A prime requirement for an accelerometer is that its resonant frequency be several times greater than the component frequencies of the acceleration to be measured. Therefore careful consideration of this property was necessary in establishing the design criteria.

Harmonic motion of a simple vibratory system is governed by the relation $a = 4\pi^2 f^2 d$, where a is the peak acceleration, f the

frequency of vibration, and d the peak displacement of the mass of the system. For free undamped motion f represents the natural frequency of the system. As mentioned earlier, the parameter d for the accelerometers was specified to be 5 mils at an acceleration equal to the gage rating. Therefore the spring-mass system in itself has the property that $f^2 \simeq 2000$ a, where f is in cycles per second and a is in gravity units.

It was evident that this relation would not hold true for the accelerometer because of the presence of the damping fluid. The instrument was designed with all of the internal parts completely immersed in the fluid. Two effects were to be expected, namely buoyancy and loss of energy due to motion of the fluid. This latter effect would appear as if a virtual mass had been added to the mass of the vibrating system. The resonant frequencies of various gages measured experimentally were found to closely follow the relation $f^2 \simeq 1000$ a. A plot of the data is given in Fig. 4.14. Since $f^2$ is proportional to 1/m, it is seen that the virtual mass added by the presence of the fluid was equal to the original mass of the system.

The resonant frequency of the accelerometers was determined by means of the shake table, and was defined as that frequency at which a gage output signal was in phase with the velocity signal of the table head. According to linear theory this frequency corresponds to the natural undamped frequency of the system. Therefore, for the case where the mass is immersed in a fluid, it may be classified as the "virtual undamped" resonant frequency. Taking into account the effect of viscous damping, the resonant frequency is decreased according to the relation $f = f_0 \sqrt{1 - \beta^2}$ for free oscillations and $f = f_0 \sqrt{1-2\beta^2}$ for steady state excitation, $f_0$ being the "virtual undamped" frequency and $\beta$ the damping factor.

### 4.1.9 Transfer Characteristic

The accelerometer is an electromechanical transducer. Its transfer characteristic is the relation between the mechanical effects being measured and the electrical signals produced.

From electrical theory, the frequency of the gage oscillator varies as $\frac{1}{\sqrt{L}}$, where L is the inductance of the E-coil for any particular position of the Mu-metal pad. Denoting the initial values by $f_0$ and $L_0$, it is seen that as the inductance varies due to the motion of the pad, the frequency will vary according to the relation $\frac{f}{f_0} = \sqrt{\frac{L_0}{L}}$. Since the mechanical properties of the spring-mass system are linear, the pad

displacement is directly proportioned to the applied acceleration in the case of static calibrations. Using the L vs d plot in Fig. 4.3, a corresponding $\frac{f-f_o}{f_o}$ vs $\frac{a}{a_R}$ curve was determined, where $a_R$ is the acceleration rating of the gage corresponding to a 7.5% decrease in frequency. This curve, shown in Fig. 4.15, is the transfer characteristic of the unit, and it is essentially non-linear. For $\frac{a}{a_R} = +1$ and -1, it is seen that $\frac{f-f_o}{f_o} = -7.5\%$ and $+5.5\%$ respectively. Therefore, when analyzing gage records where the amplitudes are proportional to the frequency changes, it is necessary to use a calibration curve of the type shown in Fig. 4.15 for conversion to equivalent accelerations.

Because of the limited time available for the development of the accelerometer, no effort could be made to eliminate this non-linearity. To do so would have required designing a magnetic circuit such that the inductance varied as $\frac{1}{d^2}$ over the region of operation. Coupled with the property that f varies as $\frac{1}{\sqrt{L}}$, the net result would have been a linear transfer characteristic.

It is often desirable to integrate acceleration records to find velocities and displacements associated with the phenomena being studied. However, because of the asymmetric form of the transfer characteristic about the equilibrium position, the integration errors from positive and negative phases would be cumulative. Where a gage record consists of a series of positive and negative signals, it is advisable to linearize the record by either electrical or mechanical means before integrating.

As mentioned earlier, a property of the accelerometer was that peak to peak signals were linearly proportional to acceleration. Fig. 4.16 shows a plot of $\frac{f_+ - f_-}{f_o}$ vs $\frac{a}{a_R}$ corresponding to the data of Fig. 4.15. It was assumed that sinusoidal accelerations of various magnitudes were applied to the gage, and the resultant maximum oscillator frequencies $f_+$ and $f_-$ were determined by the transfer characteristic. The divergence from absolute linearity is seen in Fig. 4.16 to be very slight and definitely within practical limits for studying steady state response properties.

4.1.10 Selectivity Factor

The ability of an accelerometer to resolve only components of acceleration directed along its sensitive axis may be called its selectivity factor. Tests were conducted using the shake table to vibrate gages successively in three mutually perpendicular directions. Results indicated that the instruments recorded on an average about 3% of the accelerations when transverse to the sensitive axes, the maximum for the group tested being 6%. The selectivity factor is completely independent of the errors introduced by improper alignment of an accelerometer in a test position. Potential errors of this type are related to the angle of misalignment by simple sine and cosine functions.

Another measure of the selectivity factor was found when calibrating the 0.1 g vertical gages with the tilt table. For maximum gage rating of 0.1 g it was necessary to rotate the unit through an angle of 26°. At this angle, the component of acceleration normal to the gage axes was sin 26° or 0.44 g. The contribution of this transverse effect was 3%, or 0.13 g, therefore resulting in an error of 13% in the gage reading. A simple method for compensating for this effect was found by rotating the gage clockwise and counterclockwise and averaging the calibration data. For these opposite directions of rotation, the transverse component acting on the spring-mass system is reversed, in one case being additive and in the other subtractive, thus essentially cancelling when averaged.

4.1.11 Temperature Dependence

As mentioned earlier in this report, there is an increase in damping coefficient with decreasing temperature. A question arose as to whether any other calibration factors were in some way temperature dependent

A group of 42 gages consisting of 3 horizontal and 3 vertical units of each of seven acceleration ranges were checked for a possible variation in sensitivity with temperature. The test consisted of determining $a_R$ and $\varphi_R$ at room temperature (about 27°C) and at 2°C. The symbol $a_R$ refers again to the gage acceleration rating and $\varphi_R$ corresponds to the percent frequency change that occurs when an acceleration equal to $-a_R$ is applied to the gage. The test data showed random differences in variation of $\frac{\Delta a_R}{a_R}$ and $\frac{\Delta \varphi_R}{R}$, where the reference values were those taken at room temperature. The mean deviations for the 42 gages were 2.46% and 3.04% for $a_R$ and $\varphi_R$ respectively, and the standard

deviations were 3.33% and 4.16%. These random effects are in all probability due to an irregular combination of the various coefficients of volume expansion.

A definite temperature effect was noted by a shift of the center frequency with no applied accelerations. In 41 cases of the group tested, the center frequency of 3.9 kc was increased by an average of + 0.5%. In an attempt to locate the source of this shift, a group of five individual E-coils was checked over the same temperature range. The increase in center frequency of 3.9 kc was 13, 14, 14, 15 and 15 cycles, which was an average of about + 0.36%. No experiments have been conducted to establish the cause for this characteristic in the E-coil. In general, the effects of this property were not significant in the accuracy of an accelerometer, provided the center frequency was accurately determined for each particular test.

### 4.1.12 Accuracy

A number of potential sources of error have been described in the various sections of this report. It is believed that in general the instrument can be used to yield accuracies of 5% and better. This accuracy is naturally subject to the use of the instrument in the frequency ranges considered satisfactory for accelerometers.

Over a period of several months, a search was made for possible aging effects in the gage. No evidence of such effects were found. Small random differences in some of the calibration factors were noted, but these were within the limits of the accuracy of measurement. Pending tests over a longer period of time, an assumption that the shelf life of the accelerometer is indefinite appears reasonable, in view of its general design features.

### 4.1.13 Recommendations For Further Development

Because of a critical time element, a number of features were incorporated in the design of the instrument without being fully explored. In the event further research is possible, several directions for improvement worth considering are as follows:

(a) Modification of the damping system such that the mass of the vibratory system is not immersed in the damping fluid. (Eliminating the virtual mass effect would tend to increase the resonant frequency by possibly 40%.)

(b) Design of a magnetic circuit such that the inductance of the E-coil varies inversely as the square of the gap spacing over the region of operation. (This property would insure a linear transfer characteristic.)

(c) Exploring the possibilities of decreasing the peak displacement of the Mu-metal pad corresponding to the gage acceleration rating. (A decrease from 5 mils to 3 mils would result in a resonant frequency greater by about 30%.)

(d) Determination of the optimum weight and geometry of the mass of the system to minimize the virtual mass effect of the fluid. (Higher resonant frequencies would be available for values of $\frac{m_f}{m_o}$ less than unity, as found in the present design.)

(e) Investigation of the effects of greater beam thickness for the cantilever springs in order to minimize the selectivity factor.

The foregoing fields of study are recommended as possible methods whereby the design of the accelerometer may be improved. The instrument in its existing form was found to be quite satisfactory for the purpose intended and should prove to be likewise for any similar test program requiring a variable inductance accelerometer.

## 4.2 CALIBRATION AND OIL FILLING TECHNIQUE OF ACCELEROMETERS

### 4.2.1 Purpose of Field Calibration

Each accelerometer, prior to shipment to the test site, underwent a static and dynamic calibration check. During the calibration procedure at the Naval Ordnance Laboratory, an investigation was carried out to determine what effects aging and handling had on the calibration properties of the gages. The aging test, which was conducted on about 20% of the accelerometers, took the form of a recheck of the calibration properties of the gages after they had been shelved for a period of from one to three months. The results of that check showed that for all but a very few gages aging had little or no effect on static calibration.

To determine the effects of handling and shipment on calibration, several 0.1 g and 0.5 g gages were subjected to a standard transportation-vibration test. A recheck of the calibration of these gages after the test indicated that some changes had occurred. The limited amount of time available at the Laboratory did not permit further investigation to determine to what degree of handling a gage could be subjected without a change occurring in its calibration.

When a 0.1 g and 0.5 g gage had been dropped accidentally onto a hard tile floor from a height of several feet, it was found at the Laboratory that the calibration characteristics of these gages were completely modified. A permanent distortion of the gage springs, which had been brought about by the large acceleration produced during the inelastic impact, was responsible for this modified calibration.

Since a change in the calibration of some of the gages was possible due to aging, handling and transportation, and dropping, it was considered good field procedure to recalibrate and check all accelerometers just prior to their installation in the capsules.

### 4.2.2 Field Calibration Procedure

The possibility that a gage would require refilling with damping fluid made it necessary to perform a dynamic test on the accelerometer. An M-B vibration table was set up in the field hut along with a Brown temperature recorder so that both the damping factor $\beta$ and temperature could be obtained simultaneously. Too low a damping factor in comparison to the value obtained for the same gage at the Naval Ordnance Laboratory indicated that a considerable amount of oil had leaked from the gage and that refilling was necessary. Once an accelerometer had passed through this phase and had been found to have a damping factor which fell within the limits allowed, it was given a calibration check. This check consisted of the determination of four quantities, the gage rating and an associated quantity $\varphi_R$, and the accelerations for which the two stops were set.

### 4.2.3 Technique For Filling Gages With Damping Fluid

In order to determine the effect of viscosity of oil, it was necessary first to develop satisfactory methods for filling the gages. The oil had to be admitted to the narrow and devious chamber around the movable element of the gage and freed of air that might be either mechanically trapped during filling or, being initially dissolved in the oil, precipitated as bubbles as a result of the oil changing. A hypodermic needle and a 10 cc graduate, depending on the viscosity of the oil, was used in filling the gages. The gages were then subjected to a vacuum to remove any entrapped air.

The procedure for filling gages was changed in accordance with sensitivity because the optimum viscosity was approximately 20 cs with 0.1 g gages and nearly 700 cs with 38 g gages. The light, free flowing oil could easily be poured through the narrow hole directly above the Mu-metal pad in the gage. The heavy, viscous oil might be admitted in the space around the movable element of the gage only if the nameplate on the bottom were removed to allow frequent stirring to avoid air pockets. While the oil was being poured, the gages were tapped continuously and frequently tilted to assist the dislocation of bubbles. After being filled, the gages were placed under repeated vacuum in the glass bell jar where evolution of bubbles might be closely observed.

The vacuum was increased to the boiling point of the Silicone oil and kept to that level for a short period of time. With light oils excessive boiling began at from two thirds to one half atmosphere. With heavy oils little serious boiling occurred above one eighth to one quarter atmosphere. Enough air and some incidental oil was removed by the vacuum treatment, particularly of the moderately high range gages, to require two and possible three refillings each of about five percent of the volume of the cavity of the gages. After the last refilling the gage was given a final vacuum test and a plug screwed into the gage with the oil filled to nearly overflowing. As a final operation, the gage was sprayed with a clear lacquer to prevent leakage.

### 4.2.4 Advisability of Use of Normalized Calibration Curves

When the first set of accelerometers was delivered to the Naval Ordnance Laboratory, a check of the calibration curves submitted by the manufacturer was conducted.

Considerable discrepancy was found to exist in some cases between the calibration values determined independently and those read from the curves supplied by the manufacturer. On the basis of these checks, it was felt that the original calibration curves could not be considered reliable. A decision was made to disregard those curves, and in their place new curves were to be plotted from the data obtained during the calibration conducted at the Laboratory. However, because too much time had been devoted to gathering the data for the new curves, the limited amount of time left was considered to be insufficient for plotting separate calibration curves for all the accelerometers. This led to the advisability and final plotting of a set of normalized curves which represented the calibration characteristics of all the accelerometers to within a reasonable degree of accuracy.

### 4.2.5 Establishment of Normalized Calibration Curves

As stated in detail in Section 4.1 of this report, the accelerometer furnished information by frequency-modulating a known carrier frequency A modified Hartley oscillator in conjunction with the E-coil of an accelerometer supplied the carrier signal. Since the output frequency of the oscillator was dependent only on

the circuit components L, the inductance of the E-coil, and C, the capacitance of the tank circuit, any change in the inductance $\Delta L$ of the E-coil resulted in a change in the frequency of the oscillator. This change in frequency $\Delta f$ was represented by the expression

$$\Delta f = f_o\left(\frac{1}{\sqrt{1 + \frac{\Delta L}{L_o}}} - 1\right).$$

Here $L_o$ was that inductance which provided a carrier frequency of $f_o$. When the above equation was divided by $f_o$, the expression $\Delta f/f_o$ resulted, which was independent of the carrier frequency, but depended only on the original inductance and the change in inductance of the E-coil. Since an acceleration applied to the gage resulted in a change of inductance $\Delta L$, there existed a definite relationship between the applied acceleration and the expression $\Delta f/f_o$.

That value of applied acceleration which produced a $\Delta f/f_o$ of -7.5% was defined as the gage rating and was designated by the symbol $a_R$. However, when an acceleration equal to $a_R$ was applied to the gage in the opposite direction, a value considerably lower than + 7.5% for $\Delta f/f_o$ was obtained. This value of $\Delta f/f_o$ received the symbol designation $\varphi_R$, and varied within 12% of + 5.4%. The reason for this deviation from + 7.5% was attributed to the non-linear inductance vs pad-spacing relationship for each gage.

The calibration data for a large number of gages were superimposed on a single normalized plot of "$a/a_R$ vs $\Delta f/f_o$ in %". (Both "g" units.) After a smooth curve had been drawn through the mean of the data, no value of $a/a_R$ corresponding to negative values of $\Delta f/f_o$ deviated from the curve by more than 2%. On the other hand, for positive values of $\Delta f/f_o$ the deviation was as high as 12% at an $a/a_R$ of -1.0 and it progressively increased with larger values of $a/a_R$. In order to reduce the large deviation in the $\varphi_R$ values, three normalized curves instead of one were drawn through the data. This step reduced the deviation to approximately 4%. Since for negative values of $\Delta f/f_o$ there was excellent agreement between the $a/a_R$ data and the values expressed by the curve, one normalized curve sufficed in this region.

The following procedure was used in drawing the three normalized calibration curves: First, from the $\varphi_R$ values representing all the gages the two most widely diverted values were chosen.

The difference in these two values, $\Delta \varphi_R$, was then multiplied by the factors 1/6, 1/2, and 5/6, and the resulting numbers were added to the lowest value of $\varphi_R$. Each of these three final numbers served as a nucleus for a normalized calibration curve. In order to draw the proper curve through each of these three points, the normalized calibration data of an accelerometer having the same $\varphi_R$ value as the point under question were plotted in. That curve having the lowest $\varphi_R$ value was designated as curve A; the curve with the highest $\varphi_R$ was called C.

To each accelerometer there was assigned only one normalized calibration curve from the set of three. Selection of the proper curve depended solely on the $\varphi_R$ value for the gage. Those gages whose $\varphi_R$ fell between -4.77% and -5.19% used curve A for calibration purposes. For $\varphi_R$ values lying in the region -5.19% to -5.62%, curve B was chosen. Curve C was used to represent the calibration of those gages whose $\varphi_R$ assumed a value greater than -5.62%. By this scheme it was possible to supply a pre-drawn calibration curve for each gage, accurate to within 4%. However, had more time been available for calibration, a separate curve would have been plotted for each gage, and this degree of inaccuracy would never have been tolerated.

Since the values of acceleration for which the stops were set varied from gage to gage, it was necessary to determine these values separately for each accelerometer. Thus, field calibration required the determination of only four quantities for each accelerometer, those quantities associated with the stops as well as the gage rating $a_R$ and the $\varphi_R$ value.

### 4.2.6 Calibration Techniques

Two independent methods were used to furnish static accelerations. One of the methods employed a vertical rotation head, the other made use of a spin table whose arm was rotated at some known velocity in a horizontal plane.

The rotation head, in addition to having a scale in degrees, was provided with a vernier enabling angles to be read accurately to tenths of a degree. For a horizontal gage mounted on the rotation head, the acceleration in g's applied by rotating it through gravity was expressed by the equation $a = \sin \theta$, where $\theta$ was the angle the sensitive axis of the gage made with the horizontal. Acceleration applied to the



[redacted]

vertical gages was determined by the expression $a = 1 - \cos \theta$. In this case $\theta$ was the angle between the sensitive gage axis and the vertical. Thus by means of the rotation head it was possible to simulate accelerations from 0 to 1.0 g when dealing with horizontal gages, and from 0 to 2.0 g for the vertical accelerometers.

Accelerations could be applied in both the positive and negative direction for the horizontal gages, whereas the verticals could be subjected only to positive accelerations. Because of this drawback, it became necessary to mount the vertical gages on the spin table to provide accelerations in the negative direction.

The spin table was designed to furnish accelerations from 0.1 g to about 55 g. Due to the presence of some vibration in the spin table, it was not possible to obtain calibration values for the 0.1 g accelerometers. Since neither the spin table nor rotation head could be used to determine the values of $\varphi_R$ for the 0.1 g vertical gages, the normalized calibration curve B was assigned to represent the calibration of these accelerometers. The error incurred in the calibration by making this assignment could be as large as 12% at the $\varphi_R$ point.

Except for these 0.1 g vertical accelerometers, all other gages were able to be completely calibrated by using either the rotation head or the spin table, or a combination of the two. The 0.1 g and 0.5 g horizontal accelerometers were completely calibrated on the rotation head. The 1.0 g horizontal gages and the 0.5 g and 1.0 g vertical gages had to undergo partial calibration on the spin table as well, in order to determine $\varphi_R$ and the acceleration corresponding to the "negative" step.

For all other gages having ranges higher than 1.0 g, the spin table was used exclusively to provide the required accelerations. The centrifugal acceleration obtained from the spin table was expressed by the equation $a = \frac{4\pi^2}{386} f^2 D$, (or $a = 0.1 f^2 D$) where f was the frequency of rotation in rps, and D equaled the distance in inches between the center of rotation and the center of mass of the mass-spring system of the gage, with a in g units.

Since all gages had to be mounted on the spin table in a horizontal position, i.e. with the Mu-metal pad vertical, the vertical gages, when in this position, acted as if they were being subjected to 1.0 g acceleration in addition to the centrifugal acceleration produced by the spin table. Thus, when a vertical gage was being subjected to a

centrifugal acceleration in the positive direction, it acted as if an acceleration $a = 1 + 0.1f^2D$ was being applied. Similarly, for accelerations in the negative direction, the gage acted as though the acceleration applied were $a = 1 - 0.1f^2D$.

### 4.2.7 Electronic Equipment Used

In order to completely calibrate the accelerometers, the following electronic equipment was used: A modified Hartley oscillator, a 16-20,000 cps Hewlett-Packard Audio Oscillator, a General Radio Interpolation Oscillator, a Hewlett-Packard 100-100,000 cps crystal-controlled frequency standard, a Dumont 5" oscilloscope, a switching panel and a variable "tuning" capacitor.

The modified Hartley oscillator was used in conjunction with an accelerometer, it being frequency-modulated by the gage. By means of standard Lissajous figures, the oscilloscope served as a visual aid in determining when the output frequency of the oscillator equaled that of the interpolation oscillator. By this means the exact value of the Hartley oscillator's output frequency could be obtained. The oscilloscope was also used for "Lissajousing" the output of the tachometer located on the spin table with a known frequency from the Hewlett-Packard Audio Oscillator. In this way the speed of rotation of the spin table was able to be accurately determined. The regular dial of the audio oscillator was replaced by one calibrated directly for acceleration in g's. This proved to be a considerable time saver in calibrating the accelerometers.

Because of differences in the characteristic inductance of the gages, a variable tuning capacitor was installed in the tank circuit of the Hartley oscillator, thus allowing for an adjustment in the carrier frequency to 3900 cps.

The frequency standard was used several times a day to check the frequency calibration of both the Interpolation and Audio oscillators.

### 4.2.8 Calibration Procedure

The following steps were followed in calibrating each gage:

(1) The gage was mounted in position on either the spin table or rotation head.

(2) When no acceleration was being applied to the gage, the output of the Hartley oscillator was Lissajoussed against the G-R interpolation oscillator

frequency of 3900 cps. The variable tuning capacitor was adjusted until a 1 to 1 pattern was obtained on the oscilloscope.

(3) In order to obtain $a_R$, the gage rating, the interpolation oscillator was first set for a frequency of 3607.5 cps. Then an acceleration in the positive sense was applied to the gage, its amplitude being increased until the output frequency of the Hartley oscillator was also 3607.5 cps. The acceleration required for this change in frequency of -7.5% was designated as the gage rating.

(4) In order to determine $\varphi_R$, an acceleration in the negative direction equal in amplitude to the gage rating was applied to the accelerometer. The frequency of the Hartley oscillator resulting from the acceleration was entered in the expression $\left(\frac{f_{\varphi_R}}{3900} - 1\right)100$, the exact value of which was equal to $\varphi_R$.

(5) In order to find at what values of positive and negative acceleration the gage stops were set, it was necessary to increase the amplitude of acceleration beyond the point where no further change occurred in the Hartley oscillator's frequency with a change in acceleration. Then the acceleration was gradually reduced until the Lissajous pattern on the oscilloscope became disturbed. It was at this point that both the acceleration and the $\Delta f/f_0\%$ values associated with the stop were obtained.

## 4.3 THE GAGE CAPSULE

The gage capsule was designed to provide a rugged, moisture-proof mounting for the gages which were to be placed in the ground. It is essentially an aluminum block with three mutually perpendicular faces, and a watertight case. When aligned vertically and in azimuth and coupled to the earth it provided a dry, rugged, properly positioned housing for the instruments. The assembly consists of (1) a gage block, (2) a top cap and a stem, (3) a sleeve, and (4) a nose cap.

4.3.1 The Gage Mounting Block

The fundamental problem of design for the capsule was found to be in the requirement for the three mutually perpendicular faces upon which the accelerometers were mounted. This requirement was satisfied by accurately machining the three surfaces into a quadrant section of a solid cylindrical block of aluminum ( Fig. 4.17) after these surfaces were prepared holes were drilled through the block to receive the mounting screws for fastening the gages to the block. Additional holes were drilled for cable entry, and threads were provided for the nose cap and for six bolts which held the block to the top cap. Terminal strips were installed in the top section of the block to receive the gage and oscillator wiring.

4.3.2 The Stem and Top Cap

The construction of the stem and top cap (Fig. 4.18) was sufficiently rugged to permit a large strain to be exerted for recovery of the capsule. The cap contained five holes and stuffing tubes for oscillator cable entry and six three-eighths inch holes for bolts which fastened the cap to the gage mounting block. An alignment pin in the cap which fitted into a hole in the gage mounting block insured the proper orientation of parts during assembly. An index mark on the cap, to match a mark on the alignment gear conduit, (Chapter 4.5) insured proper alignment of the capsule assembly with the head block of the assembly gear.

The stem on the top cap was accurately machined for insertion into the placement gear conduit and a pin was fitted as shown to receive the bayonet joint slots on the conduit. The stem was anchored securely into the cap by a press fit and a one-half inch allen set screw. A one-half inch diameter hole at the top axis of the stem was threaded to receive the connector on the retrieving cable.

4.3.3 The Sleeve

The sleeve, (Fig. 4.19) a hollow steel cylinder, was manufactured to slide over the gage mounting block and against a neoprene gasket which was recessed into the top cap. One-half inch walls were provided to insure ruggedness.

4.3.4 The Nose Cap

The nose cap (Fig. 4.20) which held a neoprene gasket similar to that on the top cap, was manufactured from aluminum. It

contained threads which allowed it to be screwed onto the bottom of the gage block and to be tightened against the bottom of the sleeve.

### 4.3.5 Assembly of Capsule

A photograph of the components of the capsule are shown in Fig. 4.21. An assembled capsule is shown in Fig. 4.22.

As designed and manufactured the capsule assembly was not completely satisfactory because of leakage around the cable entry points and bolt holes. These deficiencies were corrected in the field prior to installation in the ground by methods described in Sec. 4.4. Figures 4.17, 4.18, 4.19, and 4.20 include certain design changes to correct the deficiencies and capsules manufactured from these designs should be completely satisfactory.

## 4.4 GAGE MOUNTING, CAPSULE ASSEMBLY, AND WATERPROOFING PROCEDURE

### 4.4.1 Procedure for Mounting Gages in Capsule

The gage capsules were marked on top with a small arrow to position the assembled unit with relation to ground zero and gages were mounted on the gage mounting block with respect to this zero mark. The horizontal gages were mounted on the side face of the gage mounting block with coils toward the zero and with name-plates up (Fig. 4.23, upper two gages). Vertical gages were mounted on the lower base of the mounting block with coils up and name-plates away from the mounting plate face and toward zero (Fig. 4.23, lower two gages). The transverse gages (horizontal type) used at stations 2-10, 5-10, 8-10, 10-10 and 12-10 were mounted on the vertical face of the mounting block, at right angles to the horizontal gages, with name-plates up and coil away from the mounting block face. Figure 4.23 shows a vacant mounting-screw hole to the right of terminal block as there was no transverse gage present in this capsule.

Experiments showed that pressure on the back side of the gage case, exerted by the tightening of the mounting screws, changed the inductance of the gage coil. This was due to warping of the case which caused a change in the spacing between the coil and the pad internally, and had to be corrected. A 25 mil dural shim plate with four mounting-screw holes and dimensions the same as the back face of the gage was placed behind each gage before mounting. This relieved the pressure on the gage case and eliminated the inductance changes from this source.

Each gage was wired with three leads (Fig. 4.23), two to the E-coil, and the third was a center tap. Two terminal blocks within the capsule (Fig. 4.23) facilitated electrical coupling of these gage leads to the RG-22/U cables from the oscillator (Fig. 4.21).

Gages were mounted in correct positions, using appropriate length screws and shim plates. Terminal connections were then made and a desiccant bag was inserted in the remaining space near the terminal blocks to absorb any moisture present (Fig. 4.21).

### 4.4.2 Assembly of Capsule

The top neoprene washer was placed in its proper position and the cylindrical housing was fitted over the base. A second neoprene washer was then placed over the threaded end of the capsule and the nose cap threads were wire brushed and lubricated with a small amount of petroleum jelly to facilitate assembly. The cap was then screwed on, caution being taken at all times to handle the capsules and gages carefully to prevent any damage to low g gages.

### 4.4.3 Tuning Oscillator for Center Frequencies

As any variations from a true horizontal position of a gage introduced changes in the center frequencies at which the low range gages were oscillating, it was essential that the capsule be in a vertical position before the center frequencies of the oscillators were adjusted. The capsule was suspended from a tripod (Fig. 4.24) by means of a free pendulum device with centering adjustments. A 20-minute spirit level was used to insure perpendicularity in two directions. Each capsule was suspended and checked for vertical alignment with the level before center frequencies were set.

A General Radio standard interpolation oscillator was used to determine center frequencies. Channels of 3,900, 5,400, 7,350, 10,500 and 14,500 cps were utilized for recording pulses. An oscilloscope, WD-55A in a portable panel (Fig. 4.25), gave a visual Lissajous pattern when frequency standard and oscillator frequency were impressed. Adjustment of center recording-frequencies was accomplished by adding capacitance to each individual gage circuit in the oscillator and then making a final fine-adjustment of the corresponding capacitance trimmer.

Figure 4.24 shows the tripod, suspended capsule and oscillator in position for center frequency adjustment. The Console with power supply to oscillator is visible to the right. The banks of capacitors were then bolted tightly to the oscillator chassis with spacers being utilized for firm mounting.

A bakelite or plastic strip was installed over the tube shields to prevent them from jarring loose and shorting the oscillator circuit. After a recheck of center frequencies, the oscillator was installed in a cast iron housing to await shipment to the blast line. The capsule was then removed from the tripod and waterproofed.

### 4.4.4 Waterproofing of Capsule and Connectors

An investigation of the gages which failed to give reliable readings on the HE-2 shot disclosed that all of the gages concerned were operating properly when subjected to calibration tests after removal from their respective capsules. Careful observations of the conditions surrounding the capsule and of the capsule itself during removal of the gages concerned showed that a small quantity of water was present in each capsule from which faulty gage-readings had been obtained. It was found that a small amount of water on the terminal block or leads would cause a dead short of the induction leads of the gage and prevent the coil from oscillating. It was therefore determined that inadequate waterproofing of the capsule and its wiring connections was responsible for failure to secure records from these gages.

After a series of tests a practical waterproofing technique was developed. This technique was declared satisfactory after a test capsule was prepared and failed to disclose any leakage after being immersed in water for a twenty four hour period.

The waterproofing technique adopted and used for all capsules of the underground surface shots was as follows:

(1) A small silica-gel bag (Fig. 4.21) was placed with the gages in each capsule to absorb any small amount of moisture that might enter the capsule.

(2) After the capsule was assembled and tightened with strap wrenches, No. 2 non-hardening Permatex gasket compound was spread liberally on the two sleeve joints of the capsule. These joints were then taped with plastic electrical tape to hold the Permatex in place as well as to serve as additional protection from water entry.

(3) The rubber O-ring washers used on the assembly bolts for the top main joint of the capsule were replaced with lead washers coated with Permatex gasket compound.

(4) Rubber tape was placed over the sharp corners of the connectors of the RG-22/U cables from the oscillator and the MCOS-6 power cable.

(5) Plastic tubes (available commercially as "Shellie Nursing Bottles") were cut open at both ends and placed on these cables before they were connected to the top of the capsule. After the cables were connected, the Shellies were placed so as to completely cover the cable connections on the capsule and extend a small distance above and below the connectors. (Fig. 4.21 and 4.26) The bottom of each Shellie was then secured to the capsule cable connector with wax cord. The Shellies were filled with Bostick cement and then secured at the top with wax cord.

(6) A double layer of cheese cloth was wrapped around the cable connections and taped into place with masking tape to prevent damage to the Shellies. (See completely waterproofed capsule, Fig. 4.27) The completed capsule was then placed in a rack to await shipment with the corresponding oscillator unit to the blast line.

## 4.5 CAPSULE PLACEMENT

### 4.5.1 The Placement Gear

The placement gear and associated equipment were designed to accurately position the cylindrical gage capsule which contained the accelerometers. The gear is essentially a sectional thin-walled conduit supported by an adjustable leg tripod. When it is set up over a hole of nominal diameter, it controls the distance below the tripod, the verticality, and the orientation of a capsule suspended from the tripod assembly by sections of a thin walled conduit. The assembled gear is shown in Fig. 4.28.

### 4.5.2 The Problem of Alignment

The fundamental problem was to find a means of positioning a cylindrical capsule so that its vertical axis would be within one-half degree of true vertical, the practical limit of allowable tilt. Since a

plumb-bob is a standard means of establishing a vertical reference, its principal was utilized in suspending the capsule. The capsule and conduit were hung from a ball-and-socket type bearing so that ideally the capsule would assume a true vertical position. In practice the balance of forces was such that the capsule did not always rest in a true vertical position due to interference of the oscillator cables with the sides of the hole.

In anticipation of this difficulty the top of the ball was machined flat and at right angles to the tube insert to which the conduit was pinned. A vertical alignment was then accomplished by placing a spirit level on the flat surface of the head and by making adjustment to the head tubing until readings taken 90° apart indicated a true horizontal surface. The operation of the equipment was such that when these two readings were obtained, the capsule was within the allowable limits of tilt.

### 4.5.3 Alignment and Placement Procedure

When a capsule was to be placed in the ground, the depth and verticality of the hole to be used was determined. This was accomplished by using a plumb-bob assembly. In borderline cases, a dummy capsule with a light on the bottom was suspended in the hole to indicate whether or not the hole was drilled so that the capsule would swing freely. The depth of the holes, nominally 10, 20, 30 feet, was determined by measuring the length of the plumb line required to reach to the bottom of the hole. The tripod was then assembled and set up over the hole. Experience indicated that boards under the tripod legs could serve two useful purposes: (1) to provide a surface on which to slide the tripod assembly, (2) to prevent cave-ins on those holes which had been drilled in the bottom of the three-foot lateral trench.

The tripod was levelled, centered over the hole, and a short section of tubing was used to suspend the capsule in a vertical position while electrical checks were made. When the electrical checks showed normal operation on all of the gages within the capsule, the capsule was disconnected from the short section of tubing. A steel retrieving cable which was attached to the shank of the capsule was passed through the lower end of a long conduit section and out through a slot in the side. The conduit was then connected to the shank of the capsule by a bayonet joint, matching the zero marker on the capsule to an index mark on the conduit. All gear needed for the placement of the capsule was located nearby and the grouting material was mixed and poured into the hole.

These operations are illustrated in Fig. 4.29. For lowering the capsule into the hole, one man held the retrieving cable, a second man handled the electrical cables, and a third man guided the capsule with the attached conduit. This operation is illustrated in Fig. 4.30. If the hole had a depth of more than ten feet, couplings and additional conduit sections were added through the hole in the centering plate in the tripod.

When more than one conduit section was required a clamp, supported by pieces of 2" x 4" lumber laid across the hole, was attached to the conduit. The clamp was used as a friction brake allowing the conduit to descend slowly until the second coupling and third conduit section could be attached. (Figure 4.31) When the entire assembly had been lowered to within six inches of the final depth, the head tube was inserted and the conduit and tubing were pinned together. A light was lowered into the hole and the position of the capsule and the condition of the hole were checked. If both were satisfactory, the capsule was then lowered to its final position. An alidade was used to align the capsule and head with a number at the "U" zero or "S" zero and a level check was made to establish the verticality of the suspended capsule. The grouting material hardened in about one hour coupling the capsule firmly to the surrounding medium. After the grouting material had set it was found that in some cases the level of the mix had receded due to absorption by the ground. To replace the lost grouting, a pipe was lowered so that the grouting material would be placed alongside of, rather than on top of, the capsule. An inspection light was lowered so that it could be noted when the grouting material reached a level about one-half inch above the top of the capsule.

Experience indicated that having a level tripod top and a clean, lightly lubricated ball-and-socket bearing reduced the time necessary to place the capsule. Precautions which were found necessary to be observed were: (1) to make sure that the grouting material level was never high enough to interfere with the bayonet joint disconnecting process, (2) that the capsule did not rest against the bottom or side of the hole, and (3) to ascertain that the index markings on the capsule and the head tubing were in line.

For further detailed information including charts, drawings, and photographs, the reader is referred to Technical Report No. 3, dated September 1, 1951, entitled "Installation Manual, Placement of Gear and Associated Equipment" of Silver Spring Laboratory, Vitro Corporation of America.

## 4.6 RECOVERY OF CAPSULES

### 4.6.1 Desirability of Recovery

Recovery of the capsules containing gages was desirable because of the possibility of re-use of the gages and the need for checking the capsules for moisture tightness. The likelihood of initial gage conditions changing unintentionally during placement, or simply with time, and the fact that the site would probably be cleared for future tests were also factors to be considered. The recovery of the capsules containing gages was the concluding operation at the test site.

### 4.6.2 Procedure for Recovery

The process of retrieving capsules was inherently difficult because a firm bond between capsule and ground was a prime requisite in planting the instruments. To this end the capsules had been firmly coupled to the earth by the Cal-seal. In addition the capsule holes had been filled with loose dirt.

For retrieving the capsule a half inch cable had been attached to the capsule and extended from the buried capsule to the surface of the ground. No success whatever was achieved by direct tension on the steel retrieving cable attached to the capsule unless other steps were taken simultaneously. It was necessary to remove the dirt in the narrow 8" to 10" diameter holes down to the 10, 20, and 30 ft. levels and then break the strong Cal-seal covering. This was readily accomplished by means of a special water-spray technique combined with the probing action of the spray pipe.

Major equipment for the removal operation included a fifteen-ton Bay City Crane with a boom sufficient for hoisting at least 35 foot lengths of steel pipe and with double block and tackles for simultaneous lifting. Also included in major equipment was a water truck and trailer of total capacity 6000 gallons, provided with a four speed pump. A shackle for wire cable, shovels, large pipe wrench, 150 foot length of fire hose, and 11 foot sections of 2" diameter pipe threaded for suitable coupling comprised the remaining equipment.

In a typical removal operation a circular mound of earth was first built up around the entrance of the capsule hole and a connecting trench dug leading down hill from the enclosed area to channel any excess water and dirt. The steel cable from the capsule was next attached to one block and tackle of the crane and a pipe section

of length commensurate with depth of hole to the other. The fire hose made a connection between the water truck and the tackle end of the pipe. Moderate tension was applied to the wire cable, the pipe was then hoisted vertically over the hole and, as water was sprayed at the ground, the pipe was lowered gradually as close as possible to the wire cable. The lowering was not continuous except in one or two unusual instances. An up-and-down motion of two to three feet travel was frequently necessary particularly when the water jet reached the Cal-seal surrounding the capsule. At this time the tension on the cable was at maximum and the rear wheels of the crane were usually about one foot off the ground. Water flow was increased to the highest pressure and the pipe moved on all sides of the cable and capsule to insure removal of as much dirt as possible. About five to ten minutes after the initial water jet action began at the surface of the ground, the capsule began to move slowly upward under the continuous action of the water jet, the capsule and pipe section being pulled simultaneously upward by the crane operator. Invariably if the flow of water were stopped, the capsule became wedged in the hole by pieces of gravel that had been dislodged from the sides of the hole or had fallen in during filling. In general six capsules could be removed with 6000 gallons of water. Curiously, the capsules at thirty feet depth were easier to remove than those at twenty feet, and the capsules at twenty likewise easier to withdraw than those buried at ten feet.

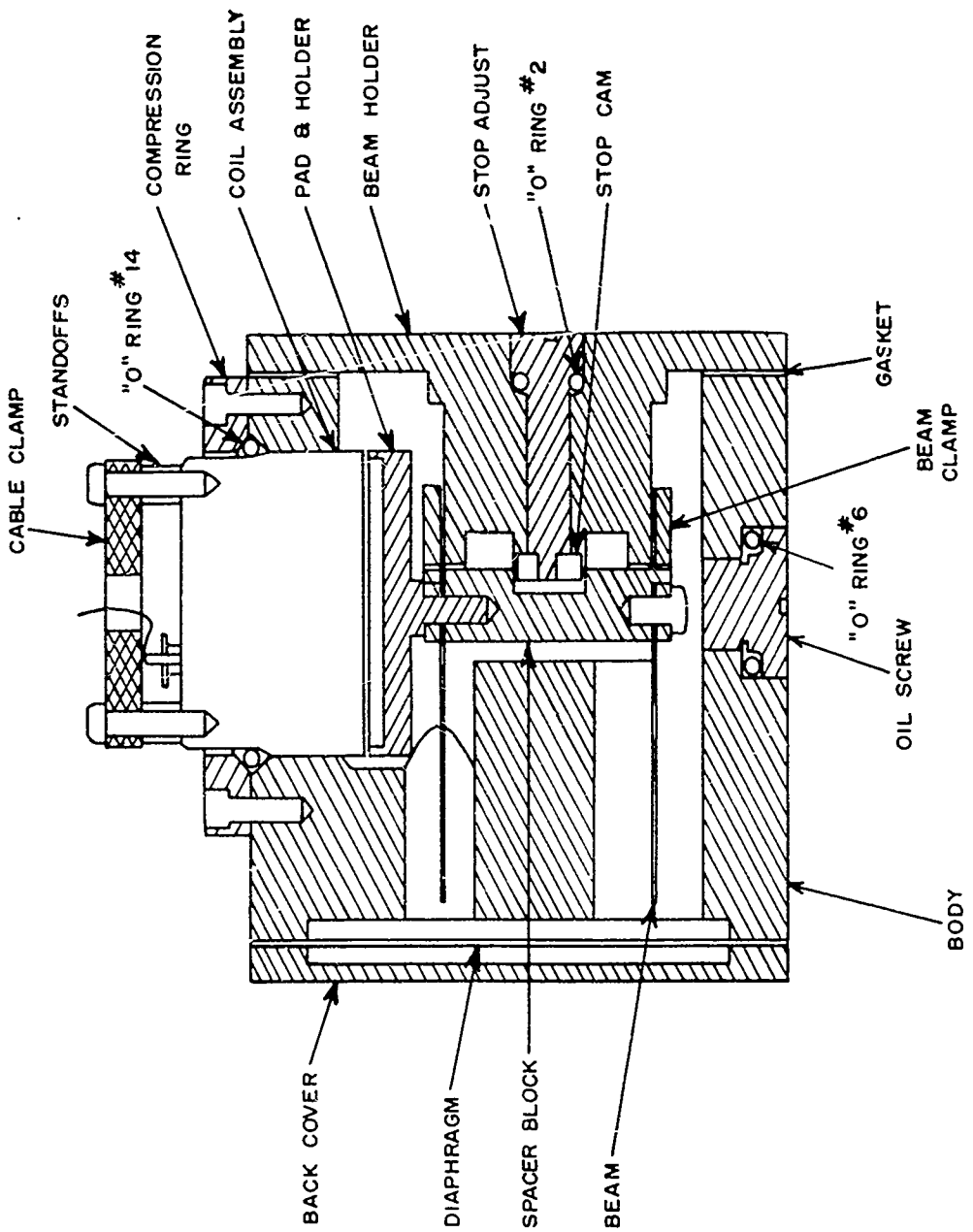


**Fig. 4.1 Sectional Diagram of Gage Construction**

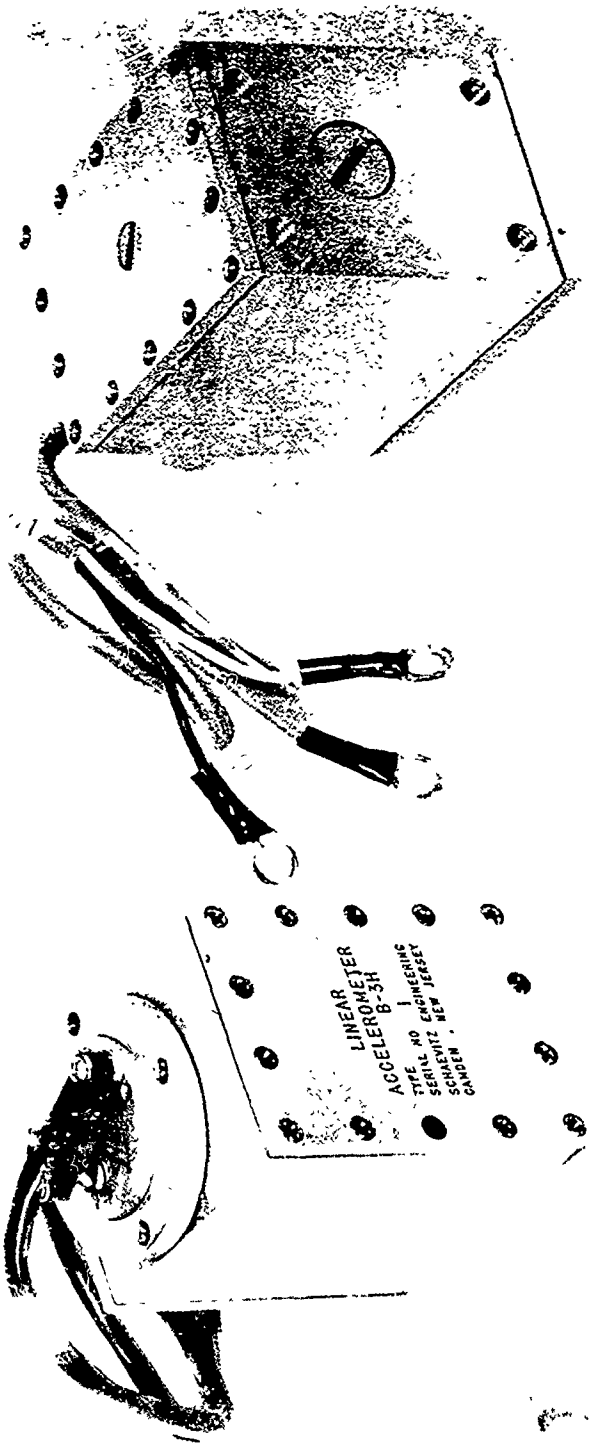


Fig. 4.2 Schaevitz Type B Accelerometer

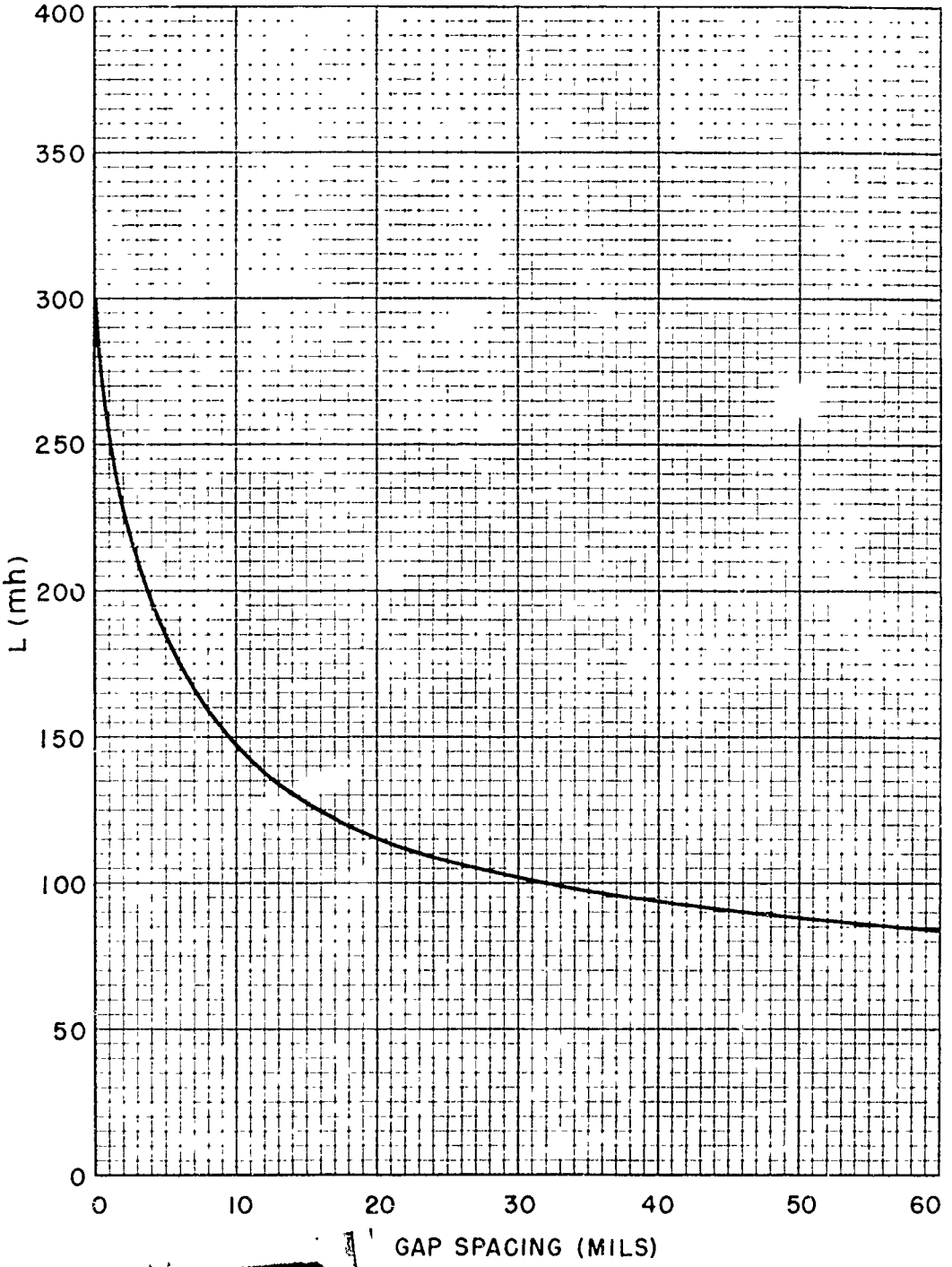


[redacted] Fig. 4.3 Inductance of Coil vs Gap Spacing

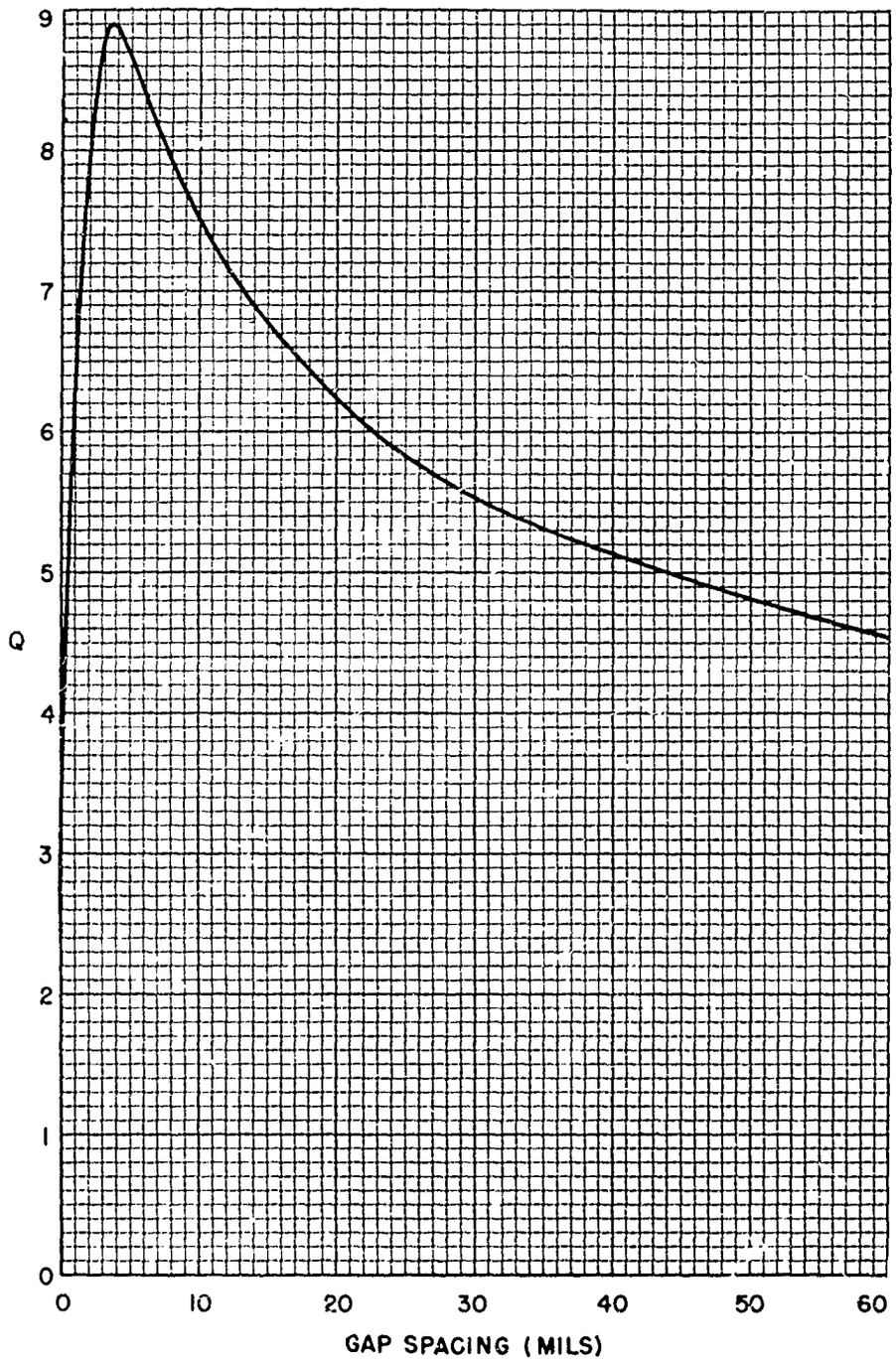


**Fig. 4.4 Q of Coil vs Gap Spacing**

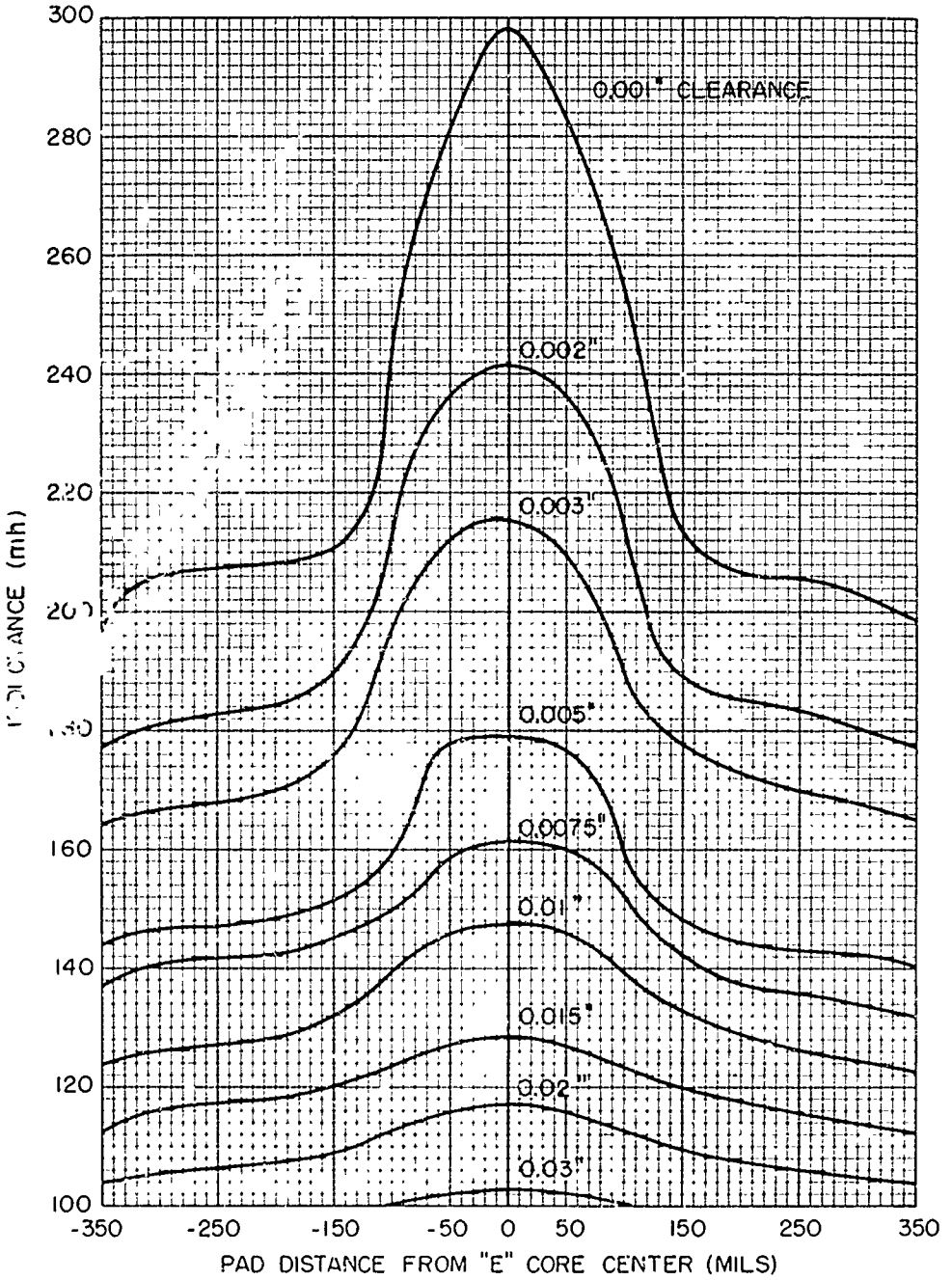


**Fig. 4.5 Variation of Inductance Due to Lateral Displacement of Pad Along Line of Pole Faces**

[redacted]



[redacted]

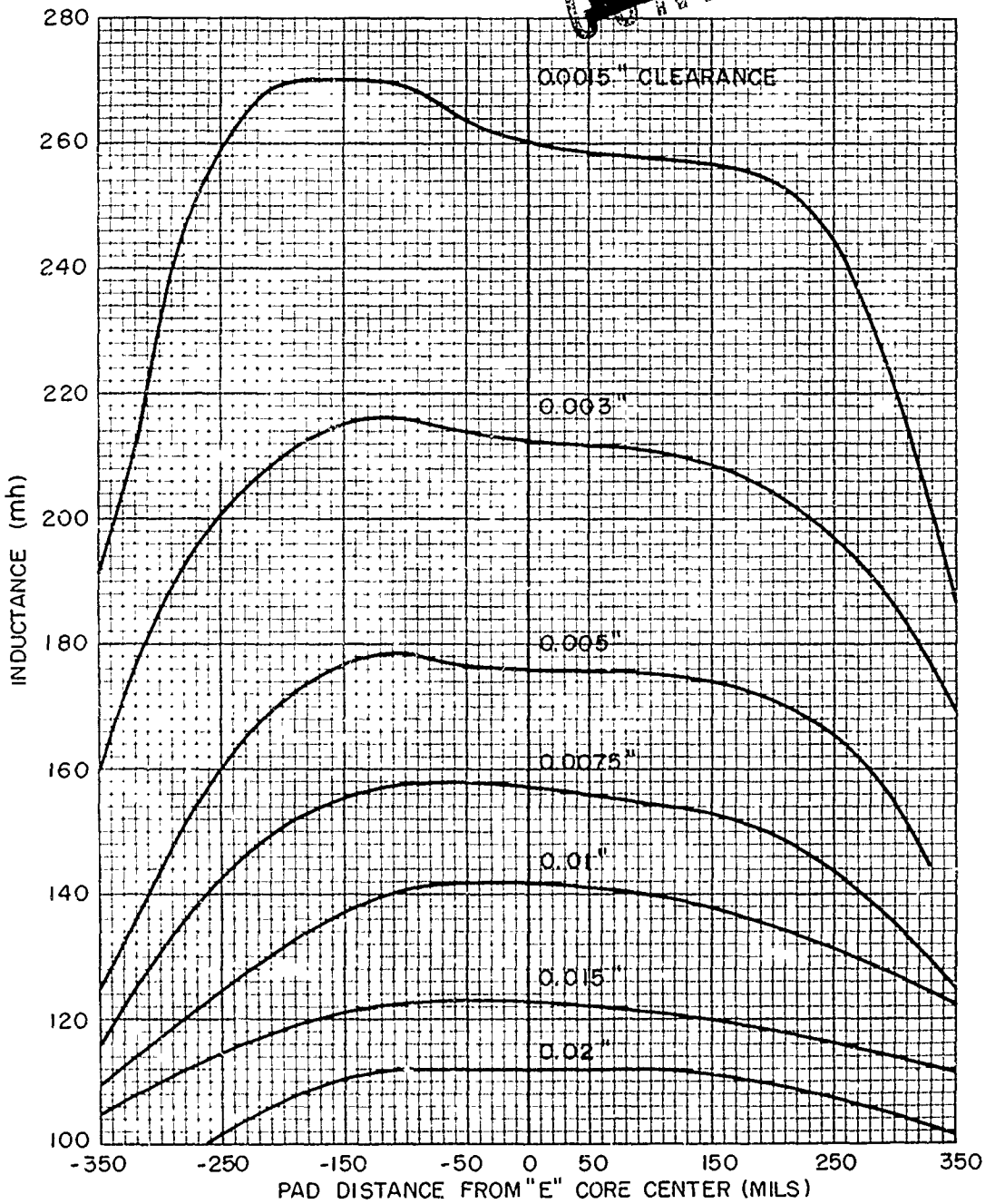


**Fig. 4.6 Variation of Inductance Due to Lateral Displacement of Pad in a Direction Normal to the Line of Pole Faces**



[redacted]

[redacted]

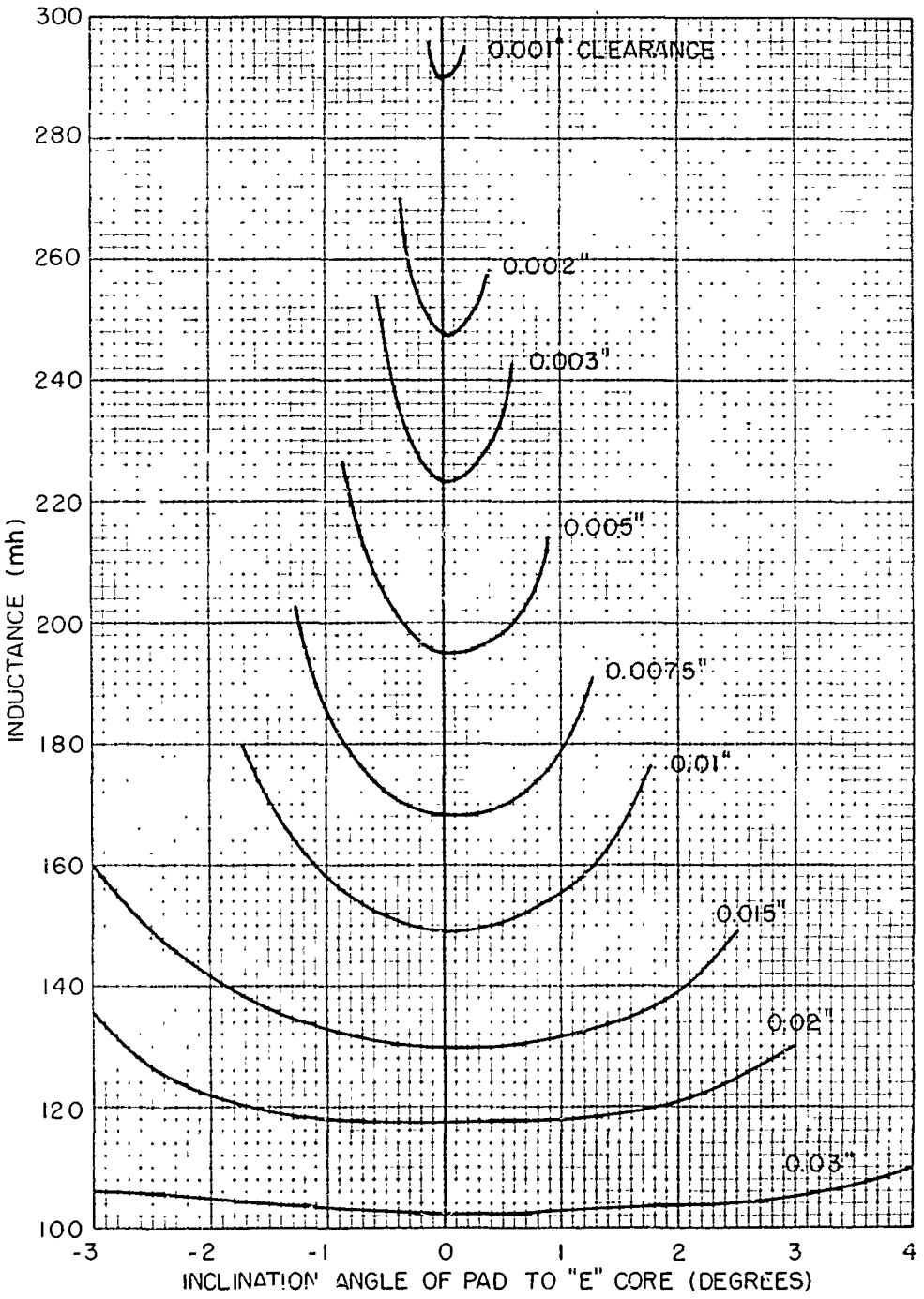


FIG. 4.7 VARIATION OF INDUCTANCE DUE TO ROTATION OF MU-METAL PAD



[redacted] [redacted]

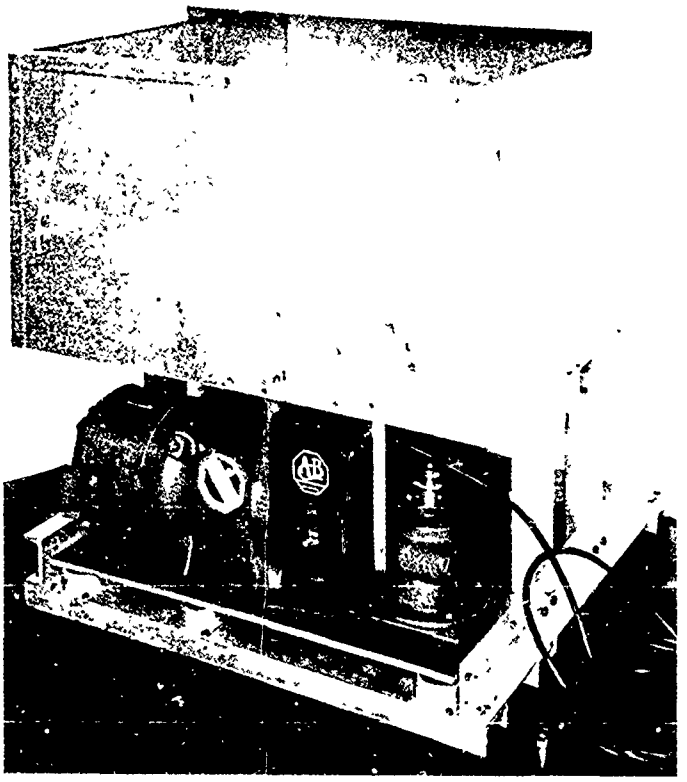

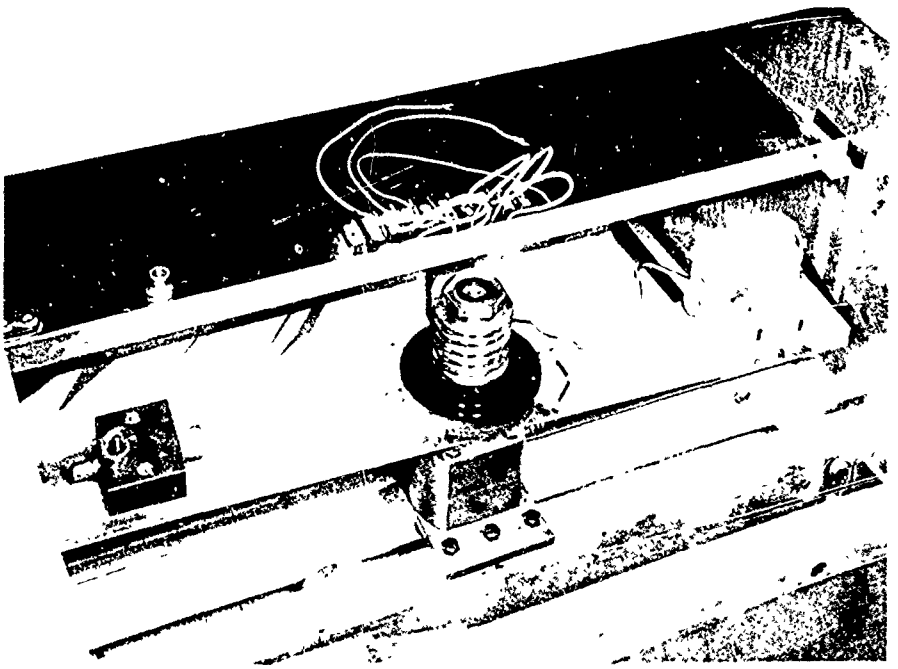

Fig. 4.8 NOL Spin Table Used for Static Calibration

Fig. 4.9 Tilt Table Used for Static Calibration

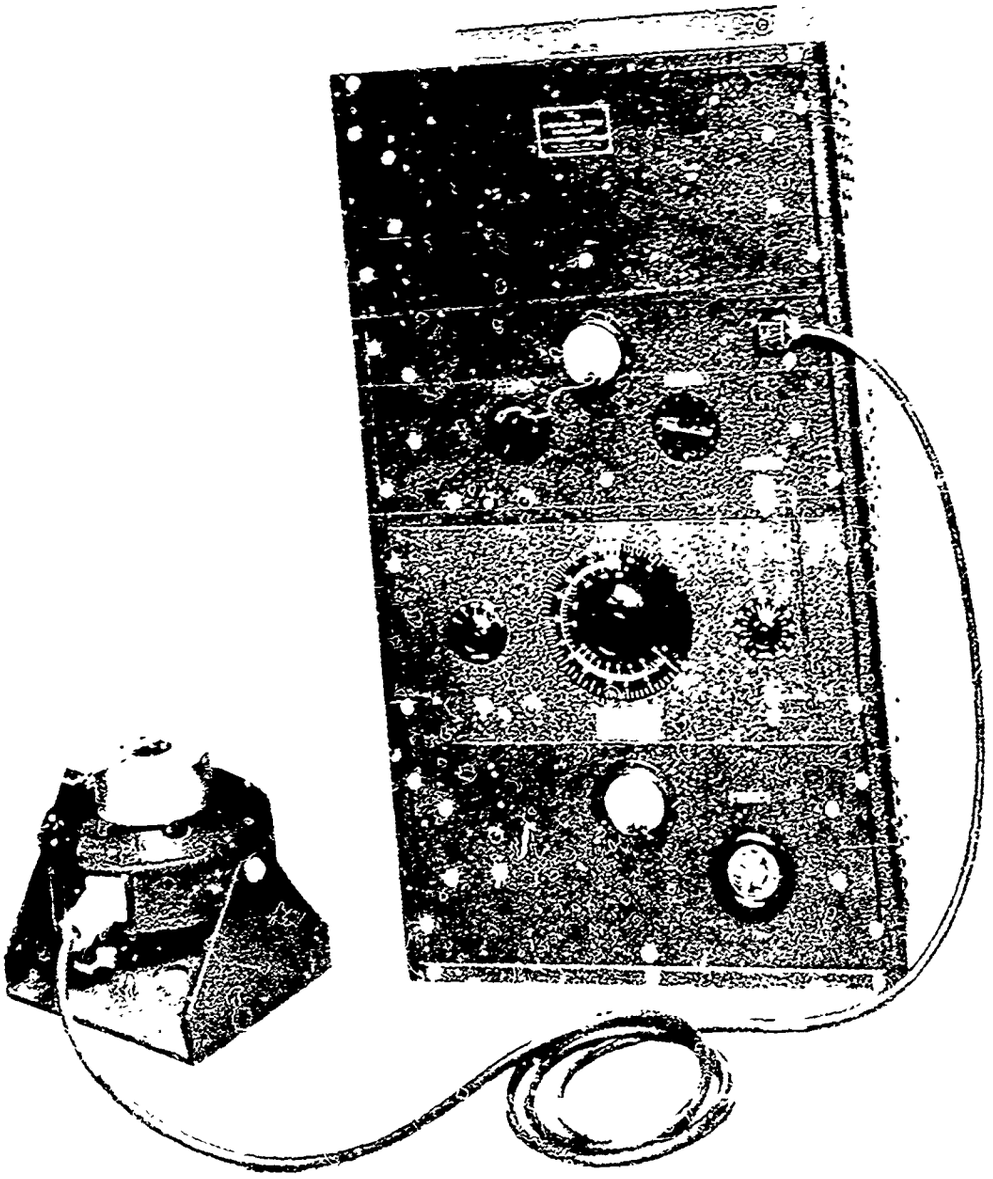

Fig. 4.10 MB Shake Table Used for Dynamic Calibrations

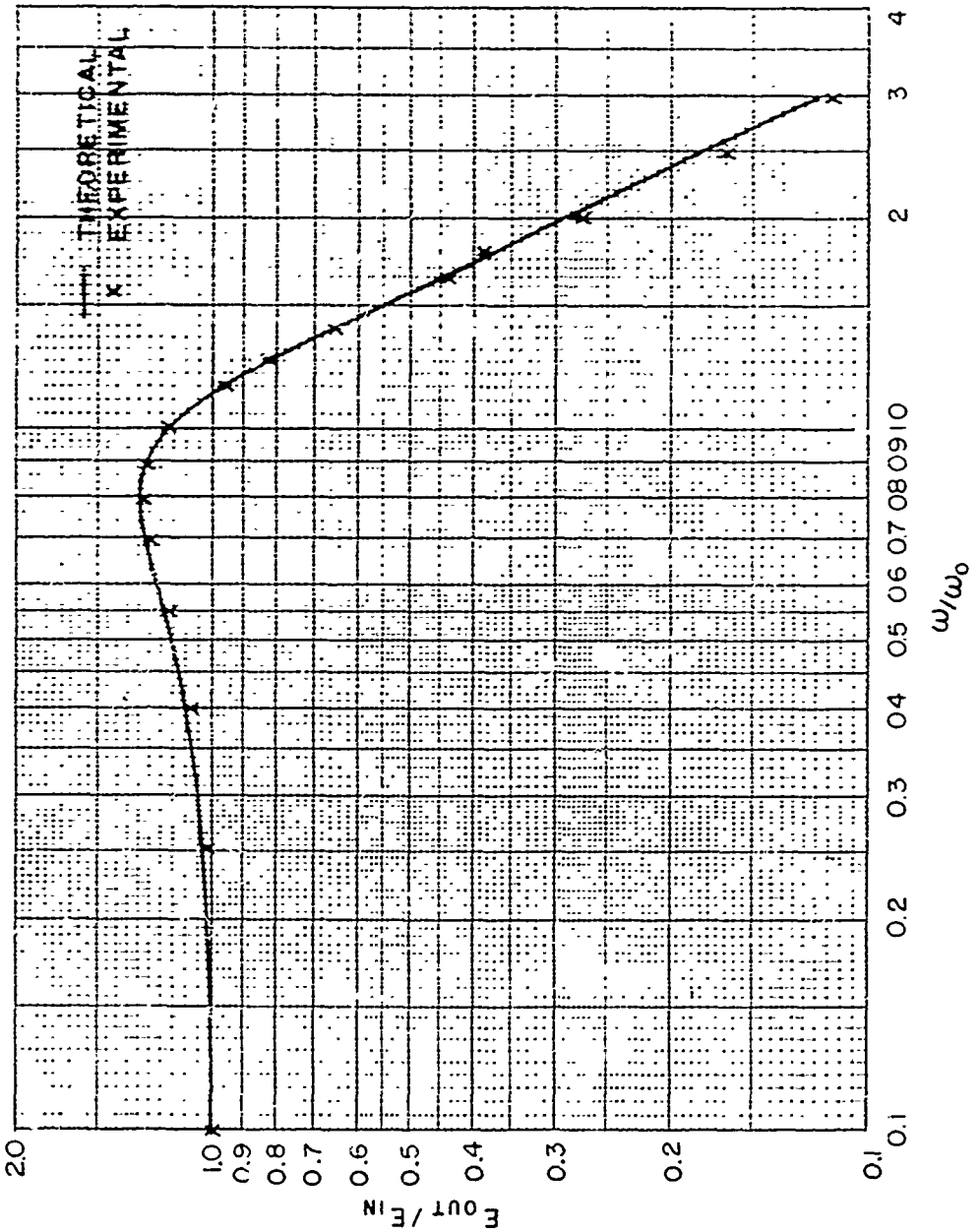


Fig. 4.11 Frequency Response to Sinusoidal Excitation

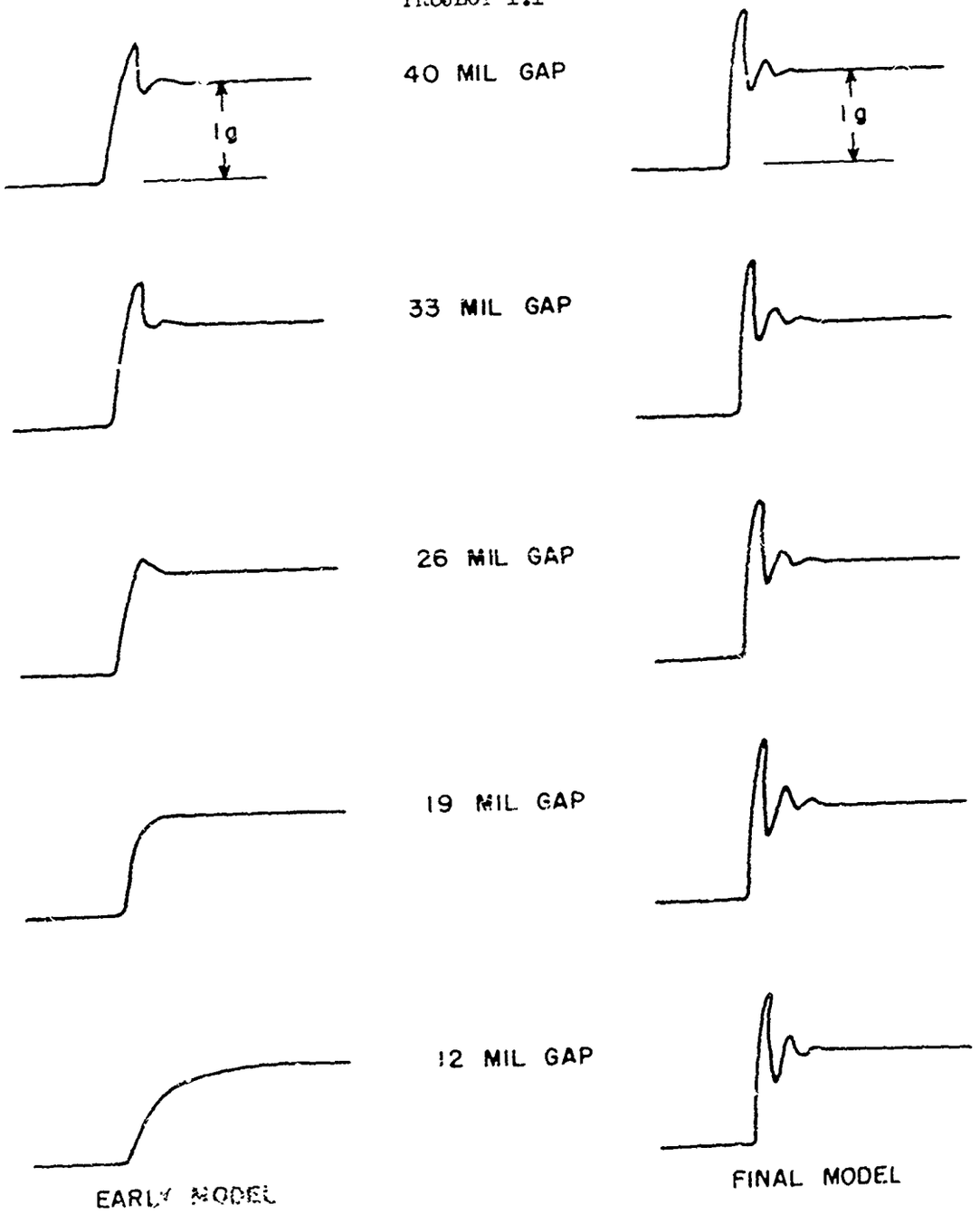


Fig. 4.12 Study of Damping Properties by Drop Tests

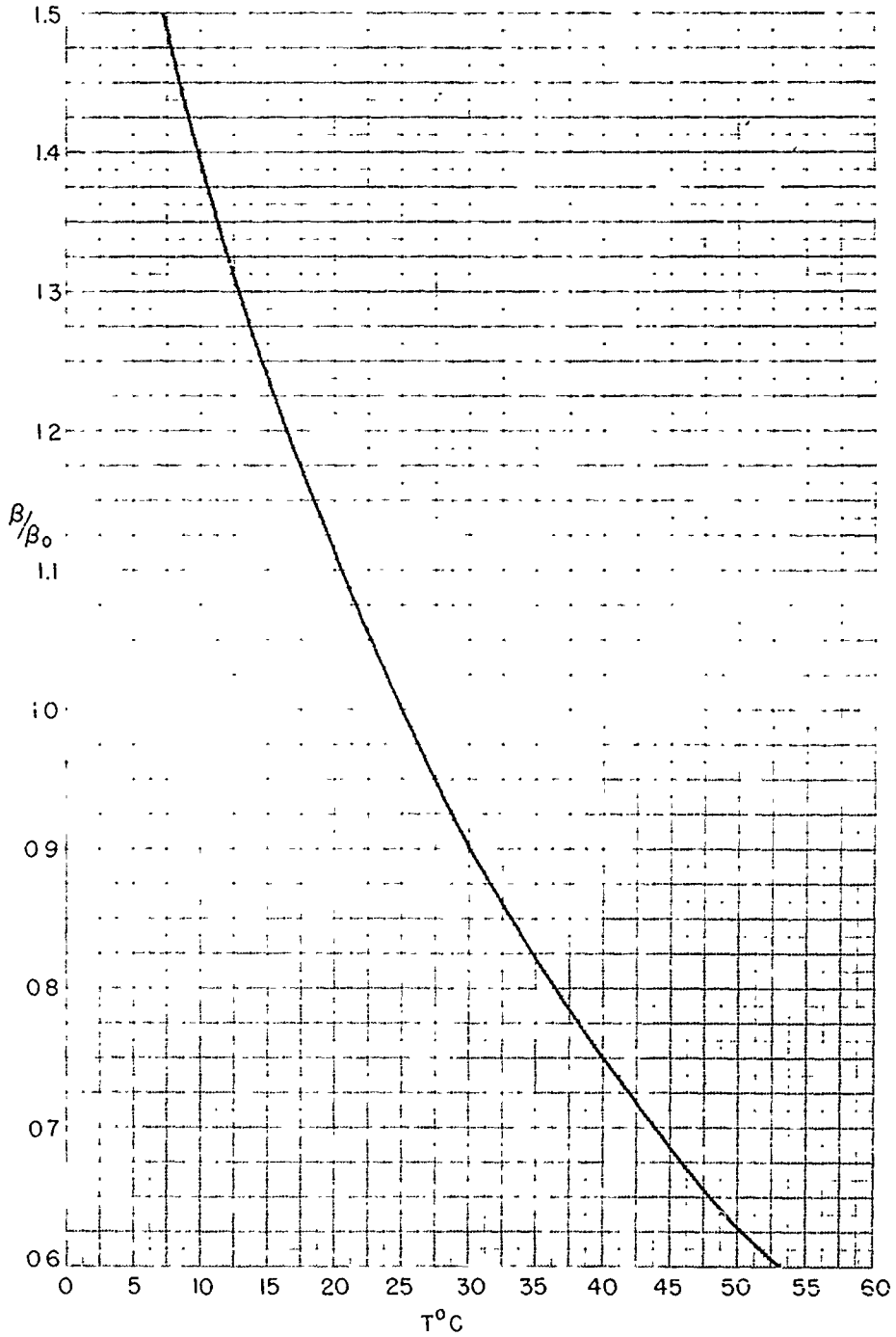


FIG. 4.13 NORMALIZED VARIATION OF DAMPING FACTOR WITH TEMPERATURE

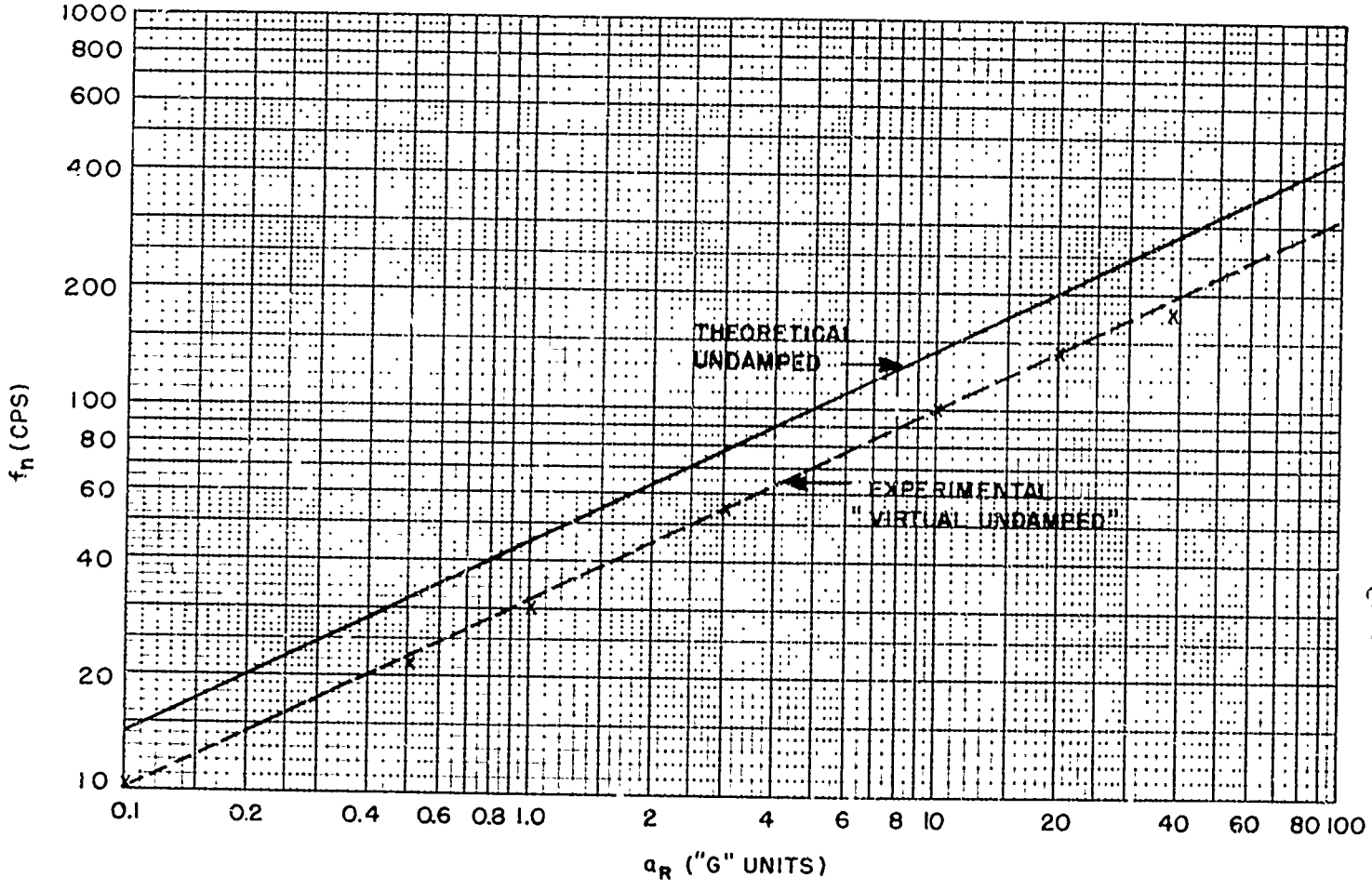


Fig. 4.14 Natural Frequency vs Gage Rating

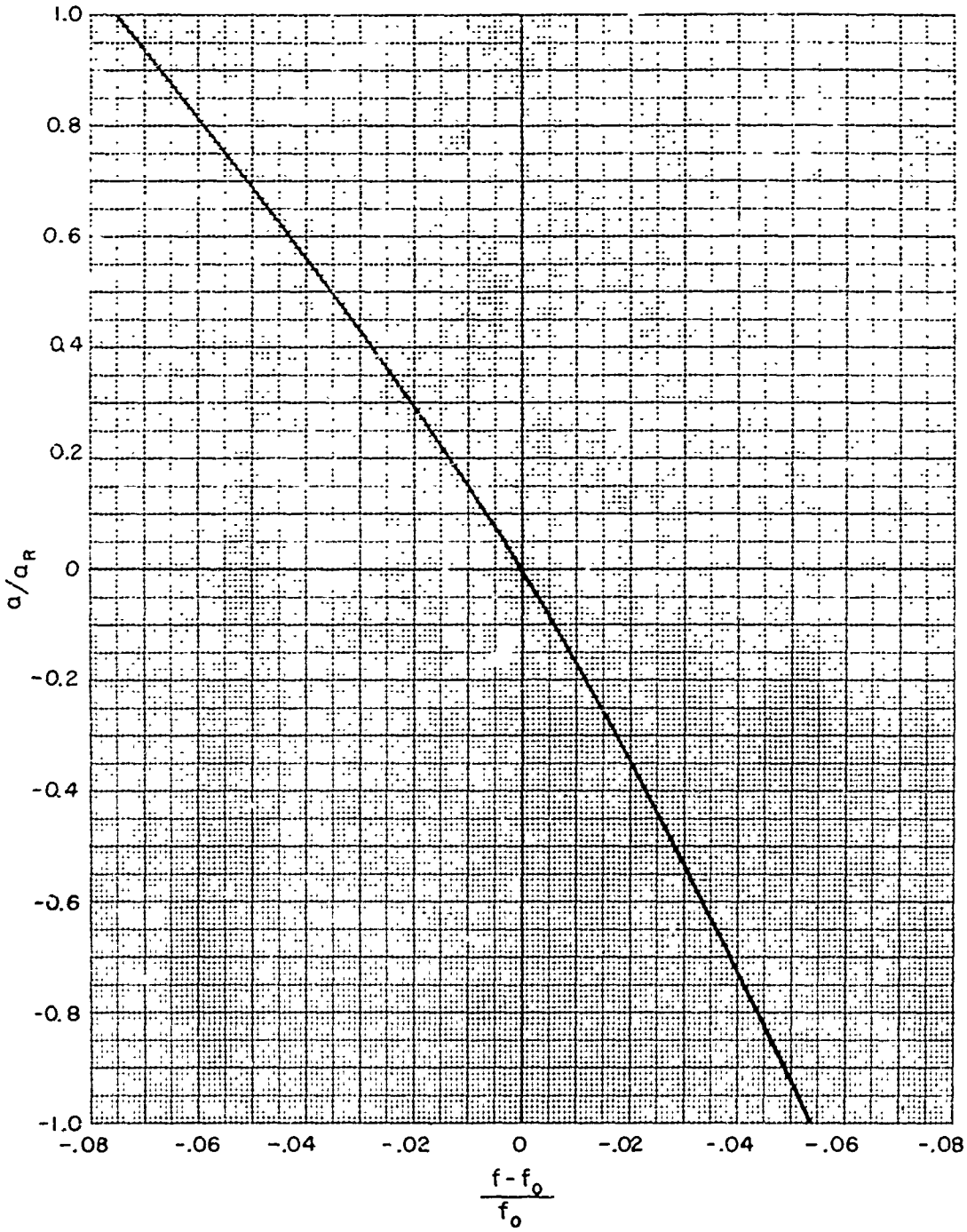


Fig. 4.15 Gage Transfer Characteristic

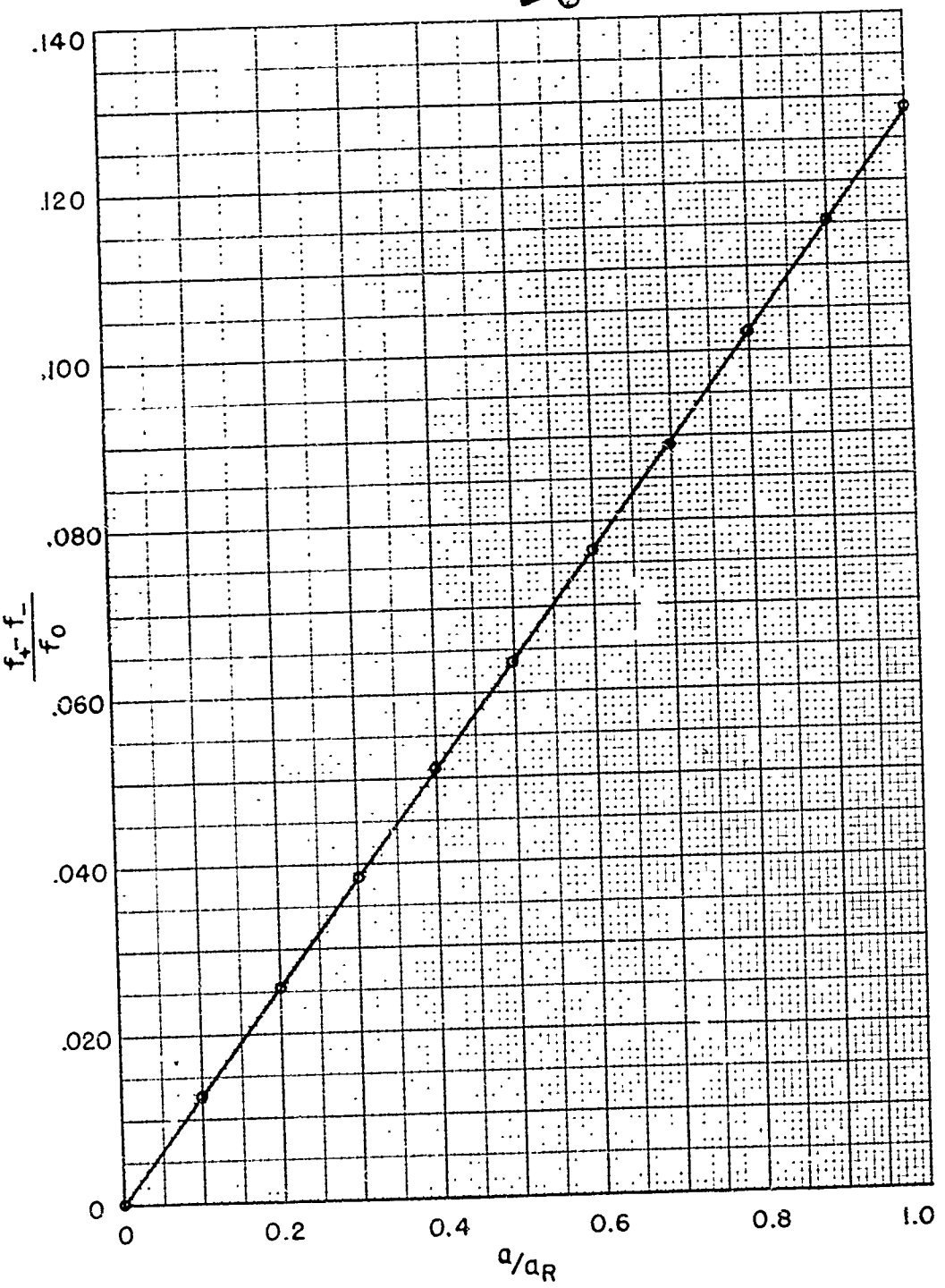


Fig. 4.16 Peak to Peak Response to Sinusoidal Excitation

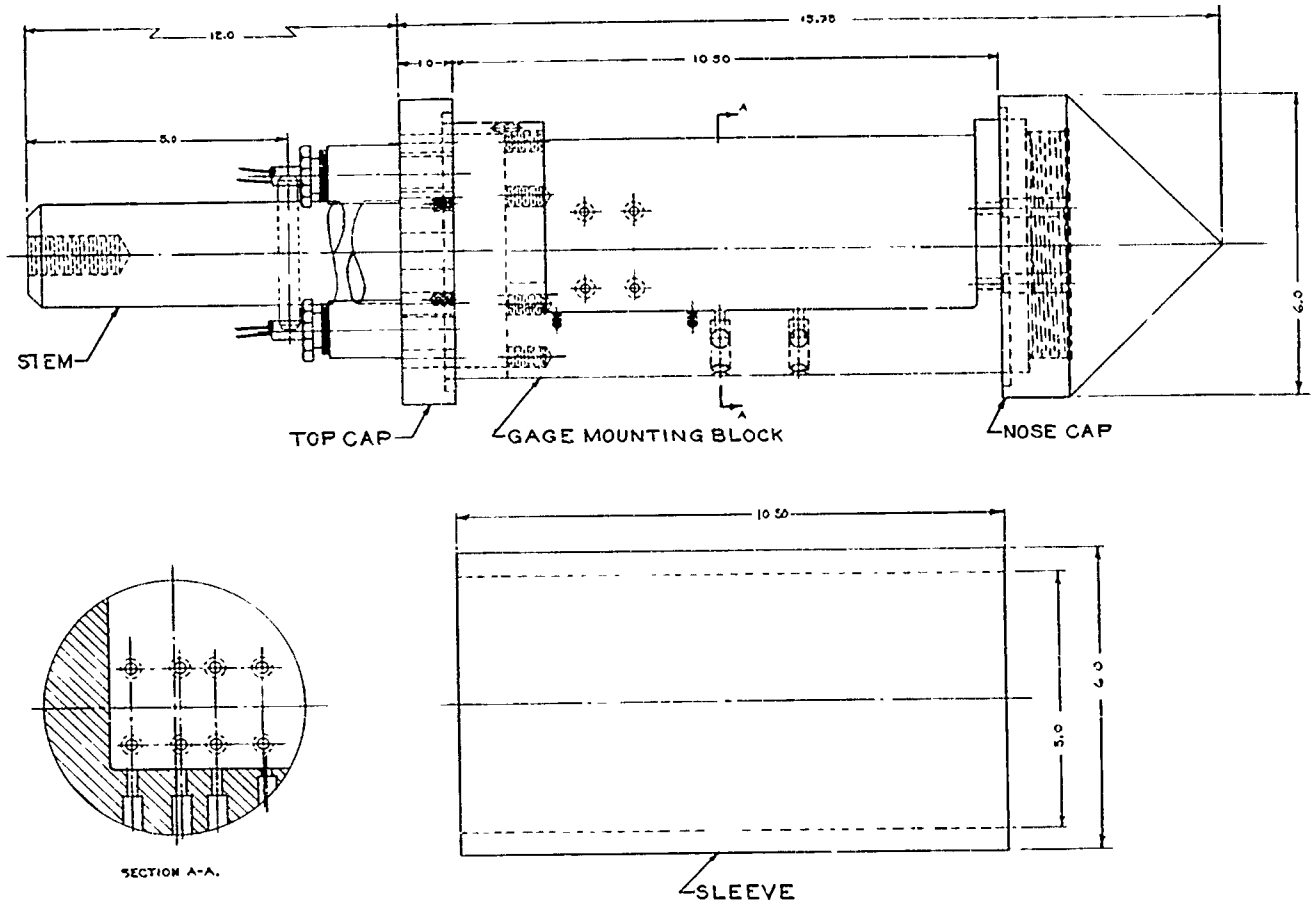


**Figs. 4.17, 4.18, 4.19, 4.20 Capsule Assembly**

[redacted]



[redacted]

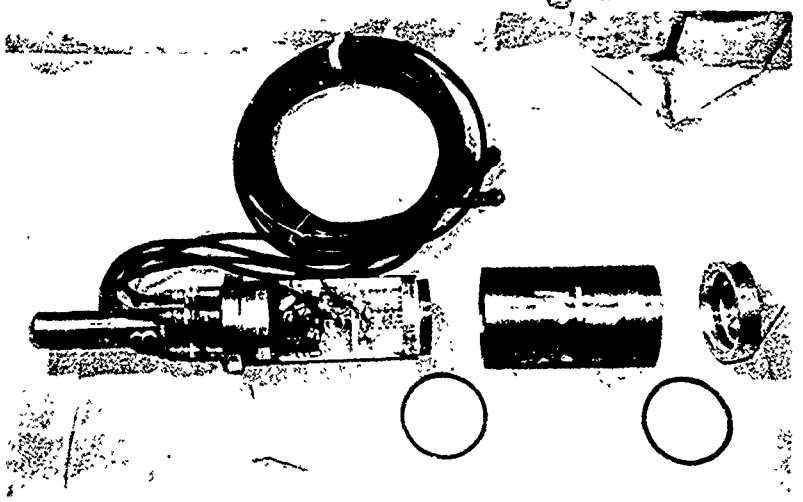

Fig. 4.21 Components of Capsule Assembly

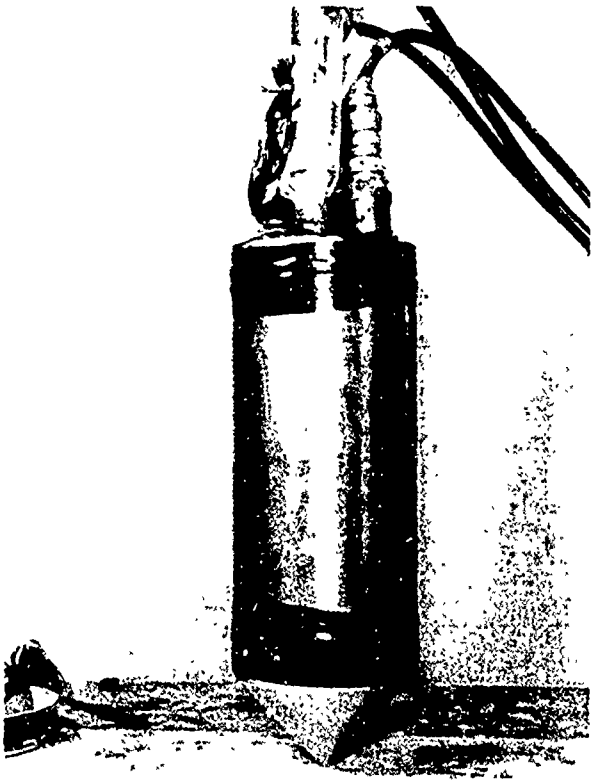

Fig. 4.22 Assembled Gage Capsule



[redacted]

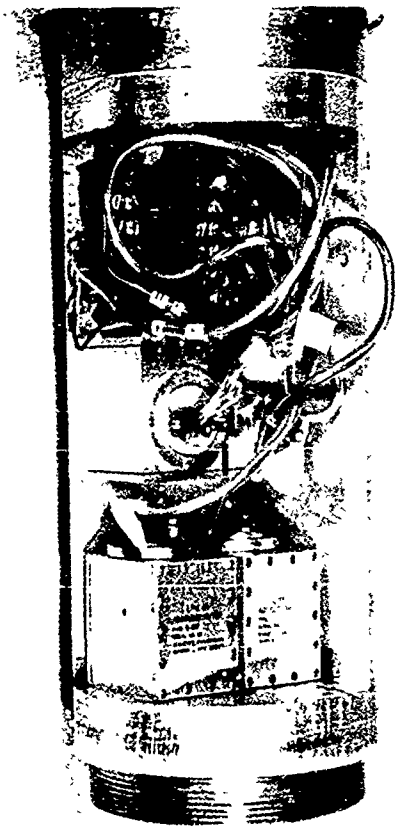

Fig. 4.23 Gages Installed on Mounting Block

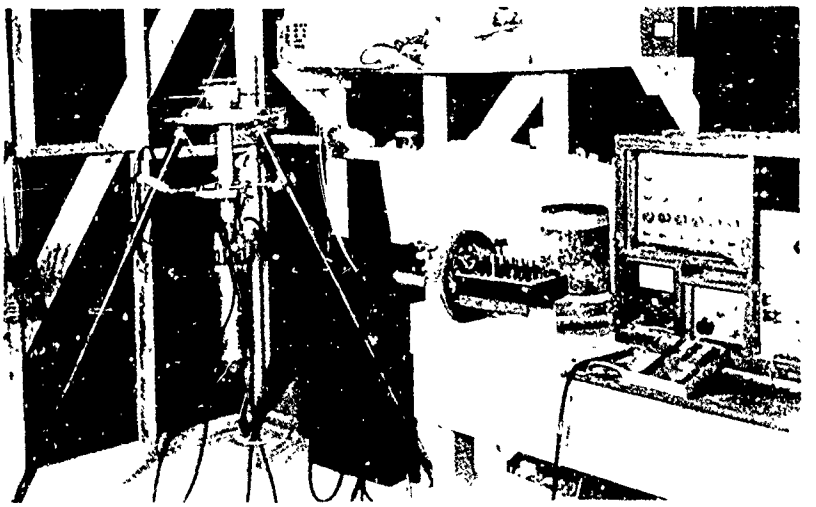

[redacted] Capsule on Calibration Tripod

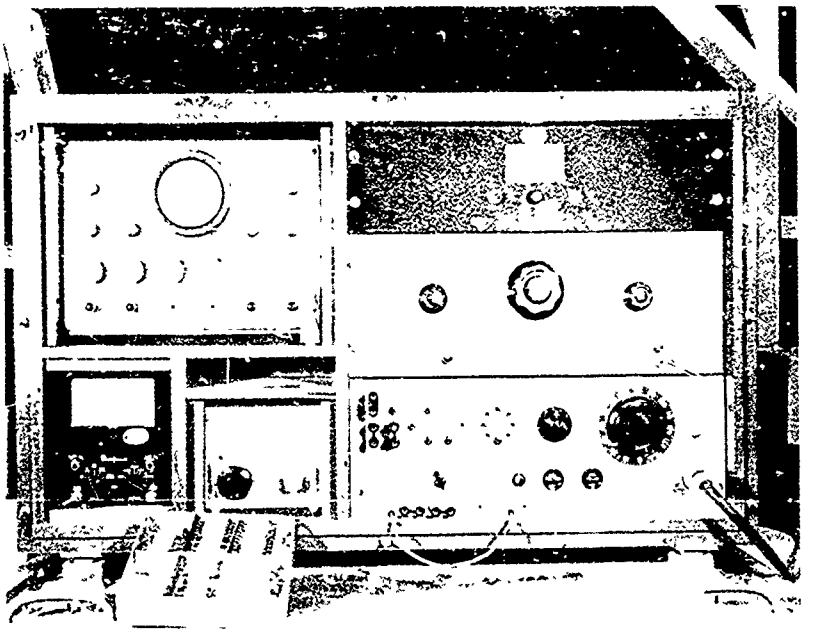

Fig. 4.25 Field Calibration Console

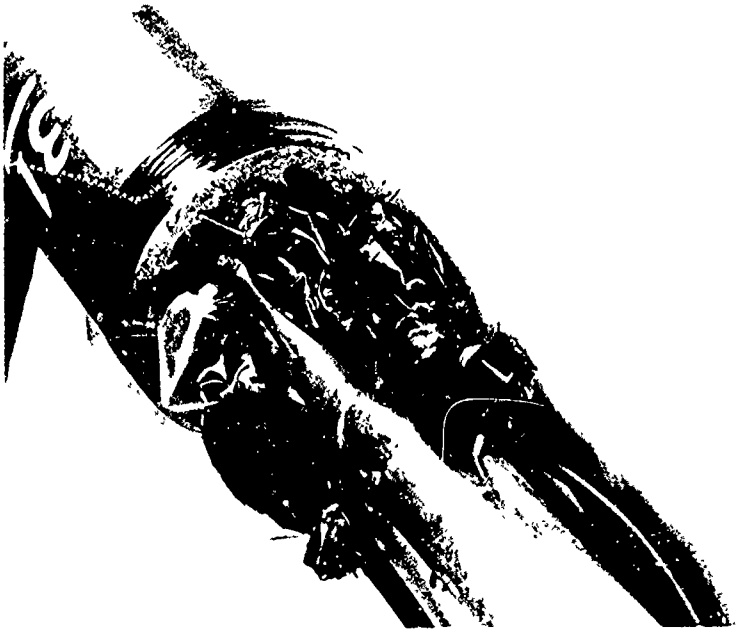

Fig. 4.26 End View of Waterproofed Capsule

[redacted]

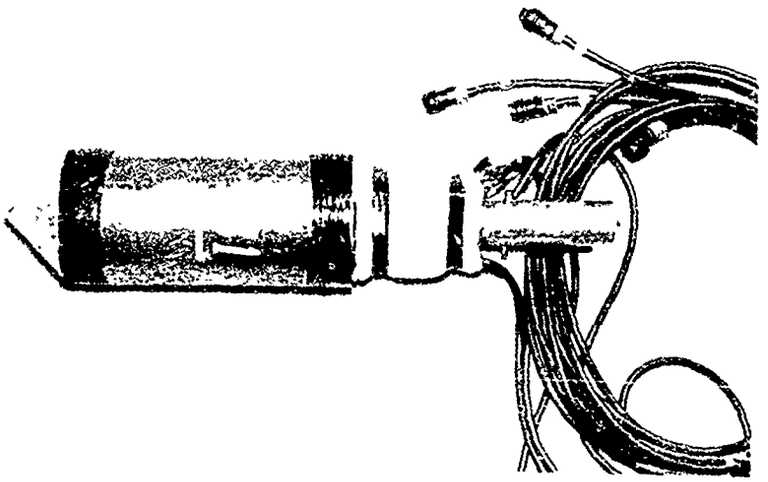

Fig. 4.27 Assembled and Waterproofed Capsule
(See page 73 for Fig. 4.28)

[redacted]29 Pouring Cal-Seal



[redacted]

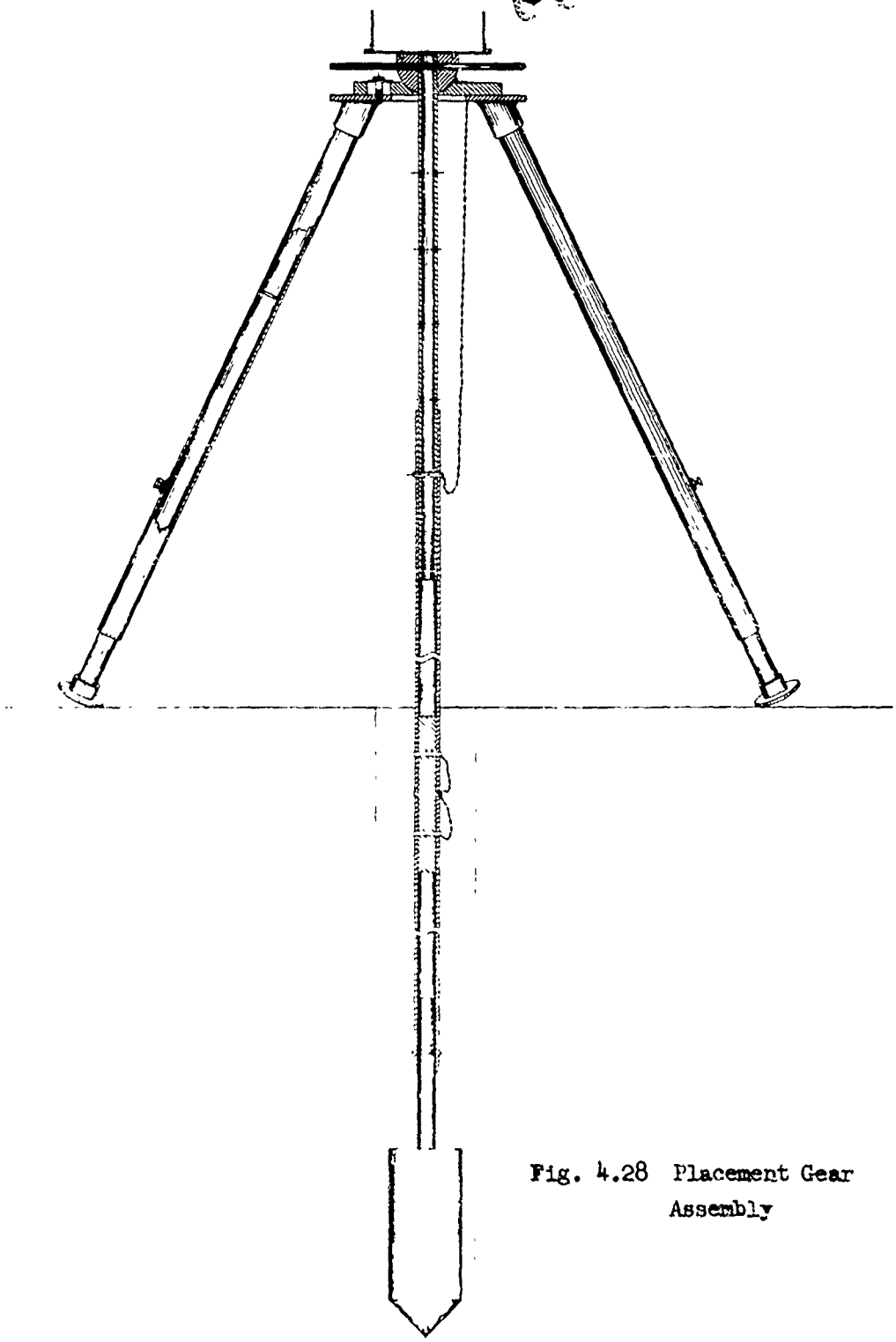

Fig. 4.28 Placement Gear Assembly

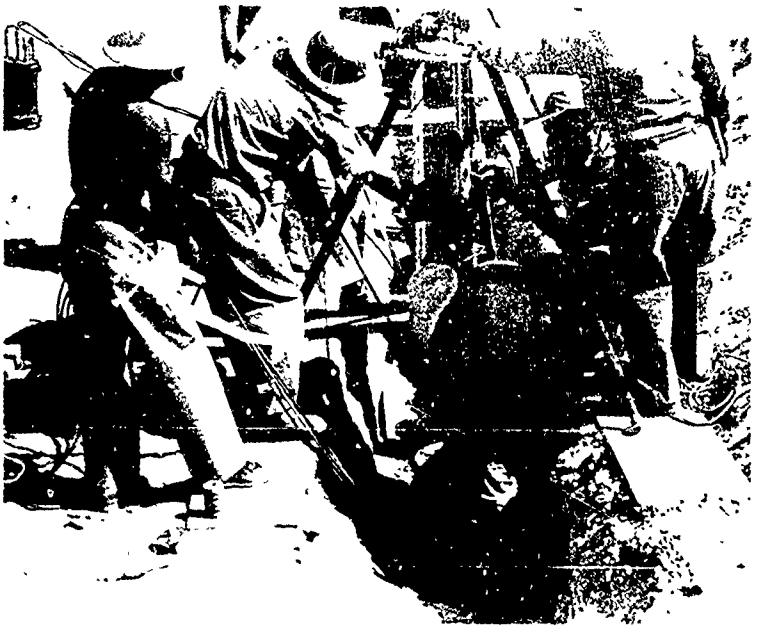

Fig. 4.30 Lowering Capsule into Gage Hole

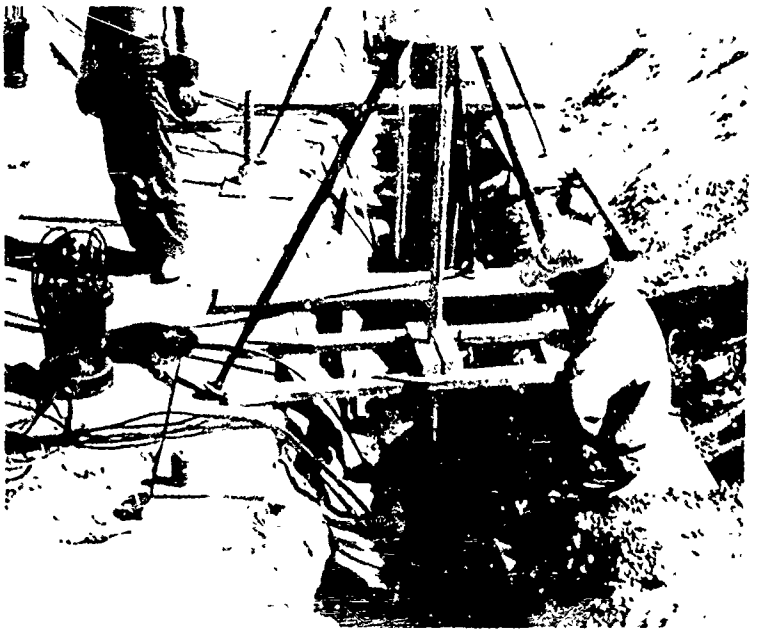

Fig. 4.31 Friction Block Arrangement for Lowering Gage Capsule

[redacted]

CHAPTER 5

## RECORDING AND PLAYBACK

The general features of the instrumentation system developed by the Naval Ordnance Laboratory for Operation Jangle, and the factors which influenced this design are briefly described in earlier portions of this report. The general features of the system are depicted in block diagram form in Fig. 5.1 through Fig. 5.4.

This chapter describes in detail the units comprising the overall recording and playback instrumentation and presents the salient characteristics of the system.

### 5.1 DESIGN CONSIDERATIONS:

(1) Frequency Response - The expected range of frequencies for accelerations was from approximately 1 cps to 20 cps for the main disturbance with superimposed higher frequencies up to 50 cps. The upper frequency range for the pressure phenomenon was expected to be higher.

(2) Amplitude Range - The expected magnitudes of the accelerations and pressures to be measured were known only to a poor degree of approximation.

(3) Number of Measurements - One hundred gage signals were to be recorded on each shot.

(4) Ionization - As with all nuclear explosions, ionization hazards and possible interference with signal transmission was expected.

(5) Remote Control - For personnel safety, and safety of equipment, remote control of all operations during the shots was required.

(6) Simplicity - The large number of measurements to be made indicated the desirability of uncomplicated equipment with a minimum number of parts and simple field adjustments.

(7) Reliability - The great expense involved on operations of this nature and the need for the information sought, made it mandatory that all the required data be obtained.



[redacted]

(8) Time - Very little time was available for the design, procurement and testing of the system.

(9) Previous Experience - The experiences of previous groups on similar operations was drawn upon in deciding individual features of the instrumentation.

5.2 DESIGN FEATURES:

(1) Frequency Modulation - The FM system was used. With this system, small interference could be expected from amplitude modulation producing signals such as ionization or other extraneous signals caused by the detonation of the weapon or signals emitted by power lines or other equipment.

(2) Multiplexing - Because of the large number of measurements to be made on each shot, the multiplexing system was used. This permitted the use of only twenty channels per shot for signal transmission; each channel contained five carrier frequencies, frequency modulated by five different gages.

(3) Magnetic Tape Recording - This mode of recording was chosen because of its freedom from the need for critical field adjustments, simplicity of operation, and adaptability to remote control. Further, the tape recording medium is insensitive to gamma radiation thus obviating the need for concern over this factor as would be the case if photographic film were used.

(4) Cable Telemetry - In the interest of simplicity, cable was used to transmit the signal from the field oscillators to the instrumentation trailer. Radio telemetry would have unnecessarily complicated the field instrumentation with transmitters, antennas, and receivers.

(5) Reliability - To enhance the reliability of the overall recording system and to insure obtaining the maximum amount of significant data, wide use was made of "back-up" units. Four complete, identical, and independent banks of equipment were used in each trailer, each bank operating five channels, one for each of five stations. The stations for each bank were selected so that in case of failure of one complete bank, recorded signals from no more than two distances would be lost. The five stations lost were so staggered as to minimize this loss (see Table 5.1). Each recorder had its inputs paralleled with the inputs of a second recorder to minimize the loss of records in case of tape or recorder failure. Each motor-generator set was powered by paralleled banks of batteries. Reference and timing signals were generated from a multiplicity of sources and recorded on two tracks of each tape. (These signals were used as fiducials, therefore they were common to all recording banks.)

TABLE 5.1

**Station Distribution to Instrumentation Banks**

| | Instrumentation Bank | | | Distances Lost With Failure of Bank | | | | Stations Lost With Failure of Bank | | | |
|---|---|---|---|---|---|---|---|---|---|---|---|
| Distances | 10 ft Depth | 20 ft Depth | 30 ft Depth | 1 | 2 | 3 | 4 | 1 | 2 | 3 | 4 |
| 1 | 1 | | | X | | | | X | | | |
| 2 | 3 | 4 | 2 | | | | | | X | X | X |
| 3 | 3 | | | | | X | | | | X | |
| 4 | 4 | | | | | | X | | | | X |
| 5 | 2 | 3 | 1 | | | | | X | X | X | |
| 6 | 4 | | | | | | X | | | | X |
| 7 | 2 | | | | X | | | | X | | |
| 8 | 4 | 1 | 3 | | | | | X | | X | X |
| 9 | 2 | | | | X | | | | X | | |
| 10 | 1 | 2 | 4 | | | | | X | X | | X |
| 11 | 1 | | | X | | | | X | | | |
| 12 | 3 | | | | | X | | | | X | |

5.3 PERFORMANCE CHARACTERISTICS:

(1) Frequency Response from D.C. to approximately 150 cps on the 3.9 kc channel, and to approximately 1,000 cps on the 14.5 kc channel. The upper frequency limits of any particular channel were limited by the frequency response of the gages used on that channel.

(2) Dynamic Range approximately a factor of 100, realized by the use of "back-up" gages.

(3) Resolution sufficient to read down to 1/20 of nominal full scale gage range. This resolution was limited by the noise - "wow-and-flutter" - inherent in the magnetic tape recording and playback mechanisms.

(4) Accuracy of reading the records varied from approximately ± 3% for signals produced near the nominal gage range to approximately 10% for the signals which were nearer 1/20 of the gage range.

(5) Recording Time of 15 minutes was availalbe.

5.4 FIELD UNITS:

5.4.1 Gage

The frequency modulating elements in both the acceleration and pressure gages consisted of iron-core inductors whose actual inductance value varied with the instantaneous position of a high permeability pad relative to the inductor core.

The accelerometers were manufactured by Schaevitz Engineering Company of Camden, New Jersey and are described in detail in Chapter 4 of this report; the pressure gages were manufactured by Wiancko and are described in detail in a Ballistics Research Laboratory report now under preparation.

5.4.2 Gage Cable

Each gage was connected to its oscillator circuit by a 10, 20, or 30 foot length of two conductor, low capacitance, shielded cable, RG-22/U. This cable had two particularly desirable features - low linear capacitance, 16 mmf per foot, and rugged mechanical construction. Low capacitance cable was a requisite since the cable capacitance comprised part of the tank capacitance of the oscillator; good design considerations called for as much as possible of the tank

capacitance to be of a fixed type. Even with this design criterion, on the 14.5 kc channels with the 35 foot length of cable (required for the 30 foot deep gages) only approximately 10% of the total tank capacitance was fixed. However, the rugged construction of the cable made this situation tolerable. Under hydrostatic and shock testing up to 1,000 psi levels, negligible change in cable capacitance was observed.

### 5.4.3 Oscillator-Amplifier[1] (Fig. 5.5)

The oscillator-amplifier unit was designed by the Vitro Corporation[2] in accordance with specifications supplied by NOL. It consisted of five input circuits and a combined output circuit. The input oscillator circuits were of the Hartley shunt feed type, with one section of a dual triode tube (12AU7) serving in the oscillator. The Hartley circuit was chosen because of its inherent stability; shunt feed was necessary in order to prevent the introduction of objectionable magnetic bias into the accelerometer coils. The second half of the tube was directly coupled to the oscillator section and served as the amplifier stage. The signals were coupled to the transmission cable, MCOS-6, by means of output transformers which provided the proper impedance match between the oscillator-amplifier units and transmission cables. The secondary windings of the output transformers of the 3.9 kc, 5.4 kc, and 7.35 kc circuits were in series across the output terminals. However, the signals from the 10.5 kc and 14.5 kc circuits were mixed and superimposed on the output through a bridge circuit (Fig. 5.6). This was necessary in order to reduce the cross-modulation between these two signals to an acceptable minimum value. It was found that without this bridging network, a 4 kc difference frequency would be produced by these two frequencies which could cause objectionable interference in the 3.9 kc band. Interference between all bands was kept to a minimum by designing the oscillator-amplifier circuits so that the total harmonic distortion was less than 3%. In this way, for example, the second harmonic of the 5.4 kc circuit was kept from distorting the signal in the 10.5 kc band.

The filament and plate power necessary to operate the units was furnished by means of the multi-conductor MCOS-6 cables. All power originated at the trailer.

The oscillator units were extremely stable and free from extraneous influences. For a change in B+ voltage from 225 volts to 325 volts the oscillator frequencies changed approximately 17 parts per million per volt on all channels except the 14.5 kc, where the change

[1]See Technical Report No. 28 of the Vitro Corp. of America, "Instruction Book - Oscillator Set TT-1/36-A and Housing.
[2]Formerly the Kellex Corporation.

was approximately 50 parts per million per volt. The frequency change due to filament voltage variations was approximately 10 parts per million per volt. Temperature changes from 20°F to 130°F resulted in frequency changes of 10 parts per million per degree F. Tests in an air gun for producing transient accelerations were made with the units operating normally while high acceleration shocks up to 50 g were applied. There were no discernible effects on the output frequency at accelerations below 30 g, and only a 15 cps change at 50 g. All the above frequency deviations were considered negligible over the limited range of voltages, temperatures and shocks to which the oscillators were to be subjected.

The oscillator units were not designed primarily for repeated operations, therefore the use of long-life components was not justified. However, operation during use had to be dependable and it was very important that as many circuits as possible function properly at that time. The circuits had a minimum number of components to reduce the chances of component failure. Except for the common filament and plate supplies, a failure in one circuit would not seriously affect the operation of the other circuits.

### 5.4.4 Transmission Cable

The cable used for the transmission of the signal from the field stations to the instrument trailers was a standard Navy type, MCOS-6. This cable consisted of two shielded pair and an unshielded pair of conductors, the overall cable being approximately 1/2 inch in diameter and covered with a neoprene jacket. The characteristic impedance of the signal conductors was approximately 70 ohms; for maximum signal transmission the cable was terminated at both ends with this impedance value. The attenuation of signals varied with the frequency of the signal carrier, the attenuation for the 3.9 kc carrier being 1.1 db per 1,000 feet and for the 14.5 kc carrier being 1.6 db per 1,000 feet (Fig. 5.7). (The oscillator-amplifier units were designed to equalize this variation by providing higher outputs for the higher frequency channels than for the lower frequency channels.) The conductors were utilized as shown in Fig 5.7. The individual pairs of leads were used for separate functions so as to achieve simplicity and reliability, and the signal leads were paralleled to reduce attenuation.

It was estimated that approximately 250,000 feet of cable would be required in Operation Jangle. This cable was available on reels each holding approximately 1,500 feet which made it convenient for laying (Fig. 5.8). To facilitate the task in the field of joining the individual cables to provide the proper lengths, connectors were attached to the ends of the cable at NOL. All that was required in the field was to join the connectors and waterproof the joint (Fig. 5.9). In this way, good electrical continuity was obtained along with strong mechanical linkage all with a saving in manhours in the field over either solder or cold splice methods.

## 5.5 INSTRUMENTATION TRAILER UNITS:

All recording and power equipment and necessary auxiliary units were housed in van-type trailers. These units are described below and the units directly associated with the recording of the signal are shown in Fig. 5.10.

### 5.5.1 Auxiliary Signal Units

(1) Distribution Panel (Fig. 5.11) - This panel served as a master distribution panel. It fed filament and plate voltages to the five stations of each bank. It also distributed the output signals of each oscillator set, through two impedance matching transformers in each signal channel, to a recording channel in each of two different recorders. The primary circuits of the transformers were connected together and matched to the characteristic impedance of the MCOS-6 cable, and the individual secondary windings were matched to the input impedance of each recorder. An attenuation network was added to the primary circuit of the transformers to reduce the signal level input to the recorders.

(2) D. C. Power Supply Panel (Fig. 5.12) - This panel received 36 volts D.C. to operate five DM-36 dynamotors (Fig. 5.13). The 300 volt filtered outputs of these units were fed to the Distribution Panel for coupling to the transmission cables and thence to the field oscillator sets. Dynamotor plate supplies were used in this operation rather than electronic power supplies because of the greater simplicity, and the ready availability of the battery source.

(3) D. C. Junction Panel - Power for this panel was received from the same 36 volt battery banks that powered the motor-generators. The five output receptacles distributed power to the D.C. Power Supply Panel.

(4) Filament Supply Panel (Fig. 5.14) - This panel received 115 volts A.C. which operated an auto transformer adjusted to produce a 145 volt output. This voltage level was needed to compensate for the voltage drop incurred over approximately 1-1/2 miles of cable in furnishing 130 volts A.C. at the filament transformer in each oscillator set. Each output receptacle fed only one cable and was individually fused with a slow-blow fuse. In this way, short circuiting of one oscillator set would not affect the other oscillator sets operating off the same auto transformer.[3]

---

For more detail on the above four panels, see Vitro Corporation Technical Report No. 29 "Installation Manual - Distribution Panels TF-1/36-A, J-1/36-A, DY-1/36-A, and J-2/36-A".

(5) A. C. Junction Panel - All A.C. power for the auxiliary units and the recorders was distributed from this panel. It received power from its associated motor-generator set.

The above panels were connected by means of cables in order to facilitate isolation of any particular component for trouble shooting purposes. A sufficient variety of types of connectors were used so that improper connections were not likely.

5.5.2 Magnetic Tape Recorder (Fig. 5.15)

The recorders were modified Ampex Model 301 commercial magnetic tape sound recorders similar to those used by the NOL group on Operation Greenhouse.[4] The salient features of these recorders are listed below:

(1) Seven separate heads in one assembly were employed to record seven channels simultaneously on 1/2" wide magnetic tape. Each channel track was 0.050 inches wide and separation between tracks was 0.020 inches.

(2) Frequency response of the recorders was flat within ± 3 db from 1 kc to 18 kc.

(3) Signal to noise ratio was greater than 20 db below a 3% distortion recording level. Cross-talk between adjacent channels was at least 45 db down.

(4) Tuning fork controlled capstan motor drive was employed to keep tape speed variations to a minimum resulting in less than 0.1% r.m.s. "wow-and-flutter".

(5) Remote control was provided for all necessary operations - application of power, start of tape transport, and recording of signal.

(6) Only the recording (not playback) operation was possible on this recorder. Further simplifications and fool-proof features of the recorders were the elimination of erase heads and the use of only forward speed at 30 inches per second.

The recorder contained seven identical two-stage amplifiers with inputs located on the front of the unit (Fig. 5.16). The power for this chassis was provided by the power supply chassis

[4] Greenhouse Report Annex 1.6, Part IV, Section 1; also "Instruction Book-Multi-Channel Magnetic Tape Recorder and Reproducer produced under Kellex Corp. Purchase Order SS No. 21223" by Ampex.

below it. For each channel the record amplifier had separate Bias Control and Signal Level Metering Jacks, Bias Adjustment and Record Level Adjustment Controls.

The power supply unit (Fig. 5.17) was of the conventional full-wave high vacuum type with adequate filtering. The high frequency (70 kc) bias supply also was located on this chassis. This push-pull oscillator had very low harmonic content in its output.

The capstan motor amplifier unit (Fig. 5.18) contained a 69 cps tuning fork which controlled the frequency of an amplitude limited oscillator circuit. The output from the oscillator was subsequently amplified and used to operate the capstan motor drive.

The prime requisite of magnetic tape recorders when used in frequency modulating systems is to keep the speed variations of the tape to a minimum. Speed variations are equivalent to frequency modulations of the signal and are, therefore, reproduced along with gage signals as extraneous and objectionable noise. The bouncing of the tape on the recording head also produces objectionable speed modulation of the tape; this "flutter" was kept to a minimum by the careful design of all parts in the tape transport mechanism and some mechanical filtering by the use of tension arms. However, irregularities on the tape surface and dust on the tape and heads were difficult to control or eliminate. As a result, the noise due to "flutter" varied from recorder to recorder and from shot to shot.

### 5.5.3 Auxiliary Units

#### (1) Timing Oscillator (Fig. 5.19)

In addition to the gage signals, calibration signals were recorded simultaneously on the tape. A composite signal of two frequencies was produced by each of two Timing Oscillator units. One unit produced a standard unmodulated frequency of 400 cps and a modulated center frequency of 2,300 cps. The other unit produced a standard unmodulated frequency of 1,000 cps and a modulated center frequency of 3,900 cps. Although only one standard frequency and one modulated frequency was required, two Timing Oscillator units were used to insure against failure of either of the units. The standard frequency signals were required to adjust the tape speed on playback to that speed which would reproduce the recorded information faithfully. These frequencies were produced by tuning fork oscillators of the General Radio type 723.

The modulated frequencies centered at 2,300 cps and 3,900 cps were produced by phase shaft oscillator circuits. These frequencies were modulated by timing signals from Blue Box and relay sources. At minus 1 second, an EG&G timing relay signal produced a frequency [redacted]

shift in the oscillator. This signal was used as an aid in playback to automatically trigger the playback sequence; it could also be used as a fiducial marker since its time with respect to zero could be accurately determined and it was common to all recorders. However, the Blue Box signals (photo-electric signals), initiated by the visible fire ball of the test weapon were used as the timing fiducial on the surface shot. Two Blue Boxes were used, each feeding its signal into the phase shift oscillators of each Timing Oscillator unit. These signals produced frequency shifts of opposite sense and different time durations from the minus 1 second signal. On the underground shot, where there was a question as to the efficacy of the fire ball light to trigger the Blue Boxes, one Box was replaced by an EG&G relay actuated near to zero time by the weapon-firing relay circuit. The time of closure of this relay could be determined with a fair degree of accuracy so that it could be used as a timing fiducial. It was this relay signal that was used as the fiducial on the underground shot.

In operation, the minus 1 second relay closed, triggering a one-shot multi-vibrator which then produced a 0.13 second pulse. To prevent multiple triggering due to possible relay chatter, a 1/200 ampere fuze was blown, thus opening the input circuit. At zero time, the Blue Box (or timing relay) closed and triggered another similar multi-vibrator which produced a 0.05 second pulse. The outputs from the two multi-vibrators were mixed and frequency modulated the phase shift oscillator producing 5% frequency shifts.

(2) Timing Oscillator Distribution

The two output signals of each Timing Oscillator unit were fed into this Timing Oscillator Distribution Panel where all four signals were added by a resistive network. Eight outputs were provided carrying the composite signals to one head of each of the eight recorders. Each output was decoupled sufficiently to prevent interference among recorders.

(3) Reference Oscillator (Figs. 5.20 and 5.21)

An oscillator unit providing stable oscillations at the five signal frequencies used (3.9, 5.4, 7.35, 10.5 and 14.5 kc) was constructed to provide a convenient reference source for checking the frequencies of the field oscillators. As a second function, the mixed frequencies of the oscillator unit were recorded on one head of each recorder to provide a reference calibration signal during playback. As a third possible function, this signal was recorded with a view to using it in a tentative scheme for "wow-and-flutter" reduction. (This function was not realized on this operation because of the lack of time required to fully develop the design.)

The circuit for this unit consisted of five cathode-coupled 12AT7 oscillators, followed by five grounded grid amplifiers whose outputs were added linearly in a resistive network. Grounded-grid amplifiers rather than conventional amplifiers were used only because a coupling condenser was thereby eliminated. The low output impedance of the cathode-coupled oscillators, moreover, permitted direct coupling to the grounded grid amplifiers. Dropping resistors were needed to adjust the voltage level in the amplifiers for equal output voltages. A sixth triode amplifier for a modulated signal from the Timing Oscillator had its output added into the same network and the composite signal was then fed in parallel to four cathode follower output stages. The six amplifiers and four cathode followers were contained in five 12AX7 tubes.

Each cathode follower fed a recording channel in each of two tape recorders, the two output terminals being isolated by two 22 kilo-ohm resistors to prevent loss of signal to one recording channel if the other should become short circuited. The output from the driven cathode in each of the five oscillators was brought out to a separate terminal through an 8.2 kilo-ohm isolating resistor. Air-dielectric trimmer capacitors for each oscillator were located beneath these output terminals to provide fine tuning of the individual oscillators. The stability of these oscillators was approximately a factor of ten greater than that of the field oscillators.

(4) Filter Scope (Fig. 5.22)

In order to measure and inspect each of the five frequencies put out by each of the field oscillators, narrow-band-pass filters, tuned to the frequencies 3,900, 5,400, 7,350, 10,500, and 14,500 cps were needed. This function was provided by the "Filter Scope" which, in addition to permitting selective amplification at each of the five frequencies, permitted two signals, one from the field oscillator and the other from a reference source such as the Reference Oscillator, to be presented on a cathode ray tube for frequency comparison by Lissojous patterns. Both horizontal and vertical amplifiers, identically constructed, had separately accessible input and output terminals.

Each tuned amplifier stage consisted of a bridge-T feedback amplifier using a "cascoded" 12AX7 tube.[5] The deflection stage was 1/2 of a 12AX7, connected as a triode amplifier, while the output stage, also 1/2 of the 12AX7, was connected as a cathode follower. In both the horizontal and vertical amplifiers, six-position

[5] G. E. Valley, Jr. and H. Wallman, "Vacuum Tube Amplifiers," M.I.T. Radiation Laboratory Series, Vol. 18, McGraw-Hill, New York (1948) Chapt. 10.

selector switches permitted a choice of either non-selective amplification (position 6) or selective amplification at any one of the five standard frequencies (positions 1 through 5). Tuning of the bridge-T networks was accomplished by adjusting the set screw in each of the VIC inductors; gain and selectivity were controlled by adjusting resistors $R_1$ through $R_5$, each having a 5 kilo-ohm potentiometer for fine adjustment. As the value of each of these resistors increased, both the gain and selectivity increased; beyond a certain value, regeneration may occur and the adjustment had to be made so as to avoid this difficulty.

A voltage doubler power supply was used to provide both positive voltage for the amplifiers and negative voltage for the cathode ray tube.

(5) Field Operation Check Panel

The purpose of this check panel was to allow monitoring of the plate and filament voltages and currents being fed to the field oscillators and of the composite signal received from these oscillators without interferring with the operation of the system. The panel contained A.C. and D.C. voltmeters and ammeters which were switched into the appropriate circuits. A coaxial output connector was bridged across the signal leads to allow for monitoring of the oscillator frequencies and wave-forms. Two jumpers were used to insert the Check Panel between the MCOS-6 field cable and the Distribution Panel. The Check Panel was used only in initially setting-up the equipment and in trouble shooting. The presence or absence of plate and filament voltages and currents was made immediately evident and by noting the amount of current flowing in the plate and filament circuits, improper operation could be localized to particular components of the system.

(6) Field Cable Tester (Fig. 5.23)

Although all cable was carefully tested before leaving the Laboratory, to forestall difficulties caused by shortened, open, or low resistance cable, all cable was checked just prior to laying by a simple Cable Tester. This two-unit tester checked the most pertinent five combinations of leads in pairs by means of switching boxes and an ohmmeter.

(7) Blue Box (Fig. 5.24)

The zero timing signal was obtained from a Blue Box manufactured by EG&G. The circuit contained a vacuum phototube (929) sensitive in the visible region, coupled to a thyratron tube (2D21) by a small capacitor so that only a sharply rising light pulse, such as emitted by the fireball of an exploding charge, would trigger the thyratron. The firing of the thyratron produced a voltage step at its cathode which was used as the zero timing signal fed into the Timing Oscillator unit.

(8) Timing Relays

The timing relays were supplied by EG&G and were manufactured by Union Switch and Signal Co., Swissvale, Pa. Seven rack mounted relays were provided to initiate the 22 separate control functions for the complete recording instrumentation at the four specified times (Fig. 5.28).

5.5.4 Primary Power

Primary power for operating the field oscillators and the trailer instrumentation during the tests was provided by battery banks housed in the battery compartments of the trailers (Fig. 5.25). In this way, except for the few timing signals required from outside sources, complete independence of operation was achieved during the test. In addition, a stable, noise-free power source was realized which could be expected to be dependable throughout and after the blast.

The batteries used were 6 volt 175 ampere-hour lead storage batteries. Each bank of equipment was supplied by twelve batteries arranged in series - parallel to provide 36 volts with 350 ampere-hours capacity; this capacity allowed for at least two hours of continuous operation of the equipment. Each battery bank ran the five dynamotors in its associated instrumentation bank, and the motor generator which provided the A.C. power for this same instrumentation bank.

The motor generators (Fig. 5.26) had a load rating of 2.5 kva; this size was quite adequate since total power consumption for the complete instrumentation bank was approximately 1,500 watts. While operating under nominal full load, the output voltage and frequency of the generators were adjusted to 60 cps and 117 volts by means of rheostats prior to the tests; the stability of the motor-generators was such as to maintain these values during the unattended test operation.

The various controllers, switches, and relays necessary to properly couple power from the batteries to the generators and to the instrumentation were incorporated into the design (Fig. 5.27). These units also provided a ready means of connecting battery charging equipment to the batteries, and A.C. power from an external source, such as a gasoline generator or a commercial-type power line, to the recording instrumentation for use during setting-up procedures.

During the test operation, a minus 15 minute relay signal actuated the controllers which started the motor generators and supplied the D.C. to the dynamotors. At this same time, a time delay mechanism

was started. After 20 minutes of operation (15 minutes before zero to provide the required time for the equipment to reach stability and five minutes after zero), the time delay mechanism opened the controller circuits and cut both A.C. and D.C. power to the instrumentation.

### 5.5.5 Instrumentation Trailer (Figs. 5.29 through 5.32)

During the history of the project when test sites, instrumentation lines, and test conditions were not definitely determined, it became evident that a mobile instrumentation trailer would be of considerable aid in setting up the field program in almost any situation. Consequently, two van-type trailers were procured and outfitted identically. Each trailer was 32 feet 3 inches long, 7-1/2 feet wide, and 11-1/2 feet high. The trailer was partitioned into three compartments, one for batteries, one for the motor generators and controllers, and the third and largest compartment for housing the recorders, auxiliary panels, testing equipment, work benches and supply cabinets (Fig. 5.33).

The motor generators and the relay racks holding the electronic equipment were shock mounted to prevent vibrations and shock from adversely affecting the operation of the equipment. An air conditioning unit was installed in each trailer to provide favorable operation conditions for the equipment and personnel regardless of outside weather conditions. To provide accessibility to the backs of the rack mounted equipment, each bank of instrumentation was secured to a platform mounted on casters. Signal cables entered the trailer through small ports located in each side of the trailers; the outside power cable, which provided the lighting and outlet power, was connected to the trailer by means of an external connector. External connectors also were used to connect the battery chargers to the power source and the batteries. (The battery chargers were located outside the trailers because of space limitations and as a safety measure.) (Fig. 5.34).

## 5.6 RECORD REDUCTION (Fig. 5.35)

5.6.1 Reproducer (Fig. 5.36) - The playback unit was designed and constructed by the Ampex Electric Corporation to reproduce the tapes recorded on the Recorder unit. It consisted of four separate component units.

(1) Tape Transport Mechanism - This unit, basically, was similar to that of the Recorder, but it had a few additions. It had a selector switch for quick choice of mode of operation to facilitate signal location and playback. With the selector switch in the "play" position the tape traveled at a velocity of 30 inches per second (approximately the same speed as the Recorder). Three other modes of operation

were provided: Fast Forward, Fast Rewind, and Slow Rewind. The take-up tension arm on the Reproducer actuated a shut-off switch which automatically shut off the mechanism in the event of tape breakage.

(2) Reproducer Amplifier (Fig. 5.37) - This unit incorporated two identical playback amplifiers which allowed for simultaneous playback of any two channels by means of selector switches. Normally one amplifier was switched from head to head in order to reproduce the gage signals on five of the tracks; the second amplifier was set to play back the signal on the track which contained the standard reference frequency and timing signals. By means of a second output on this second amplifier circuit and a phone jack to allow for the insertion of a 400 cps or 1,000 cps filter, the standard frequency was made available for tape speed control.

(3) Capstan Motor Amplifier (Fig. 5.38) - This unit, located within the Reproducer console, was very similar to the tuning fork amplifier of the Recorder. Instead of a tuning fork, however, the signal being amplified to drive the capstan motor was supplied by a Wien bridge oscillator located inside the tape speed control unit.

(4) Tape Speed Control Unit (Fig. 5.39) - This unit, coupled to the Reproducer console by means of a cable, contained a stable 69 cycle Wien bridge oscillator. Two potentiometer controls provided fine and course adjustments of this oscillator frequency within a ± 3 cycle range.

In the playback procedure, the 400 cps (or 1,000 cps) standard frequency signal obtained from the tape was fed to the vertical input of a cathode ray oscilloscope. The signal from a local tuning fork oscillator, identical to the one used in the trailer for recording, was fed to the horizontal input thus forming a Lissajous pattern. The Tape Speed Control unit was adjusted until a stationary pattern was obtained. This was the indication that the tape speed in playback was the proper one to give faithful reproduction of all recorded signal frequencies. This scheme compensates for tape length variations caused by temperature and humidity variations between time of recording to time of playback. It also compensated for possible variations in tape speed during the recording process caused by faulty drive mechanisms. It was because of this speed control feature and indication of correct frequency reproduction that it was possible to calibrate the system frequency-wise during record playback, thus simplifying the field electronics.

5.6.2 Discriminator (Fig. 5.40) - The composite FM field signal from the Reproducer was fed into five Discriminator units, with parallel inputs, each unit containing a band-pass filter to select one of the carrier frequencies modulated by the gage signal. In the

Discriminator, the frequency modulated signal was converted into amplitude variations with time and was made suitable for presentation on a string galvanometer oscillograph.

The Discriminators were made by the National Machine Shop of Silver Spring, Maryland, and originally designed by the Applied Physics Laboratory of Johns Hopkins University for the Bumble Bee system.

The input stage of the Discriminator was a cathode follower having an input impedance of 1/2 megohm, preceded by an attenuator enabling utilization of input signals ranging in level from 10mv to 10v. Following the input cathode follower was a plug-in band-pass filter which allowed selection of the desired FM signal and provided rejection of all other signals. After filtering, the desired FM signal was amplified and limited, the limited signal actuating a pulse forming circuit which delivered one pulse for each cycle of the incoming signal. Each of these pulses triggered a one-shot multivibrator which returned to its rest state after a time interval equal to half the reciprocal of the center frequency of the selected FM signal. The return time of the multivibrator was determined by the circuit constants of a plug-in network augmented by a fine adjustment. By the proper choice of one of a number of such plug-in networks, the return time of the multivibrator was adjusted to correspond to the chosen FM signal for that gage channel - 3.9, 5.4, 7.35, 10.5, or 14.5 kc.

When the return time of the multivibrator was adjusted to correspond to the center frequency of the selected FM signal, the average voltage measured between the plates of the multivibrator tubes was proportional to the deviation of the signal from the center frequency. This averaging was performed by a low-pass filter inserted between the multivibrator plates and the following cathode followers. These were followed by another push-pull cathode-follower stage, providing a balanced output having an effective source impedance of 330 ohms. Overload protection incorporated in the output circuit automatically limited the output current to ±15 ma. With the output load 330 ohms, the load current was 10 ma when the FM signal deviated 7-1/2% from its center frequency.

The timing signal from the standard reference track of the tape was reproduced by means of a sixth discriminator operating on a center frequency of 2.3 kc or 3.9 kc.

5.6.3 <u>String Galvanometer Oscillograph</u> (Fig. 5.41) - The String Galvanometer Oscillograph unit changed the electrical signal outputs of the Discriminators into a visual and photographic presentation. This unit was manufactured by the Century Geophysical Corporation of Tulsa, Oklahoma. Although sixteen strings could be accommodated in this unit,

only six were used - one for each of the five gage signals played back simultaneously, and one for the timing fiducial signal.

The resonant frequency of the galvanometers was 200 cps and each had a resistance of 60 ohms and required an external shunt of 120 ohms for critical damping. These resistors and the network required to properly match the impedance of the galvanometers to the Discriminators were built on an auxiliary panel. This panel also provided attenuation of the signals into the galvanometers so as not to overload these elements.

The oscillograph unit contained a tuning fork controlled oscillator which produced 100 and 10 millisecond timing lines transversely across the eight inch wide photographic paper used. The paper used was Kodak Linograph 1127, selected because of its high sensitivity. The paper feed speed used was approximately 10-15 inches per second.

5.6.4 Calibration Oscillator (Fig. 5.42) - The function of the calibration oscillator was to provide for each of the five gage frequency bands a sequence of calibrating frequencies which when fed through the playback system, produced stepwise calibration marks on the photographic records. For convenience and accuracy, these calibration marks were made to appear during the one second interval preceding the zero time mark. The calibration sequence, which was obtained by means of an automatic stepping 5-pole, 22-position relay, corresponded to frequency deviations from center frequency in the order: 0%, +6%, +3%, +1.5%, +0.5%, 0%, -0.5%, -1.5%, -3%, -6%, 0%, +6%, +3%, +1.5%, +0.5%, 0%, -0.5%, -1.5%, -3%, -6%, 0%, the center frequencies being 3,900, 5,400, 7,350, 10,500, and 14,500 cps.

The basic oscillator design used a cathode follower coupled to a grounded-grid amplifier by means of a series resonant LC circuit. Each of the five oscillators used a single 12AT7 tube and contained a high-Q inductor with an appropriate set of capacitors tuned to the desired frequencies and selected in turn by a stepping relay. Positions 1 through 10 were connected so as to provide the first half of the calibration sequence while positions 11 through 20 were appropriately paralleled with the first ten positions so that the first half of the sequence was repeated. Positions 21 and 22 provided center frequencies again. The output of each oscillator was taken from the cathode of the cathode follower at an impedance level of something less than 200 ohms. In this way, cross-talk between the five calibration oscillators was minimized.

The power supply, constructed on a separate chassis (Fig. 5.43), was electronically regulated and used a "cascode" regulator circuit. In order to prevent cross-talk between the five oscillators and the playback signal, the B+ lead to the oscillators was disconnected except during the calibration interval. Low voltage

(up to 12 volts) D.C. for the relays was furnished by means of a full-wave selenium rectifier and this voltage was controlled by a Variac. In this way, the calibration cycle could be varied from 1/2 to 2 seconds. A connector was provided on the skirt of the oscillator chassis to feed low voltage D.C. to the sequencing unit chassis and to receive therefrom the triggering short-circuit for the stepping relay.

Under laboratory conditions, the stability of the oscillators was in the order of ± 2 to ± 5 cps over periods of several weeks. Under field conditions, this stability was not observed.

5.6.5 Sequencing Unit (Fig. 5.44) - In order to facilitate the playback of records and presentation in final form, a unit was constructed which controlled the necessary playback operations in orderly sequence. This unit had two modes of operation, "Automatic" which was normally used in playback, and "Manual" which was normally used in setting-up procedures. By means of this Sequencing unit the locally generated frequencies from the Calibration Oscillator unit and the recorded gage signals from the Reproducer were applied through the playback system in proper sequence and in synchronization with the string oscillograph operation.

With the unit set to "Automatic", the playback procedure was as follows:

The tape transport was started manually well before the appearance of signals on the tape. When the signal appeared, the Tape Speed Control was adjusted until a stationary Lissajous pattern was formed. Approximately 30 seconds were available for this manually performed operation before the automatic operation started. With the appearance of the minus one second signal on the standard reference track, a voltage pulse was formed in the Discriminator, and passed on to the sequencing unit. Here the signal was amplified before triggering a thyratron circuit. The thyratron output pulse initiated the calibration sequence by actuating the stepping relay in the Calibration Oscillator unit. Simultaneously, a five-pole, double-throw relay was actuated. This relay switched from the Reproducer output to the Calibration Oscillator outputs so that each of the five calibration signals was fed individually into the proper Discriminator. After the calibration cycle which had a duration of approximately one second, when the stepping relay came to rest again, the five-pole, double-throw relay switched back to the Reproducer output, thus feeding the gage signals into all five Discriminators simultaneously. Coincident with the start of the calibration cycle, the circuit providing for automatic operation of the string oscillograph was closed. This started the paper drive and illuminated the galvanometer mirrors and record identification numerals. After the gage signals on the tape were recorded, as evidenced by the meter movements on the Discriminators, the playback was stopped, the tape rewound, and the above procedure followed for the other gage

At times it was desirable to record on the string oscillograph only one of the gage signals making up the composite signal on a track. This was accomplished by the simple expedient of connecting only the required lead to the string oscillograph.

In "Manual" operation, the various operations described above were initiated by switches. In this way it was convenient to cycle the calibration oscillators one step at a time and to check and adjust the calibration frequencies to close tolerances. Also, it provided a means of initiating automatic operation when the minus one second signal circuit failed to operate.

5.6.6 Photographic Technique - The photographic paper obtained from the string oscillograph magazines varied in length from five feet to 150 feet depending on the number of tape runs that were made. For the shorter lengths, tray developing was used. For the longer lengths of paper, a portable automatic tank method was used (Fig 5.45). Because of the high photographic speed of the paper, to obtain best results, all loading and unloading of the magazines and developing of the paper was done in a darkroom without benefit of safe lights.

The paper was dried on a small, commercial drum dryer with an automatic paper feed and take-up device added (Fig. 5.46).

## 5.7 PERFORMANCE AND RECOMMENDATIONS:

The present over-all instrumentation system performed satisfactorily on Operation Jangle; however, improvements in design are indicated for future use so as to realize even better performance. The most serious shortcoming of the system was the low signal to noise ratio obtained in the field. Although the recorders and playback machines met or even exceeded specifications for "wow-and-flutter", less than 0.1% rms, in the laboratory, this figure was exceeded by as much as a factor of 2.5 in the field. For the most part, this was due to the ever-present dust problem and the inability to keep recording and playback heads, the capstans, idlers and magnetic tapes completely free of dust. However, even under laboratory conditions it would be advisable to decrease the "wow-and flutter", thus increasing the dynamic range of the equipment and obviating the need for "back-up" gages. This, of course, would free gage circuits for additional measurements.

This decrease could be accomplished in many ways - by redesigning the recorder and playback machines, by employing some "wow-and-flutter" compensation scheme, or by producing a larger signal. The redesign of the recorder and reproducer could proceed along the lines of developing smoother motor drives and better mechanical filtering possibly using compliance loops similar to those used in sound-on-film recording.

Compensation methods could be designed including servo-mechanisms to correct for "wow" and mixing and "beating" schemes for "flutter" reduction. It was this latter scheme that was attempted in the NOL instrumentation and abandoned temporarily because of the lack of time.

Essentially, it was a system to make "wow-and-flutter" a function of the frequency deviation produced by the acceleration or pressure phenomenon, rather than the carrier center frequency. Since the frequency deviation could be at most approximately 10% of the center frequency, a minimum noise reduction factor of 10 could be expected, with greater reduction for smaller signals. In this method, the compensation was accomplished in playback. The signal frequency was beat with the output of a local oscillator, the sum frequency filtered and passed into another non-linear mixer circuit. The unmodulated reference frequency from the tape also was fed into this mixer, the difference frequency filtered and passed into a discriminator where amplitude variations were produced corresponding to the original signal phenomenon. Early tests on this system were encouraging and further work should be undertaken.

Increase of signal to "wow-and-flutter" induced noise can be accomplished by producing larger signals. This indicates a gage development problem with a view towards increasing the frequency deviation produced by any given forcing function. (Of course, this would limit the spacing of adjacent bands, but this may not be detrimental in some applications.)

New gage development should also seek a linear end instrument as stated in Chapter 4. This would lead to a simple expansion of the playback system permitting more complete data reduction and enabling acceleration records to yield velocity and displacement data electronically.

In conjunction with decreased "wow-and-flutter" endeavors, work should be done on oscillator-amplifier design. In a multiplexing system it is important to keep intermodulation products at a low level so as not to cause interference in other bands. This indicates that the total harmonic content of oscillators and amplifiers should be low. The 3% level obtained in Operation Jangle was tolerable because it was masked by the "wow-and-flutter" noise; with better noise characteristics, lower harmonic distortion limits will have to be maintained.

The physical design of the trailer instrumentation could be improved by combining all the components included in one recording channel (exclusive of the Recorders) on one small chassis. Field experience showed very little need for trouble shooting on the trailer equipment thus eliminating the need for multiple-disconnect elements with its encumbering cabling.

A modification in the filament supply design would be advisable. At present, with only one transformer feeding the filaments of the five oscillator-amplifier units in one instrumentation bank, the output voltage of the auto-transformer is set to the optimum value for the mid-distance station. Because of the difference in lengths of cables and the resultant difference in line attenuation, some stations operated with an over-voltage, and others with an under-voltage. Although no tube failure or other adverse effects resulted from this condition, in future operations with possibly longer lines, detrimental voltages may be incurred at the extreme stations. Individual transformers for each station would eliminate this condition, and lead to a more reliable and flexible design.

As an aid to overall field operation and as a step toward coping with the dust problem, it is suggested that a trailer be outfitted to house the playback instrumentation. This trailer should also contain the photographic processing facility and it could contain the necessary laboratory work space and storage space for the project group.

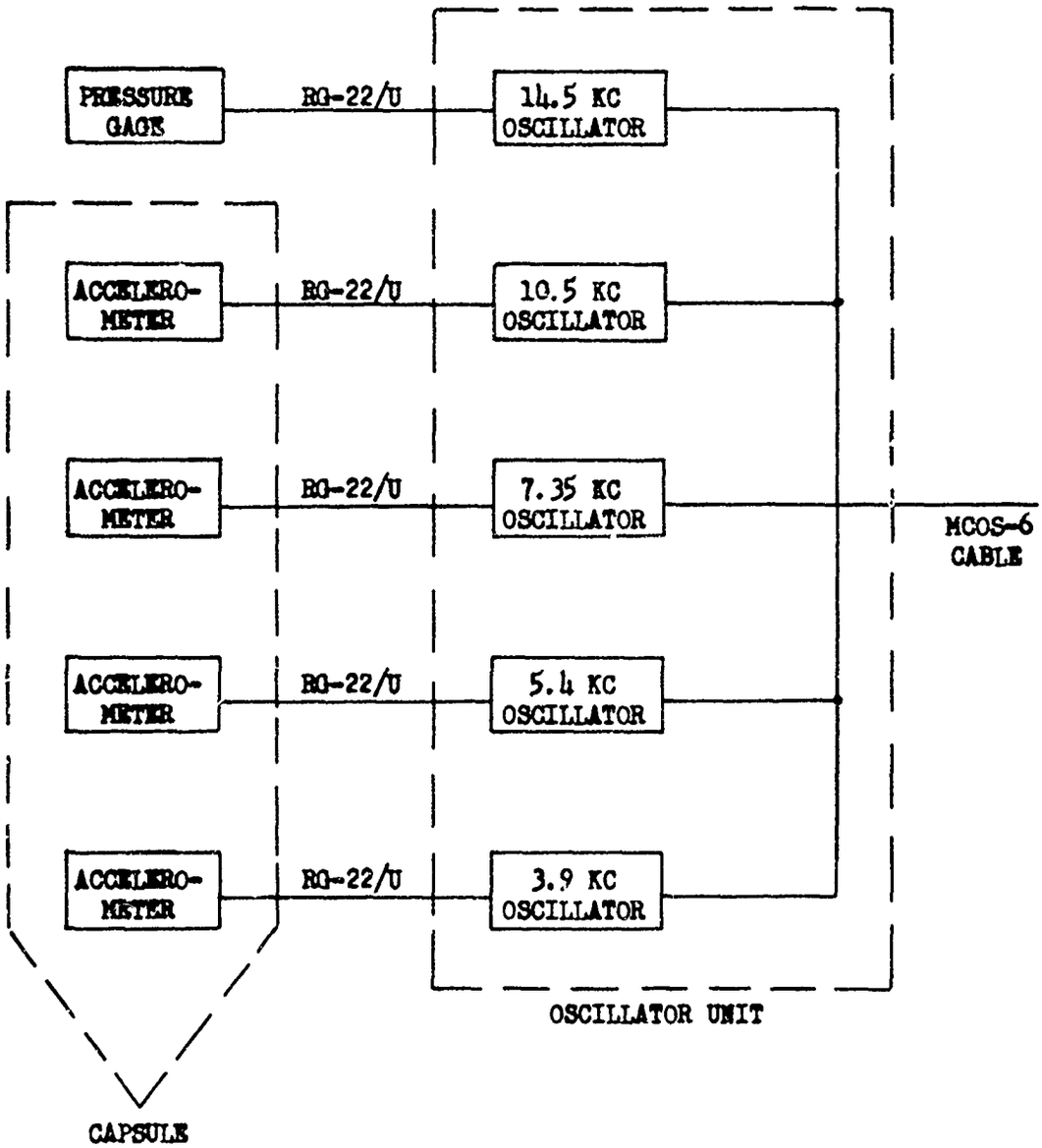


FIG. 5.1 TYPICAL STATION INSTALLATION

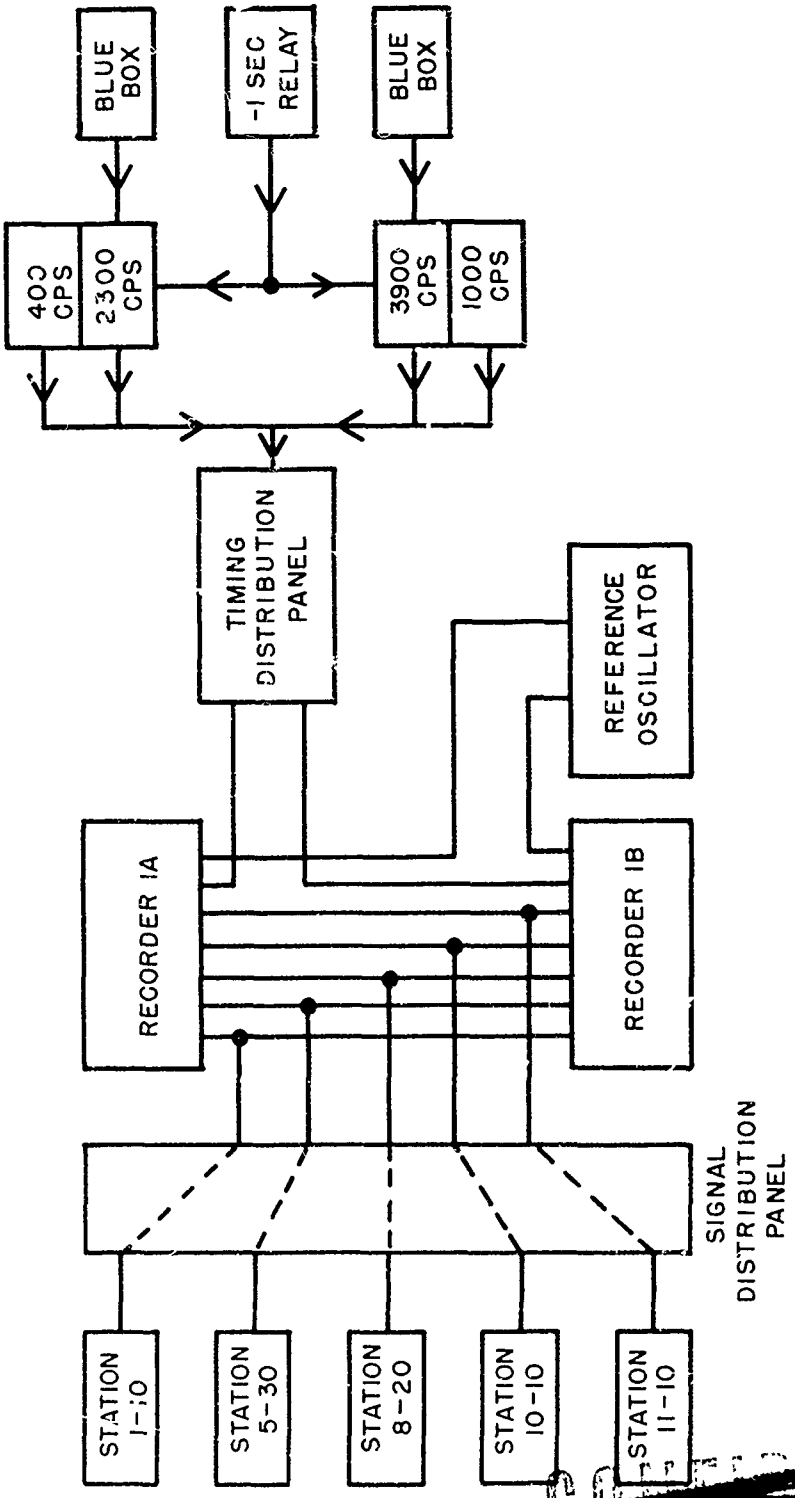


FIG. 5.2
SIGNAL DISTRIBUTION FOR TYPICAL BANK

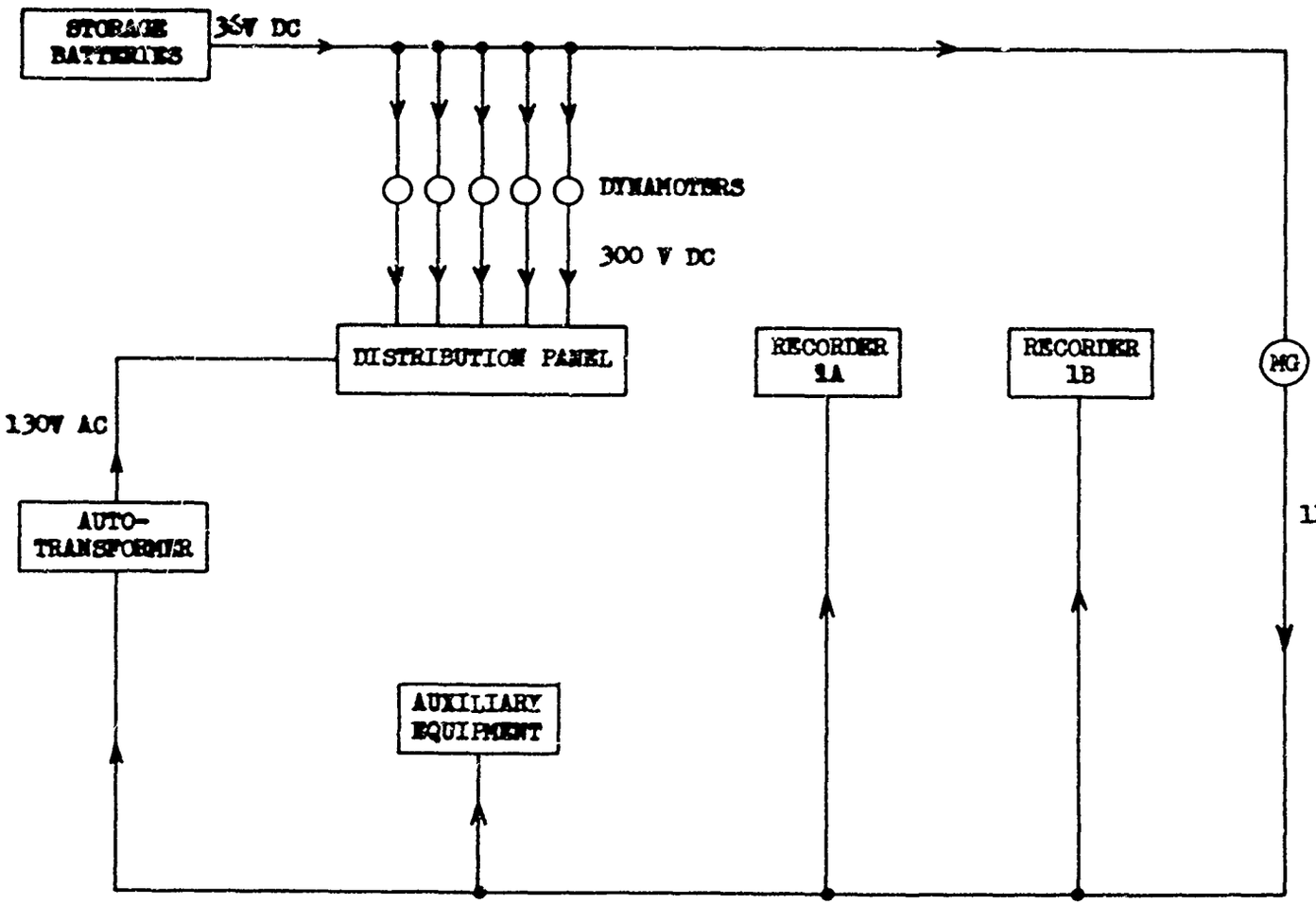


FIG. 5.3 POWER DISTRIBUTION FOR TYPICAL BANK

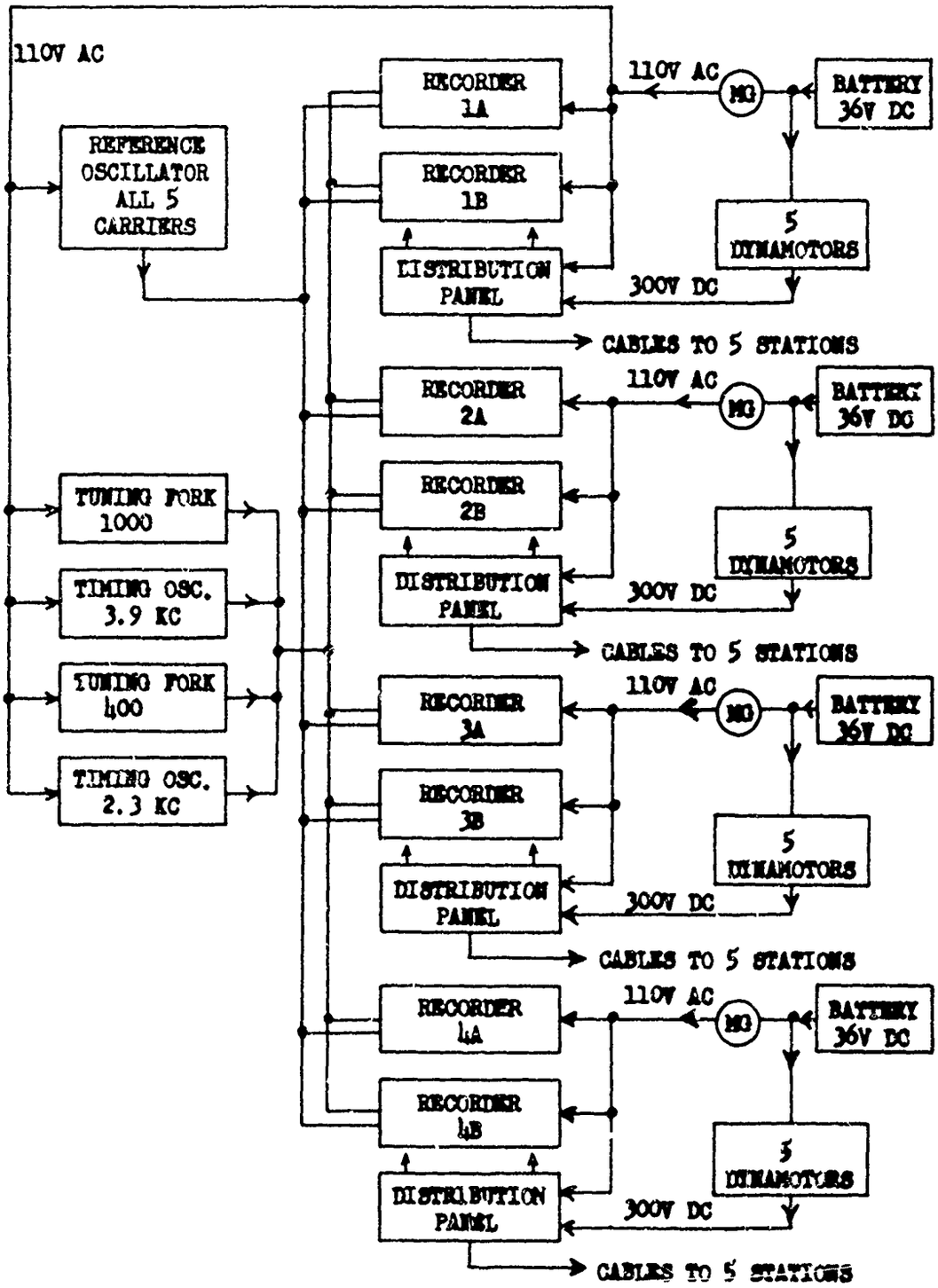


FIG. 5.4 OVER-ALL RECORDING SYSTEM

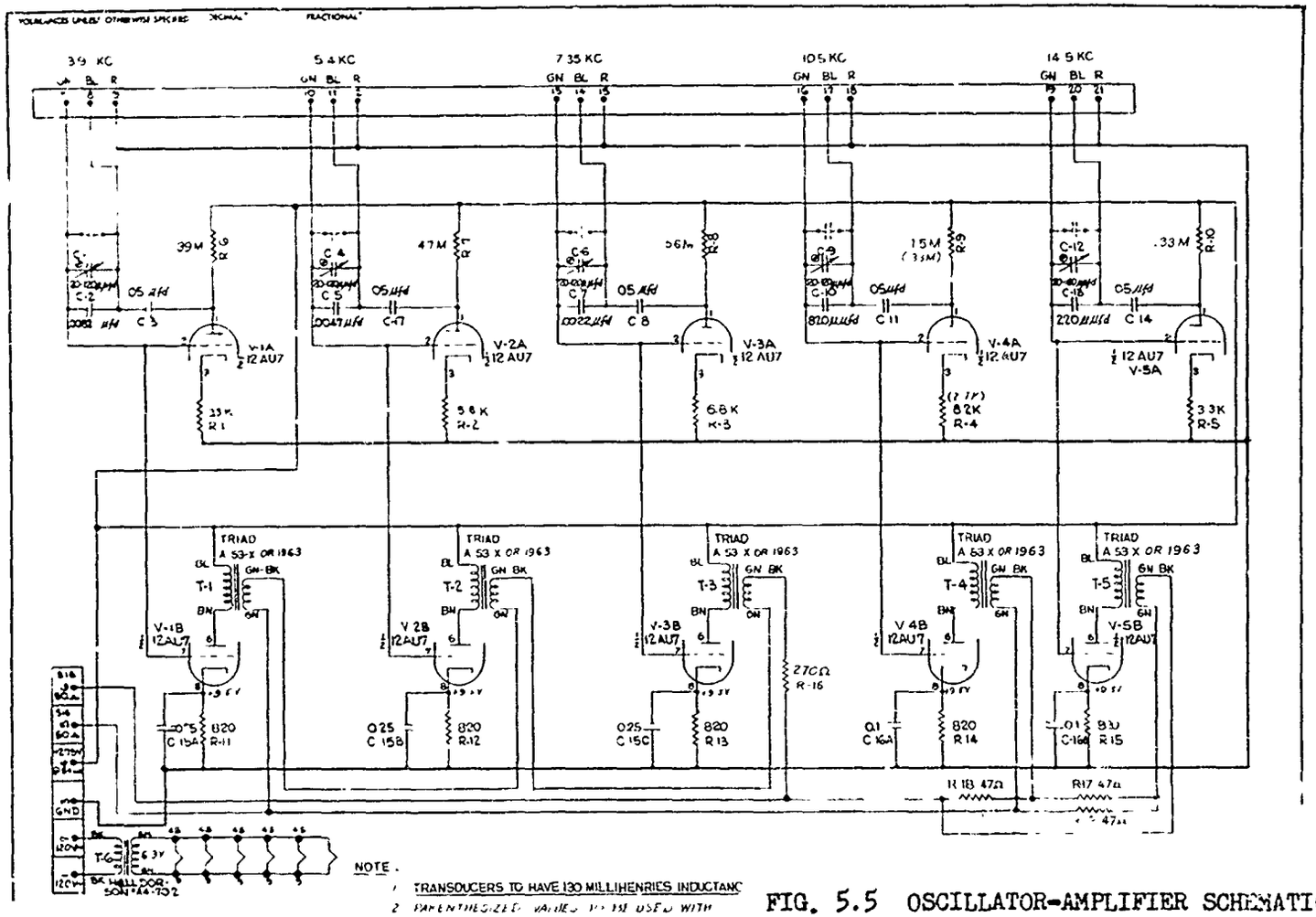


NOTE.

1. TRANSDUCERS TO HAVE 130 MILLIHENRIES INDUCTANC
2. PARENTHESIZED VALUES TO BE USED WITH WIAN NO GAUGES

FIG. 5.5 OSCILLATOR-AMPLIFIER SCHEMATIC

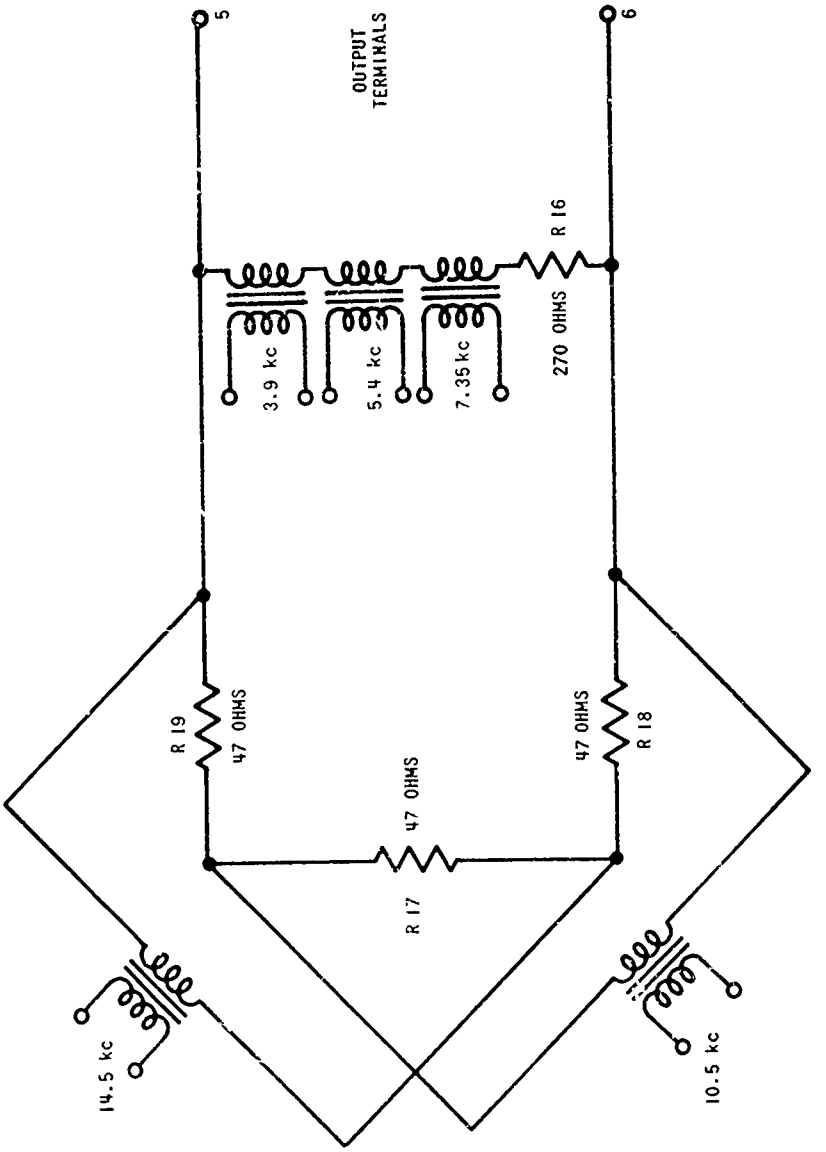


FIG. 5.6 BRIDGE CIRCUIT FOR COMBINED OUTPUT

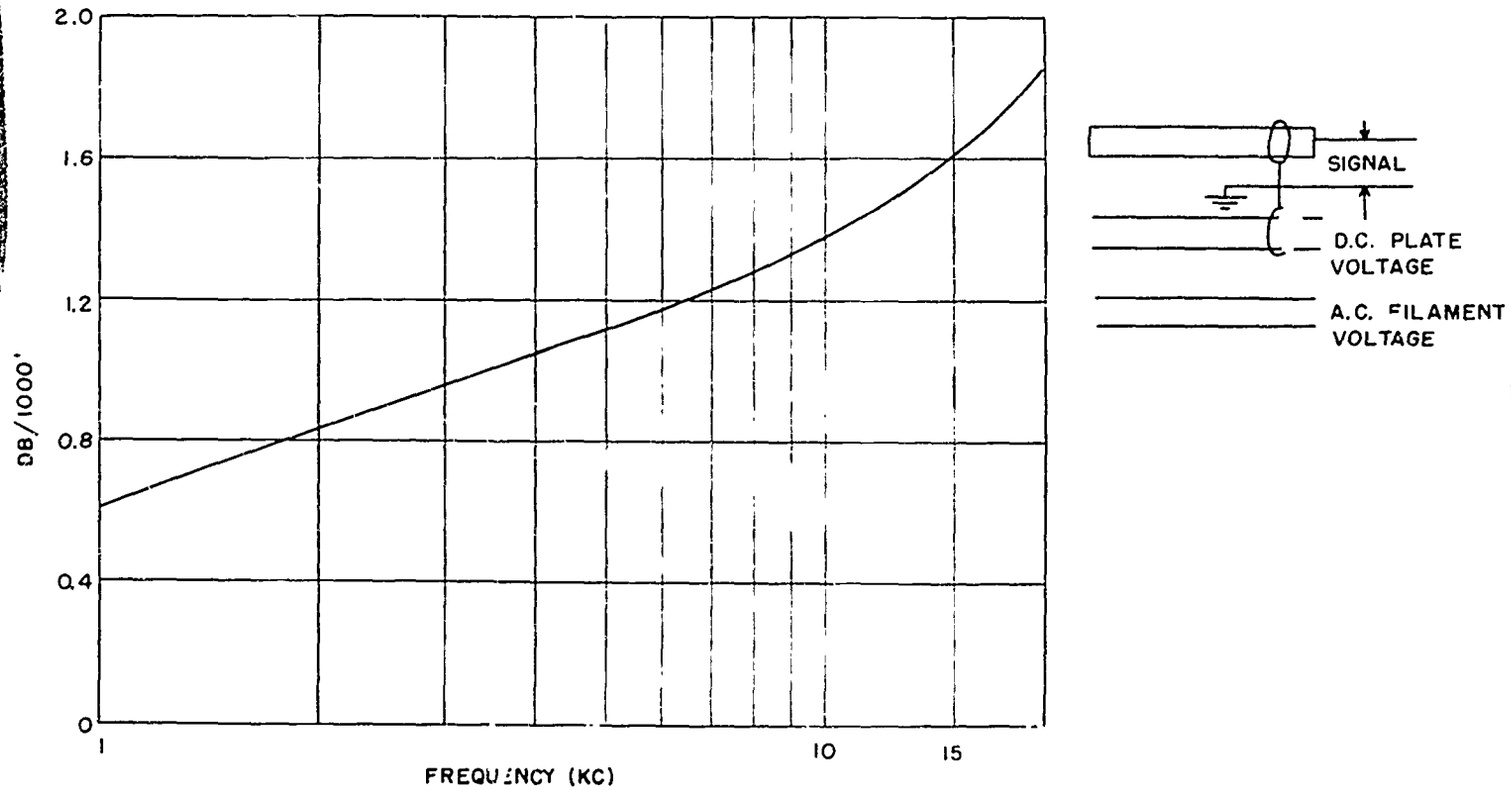


Fig. 5.7 Signal Attenuation in MCOS-6 Cable

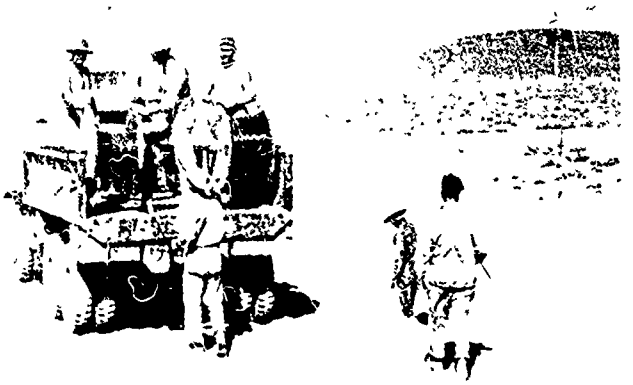

Fig. 5.8 Cable Laying

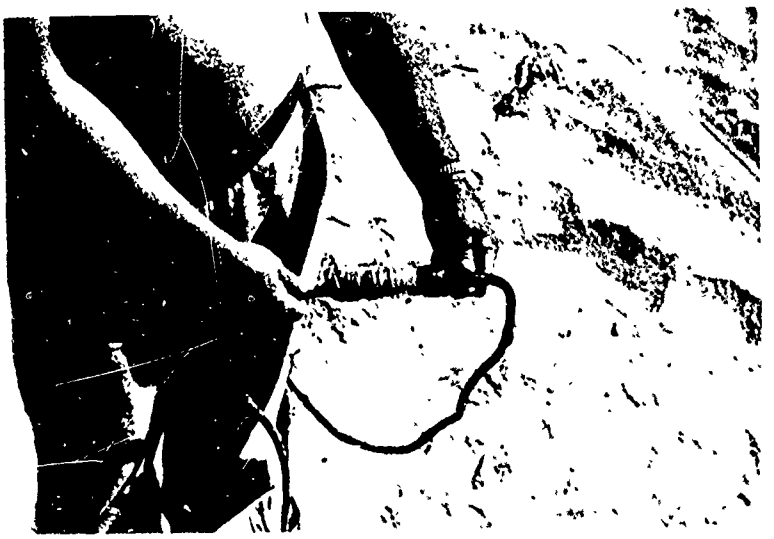

Fig. 5.9 Cable Connector

[redacted]

PROJECT 1.1

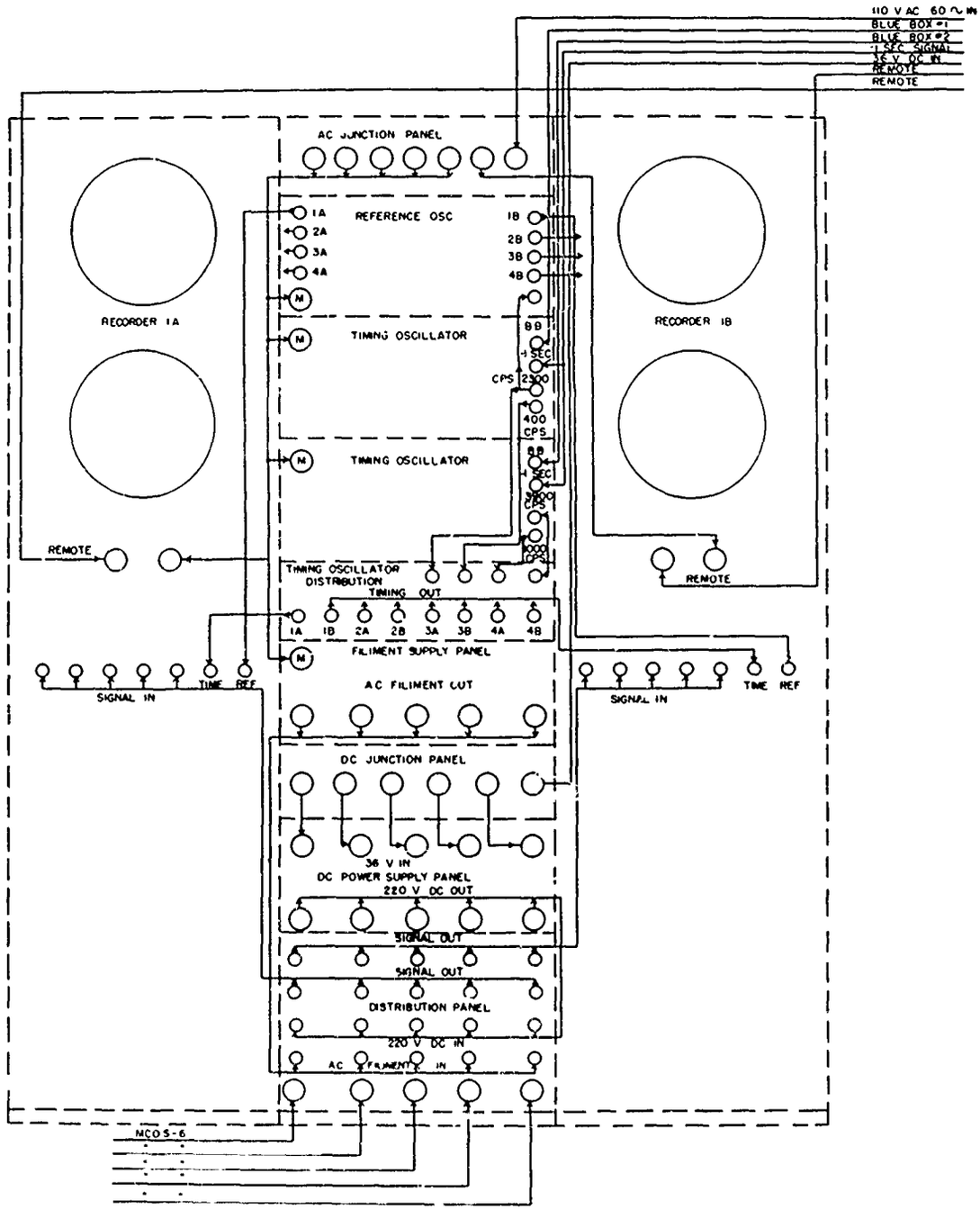


Fig. 5.10 Inter Cabinet Layout

[redacted]



[redacted]

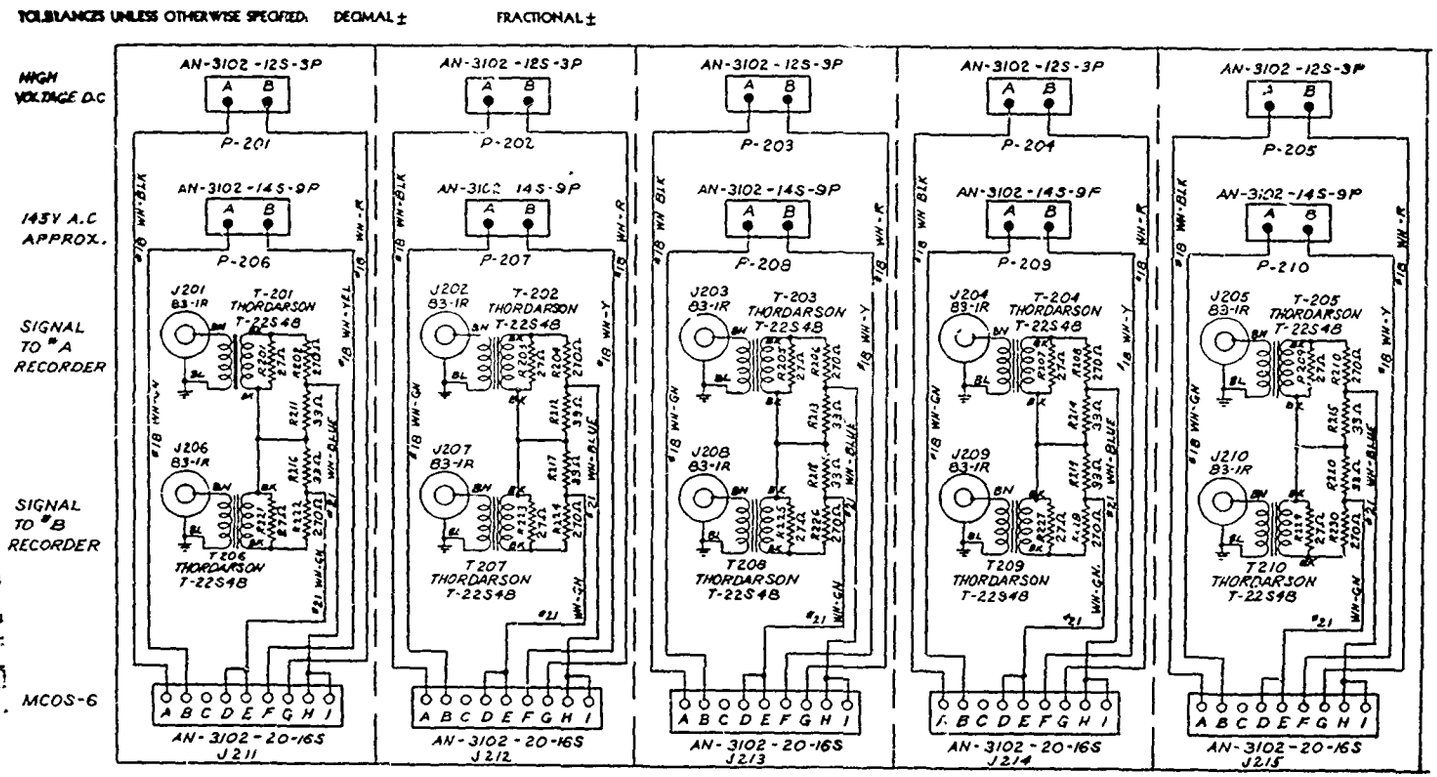


NOTE
1- ORIENT CONNECTOR KEYWAYS UP

FIG. 5.11 DISTRIBUTION PANEL SCHEMATIC

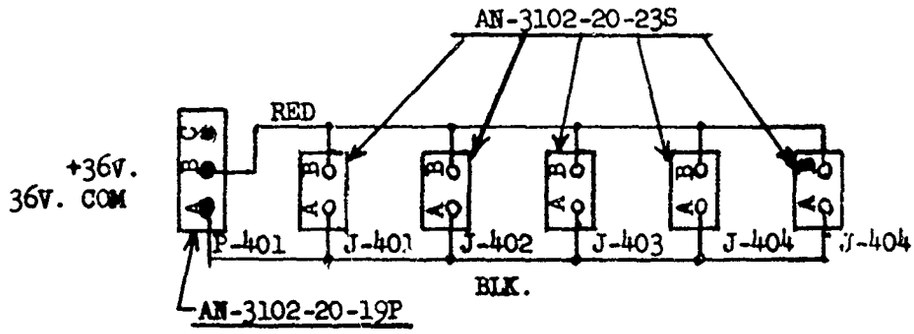


NOTE:

1. - ORIENT CONNECTOR KEYWAYS UP

FIG. 5.12
D.C. POWER SUPPLY PANEL

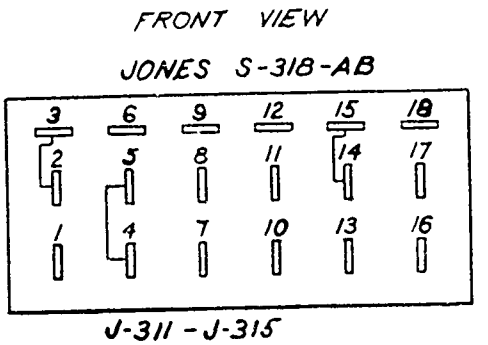


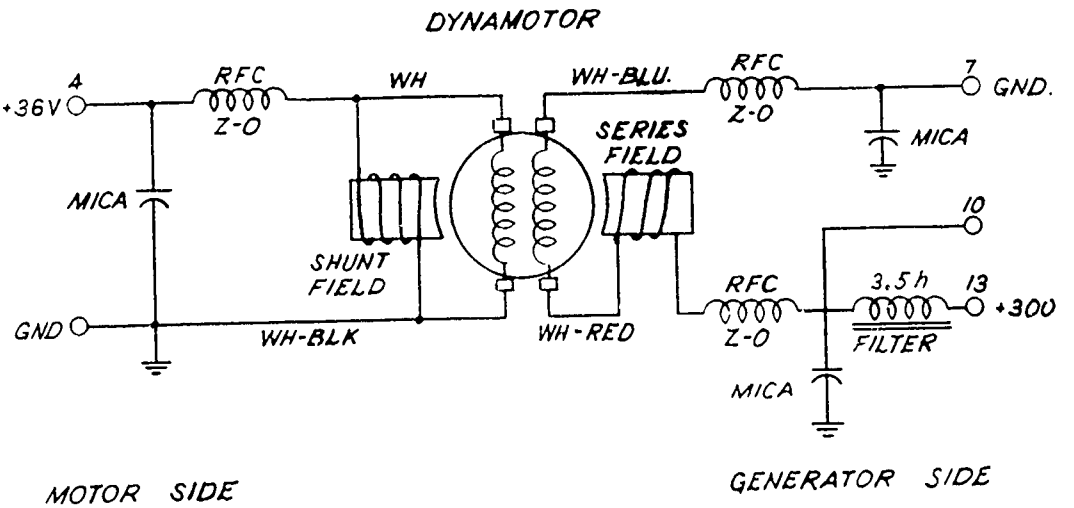


Fig. 5.13 Dynamotor Circuit

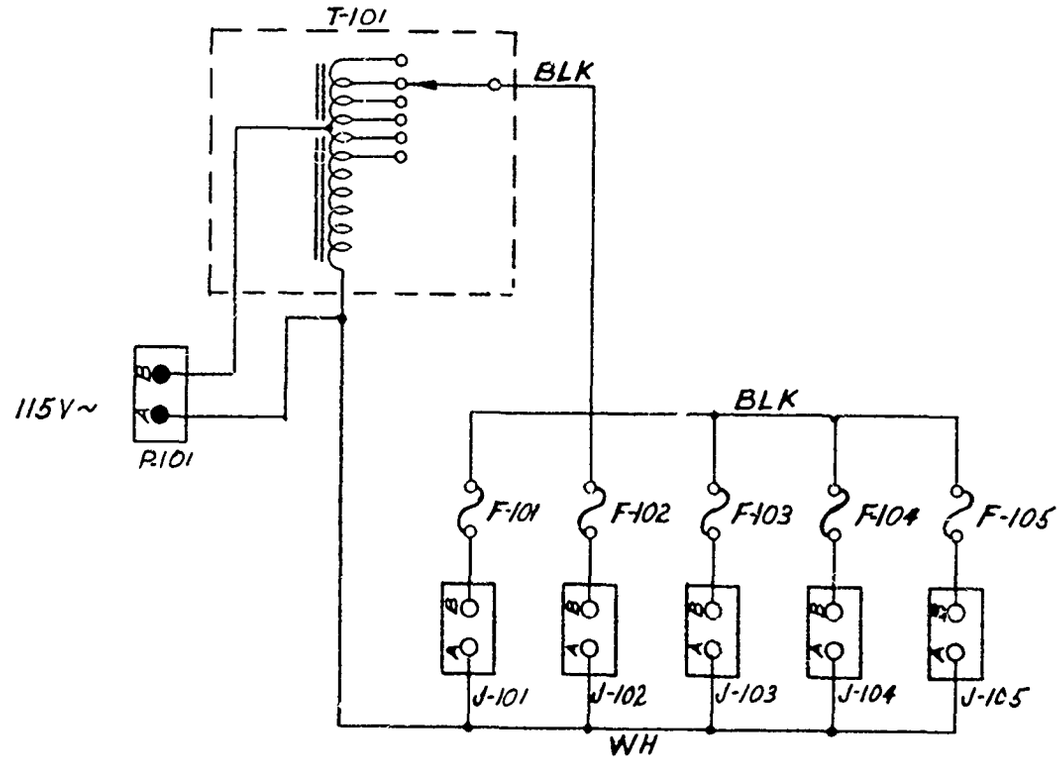


F-101 - F-105 $\frac{1}{2}$A SLO-BLO FUSE
J-101 - J-105 AN-3102-14S-9S
P101 AN-3102-20-23P
T-101 STANCOR P-6299

NOTE:
1 - ORIENT CONNECTOR KEYWAYS UP

Fig. 5.14 Filament Supply Panel

[redacted]

PROJECT 1.1

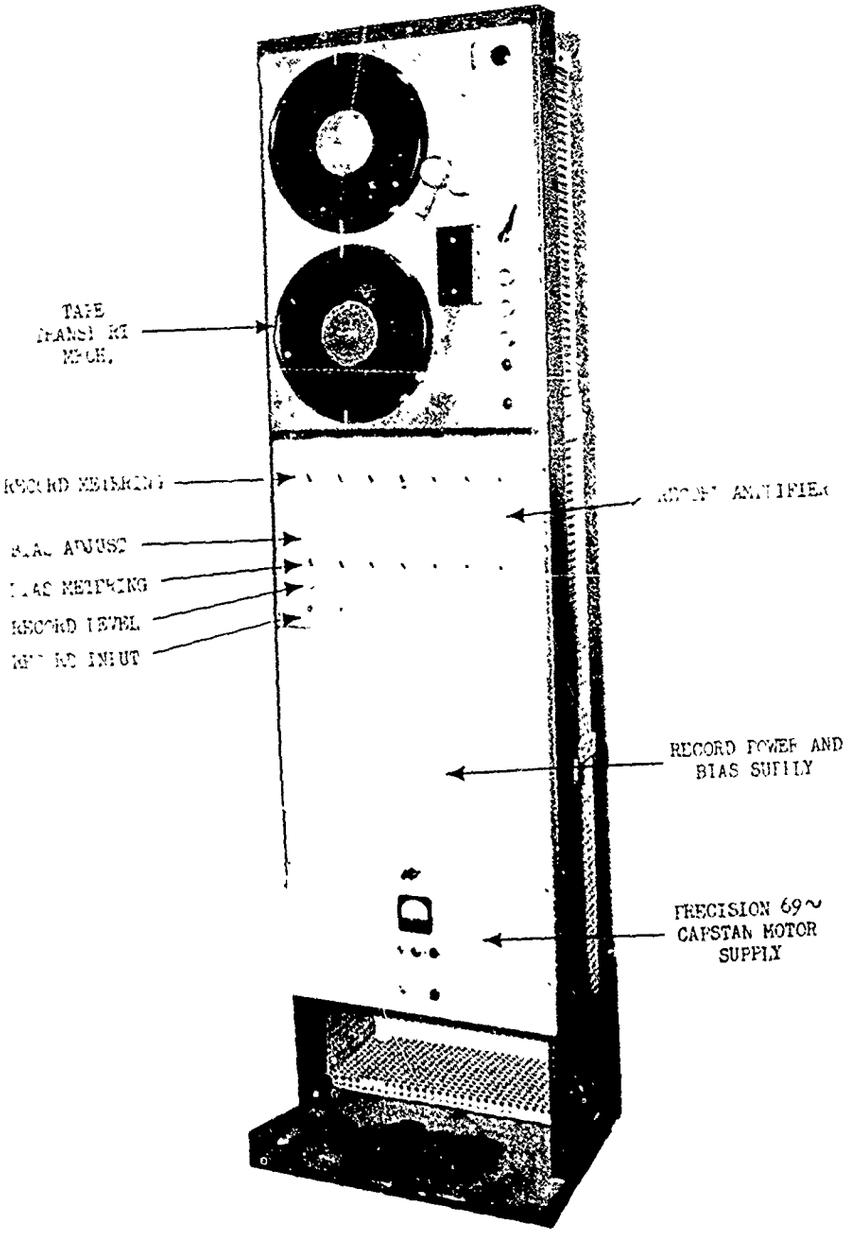


Fig. 5.15 Ampex Magnetic Tape Recorder

[redacted]



[redacted]

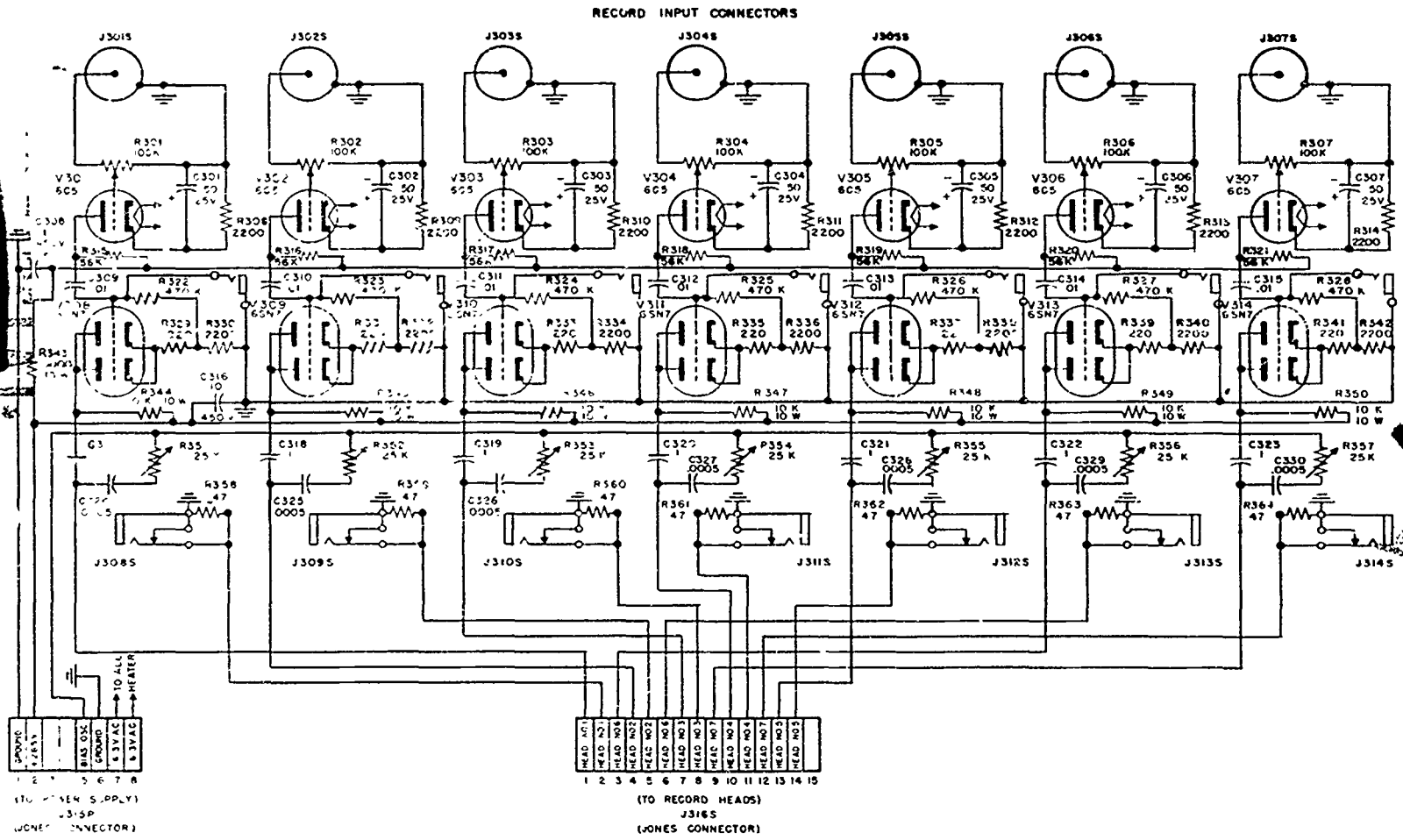


Fig. 5.16 Seven Channel Record Amplifier

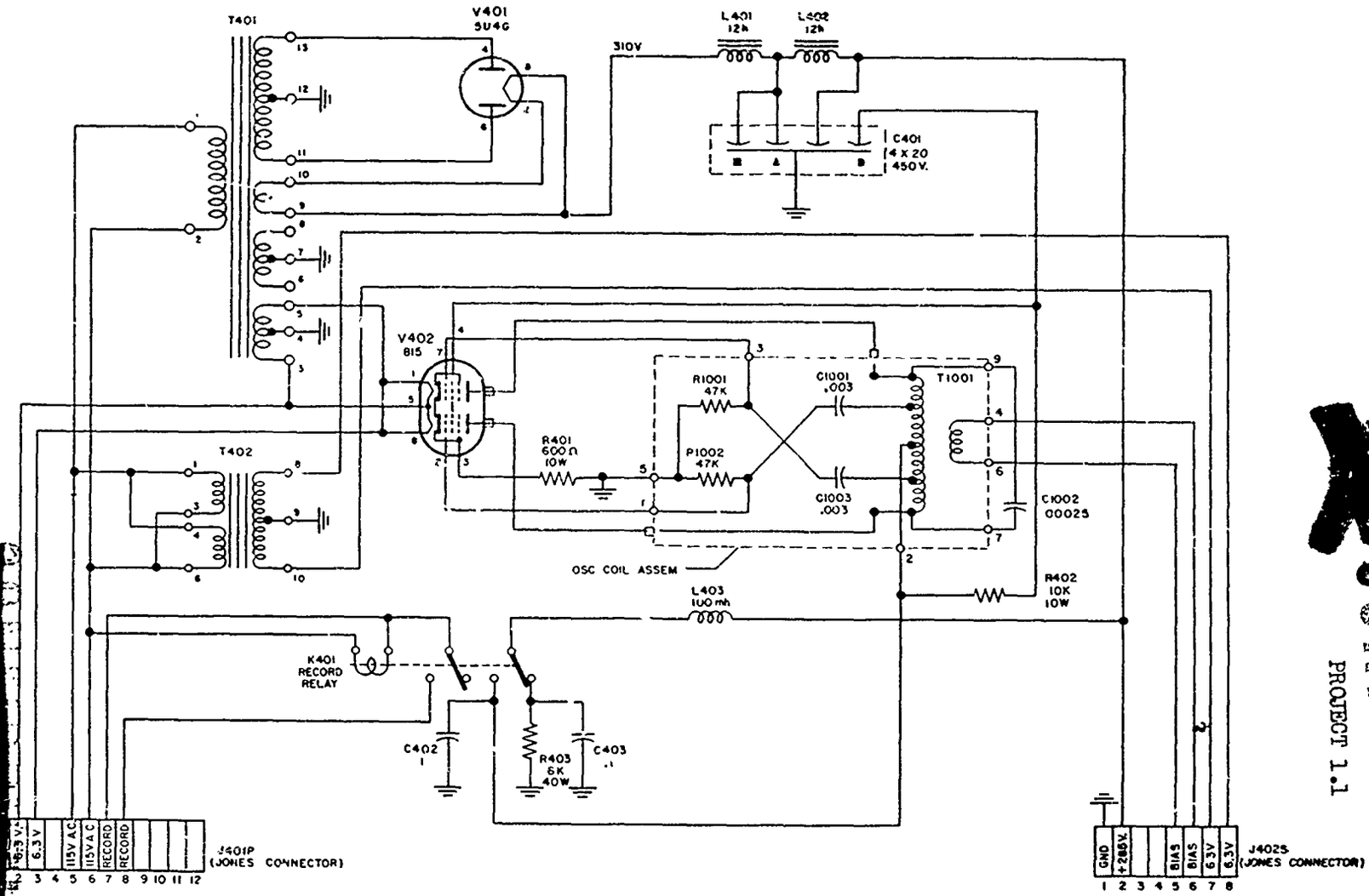


Fig. 5.17 Record Amplifier Power Supply and Bias Oscillator



PROJECT 1.1

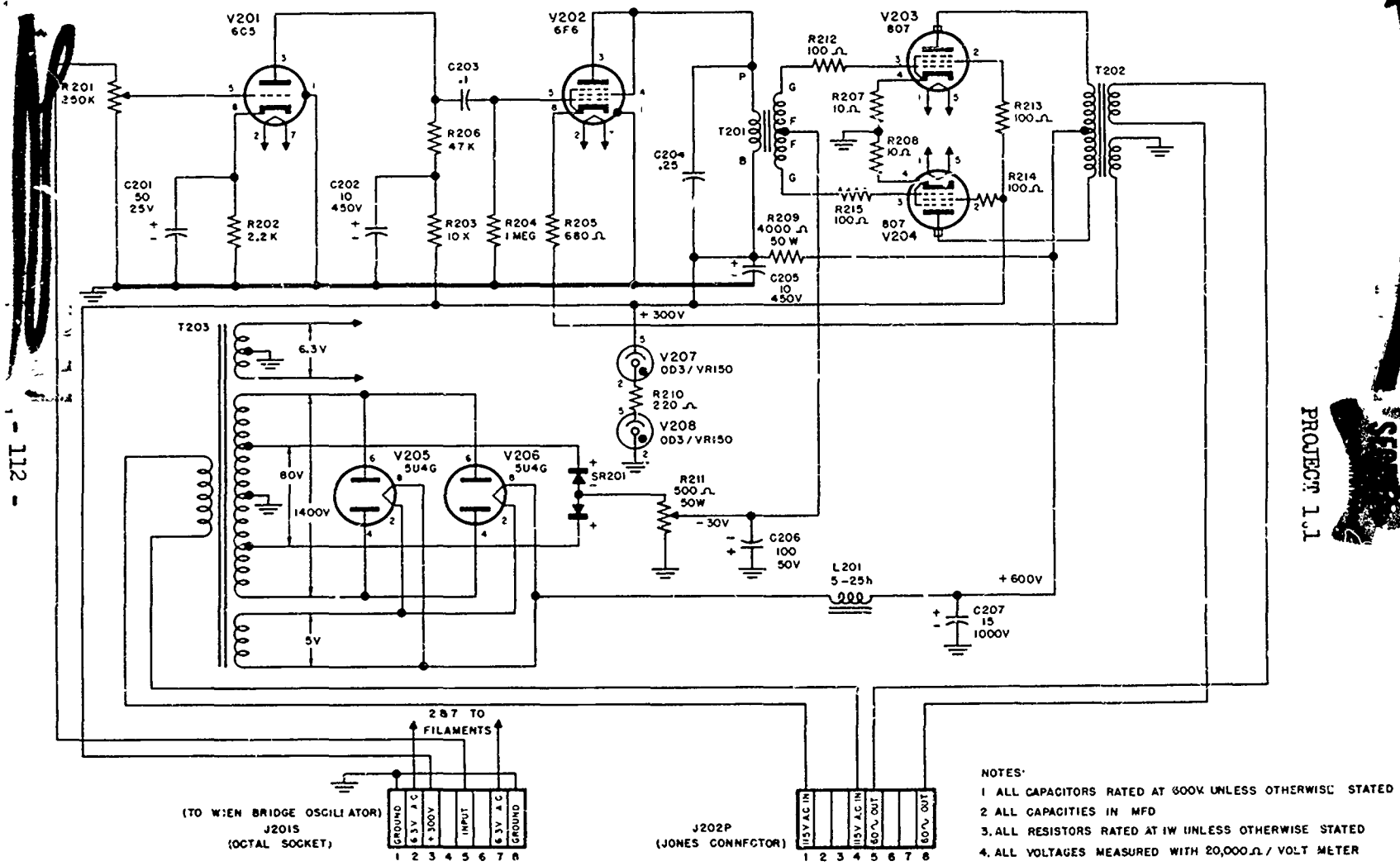


NOTES:
1. ALL CAPACITORS RATED AT 600V UNLESS OTHERWISE STATED
2. ALL CAPACITIES IN MFD
3. ALL RESISTORS RATED AT 1W UNLESS OTHERWISE STATED
4. ALL VOLTAGES MEASURED WITH 20,000Ω / VOLT METER

FIG. 5.18 POWER AMPLIFIER FOR CAPSTAN MOTOR SUPPLY

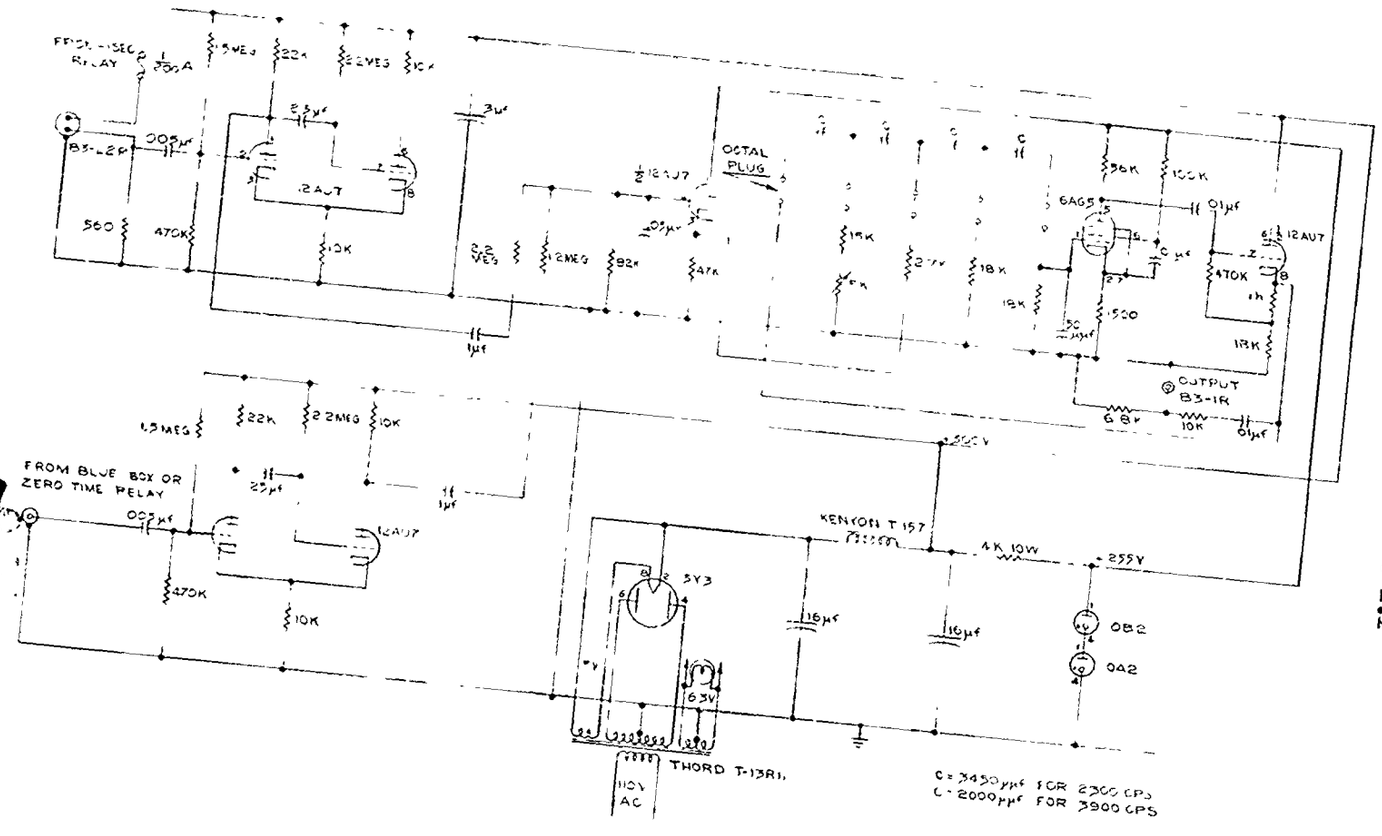


Fig. 5.19 Timing Oscillator

[redacted]

[redacted]

PROJECT 1.1

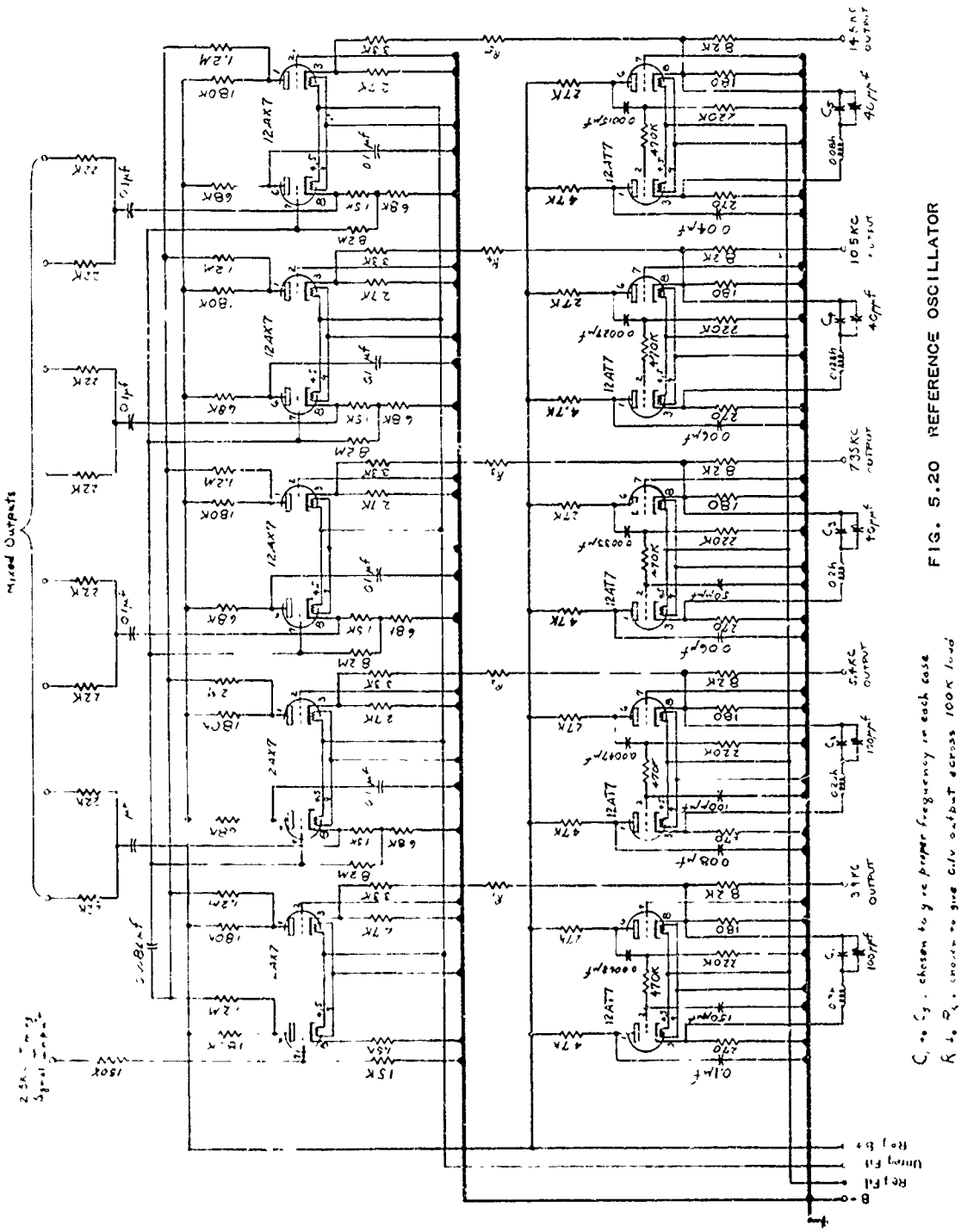


FIG. 5.20 REFERENCE OSCILLATOR

$C_1$ to $C_5$ - chosen to give proper frequency in each case

$R_1$ to $R_4$ - chosen to give c/v output across 100K load

[redacted]



[redacted]

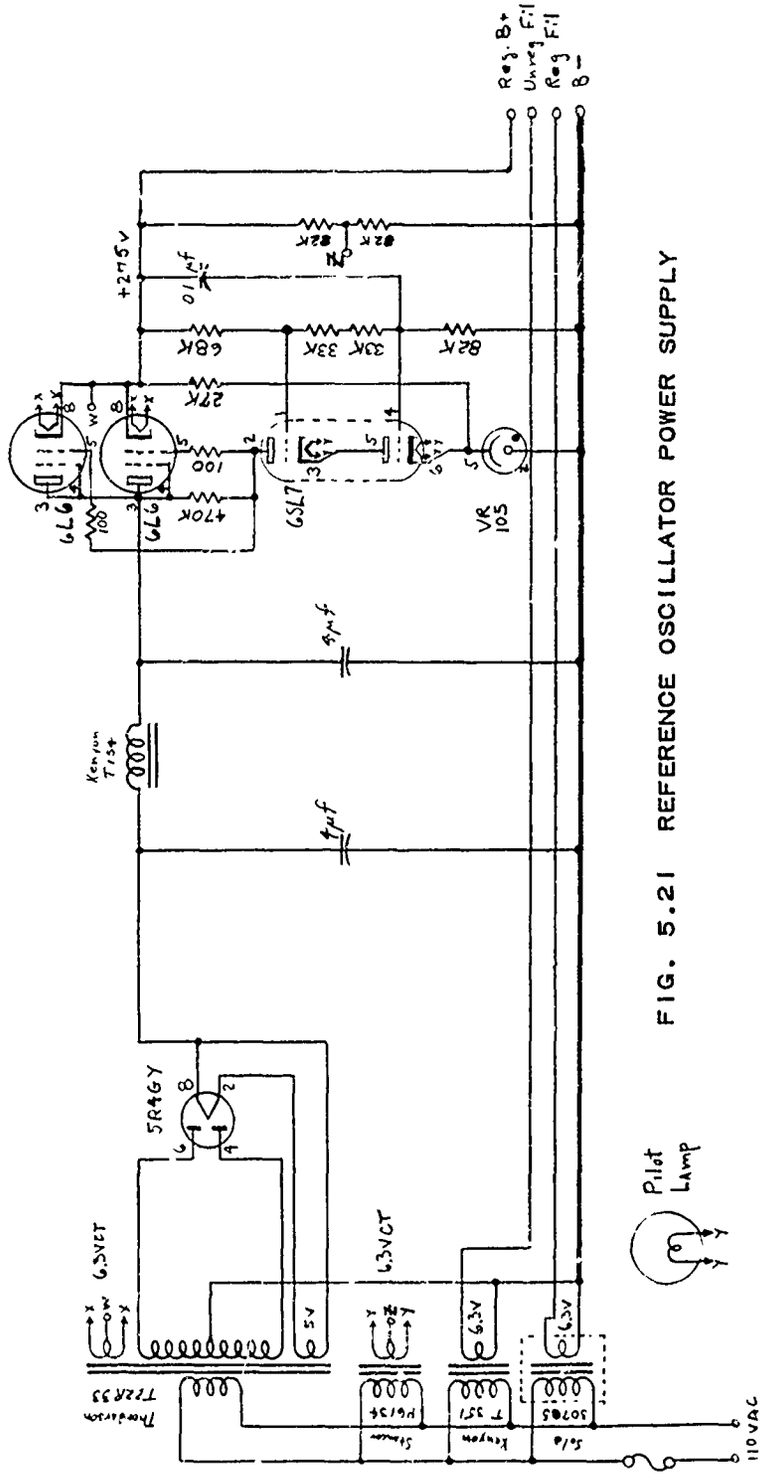


FIG. 5.21 REFERENCE OSCILLATOR POWER SUPPLY

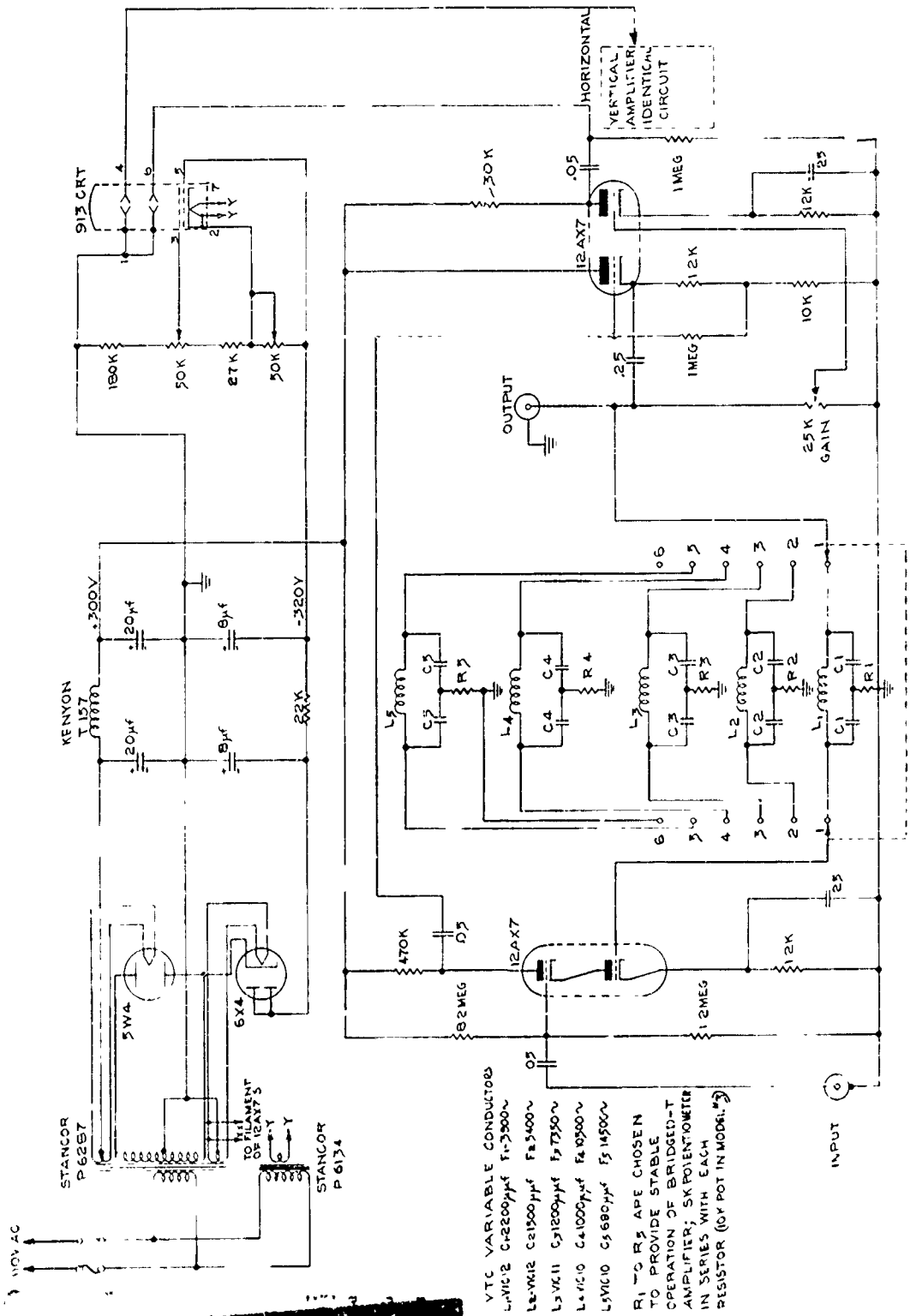


FIG. 5.22 FILTER SCOPE

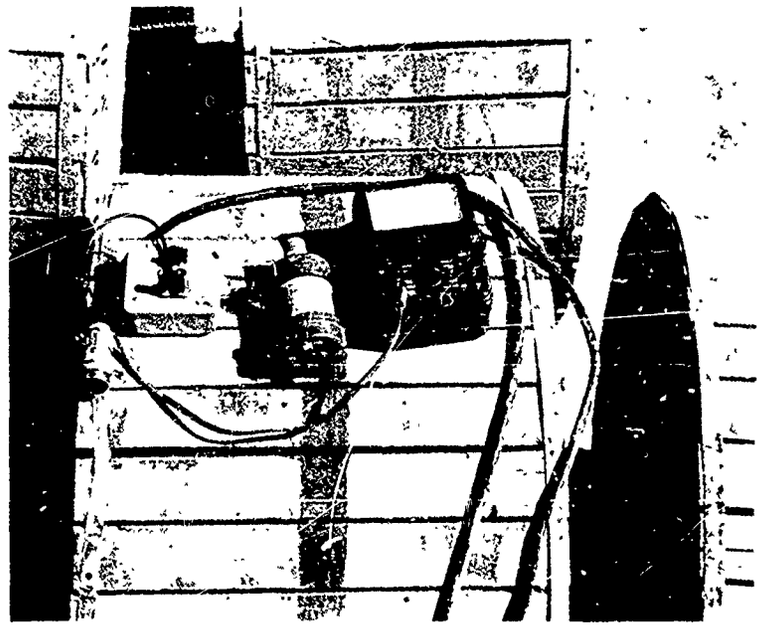

Fig. 5.23 Field Cable Tester

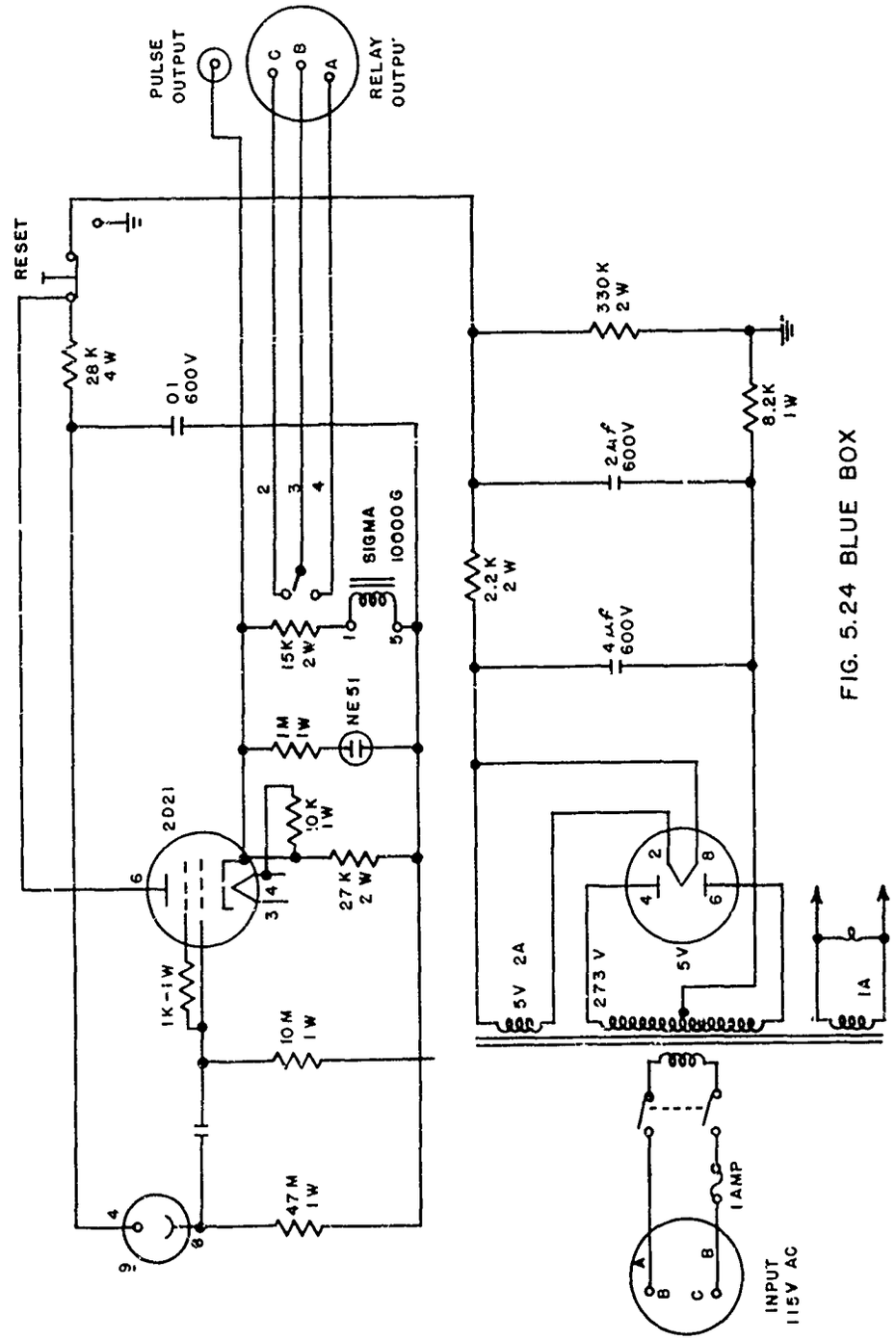


FIG. 5.24 BLUE BOX

Fig. 5.25 Battery Bank in Trailer

Fig. 5.26 Motor Generator in Trailer

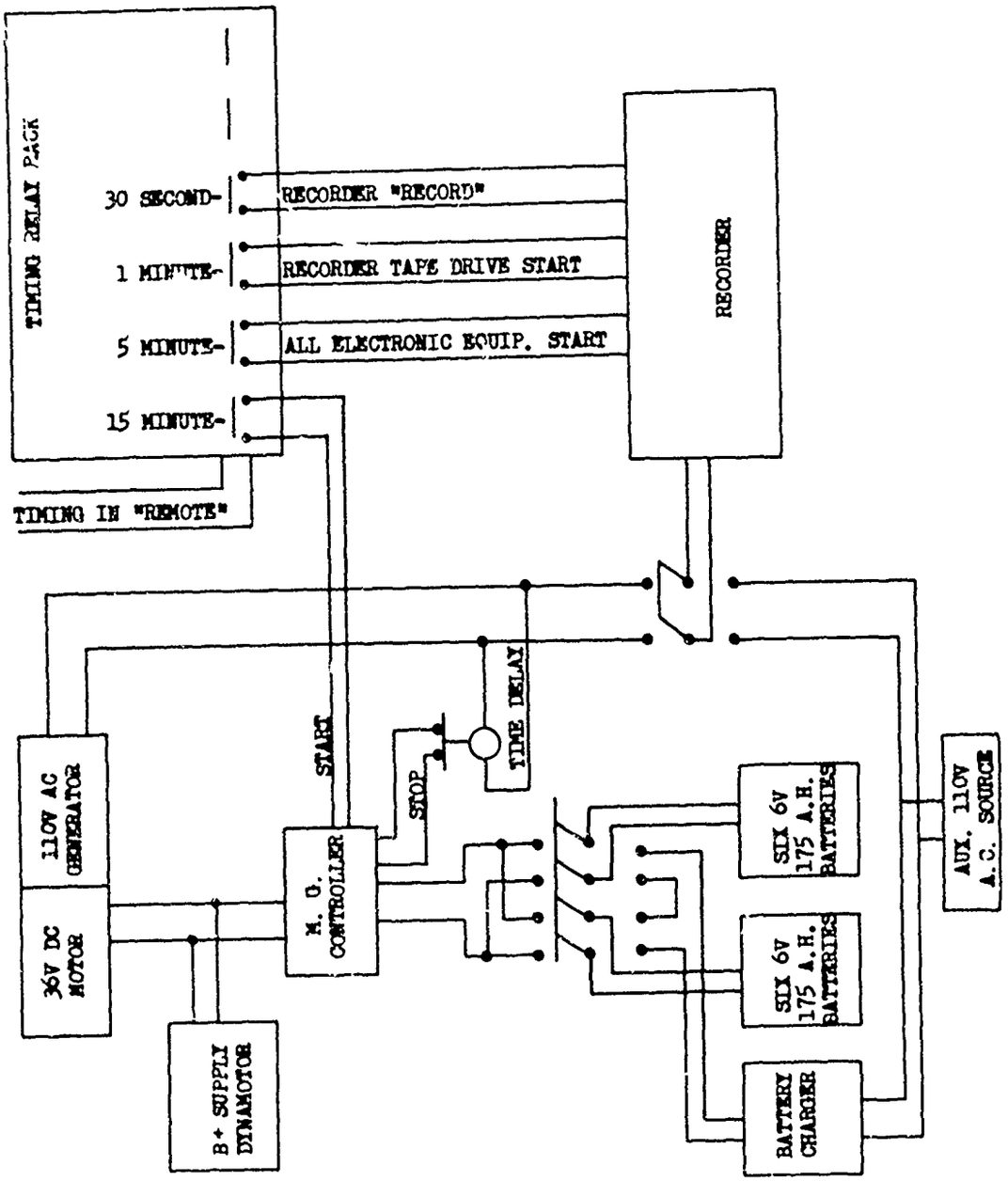


FIG. 5.27 POWER CONTROLS FOR TYPICAL BANK

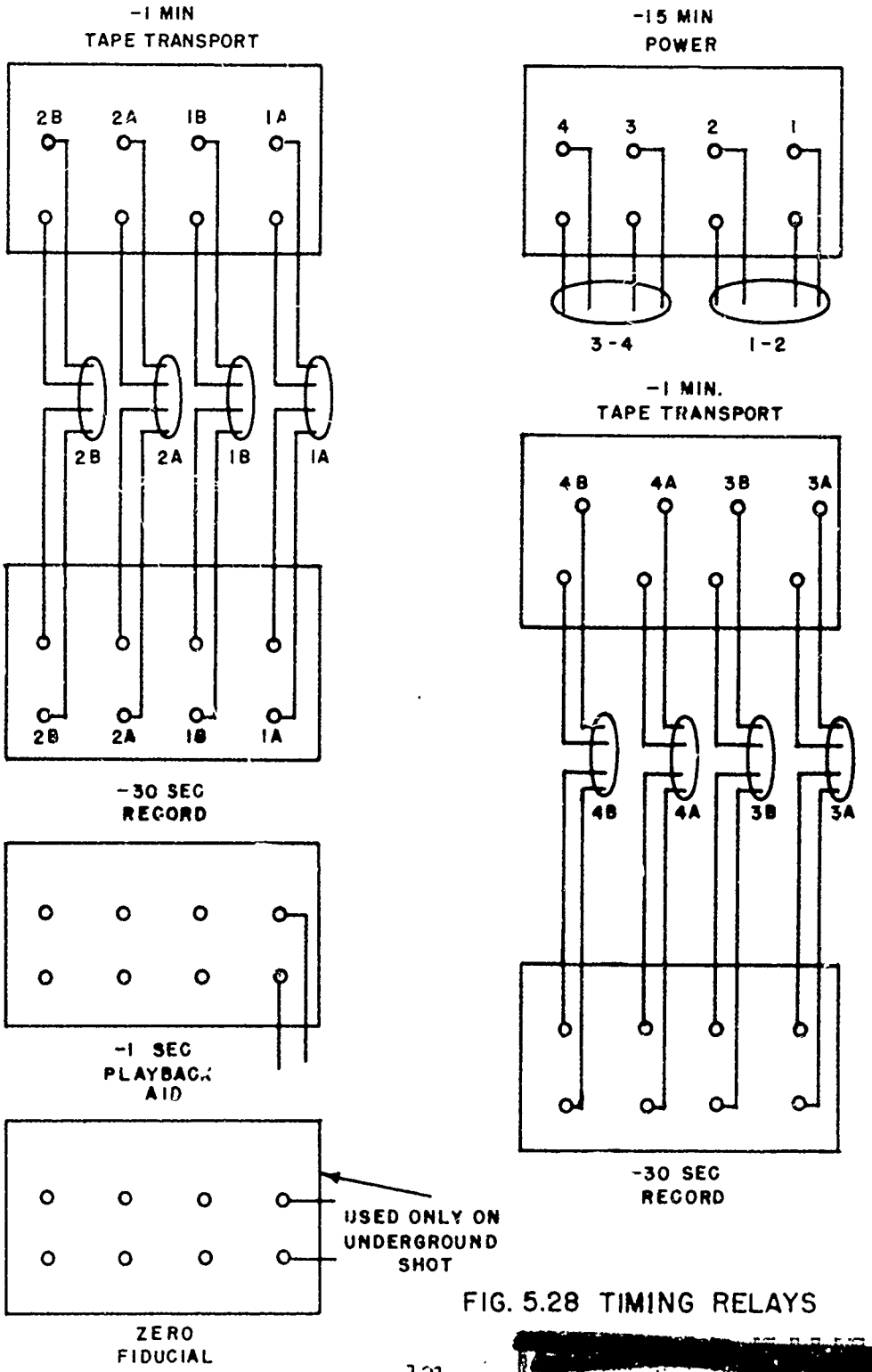


FIG. 5.28 TIMING RELAYS

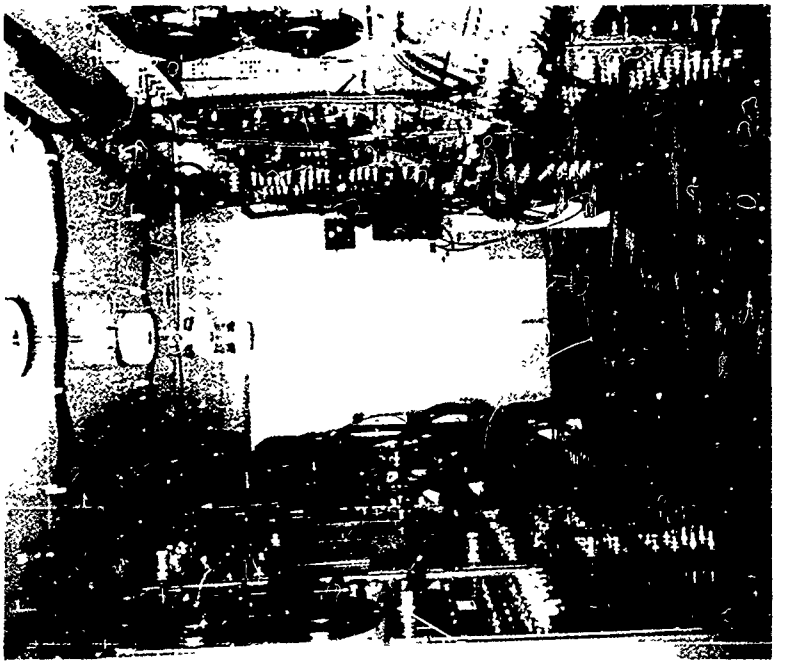

Fig. 5.30 Instrumentation Trailer
Inside - Towards Rear

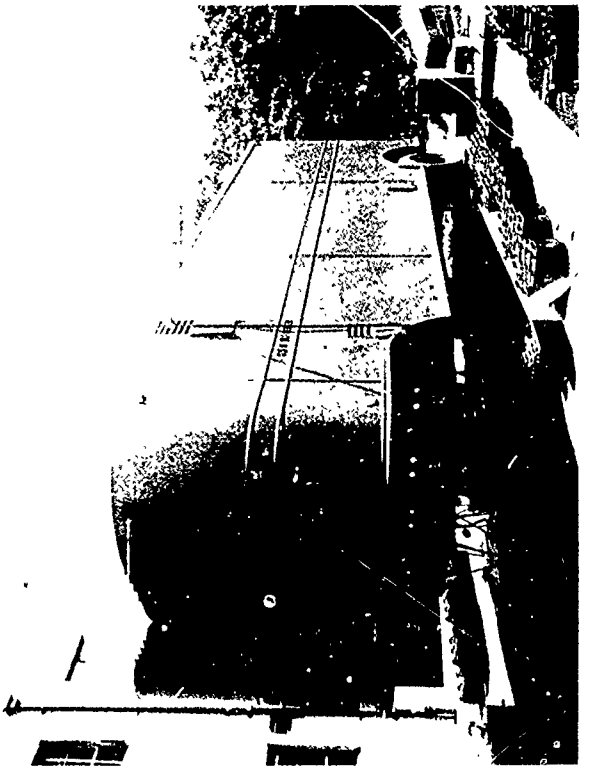

Fig. 5.29 Instrumentation Trailer

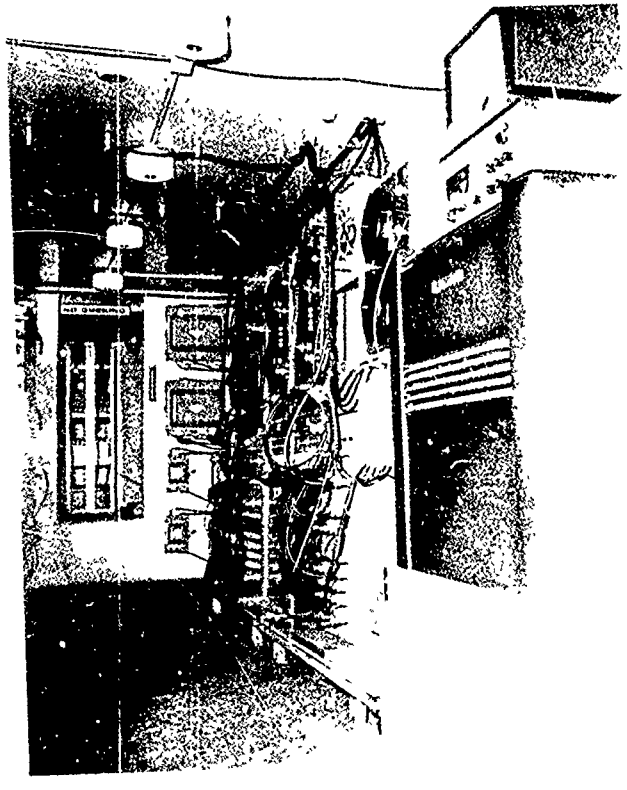

Fig. 5.31 Instrumentation Trailer
Inside - Right Side

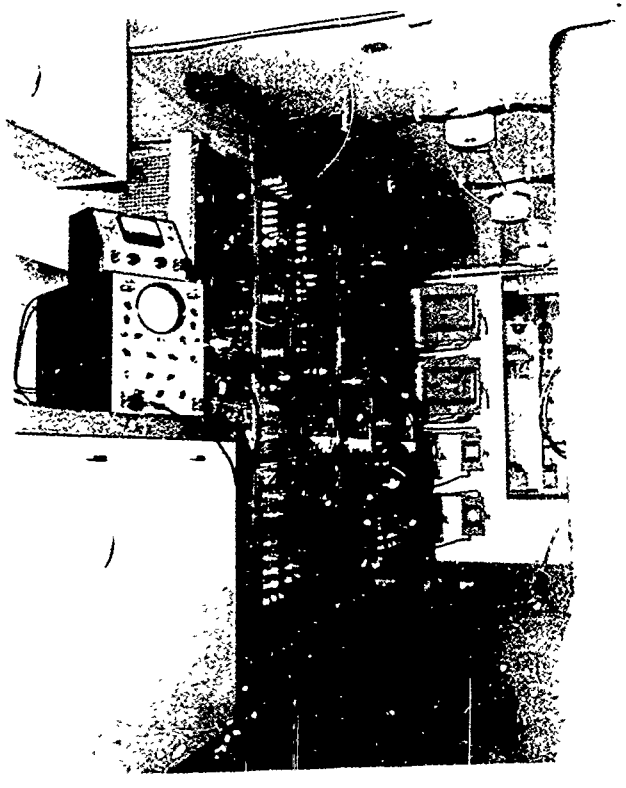

Fig. 5.32 Instrumentation Trailer
Inside - Left Side

[redacted]

PROJECT 1.1

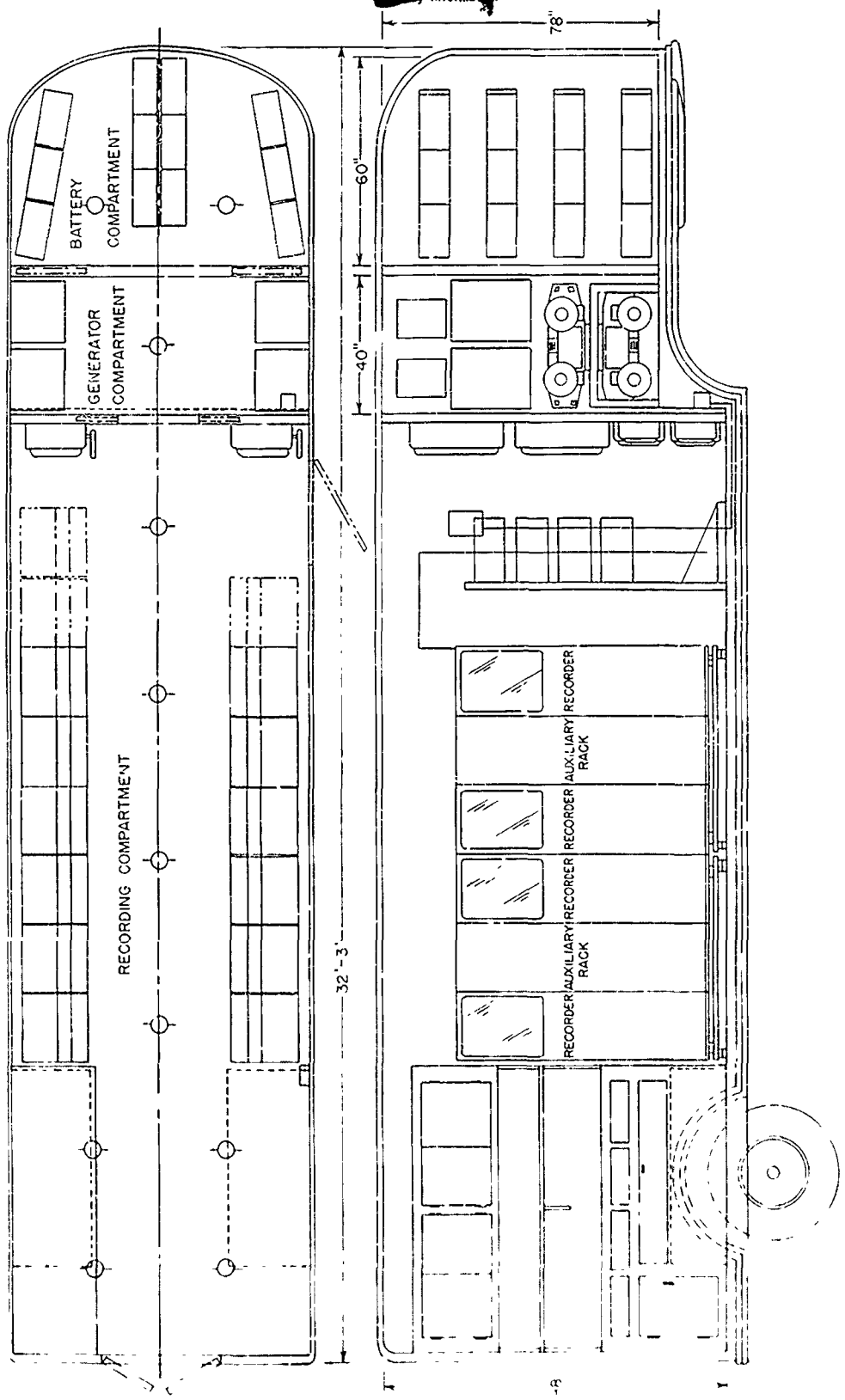


FIG 5.33 INSTRUMENTATION TRAILER - LAYOUT

[redacted]

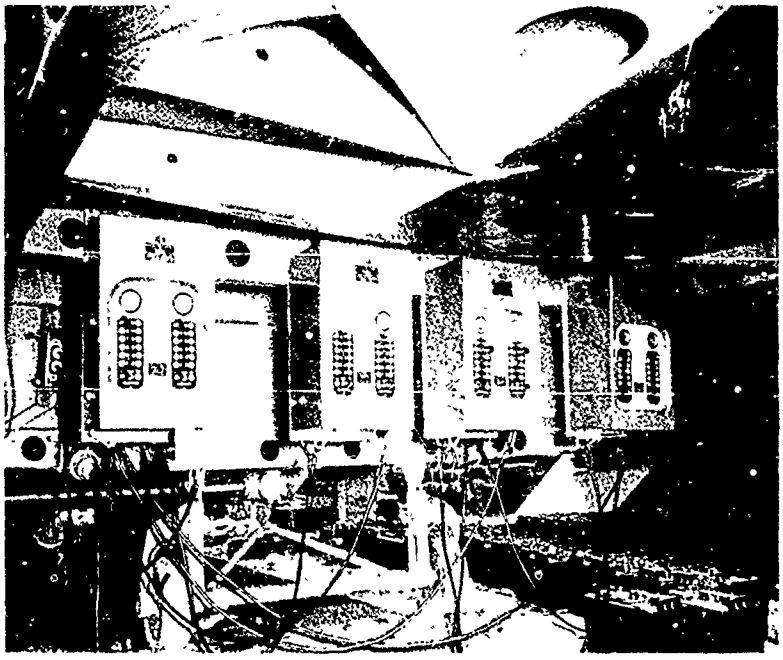

Fig. 5.34 Instrumentation Trailer - Battery Chargers

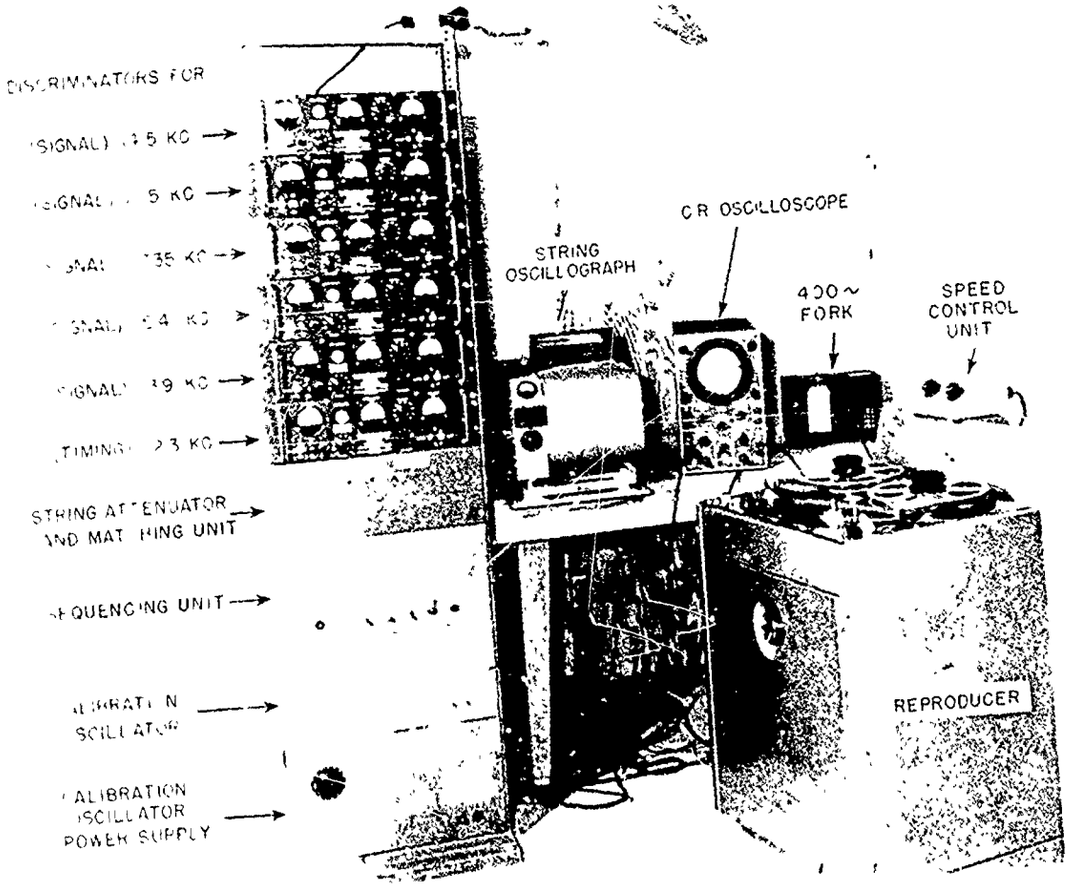


Fig. 5.35 Playback System

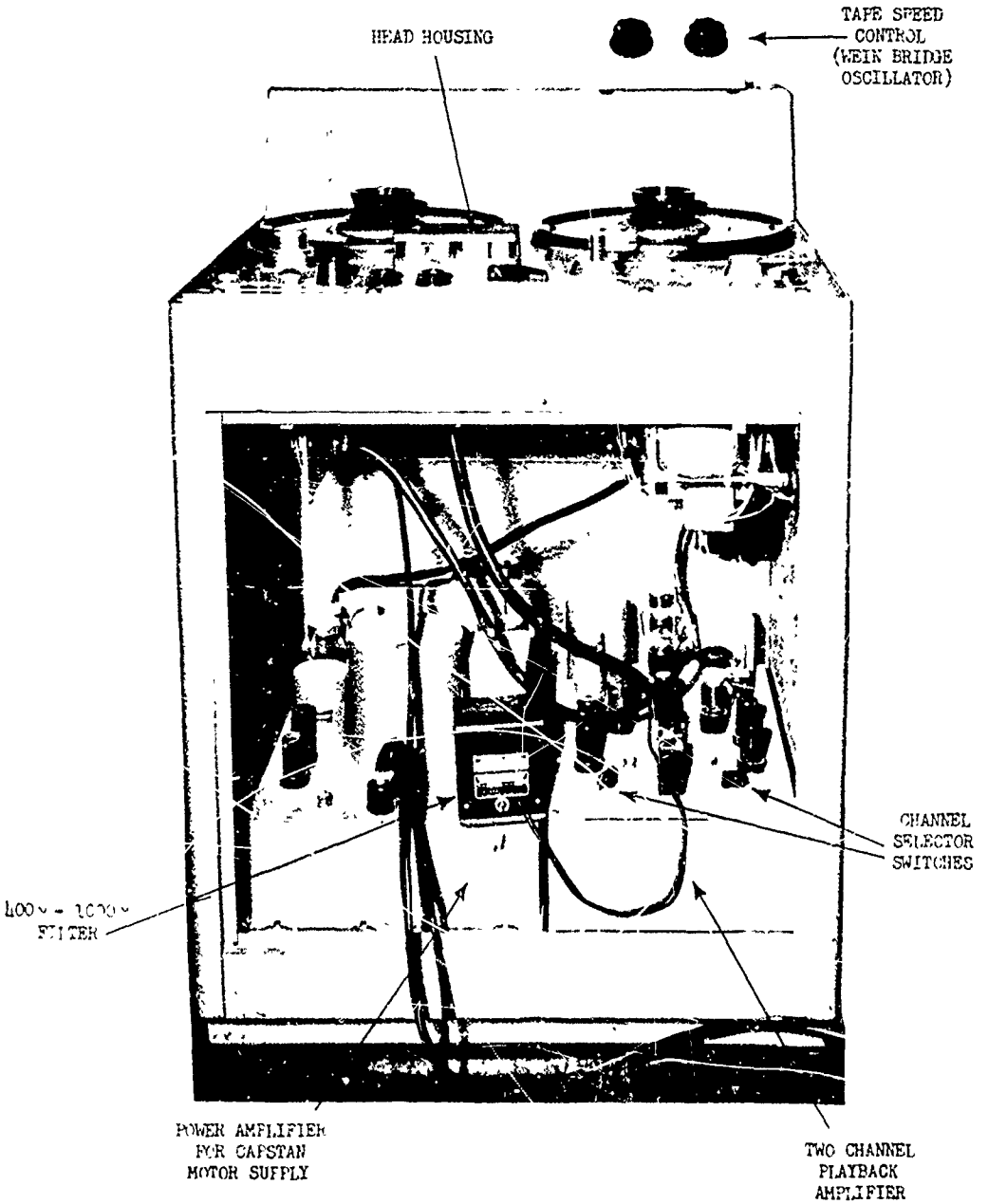


**Fig. 5.36 Ampex Magnetic Tape Recorder**

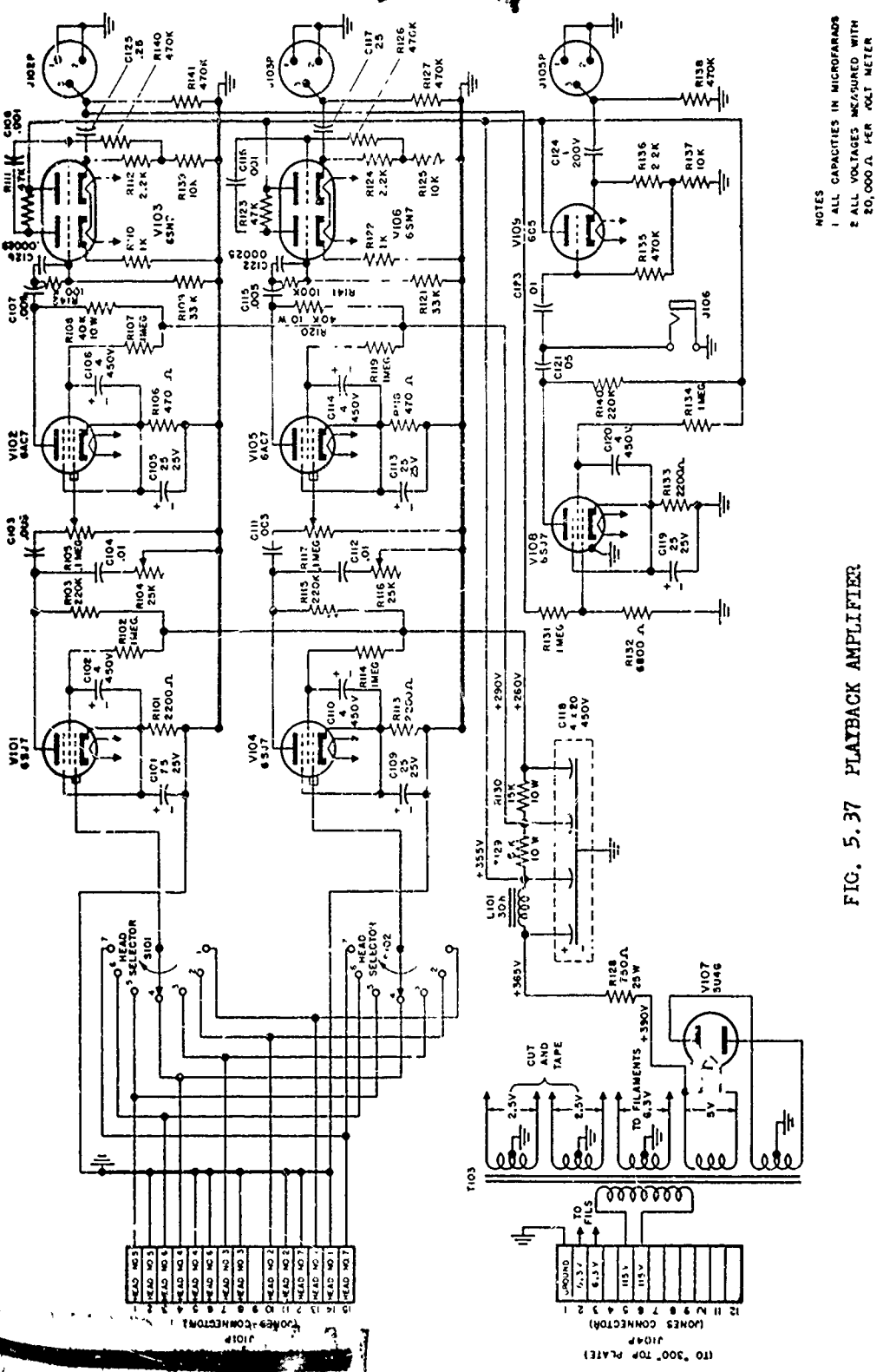


FIG. 5.37 PLAYBACK AMPLIFIER



[redacted]

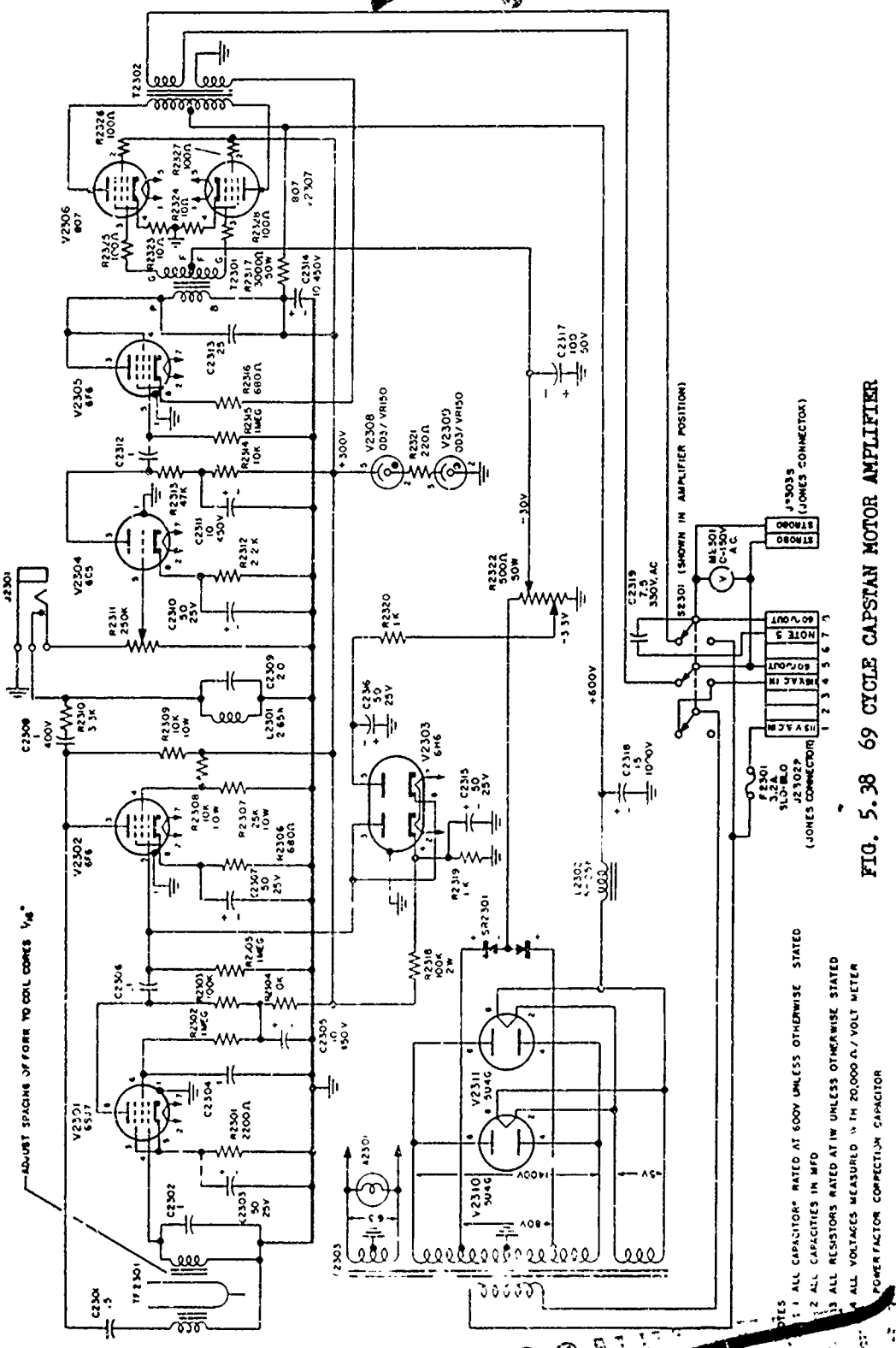


FIG. 5.38 69 CYCLE CAPSTAN MOTOR AMPLIFIER

NOTES
1. ALL CAPACITORS RATED AT 600V UNLESS OTHERWISE STATED
2. ALL CAPACITIES IN MFD
3. ALL RESISTORS RATED AT 1W UNLESS OTHERWISE STATED
4. ALL VOLTAGES MEASURED WITH 20,000 Ω/VOLT METER
5. POWER FACTOR CORRECTION CAPACITOR

RESTRICTED DATA
ATOMIC ENERGY ACT 1946

PROJECT 1.1

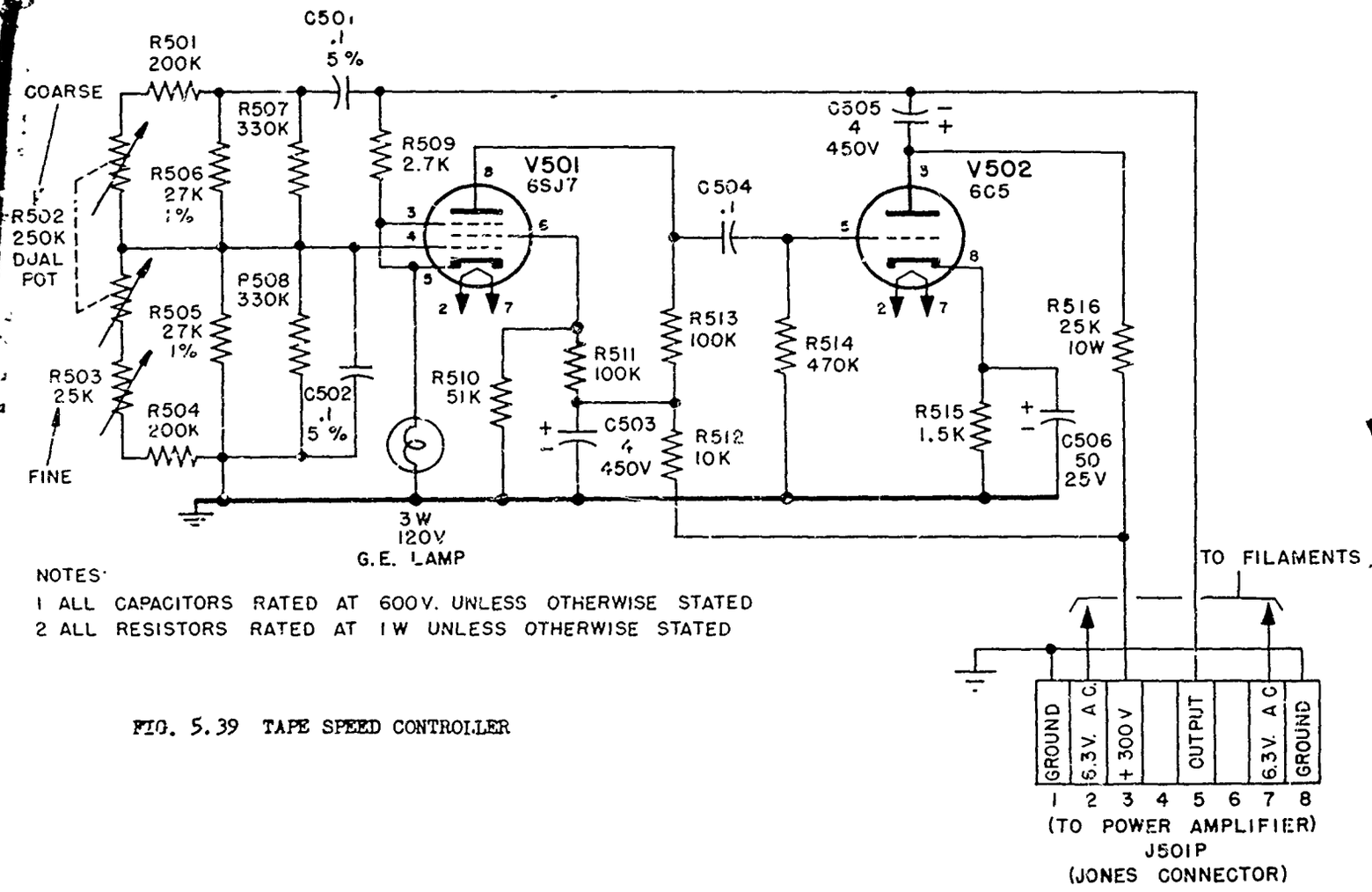


NOTES:

1 ALL CAPACITORS RATED AT 600V. UNLESS OTHERWISE STATED

2 ALL RESISTORS RATED AT 1W UNLESS OTHERWISE STATED

FIG. 5.39 TAPE SPEED CONTROLLER

SECRET
Security Information

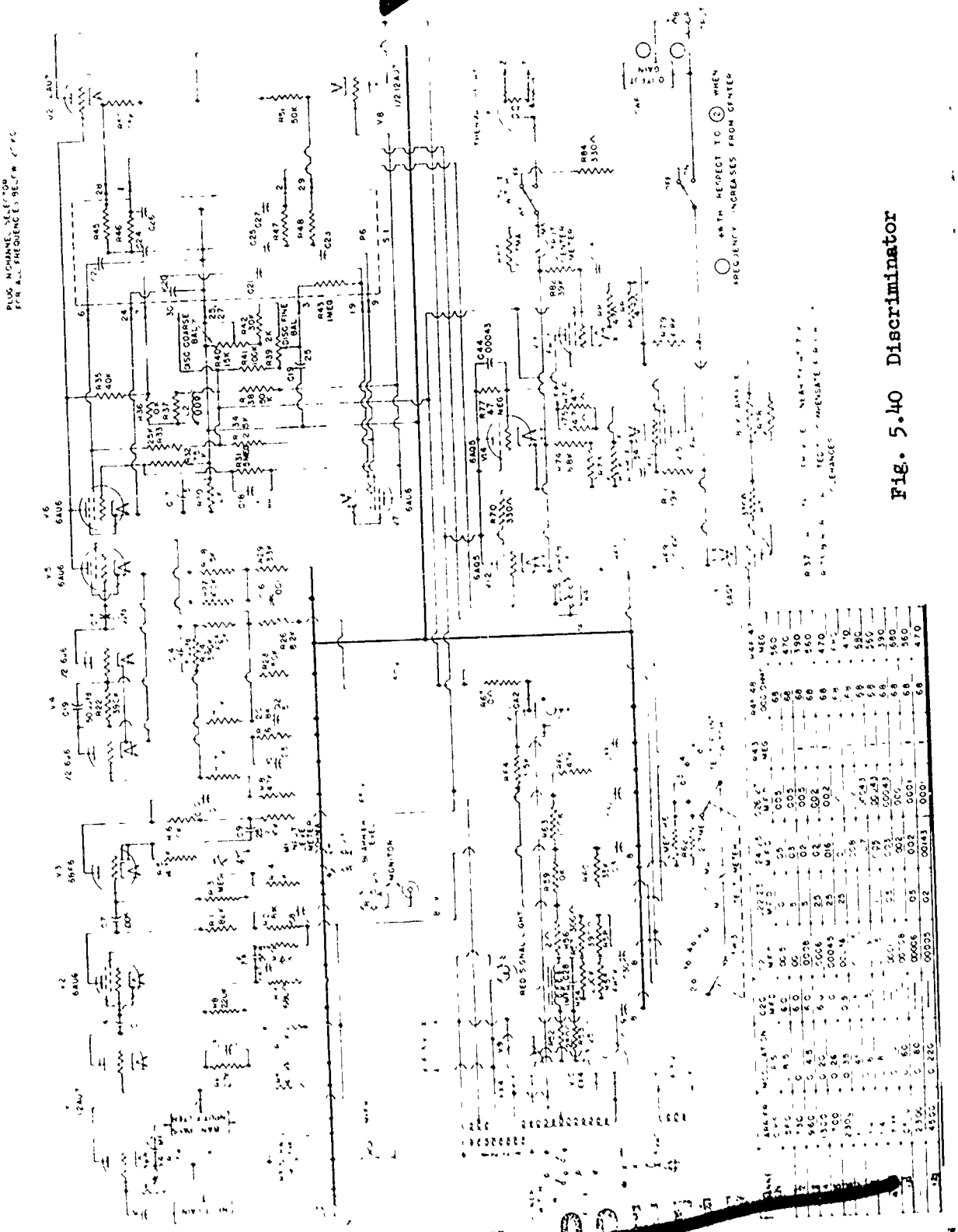

Fig. 5.40 Discriminator

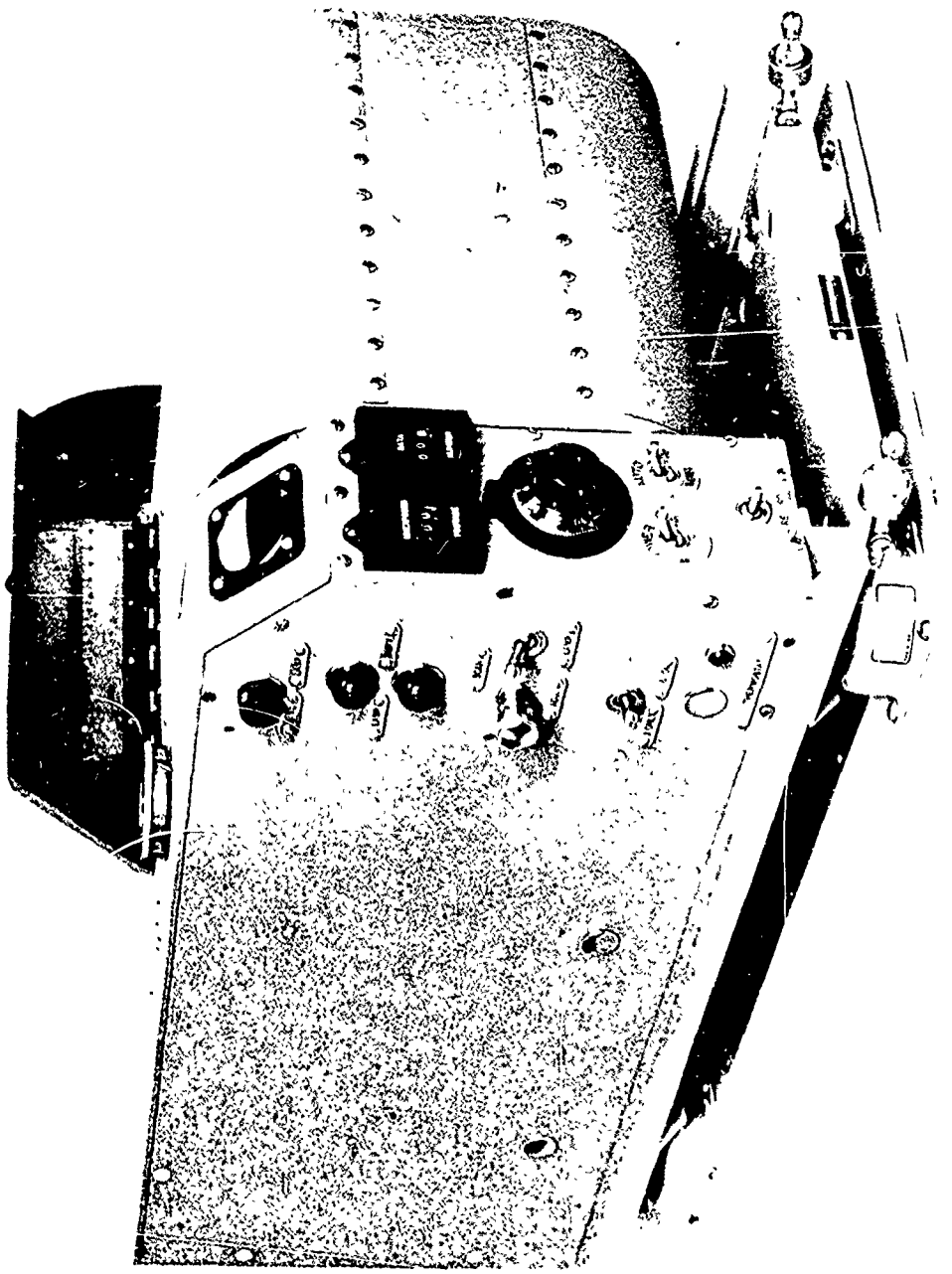

Fig. 5.41 String Galvanometer Oscillograph



RESTRICTED DATA
ATOMIC ENERGY ACT 1946

SECRET
Security Information

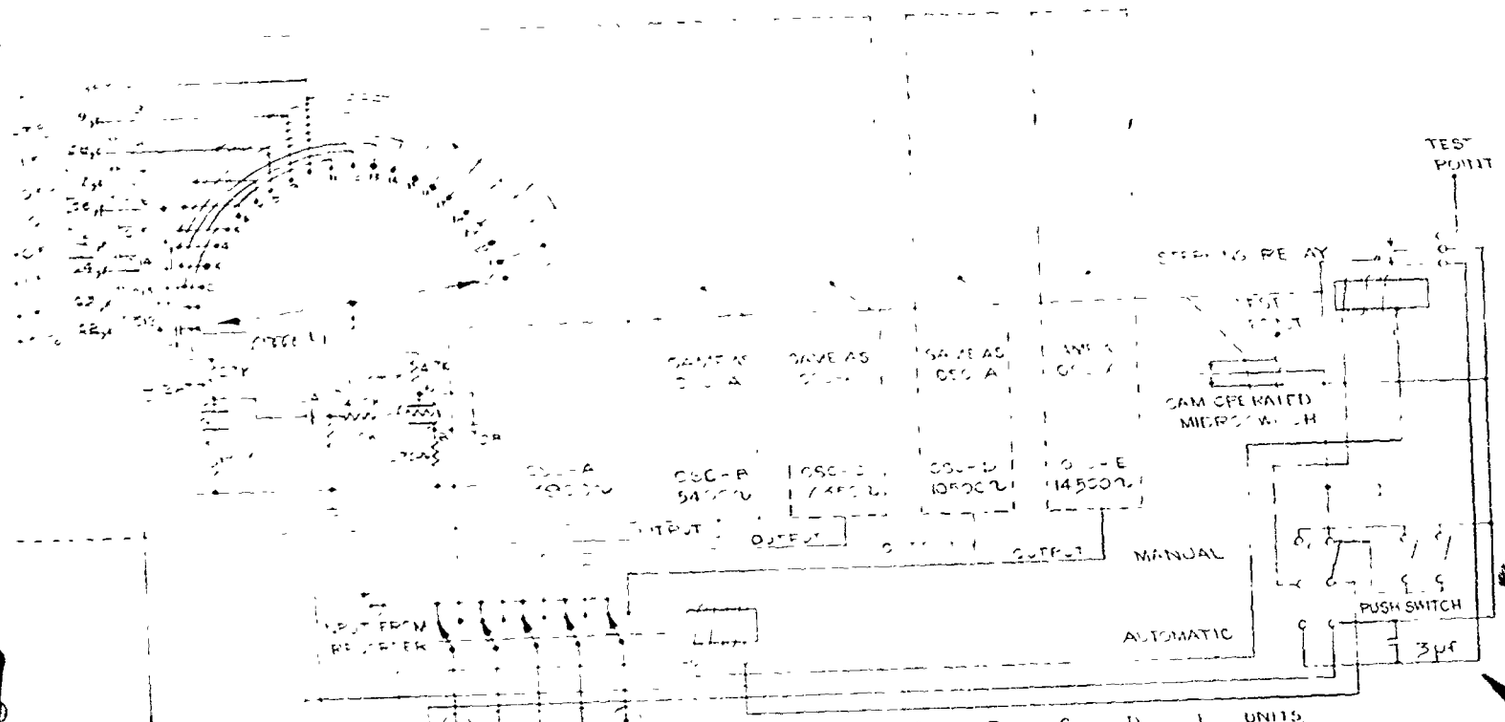


| OSC 30 KC | A 3.3 | B 3.4 | C 7.55 | D 10.5 | E 14.5 | UNITS KC |
|---|---|---|---|---|---|---|
| CA | 0.001 | 4700 | 2200 | 2700 | 1500 | μμf |
| CB | 0.1 | 0.03 | 0.06 | 0.02 | 0.04 | |
| C1 | 4896 | 3098 | 1980 | 1260 | 1168 | |
| C2 | 20-125 | 12-52 | 12-62 | 10-62 | 6-35 | |
| C3 | | | | | | |
| C4 | | | | | | |
| C5 | | | | | | |
| C6 | | | | | | |
| C7 | | | | | | |
| C8 | | | | | | |
| C9 | | | | | | |
| C10 | 20-125 | 12-60 | 10-60 | 10-60 | 6-45 | |
| C11 | 360 | 183 | 117 | 151 | 85 | |
| C12 | 443 | 281 | 188 | 232 | 120 | |
| C13 | 521 | 348 | 234 | 288 | 150 | |
| C14 | 604 | 382 | 257 | 316 | 180 | |
| C15 | 660 | 418 | 279 | 345 | 180 | |
| C16 | 773 | 489 | 329 | 404 | 220 | |
| C17 | 930 | 600 | 404 | 496 | 247 | |
| C18 | 1320 | 841 | 565 | 695 | 330 | μμf |
| L1 | 0.3 | 0.21 | 0.2 | 0.08 | 0.06 | H |

FIG. 5.42 CALIBRATION OSCILLATOR



SECRET
Security Information
DECLASSIFIED DATA

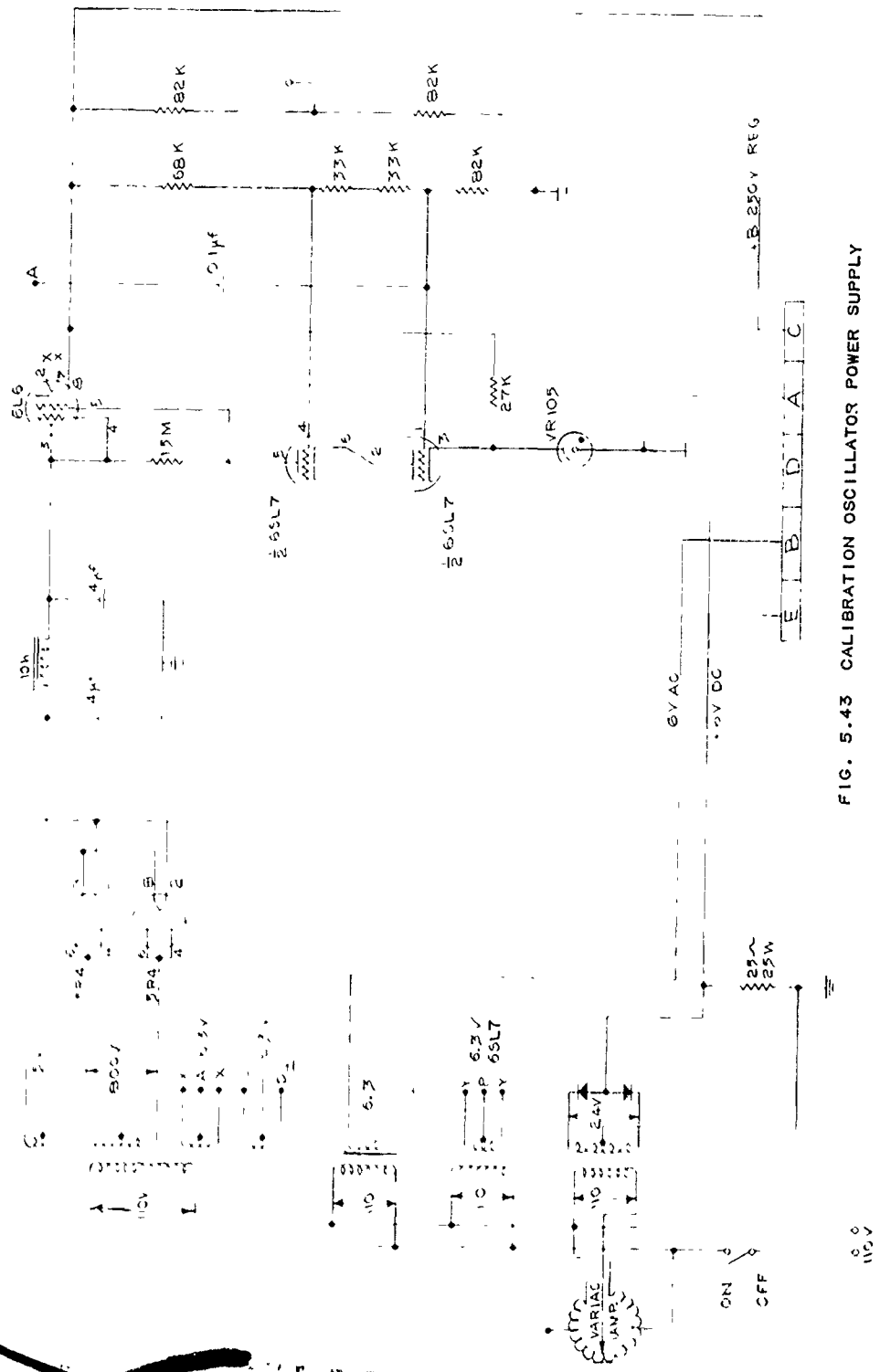


FIG. 5.43 CALIBRATION OSCILLATOR POWER SUPPLY



[redacted]

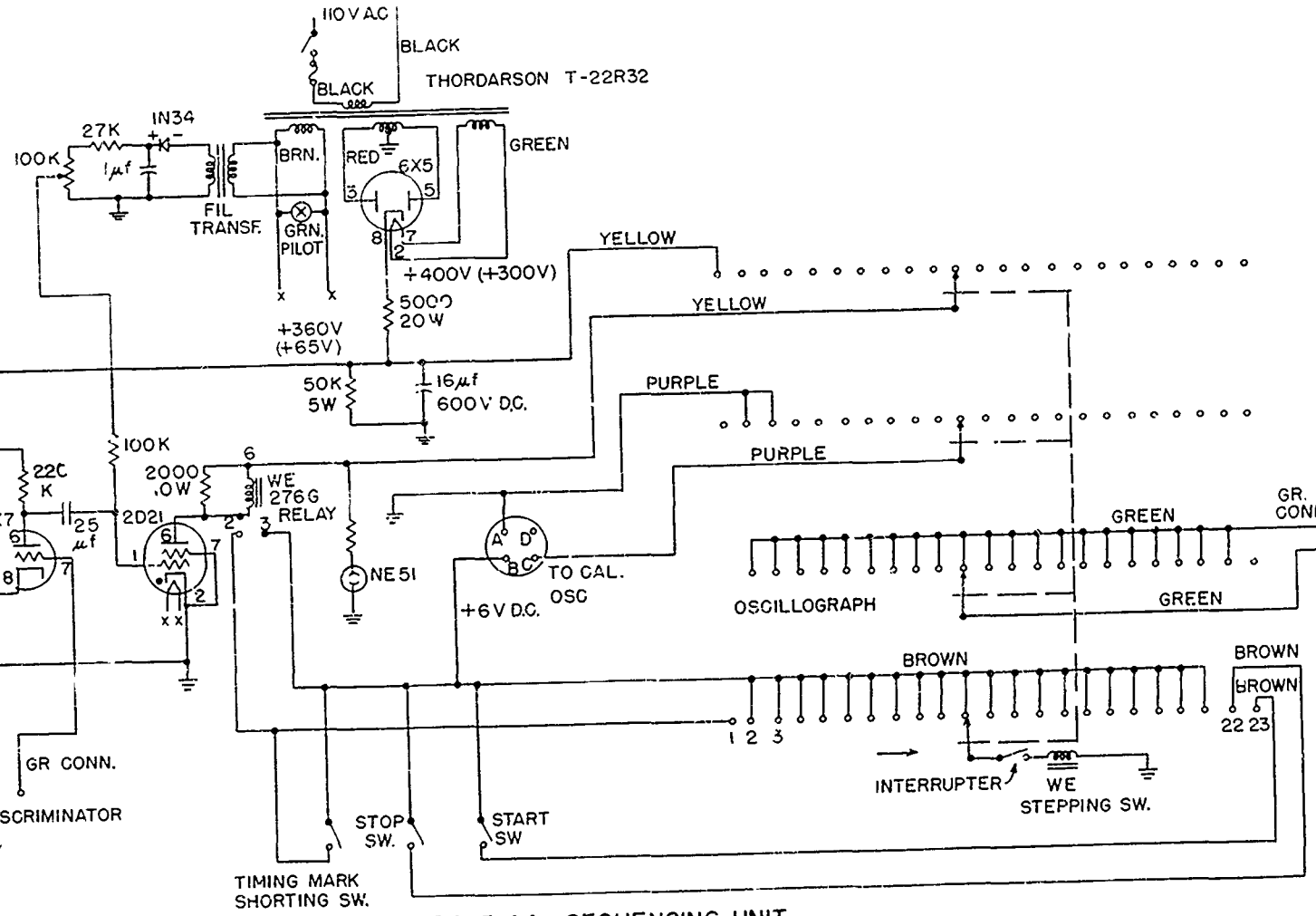


FIG. 5.44 SEQUENCING UNIT

PROJECT 1.1

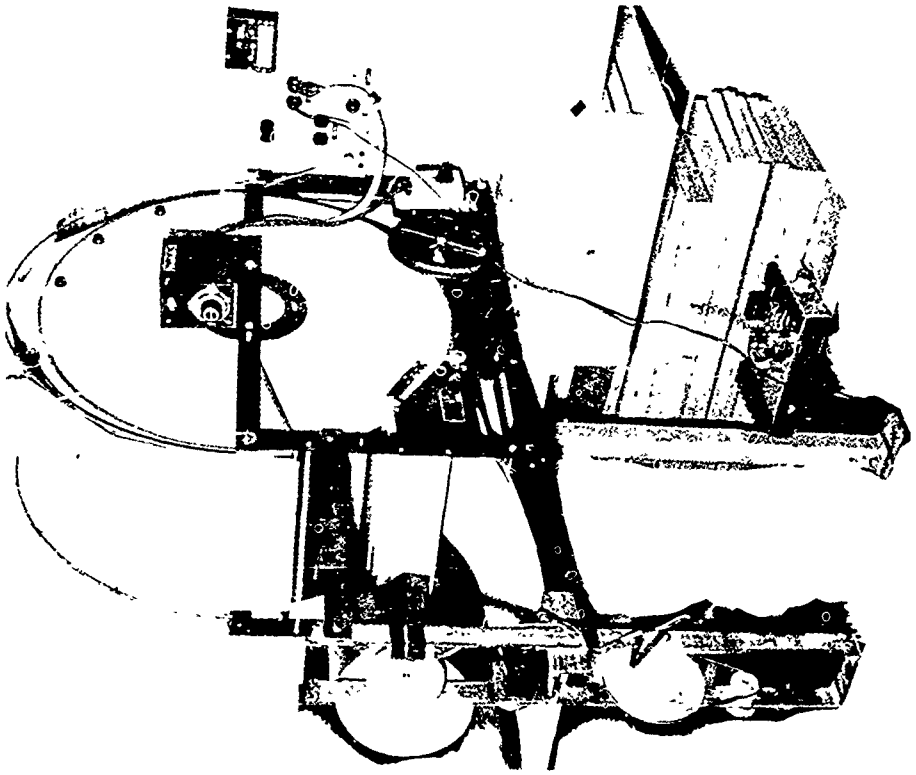

Fig. 5.46 Print Dryer

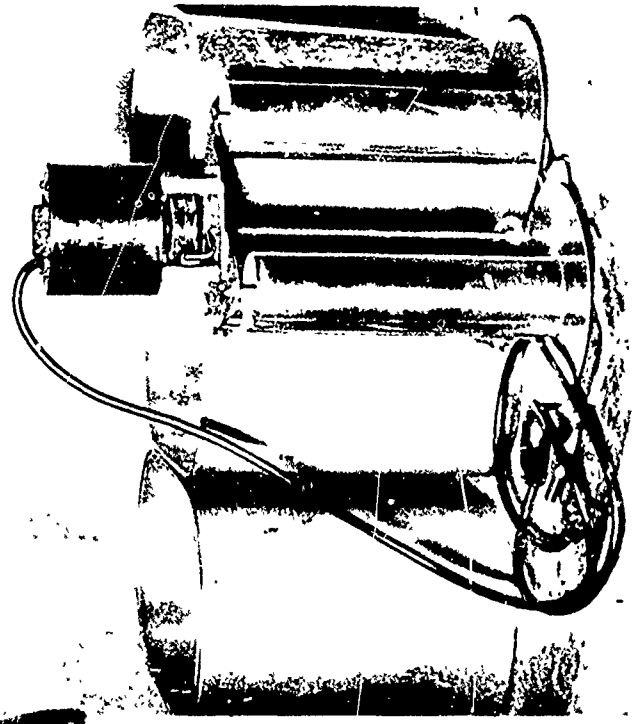

Fig. 5.45 Developing Tanks

# CHAPTER 6

## FIELD CONSTRUCTION

A general layout of the two nuclear and the HE blast lines is shown in Fig. 3.1. A more detailed presentation of the gage locations is shown in Fig. 3.2. Engineering design and construction of the items shown in these figures and other field installations was carried out by the Haddock Engineers IV, Ltd., based upon requirements submitted jointly by NOL and BRL. The more important items of construction were: the trailer revetments, gage holes, cable trenches, blast line roads and work shop space. Other items of lesser importance which are mentioned herein for future planning purposes are a photographic dark room, a dust proof laboratory space, and a field office.

### 6.1 TRAILER REVETMENTS

The two revetments, one for each blast line, were provided to afford protection from blast, shock, and contamination to the NOL and BRL instrument trailers. They were located at 8,000 ft from zero on an extension of the instrument lines where the expected air overpressures were .4 psi for the underground shot and .6 psi for the surface shot. The full 8,000 ft of distance was thus not required for blast protection but was considered to be necessary to locate the trailers out of range of contamination hazards.

The revetment design utilized was similar to one which had been used by the Office of the Chief of Engineers at the Dugway Proving Grounds. This design was modified in length and width to meet the requirements for housing the BRL and NOL trailers within a common shelter and proved to be satisfactory. Figure 6.1 is a detailed drawing of the shelter and Figs. 6.2 and 6.3 show two phases of construction. Prior to shot time, heavy tarpaulins were fastened across each end of the revetment by battens to prevent contaminated dust particles from entering and settling in and around the trailers. As constructed the revetment allowed only a few inches of overhead clearance for the NOL trailer, which necessitated having a low-bed tractor to tow the trailers into position. Fortunately, one of this type was always available but this factor could have been a critical one in the time schedule. Such a requirement can be avoided in the future by having at least 1-1/2 ft of overhead clearance. The revetments contained power panels which provided 30 amp, 110v or 220v

circuits for lighting, battery charging, and general utility purposes. During most of the field period power was furnished by mobile generators, but during the last three weeks the test site power net-work was tied into the panel. The utility items of lighting circuits, field telephones and a telephone on the test site hook-up were installed in the revetment and were most useful. The phones were of collateral value after the shots when they were used by field monitoring groups for contacting other Rad-Safe parties.

## 6.2 GAGE HOLES

### 6.2.1 Hole Requirements

A detailed layout of the plan for the gage holes which were required along the instrument lines are shown in Figs. 3.2 and 3.3. In order to align the accelerometer capsules at the bottom of the 10 in. diameter holes it was necessary that the run-out of a hole be not more than about 6 in. If greater than this, the capsule could not be mounted in a sufficiently vertical position so that an appreciable gravity component was imposed on the accelerometer. This proved to be quite a critical factor for the holes which were 30 ft deep. Inasmuch as the holes for pressure gages were drilled adjacent to the accelerometer holes, it was possible to select the better of the two holes for the accelerometer capsule, verticality not being critical for installing the pressure gage. The drilling operations were performed by the Casey and Case Company of Los Angeles, California, using bucket and geophysical type rotary drill rigs. A summary of the total drilling requirements for NOL and BRL is listed below. Although 8 in. diameter holes were specified to the contractors, various sizes ranging from 8 to about 12 in. diameters were drilled because of the limited availability of bits and rigs of the required size and type.

Surface Shot Instrument Line

| | | |
|---|---|---|
| 10 ft depth | - | 40 |
| 20 ft depth | - | 8 |
| 30 ft depth | - | 8 |
| | | 56 |

Underground Shot Instrument Line

| | | |
|---|---|---|
| 10 ft depth | - | 42 |
| 20 ft depth | - | 8 |
| 30 ft depth | - | 8 |
| | | 58 |
| Total | | 114 |

### 6.2.2 Drilling Operation

Figures 6.4, 6.5, and 6.6 illustrate the drill crews in operation. Attention is directed to the bucket type bit which, though not as fast as a geophysical rig, drilled a cleaner and more satisfactory hole. It was not necessary to case the holes and in only one instance did a hole cave in prior to installation of the capsule. This hole was cleaned out in a few minutes by a bucket drill and proved satisfactory for use. Figure 6.7 illustrates the appearance of the holes in one of the lateral trenches in which they were located.

### 6.2.3 Composition of Overburden

The soil conditions imposed few problems to the drilling crews, intermittent layers of calechi and an occasional rock being the only deterrent. Table 6.1 contains information as to the strata and overburden through which drilling was accomplished. This information was furnished by Thomas Patterson, Chief of the drill crews, upon completion of the drilling operation.

## 6.3 CABLE TRENCHES

Cable trenches were required to protect the power, instrument and telephone cables from damage due to vehicles prior to shot time and from blast damage after shot time. It is questionable as to which is the greater hazard to field installations. The trenches required for each blast line were (1) a main cable trench starting at 275 ft from zero and extending to the trailer revetment at 8,000 ft from zero and (2) lateral trenches at each of the 12 gage locations.

A "V" type trench was dug with a tilted grader blade for the main trench while a ditching machine was used for the lateral trenches. Figure 6.8 shows the "V" type trench and its intersection with several lateral trenches. Figures 6.7 and 6.9 show the square type lateral trenches with holes drilled in the trench alongside the trench. Both methods were used. All trenches were dug 2 to 3 ft deep, which proved to be sufficient as no damage occurred to the cables on either blast line. The square type trench dug with a ditching machine is considered to be the most desirable as it affords better protection from vehicles, is easier to work in and around, and results in less disturbance to the medium.

TABLE 6.1

Composition of Overburden Along Instrument Lines

Surface Shot Instrument Line

Station No. 2 - 340 ft from zero

| | |
|---|---|
| 0 ft | - 15 ft - Soft broken calechi |
| 15 ft | - 17 ft - Soft sand mixed with calechi |
| 17 ft | - 17-1/2 ft - or 18-1/2 ft - Hard layer of calechi |
| 18 ft | - 30 ft - Fine dirt and broken calechi |

Station No. 5 - 642 ft from zero

| | |
|---|---|
| 0 ft | - 4 ft - Loose dirt and calechi |
| 4 ft | - 5 ft - Hard calechi layer |
| 5 ft | - 18 ft - Dirt with large chunks of hard calechi |
| 18 ft | - 18-1/2 ft - Hard calechi |
| 18-1/2 ft | - 30 ft - Dirt and loose bits of calechi |

Station No. 8 - 1213 ft from zero

| | |
|---|---|
| 0 ft | - 4 ft - Loose dirt and calechi |
| 4 ft | - 5 ft - Hard calechi layer |
| 5 ft | - 18 ft - Dirt with large chunks of hard calechi |
| 18 ft | - 18-1/2 ft - Hard calechi |
| 18-1/2 ft | - 30 ft - Dirt and loose bits of calechi |

Station No. 10- 1890 ft from zero

| | |
|---|---|
| 0 ft | - 4 ft - Loose dirt and calechi |
| 4 ft | - 5 ft - Hard calechi layer |
| 5 ft | - 18 ft - Dirt with large chunks of hard calechi |
| 18 ft | - 18-1/2 ft - Hard calechi |
| 18-1/2 ft | - 30 ft - Dirt and loose bits of calechi |

TABLE 6.1 (cont'd)

Underground Shot Instrument Line

Station No. 2 - 340 ft from zero

| | | |
|---|---|---|
| 0 ft | - 5 ft | - Fine silt and a few rocks with a little sand at about 4 ft. |
| 5 ft | - 8 ft | - Fine silt |
| 8 ft | - 17 ft | - Very loose dirt mixed with small bits of calechi |
| 17 ft | - | - 4 in. layer of hard calechi |
| 17 ft | - 20 ft | - Dirt and sand |
| 20 ft | - 24 ft | - Dirt and rocks - some 8 to 10 in. in diameter |
| 24 ft | - 30 ft | - Dirt and calechi |

Station No. 5 - 642 ft from zero

| | | |
|---|---|---|
| 0 ft | - 7 ft | - Sand and gravel mixed with a few rocks 7 to 12 in. in diameter |
| 7 ft | - 18 ft | - Dirt mixed with loose calechi |
| 18 ft | - | - 4 in. layer of hard calechi |
| 18 ft | - 30 ft | - Dirt mixed with small bits of broken calechi |

Station No. 8 - 1213 ft from zero

| | | |
|---|---|---|
| 0 ft | - 8 ft | - Sand and gravel with some rocks up to 10 in. in diameter |
| 8 ft | - 12 ft | - Sand, gravel, and dirt mixed with a few rocks |
| 13 ft | - 14 ft | - Hard calechi |
| 14 ft | - 20 ft | - Firm dirt |
| 20 ft | - 22 ft | - Loose gravel |
| 22 ft | - 30 ft | - Firm dirt mixed with calechi |

Station No. 10 - 1890 ft from zero

| | | |
|---|---|---|
| 0 ft | - 6 ft | - Very fine silt |
| 6 ft | - 12 ft | - Loose dirt and calechi |
| 12 ft | - 13 ft | - Hard calechi layer |
| 13 ft | - 21 ft | - Hard dirt and calechi |
| 21 ft | - 30 ft | - Hard dirt mixed with gravel |



[redacted]
[redacted]

## 6.4 ROADS

A cross section of a typical station with its adjacent clearing, access roads, and stabilized work area is shown in Fig. 6.10. This arrangement made possible the entry of trucks and other vehicles directly adjacent to the gage holes. The construction of this work area was easily accomplished by grading, and compacting and contributed materially to good working conditions. Figure 6.8 illustrates convenience of access to the immediate work area.

## 6.5 GENERAL CONDITIONS IN AREA

To provide a general description of the appearance of the area and to point out conditions which may be of interest in future planning for a similar operation, the reader is referred to the United Geophysical report[1] of the test area and to Figs. 6.11 and 6.12. The dust conditions illustrated in Fig. 6.12 prevailed nearly every afternoon during September and are a real factor to contend with in regard to equipment, personnel, and time schedules. The flatness of the area, the dry climatic conditions, and the near homogeneity of the soil were favorable factors which contributed to the success of the project.

---

[1] United Geophysical Co., Inc., "Seismic Refraction for Nye County, Nevada", July 1951.

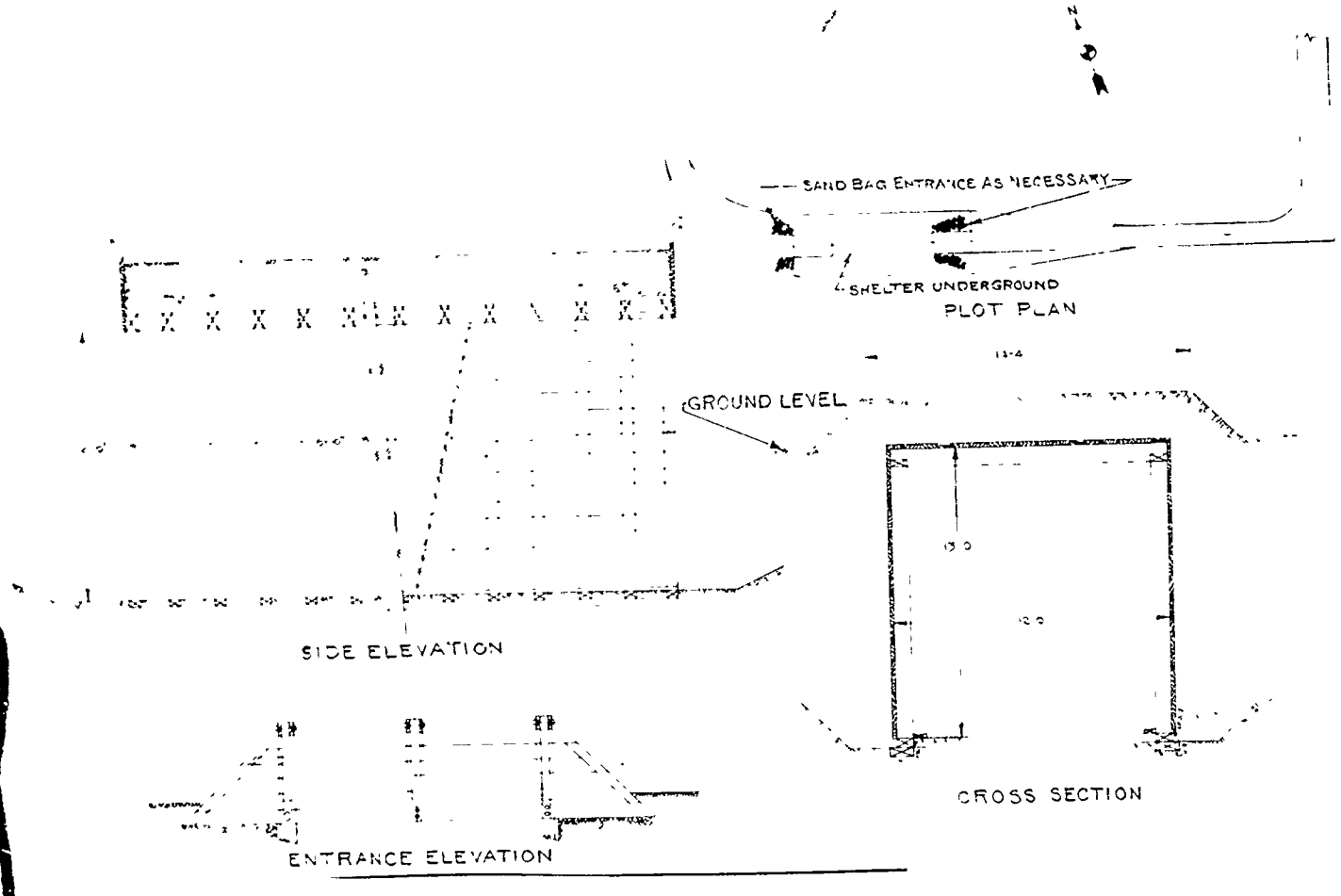


FIG 6.1 UNDERGROUND SHELTER

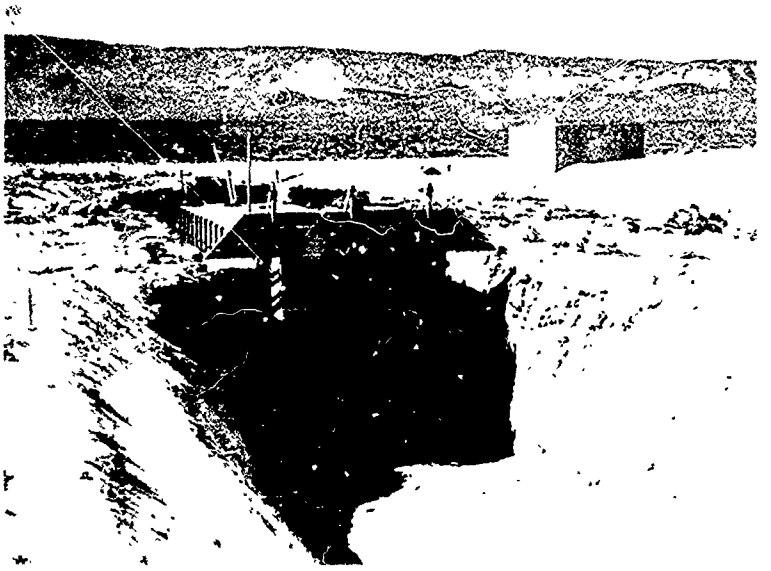

Fig. 6.2 Trailer Shelter Construction

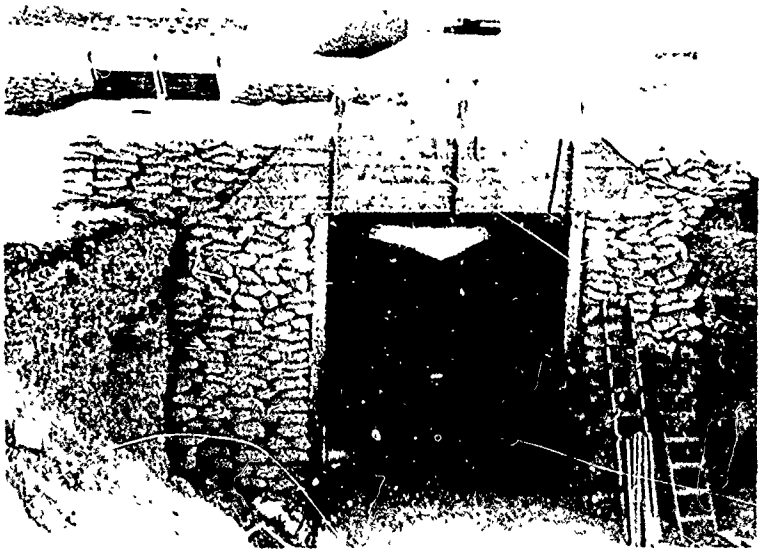

Fig. 6.3 Trailer Shelter and Trailer

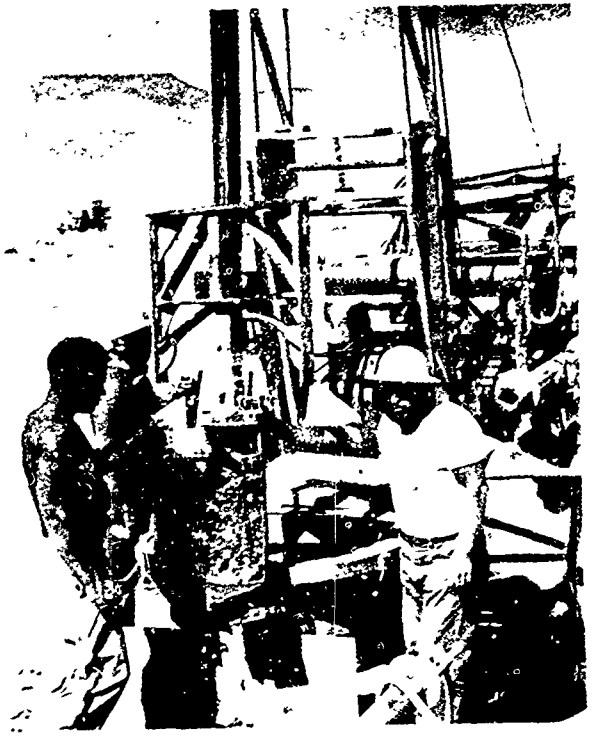

Fig. 6.4 Rotary Drill Rig Showing Bucket Type Bit

Fig. 6.5 Rotary Drill Rig and Crew



Security Information
ATOMIC ENERGY ACT

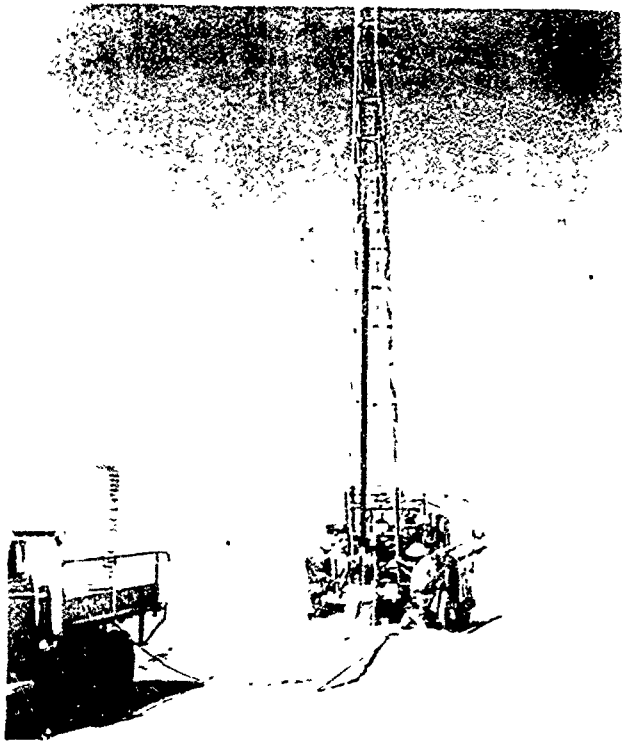

Fig. 6.6 Geophysical Drill Rig and Crew

Fig. 6.7 Gage Holes Drilled in Bottom of Lateral Cable Trench



RESTRICTED DATA
ATOMIC ENERGY ACT 1946

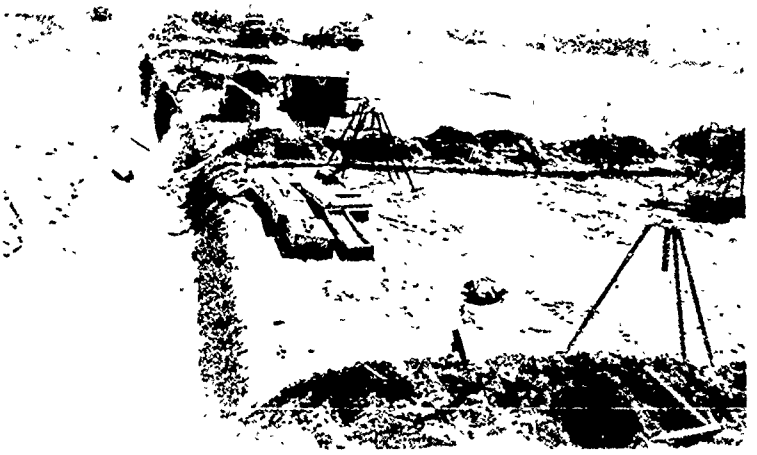

Fig. 6.8 General View of Blast Line Showing Main and Lateral Cable Trenches

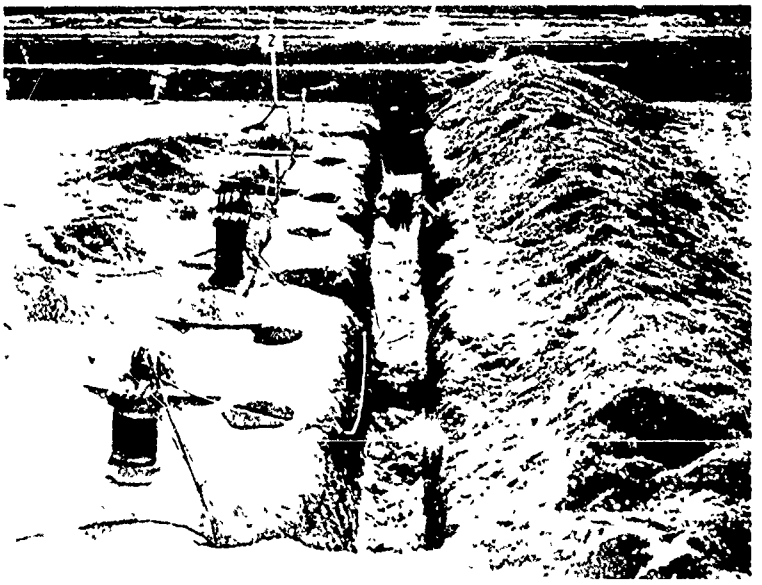

Fig. 6.9 Gage Holes Drilled at Sides of Lateral Cable Trench

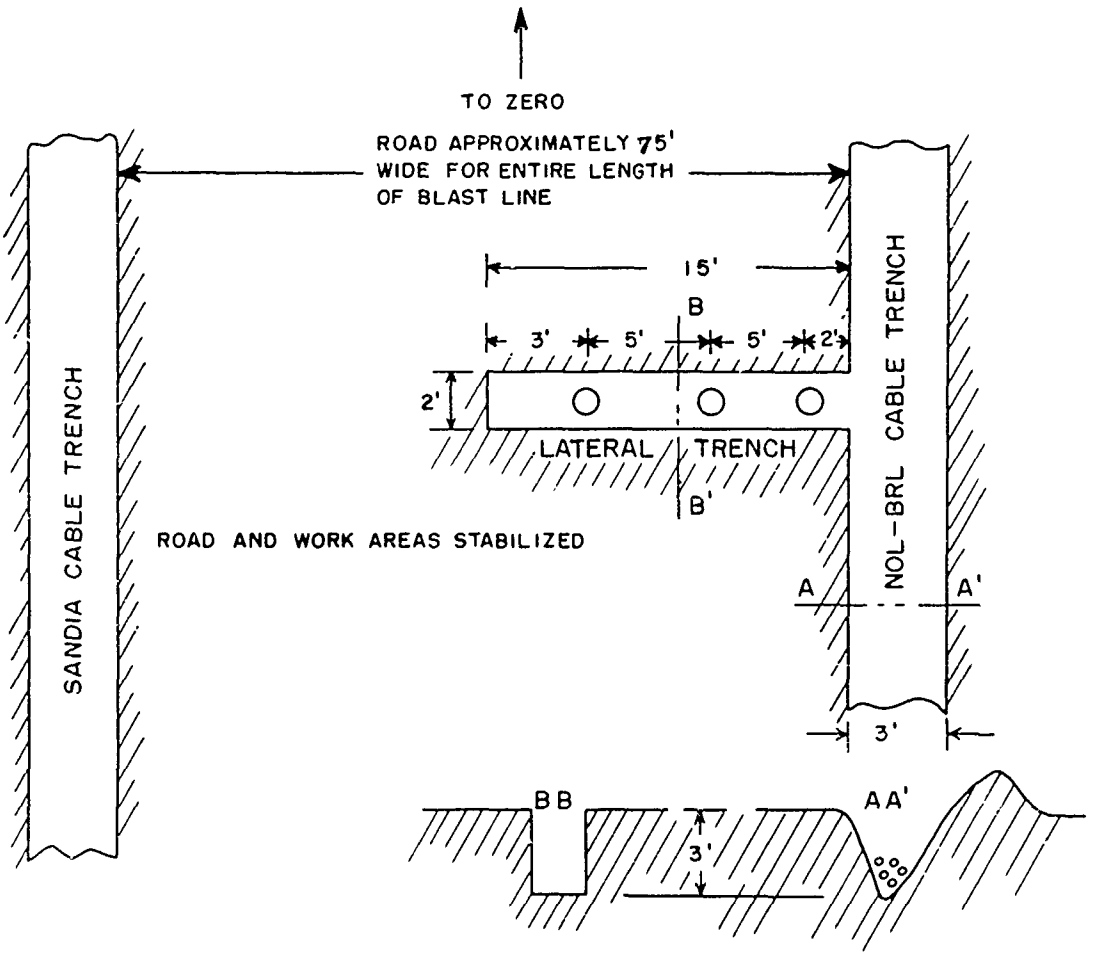


Fig. 6.10 Details of a Typical Station on NOL - BRL Blast Line

Fig. 6.11 View Along Blast Line

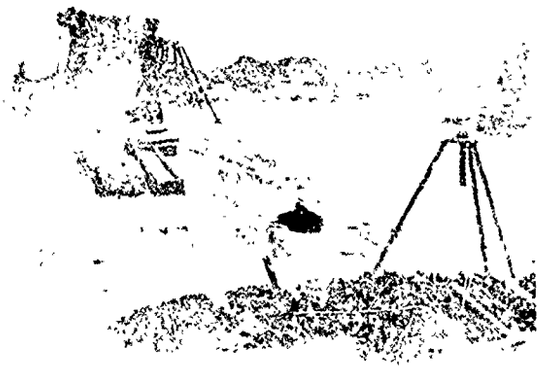

Fig. 6.12 Working Conditions in the Dust Along the Blast Line.

[redacted]

CHAPTER 7

# RESULTS AND DISCUSSION

## 7.1 SUCCESS OF THE TESTS

Excellent results were obtained from both the surface and underground shots. Acceleration records were obtained from 75 of the 76 gages installed on the surface shot, and from all of the 80 gages installed on the underground shot. The magnitudes and frequencies of the accelerations were generally within the range of the gages.

## 7.2 ARRANGEMENT OF THE ACCELEROMETERS

As discussed in Chap. 3, acceleration was measured in three components: vertical, horizontal (radial from zero) and transverse (perpendicular to the vertical and horizontal). For the surface shot, there were twelve stations at a depth of 10 ft spaced logarithmically from 275 ft to 3000 ft from zero, and four stations each at depths of 20 ft and 30 ft (see Fig. 3.2 and Table 3.1.) For the underground shot there were thirteen stations at a depth of 10 ft spaced logarithmically from 200 ft to 3000 ft from zero, and four stations each at depths of 20 ft and 30 ft. For both shots there were five transverse stations at a 10 ft depth. Of the 76 accelerometers on the surface shot, 45 were primary gages and 31 were back-up gages. On the underground shot 47 of the 80 accelerometers were primary gages and 33 were back-up gages.

## 7.3 PRESENTATION OF THE DATA

Tracings of most of the original acceleration records (Fig. A.9) and analysis of the results of the 40,000 lb HE test at Yucca Flats (Figs. A.1 to A.8) are contained in Appendix A. Since no previous publication of these records has been made, they are included in this report for comparison with the nuclear shots.

Tracings of all of the original nuclear records are reproduced in Appendix B, which is divided into surface shot records (Figs. B.1 to B.7), and underground shot records (Figs. B.8 to B.14). These

[redacted]



[redacted]

tracings show the horizontal, vertical, and transverse acceleration records as a function of time at the various distances and depths. For a complete list of the tracings, refer to the list of illustrations, Appendix B.

Each record has a designation such as U1-10. The interpretation of this designation is: underground shot, station 1, 10 ft depth. Likewise, record S5-30 would be: surface shot, station 5, 30 ft depth.

All data reduction has been made from the original records. Where there are back-up gages, the best record was used for the analysis, the best record being determined by such things as signal to noise ratio and gage frequency response. In some instances where the range of the primary gage was not adequate to cover the magnitude of the signal, parts of the back-up gage records have been reproduced along with the primary records.

The analysis of the records are presented in the form of graphs at the end of this Chapter. Figures 7.1 to 7.20 are concerned with the surface shot, Figs. 7.21 to 7.40 are concerned with the underground shot, and the underground and surface shots are compared in Figs. 7.41 to 7.43. The data presented in these figures include time of arrival, velocity of propagation, and horizontal, vertical, and transverse acceleration components as a function of distance and depth.

## 7.4 GROUND SHOCK PHENOMENA DEDUCED FROM INSPECTION OF THE ACCELERATION RECORDS

### 7.4.1 Appearance of Acceleration Records

The general form of the acceleration-time records of Appendix B are similar to acceleration records obtained from HE underground tests: close in to zero the acceleration is attributed primarily to the directly propagated ground shock, which is characterized by a short duration record of irregular pulses comprised of many high frequency components; far out the directly propagated shock has become attenuated, and the ground shock is propagated in large part by reflection and refraction from underlying rock strata, and this type of propagation is characterized by a long duration record of periodic low frequency pulses.

### 7.4.2 Ground Shock Induced by Air Blast

Examination of the acceleration records shows that the air blast induced ground shock is responsible for a very important part of the acceleration pattern. As the air blast shock wave produced



[redacted]
Security Information
ATOMIC ENERGY ACT 1946

by the explosion progresses along the ground, it exerts pressure on the ground and the ground is accelerated. The evidence of the existence of this so called air blast acceleration or air blast effect is very clear. On every record there appears a dotted line designated A. B. (air blast). This line represents the arrival time of the air blast shock wave as measured by BRL in their air blast measurements. In every case, a characteristic high frequency pulse of one and one half cycle duration is observed immediately following this line. A plot of the arrival time of this characteristic pulse as a function of distance is identical with a plot of air blast arrival times. This air blast acceleration appears in the records of the three acceleration components - horizontal, vertical and transverse. The air blast induced acceleration was first identified by the NOL group on the 40,000 lb HE test at Yucca Flats, and it is characteristic of a surface or shallow underground shot. Typical air blast acceleration pulses are observed in Fig. B.1, station S1-10; Fig. B.2, station S9-10; and Fig. B.9, station U6-10. Distortions of this typical pattern occur, and this is discussed in Sec. 7.4.5.

### 7.4.3 Reflected and Refracted Ground Shock

On the underground shot, secondary and tertiary ground shock pulses arrive 0.35 and 0.55 sec respectively after the arrival of the initial shock at the nearest station, UA-10 (Figs. B.8 and B.9). Furthermore, the secondary shock arrives at station 2 before it arrives at station 1, and it arrives at station 1 before it arrives at station A. This secondary shock could develop in the explosion or it could be a reflected shock from the underlying rock strata. It is difficult to believe that the explosion process would have a delayed reaction of 0.35 sec, and it is impossible to explain how a directly propagated shock could arrive sooner at a more distant station than a nearer station. Almost certainly this secondary shock is a reflected shock. Further weight is added to this hypothesis by consideration of the arrival times of the vertical and horizontal components (see Sec. 7.5.2).

A reflected shock could travel a greater distance in a shorter time, and thus arrive at station 1 before arriving at the closer distance of station A, if the path to station 1 passed through a higher velocity medium than the path to station A. These secondary pulses were also observed on the 40,000 lb HE shot, but were not observed on the nuclear surface shot. This lends weight to the reflection hypothesis rather than the explosion mechanism hypothesis, since the nuclear weapons were identical. These secondary pulses appearing at the close-in stations are important because they are as great and even greater in magnitude than the primary acceleration



RESTRI[redacted] ENERGY ACT 1946

[redacted]

pulses. Why these pulses are of such magnitude is not understood, for they should suffer considerable attenuation if they travel to bedrock at 1,000 ft down and back again. It indicates that much more of the energy of the explosion is transmitted down than horizontally along the surface and that some focusing action may take place.

### 7.4.4 Recapitulation of the Origins of Ground Shock

Ground acceleration for both the surface and underground shots originates from the following three sources:

(1) Acceleration produced by the ground shock from an explosion and propagated directly from the explosion to the point in question and henceforth called primary acceleration.

(2) Acceleration produced by the ground shock from an explosion which has been reflected and refracted from underlying rock strata and henceforth called secondary acceleration.

(3) Acceleration induced in the ground by the reaction of the ground to air blast and henceforth called air blast acceleration or air blast effect.

For most of the analysis the primary and secondary acceleration are considered as a unit and henceforth will be called fundamental acceleration as distinguished from the air blast acceleration.

### 7.4.5 Superposition of Fundamental Acceleration and Air Blast Acceleration

When the arrival times of the air blast acceleration and a fundamental acceleration pulse coincide at a given distance, these two types of accelerations superimpose on one another and distort their respective wave shapes, and the magnitude of the combined air blast and fundamental acceleration may be greater or less than normal depending on phase considerations. This superposition complicates the analysis, as will be discussed later. A good example of the effect of superposition is illustrated in Fig. B.1, stations S6-10 to S8-10, which shows the distortion and change in amplitude produced on the air blast wave as the fundamental wave overtakes and passes it. This can also be observed in Fig. B.2, stations S3-10 to S7-10, and again in Fig. B.8, stations U4-10 through U8-10.

The normal initial direction for the air blast acceleration is down for the vertical and out for the horizontal component. It is interesting to note th[redacted]obably due to the effect

of superposition the initial direction of the air blast is reversed for a few stations for the horizontal acceleration on the surface shot (Fig. B.1, stations S4-10 through S7-10).

## 7.5 GROUND SHOCK PROPAGATION

### 7.5.1 Surface Shot

The arrival times of the primary ground shock and the air blast are shown in Fig. 7.1. As discussed in Sec. 7.4.2, the arrival times of the air blast and air blast induced acceleration are identical. No detectable vertical acceleration arrived ahead of the air shock out to 800 ft, beyond which it coincides with the horizontal arrival time. Out to 420 ft (3.3 $\lambda$) the air blast precedes the primary ground shock. Closer than 420 ft the primary ground shock arrival time is not known, since it is masked by the air blast effect. While initially the air blast has a greater velocity than that of the primary ground shock, the air blast velocity rapidly decreases and is soon exceeded by the steadily increasing ground shock velocity. Beyond the cross-over point the air shock lags further and further behind the ground shock. The velocity of the primary ground shock (Fig. 7.2) has been derived from the arrival time curve. Normally, as observed from previous underground HE and seismic tests, the velocity of propagation increases with distance from the explosion source, due to the fact that as the distance increases the transmission path is more and more by refraction and reflection from underlying higher velocity strata. An unusual decrease in the velocity of the primary ground shock from the surface shot is observed out to a distance of around 1,200 ft, after which it begins to increase in normal fashion. The velocity of 4,600 ft/sec at 400 ft from zero decreases to 3,500 ft/sec at 1,100 ft, and then rises to 7,900 ft/sec at 2,800 ft. It is interesting to note that ground shock velocity of the 40,000 lb HE shot (Fig. A.3) is very similar to the surface shot.

The ground shock arrival times of Fig. 7.1 are for the initial part of the acceleration curve. The arrival times of several of the corresponding peaks for the surface shot are plotted in Fig. 7.20 and indicate that these particular peaks, which consist of one portion of the acceleration pattern, proceed reasonably well with the same relative velocity. When an acceleration cycle can be identified from one station to the next, it is called a corresponding peak. These corresponding peaks can only be identified for a limited part of the acceleration pattern, and are almost impossible to identify at the close-in stations. Motion of the ground cannot be deduced from Fig. 7.20 (as will be done for the underground shot) since additional extraneous cycles interrupt the [redacted] pattern.

### 7.5.2 Underground Shot

From Fig. 7.21 it is evident that the primary ground shock arrives at the first station, 200 ft from zero, ahead of the air blast and air blast acceleration, which was not the case for the surface shot. This is to be expected, inasmuch as the air blast pressure was much lower than on the surface shot, and therefore the air blast velocity was much less. Extrapolating back to zero, it appears that the ground shock preceded the air blast from zero on out. The velocity of the ground shock (Fig. 7.22) is quite different from the normal situation where the velocity increases with distance from the explosion; in the underground shot the velocity steadily decreases from about 4,780 ft/sec at 200 ft from zero to 3,460 ft/sec at 2,800 ft. For both shots the velocity has the same initial value and decreases to the same value at 1,200 ft from zero, and then the two velocities diverge.

Repeating the procedure of the surface shots, the arrival times of the corresponding peaks for the underground shot are plotted in Fig. 7.40. Again the peaks proceed reasonably well with the same relative velocity. As indicated in the inset of Fig. 7.40, the cyclical pattern is identified and maintained. Following the arrival time pattern at a given distance, the ground motion is out, down, in, and up. This type of motion is propagated as a surface wave, and is termed a "hydrodynamic wave" by Leet[1].

As with the surface shot, this particular wave pattern occurs only for a limited part of the acceleration pattern, and it cannot be identified close in, where it is difficult to identify corresponding peaks. That other types of motion exist can be demonstrated by the second pulse that arrives at the same time of 0.4 sec for both the horizontal and vertical components (Figs. B.8 and B.9, station UA-10). In this instance the shock is in phase for both components, indicating that the ground motion is longitudinal in an upward and outward direction. This lends weight to the hypothesis that this shock is a secondary shock, having been reflected from an underlying strata.

## 7.6 ANALYSIS OF ACCELERATION AS A FUNCTION OF DISTANCE

### 7.6.1 Reasons for the Form of the Analysis

The acceleration records of the surface and underground shots (Appendix B) have a very complex wave form involving many

[1] L. Don Leet, Earth Waves (Harvard University Press), p.51

frequencies, cycles, partial cycles, and superposition of wave patterns. As discussed in Sec. 7.4.4, the record has three sources of acceleration contributing to the acceleration pattern: primary, secondary, and air blast acceleration. These sources of acceleration have their own wave shapes and frequencies, follow different propagation and attenuation laws, and interact among themselves.

Except possibly at distances close to the explosion, it is impossible to differentiate between primary and secondary acceleration, as the two merge into one pattern. Evidence of the secondary shock appears at certain distances where the reflected and refracted shock may feed back to the surface causing a shift or plateau in the acceleration-distance curve. Plateaus which may be due to this secondary shock appear in Figs. 7.3, 7.4, 7.7, and 7.27. The secondary acceleration is very sensitive to the geology of the region, and may influence the acceleration laws differently for different locations. While the desirability of separating primary and secondary acceleration is realized, the inability to distinguish between the two leaves no alternative but to lump them together into the so defined fundamental acceleration.

The air blast acceleration, on the other hand, does maintain its identity in the acceleration pattern, and it definitely follows different attenuation and propagation laws than the fundamental acceleration. Accordingly the air blast effect is separated out in the analysis, and the results are presented with and without air blast effect. Even here it is not simple to separate out the air blast effect, for when interaction occurs with the fundamental acceleration, the magnitude is affected markedly. When interaction is very apparent, that part of the data may be excluded from the analysis. However, this interaction phenomenon can be expected to produce considerable variation or apparent scatter in any acceleration plot. Much of the apparent scatter in the analysis to follow is not due to errors in instrumentation etc., but is caused by the various factors contributing to the total acceleration.

Many pulses and cycles go to make up the acceleration pattern. One peak has no preference over any other peak, so major emphasis was placed on the maximum peak. The first peak, which has sometimes been considered, was usually of small amplitude and was not deemed important except to show the attentuation of the primary acceleration which is often associated with the inital or first peak.

Mention is made of the fact that the $\lambda$ scale used in the plots is based on the assumption that the effective charge weight is

1 kt. ($W^{1/3}$ = 126).

7.6.2 Surface Shot Analysis

As mentioned in the previous section, the air blast acceleration can be identified and the following analysis separates it from the fundamental acceleration; accordingly, the air blast effect is first excluded (Figs. 7.3 to 7.7) and then included (Figs. 7.8 to 7.12). The plot of the first acceleration peak (Fig. 7.3), which is outward horizontal, has a plateau and its slope of 4 is the largest slope of any of the acceleration curves. A plateau is also evident in the maximum inward horizontal acceleration curve (Fig. 7.4) but is not apparent in the maximum outward horizontal curve (Fig. 7.5). Plateaus are evident in the maximum upward and downward vertical acceleration curves (Figs. 7.6 and 7.7), but they do not occur at the same distance. The slopes of these curves excluding air blast vary from 1.0 to 1.7.

Figures 7.8 to 7.12 are curves of the maximum outward and inward horizontal acceleration, maximum upward and downward vertical acceleration, and right and left transverse acceleration, all with air blast effect included. It is clear from inspection of the acceleration records (Figs. B.1 and B.2) that these latter curves with air blast effect included are really plots of the peak of the air blast effect alone, since the maximum fundamental acceleration, in all cases except the horizontal far out, is less than the air blast acceleration. No plateaus are expected or observed, since no secondary acceleration is involved. Slopes of the horizontal and vertical components vary from 1.7 to 2.3. Appreciable transverse acceleration is evident (Fig. 7.12), though it is much less than the horizontal or vertical. The left transverse component is slightly greater than the right component.

The various acceleration curves of the surface shot are combined in several ways in Figs. 7.13 to 7.15. First the air blast effect is excluded and the inward and outward horizontal and upward and downward vertical acceleration are combined in Fig. 7.13. Then the air blast effect is included and the same components are combined in Fig. 7.14. Lastly, the horizontal, vertical, and transverse components with and without the air blast acceleration are combined in Fig. 7.15. Here the inward and outward component are not plotted separately but are combined into an overall maximum horizontal component. Likewise the upward and downward vertical and the right and left transverse have been combined into an overall maximum vertical and maximum transverse acceleration.

The results of the surface shot may be summarized as follows:

(1) With the air blast effect excluded, (Fig. 7.13) the various components tend to follow the same acceleration distance curve, with the exception of the outward horizontal component which is 1.5 to 2 times greater than the others close in ($2.5\lambda$). All components merge at $15\lambda$ and beyond.

(2) With the air blast effect included (Fig. 7.14), the various components again follow a common acceleration curve with the exception of the upward vertical component which is a factor of 2 less than the other components close-in.

(3) One of the most important results is illustrated in Fig. 7.15: the horizontal and vertical air blast acceleration is larger by a factor of 10 to 15 at the close-in distances than the fundamental horizontal and vertical acceleration.

(4) The vertical component of the air blast acceleration is a little larger than the horizontal component, while the horizontal component of the fundamental acceleration is 1.5 times as large as the vertical component at $2\lambda$.

(5) The transverse component is about a factor of 4 less than the other fundamental acceleration components.

(6) All of the acceleration curves attenuate to about the same value far out (beyond $25\lambda$).

(7) The average slope of the air blast acceleration is about 2.2, and the slope of the fundamental acceleration is about 1.2, and it is obvious (Fig. 7.15) that the air blast acceleration attenuates more rapidly than the fundamental acceleration.

### 7.6.3 Underground Shot Analysis

The underground acceleration analysis follows the same order as the surface shot; the air blast effect is first excluded (Figs. 7.23 to 7.27) and then included (Figs. 7.28 to 7.32). A plot of the first outward horizontal acceleration peak (Fig. 7.23) is followed by the maximum inward horizontal acceleration (Fig. 7.24), the maximum outward horizontal (Fig. 7.25), the maximum upward vertical (Fig. 7.26), and the maximum downward vertical acceleration (Fig. 7.27). Plateaus appear in the upward and downward vertical acceleration curves. The slopes of these curves excluding air blast acceleration vary from 1.2 to 1.6 except the upward vertical acceleration curve which starts out at a slope of 2.4.

The maximum acceleration with the air blast included follow in order: maximum inward horizontal (Fig. 7.28), maximum outward horizontal (Fig. 7.29), maximum upward vertical (Fig. 7.30), maximum downward vertical (Fig. 7.31), and maximum transverse (Fig. 7.32). The unusual plateau-like part of the curve for the maximum inward horizontal acceleration (Fig. 7.28), which starts at the closest station (1.6 $\lambda$), may possible be due to interaction between the outward fundamental acceleration and the inward phase of the air blast acceleration, inasmuch as the phenomenon is not observed with the air blast effect excluded. This can be seen in Fig. B.8.

Inspection of the acceleration records for the underground shot (Figs. B.8 and B.9) show that the magnitude of fundamental vertical acceleration is somewhat smaller than the air blast acceleration, while the horizontal acceleration is about the same as the air blast acceleration. The slopes of the horizontal and vertical components with the air blast effect included vary between 1.2 and 1.6. Appreciable transverse acceleration is evident, with the left transverse component being slightly larger than the right, the same as for the surface shot.

The various acceleration curves of the underground shot are combined in several ways in Figs. 7.33 to 7.35. First the air blast effect is excluded and the inward and outward horizontal and the upward and downward vertical acceleration components are combined in Fig. 7.33. Then the same maximum acceleration components with the air blast acceleration included are combined in Fig. 7.34. Lastly, the overall maximum horizontal, vertical, and transverse components with and without the air blast effect are combined in Fig. 7.35, where the overall acceleration is defined for the surface shot.

The results of the underground shot may be summarized as follows:

(1) With the air blast effect excluded (Fig. 7.33), the horizontal and vertical components start [redacted]



[redacted]

the same magnitude at 1.6 $\lambda$, but then the vertical component attenuates more rapidly until at 10 $\lambda$ and beyond the plateau effect brings the components together and they tend to merge beyond 20 $\lambda$. Close in, the outward horizontal is somewhat greater than the inward horizontal, and the upward vertical is somewhat greater than the downward vertical. This same relationship held on the surface shot.

(2) With the air blast acceleration included (Fig. 7.34) the horizontal and vertical components follow a common acceleration curve except the maximum downward vertical component which starts out at about the same value at 1.6 $\lambda$, but at 3 $\lambda$ it has become 1.5 times larger than the other components.

(3) When the air blast effect is included in the acceleration pattern, both the horizontal and vertical components are greater than with the air blast effect excluded (Fig. 7.35). The acceleration with the air blast effect included is nowhere near as large as was the surface shot acceleration, and the difference between acceleration with and without air blast effect is only a factor of between 1.3 and 3 in the region of 1.6 $\lambda$ to 3 $\lambda$. With the air blast acceleration excluded, the overall horizontal acceleration is larger than the vertical acceleration, but with the air blast acceleration included, the vertical acceleration becomes greater than the horizontal.

(4) The transverse acceleration component is appreciable and close in is a factor of 3 or 4 less in magnitude than the horizontal or vertical component.

(5) The slopes of the fundamental acceleration curves (air blast effect excluded) varies between about 1.3 and 2.3, with an average of all the components being around 1.6. With the air blast effect included, the average slope of the acceleration curves is about 1.4. As contrasted to the surface shot, the attenuation factor for the fundamental acceleration is about the same as for the acceleration curve with air blast effect included.

### 7.6.4 Comparison of Acceleration from the Surface Shot with Acceleration from the Underground Shot

All of the horizontal and transverse acceleration components for the surface and underground shots are compared in Fig. 7.41, the vertical components are compared in Fig. 7.42, and all the horizontal, vertical and transverse components are combined in Fig. 7.43. From these graphs a compilation of the values of the acceleration components is presented in the order of their magnitude in Table 7.1

As is evident from Fig. 7.43 and Table 7.1, the acceleration from the surface shot is the largest by a considerable factor, and as shown in the analysis this large acceleration is the air blast induced acceleration. It is logical that the air blast acceleration for the surface shot be larger than the air blast acceleration for the underground shot by a factor of four, because of the fact that the air blast was much greater on the surface shot. That this air blast acceleration is a factor of as much as eighteen greater than the fundamental (air blast effect excluded) acceleration on the surface shot, and a factor of seven greater than the fundamental acceleration on the underground shot is surprising and unexpected.

When only the fundamental acceleration is considered (and most of the previous underground tests have considered only this), a true comparison is obtained between a surface shot and a shallow underground shot as a means of transmitting a ground shock through the ground. From Table 7.1 this comparison is made by considering the acceleration for the surface and underground shot with the air blast effect excluded, and it is found that at $2\lambda$ the horizontal and vertical components for the surface shot are larger by factors of 1.8 and 2.7 respectively than the corresponding components for the underground shot.

As previously observed, the transverse components are considerably less than the horizontal and vertical components, and it is further evident from Fig. 7.43 that at $3\lambda$ the transverse acceleration for the underground shot is larger by a factor of 1.8 than for the surface shot.

From the comparison of the underground and surface shots, it would appear that the surface shot would be much more effective since it produces by far the greatest acceleration. This coupled with the much larger air blast would indicate in no uncertain terms that the surface shot is preferred. This is probably the correct conclusion; however, the advantage of the surface shot is due to the air blast acceleration, and this is a high frequency, short duration pulse.

TABLE 7.1

Compilation of the Magnitudes of Acceleration Components at Several Distances for the Surface and Underground Shots

| Surface Shot -S<br>Underground Shot -U | Horizontal -H<br>Vertical -V<br>Transverse -T | Including Air Blast Effect -I<br>Excluding Air Blast Effect -X | Acceleration G Units | | | | | |
|---|---|---|---|---|---|---|---|---|
| | | | 1.6λ | 2λ | 3λ | 4λ | 10λ | 25λ |
| S | V | I | | 16 | 7.2 | 4.1 | 6.1 | 0.11 |
| S | H | I | | | 6.2 | 3.6 | 0.47 | .066 |
| U | V | I | 4.6 | 4.0 | 2.8 | 1.9 | 0.56 | 0.17 |
| U | H | I | 4.8 | 3.2 | 1.8 | 1.2 | 0.31 | .080 |
| U | H | X | 3.6 | 2.5 | 1.5 | 1.0 | 0.31 | .088 |
| U | V | X | 4.4 | 2.4 | 0.88 | 0.54 | 0.22 | .088 |
| S | H | X | | 1.4 | 0.90 | 0.66 | 0.26 | .080 |
| S | V | X | | 0.9 | 0.60 | 0.47 | 0.20 | .088 |
| U | T | I | | | 0.46 | 0.35 | 0.14 | .060 |
| S | T | I | | | 0.26 | 0.21 | 0.11 | .060 |

If it should turn out that from a damage standpoint this air blast acceleration was not important, then the underground shot, which has an advantage of two or more in fundamental acceleration over the surface shot, may prove to be the most effective. It might also be mentioned that the overall frequency pattern for the underground shot is considerably lower than that of the surface shot. This is discussed more fully in Sec. 7.8.2 and 7.8.3. Correlation with damage to structures will give the final answer as to the effectiveness of a surface vs an underground shot.

### 7.6.5 Attenuation of Air Blast Acceleration

Inasmuch as the air blast acceleration is due entirely to the air blast, it follows that the two should attenuate in similar fashion. To test this, the air blast peak pressure measured by BRL, was compared to the air blast acceleration and is presented in Table 7.2.

TABLE 7.2

Comparison of Air Blast and Air Blast Acceleration for the Surface and Underground Shots

| | Surface Shot | | | Underground Shot | | |
|---|---|---|---|---|---|---|
| $\lambda$ | Air Bl. (psi) | Air Bl.Accel. (G) | Air Blast / Air Bl.Accel. (psi/G) | Air Bl. (psi) | Air Bl.Accel. (G) | Air Blast / Air Bl.Accel. (psi/G) |
| 3 | 110 | 6.4 | 17.4 | 26.0 | 2.95 | 8.8 |
| 4 | 60.0 | 3.8 | 16.2 | 16.5 | 2.07 | 7.8 |
| 5 | 34.0 | 2.0 | 17.0 | 12.5 | 1.50 | 8.3 |
| 6 | 21.5 | 1.35 | 15.9 | 10.0 | 1.12 | 8.9 |
| 7 | 15.0 | 0.96 | 15.6 | 8.3 | 0.86 | 9.6 |
| 8 | 11.2 | 0.70 | 16.0 | 7.1 | 0.70 | 10.1 |
| 10 | 7.0 | 0.42 | 16.6 | 5.6 | 0.48 | 11.7 |
| 15 | 3.5 | 0.17 | 20.6 | | | |
| 20 | 2.2 | 0.09 | 24.4 | | | |

The ratio of air blast to acceleration shows remarkable agreement out to 10 $\lambda$. This is further evidence that the air blast acceleration is produced by the air blast in accordance with Newton's second law (acceleration proportional to force). The constancy of the ratio proves that the air blast acceleration attenuates the same as the air blast. The interesting fact that the average ratio of 16.4 for the



SECRET
Information
RESTRICTED DATA
ATOMIC ENERGY ACT 1946

surface shot differs from the average ratio of 9.3 for the underground shot indicates that more efficient coupling of air blast to ground shock occurs for the underground shot. The reason for this is not known.

The constancy of the ratio of air blast to acceleration suggests a way to predict the air blast acceleration if the air blast is known. Further study for different charge weights at different depths is suggested.

## 7.7. STUDY OF ACCELERATION AS A FUNCTION OF DEPTH

### 7.7.1 Surface Shot

In addition to the measurements at the 10 ft depths, acceleration measurements were made at depths of 20 ft and 30 ft at stations 2 (340 ft from zero), 5 (642 ft), 8 (1213 ft), and 10 (1890 ft). Tracings of the acceleration records at the 10, 20, and 30 ft depths are reproduced in Figs. B.6 and B.7. As can be seen, the characteristic of the acceleration curves repeat remarkably well at the different depths. The horizontal and vertical acceleration as a function of depth is presented in Figs. 7.16 to 7.19. The horizontal acceleration component shows no variation with depth when the air blast effect is excluded (Fig. 7.16), but gives an indication of decrease with depth when the air blast effect is included in the analysis (Fig. 7.18). With the air blast effect excluded (Fig. 7.17), the vertical acceleration component shows a definite decrease at station 2, the nearest station, and with the air blast effect included (Fig. 7.19) there is an even greater decrease at station 2, and an indication of a decrease at stations 5 and 8.

### 7.7.2 Underground Shot

Identical depth measurements were made on the underground shot, and are presented in Figs. 7.36 to 7.39. Tracings of the acceleration records at the various depths are reproduced in Figs. B.13 and B.14. With the air blast effect excluded (Fig. 7.36) the horizontal acceleration component shows no variation with depth, but with the air blast effect included in the analysis (Fig. 7.38), stations 2 and 5 show a decrease of acceleration with depth. Station 5 curiously shows a greater depth decrease than the nearer station 2. With the air blast effect excluded (Fig. 7.37), the vertical acceleration decreases considerably with depth at station 2, and slightly at station 5. With the air blast effect included (Fig. 7.39),

the vertical acceleration shows considerable decrease with depth at station 2.

### 7.7.3 Summary of Depth Studies for the Surface and Underground Shots

At the close-in distances, a definite decrease of acceleration with depth is noted. The vertical component shows more of a decrease than the horizontal component, and a greater depth effect is noted with the air blast acceleration than with the fundamental acceleration. This is to be expected, since the air blast is incident on the surface of the ground, and rapidly attenuates with depth. At the far out distances (station 8 and beyond), no variation of acceleration with depth is observed. The downward vertical component is larger than the upward component when the air blast acceleration is included, and the upward component is larger when the air blast acceleration is excluded.

In any case, whether horizontal or vertical components, the largest acceleration occurs at the depth nearest the ground surface. Because the earth near the surface is more loosely packed and of lower density, and because the movement of the earth can be relieved at the surface, there is effectively a weaker restoring force at the surface. This results in a greater acceleration being produced at the surface than at a deeper depth in the ground.

## 7.8 GROUND SHOCK FREQUENCIES

### 7.8.1 General Comments on Acceleration Record Frequencies

The discussion of the frequencies associated with the nuclear explosions is complicated by the complex nature of the acceleration records, which consist of full cycles, half cycles, and square wave transient type pulses having many high frequency components. A Fourier analysis would be necessary to give the complete frequency spectrum. In the analysis to follow, the high frequencies have been ignored and the more fundamental low frequency waves have been considered. More often than not, half cycles and pulse durations are interpreted as frequency, even though these transient cycles do not repeat themselves. By defining frequency in this loose sense, certain conclusions become evident and are discussed.

### 7.8.2 Comparison of Surface Shot and Underground Shot Frequencies

The characteristic frequencies associated with the surface shot are tabulated in Table 7.3. The air blast acceleration frequencies

Table 7.3

Tabulation of Surface Shot Frequencies and Associated Accelerometer Characteristics

| Sta. | Gage | Accelerometer | | | Ground Acceleration | |
|---|---|---|---|---|---|---|
| | | $\beta$ Coeff. of Damping | $f_o$ Undamped Natural Frequency (cps) | f Damped Natural Frequency (cps) | Air Blast Acceleration Frequency (cps) | Fundamental Acceleration Frequency (cps) |
| 1-10 | 20H14 | 0.54 | 138.0 | 115.8 | ---- | 10.0 |
| | 3H19 | 0.44 | 53.1 | 47.7 | ---- | 6.0 |
| | 20V4 | 0.54 | 138.0 | 116.7 | 58.2 | ---- |
| | 3V19 | 0.47 | 55.5 | 48.9 | 41.3 | 9.5 |
| 2-10 | 20H11 | 0.52 | 140.0 | 119.3 | 71.5 | 10.0 |
| | 3H20 | 0.48 | 54.3 | 47.7 | ---- | 4.7 |
| | 10V2 | 0.54 | 96.8 | 81.6 | ---- | ---- |
| | 0.5H26 | 0.51 | 22.1 | 19.0 | 38.2 | 10.9 |
| 2-20 | 10H16 | 0.62 | 102.0 | 80.4 | 71.5 | 5.5 |
| | 20V1 | 0.52 | 149.0 | 127.2 | 38.6 | ---- |
| | 3V16 | 0.48 | 54.0 | 47.4 | 33.8 | 10.8 |
| 2-30 | 10H10 | 0.54 | 100.0 | 84.2 | ---- | 5.7 |
| | 3H23 | 0.44 | 54.2 | 48.6 | 83.0 | 3.4 |
| | 10V5 | 0.59 | 101.0 | 81.5 | ---- | ---- |
| | 3V17 | 0.45 | 52.9 | 47.3 | ---- | ---- |
| 3-10 | 10H9 | 0.54 | 104.8 | 88.3 | ---- | ---- |
| | 1H4 | 0.63 | 30.2 | 23.3 | ---- | 19.4 - 4.6 |
| | 10V4 | 0.65 | 107.0 | 81.0 | 36.2 | ---- |
| | 1V2 | 0.49 | 31.0 | 26.9 | 36.2 | 16.6 |
| 4-10 | 3H1 | 0.50 | 52.8 | 45.8 | ---- | ---- |
| | 1H8 | 0.65 | 28.9 | 21.8 | ---- | 16.2 |
| | 3V20 | 0.52 | 53.9 | 46.0 | 36.7 | 6.4 |
| | 1V18 | 0.66 | 31.2 | 23.4 | 36.7 | 25.0 - 6.2 |

Table 7.3 (Continued)

| Sta. | Gage | Accelerometer | | | Ground Acceleration | |
|---|---|---|---|---|---|---|
| | | $\zeta$ Coeff. of Damping | $f_o$ Undamped Natural Frequency (cps) | $f$ Damped Natural Frequency (cps) | Air Blast Acceleration Frequency (cps) | Fundamental Acceleration Frequency (cps) |
| 5-10 | 3H4 | 0.51 | 53.8 | 45.7 | ---- | ---- |
| | 3V4 | 0.43 | 55.0 | 49.6 | ---- | ---- |
| | 1V3 | 0.71 | 29.1 | 20.5 | 35.0 | 12.6 - 6.4 |
| | 0.1H3 | 0.48 | 11.1 | 9.75 | ---- | 8.5 |
| 5-20 | 3H3 | 0.50 | 54.0 | 46.6 | ---- | 12.7 - 4.8 |
| | 1H20 | 0.66 | 31.1 | 23.4 | ---- | 12.7 - 4.8 |
| | 3V14 | 0.49 | 52.5 | 45.8 | 41.5 | ---- |
| | 1V20 | 0.51 | 28.2 | 24.3 | 41.5 | 6.1 |
| 5-30 | 3H8 | 0.38 | 57.8 | 53.4 | 36.8 | ---- |
| | 1H6 | 0.68 | 29.2 | 21.5 | 33.0 | ---- |
| | 3V7 | 0.46 | 53.5 | 47.4 | 44.6 | 6.4 |
| 6-10 | 3H9 | 0.39 | 56.8 | 52.4 | 31.0 | ---- |
| | 0.5H25 | 0.53 | 20.4 | 17.2 | 25.5 | 13.9 - 5.1 |
| | 3V1 | 0.45 | 54.2 | 48.4 | 53.7 | 9.1 |
| | 0.5V26 | 0.59 | 21.0 | 16.9 | ---- | 11.0 |
| 7-10 | 1H11 | 0.62 | 29.5 | 23.2 | 36.2 | 11.2 |
| | 0.5H21 | 0.58 | 20.4 | 16.6 | 32.3 | 10.7 |
| | 1V10 | 0.64 | 30.3 | 23.2 | 23.0 | 10.0 |
| | 0.5V9 | 0.44 | 21.6 | 19.4 | 21.2 | 9.2 |
| 8-10 | 1H9 | 0.60 | 30.0 | 24.0 | ---- | 11.8 |
| | 0.5H20 | 0.51 | 21.0 | 18.0 | ---- | 11.8 |
| | 1V13 | 0.60 | 31.0 | 24.8 | 19.7 | 20.4 - 8.1 |
| | 0.1H22 | 0.35 | 9.9 | 9.29 | ---- | 10.4 |
| 8-20 | 1H21 | 0.59 | 30.0 | 24.3 | ---- | 11.8 |
| | 1V11 | 0.60 | 31.0 | 24.9 | 17.1 | 17.4 - 8.8 |
| | 0.5V20 | 0.51 | 20.9 | 18.0 | 14.5 | 16.9 - 8.8 |

Table 7.3 (Continued)

| Sta. | Gage | Accelerometer | | | Ground Acceleration | |
|---|---|---|---|---|---|---|
| | | $\beta$ Coeff. of Damping | $f_o$ Undamped Natural Frequency (cps) | f Damped Natural Frequency (cps) | Air Blast Acceleration Frequency (cps) | Fundamental Acceleration Frequency (cps) |
| 8-30 | 1H7 | 0.62 | 29.6 | 23.3 | ---- | 12.3 - 5.0 |
| | 0.5H12 | 0.54 | 21.2 | 17.9 | ---- | 11.8 - 5.0 |
| | 1V9 | 0.59 | 32.2 | 26.1 | 20.0 | ---- |
| | 0.5V12 | 0.54 | 21.7 | 18.3 | 20.0 | 15.9 |
| 9-10 | 0.5H4 | 0.49 | 21.2 | 18.4 | ---- | 14.0 |
| | 0.1H4 | 0.46 | 10.6 | 9.41 | ---- | 8.3 |
| | 0.5V3 | 0.63 | 20.0 | 16.1 | 20.4 | 16.8 |
| | 0.1V16 | 0.38 | 11.8 | 10.9 | 20.4 | 10.8 |
| 10-10 | 0.5H9 | 0.50 | 21.5 | 18.6 | ---- | 12.7 |
| | 0.5V8 | 0.57 | 20.9 | 17.2 | 32.3 | 13.9 |
| | 0.1V14 | 0.30 | 11.3 | 10.8 | ---- | 12.7 - 5.5 |
| | 0.1H19 | 0.52 | 10.6 | 9.05 | ---- | 7.4 |
| 10-20 | 0.5H7 | 0.52 | 21.5 | 18.4 | ---- | 10.9 - 3.6 |
| | 0.1H8 | 0.35 | 11.4 | 10.7 | ---- | 10.9 - 3.6 |
| | 0.5V6 | 0.50 | 21.2 | 18.4 | ---- | 12.4 |
| | 0.1V4 | 0.59 | 10.4 | 8.4 | ---- | 13.0 - 4.8 |
| 10-30 | 0.5H11 | 0.54 | 22.3 | 18.8 | ---- | 3.6 |
| | 0.1H26 | 0.51 | 10.2 | 8.75 | ---- | 11.0 |
| | 0.5V11 | 0.53 | 22.75 | 19.3 | ---- | 12.9 - 7.3 |
| 11-10 | 0.5H8 | 0.64 | 21.0 | 16.2 | ---- | 5.8 |
| | 0.1H24 | 0.50 | 10.0 | 8.65 | ---- | 5.8 - 6.4 |
| | 0.5V7 | 0.64 | 21.6 | 16.5 | 37.0 | 20.4 - 9.3 |
| | 0.1V6 | 0.27 | 12.3 | 11.8 | ---- | 17.8 - 7.1 |
| 12-10 | 0.5H13 | 0.53 | 22.1 | 18.7 | ---- | 6.7 |
| | 0.1H14 | 0.40 | 11.7 | 10.7 | ---- | 6.7 - 7.8 |
| | 0.5V13 | 0.55 | 21.5 | 17.9 | 35.7 | 6.25 |
| | 0.1H16 | 0.40 | 9.42 | 8.62 | ---- | 7.2 |

Table 7.4

Tabulation of Underground Shot Frequencies and Associated Accelerometer Characteristics

| Sta. | Gage | Accelerometer | | | Ground Acceleration | |
|---|---|---|---|---|---|---|
| | | $\beta$ Coeff. of Damping | $f_o$ Undamped Natural Frequency (cps) | $f$ Damped Natural Frequency (cps) | Air Blast Acceleration Frequency (cps) | Fundamental Acceleration Frequency (cps) |
| A-10 | 38H3 | 0.59 | 179.0 | 144.3 | 40.0 | 3.4 |
| | 10H1 | 0.39 | 102.0 | 93.7 | 34.5 | 3.4 |
| | 38V3 | 0.56 | 176.0 | 146.1 | ---- | 6.2 |
| | 10V7 | 0.45 | 100.0 | 89.2 | 59.0 | 6.8 |
| 1-10 | 38H5 | 0.62 | 174.0 | 136.9 | 30.3 | 4.0 |
| | 10H5 | 0.61 | 93.0 | 73.9 | 30.3 | 4.0 |
| | 38V2 | 0.60 | 177.0 | 141.4 | 55.6 | 8.7 |
| | 10V16 | 0.58 | 100.0 | 81.2 | 55.6 | 8.7 |
| 2-10 | 20H2 | 0.54 | 140.0 | 118.0 | 42.0 | 4.0 |
| | 10H3 | 0.61 | 93.5 | 74.1 | 40.0 | 4.0 |
| | 20V5 | 0.52 | 138.0 | 117.6 | 32.4 | 3.4 |
| | 1H3 | 0.56 | 30.2 | 25.0 | 32.3 | 3.5 |
| 2-20 | 20H3 | 0.52 | 139.0 | 123.1 | 34.0 | 4.5 |
| | 20V3 | 0.52 | 143.0 | 122.4 | 24.6 | 3.1 |
| | 10V15 | 0.58 | 103.0 | 83.7 | 20.8 | 3.0 |
| 2-30 | 10H11 | 0.60 | 99.0 | 79.4 | ---- | 4.2 |
| | 3H11 | 0.51 | 55.0 | 47.3 | ---- | 4.4 |
| | 10V11 | 0.66 | 105.0 | 79.0 | ---- | --- |
| | 3V9 | 0.52 | 53.5 | 45.8 | 21.4 | 3.3 |
| 3-10 | 10H12 | 0.75 | 95.0 | 62.5 | 35.7 | 4.4 |
| | 3H14 | 0.47 | 55.0 | 48.6 | 41.7 | 4.4 |
| | 10V13 | 0.64 | 90.0 | 69.4 | 35.7 | 8.7 |
| | 3V11 | 0.46 | 55.0 | 48.8 | 35.7 | 8.7 |

Table 7.4 (Continued)

| Sta. | Gage | Accelerometer | | | Ground Acceleration | |
|---|---|---|---|---|---|---|
| | | $\zeta$ Coeff. of Damping | $f_o$ Undamped Natural Frequency (cps) | $f$ Damped Natural Frequency (cps) | Air Blast Acceleration Frequency (cps) | Fundamental Acceleration Frequency (cps) |
| 4-10 | 10H6 | 0.62 | 100.0 | 78.9 | 50.0 | 4.4 |
| | 3H17 | 0.51 | 54.5 | 46.8 | 50.0 | 4.2 |
| | 10V3 | 0.62 | 105.0 | 82.4 | 50.0 | 6.2 |
| | 3V3 | 0.45 | 56.5 | 50.4 | 45.5 | 6.2 |
| 5-10 | 3H12 | 0.39 | 53.5 | 49.3 | 42.0 | 4.7 |
| | 3V10 | 0.43 | 58.5 | 52.9 | 34.5 | 4.8 |
| | 1V6 | 0.69 | 29.0 | 21.1 | 19.3 | 5.9 |
| | 0.5H14 | 0.53 | 20.8 | 17.6 | 45.0 | 6.8 |
| 5-20 | 10H8 | 0.62 | 98.5 | 77.5 | 36.0 | 4.4 |
| | 3H10 | 0.50 | 52.2 | 45.5 | 29.4 | 4.7 |
| | 10V17 | 0.62 | 102.0 | 79.8 | ---- | 5.8 |
| | 3V12 | 0.52 | 54.0 | 46.2 | 18.5 | 5.6 |
| 5-30 | 10H14 | 0.63 | 99.8 | 77.1 | ---- | 4.3 |
| | 3H15 | 0.45 | 55.0 | 49.2 | ---- | 4.6 |
| | 10V14 | 0.63 | 101.0 | 78.7 | ---- | --- |
| 6-10 | 3H5 | 0.50 | 54.2 | 46.9 | 53.0 | 4.3 |
| | 1H5 | 0.68 | 28.3 | 20.7 | 53.0 | 4.3 |
| | 3V5 | 0.50 | 55.8 | 48.4 | 33.4 | 6.6 |
| | 1V4 | 0.68 | 28.4 | 20.7 | 24.4 | 6.6 |
| 7-10 | 3H16 | 0.38 | 56.0 | 51.7 | 71.0 | 4.4 |
| | 0.5H15 | 0.52 | 20.6 | 17.6 | 35.5 | 4.4 |
| | 3V13 | 0.44 | 57.0 | 51.3 | 43.5 | 6.1 |
| | 0.5V14 | 0.58 | 21.8 | 17.7 | 27.0 | 6.5 - 10.3 |

Table 7.4 (Continued)

| Sta. | Gage | Accelerometer | | | Ground Acceleration | |
|---|---|---|---|---|---|---|
| | | $\beta$ Coeff. of Damping | $f_o$ Undamped Natural Frequency (cps) | $f$ Damped Natural Frequency (cps) | Air Blast Acceleration Frequency (cps) | Fundamental Acceleration Frequency (cps) |
| 8-10 | 1H14 | 0.66 | 30.2 | 22.8 | 53.0 | 4.0 - 6.9 |
| | 0.5H17 | 0.51 | 22.7 | 19.5 | 50.0 | 4.0 - 6.9 |
| | 1V14 | 0.72 | 29.4 | 20.3 | 28.4 | 5.5 |
| | 0.1H17 | 0.41 | 10.0 | 9.1 | ---- | --- |
| 8-20 | 1H16 | 0.68 | 27.4 | 20.0 | ---- | 3.9 - 5.5 |
| | 1V15 | 0.73 | 29.4 | 20.2 | 22.2 | 4.3 - 2.5 |
| | 0.5V16 | 0.51 | 23.0 | 19.8 | 21.0 | 4.2 - 3.0 |
| 8-30 | 1H13 | 0.78 | 28.9 | 17.9 | ---- | 4.3 |
| | 0.5H16 | 0.51 | 21.3 | 18.3 | ---- | 4.4 |
| | 1V12 | 0.68 | 30.8 | 22.6 | 29.2 | 4.4 - 2.65 |
| | 0.5V15 | 0.56 | 22.1 | 18.4 | 25.0 | 5.7 - 2.2 |
| 9-10 | 1H17 | 0.67 | 28.6 | 21.2 | 34.0 | 3.7 - 7.0 |
| | 0.5H18 | 0.53 | 22.7 | 19.2 | 29.2 | 3.8 - 4.9 |
| | 1V16 | 0.66 | 29.5 | 22.1 | 25.6 | 6.0 |
| | 0.5V17 | 0.49 | 22.5 | 19.7 | 24.0 | 4.7 |
| 10-10 | 1H18 | 0.66 | 31.1 | 23.3 | 36.0 | 3.8 |
| | 1V17 | 0.74 | 28.7 | 19.3 | 30.0 | 3.7 - 3.5 |
| | 0.5V25 | 0.52 | 29.1 | 24.9 | 25.6 | 3.3 - 2.6 |
| | 0.1H13 | 0.47 | 10.1 | 8.9 | ---- | --- |
| 10-20 | 1H12 | 0.72 | 28.9 | 20.1 | 42.0 | 3.5 |
| | 0.5H3 | 0.55 | 21.1 | 17.7 | 37.0 | 3.5 |
| | 1V5 | 0.66 | 29.4 | 22.2 | 24.0 | 3.3 |
| | 0.5V1 | 0.48 | 21.5 | 18.9 | 20.0 | 3.3 |

Table 7.4 (Continued)

| Sta. | Gage | Accelerometer | | | Ground Acceleration | |
|---|---|---|---|---|---|---|
| | | $\beta$ Coeff. of Damping | $f_o$ Undamped Natural Frequency (cps) | $f$ Damped Natural Frequency (cps) | Air Blast Acceleration Frequency (cps) | Fundamental Acceleration Frequency (cps) |
| 10-30 | 1H19 | 0.77 | 28.4 | 18.0 | 26.0 | 3.7 - 2.4 |
| | 0.5H30 | 0.13 | 20.0 | 15.6 | 26.0 | 3.6 - 2.4 |
| | 1V19 | 0.60 | 31.4 | 25.2 | 22.2 | 2.8 |
| 11-10 | 0.5H1 | 0.42 | 23.1 | 21.0 | 24.0 | 3.3 - 2.7 |
| | 0.1H18 | 0.47 | 10.1 | 8.9 | ---- | 3.2 - 2.7 |
| | 0.5V18 | 0.54 | 21.4 | 17.3 | 21.8 | 4.6 |
| | 0.1V12 | 0.27 | 10.3 | 5.2 | 13.7 | 3.3 - 9.5 |
| 12-10 | 0.5H24 | 0.46 | 22.1 | 19.7 | 23.0 | 3.1 - 2.7 |
| | 0.1H36 | 0.63 | 10.1 | 7.8 | ---- | 3.0 - 2.6 |
| | 0.5V24 | 0.50 | 22.7 | 19.7 | 19.6 | 3.3 |
| | 0.1H1 | 0.47 | 9.4 | 8.3 | ---- | --- |

vary primarily from 20 to 40 cps. The frequencies associated with the fundamental acceleration vary primarily from 5 to 16 cps, with a predominance of frequencies in the 10 to 14 cycle range.

The characteristic frequencies associated with the underground shot are tabulated in Table 7.4. The air blast frequencies vary from 20 to 55 cps, and the fundamental acceleration frequencies vary from 3 to 6 cps.

The air blast frequencies are about the same for each shot. A definite difference in fundamental frequencies is noted between the two shots, with the underground shot having frequencies lower by a factor of two or three.

### 7.8.3 Implications of the Frequency Analysis

In the analysis of acceleration from both the surface and underground shots (Sec. 7.6.4), the air blast acceleration was observed to be considerably greater than the fundamental acceleration. The fact that the surface shot acceleration is much greater than that of the underground shot is due to the predominance of the air blast acceleration which occurs on the surface shot. When damage to structures is considered, it is also important to consider the frequencies involved; since the air blast frequencies as tabulated in Sec. 7.8.2 are much higher than the fundamental frequencies, it might well be that the short duration, high frequency pulses are not very important in producing damage to structures even though they are of greater magnitude. If this is so, then the effectiveness of the surface and underground shot should be compared from the standpoint of the fundamental acceleration. Here again, the fact that the underground fundamental frequencies are a factor of two to three lower than surface shot fundamental frequencies may be important when considering response of structures.

## 7.9 GAGE FREQUENCIES AND THEIR INFLUENCE ON THE RECORDING OF ACCELERATION

The steady state theory of accelerometers is well known, and the relationship of response and phase as a function of frequency are illustrated in Fig. 7.44. The majority of the gages (Tables 7.3 and 7.4) turned out to have a damping coefficient, $\beta$, between 0.5 and 0.6 critical at the underground temperatures that were obtained. Figure 7.44 indicates that in this range of $\beta$, $(c/c_0)$ the output of the gage, will have an error of between 5 per cent and 10 per cent for a signal frequency up to 0.8 the natural frequency of the gage. (For an

accelerometer to reproduce a signal without error the signal frequency should be less than 0.2 the gage frequency.) When the signal frequency equals the gage frequency ($\omega/p = 1$), the output error is between 10 per cent and 20 per cent, and this error increases rapidly as the signal to gage frequency increases. In reality, when the signal frequency is equal to the gage frequency the accelerometer becomes a velocity meter according to theory, though it may still be considered an accelerometer with considerable error in phase and amplitude.

The acceleration records more often than not are transient in nature, which if idealized would vary between a half sine wave to a square step wave. Unfortunately, much less is known concerning the response of accelerometers to transient excitation. Figure 7.45[2] presents accelerometer response for several types of transient accelerations. This transient analysis shows that for damping between 0.5 and 0.6 critical, the transient pulses are reproduced fairly well for a pulse duration up to 3 times the natural period of the gage (pulse frequency 1/6 the gage frequency). When the pulse duration is equal to the gage period (pulse frequency 1/2 gage frequency), considerable error in gage response results along with phase distortion; inspection of the curves for half sine wave, triangular, and square excitation indicates that the error in gage response could be as much as 10 to 20 per cent in this case. No information is available for a transient pulse frequency equal to the natural frequency of the gage, but response error up to 50 per cent would not be improbable.

The importance of gage frequency in relation to the frequencies of the acceleration records is apparent when the two are compared in Tables 7.3 and 7.4. It can be seen that the frequency of the transient air blast pulse equals or surpasses the gage frequency in a number of cases; particularly is this true at some distances from zero where low frequency gages were installed. In these cases, the phase and amplitude errors will be large. One consequence of this, whereby the error increases with distance for the air blast acceleration case, is that the air blast acceleration attenuation appears to be greater than it really is.

The frequency relationship is much more favorable for the so-called fundamental acceleration. For the surface shot there are a fair number of cases wherein the signal frequency is 1/2 or more that of the gage frequency, and here the error might be as high as 30 per cent.

---

[2] From Levy and Kroll, Response of Accelerometers to Transient Accelerations. Research Paper 2138 Jour. of Res. Nat. Bur. Stand. 45, Oct 1950.

The frequency relationship is most favorable for the fundamental acceleration frequency on the underground shot. Practically all of the record frequencies are less than 1/3 the natural frequency of the accelerometer, and so, in general, the true acceleration is faithfully reproduced.

Mention is again made that the frequencies tabulated in Tables 7.3 and 7.4 are the low frequency components of the records. There are many high frequency components that will be poorly resolved and reproduced, if at all. This is not serious since these higher frequencies are of little importance from the structural response standpoint.

As explained in Chap. 3, a large number of back-up gages were used to increase the range of acceleration that could be recorded. The back-up and primary gage were, of course, of different ranges and therefore had different natural frequencies. In almost all cases the acceleration was identically reproduced by both gages, within the limitations of range and frequency. This was good evidence of the proper functioning of the gages. Examples of records of primary and back-up gages on the surface and underground shots are presented in Figs. B.4, B.5, B.11, and B.12.

## 7.10 SCALING OF HE AND NUCLEAR CHARGES

### 7.10.1 General Difficulties in Scaling

The problem of scaling ground acceleration from an underground or surface shot is complicated by many factors. In the first place, the three types of acceleration, primary, secondary, and air blast (defined in Sec. 7.4.4) obey different laws of propagation, attenuation, and scaling. In the second place, the non-homogeneous nature of the ground introduces variability in the data and confuses attempts to discover laws of propagation or scaling. In the third place, the interaction of the air blast acceleration with the fundamental acceleration produces abnormal effects which distort any acceleration curve that is plotted. In the fourth place, the secondary reflected and refracted ground shock distorts the directly propagated primary shock, producing plateaus in the acceleration curves and affecting their decay with distance.

As originally pointed out by Lampson, ground shock laws are very dependent on the type of soil. The Lampson Eq.2.1 accommodated this variation by incorporating a soil constant, k, which varied by as much as a factor of 100 for different soils. As the result of the

Dugway and Yucca Flats underground HE tests, the dependence on soil and geological conditions is even more pronounced, since the rate of decay is affected in addition to the magnitude of the acceleration. Due to this great dependence on soil and geological conditions. considerations of scaling must be confined to experiments conducted at the same location. This means that for the Yucca Flats site, we have only one surface HE shot and two HE underground shots at the scale depth of the nuclear underground shot upon which to base scaling. These are not enough shots to base sound conclusions.

7.10.2 Scaling for the Underground Shot

The prediction for the underground shot (Fig. 2.2) was based on results of the 40,000 lb HE shot at Yucca Flats (Fig. A.1). The HE curve was a straight line curve when plotted on a log-log scale, had a slope of -1.66, and was the same for both horizontal and vertical acceleration componets. Analytically the acceleration curve is of the form (if $W^{1/3}$ scaling is assumed):

$$A = \frac{A_o \lambda^{-n}}{W^{1/3}} \qquad (7.1)$$

Where A = acceleration in units of gravity

$A_o$ = a constant which is a function of the soil and geology and charge depth

W and $\lambda$ are as defined in Chap. 2

For the particular curve used in the predictions

$$A = \frac{880 \lambda^{-1.62}}{W^{1/3}} \qquad (7.2)$$

To compare with the Lampson eq for acceleration. $A_o$ would equal $\frac{kF}{\rho W^{1/3}}$, where k is the soil constant and F is the depth factor. It is believed that k, which is proportional to the square of the seismic velocity, does not have much meaning as a constant, since the seismic velocity varies with distance over the distance range of these experiments. Also the ratio of surface to underground acceleration is not 2/3, as defined by the depth factor F, but is more complicated (see Sec. 7.6.4.) Thus $A_o$ is not related to the soil properties and charge depth as defined by the constants k and F.

It was arbitrarily assumed that the 1.2 kt atomic bombs that were used would be equivalent to one kt of TNT as far as ground shock energy was concerned. With this assumption, the HE acceleration was scaled to one kt from the HE acceleration curve in accordance with Eq. 7.2, and this scaled prediction is shown as a dotted line in Fig. 7.33. Here the air blast acceleration is excluded, and therefore the scaling of the fundamental acceleration is observed. As can be seen, the predicted acceleration agrees very well with the results at the close in distance of 2 $\lambda$, but then as $\lambda$ increases the vertical acceleration begins to attenuate faster than the predicted curve and the horizontal attenuates more slowly. The predicted curve turns out to be a pretty good average of the two acceleration components.

When the predicted acceleration is compared to the acceleration with the air blast effect included, (Fig. 7.34), the results are greater than predicted. The reason for this is that the air blast acceleration should scale the same way as air shock, since it is produced by the air blast, and it has already been demonstrated that the air blast acceleration is intimately related with air blast and follows the air blast attenuation law. In accordance with Eq. 7.2, the HE results were divided by a scale factor of $(1\ \text{kt}/40{,}000)^{1/3} = 3.68$ to give the predicted acceleration value for the nuclear shot at the same $\lambda$. Now, if the acceleration scaled as air blast, then it would have the same value for the nuclear shot as it had for the HE shot at the same $\lambda$. It is observed (Fig. A.9) that the air blast acceleration for the HE shot was about the same magnitude as the overall maximum acceleration which was the basis for the nuclear predictions. Assuming, then, that the air blast acceleration scaled as does air blast, it follows that the air blast acceleration on the nuclear shot should be a factor of 3.68 greater than the predicted curve. This increase was not realized; however, a sizeable increase of air blast acceleration over the predicted value by a factor of between two and three was realized.

In summary, the results indicate that the fundamental acceleration scales from HE to nuclear, and for Yucca Flats, it scales in accordance with Eq. 7.1 and 7.2. The air blast acceleration scales more nearly as the air blast does, and could be predicted from the air blast to air blast acceleration ratio as discussed in Sec. 7.6.5. It could also be scaled directly from smaller charges, although it is not exactly clear from these few experiments what the scaling factor is.

7.10.3 Scaling for the Surface Shot

As discussed in Chap. 2, the surface shot acceleration was somewhat arbitrarily assumed to be 1/2 the underground acceleration. There was no direct experimental evidence at the time to support this assumption. Accordingly, scaling for the surface shot cannot be placed on a sound basis until compared with scaled surface shot data.

The dotted line in Fig. 7.13 is the predicted acceleration. With the air blast acceleration excluded, the predicted acceleration agrees very well out to 4 $\lambda$ with all the acceleration components except the outward horizontal component which is 1.5 to 5 times larger. Beyond 4 $\lambda$ , plateau effects set in and the predicted curve diverges more and more until at 20 $\lambda$ the predicted curve is a factor of four less than the measured results.

When the air blast acceleration is included in the acceleration curves (Fig. 7.14), there is no agreement at all with the prediction. While it was known that the air blast would be much greater, such a large air blast acceleration was not anticipated. More so than for the underground shot, the fundamental and air blast acceleration must be scaled separately. The fundamental acceleration can probably be scaled, though no comparison has been made with scaled shots. The air blast acceleration can be estimated if the air blast is known by means of the air blast to air blast acceleration ratio as discussed in Sec. 7.6.5.

7.10.4 Several Observations Concerning Scaling

At Yucca Flats prediction of ground shock from HE and nuclear underground shots can be made that will be good to within a factor of two. Predictions of ground shock for a different location would still be very uncertain. In such a case preliminary HE tests would be imperative for the purpose of predicting effects for a nuclear shot.

Because of the variable nature of ground shock, accurate estimates of the yield or TNT equivalent from ground shock measurements will never be feasible.

If bedrock and the water table were close to the surface, large damaging ground shock waves might be transmitted for some distance from zero by refraction and reflection of the shock wave. These ground shock waves would probably be greater in magnitude and

attenuate more slowly than when the bedrock and water table are located at a great depth, as in the case at the Yucca Flats site.

## 7.11 ACCURACY OF THE MEASUREMENTS

The general accuracy of the measurements was good. The majority of the records were well within the range of the accelerometers and the noise in the recording system was in accordance with the specifications. The more important factors affecting the accuracy of the measurements are:

1. Accuracy of the Gages
2. Effect of ratio of signal to gage frequency on the accuracy
3. Accuracy of the recording system
4. Apparent Inaccuracies

These will be discussed in order.

### 7.11.1 Accuracy of the Accelerometers

The calibration of the accelerometers is estimated to be accurate to within 5 per cent or better (see Chap. 4). The average is between 2 and 3 per cent which appears to be about the limit of accuracy for this gage.

A guess was made as to the ground temperature that would prevail. The actual ground temperature was around 62°F, which was about 10° higher than estimated. For this reason some of the damping coefficients are too low, since the silicone damping fluid undergoes a 1 per cent change in viscosity per degree F. Even so, the majority of the accelerometers lie within the preferred range of 0.5 to 0.7 critical (Tables 7.3 and 7.4). The gages with low damping coefficients will of course introduce some phase and response error.

### 7.11.2 Effect of the Ratio of Signal to Gage Frequency on the Accuracy

The error in the accelerometer output as a function of the ratio of the signal frequency to the natural frequency of the accelerometer has been discussed fully in Sec. 7.9, and will only be summarized here. For a signal to gage frequency ratio up to 0.3, very

little error will result in a properly damped gage. For a frequency ratio from 0.3 to over 0.5, the error will be from 5 to 20 per cent, depending on the damping coefficient of the gage, and depending on whether the input signal has steady state or transient characteristics. When the frequency ratio approaches one, the response error may vary from 10 per cent to over 50 per cent. As previously stated in Sec. 7.9, the air blast acceleration will suffer the greatest error, particularly at the greater distances from zero, because the signal frequency approaches the natural frequency of the gage in some cases. The fundamental acceleration frequencies for the surface shot are on the whole favorable for good accuracy, though in a fair number of cases the frequency ratio is 0.5, and here the error might be in the neighborhood of 20 per cent or more. The fundamental acceleration frequencies for the underground shot are the most favorable of all, and the error should be small.

### 7.11.3 Accuracy of the Recording System

The wow and flutter noise for the recording system was about 0.2 per cent rms. This amounts to 3.7 per cent noise for a full range signal on the accelerometer. Thus, when the accelerometer is operating at its full range, the error due to recording noise such as wow and flutter will be less than 3.7 per cent. On the other hand when the signal being recorded is, say, 3.7 per cent of the range of the gage, then the variation in the signal magnitude due to noise is equal to the magnitude of the signal itself, and the error can be very large. In general, the records had a high signal to noise ratio and errors were small; however, there were some cases where the signal was weak in relationship to the range of the gage, and large error resulted. Figure B.15 is a photograph of two original records. One record, which is the more typical, shows very high signal to noise ratio and excellent accuracy. The other record is one of the worst records obtained having a low signal to noise ratio of around one and indicating a possible error of 100 per cent. On the acceleration curves the back-up gage value is plotted along with the primary gage result. In some instances considerable discrepancy occurs between the two accelerometers. This discrepancy can nearly always be explained by the signal to noise error or to the unfavorable signal to gage frequency.

### 7.11.4 Apparent Inaccuracies

Much of the apparent scatter in results, which at first glance is attributed to gage or recording errors, is not scatter at all but is real and is due to such things as inhomogeneity of the soil, various origins of the acceleration, and interaction of the various components making up the acceleration pattern.

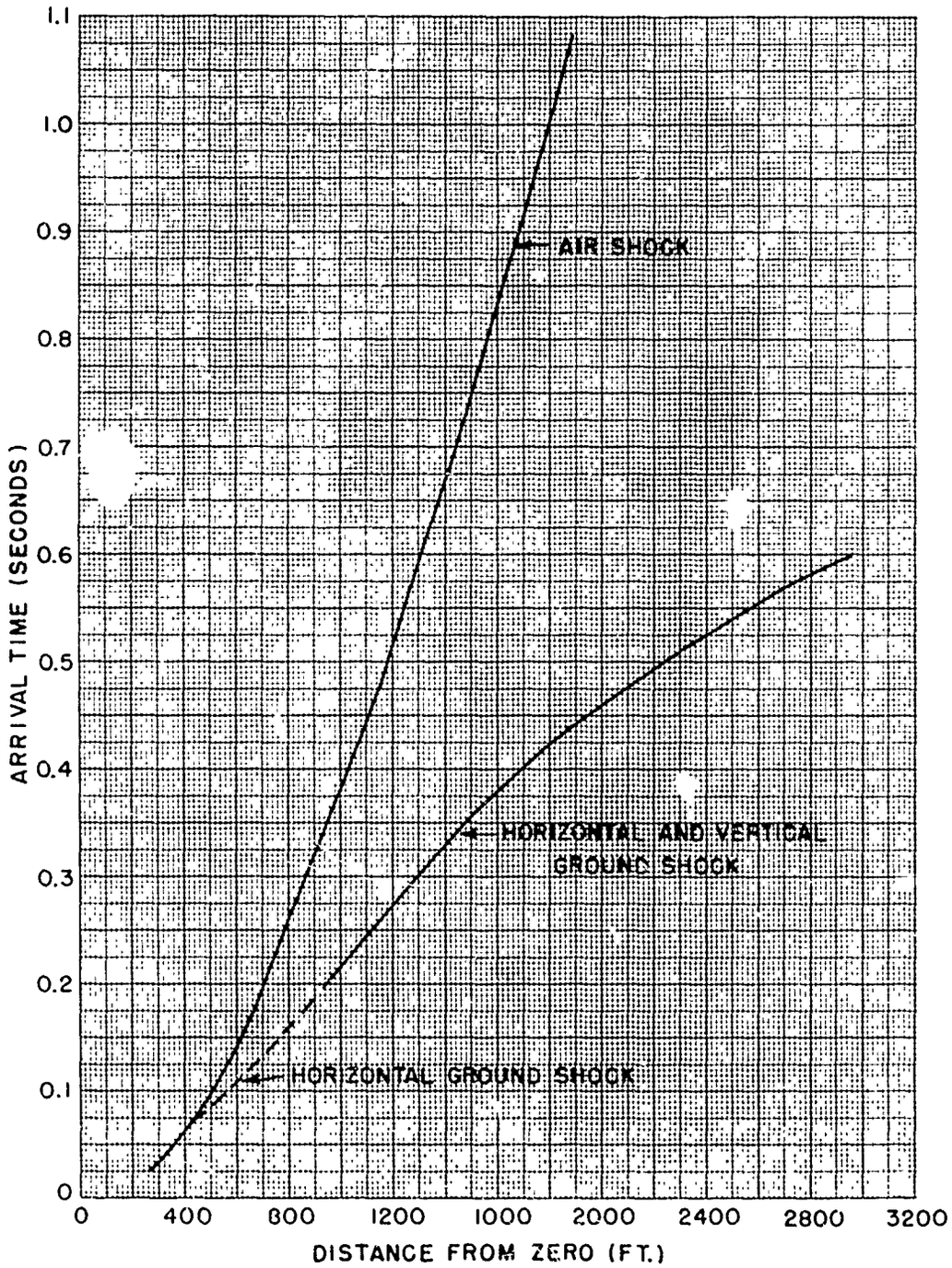


Fig. 7.1 Surface Shot - Arrival Times of Air and Ground Shock

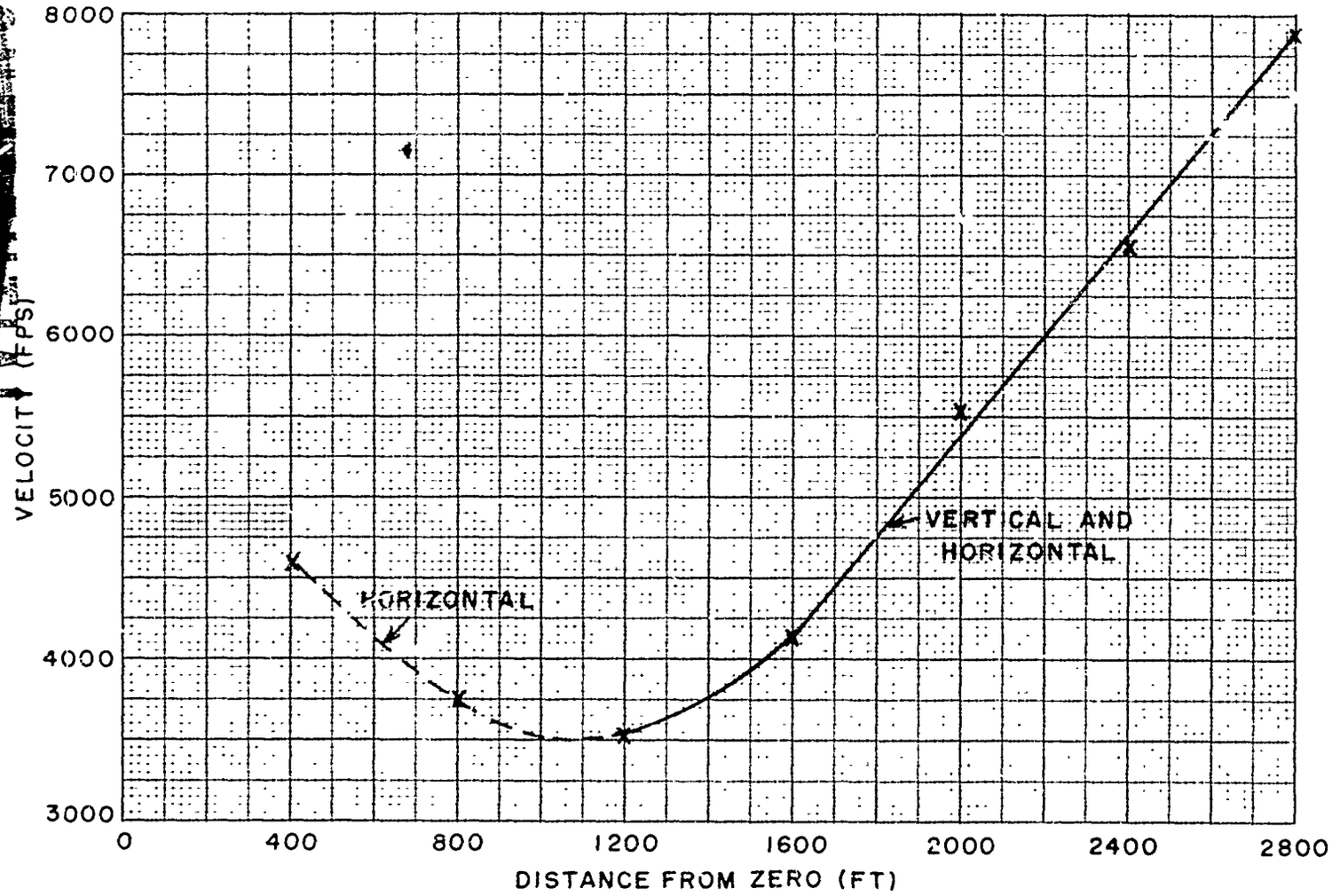


Fig. 7.2 SURFACE SHOT - Velocity of Initial Ground Shock

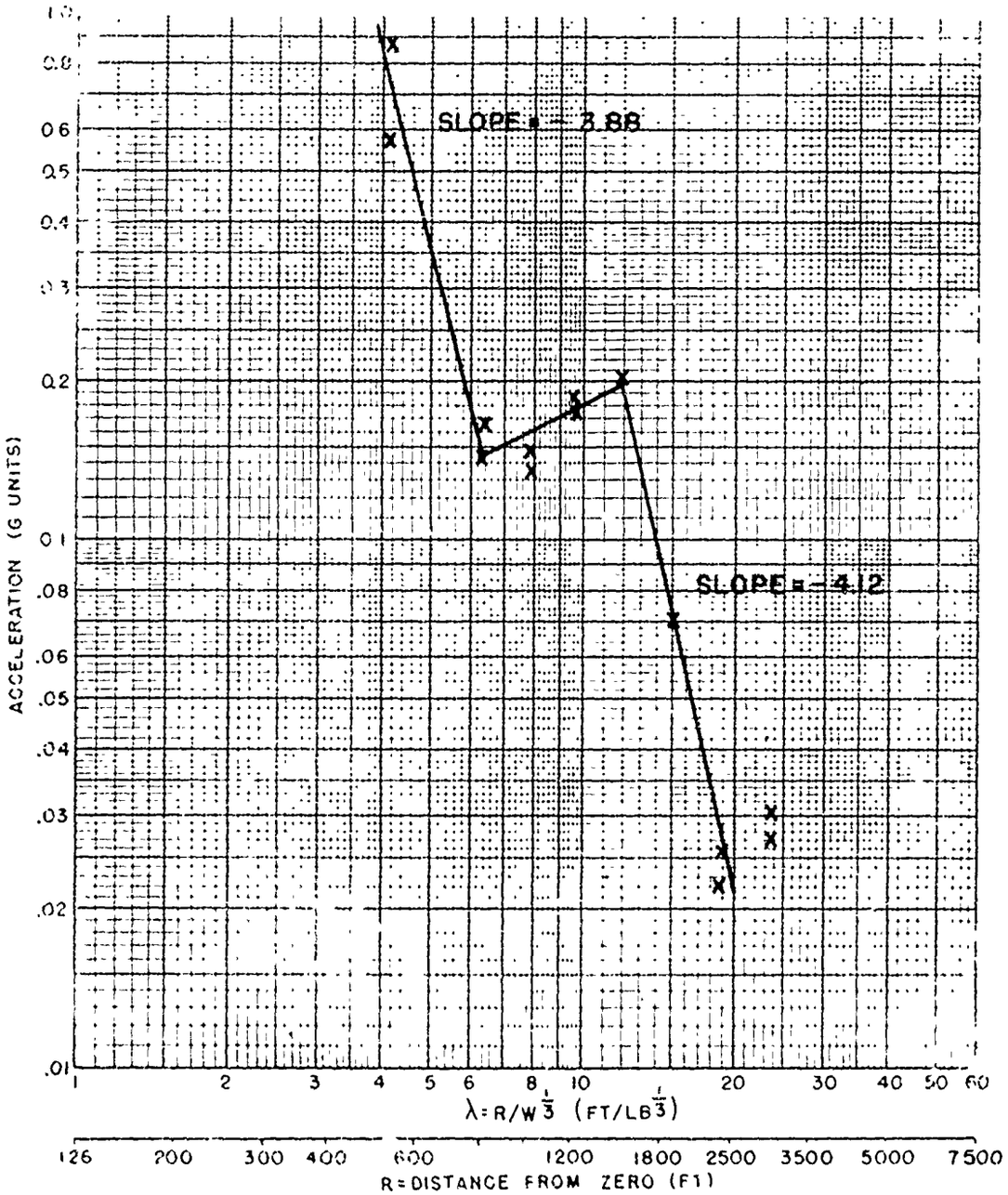


Fig. 7.3 SURFACE SHOT - First Outward Horizontal Acceleration (Excluding Air Blast Effect)

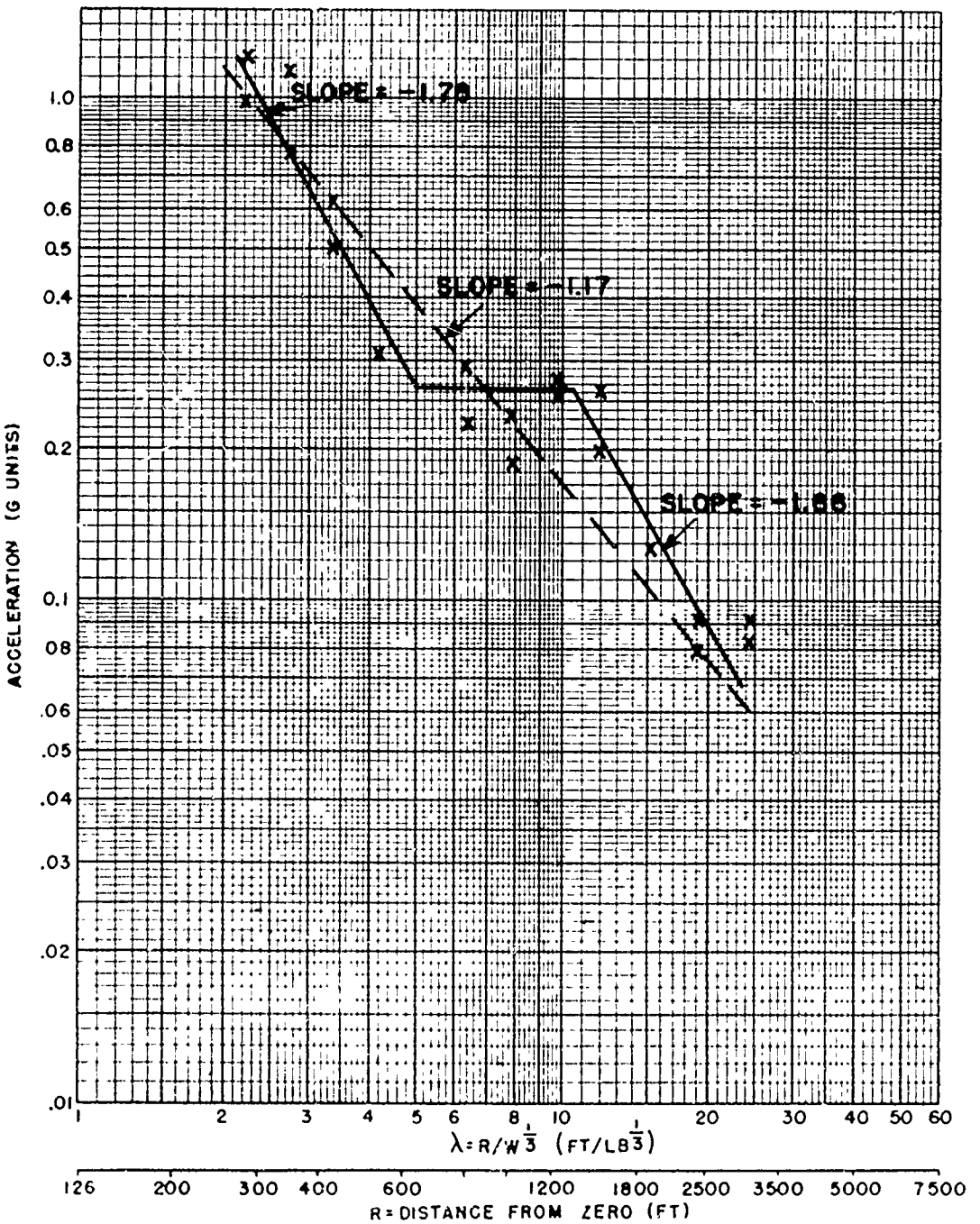


Fig. 7.4 SURFACE SHOT - Maximum Inward Horizontal Acceleration (Excluding Air Blast Effect)

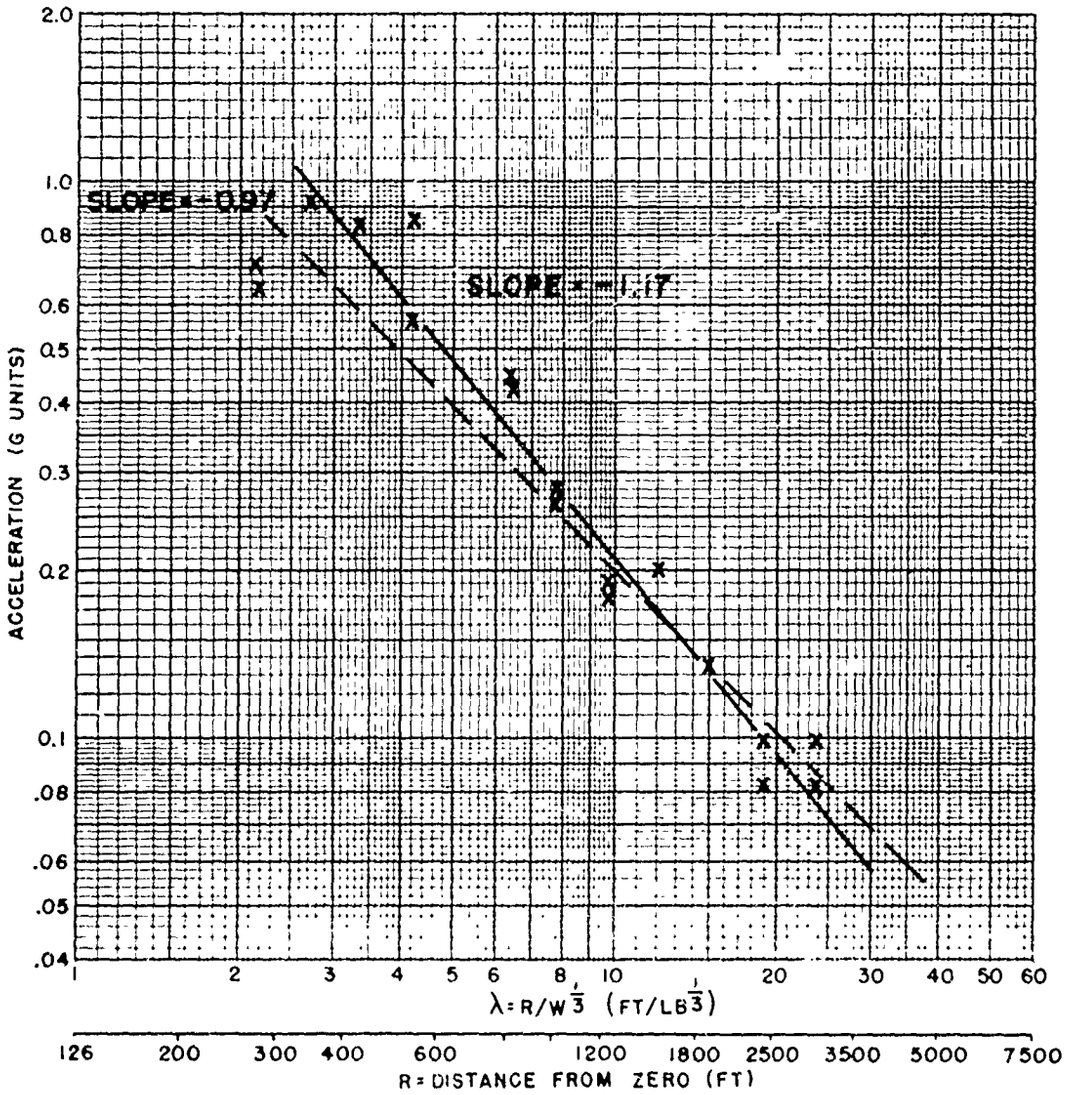


Fig. 7.5 SURFACE SHOT - Maximum Outward Horizontal Acceleration (Excluding Air Blast)

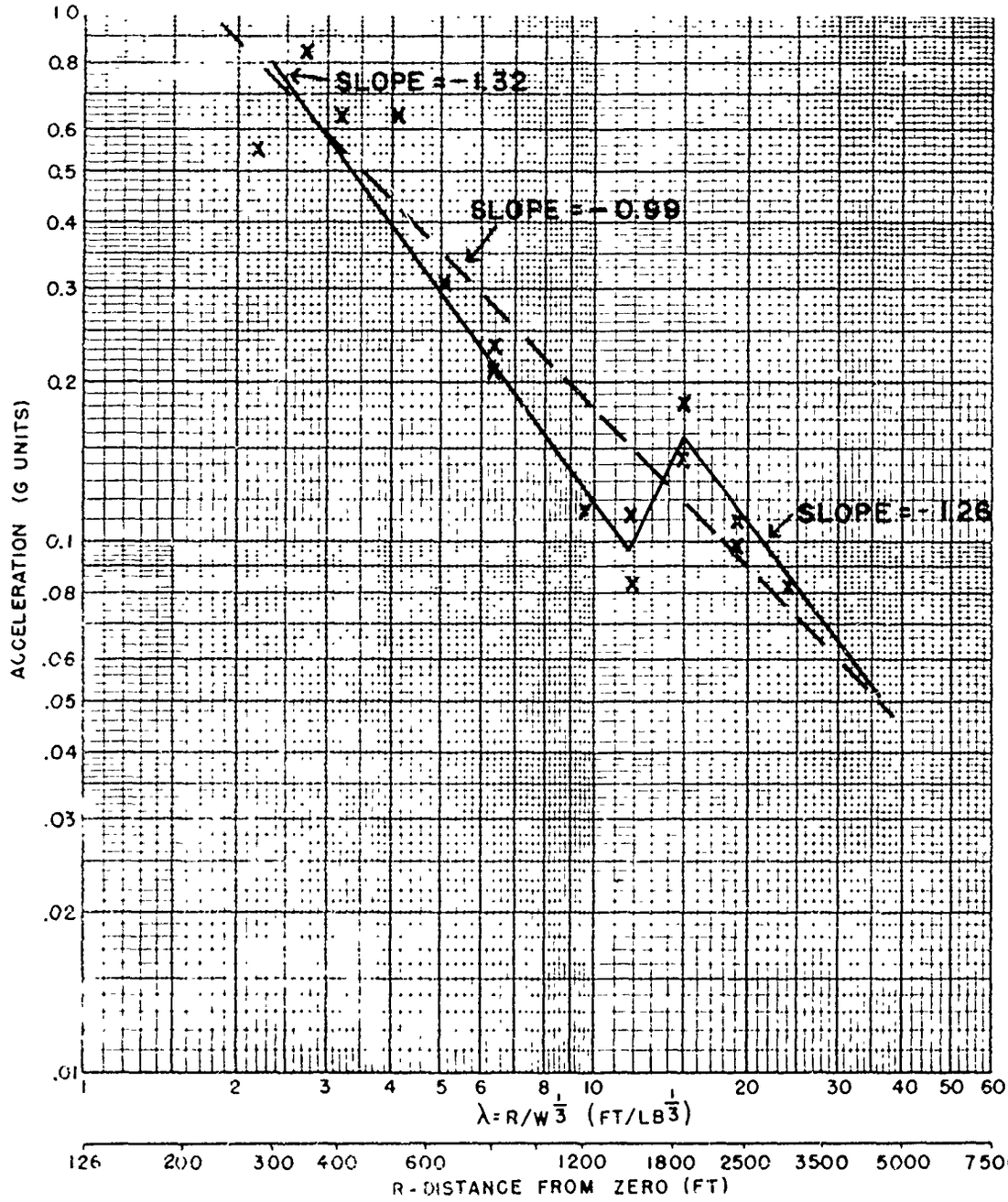


Fig. 7.6 SURFACE SHOT - Maximum Upward Vertical Acceleration (Excluding Air Blast Effect)

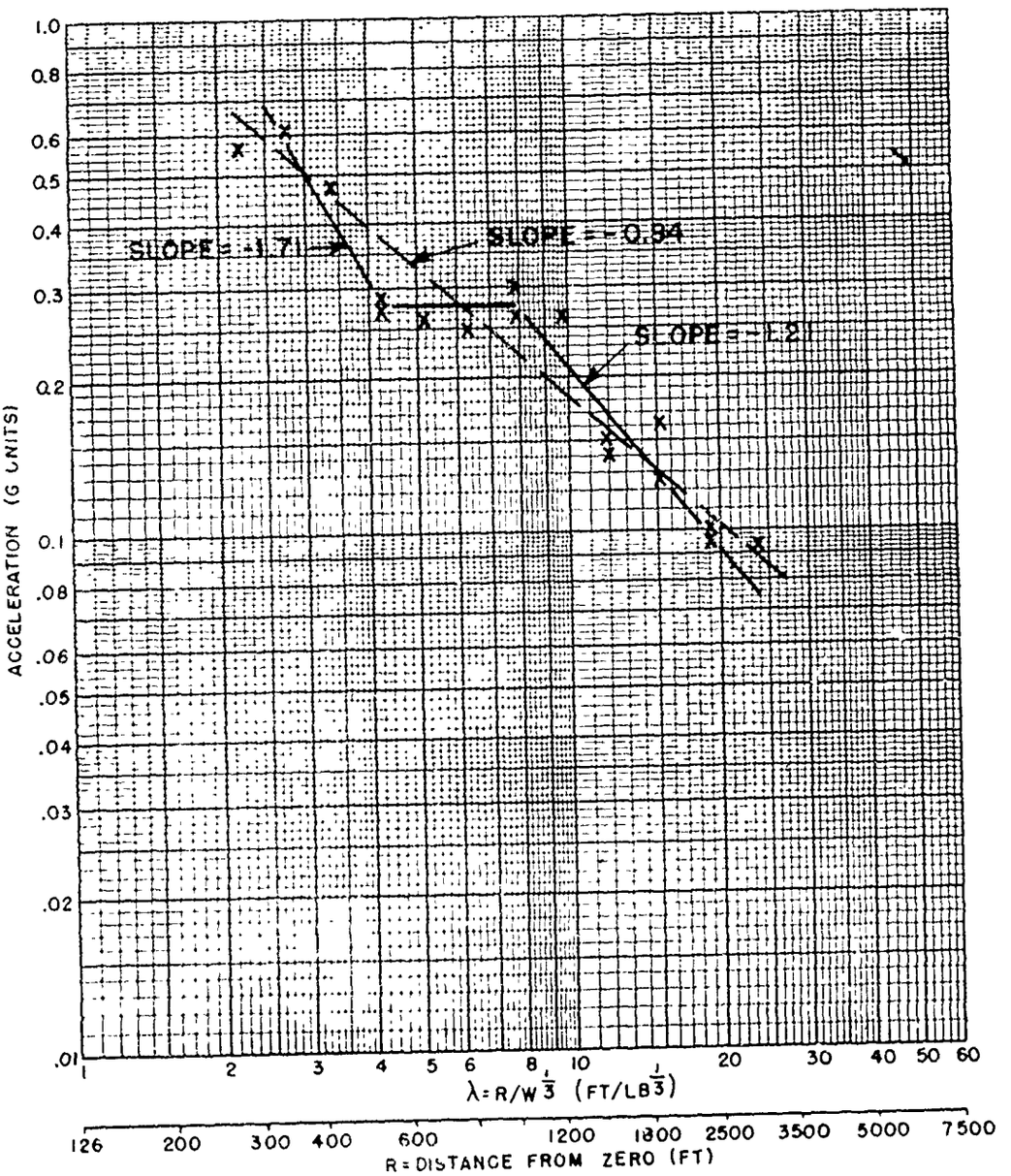


Fig. 7.7 SURFACE SHOT - Maximum Downward Vertical Acceleration (Excluding Air Blast Effect)

[redacted]

PROJECT 1.1

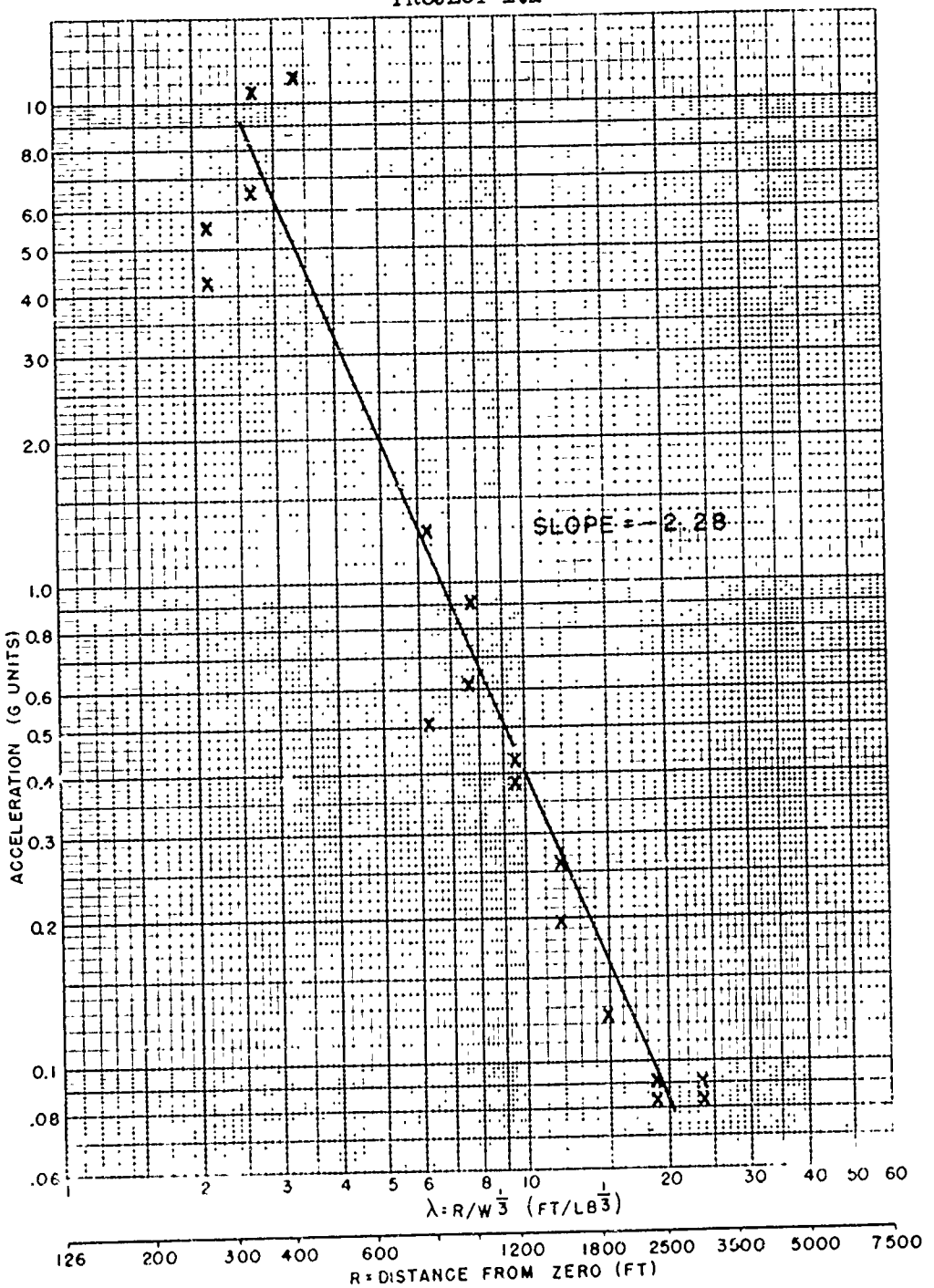


Fig. 7.8 SURFACE SHOT - Maximum Inward Horizontal Acceleration (Including Air Blast Effect)

[redacted]



[redacted]

PROJECT 1.1

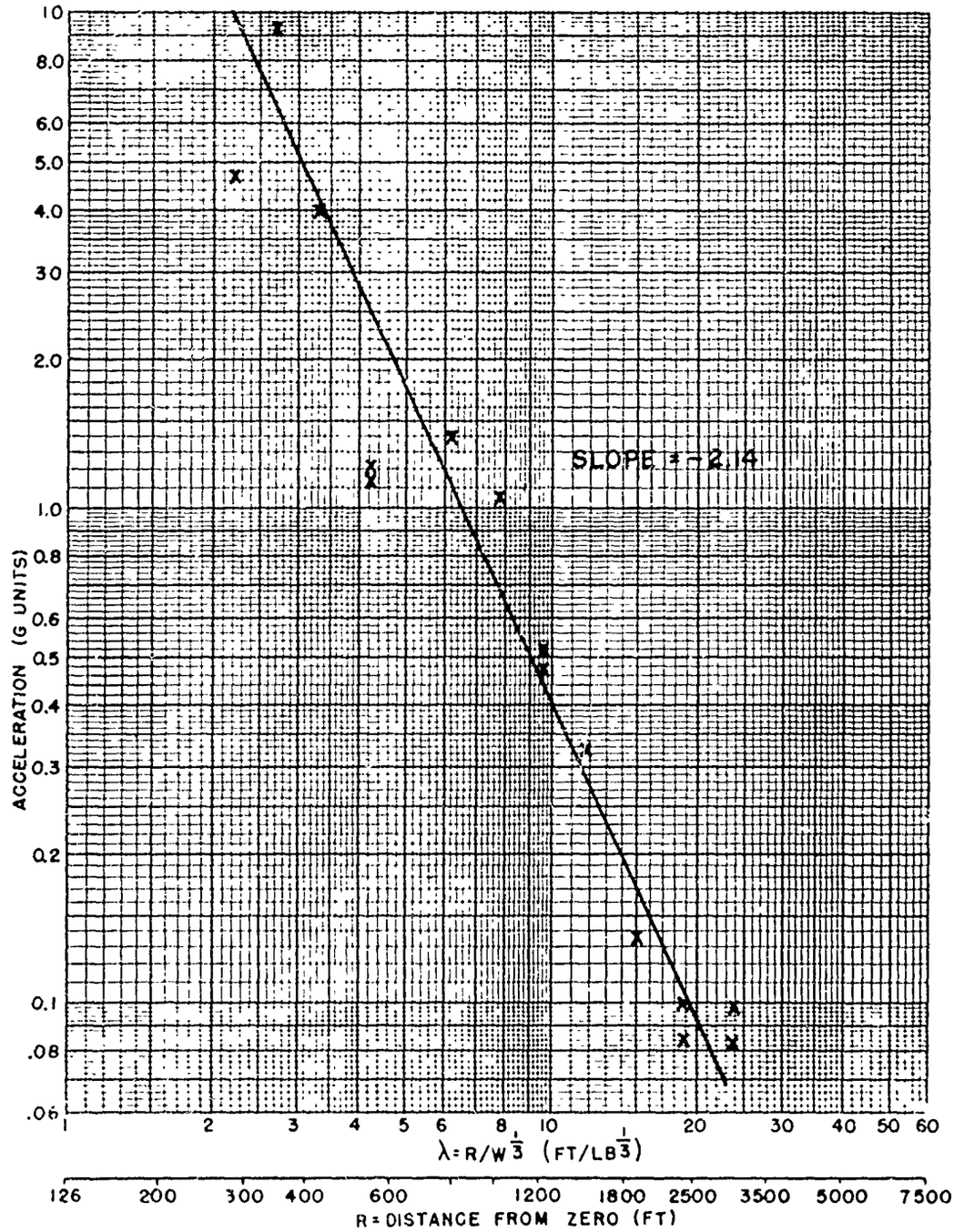


Fig. 7.9 SURFACE SHOT - Maximum Outward Horizontal Acceleration (Including Air Blast Effect)

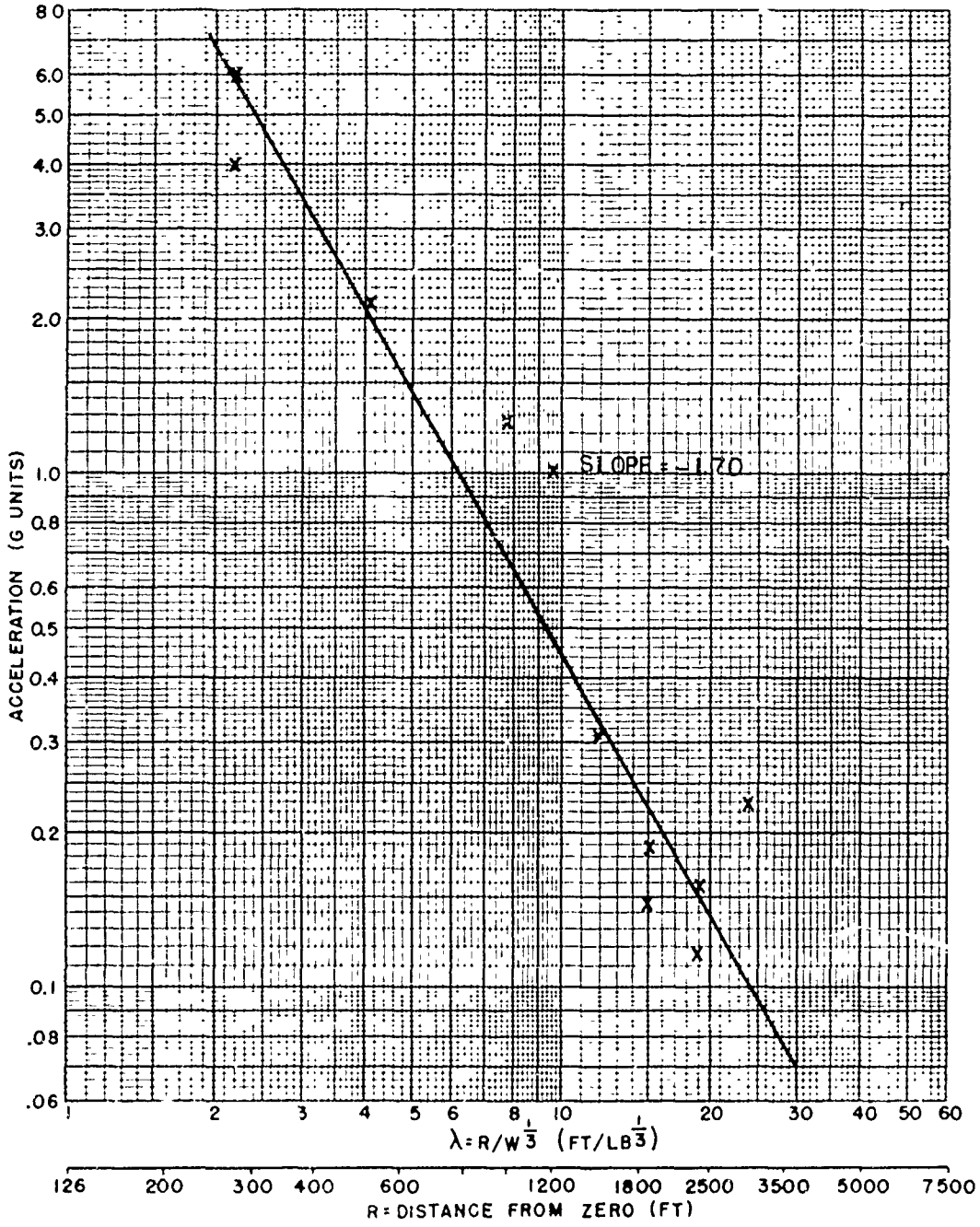


Fig. 7.10 SURFACE SHOT - Maximum Upward Vertical Acceleration (Including Air Blast Effect)

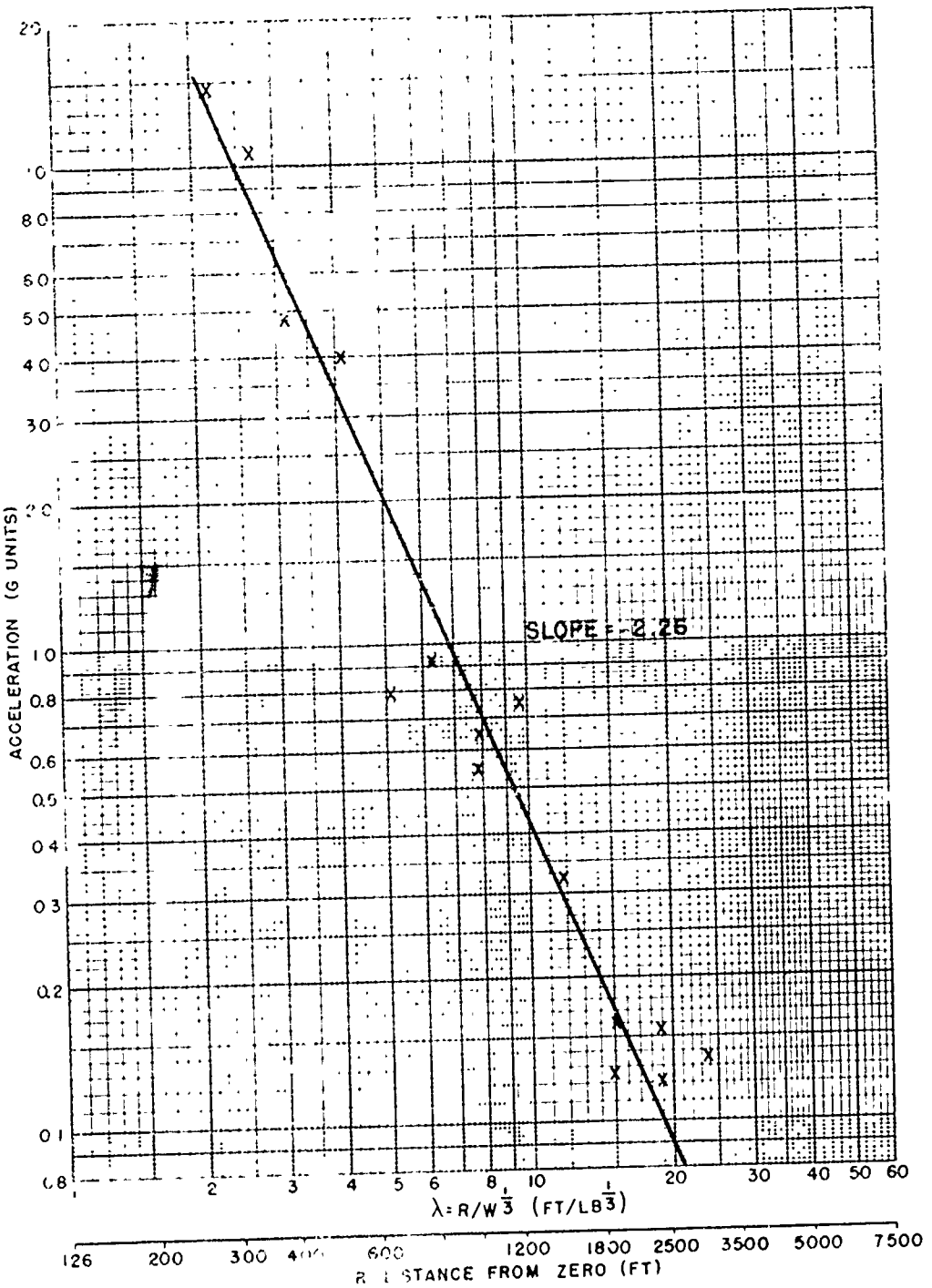


Fig. 7.11 SURFACE SHOT - Maximum Downward Vertical Acceleration (Including Air Blast Effect)

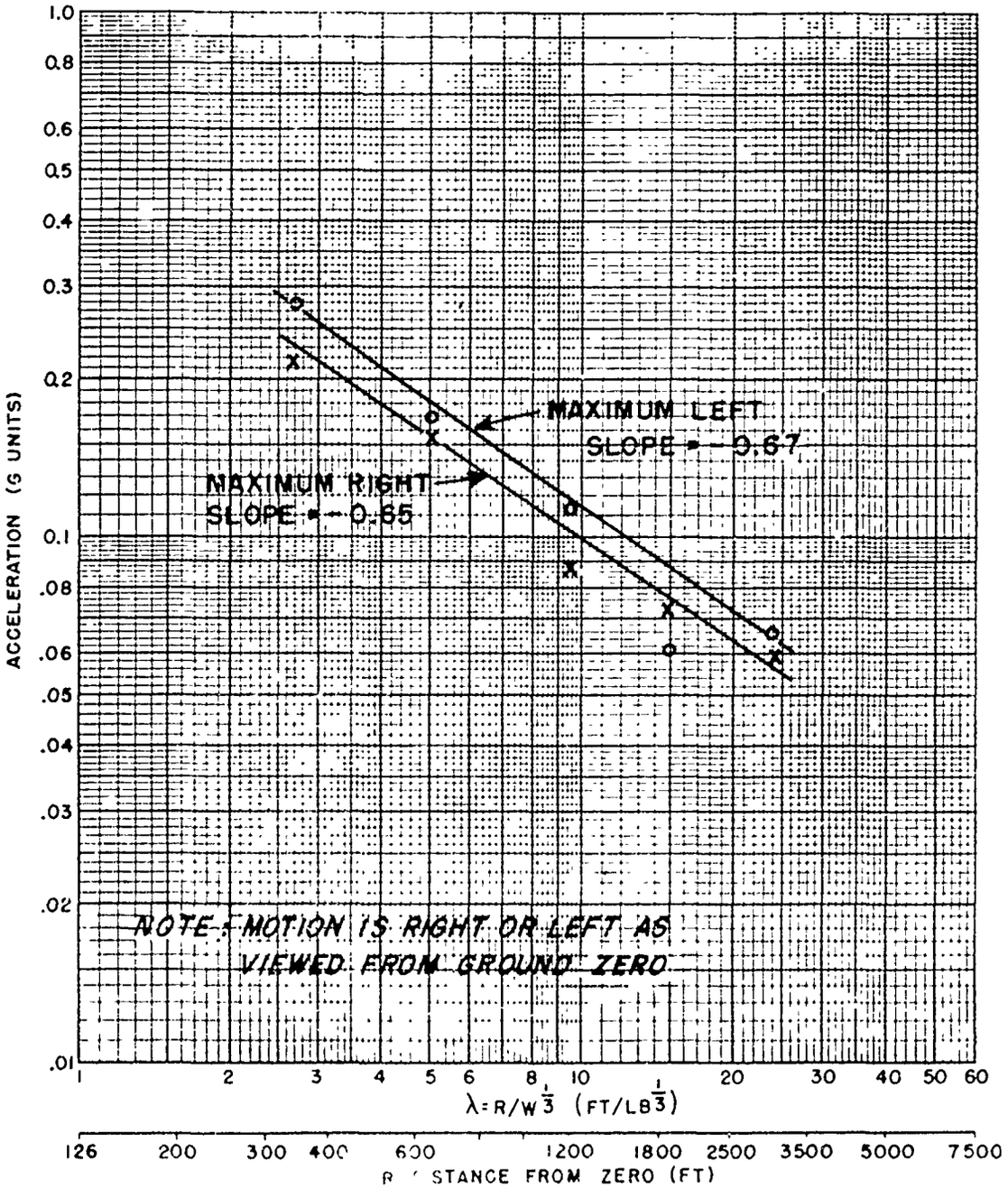


Fig. 7.12 SURFACE SHOT - Maximum Transverse Acceleration (Including Air Blast Effect)

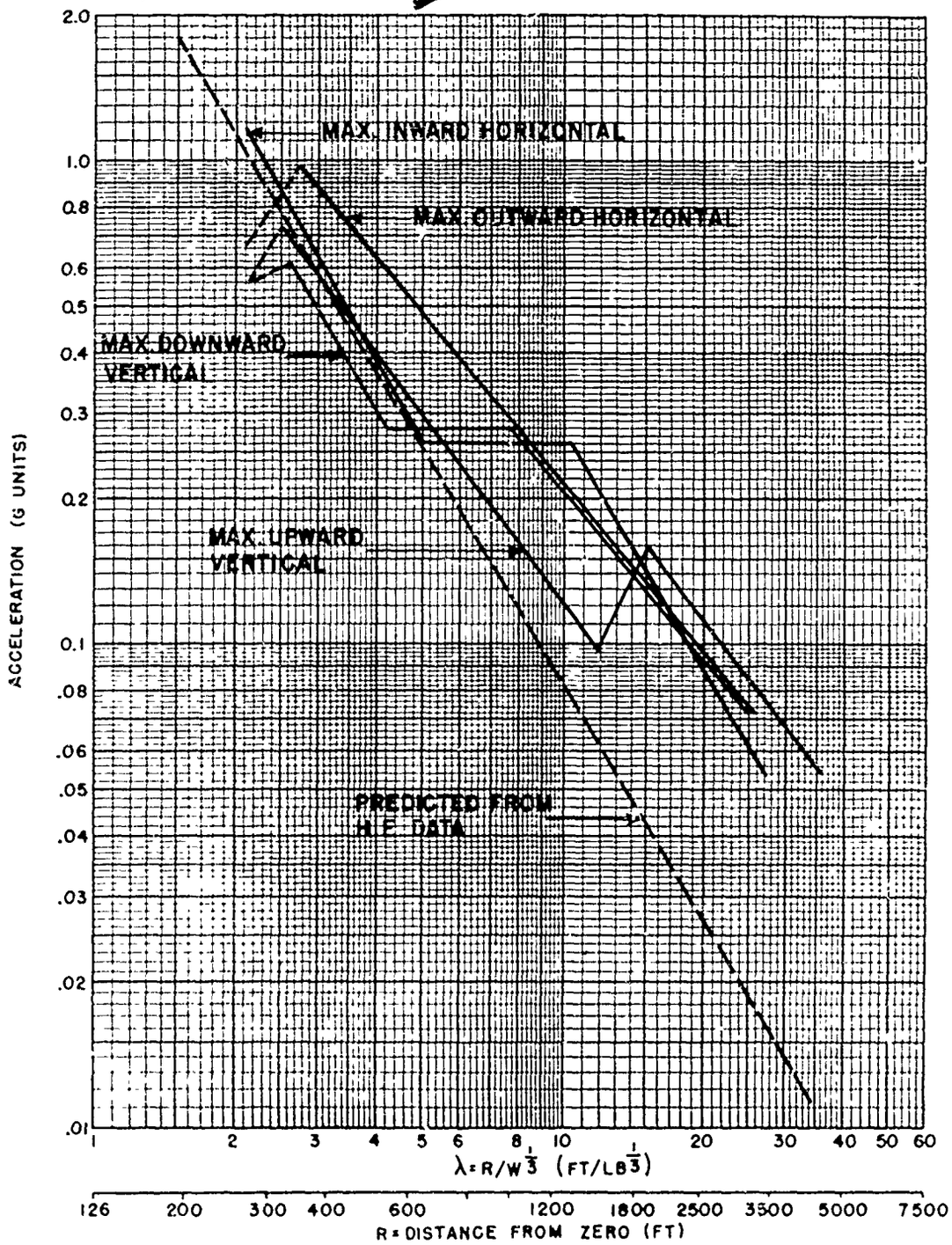


Fig. 7.13 SURFACE SHOT - Composite of All Maximum Acceleration Plots which Exclude Air Blast Effect (Figs. 7.4 to 7.7)

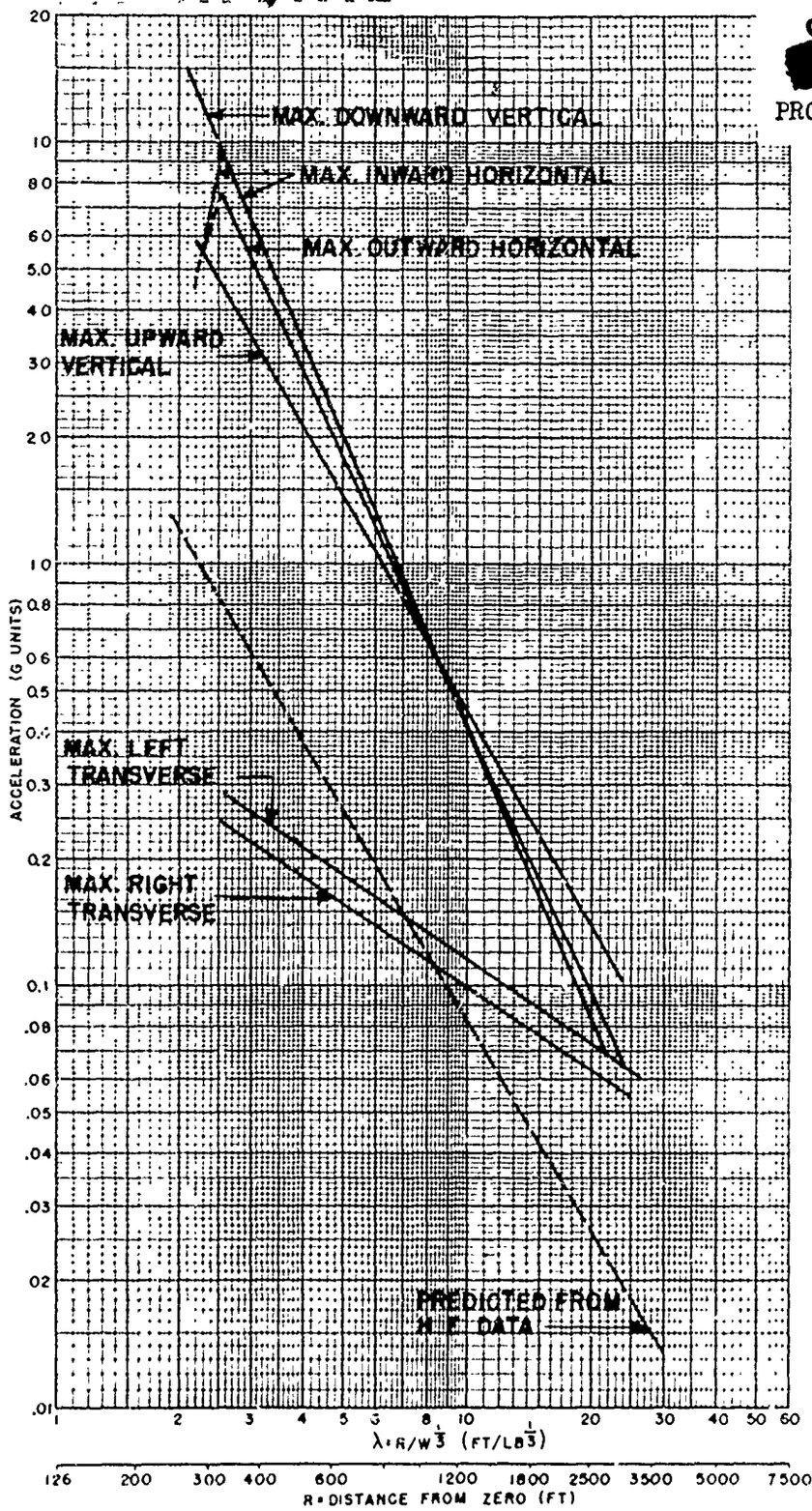


Fig. 7.14 Surface Shot - Composite of All Maximum Acceleration [redacted] Air Blast Effect (Figs. 7.8 to 7.12)

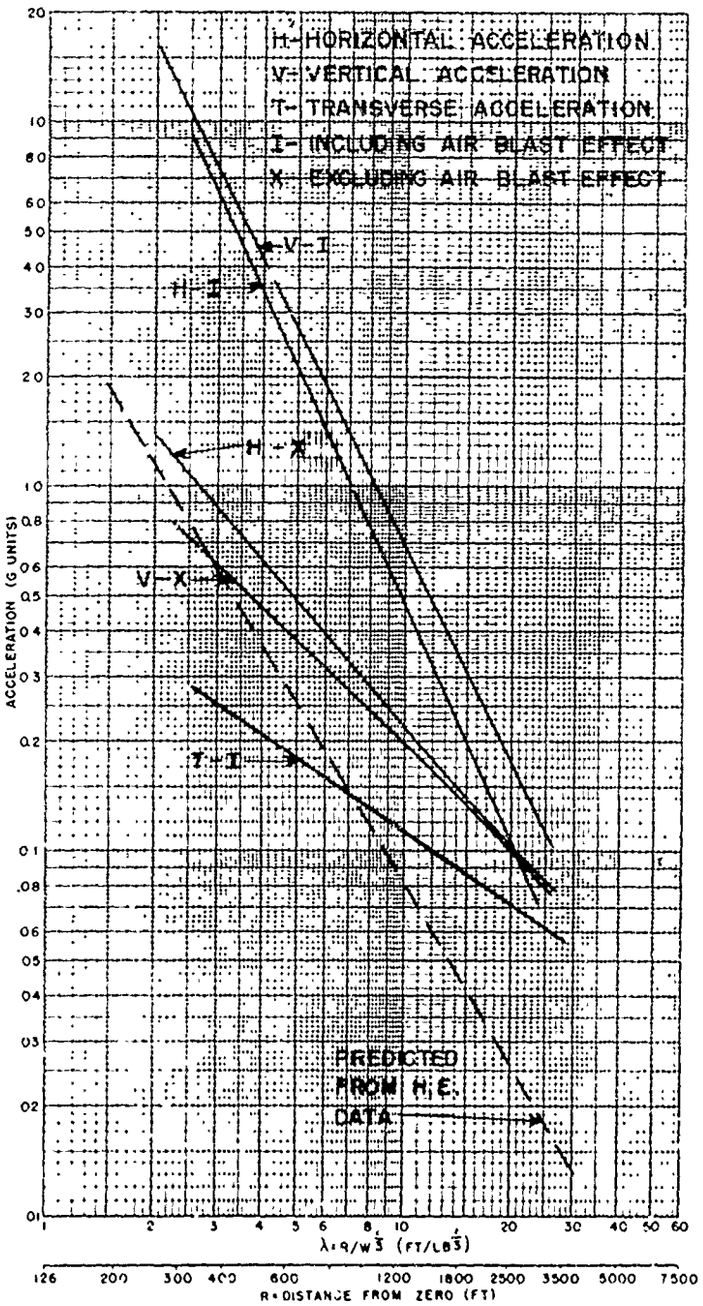


Fig. 7.15 Surface Shot - Composite Plot of Overall Maximum Horizontal, Vertical, and Transverse Acceleration (Including and Excluding Air Blast Effect)

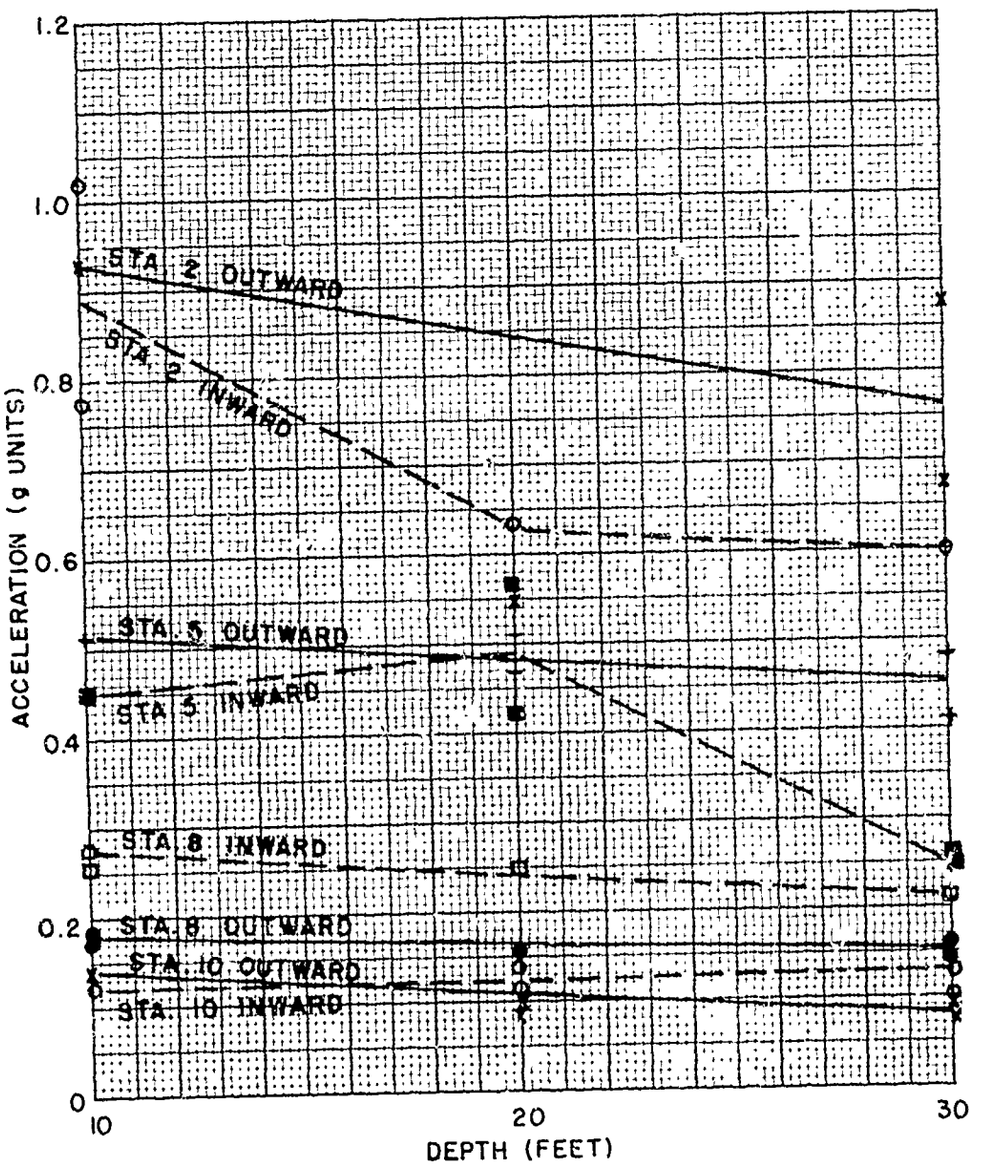


Fig. 7.16 SURFACE SHOT - Maximum Horizontal Acceleration vs Depth (Excluding Air Blast Effect)

[redacted]

PROJECT 1.1

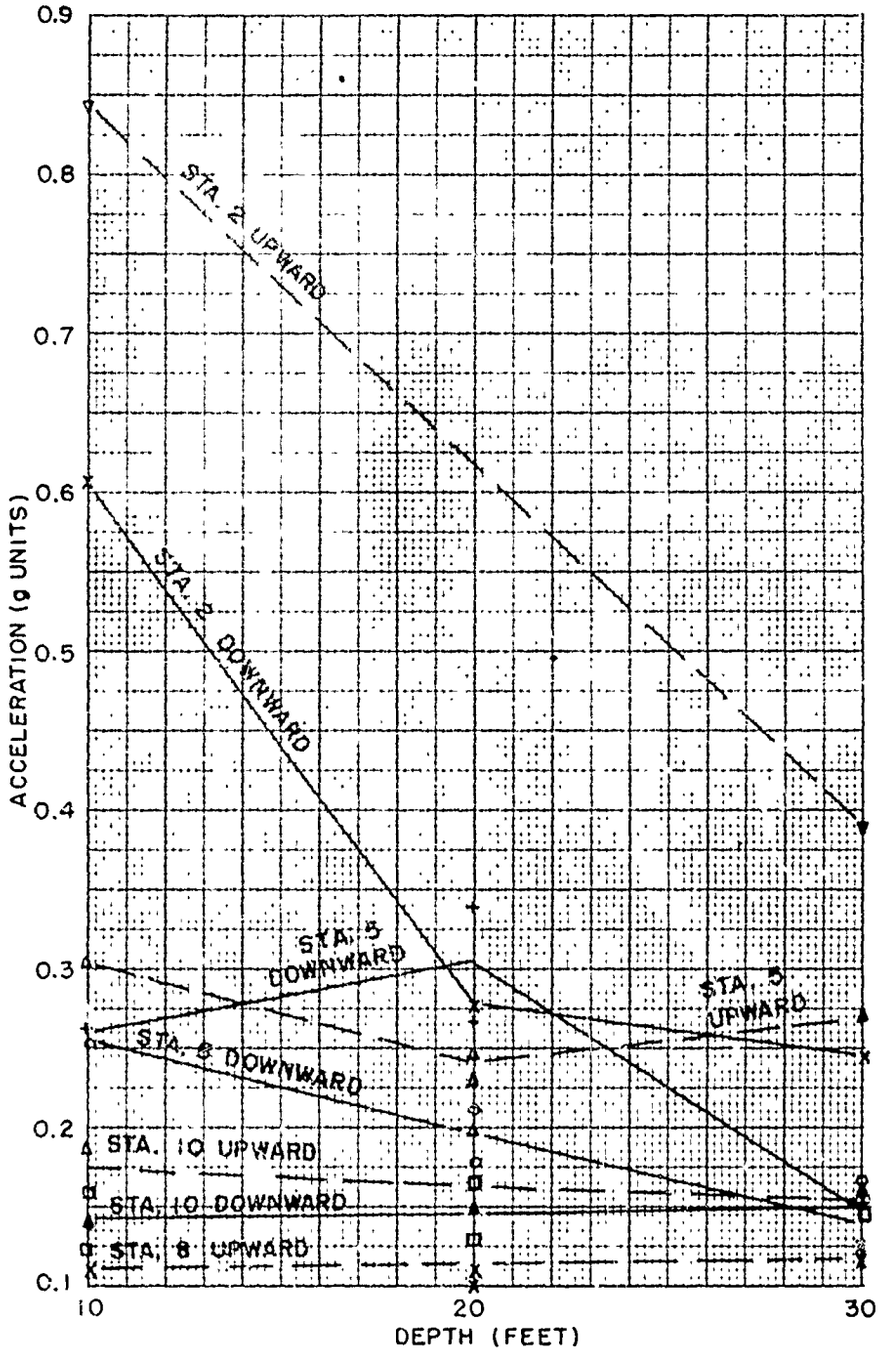


Fig. 7.17 Surface Shot - Maximum Vertical Acceleration vs Depth (Excluding Air Blast Effect)



[redacted]

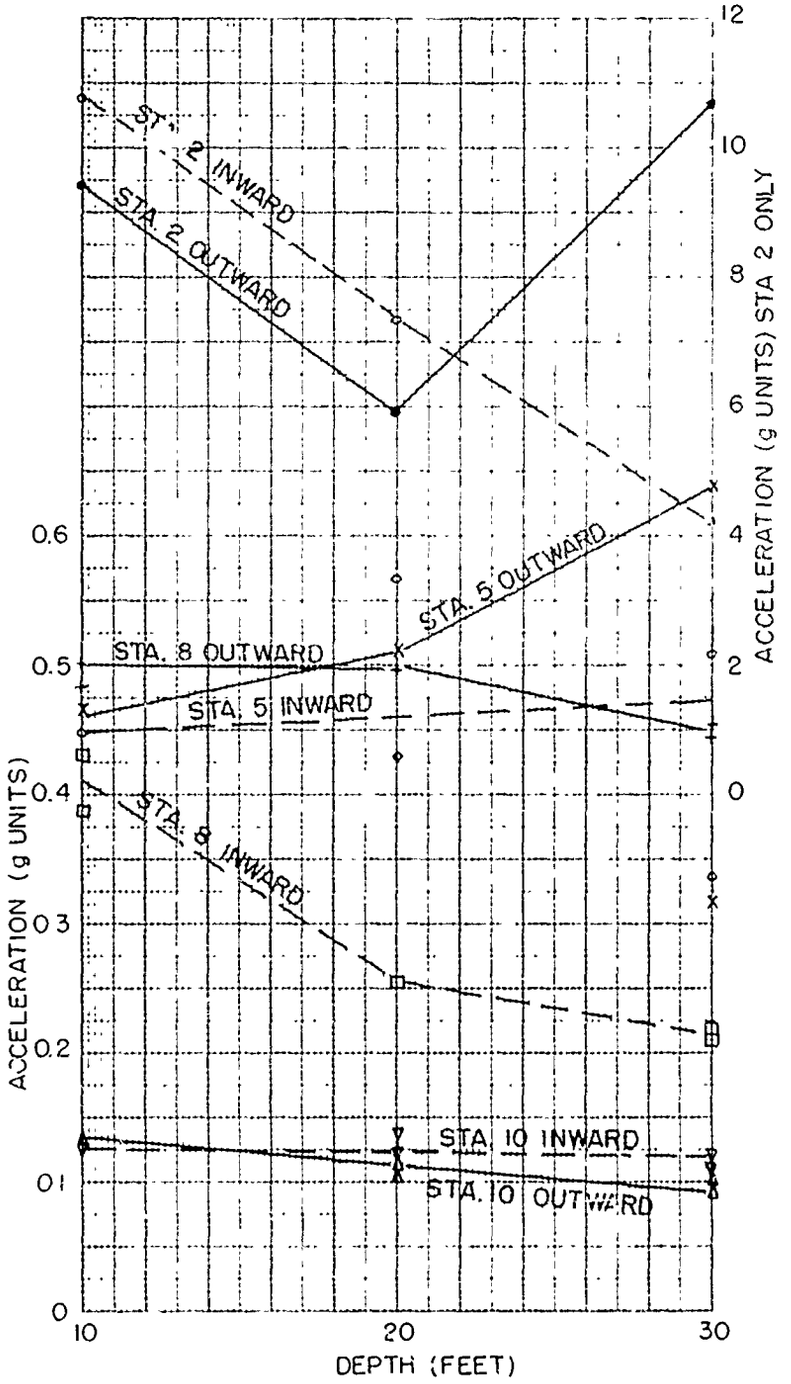


Fig. 7.18 Surface Shot - Maximum Horizontal Acceleration vs Depth (Including Air Blast Effect)

[redacted]

PROJECT 1.1

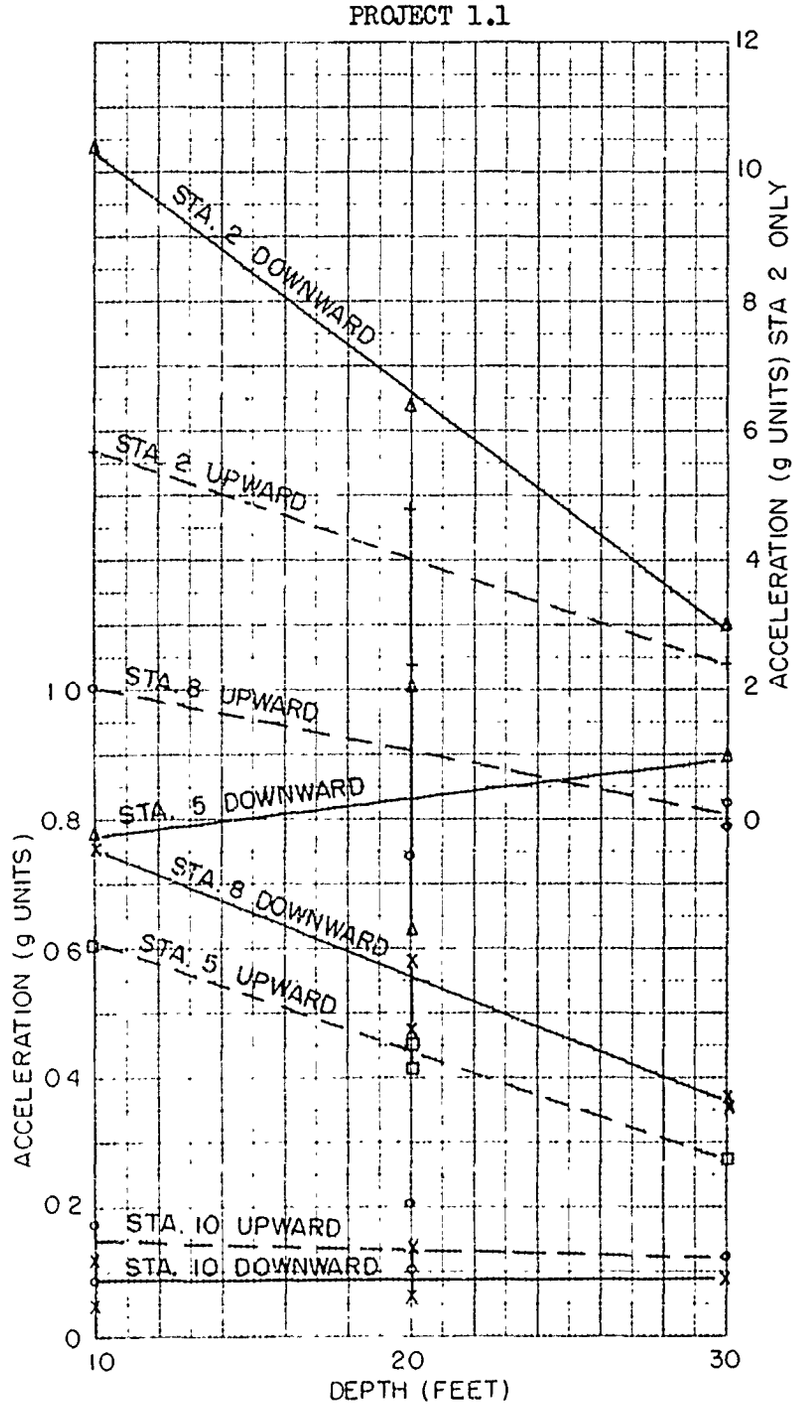


**Fig. 7.19** Surface Shot - Maximum Vertical Acceleration vs Depth (Including Air Blast Effect)

[redacted]



[redacted]

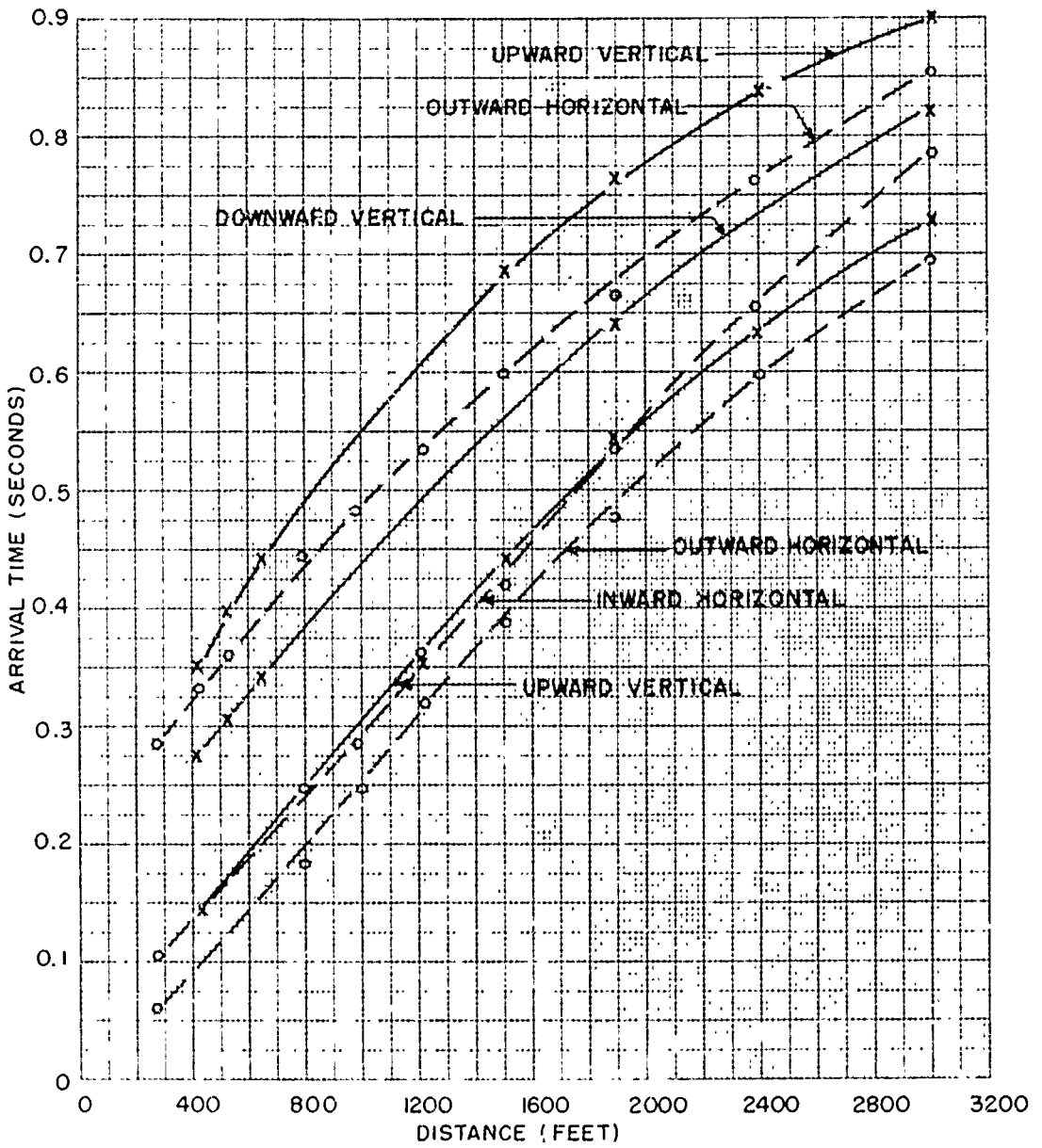


Fig. 7.20 SURFACE SHOT - Arrival Times of Corresponding Peaks

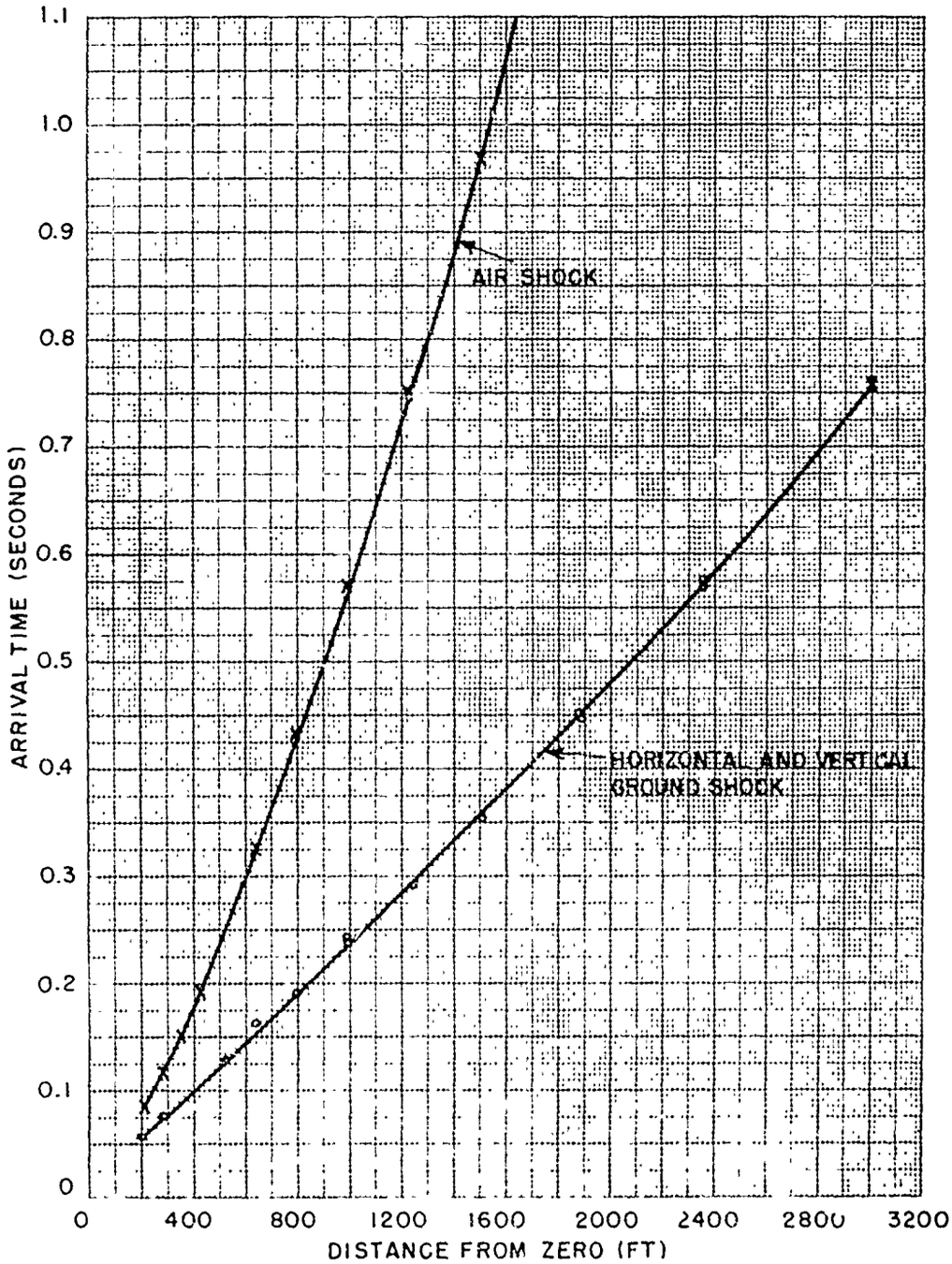


Fig. 7.21 Underground Shot - Arrival Times of Air and Ground Shock

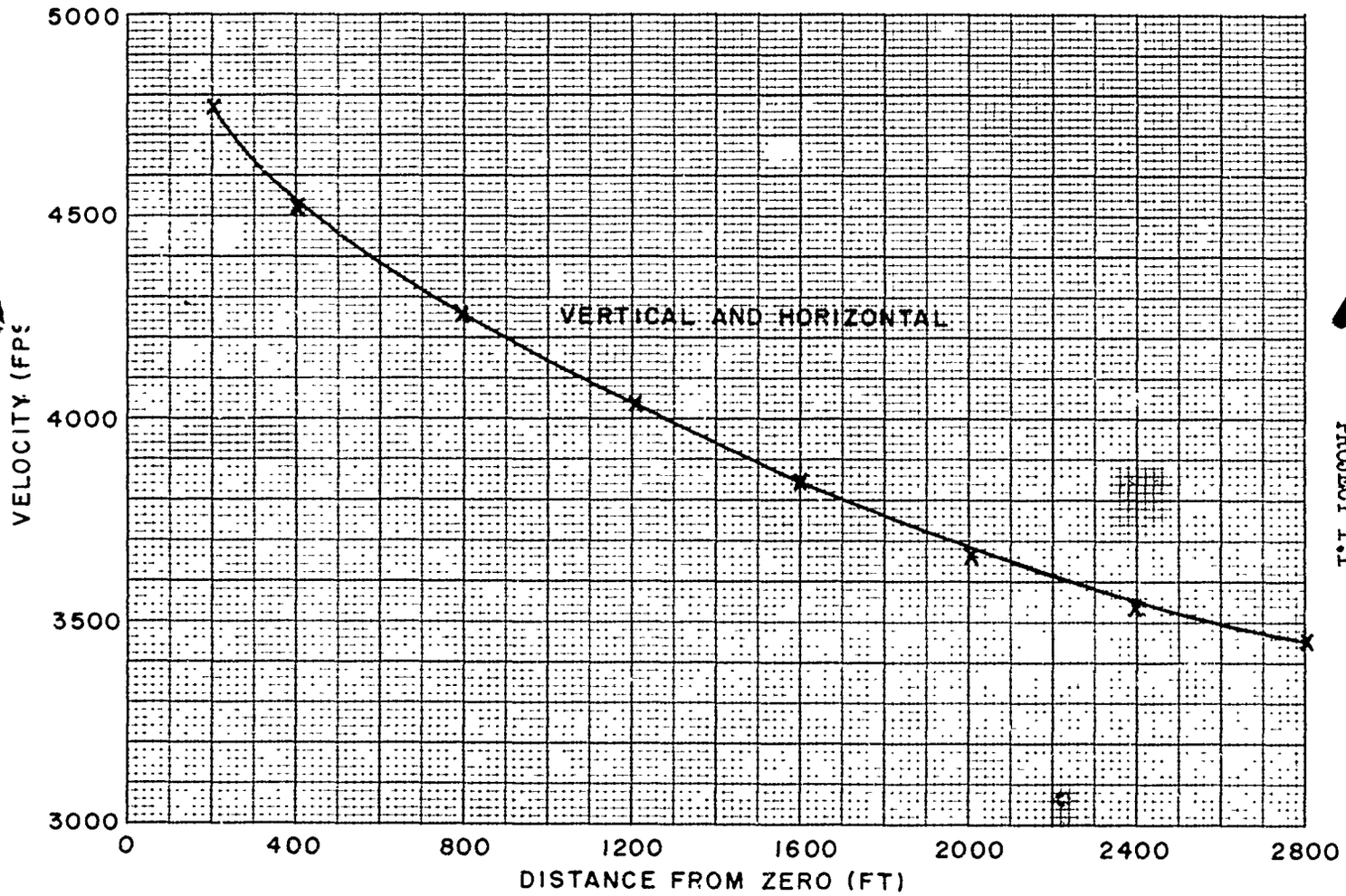


Fig. 7.22 UNDERGROUND SHOT - Velocity of Initial Ground Shock

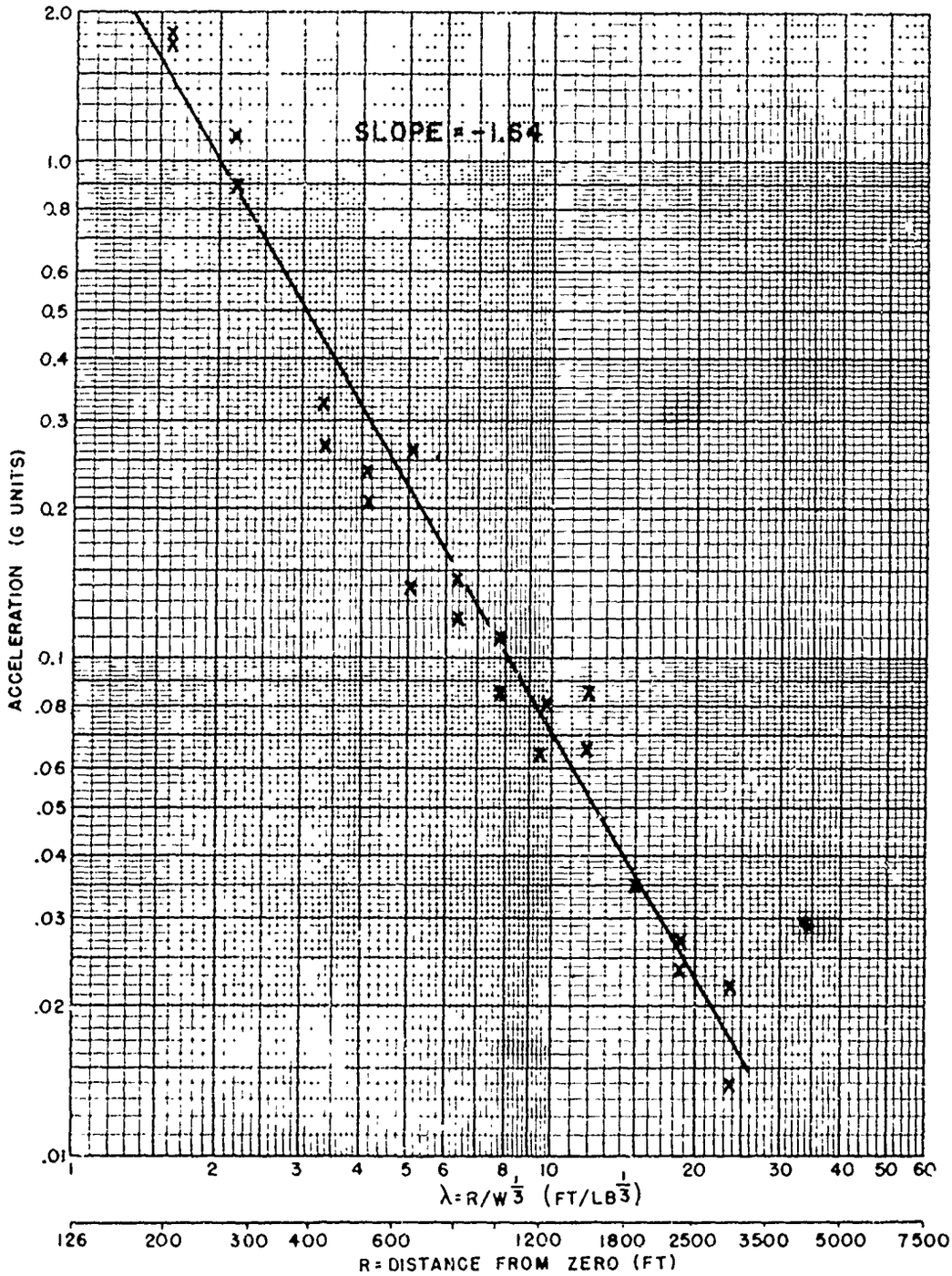


Fig. 7.23 UNDERGROUND SHOT - First Outward Horizontal Acceleration (Excluding Air Blast Effect)

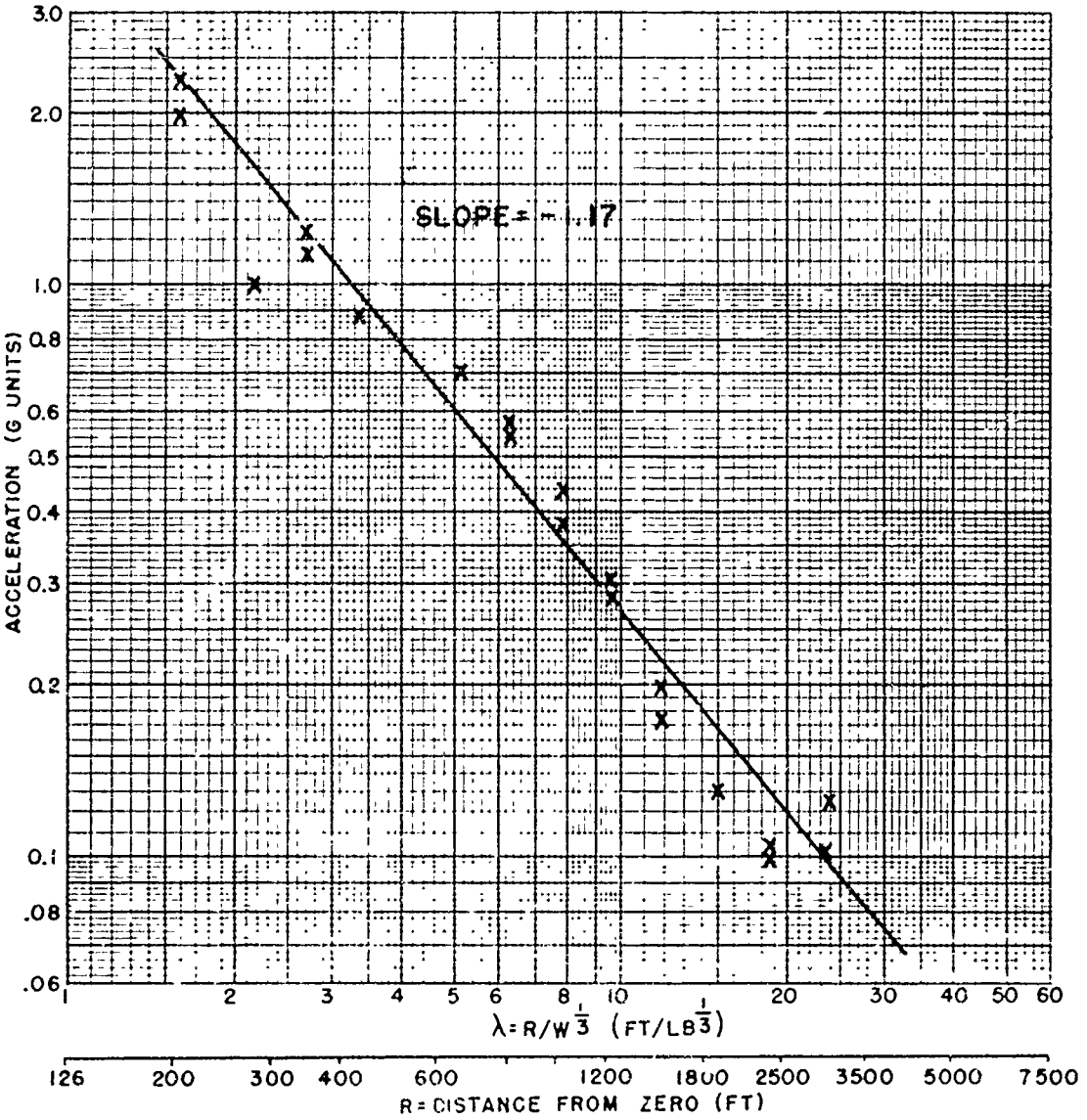


Fig. 7.24 UNDERGROUND SHOT - Maximum Inward Horizontal Acceleration (Excluding Air Blast Effect)

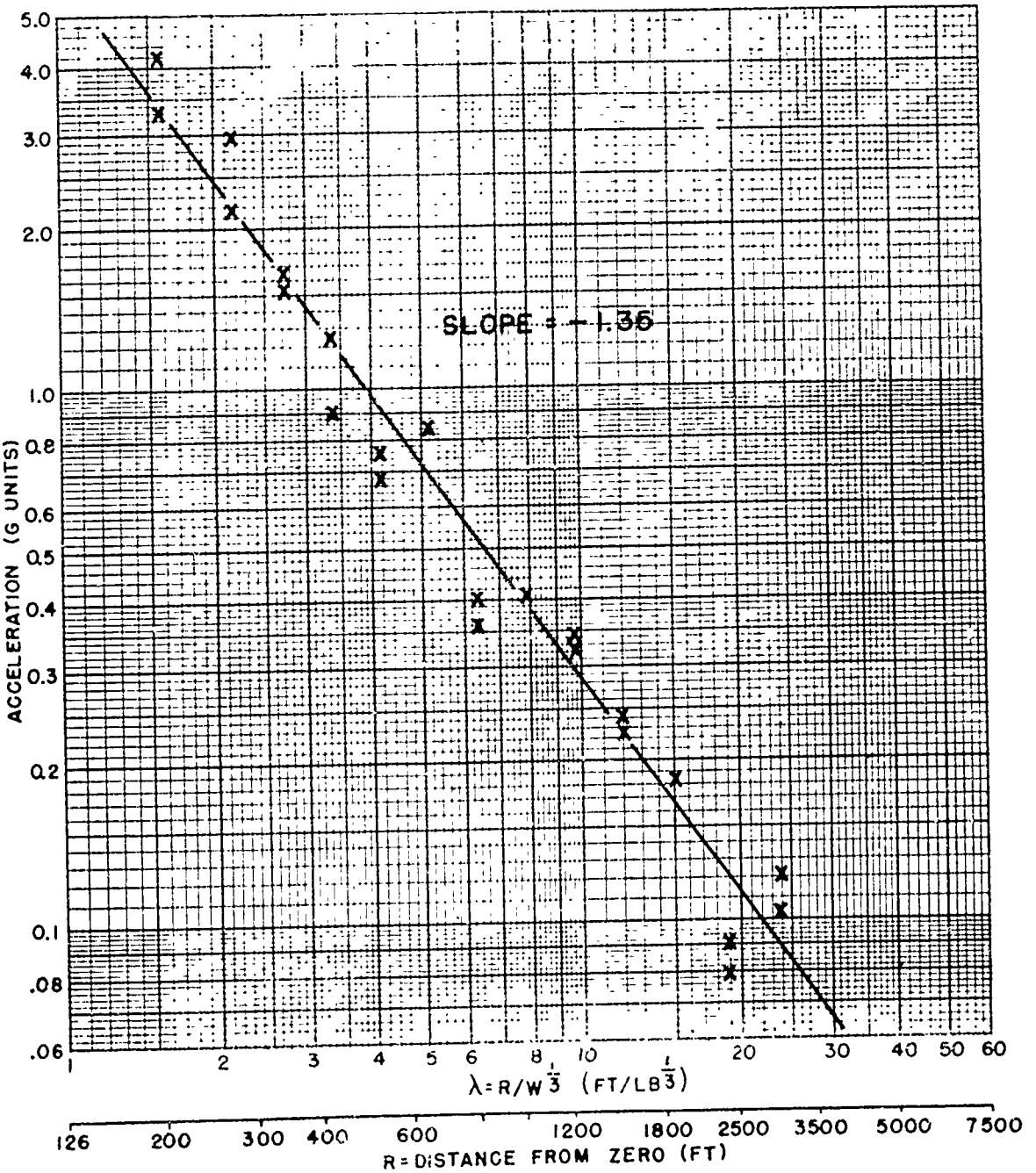


Fig. 7.25 UNDERGROUND SHOT - Maximum Outward Horizontal Acceleration (Excluding Air Blast Effect)

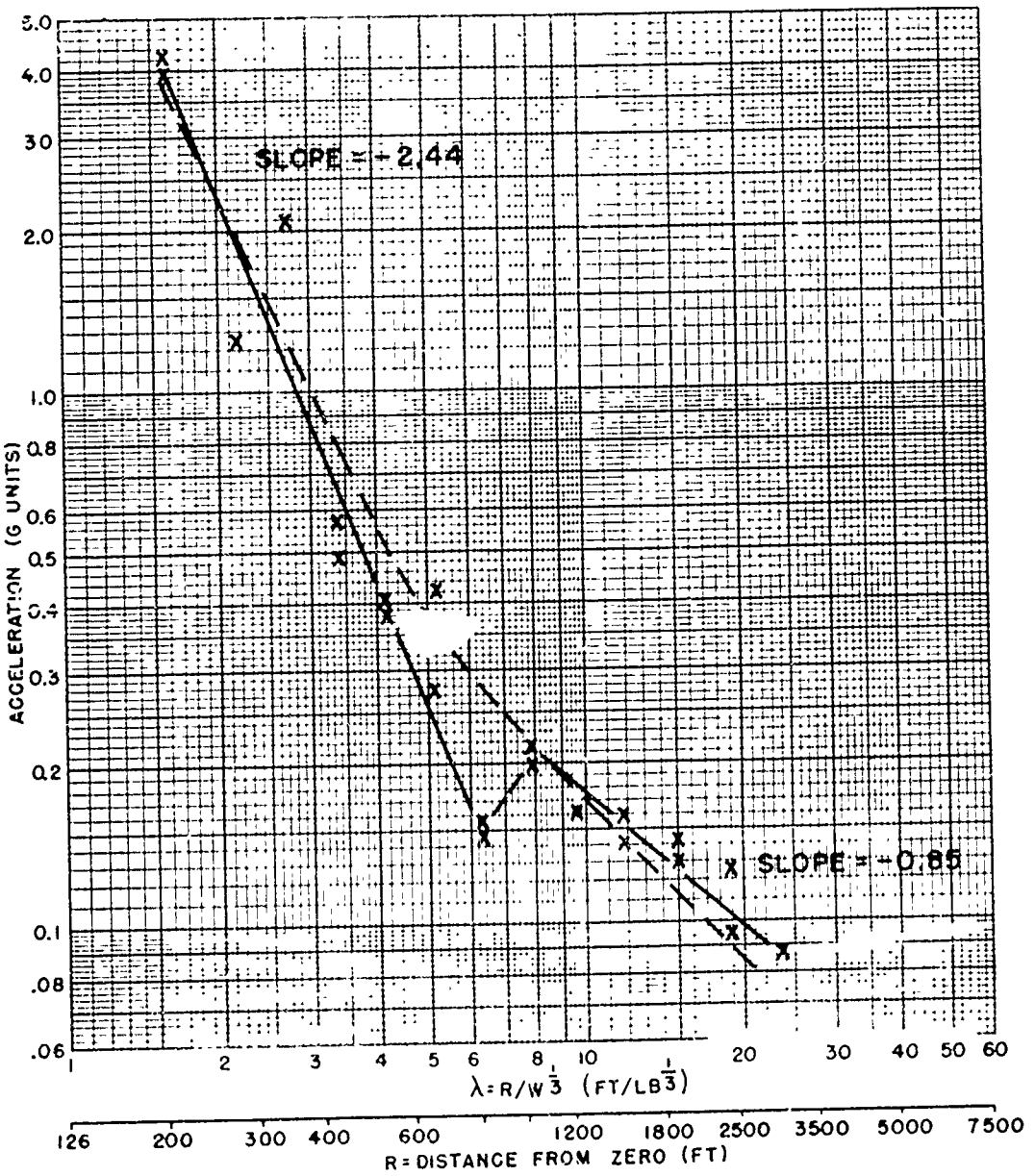


Fig. 7.26 UNDERGROUND SHOT - Maximum Upward Vertical Acceleration (Excluding Air Blast Effect)

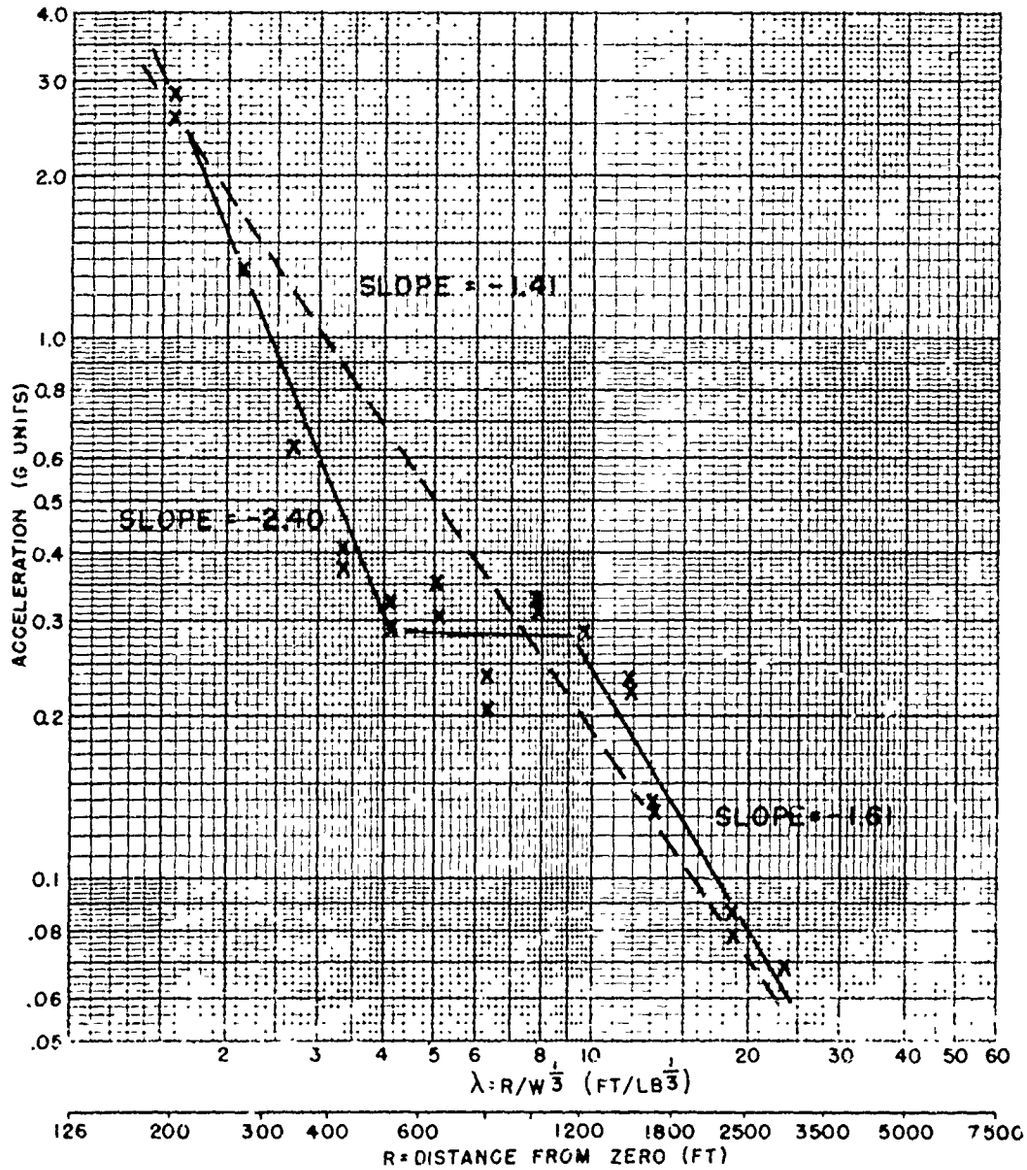


Fig. 7.27 UNDERGROUND SHOT - Maximum Downward Vertical Acceleration (Excluding Air Blast Effect)

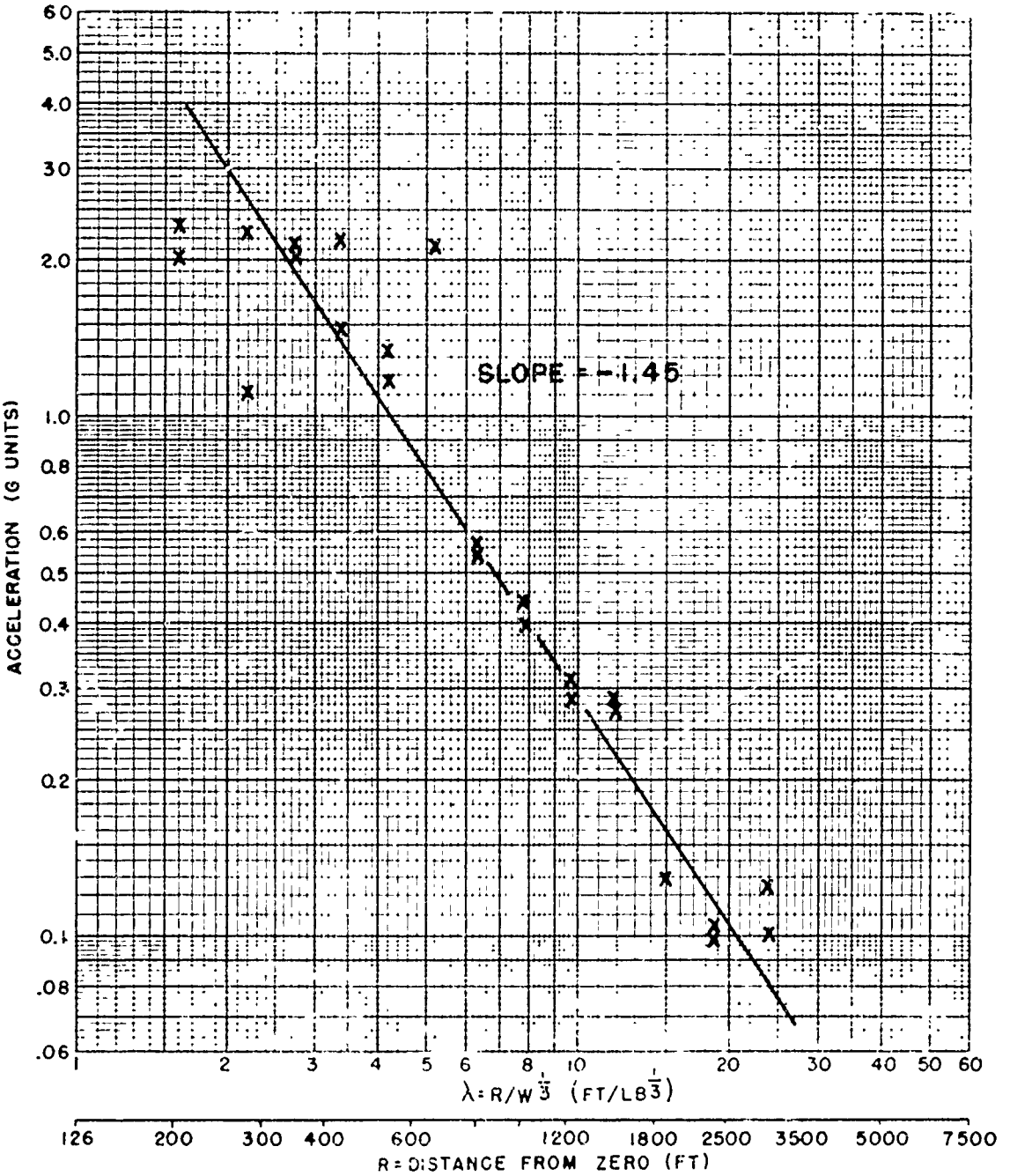


Fig. 7.28 UNDERGROUND SHOT - Maximum Inward Horizontal Acceleration (Including Air Blast Effect)

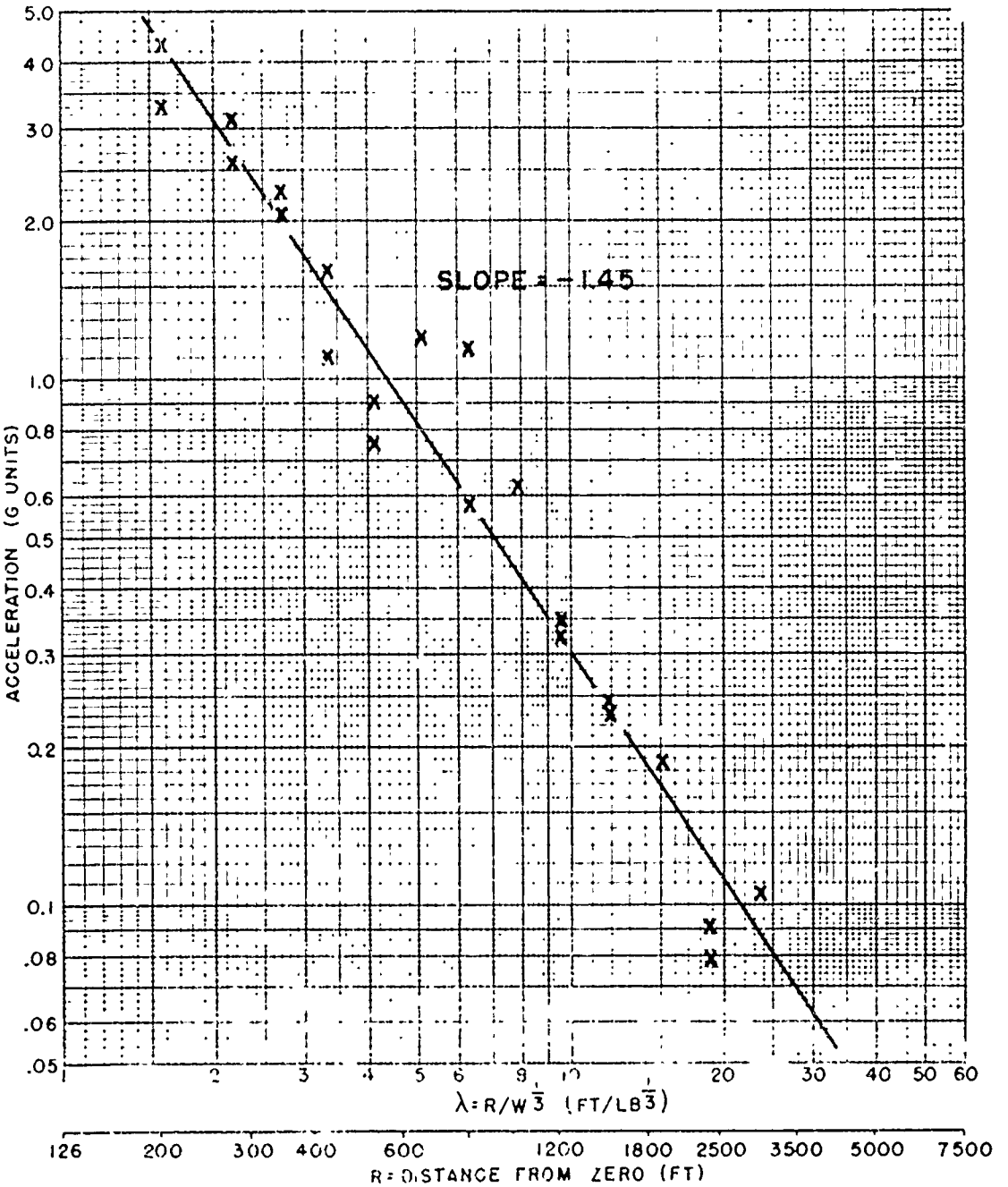


Fig. 7.29 UNDERGROUND SHOT - Maximum Outward Horizontal Acceleration (Including Air Blast Effect)

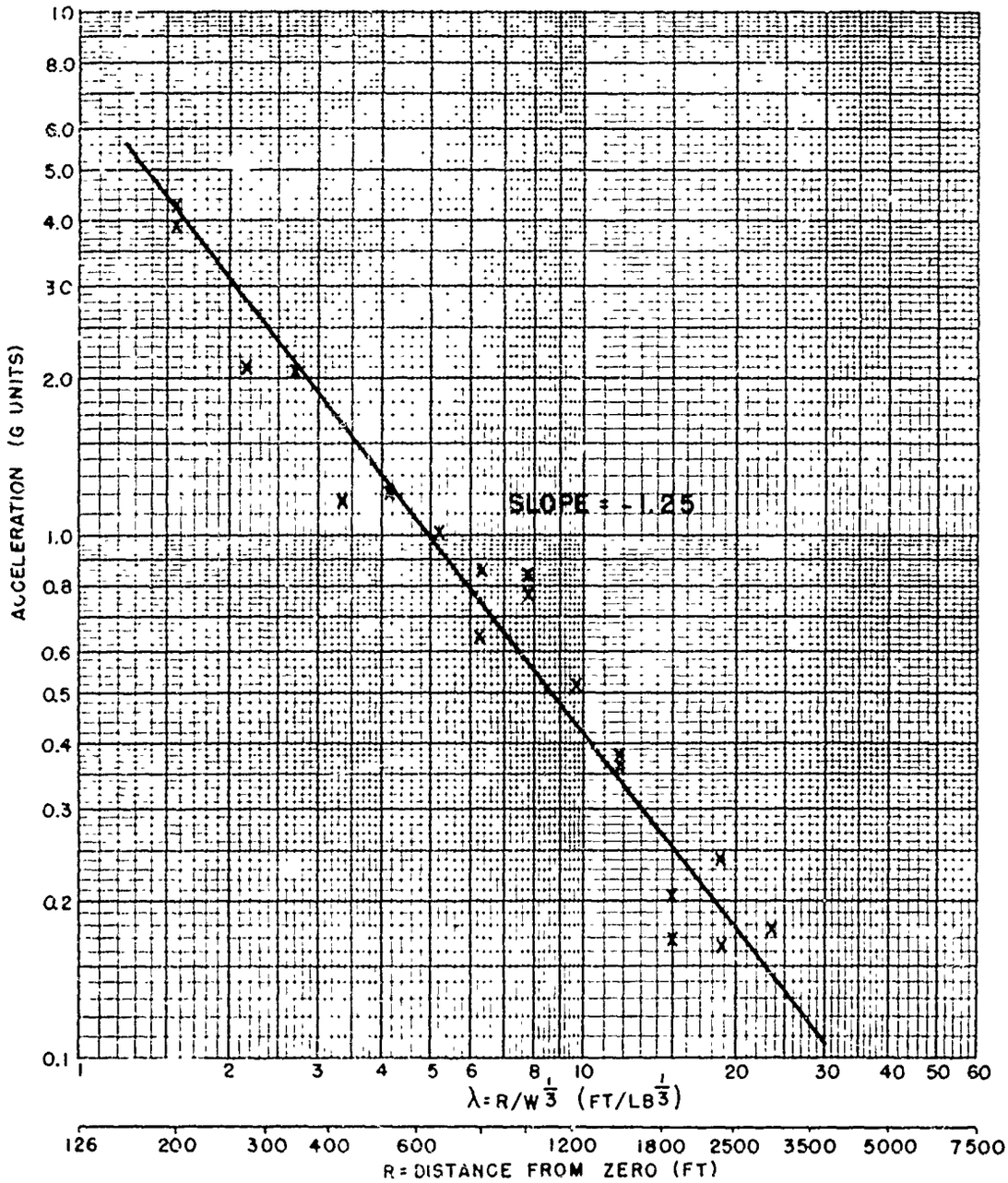


Fig. 7.30 UNDERGROUND SHOT - Maximum Upward Vertical Acceleration (Including Air Blast Effect)

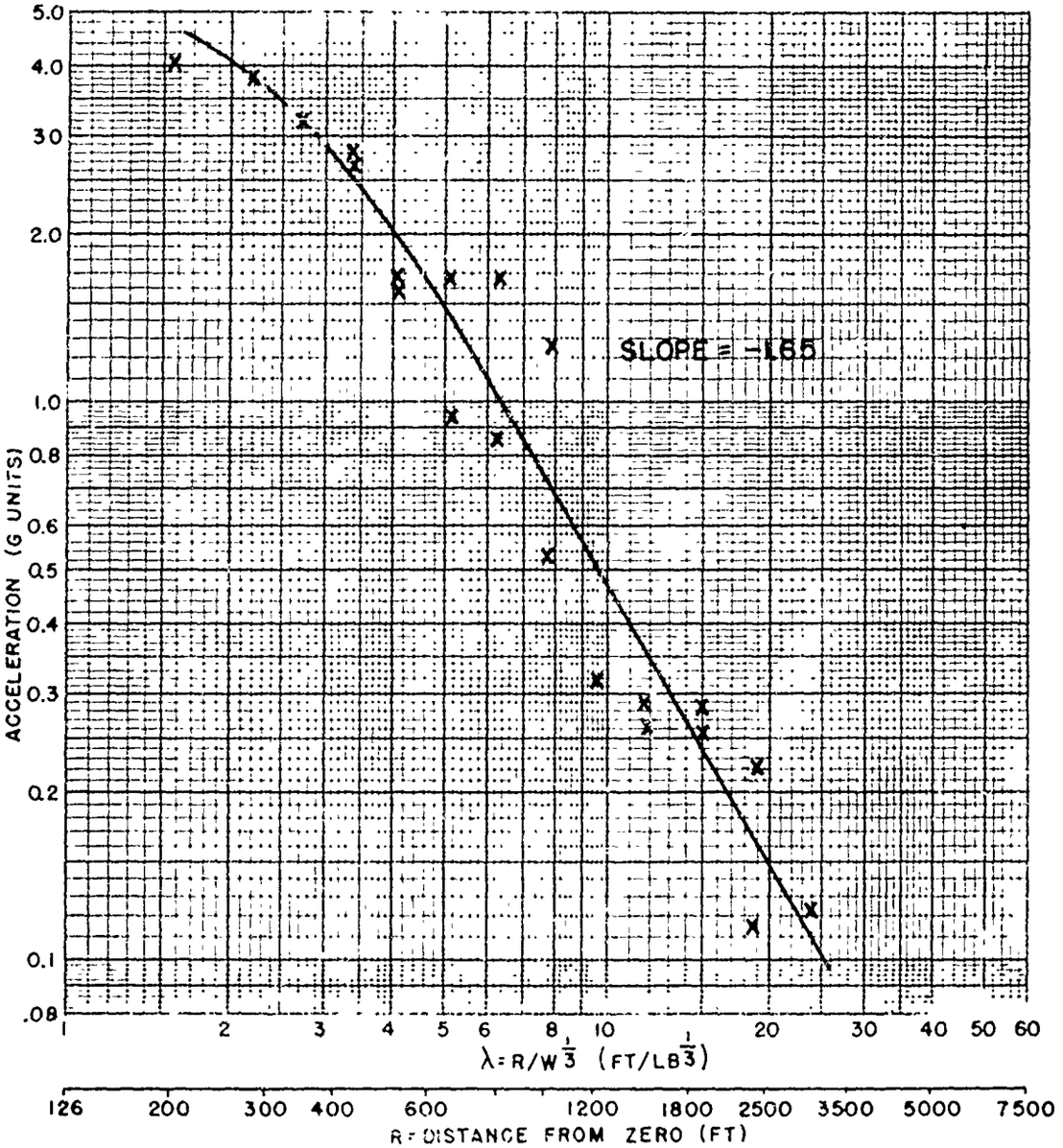


Fig. 7.31 UNDERGROUND SHOT - Maximum Downward Vertical Acceleration (Including Air Blast Effect)

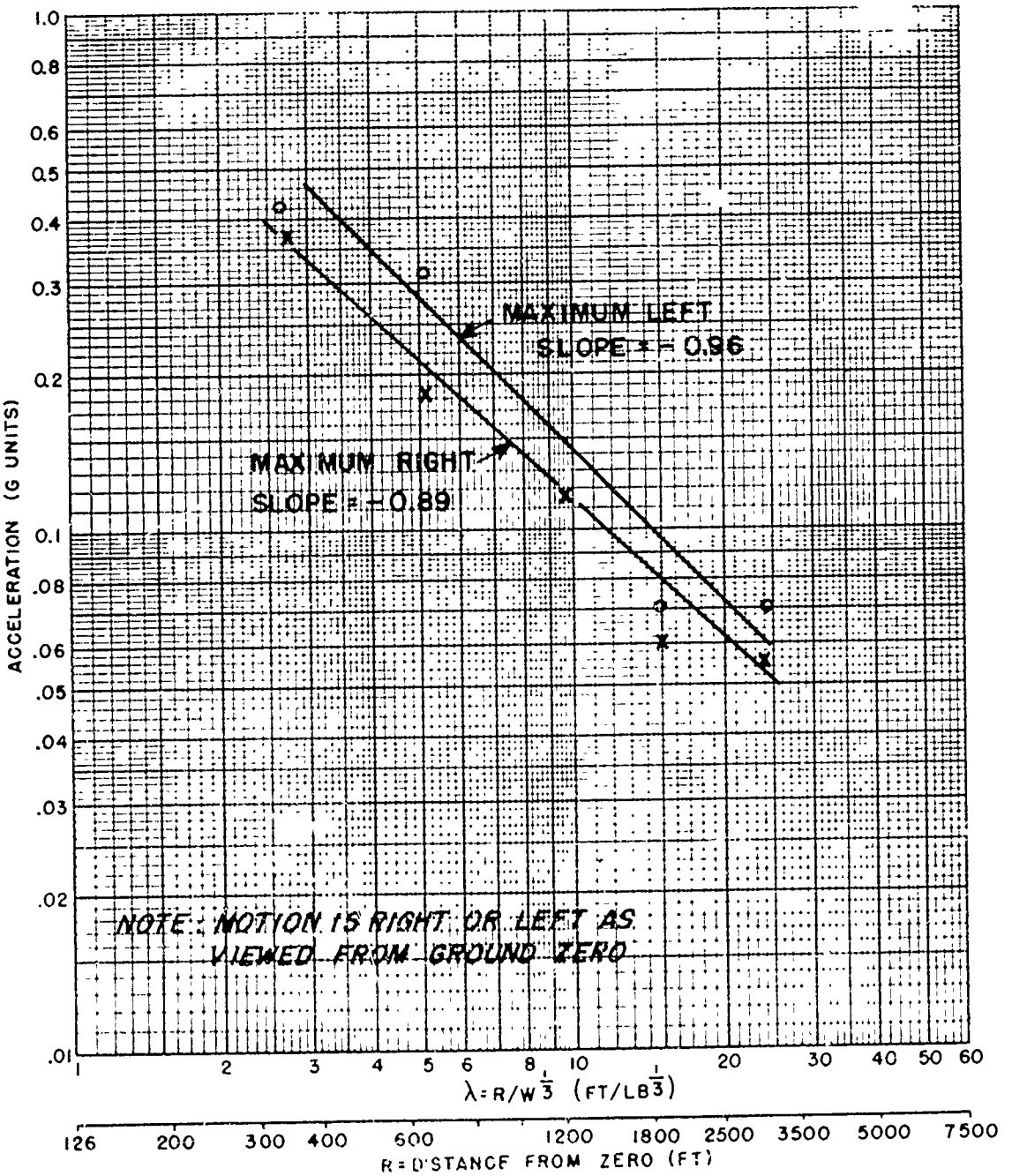


Fig. 7.32 UNDERGROUND SHOT - Maximum Transverse Acceleration (Including Air Blast Effect)

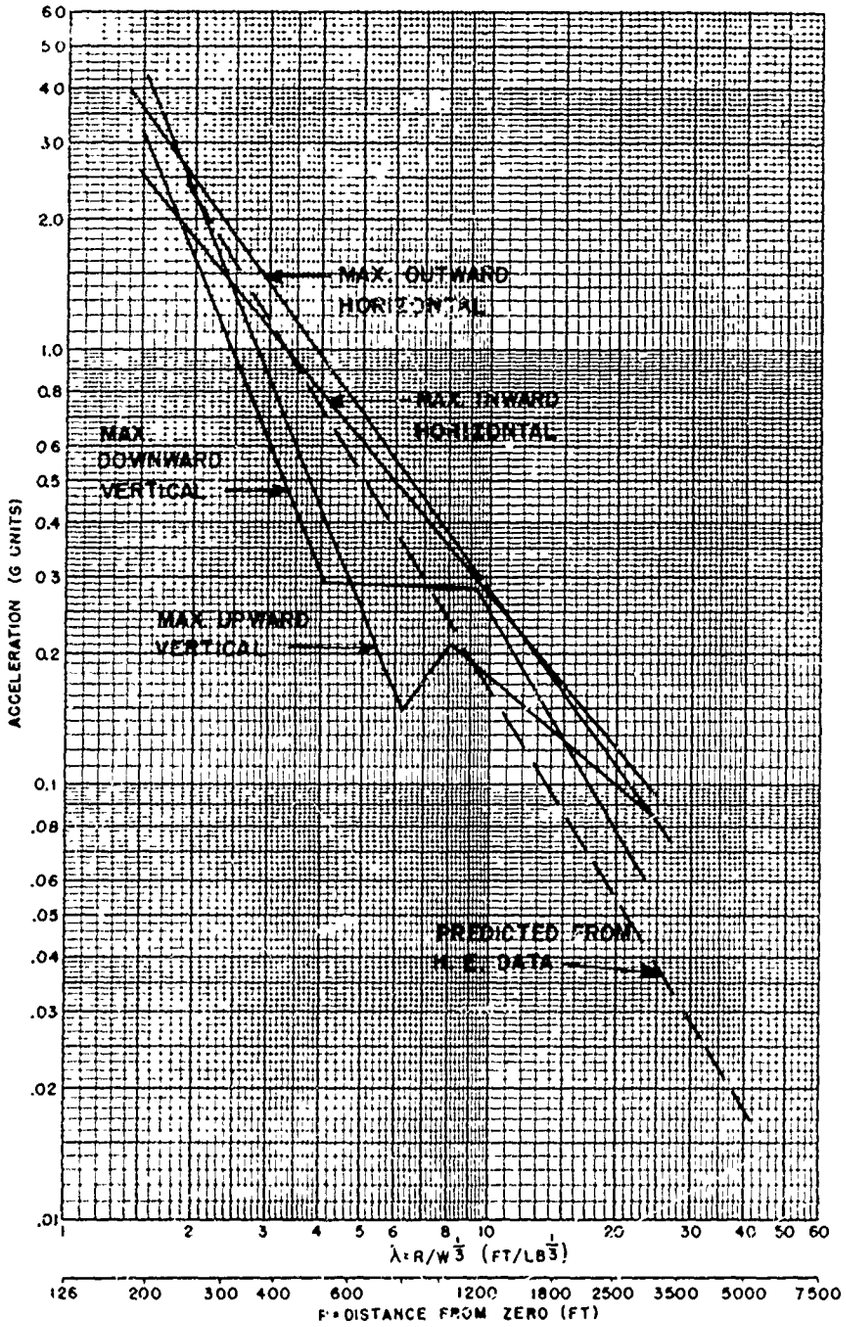


Fig. 7.33 Underground Shot - Composite of All Maximum Acceleration Plots Which Exclude Air Blast Effect (Figs. 7.24 to 7.27)

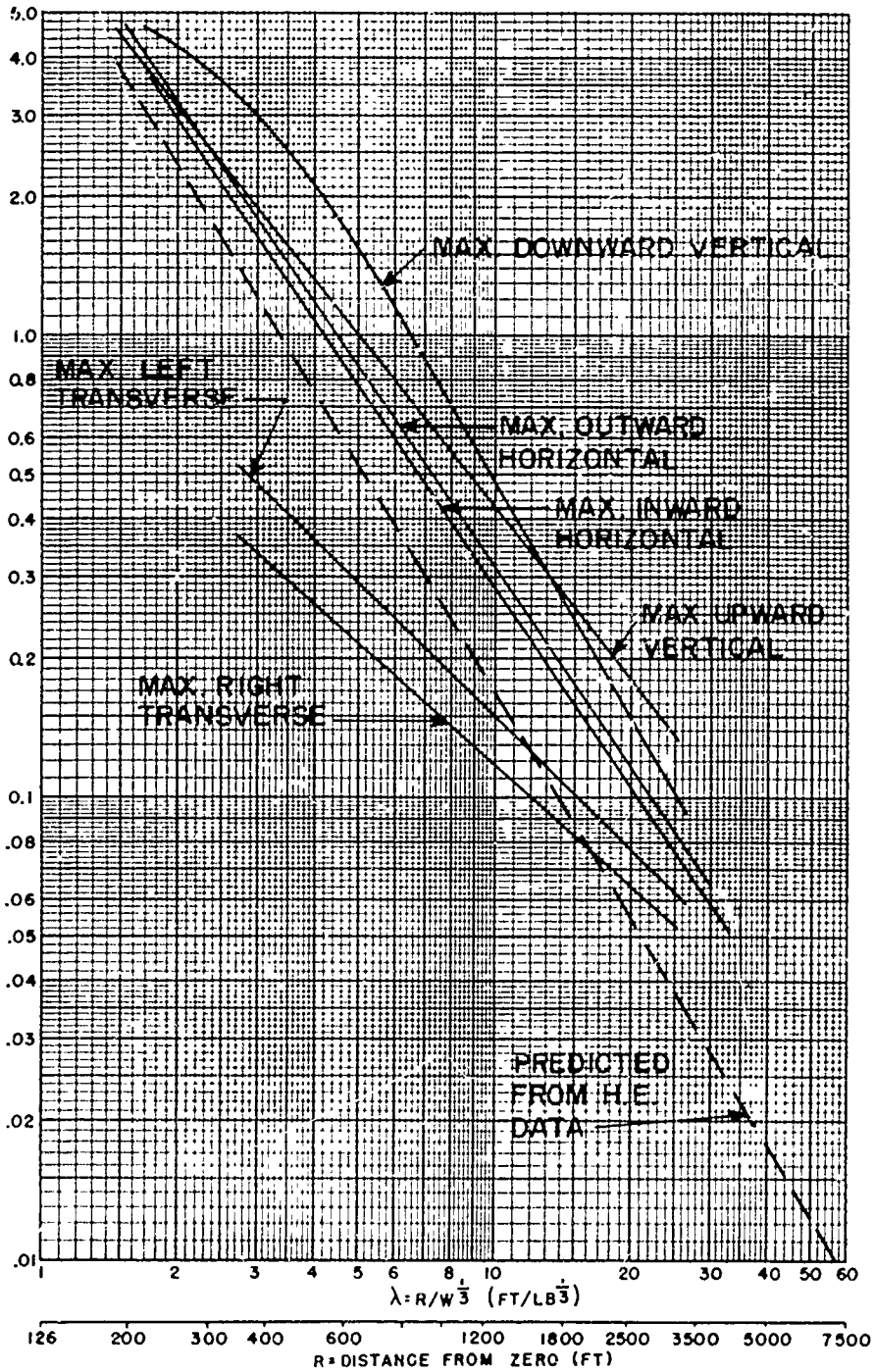


Fig. 7.34 Underground Shot - Composite of All Maximum Acceleration Plots Which Include Air Blast Effect (Figs. 7.28 to 7.32)



RESTRICTED DATA
ATOMIC ENERGY ACT 1946

[redacted]

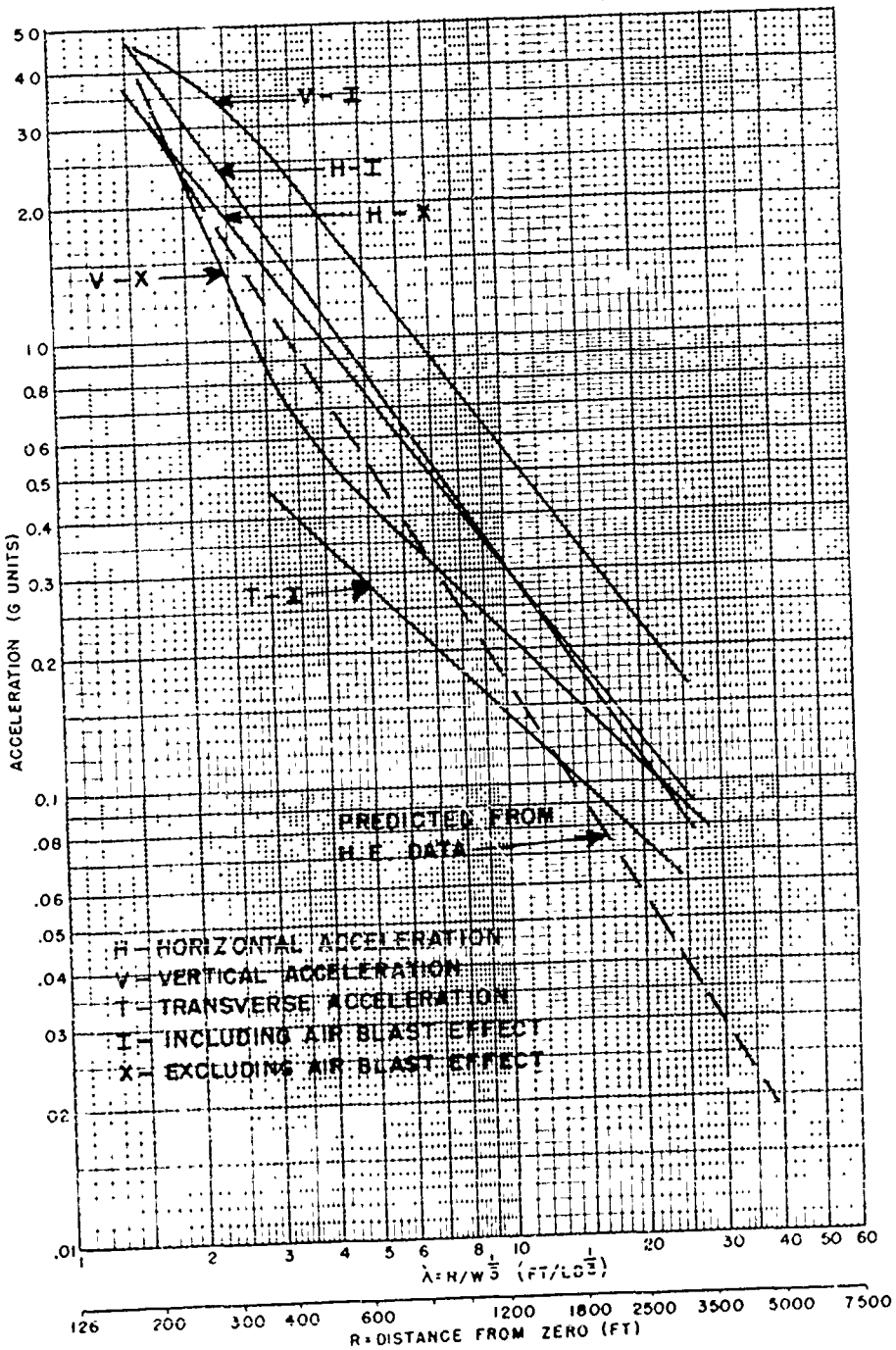


Fig. 7.35 Underground Shot - Composite Plot of Overall Maximum Horizontal, Vertical, and Transverse Acceleration (Including and Excluding Air Blast Effect)

[redacted]

PROJECT 1.1

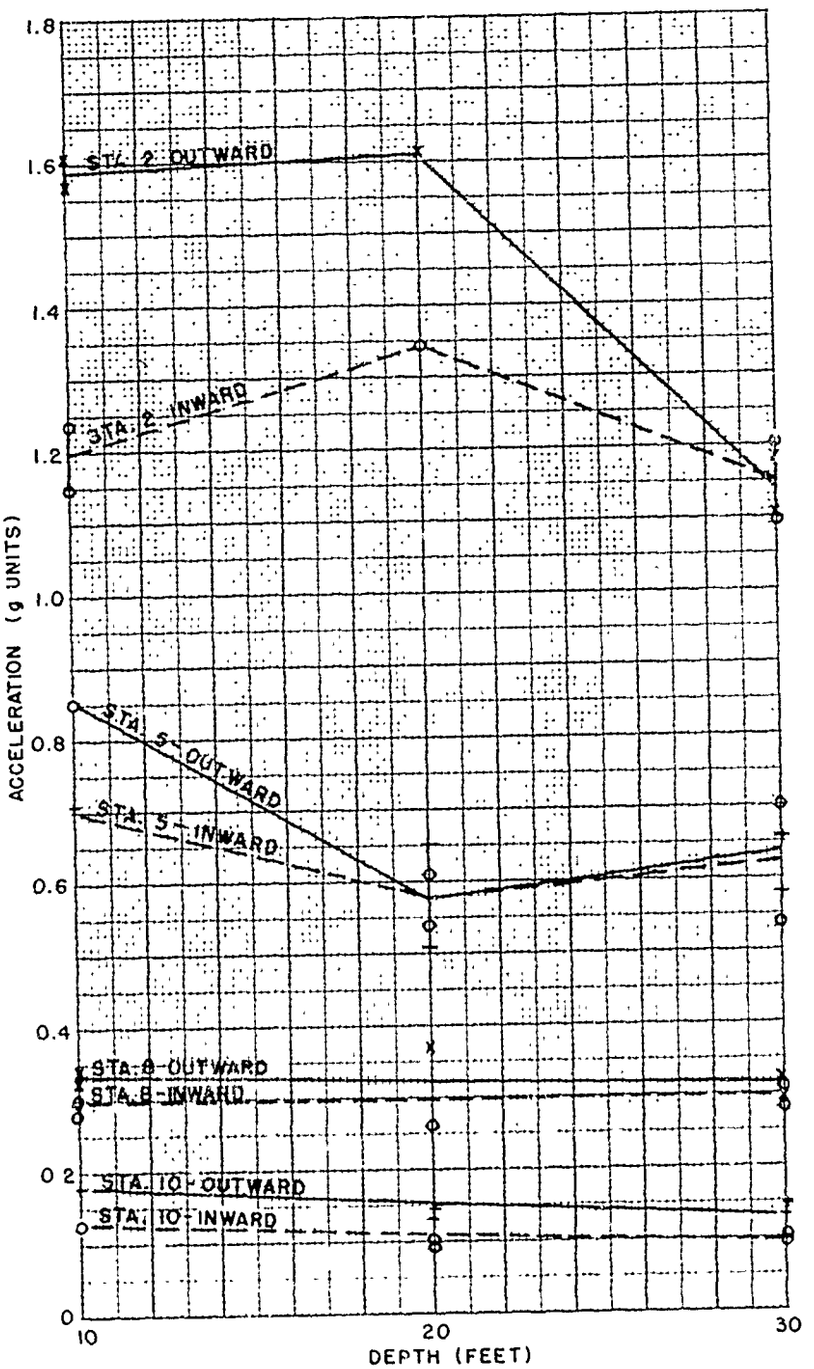


Fig. 7.36 Underground Shot - Maximum Horizontal Acceleration vs Depth (Excluding Air Blast Effect)



[redacted]

PROJECT 1.1

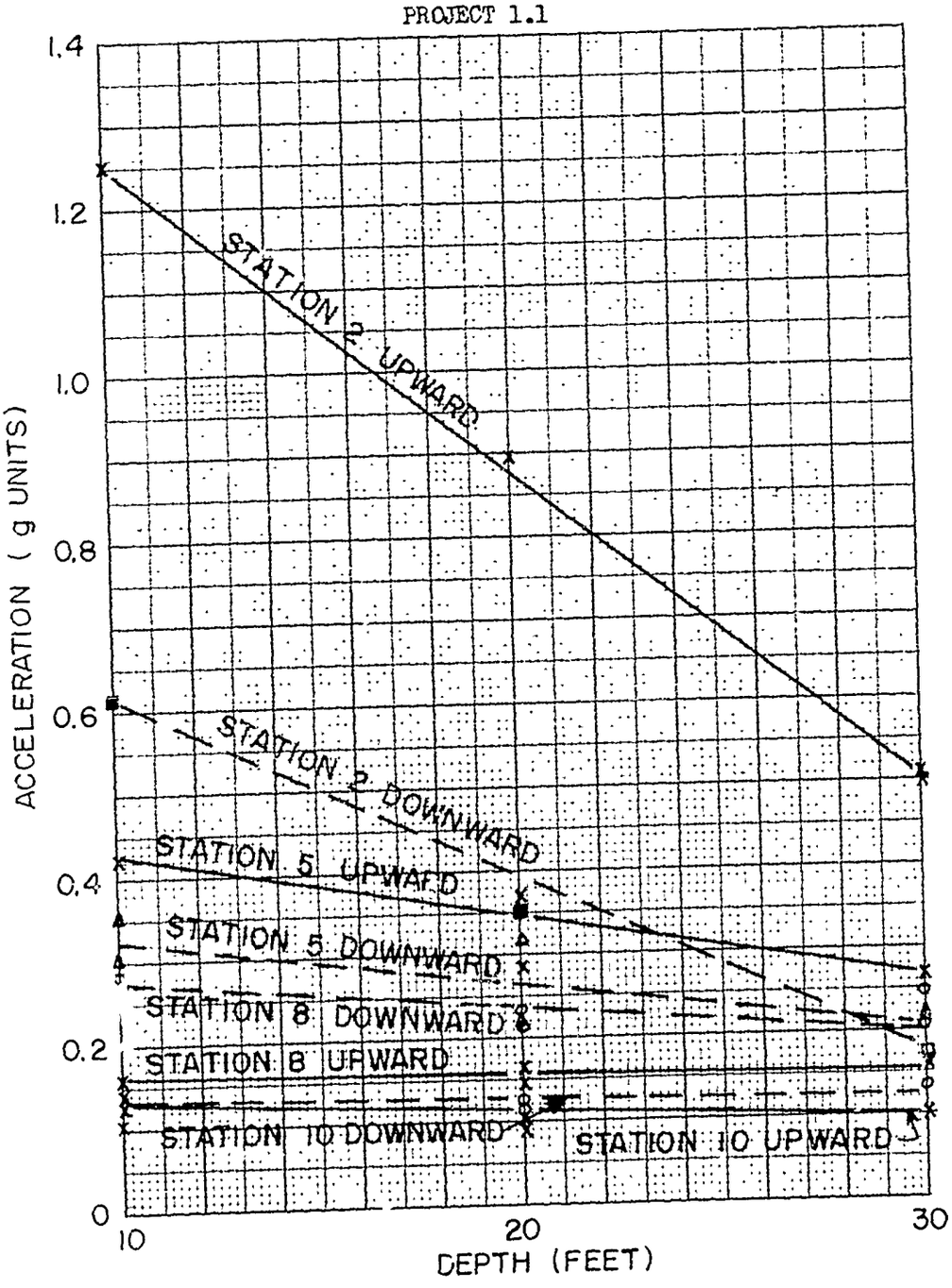


Fig. 7.37 UNDERGROUND SHOT - Maximum Vertical Acceleration vs Depth (Excluding Air Blast Effect)

[redacted]

PROJECT 1.1

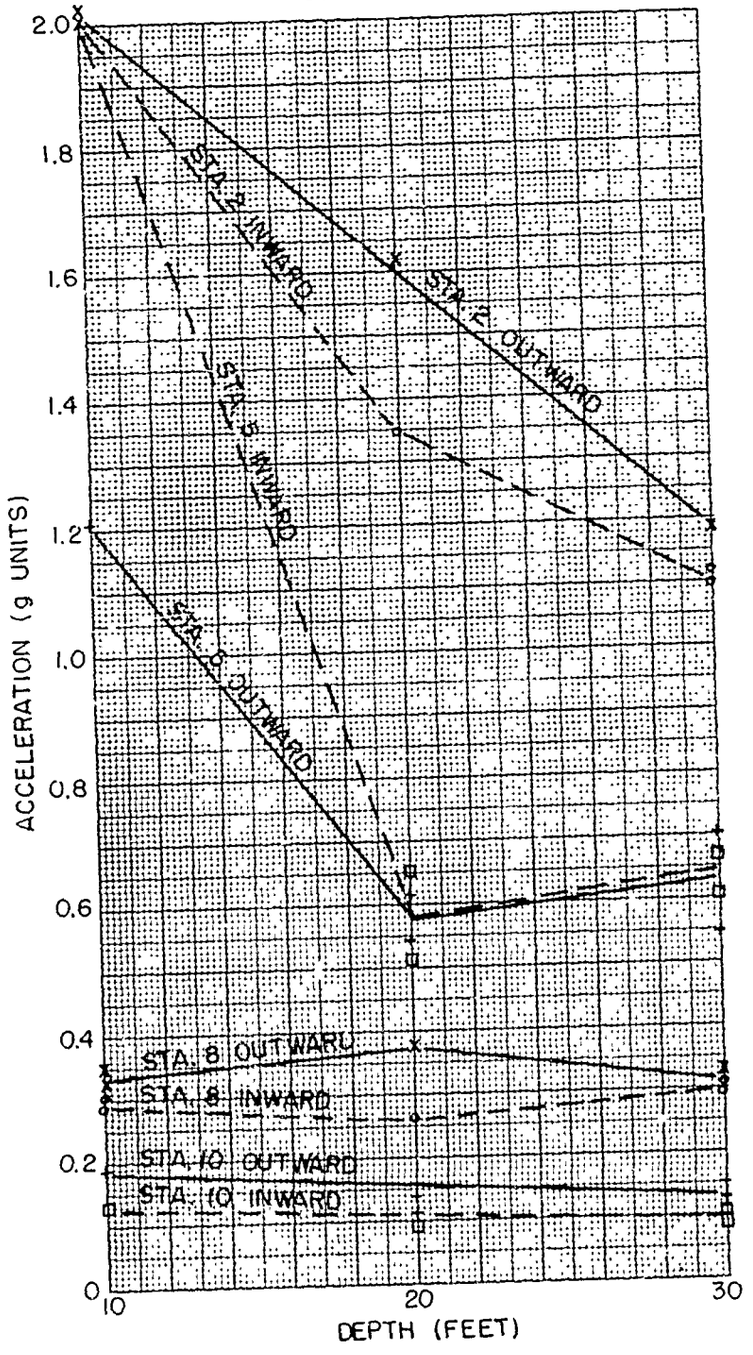


Fig. 7.38 Underground Shot - Maximum Horizontal Acceleration vs Depth (Including Air Blast Effect)



[redacted]

PROJECT 1.1

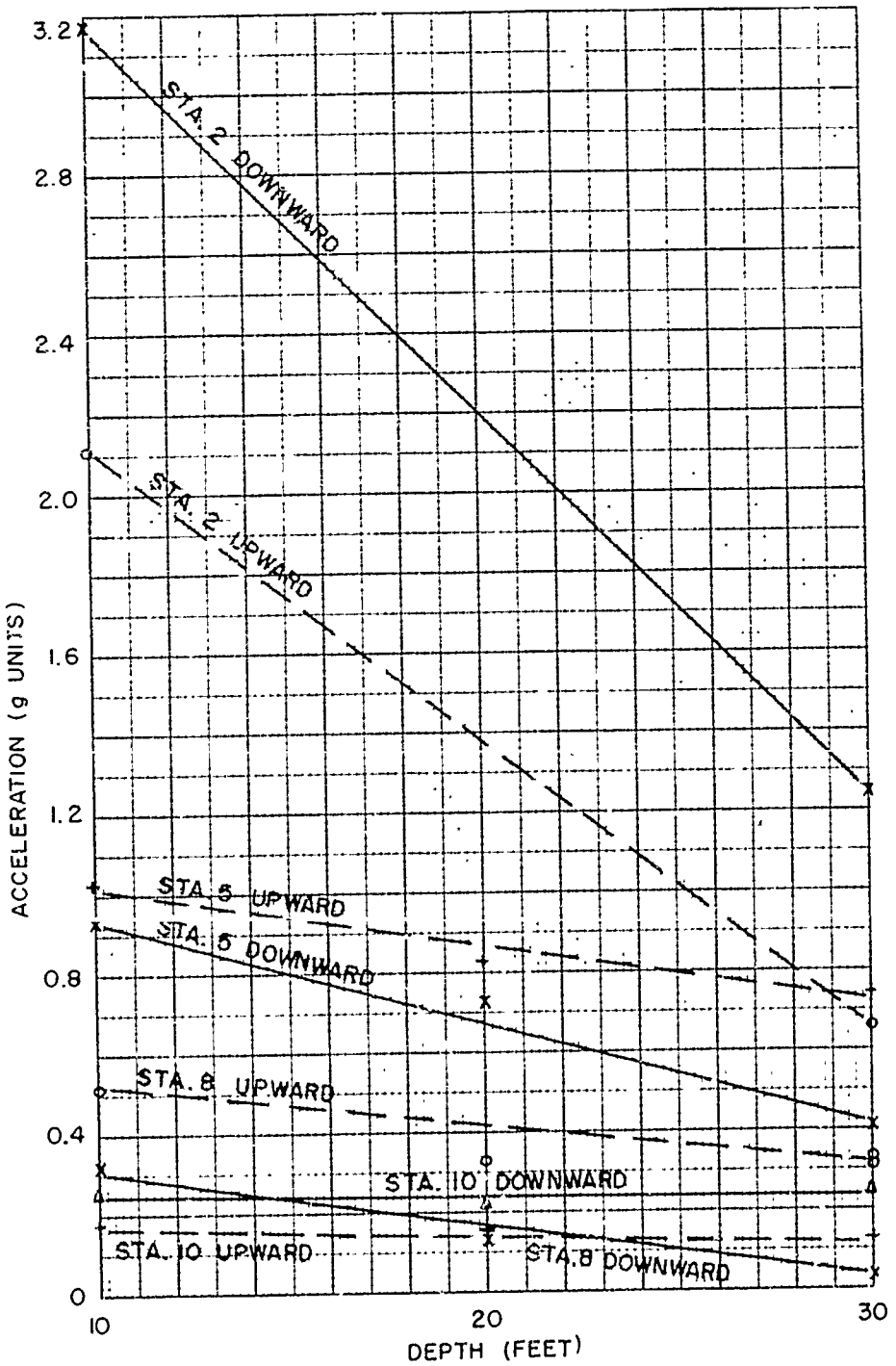


Fig. 7.39 UNDERGROUND SHOT - Maximum Vertical Acceleration vs Depth (Including Air Blast Effect)

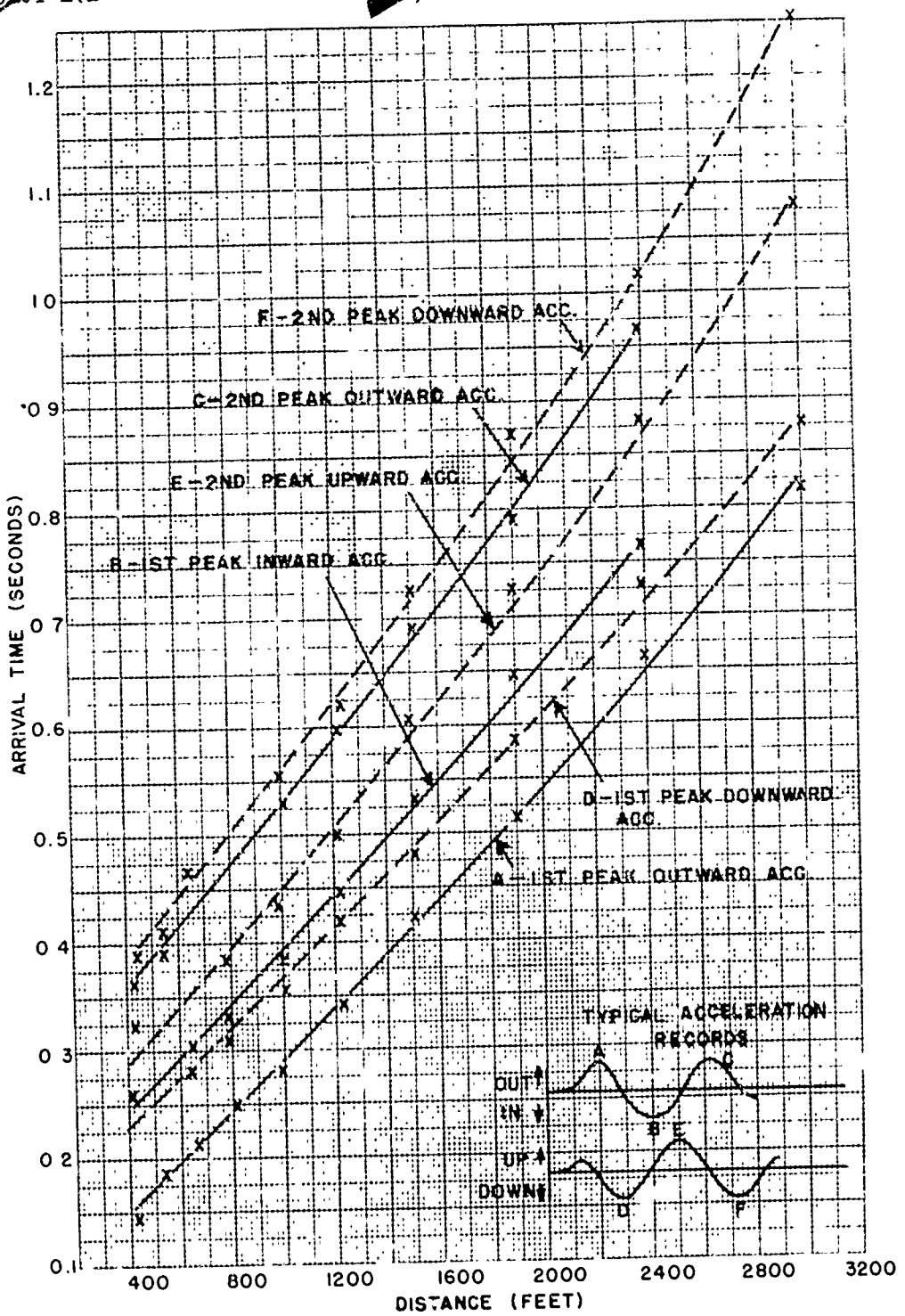


Fig. 7.40 Underground Shot - Arrival Times of Corresponding Peaks



RESTRICTED DATA
ATOMIC ENERGY ACT 1946
Security Information

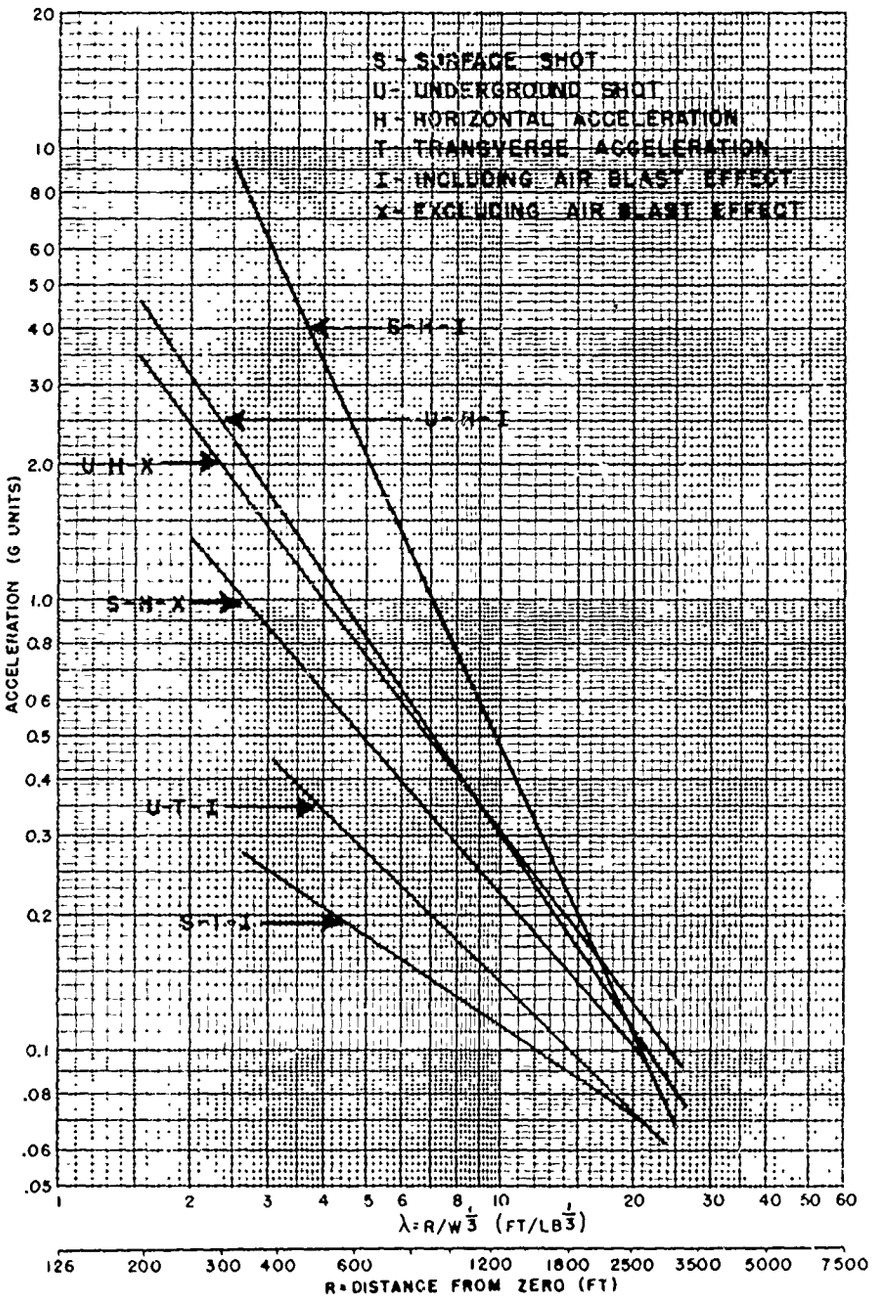


Fig. 7.41 Surface and Underground Shot - Composite Plot of Overall Maximum Horizontal Acceleration



[redacted]

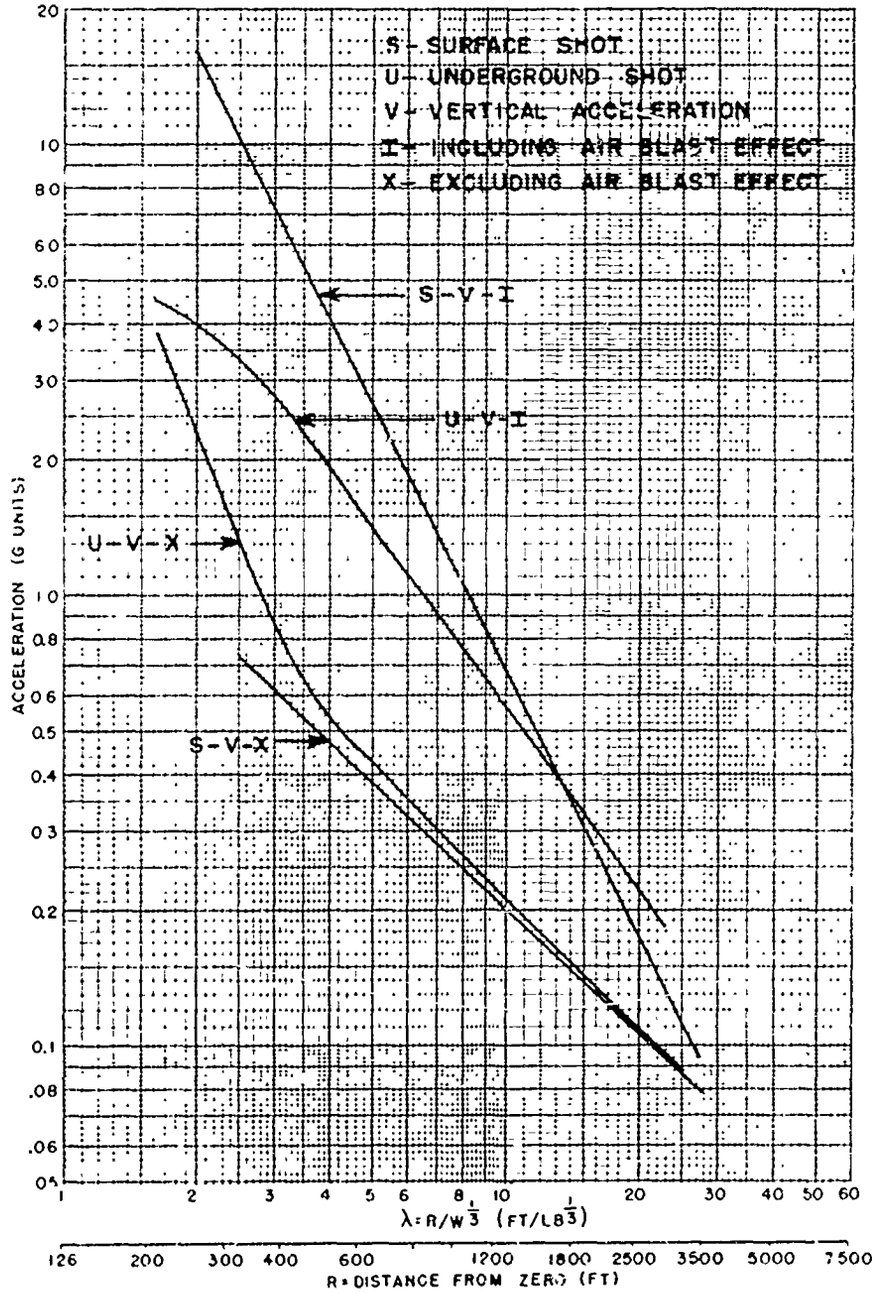


Fig. 7.42 Surface and Underground Shot - Composite Plot of Overall Maximum Vertical Acceleration

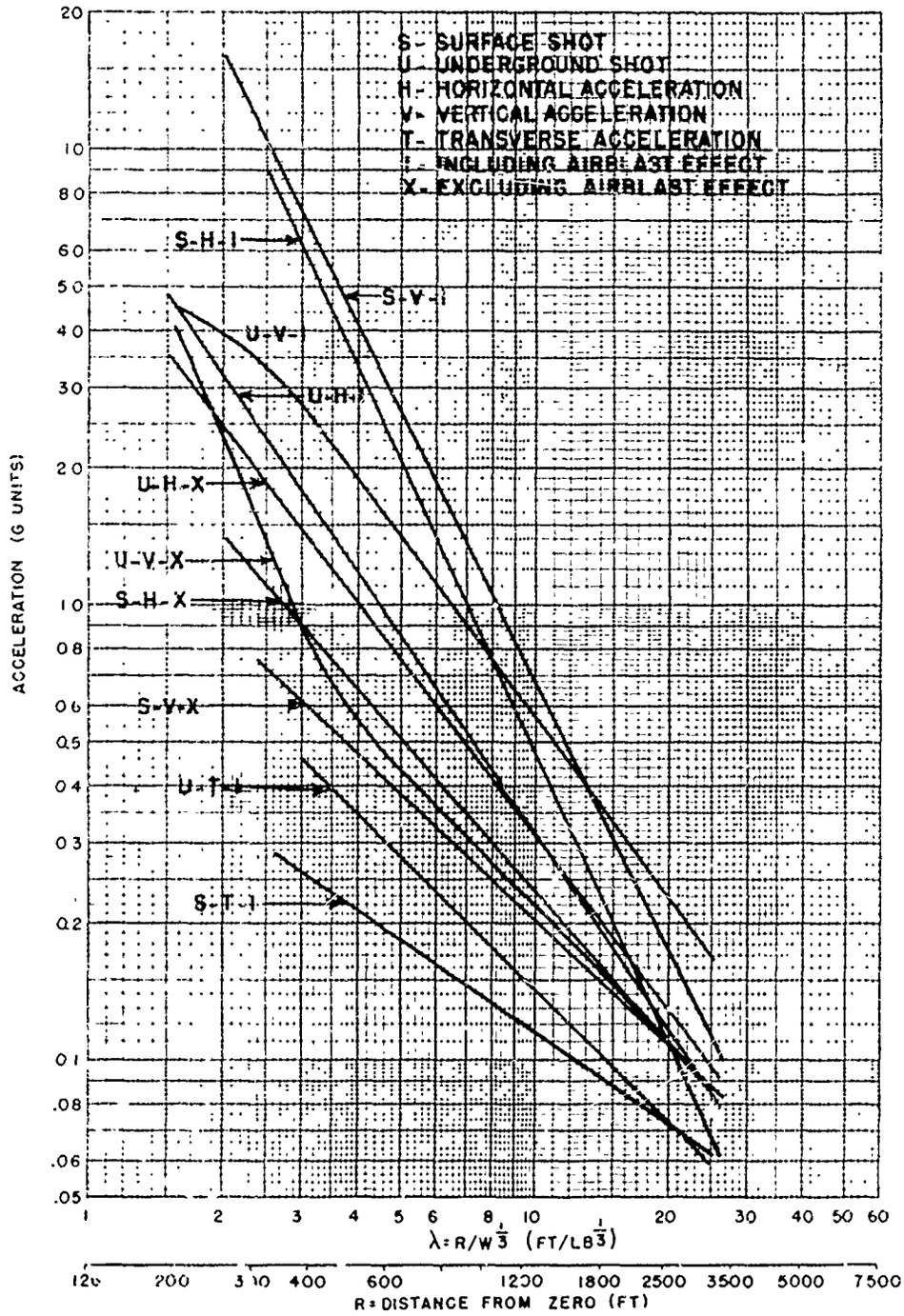


Fig. 7.43 Surface and Underground Shot - Composite Plot of Overall Maximum Horizontal, Vertical, and Transverse Acceleration

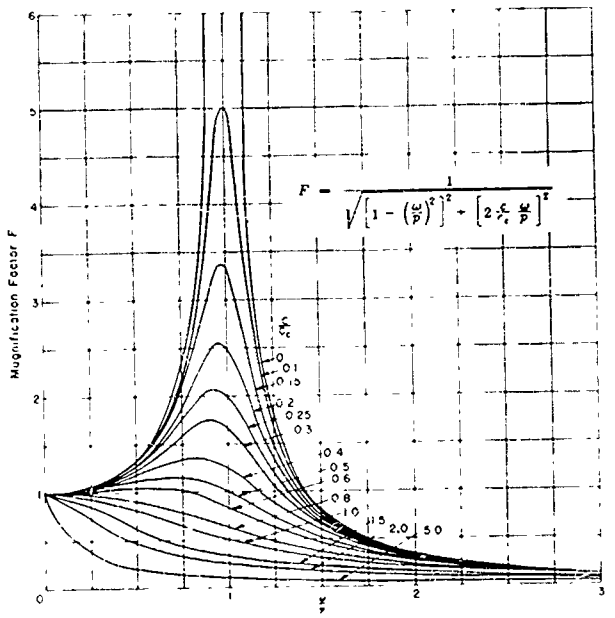


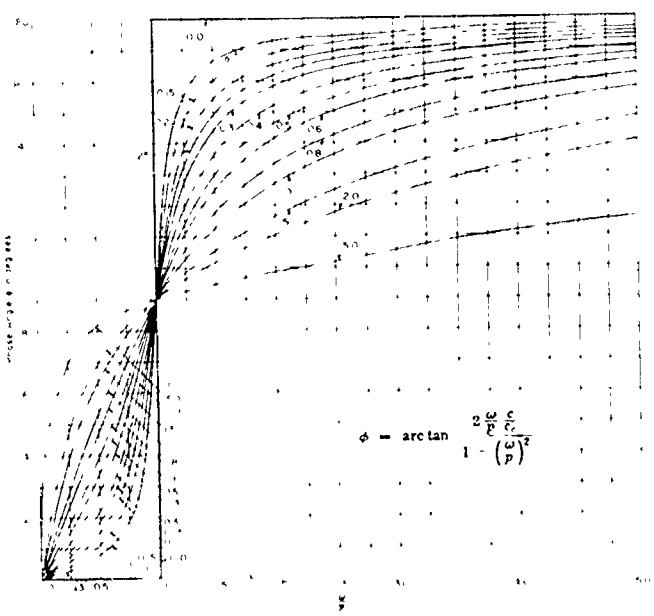


Fig. 7.44 Typical Response Characteristics of Accelerometers to Sinusoidal Acceleration

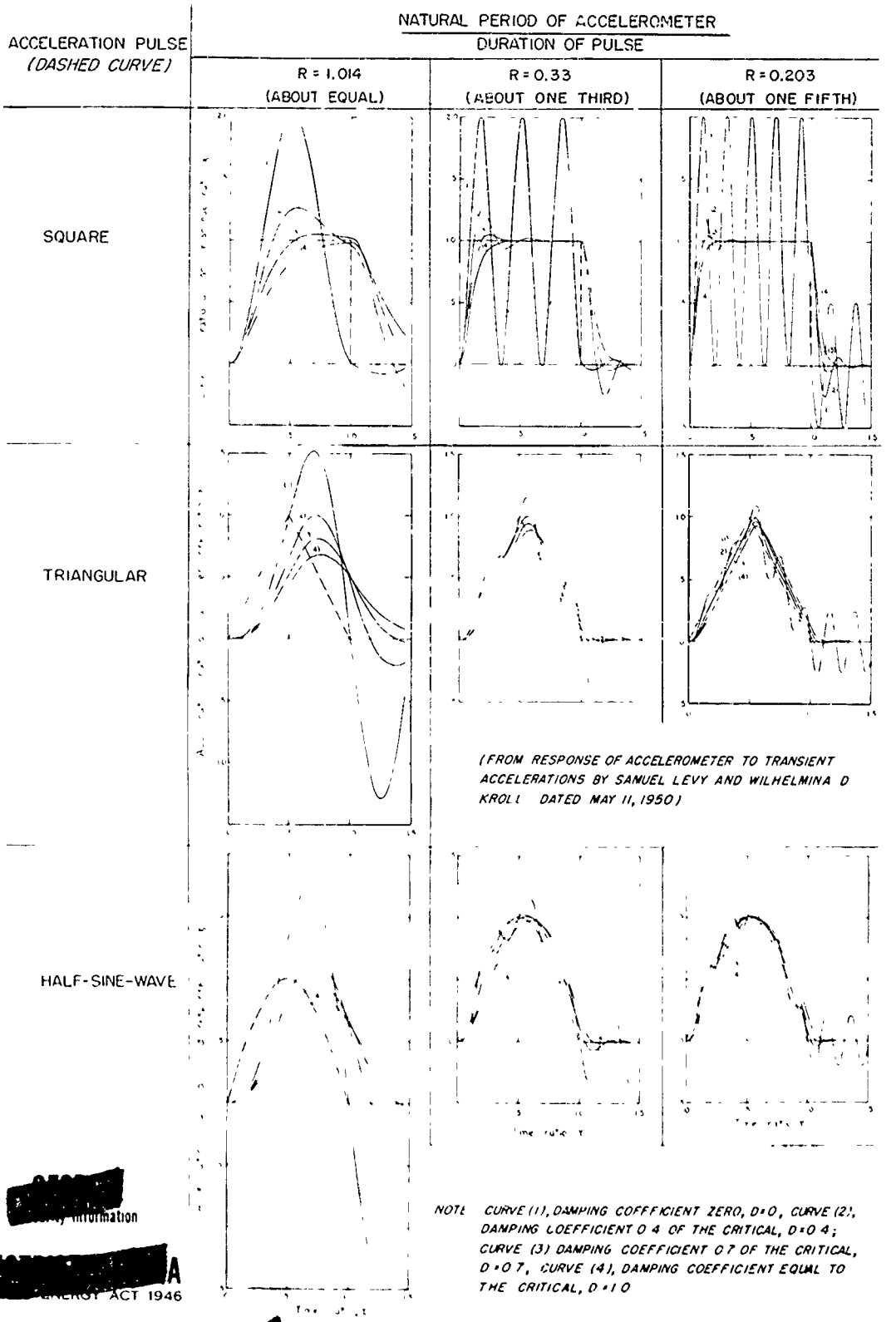


[redacted] information

[redacted]A
A[redacted] ENERGY ACT 1946

Fig. 7.45 Typical Response Characteristics of Accelerometers to Transient Accelerations

SECRET
Security Information

# CHAPTER 8

## CONCLUSIONS AND RECOMMENDATIONS

### 8.1 CONCLUSIONS

The conclusions are listed and summarized as follows:

1. Origins of Acceleration

Acceleration is produced by ground shock arising from the following three sources: (a) ground shock propagated directly from the charge (primary acceleration), (b) ground shock reflected and refracted from underlying bedrock (secondary acceleration), (c) ground shock induced by the air blast (air blast acceleration). The reflected pulses were very prominent and most pronounced at the station closest to zero. For a location where the bedrock is at a shallow depth it appears likely that the reflected acceleration would be very important. The acceleration induced in the ground by the air blast was in the form of a high frequency short duration pulse that is easily distinguishable from the rest of the acceleration pattern. This air blast acceleration pulse is very prominent and interacts with the fundamental acceleration and superposition effects were observed. The primary and secondary acceleration is, for the most part, indistinguishable and is treated as a unit termed fundamental acceleration.

2. Propagation

On the surface shot the air blast acceleration initially preceded the fundamental acceleration, while on the underground shot the fundamental acceleration preceded the air blast acceleration at all times. For both shots the velocity of propagation decreased for some distance out from zero.

3. Magnitude of Effects

When the air blast acceleration is included in the analysis, the surface shot acceleration is 4 times larger than the underground shot acceleration at a distance of 2 $\lambda$ . The air blast acceleration is of the order of 12 times the fundamental acceleration for the



RESTRICTED DATA
ATOMIC ENERGY ACT 1954
SECRET
Security Information

surface shot at $2\lambda$ and 1.6 times the fundamental acceleration for the underground shot. When the air blast effect is excluded from the analysis and only the fundamental acceleration considered, the underground acceleration is two to three times that of the surface shot acceleration. For both shots, the vertical acceleration component is the largest when the air blast effect is considered, and the horizontal component is the largest when the air blast acceleration is excluded. The transverse acceleration is appreciable, but is very much less than the horizontal or vertical components.

4. Attenuation of Acceleration with Distance

On a log-log plot the acceleration for most of the components for both shots attenuate in a straight line curve of the form of Eq. 7.1; namely,

$$A = \frac{A_o \lambda^{-n}}{W^{1/3}}$$

where the slope, n, for the various components varies between 1 and 2. The air blast acceleration closely follows the air blast attenuation, and attenuates much more rapidly for the surface shot than for the underground shot. The fundamental acceleration attenuates much the same for both shots.

5. Acceleration as a Function of Depth

For both the surface and underground shots, the acceleration decreased with the depth of measurement at the stations closest to zero, and with the greatest decrease noted at the nearest station. The attenuation of acceleration with depth was more pronounced for the air blast acceleration than for the fundamental acceleration. Far out from zero no effect of depth was observed.

6. Acceleration Frequencies

The acceleration time curves are very complex and are made up of many transient type pulses and high frequency components. The low frequency pattern of the acceleration curve was measured and this meant ascribing frequencies to pulses which were transient in nature. The air blast acceleration frequency, so measured, varied between 20 and 50 cps for both shots. The fundamental acceleration frequency was predominantly in the range of 10 to 14 cps for the surface shot and in the range of 3 to 6 cps for the underground shot.

Even though the air blast acceleration is much larger than the fundamental acceleration, it may not be effective from the standpoint

of damage to structures due to its high frequency characteristics. Likewise, the fact that the fundamental acceleration frequencies of the underground shot are lower than those of the surface shot may be important from the standpoint of structural response.

7. Effectiveness of the Surface Shot Compared to the Underground Shot

From the standpoint of maximum acceleration, the surface shot was much more effective, due to the contribution of the air blast induced acceleration. This air blast acceleration, however, consists of a single high frequency pulse; the lower frequency nature of the fundamental acceleration, which is comprised of many cycles, may be more important from the standpoint of structures. If this is so, then the air blast acceleration must be excluded from the analysis and the comparison made considering only the fundamental acceleration. When compared on this basis, the underground shot was more effective since it produced accelerations with frequencies 2 or 3 times lower and magnitudes 2 or 3 times larger than the surface shot.

8. Scaling of Nuclear Explosions with HE

It is difficult to draw conclusions concerning scaling due to the variability in results that is typical of underground explosions and due to the limited number of shots available for comparison. In scaling it is absolutely necessary to consider the air blast acceleration and the fundamental acceleration separately, as each scales differently. The air blast acceleration scales in similar manner to the air blast, but the relationship is not clear from the limited analysis that has been made. The fundamental acceleration for the underground shot appears to scale reasonably well with the 40,000 lb HE shot at Yucca Flats in accordance with Eq. 7.1. Data are not available for comparison of the surface shot with the only HE surface shot that has been detonated at the site.

8.2 Recommendations

It is recommended that:

1. Correlation be made among the medium measurements and this should include:

(a) Correlation with other acceleration measurements; namely, with ERA gages, Standard Research measurements, and shock pin measurements



RESTRICTED DATA
[redacted]

(b) Correlation with permanent displacement as measured by Shear shafts and the post test survey

(c) Correlation of ground acceleration with ground pressure

(d) Comparison of the various experiments that measured arrival times.

2. An attempt be made to integrate the acceleration records to give velocity and displacement.

3. Medium measurements be correlated with response and damage of structures, and this analysis should consider:

(a) The effect of both magnitude and frequency and the relationship of the two

(b) The importance of the air blast acceleration

4. Further underground HE tests be conducted with the objectives of:

(a) Studying the effect of depth of burial for charges both in and out of the ground

(b) Further investigating scaling between tests at a particular site and between tests at different sites

(c) Measuring displacement and velocity as well as acceleration and ground pressure

(d) Investigating scaling of air blast acceleration.

5. Underground HE tests be conducted in more typical locations where the bedrock and water table are close to the surface with the objective of testing the enhancing power of reflected and refracted ground shock that appeared to be rather important in the Yucca Flats tests.

6. Accelerometer development be carried on along lines which will provide a gage with a linear response, greater dynamic range, and higher frequency response.

7. The response of accelerometers to transient pulses similar to those produced by nuclear shots be studied.

8. Work be done to increase the signal to noise ratio of the recording system.

9. If future nuclear tests are conducted, they should:

(a) Use a larger atomic weapon of at least 20 kt

(b) Bury the charge deeper, if possible, in order to produce greater ground shock and to also study the effect of depth

(c) Make medium measurements closer to zero than on JANGLE; specifically, the measurments should start at the edge of the crater

(d) Make velocity and displacement measurements by means of velocity and displacement gages and by means of high speed photography

(e) For shallow shots determine whether air blast acceleration should be measured along with the fundamental acceleration

(f) Use improved gages and recording system as outlined in items (6) and (8)

(g) Use telephone cable instead of shielded cable to transmit the signal. The feasibility of this has been demonstrated on TUMBLER.

[redacted]

# CHAPTER 9

## ADMINISTRATIVE ARRANGEMENTS

This chapter contains information on the administrative arrangements that were used at the Naval Ordnance Laboratory and the working arrangements that existed with the Ballistics Research Laboratory and the Vitro Corporation.

### 9.1 ARRANGEMENTS WITH THE BALLISTICS RESEARCH LABORATORY

A delineation of the specific assignments of the Naval Ordnance Laboratory and the Ballistics Research Laboratory in the ground shock program is presented in Chapter 1. It will be noted that the NOL recording system was used for recording the pressure information from the BRL gages and that BRL provided back-up acceleration measurements with ERA gages. Procurement for both laboratories was accomplished through the NOL Supply Department and the Vitro Corporation. As these common features necessitated close liaison and cooperation between the two laboratories, joint meetings of the planning personnel were held about every two weeks. At these meetings the numerous problems of joint operations were resolved and future actions delegated. This arrangement accomplished much which could not have been done by correspondence or telephone within the time schedule for the operation.

### 9.2 FIELD GROUP ORGANIZATION

Due to the short time schedule of the operation and personnel shortages at the NOL occasioned by assignments to Operation Greenhouse, engineering and procurement assistance was required. This was provided in the form of a Bureau of Ordnance contract with the Vitro Corporation of Silver Springs, Maryland, which obligated that organization to assist in supply problems and to provide technical assistance and field engineering services. Vitro expended about 85 man months in technical assistance in design and development of oscillators, placement gear and distribution panels. They provided eight engineers for the field trip to the Test Site in August and September and five men during the month of November.

AFSWP supplemented the personnel available at the Laboratory by detailing six Naval officers, two Air Force officers and one civilian scientist to the group. The total field party of twenty-eight men consist[redacted]



[redacted]

of nine persons from AFSWP, eight from Vitro Corporation, and eleven from the Laboratory. The names and primary duties of these personnel are listed below:

| Name | Title | Duties | Organization |
|---|---|---|---|
| Aronson, P. W. | Physicist | Gage Group | NOL |
| Baggott, H. W. | Ordnanceman | Recording Group | NOL |
| *Brannin, F. H.,Jr. | Lt., U.S. Navy | Recording Group | AFSWP |
| Brigham, S. F. | Engineer | Record & Field Engr. | Vitro |
| Browder, L. B. | Lt., U.S. Navy | Recording Group | AFSWP |
| Burk, E. E. | Electronics Mech. | Recording Group | NOL |
| Culling, E. J. | Electronics Engr. | Gage Group | NOL |
| Denning, V. E. | Capt., U.S.A.F. | Gage Group | AFSWP |
| *Disario, N. | Engineer | Record & Field Engr. | Vitro |
| **Fannin, B. B. | Engineer | Gage & Record Group | Vitro |
| **Feldman, H. P. | Mech. Engr. | Design | NOL |
| Fleming, W. H.,Jr. | Major, U.S.A.F. | Gage Group | AFSWP |
| *Frederick, R. E. | Engineer | Record & Field Engr. | Vitro |
| Hammond, N. B. | Engineer | Record & Field Engr. | Vitro |
| **Harris, V. | Senior Engineer | Project Engineer | Vitro |
| Higgins, W. F. | Engineer | Record & Field Engr. | Vitro |
| Kee, J. W. | Engineer | Record & Field Engr. | Vitro |
| Loring, B. M. | Lt., U.S. Navy | Gage Group | AFSWP |
| Mather, J. I. | Senior Engineer | Record & Field Engr. | Vitro |
| *McGuckin, P. A. | Engineer | Record & Field Engr. | Vitro |
| Milloit, H. W. | CHRELE, USN | Recording Group | AFSWP |
| Morris, W. E. | Physicist | Project Officer | NOL |
| Nacke, E. G. | Ordnanceman | Recording Group | NOL |
| Petes, J. | Physicist | Record Group Head | NOL |
| Quick, R. G. | Engr. Aide | Gage Group | NOL |
| Robinson, G. W. | Lt., U.S. Navy | Recording Group | AFSWP |
| Shadle, P. W. | Electronics Scien. | Recording Group | NOL |
| Shisko, J. | Property Clerk | Logistics | NOL |
| Somers, F. E. | CDR. U.S. Navy | Deputy Project Officer | AFSWP |
| Sussholz, B. | Physicist | Gage Group | AFSWP |
| Vogl, J. F. | Physicist | Gage Group | NOL |

* At site during September only.
**Not at site.

## 9.3 SUPPLY ARRANGEMENTS AT THE NAVAL ORDNANCE LABORATORY

The Naval Ordnance Laboratory purchased the bulk of the materials for the Ballistics Research Laboratories, the Vitro Corporation and for

its own field party, utilizing the purchasing facilities of the Vitro Corporation, and the NOL Supply Department. The actual choice of which agency was to purchase a particular item was determined by (1) availability of the item in the Navy supply system, (2) comparative costs of the item, and (3) delivery date. In general, large electronic items and electric cable were purchased through the Vitro Corporation and the bulk of hand tools, small electrical items, etc., through the Navy sources. By number of items, the largest amount of material was purchased from Navy sources while dollar-wise Vitro purchases were greater. Some of the major items purchased and their total cost are shown below:

| | |
|---|---|
| Electric cable | $122,000 |
| Accelerometers | 36,500 |
| Oscillators | 3,250 |
| Recorders, modifications to recorders and playback equipment and string oscillograph | 60,000 |
| Trailers and modifications to trailers | 11,250 |
| Capsules | 10,000 |
| Packing | 10,000 |
| Shipping (out) | 18,000 |
| Shipping (back) | 10,000 |
| Total..... | $281,000 |

## 9.4 SHIPPING

The Naval Ordnance Laboratory Shipping Department shipped all material for their own group and for Vitro as well as sizable amounts of cable and supplies for BRL. The general procedure followed was for individual group leaders to tag their equipment or supplies so that on arrival at the site they could be claimed or reassembled easily. A second major identification was made by indicating the site at which the material was to be used. This led to expeditious distribution of the material at the site and a separation of many items reserved for possible replacement or emergency use. It also led to more expedient return shipping.

Another major item which played a prominent part in the quick "roll-up" procedure was the original insistence that all boxes be build with a one-piece plywood (plyscord grade) top, fastened with screws. This proved to have several desirable features:

(1) Increased protection for contents against weather or mishap

(2) By use of electric screwdrivers tops were quickly and easily removed without the normal prying and hammering which results in damage to contents

(3) About 96% of all boxes were successfully salvaged and used for return shipping

(4) There was a worthwhile savings in time and money.

## 9.5 AMOUNT OF SHIPPING

The amount of shipping, all of which was accomplished by truck, is shown below:

| | From NOL to NTS | From NTS to NOL |
|---|---|---|
| No. of pieces | 1119[1] | 354 |
| Tonnage | 200.5 | 106 |
| Cubic footage | 11,259[2] | 3858 |

[1] Includes two fully equipped instrument trailers of 25,000 lbs each.

[2] Does not include cube of instrument trailers.

## 9.6 RETURN SHIPPING

Inasmuch as nearly all boxes were salvaged, the NOL group accomplished its own packing by simply putting instruments and materials back into their original containers, and resealing the boxes. Two packers from the NOL arrived at the Nevada Test Site ten days prior to the underground shot and remained until three days after the underground shot. These men handled the bracing of the instrument trailers, the crating of the more delicate instruments, and assisted in general with the job. The remainder of the work was accomplished by the NOL field party. This method worked so successfully that 72 hours after the last shot, the NOL group completed the packing of approximately 100 tons of material.

It is believed that the NOL group was the first major group to complete its "roll-up".

The overall success of the procurement, packing and supply functions was due to the assignment, on a full time basis, of a Supply representative to the project. The representative, Mr. Joseph Shisko, coupled his good technical capabilities with diligence and perseverance and forestalled many of the expected supply problems.

[redacted]

APPENDIX A

Results of Acceleration Measurements from the 40,000 lb HE Shot at Yucca Flats

The HE acceleration results contain the following:

1. Observations from the data

2. Graphs of arrival times, velocity of propagation, and acceleration as a function of distance, Figs. A.1 to A.8

3. Tracings of most of the horizontal and vertical acceleration records. This is reproduced in Fig. A.9. For explanation of the records refer to Appendix B.

Observations from the Naval Ordnance Laboratory acceleration data from the 40,000 lb shot at Yucca Flats:

1. A log-log plot of maximum acceleration as a function of distance gave a straight line curve with a slope of 1.66. This attenuation of acceleration, falling off as a 1.66 power with distance, differs considerably from the previous predictions from Lampson's formulas which decay initially as a 4th power. Compared to the Lampson curves, the HE results give values of acceleration lower by a factor of 4 close in and higher farther out by a factor of 5, with the cross over at a of 3.5.

2. Maximum horizontal acceleration and maximum vertical acceleration are identical, also maximum positive and maximum negative accelerations are of the same order of magnitude for both horizontal and vertical components.

3. Log-log plots of first and last acceleration peaks give straight line curves with slopes in the range 1.6 to 2.1.

4. The magnitude of the first vertical acceleration peak is considerably below the maximum vertical acceleration. The first horizontal peak is of the same order of magnitude as the maximum horizontal acceleration.



[redacted]

5. Secondary and tertiary acceleration pulses occur of the same order of magnitude as the initial pulse. These subsequent pulses arrive 0.1 to 0.3 sec. after the initial pulse. These pulses are not transmitted with the same velocity as the initial pulse.

6. Ground shock produced by air blast was observed. Acceleration so produced was of the same magnitude as acceleration produced by directly transmitted ground shock. Considerable ground shock due to air blast can be anticipated on the nuclear shots.

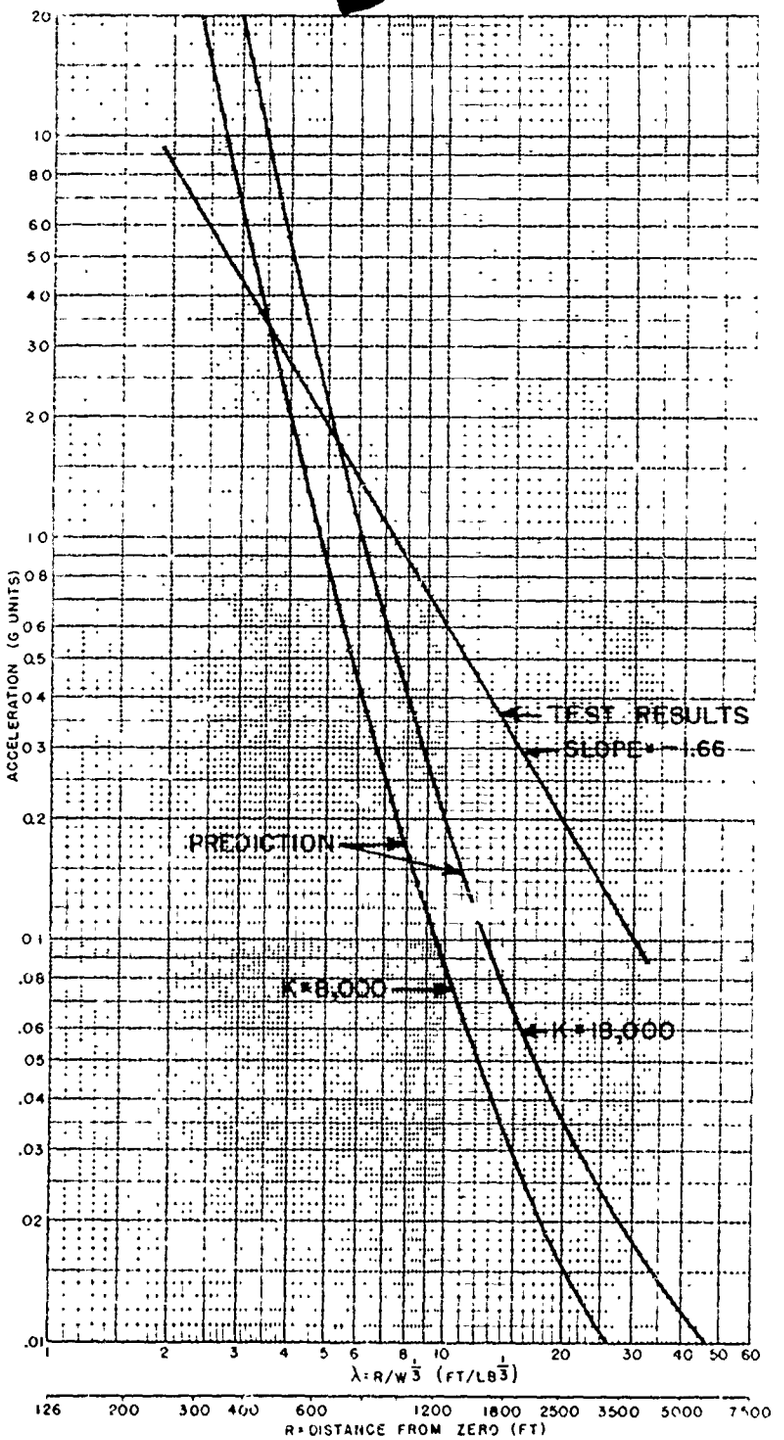


Fig. A.1 40,000 Lb Shot - Prediction of Maximum Acceleration from Lampson's Theory and Comparison with the Test Results

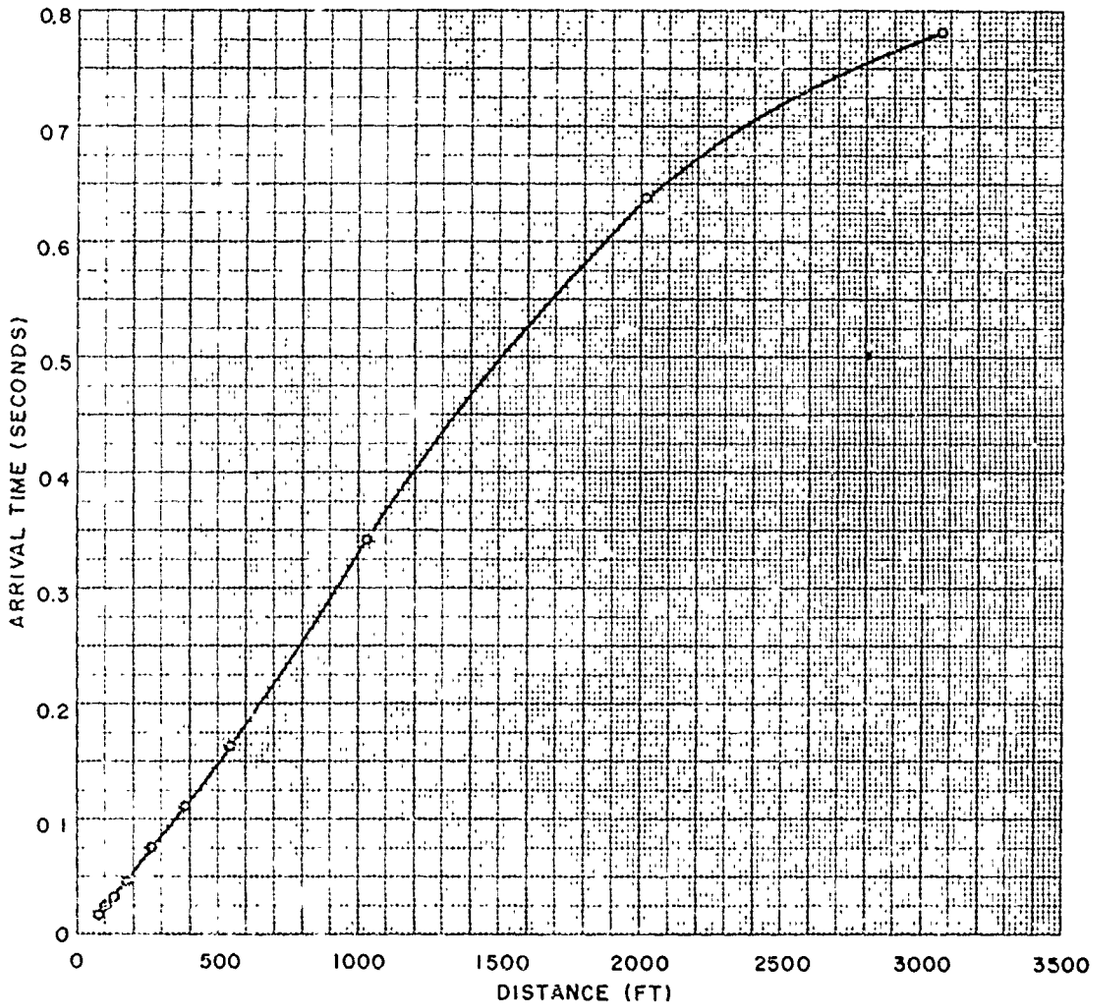


Fig. A.2 40,000 Lb Shot - Arrival Time of Initial Ground Acceleration

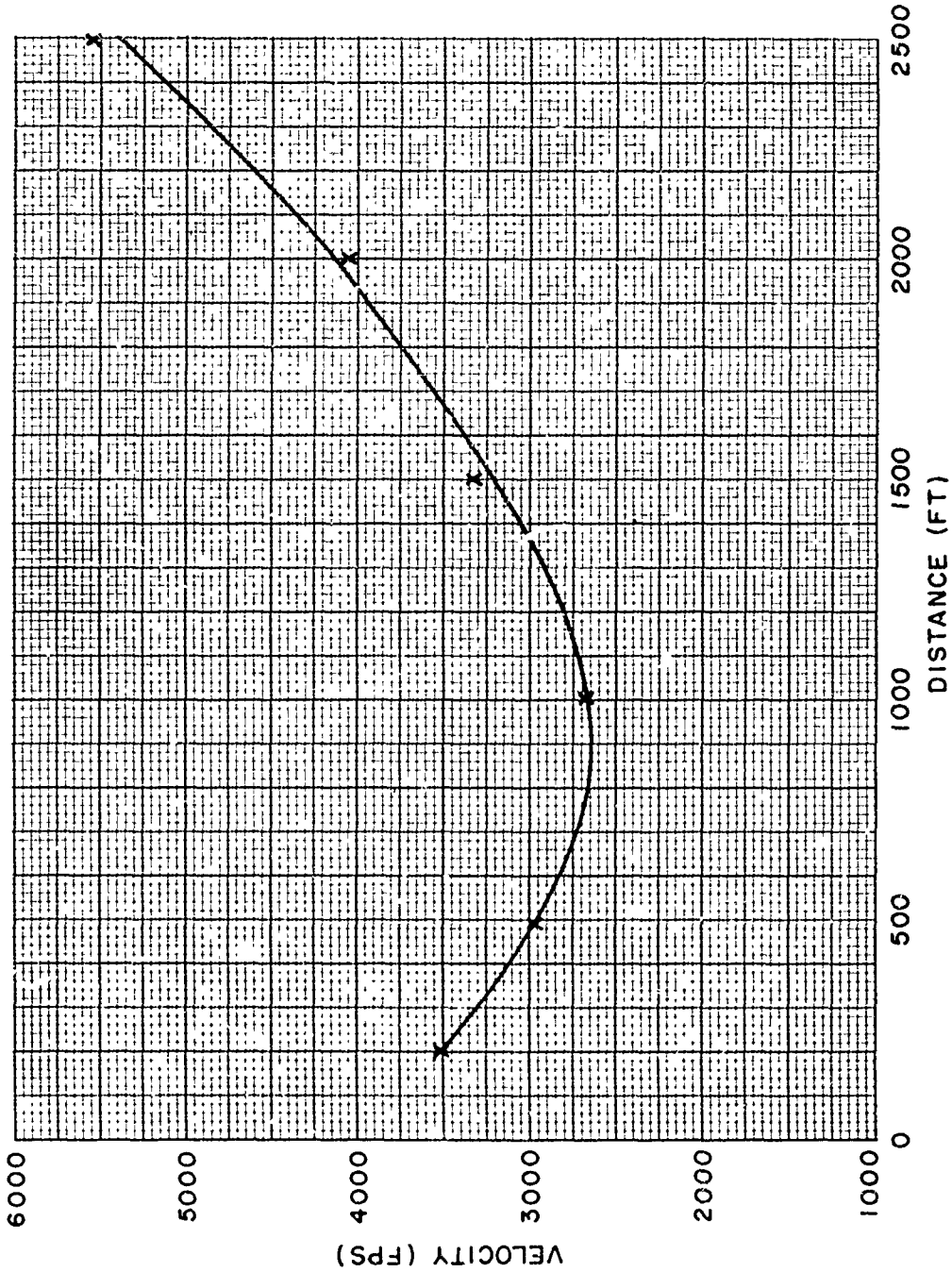


Fig. A.3 40,000 lb Shot - Velocity of Initial Ground Shock

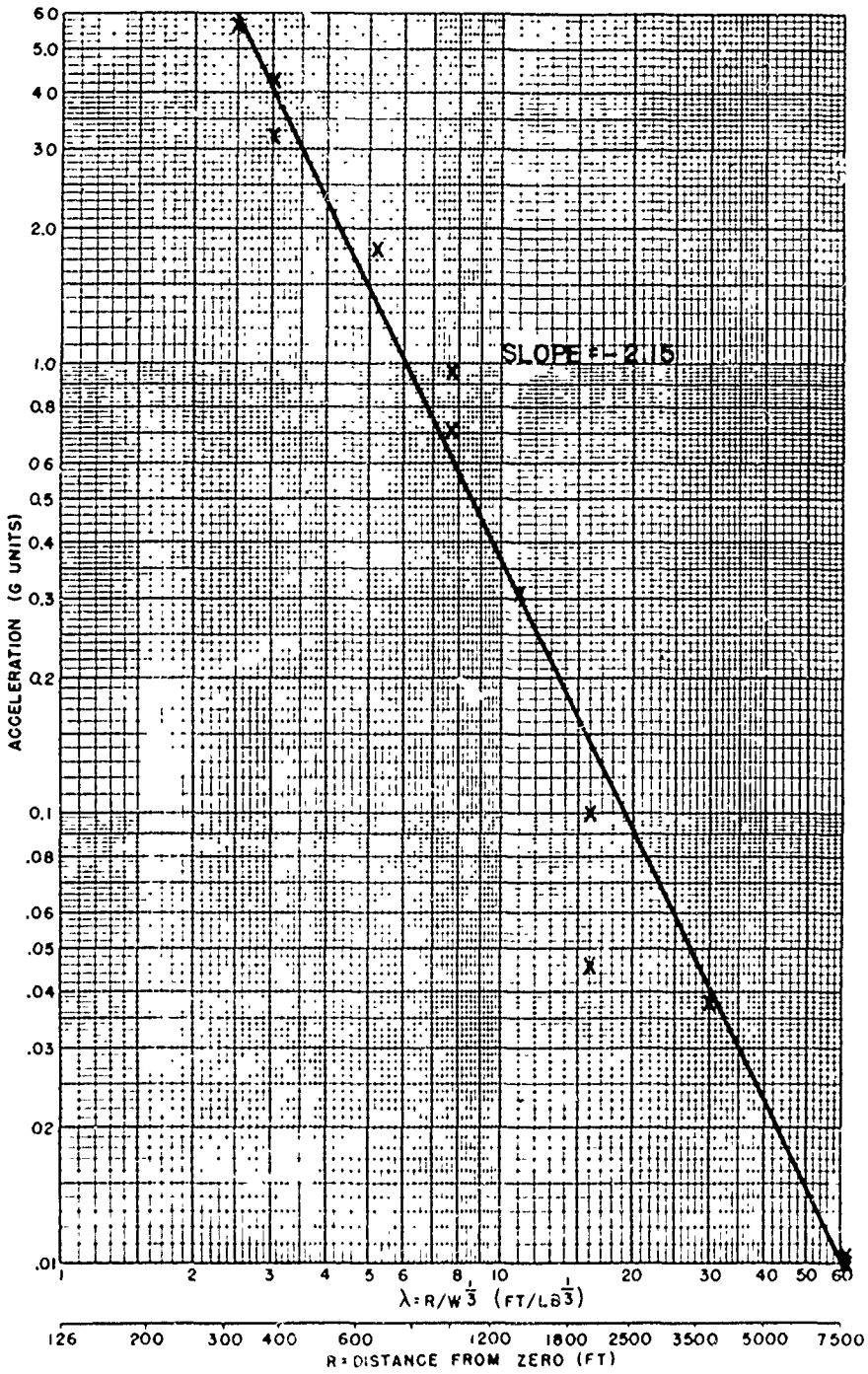


Fig. A.4 40,000 Lb Shot - First Horizontal Acceleration Outward (Including Air Blast)

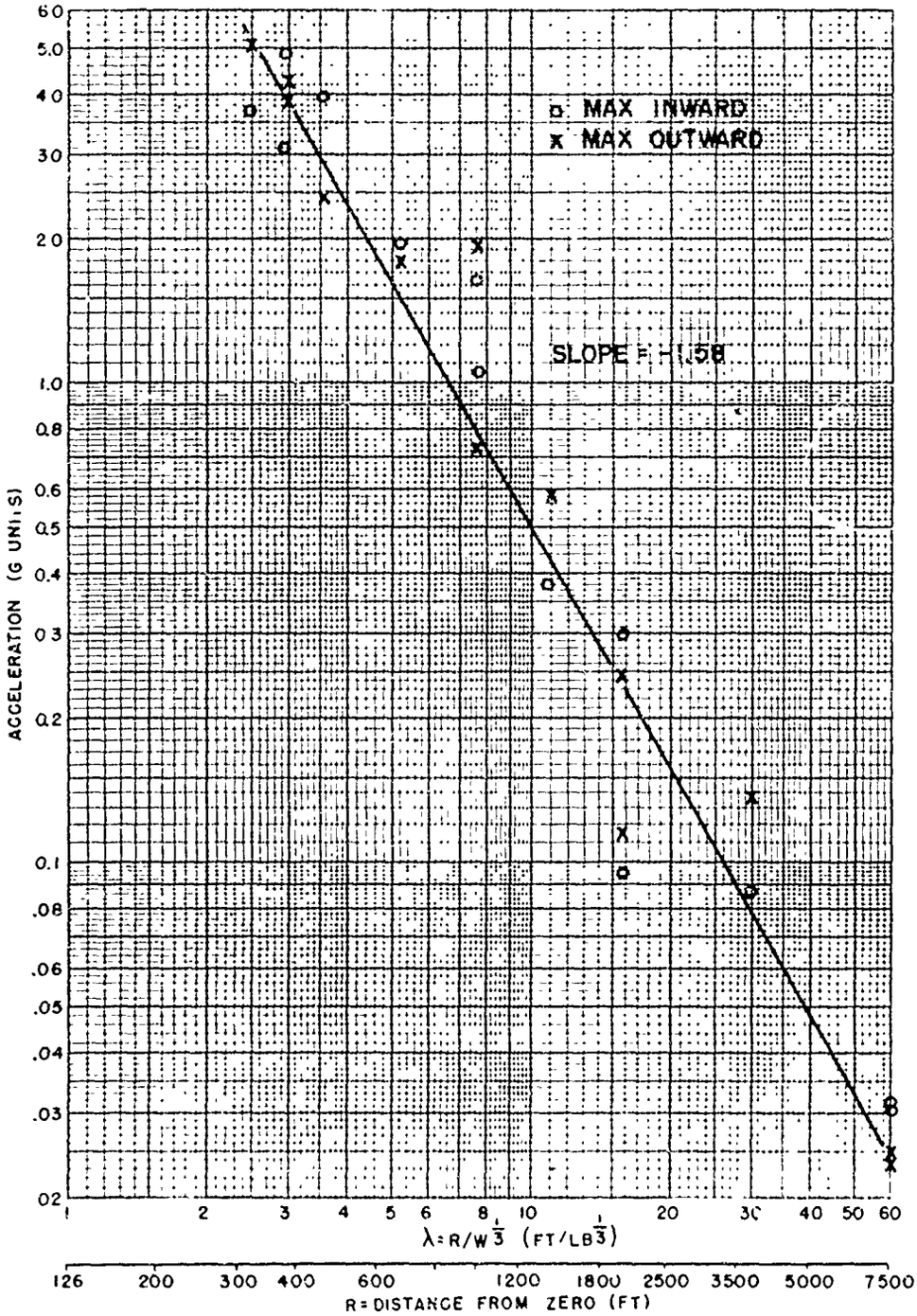


Fig. A.5 40,000 LB SHOT - Maximum Horizontal Acceleration (Including Air Blast)

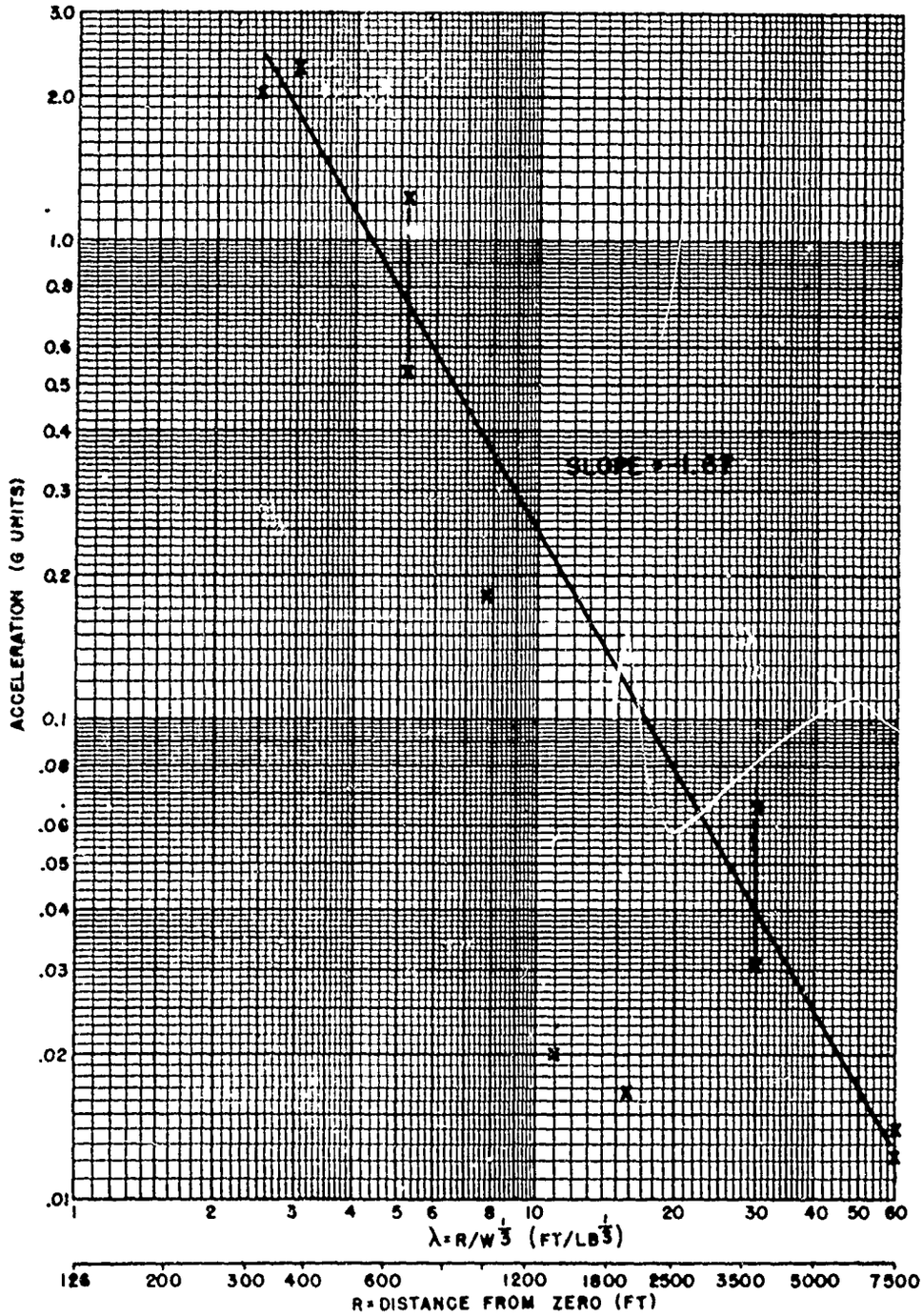


Fig. A.6 40,000 LB SHOT - First Vertical Acceleration Upward (Excluding Air Blast)

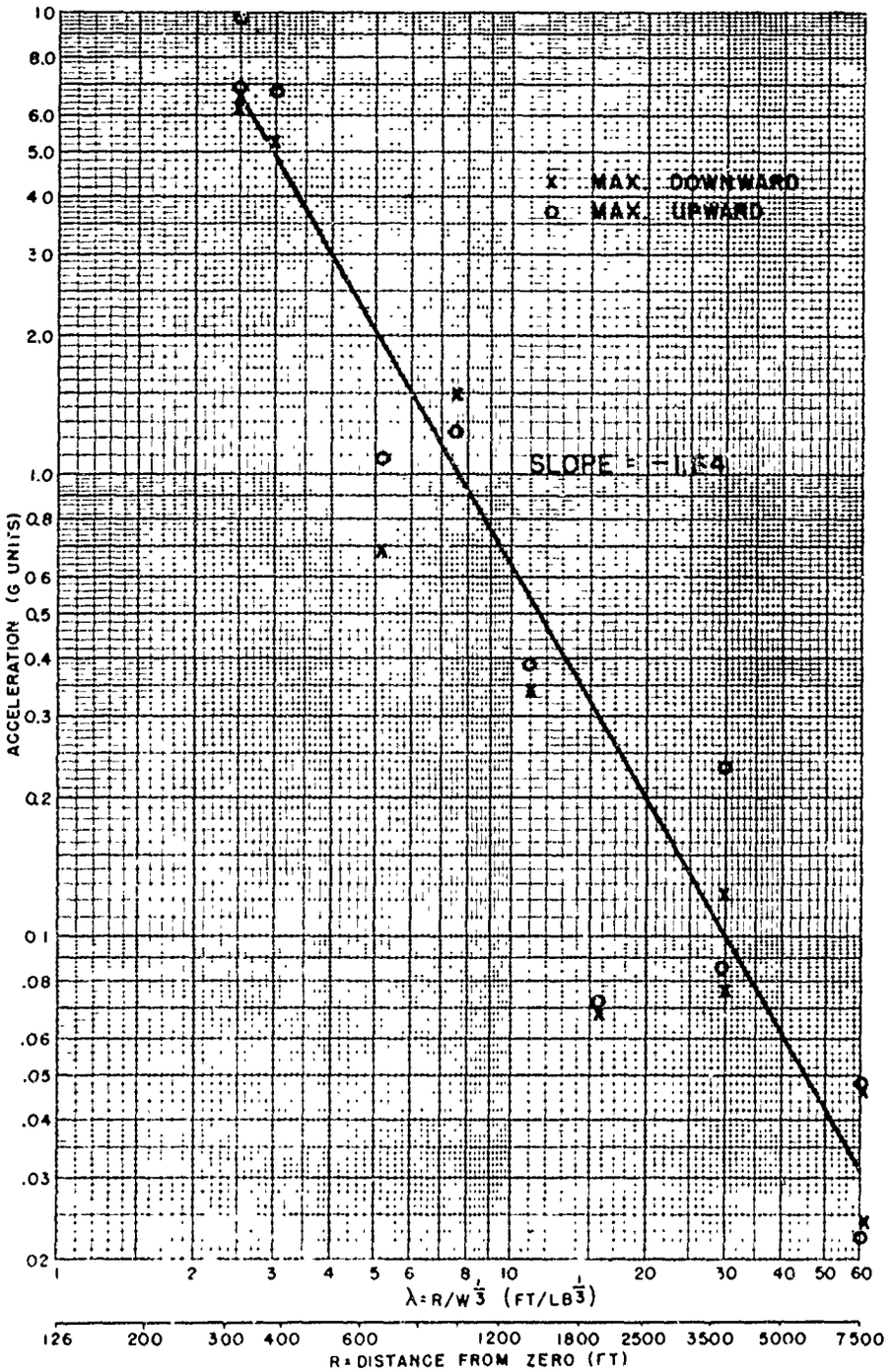


Fig. A.7 40,000 Lb Shot - Maximum Vertical Acceleration (Including Air Blast)

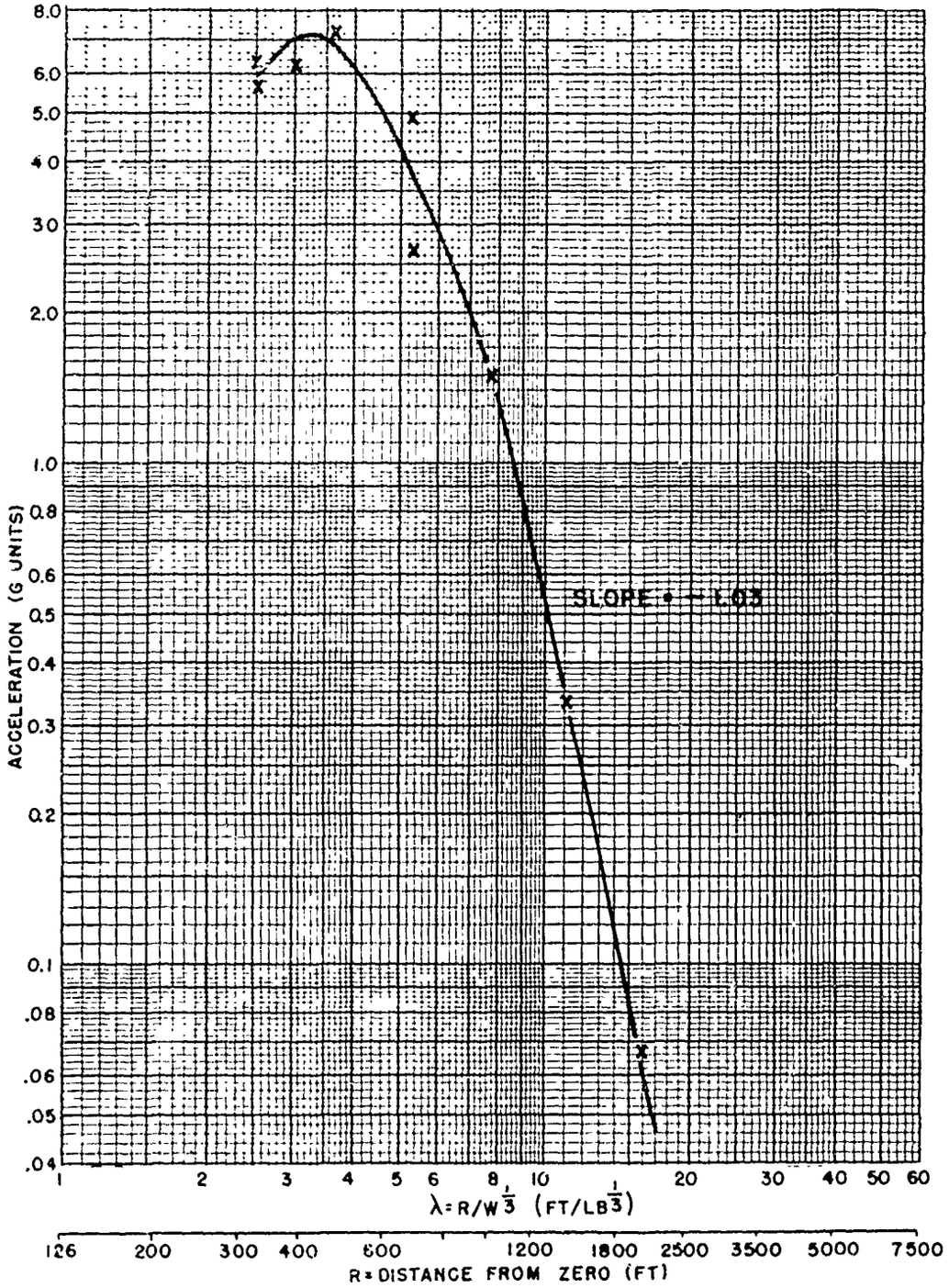


Fig. A.8 40,000 LB SHOT - Maximum Downward Acceleration Due to Air Blast Alone

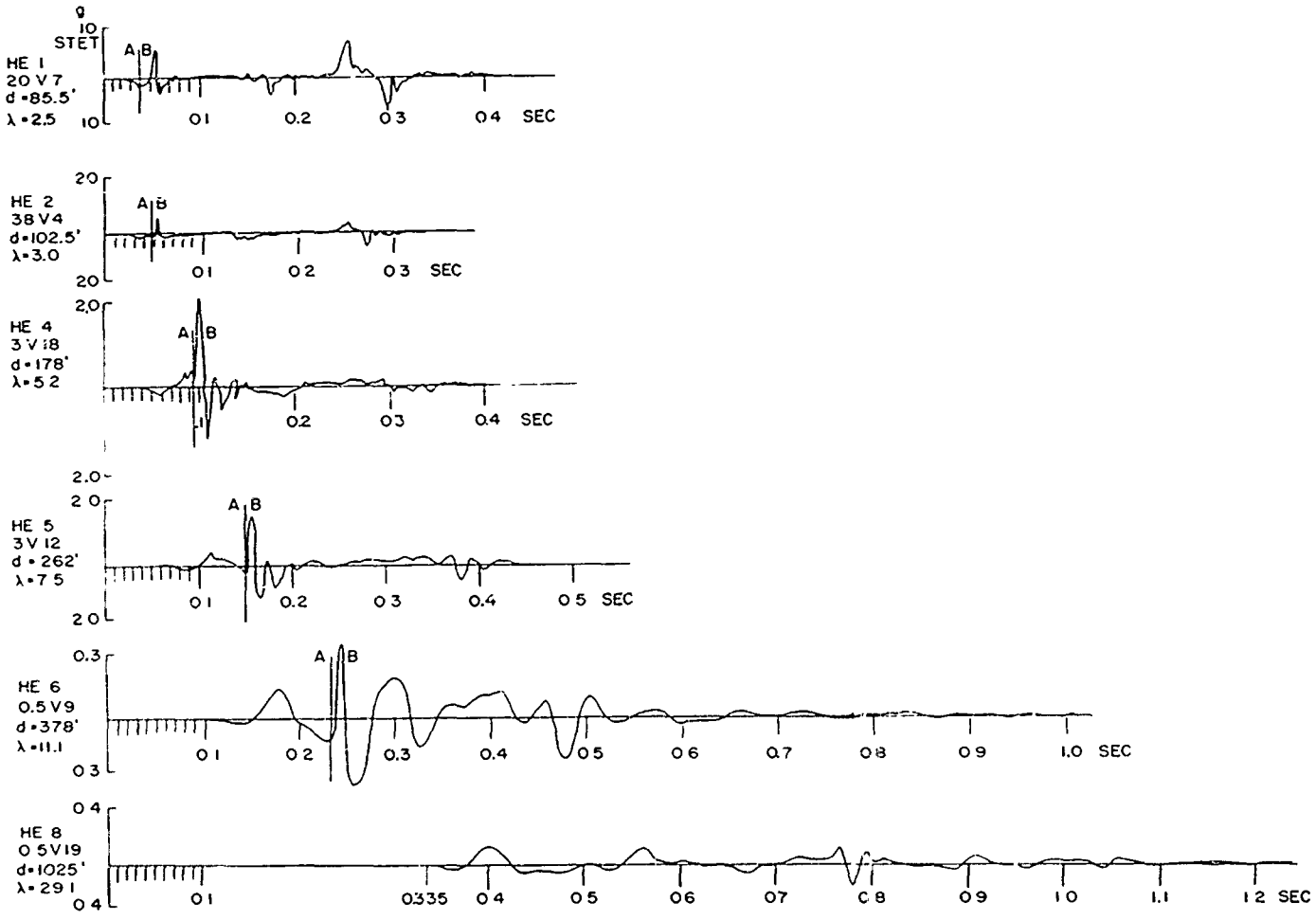


RECORDS OF VERTICAL GAGES

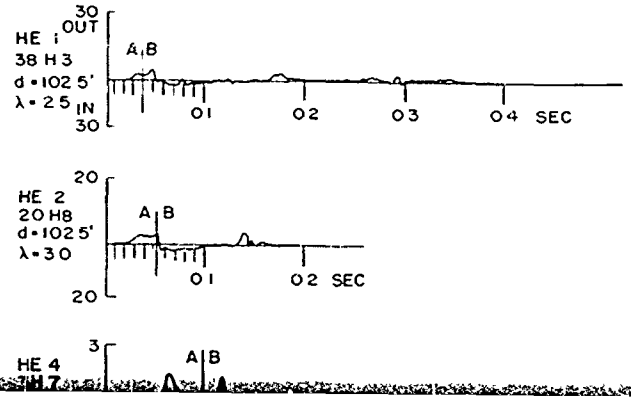


PROJECT 1.1

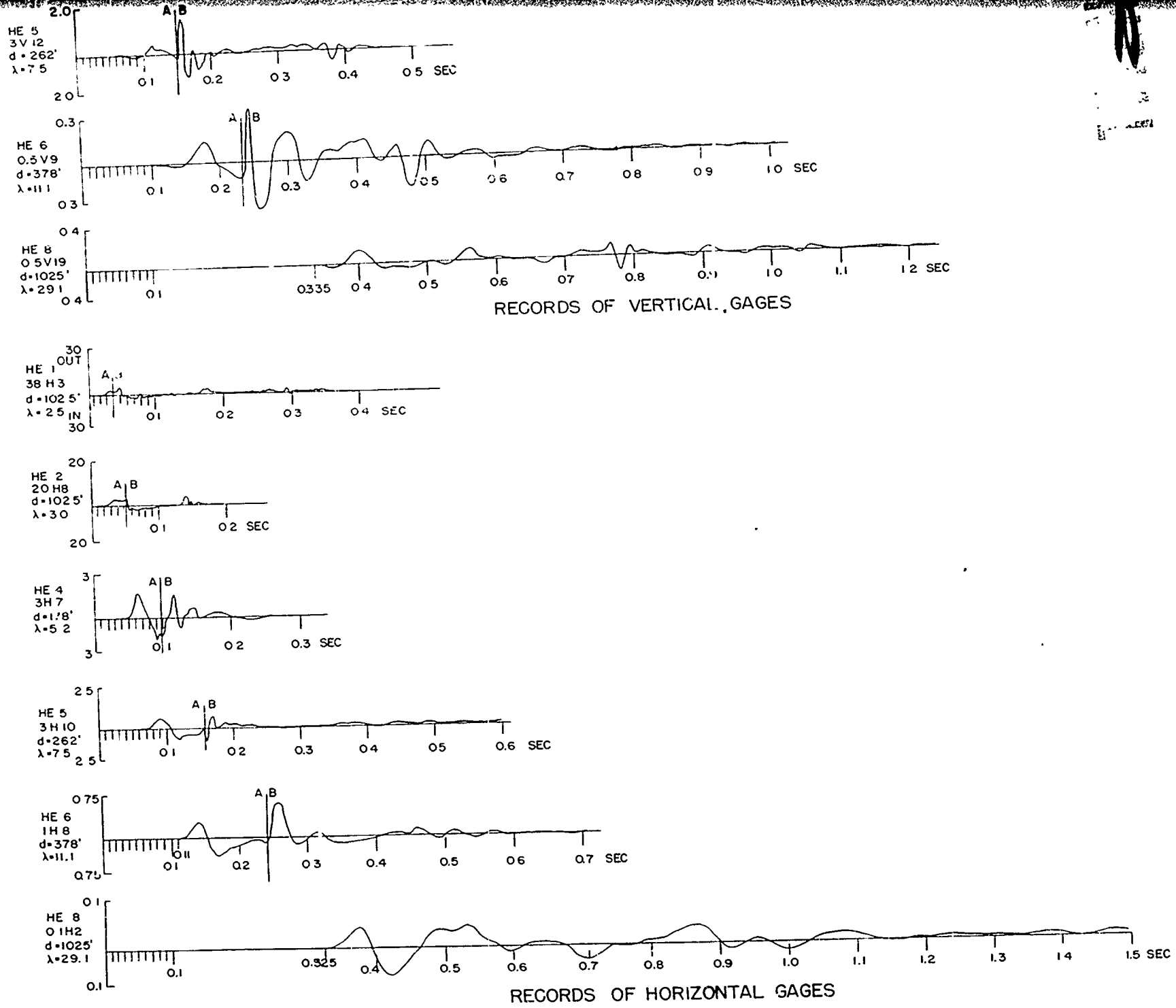


FIG. A9 NOL ACCELERATION RECORDS FROM HE-2 (40,000 LBS)

[redacted]

APPENDIX B

Copies of Acceleration Records for the Surface and Underground Nuclear Shots

Notes for Use with Acceleration Records

1. On the vertical acceleration records the trace above the base line denotes downward ground movement.

2. On the horizontal acceleration records the trace above the base line denotes outward ground movement.

3. On the transverse acceleration records the trace below the base line denotes ground movement to the left as viewed from the zero point.

4. Amplitude scales on all records are non-linear.

5. Gage numbering system is as follows:

   H denotes Horizontal accelerometer.
   V denotes Vertical accelerometer.
   T denotes Transverse accelerometer.

Example: 0.1V13
0.1 denotes ranges of accelerometer.
V denotes that instrument measures vertical acceleration.
13 denotes serial number of gage.

6. Station numbers run consecutively from closest (1) to most distant (12) station.

Example: STATION S12 - 20 ft
S denotes that record is for surface shot.
12 denotes most distant station (12).
20 ft denotes that gage was located twenty ft below surface of ground.

Note: On the underground shot a station was added closer to zero than station 1. This is designated as station A.



[redacted]

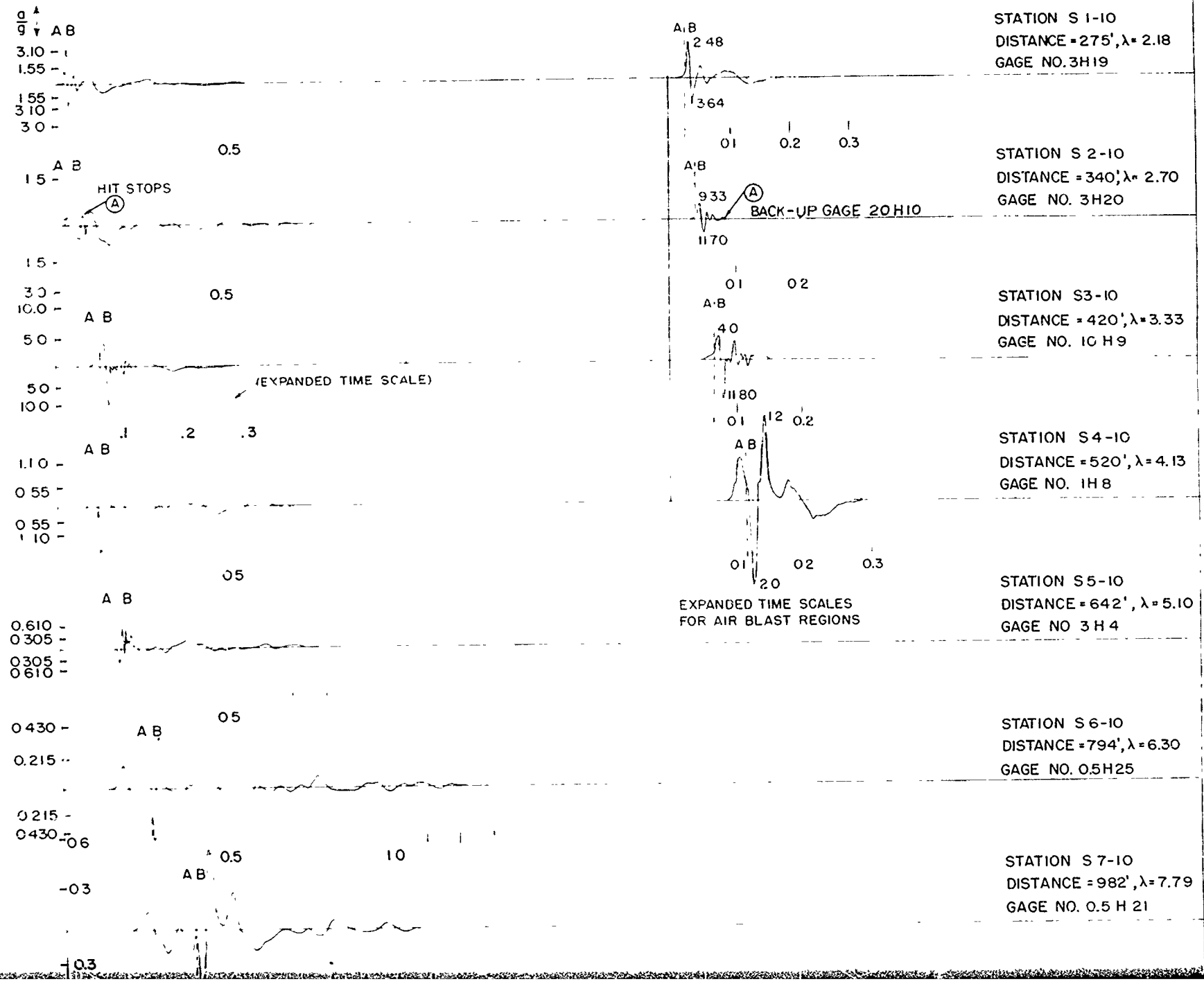
a/g
A B
3.10
1.55
1.55
3.10
3.0
0.5
A B
1.5
HIT STOPS
A
1.5
3.0
10.0
0.5
A B
5.0
(EXPANDED TIME SCALE)
5.0
10.0
.1
.2
.3
A B
1.10
0.55
0.55
1.10
0.5
A B
0.610
0.305
0.305
0.610
0.5
0.430
A B
0.215
0.215
0.430
-0.6
0.5
1.0
A B
-0.3
0.3
A B
2.48
3.64
0.1
0.2
0.3
A B
9.33
A
BACK-UP GAGE 20H10
11.70
0.1
0.2
A B
4.0
11.80
0.1
1.2
0.2
A B
0.1
0.2
0.3
2.0
EXPANDED TIME SCALES
FOR AIR BLAST REGIONS
STATION S 1-10
DISTANCE = 275', λ = 2.18
GAGE NO. 3H19
STATION S 2-10
DISTANCE = 340', λ = 2.70
GAGE NO. 3H20
STATION S3-10
DISTANCE = 420', λ = 3.33
GAGE NO. 10 H 9
STATION S4-10
DISTANCE = 520', λ = 4.13
GAGE NO. 1H 8
STATION S5-10
DISTANCE = 642', λ = 5.10
GAGE NO 3 H 4
STATION S 6-10
DISTANCE = 794', λ = 6.30
GAGE NO. 0.5H25
STATION S 7-10
DISTANCE = 982', λ = 7.79
GAGE NO. 0.5 H 21

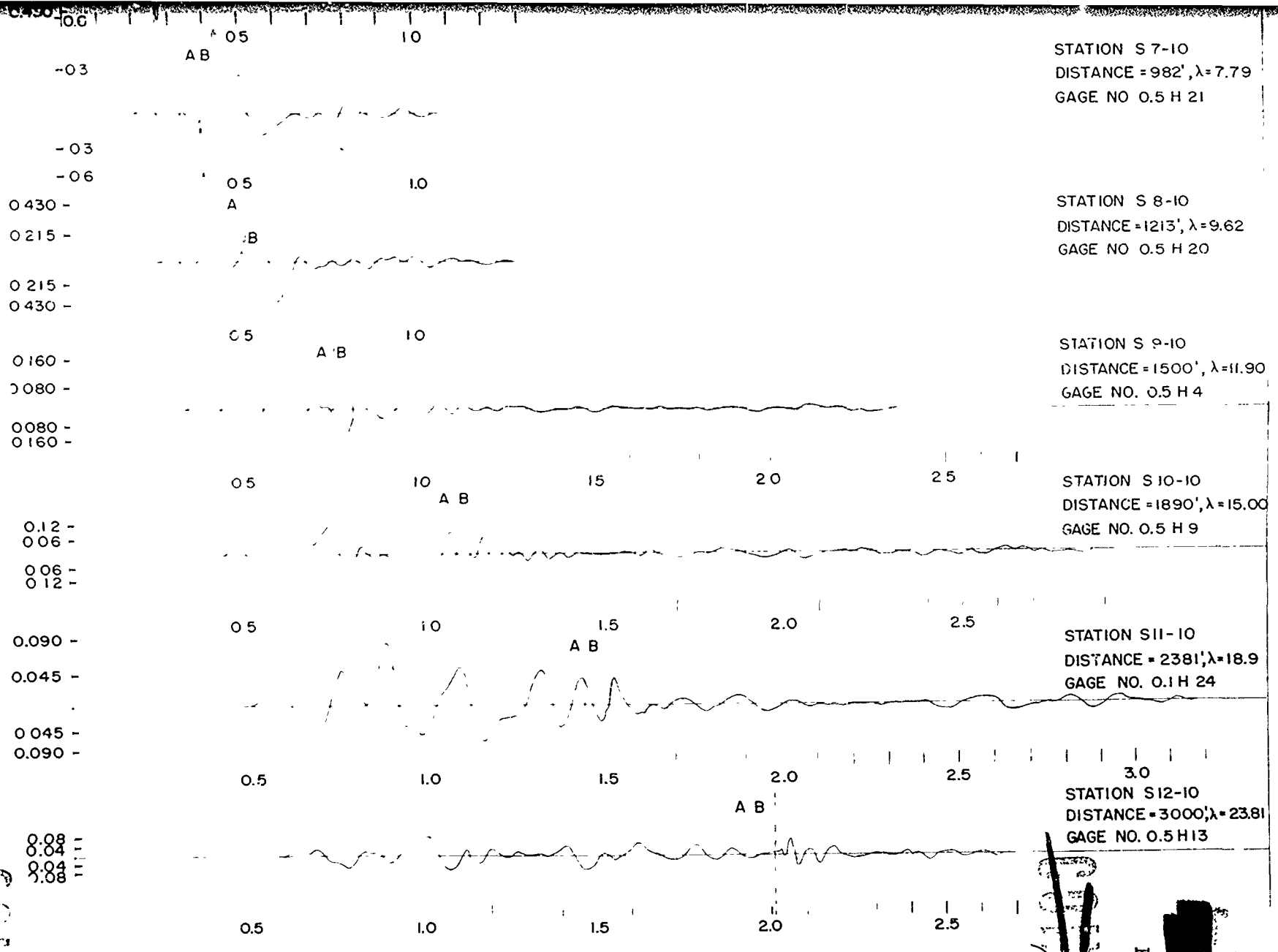


HORIZONTAL ACCELERATIONS FROM SURFACE SHOT

B.1



PROJECT 1.1

[redacted]

[redacted]

PROJECT 1.1

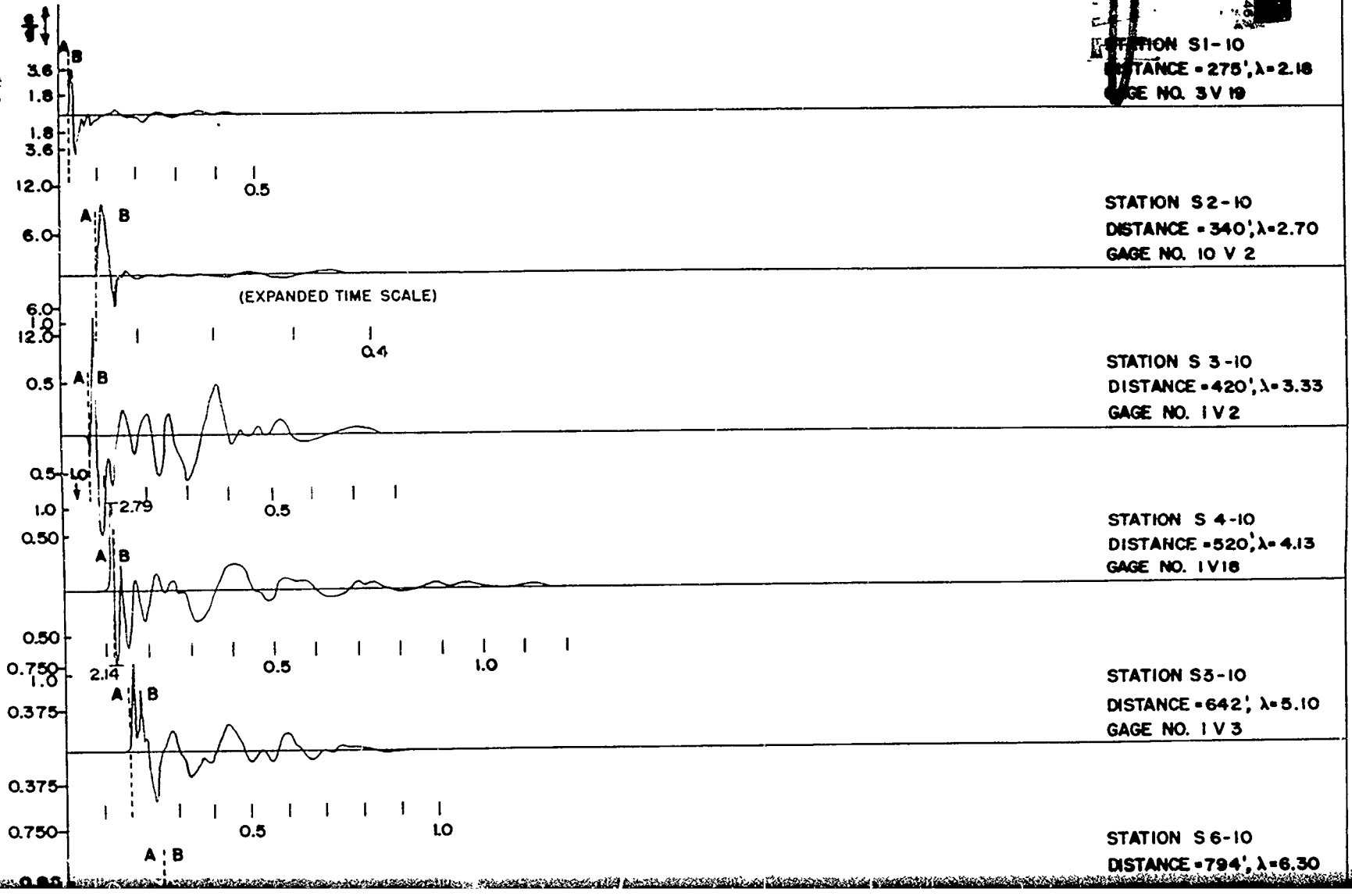

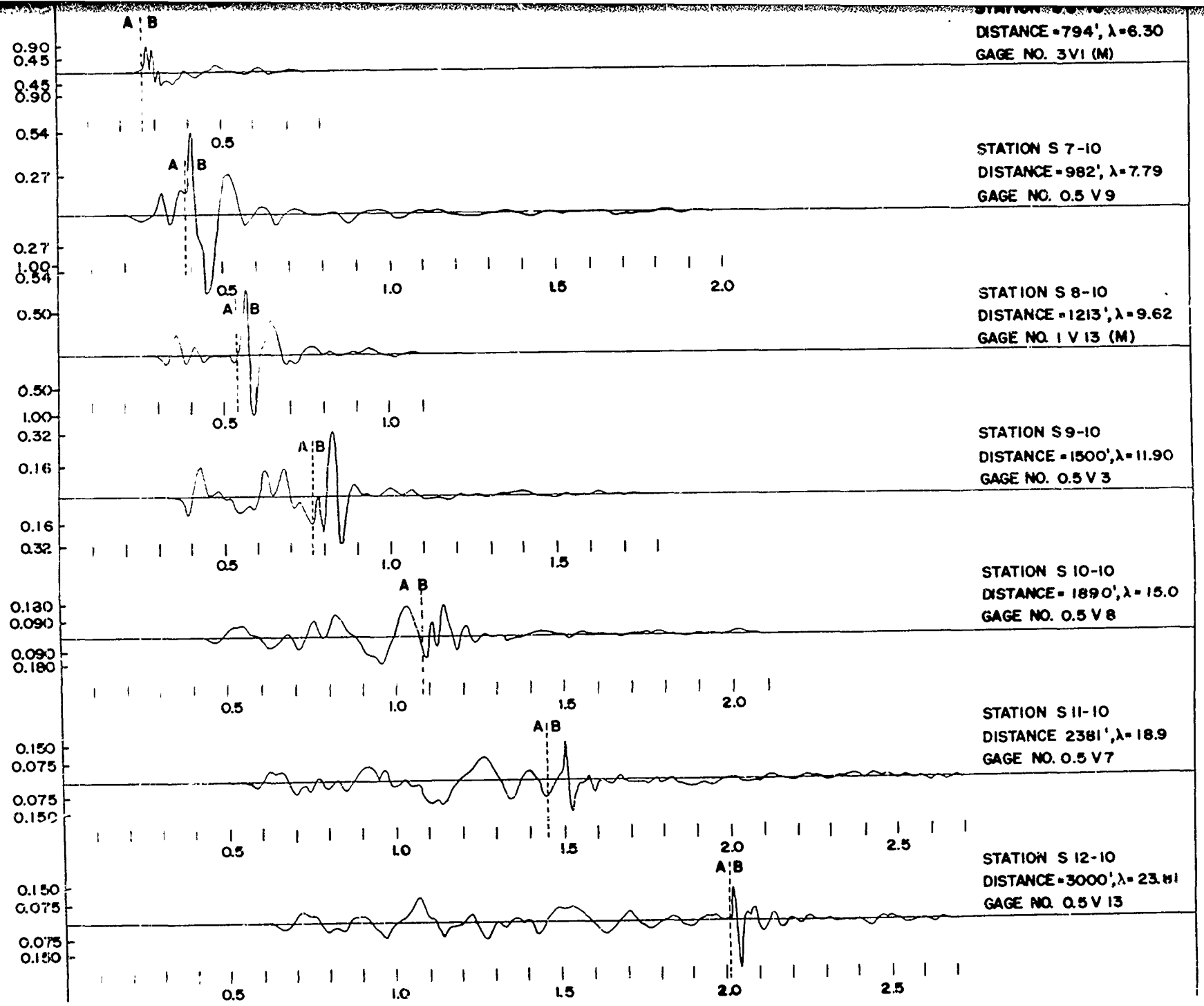


B.2 VERTICAL ACCELERATIONS FROM SURFACE SHOT

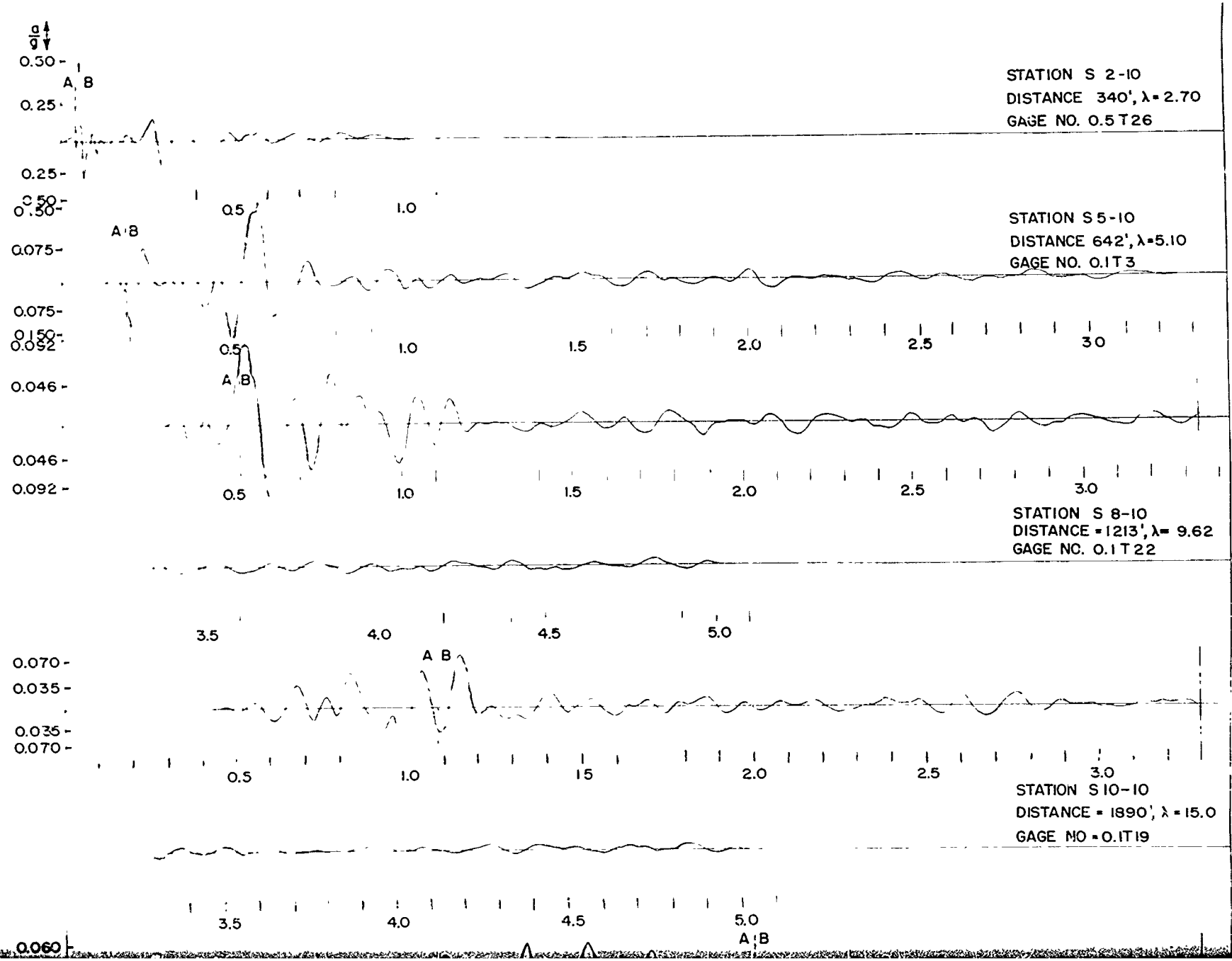
a/g
STATION S 2-10
DISTANCE 340', λ = 2.70
GAGE NO. 0.5 T26
STATION S 5-10
DISTANCE 642', λ = 5.10
GAGE NO. 0.1 T3
STATION S 8-10
DISTANCE = 1213', λ = 9.62
GAGE NO. 0.1 T22
STATION S 10-10
DISTANCE = 1890', λ = 15.0
GAGE NO = 0.1T19
A B
0.5
1.0
1.5
2.0
2.5
3.0
3.5
4.0
4.5
5.0

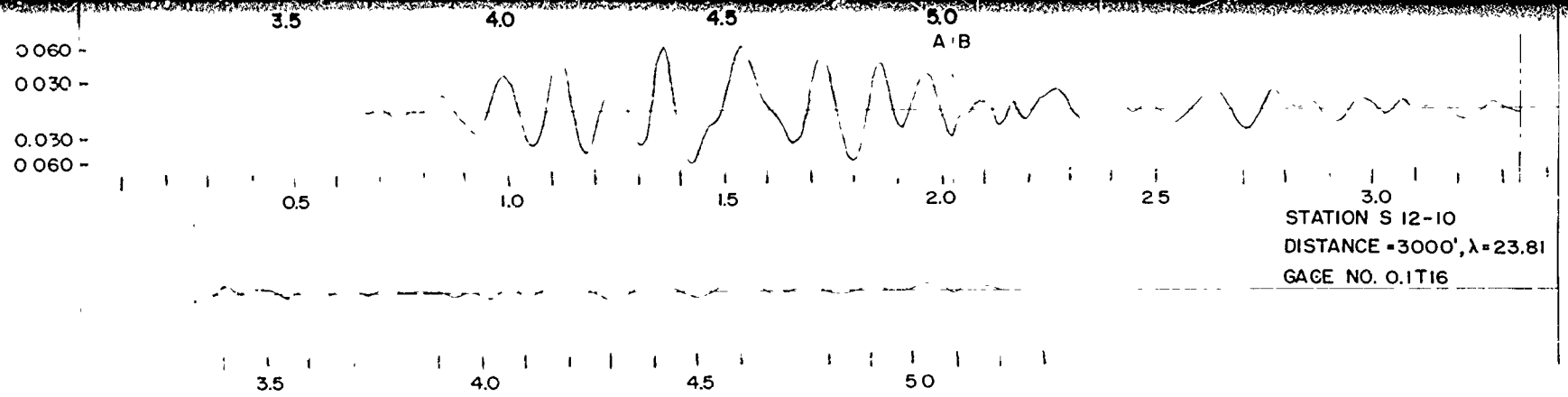


B.3 TRANSVERSE ACCELERATIONS FROM SURFACE SHOT

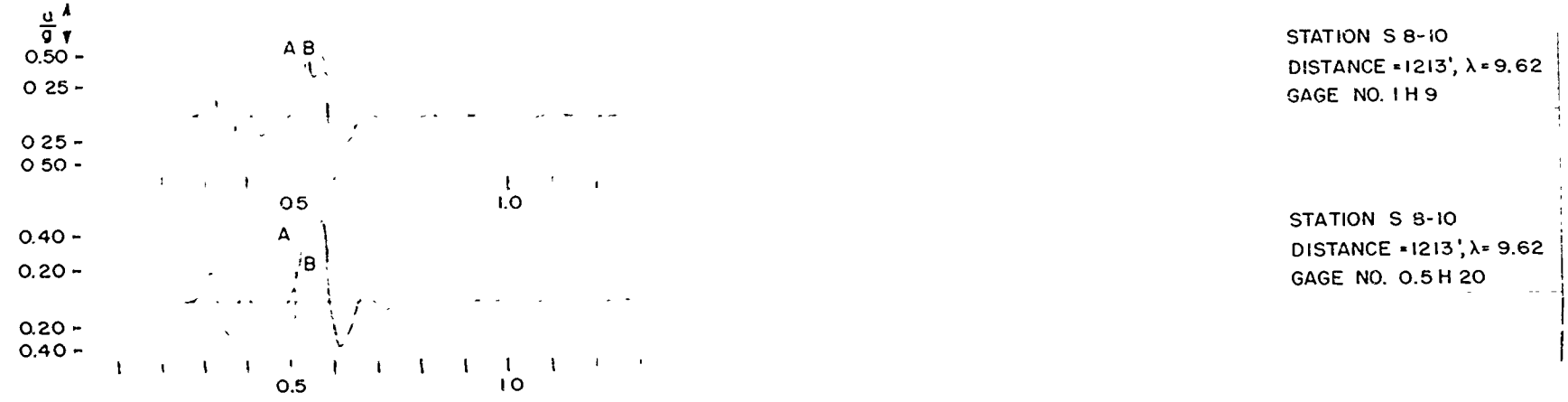


B.4 HORIZONTAL ACCELERATIONS FROM PRIMARY AND BACKUP GAGES ON SURFACE SHOT

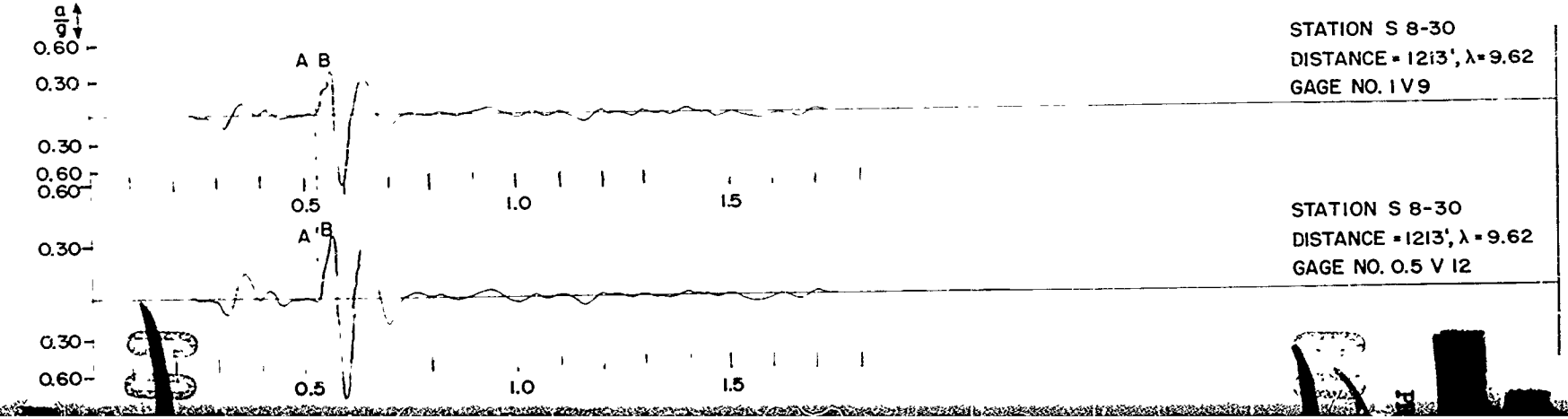

B.3 TRANSVERSE ACCELERATIONS FROM SURFACE SHOT

B.4 HORIZONTAL ACCELERATIONS FROM PRIMARY AND BACKUP GAGES ON SURFACE SHOT

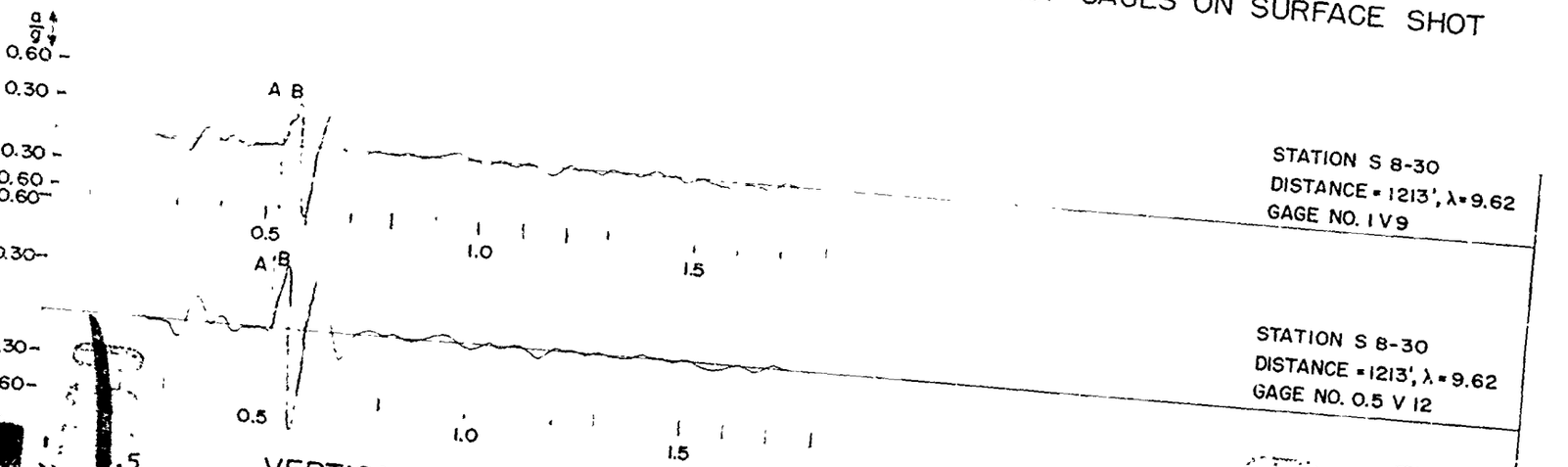


VERTICAL ACCELERATIONS FROM PRIMARY AND BACKUP GAGES ON SURFACE SHOT



PROJECT 1.1

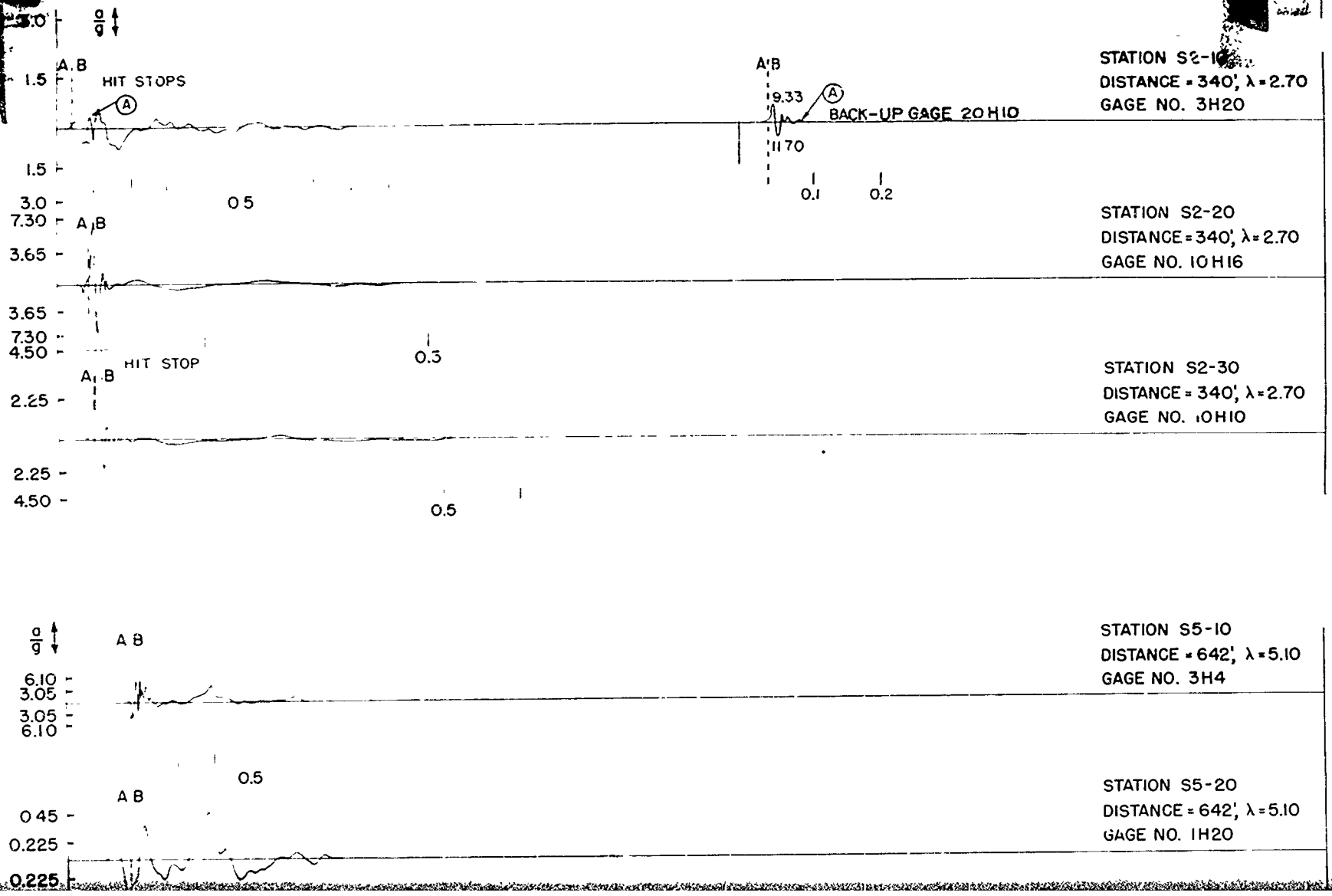
a/g
A B
HIT STOPS
A
A B
9.33
A
BACK-UP GAGE 20H10
11.70
0.1
0.2
0.5
STATION S2-10
DISTANCE = 340', λ = 2.70
GAGE NO. 3H20
A B
STATION S2-20
DISTANCE = 340', λ = 2.70
GAGE NO. 10H16
HIT STOP
0.3
A B
STATION S2-30
DISTANCE = 340', λ = 2.70
GAGE NO. 10H10
0.5
a/g
A B
STATION S5-10
DISTANCE = 642', λ = 5.10
GAGE NO. 3H4
0.5
A B
STATION S5-20
DISTANCE = 642', λ = 5.10
GAGE NO. 1H20

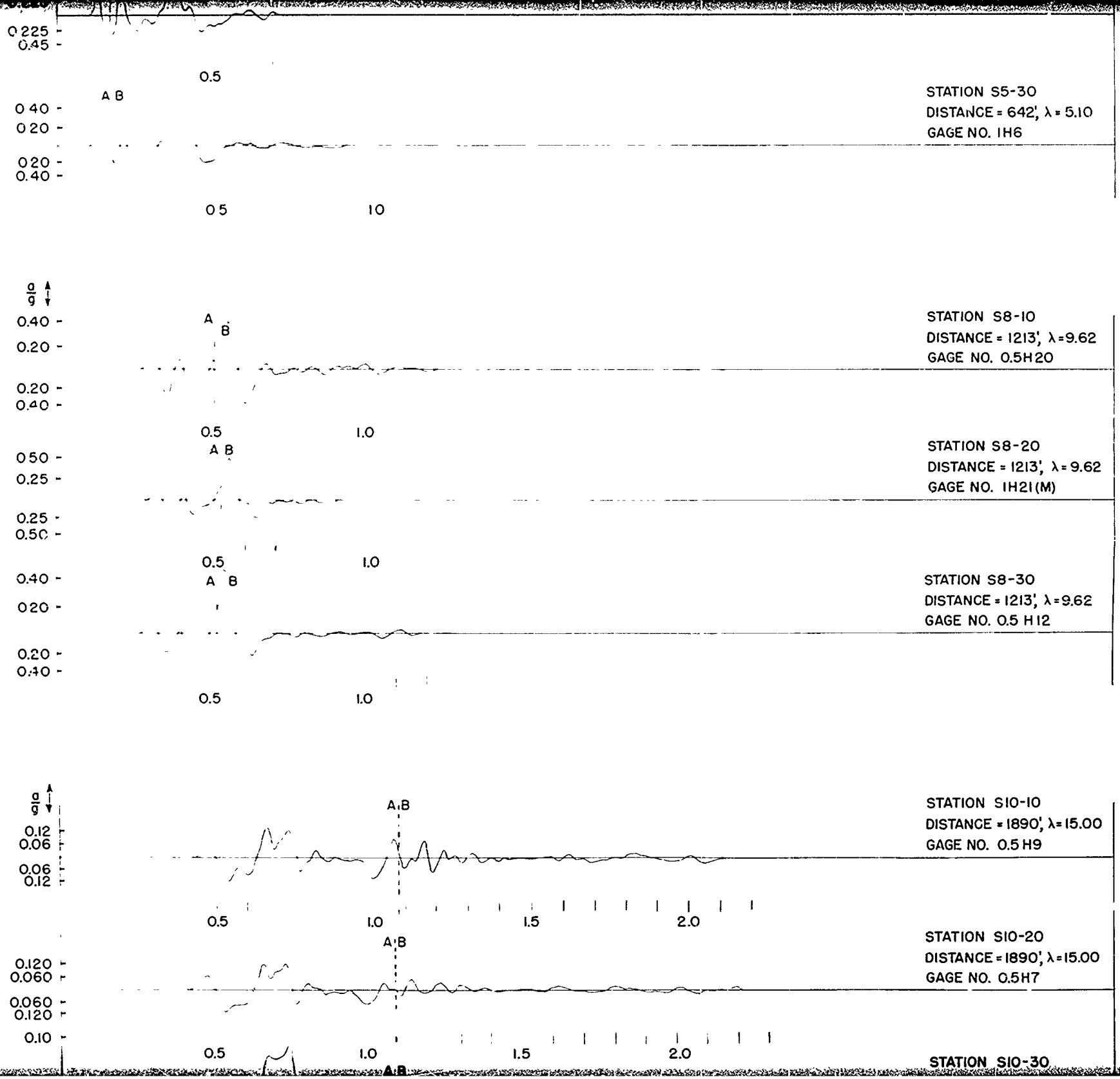
0.225
0.45
0.5
A B
0.40
0.20
0.20
0.40
0.5
1.0
STATION S5-30
DISTANCE = 642', λ = 5.10
GAGE NO. 1H6
a/g
0.40
A
B
0.20
0.20
0.40
0.5
1.0
STATION S8-10
DISTANCE = 1213', λ = 9.62
GAGE NO. 0.5H20
0.50
0.25
0.25
0.50
0.5
1.0
A B
STATION S8-20
DISTANCE = 1213', λ = 9.62
GAGE NO. 1H21(M)
0.40
0.20
0.20
0.40
0.5
1.0
A B
STATION S8-30
DISTANCE = 1213', λ = 9.62
GAGE NO. 0.5 H12
a/g
0.12
0.06
0.06
0.12
A B
0.5
1.0
1.5
2.0
STATION S10-10
DISTANCE = 1890', λ = 15.00
GAGE NO. 0.5 H9
0.120
0.060
0.060
0.120
0.10
A B
0.5
1.0
1.5
2.0
STATION S10-20
DISTANCE = 1890', λ = 15.00
GAGE NO. 0.5H7
A B
STATION S10-30

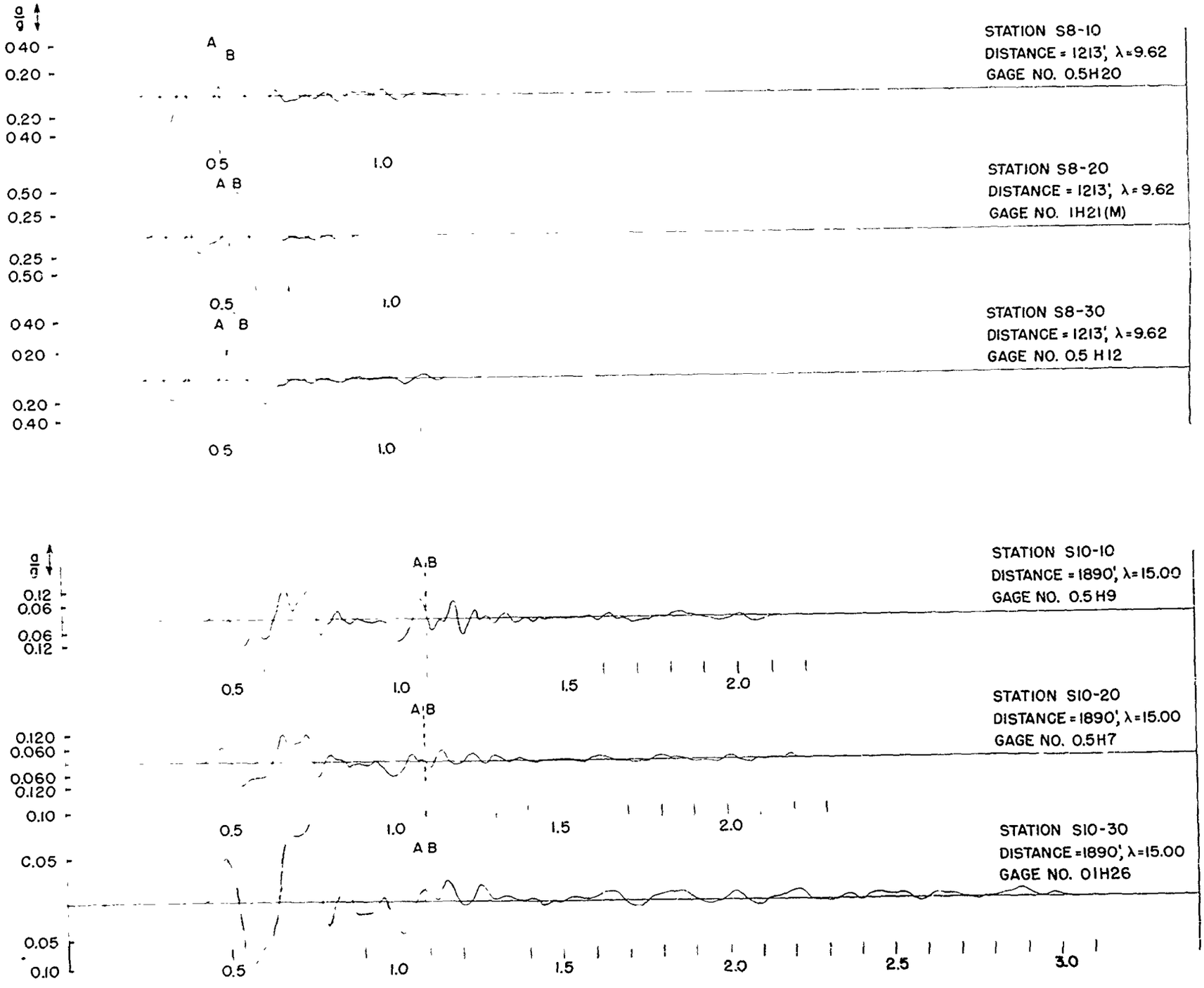


B.6 HORIZONTAL ACCELERATIONS FROM SURFACE SHOT FOR 10, 20, 30 FT. DEPTHS

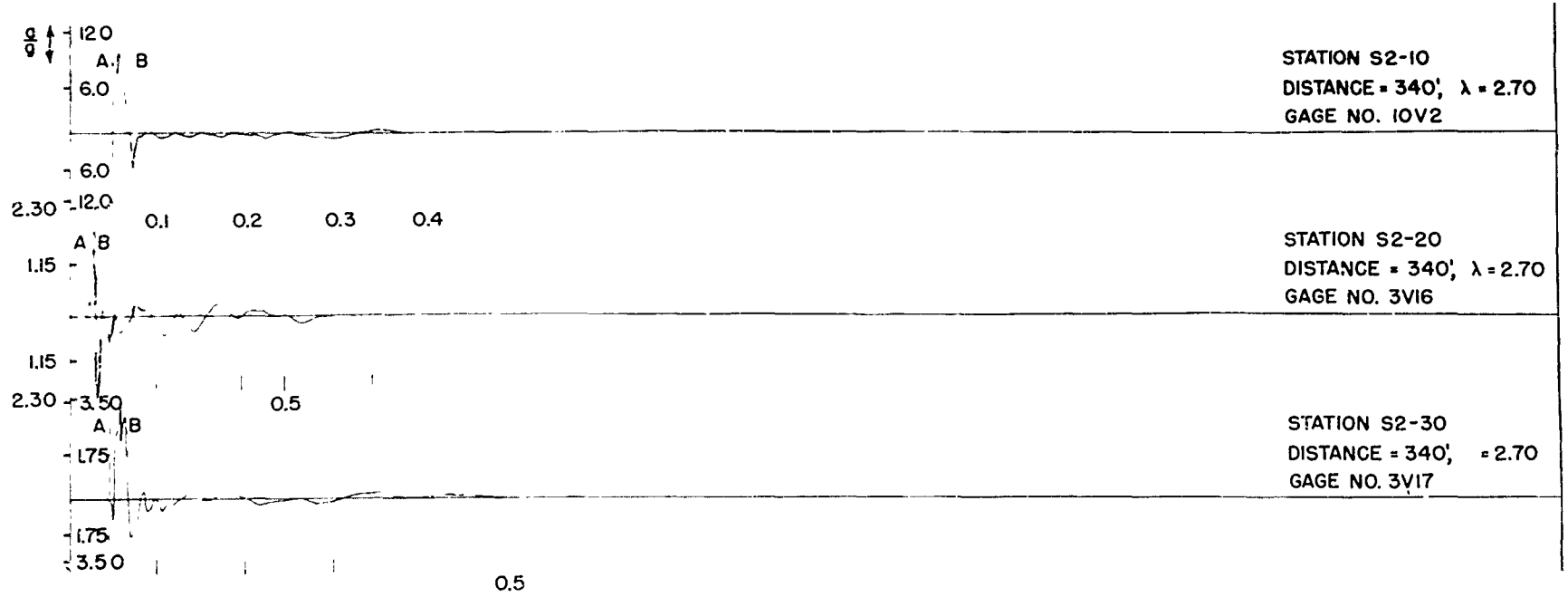
a/g
12.0
A B
6.0
6.0
2.30
12.0
0.1
0.2
0.3
0.4
A B
1.15
1.15
2.30
3.50
0.5
A B
1.75
1.75
3.50
0.5
STATION S2-10
DISTANCE = 340', λ = 2.70
GAGE NO. 10V2
STATION S2-20
DISTANCE = 340', λ = 2.70
GAGE NO. 3V16
STATION S2-30
DISTANCE = 340', = 2.70
GAGE NO. 3V17

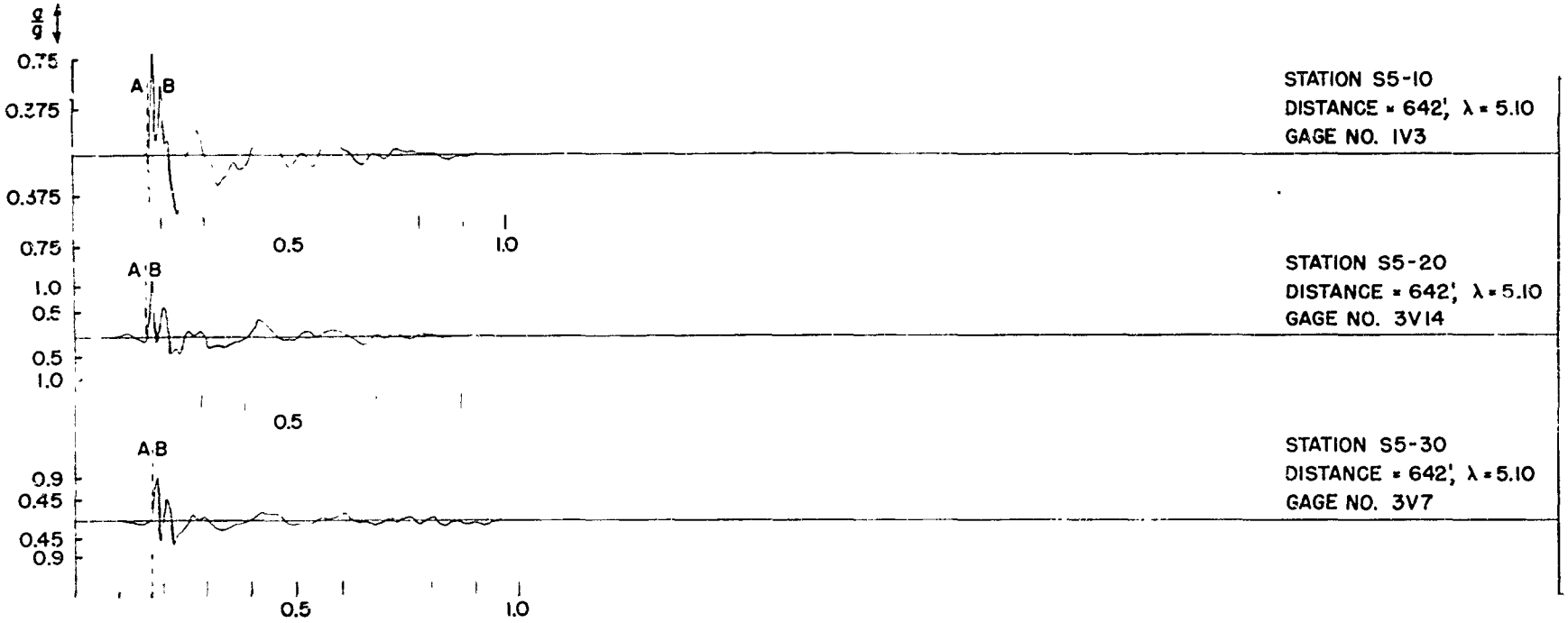
a/g
0.75
A B
0.375
0.375
0.5
1.0
0.75
A B
1.0
0.5
0.5
1.0
0.5
A B
0.9
0.45
0.45
0.9
0.5
1.0
STATION S5-10
DISTANCE = 642', λ = 5.10
GAGE NO. 1V3
STATION S5-20
DISTANCE = 642', λ = 5.10
GAGE NO. 3V14
STATION S5-30
DISTANCE = 642', λ = 5.10
GAGE NO. 3V7

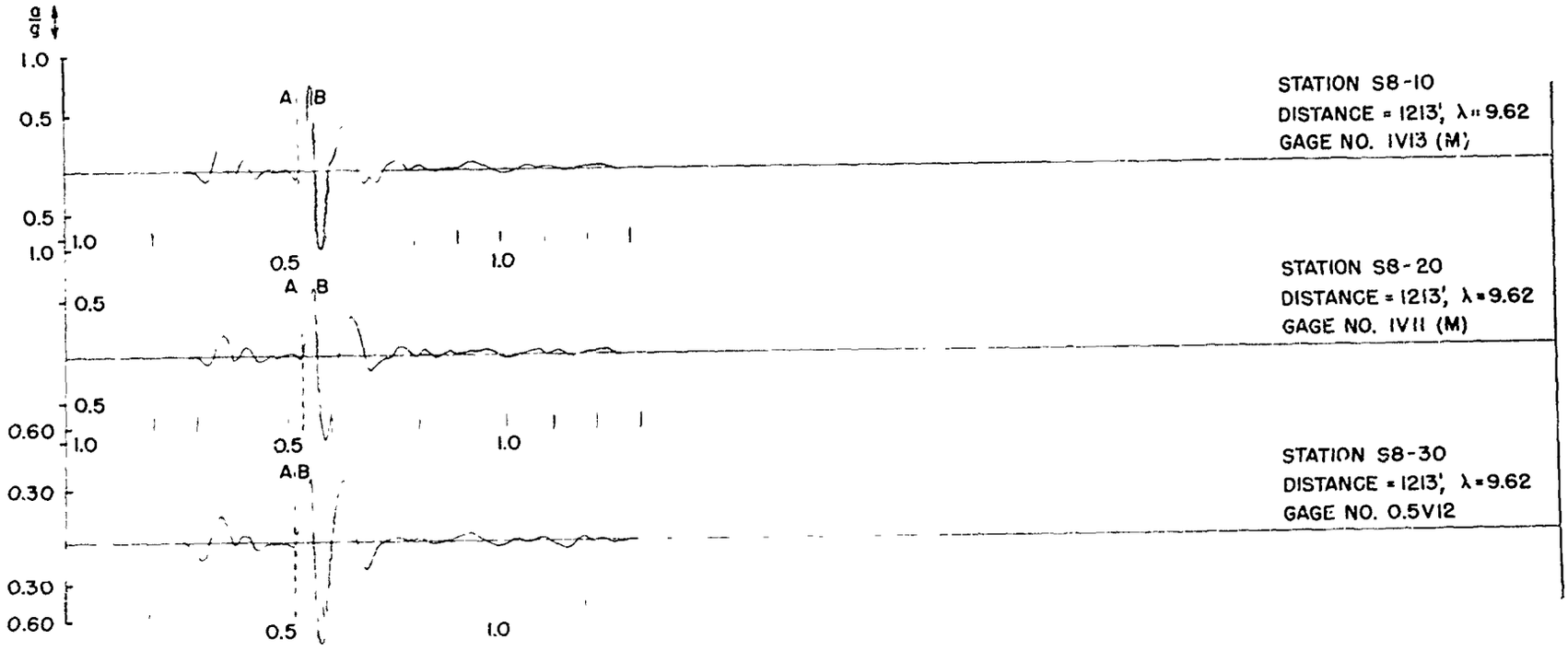
a/g
STATION S8-10
DISTANCE = 1213', λ = 9.62
GAGE NO. IV13 (M)
STATION S8-20
DISTANCE = 1213', λ = 9.62
GAGE NO. IV11 (M)
STATION S8-30
DISTANCE = 1213', λ = 9.62
GAGE NO. 0.5V12
A B

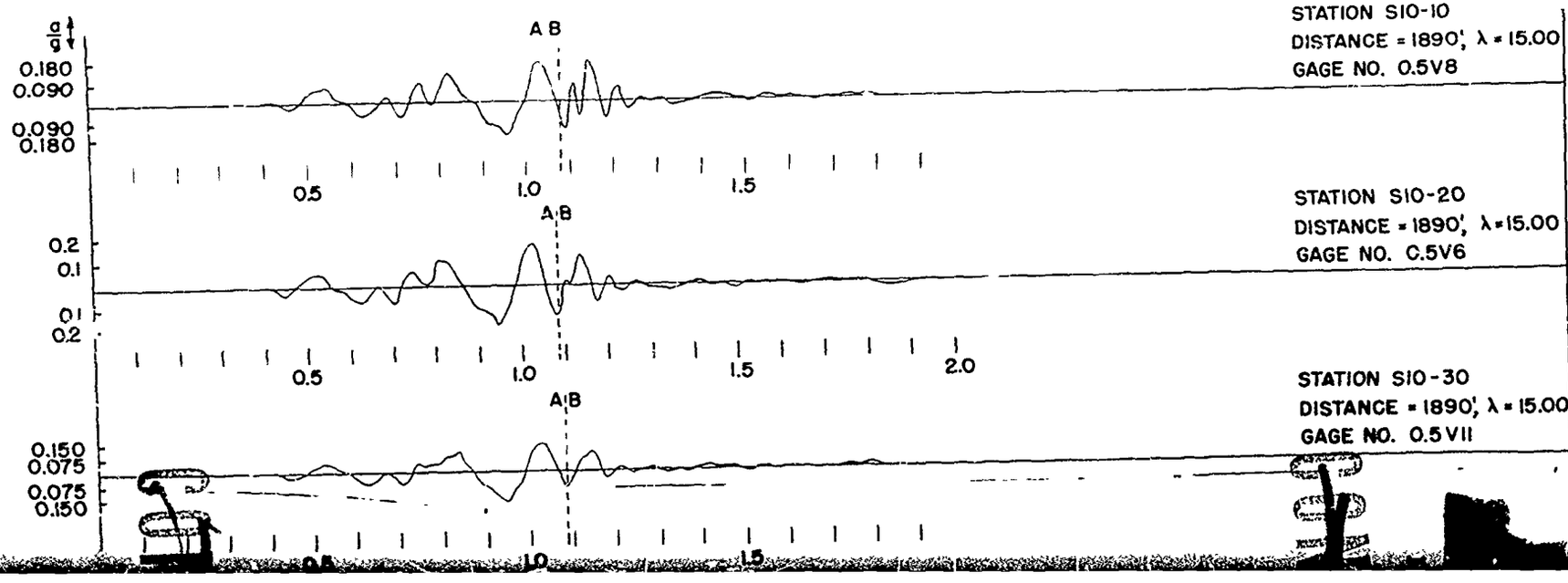
a/g
STATION S10-10
DISTANCE = 1890', λ = 15.00
GAGE NO. 0.5V8
STATION S10-20
DISTANCE = 1890', λ = 15.00
GAGE NO. 0.5V6
STATION S10-30
DISTANCE = 1890', λ = 15.00
GAGE NO. 0.5V11
A B

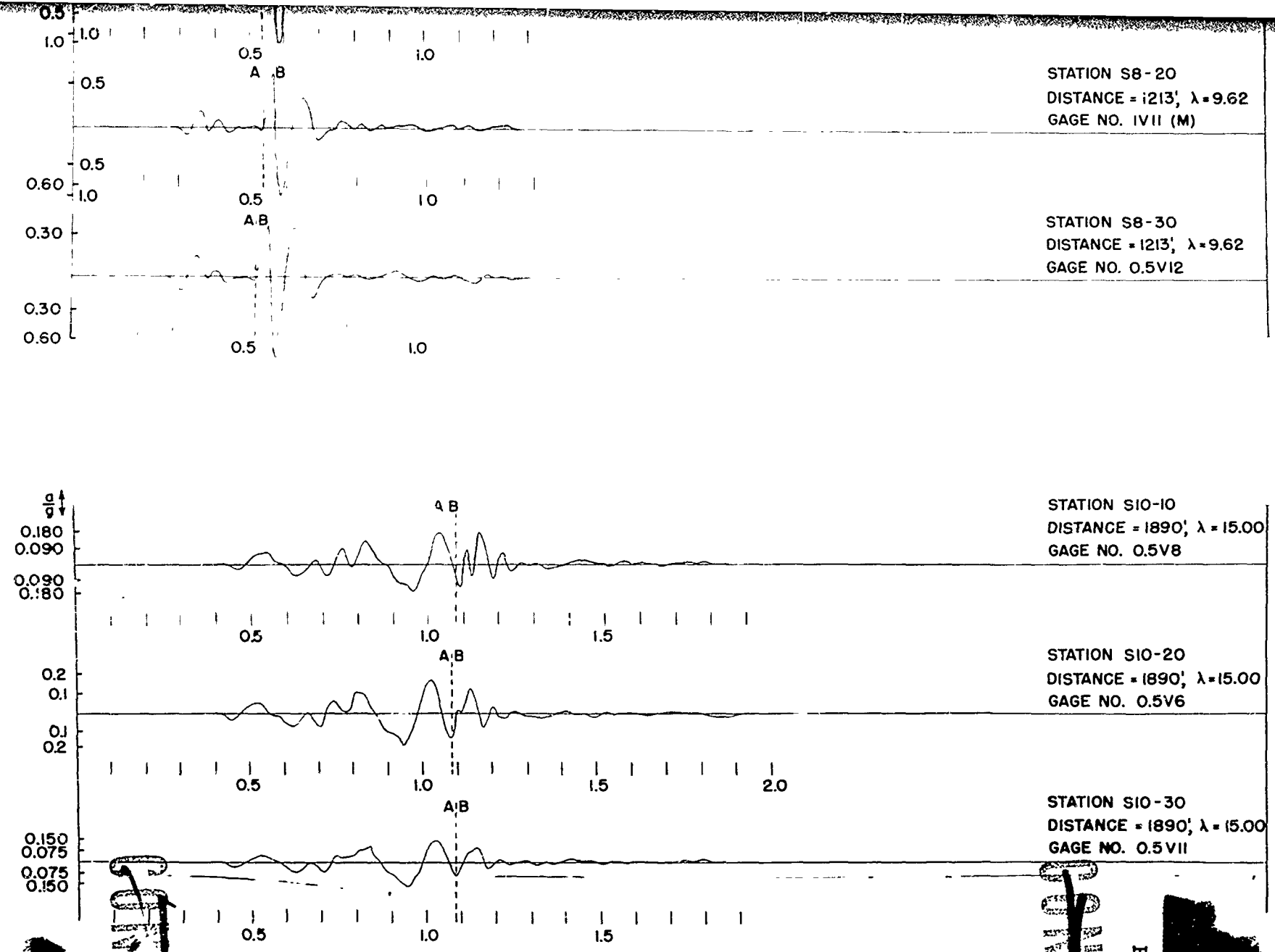


B.7 VERTICAL ACCELERATIONS FROM SURFACE SHOT FOR 10, 20, 30 FT. DEPTHS



PROJECT 1.1

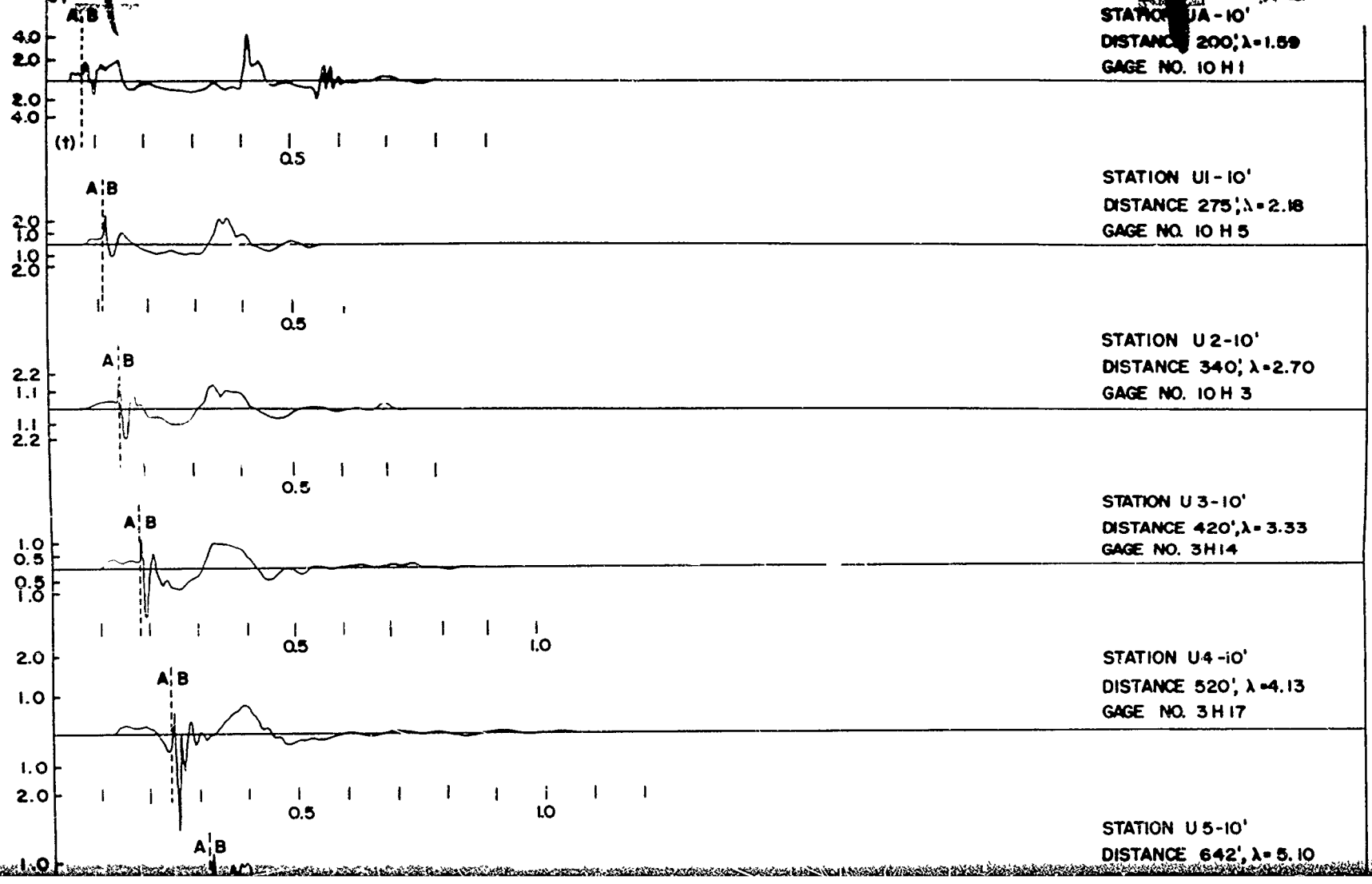
A B
4.0
2.0
2.0
4.0
(t)
0.5
STATION UA-10'
DISTANCE 200', λ=1.59
GAGE NO. 10 H 1
A B
2.0
1.0
1.0
2.0
0.5
STATION U1-10'
DISTANCE 275', λ=2.18
GAGE NO. 10 H 5
A B
2.2
1.1
1.1
2.2
0.5
STATION U 2-10'
DISTANCE 340', λ=2.70
GAGE NO. 10 H 3
A B
1.0
0.5
0.5
1.0
0.5
1.0
STATION U 3-10'
DISTANCE 420', λ=3.33
GAGE NO. 3H14
A B
2.0
1.0
1.0
2.0
0.5
1.0
STATION U4-10'
DISTANCE 520', λ=4.13
GAGE NO. 3 H 17
A B
1.0
STATION U 5-10'
DISTANCE 642', λ=5.10

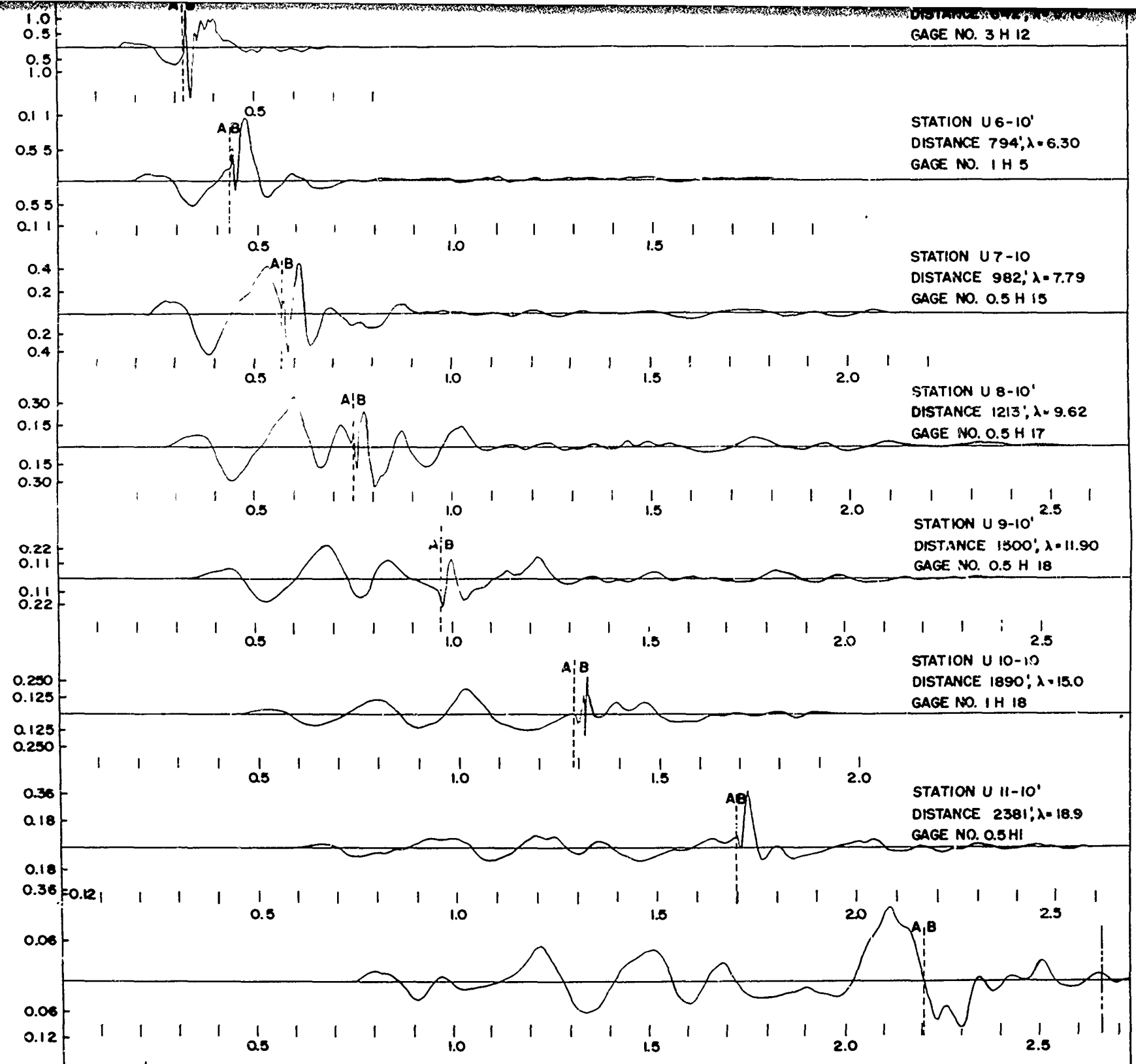
GAGE NO. 3 H 12
STATION U 6-10'
DISTANCE 794', λ = 6.30
GAGE NO. 1 H 5
STATION U 7-10
DISTANCE 982', λ = 7.79
GAGE NO. 0.5 H 15
STATION U 8-10'
DISTANCE 1213', λ = 9.62
GAGE NO. 0.5 H 17
STATION U 9-10'
DISTANCE 1500', λ = 11.90
GAGE NO. 0.5 H 18
STATION U 10-10
DISTANCE 1890', λ = 15.0
GAGE NO. 1 H 18
STATION U 11-10'
DISTANCE 2381', λ = 18.9
GAGE NO. 0.5 H1
A B

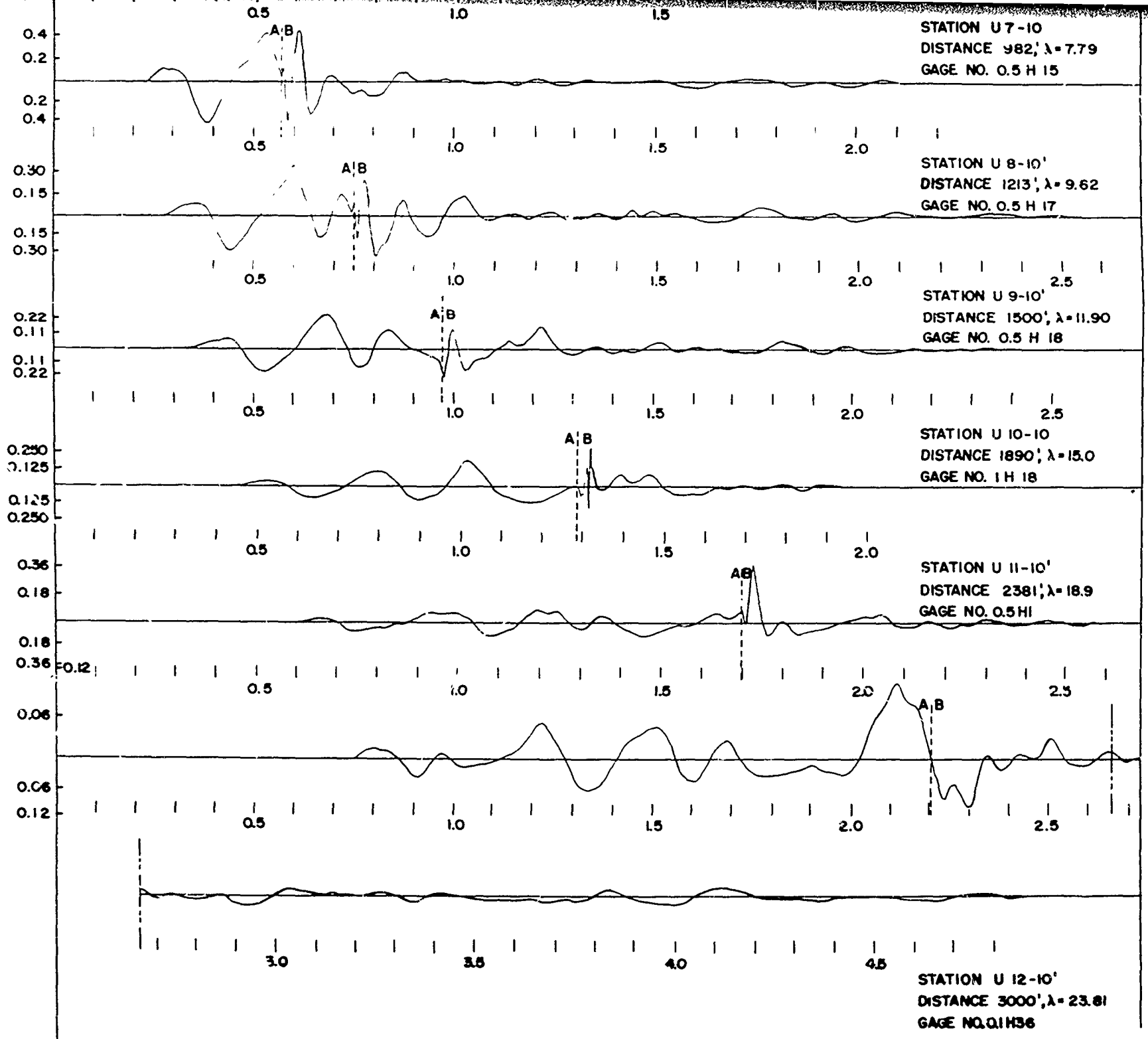


3.8 HORIZONTAL ACCELERATIONS FROM UNDERGROUND SHOT

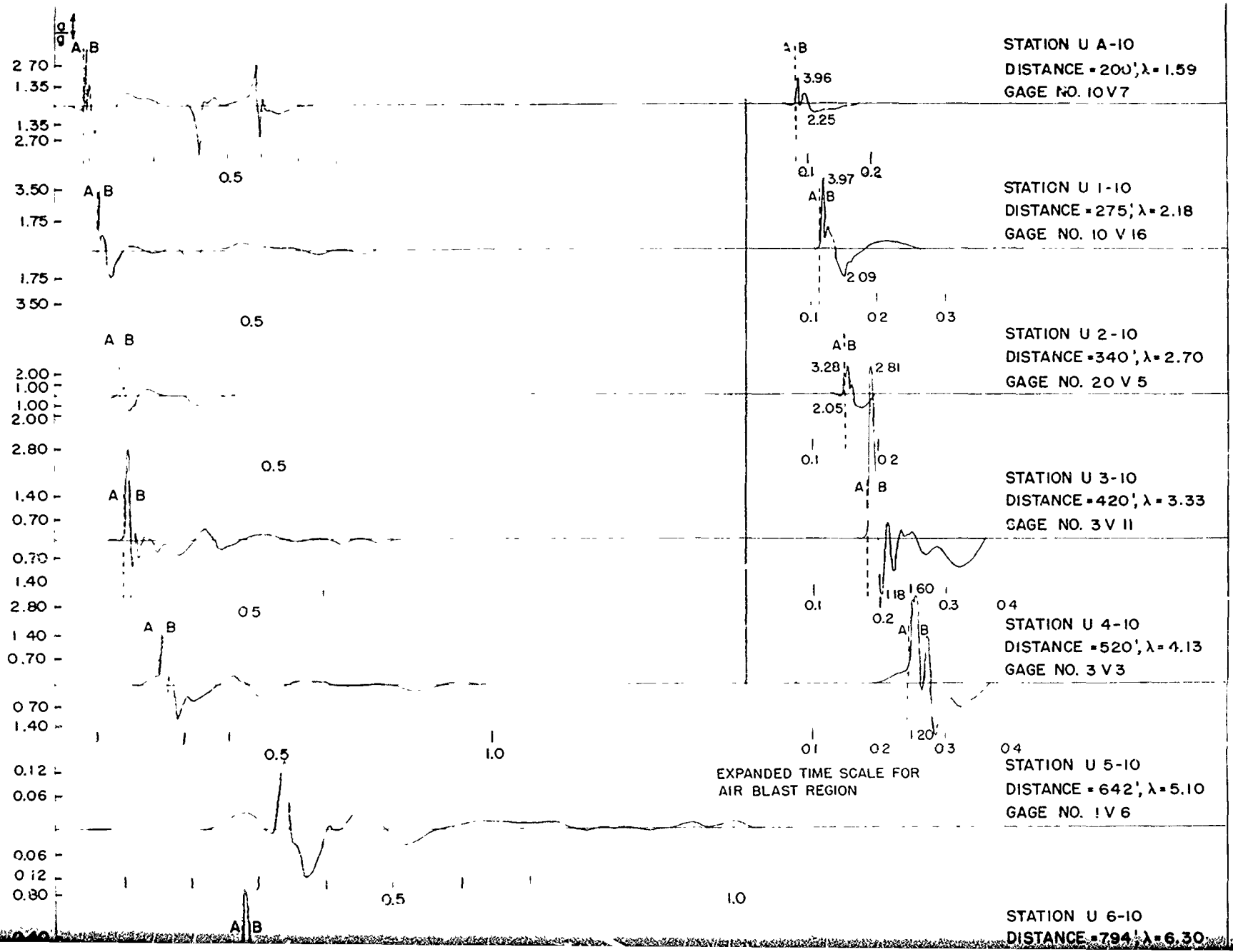
STATION U A-10
DISTANCE = 200', λ = 1.59
GAGE NO. 10 V 7
STATION U 1-10
DISTANCE = 275', λ = 2.18
GAGE NO. 10 V 16
STATION U 2-10
DISTANCE = 340', λ = 2.70
GAGE NO. 20 V 5
STATION U 3-10
DISTANCE = 420', λ = 3.33
GAGE NO. 3 V 11
STATION U 4-10
DISTANCE = 520', λ = 4.13
GAGE NO. 3 V 3
STATION U 5-10
DISTANCE = 642', λ = 5.10
GAGE NO. 1 V 6
STATION U 6-10
DISTANCE = 794', λ = 6.30
EXPANDED TIME SCALE FOR
AIR BLAST REGION

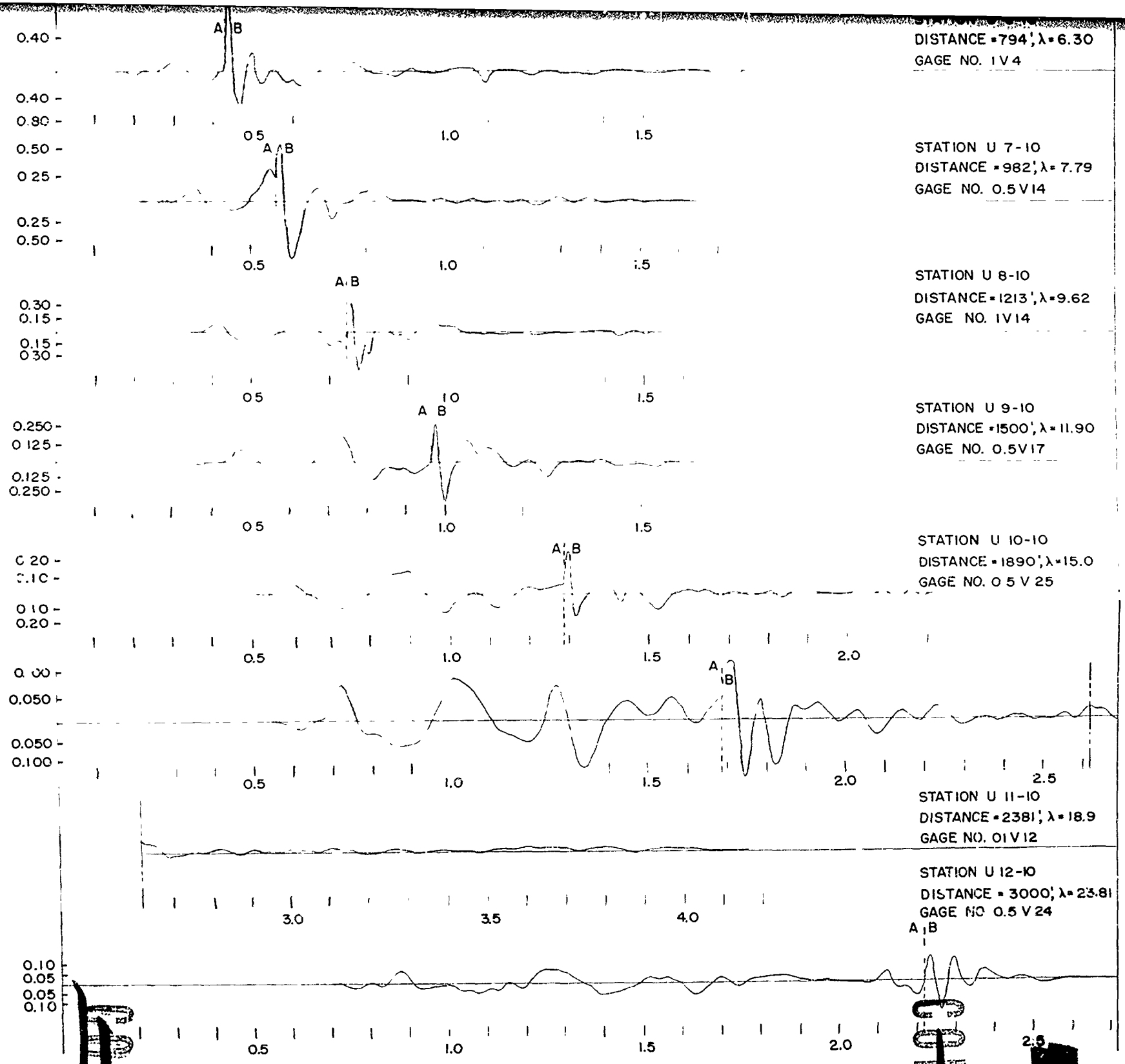
DISTANCE = 794', λ = 6.30
GAGE NO. 1V4
STATION U 7-10
DISTANCE = 982', λ = 7.79
GAGE NO. 0.5V14
STATION U 8-10
DISTANCE = 1213', λ = 9.62
GAGE NO. 1V14
STATION U 9-10
DISTANCE = 1500', λ = 11.90
GAGE NO. 0.5V17
STATION U 10-10
DISTANCE = 1890', λ = 15.0
GAGE NO. 0.5V25
STATION U 11-10
DISTANCE = 2381', λ = 18.9
GAGE NO. 01V12
STATION U 12-10
DISTANCE = 3000', λ = 23.81
GAGE NO. 0.5V24
A B

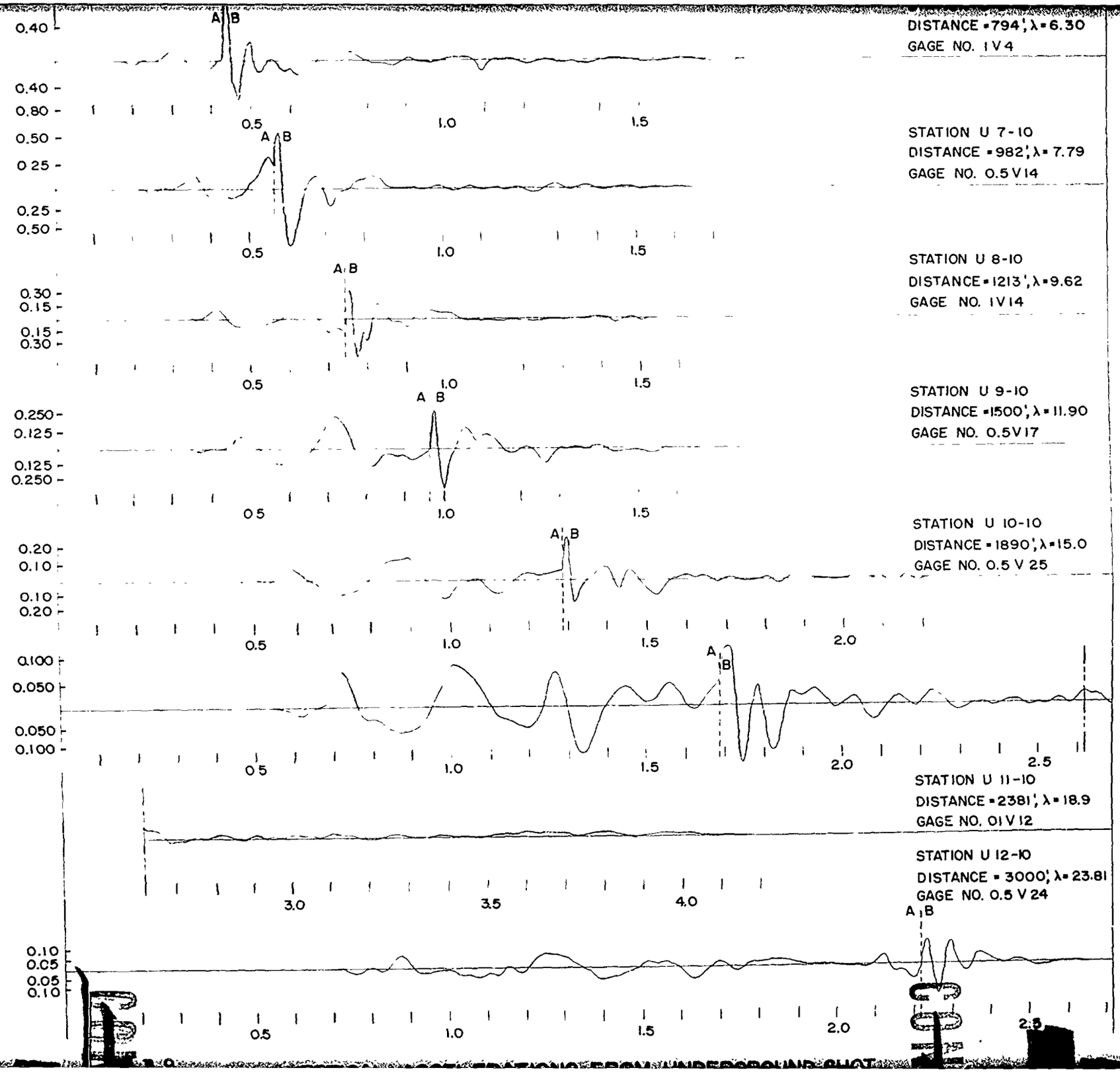
DISTANCE = 794', λ = 6.30
GAGE NO. 1V4
STATION U 7-10
DISTANCE = 982', λ = 7.79
GAGE NO. 0.5V14
STATION U 8-10
DISTANCE = 1213', λ = 9.62
GAGE NO. 1V14
STATION U 9-10
DISTANCE = 1500', λ = 11.90
GAGE NO. 0.5V17
STATION U 10-10
DISTANCE = 1890', λ = 15.0
GAGE NO. 0.5 V 25
STATION U 11-10
DISTANCE = 2381', λ = 18.9
GAGE NO. 01 V 12
STATION U 12-10
DISTANCE = 3000', λ = 23.81
GAGE NO. 0.5 V 24
A B

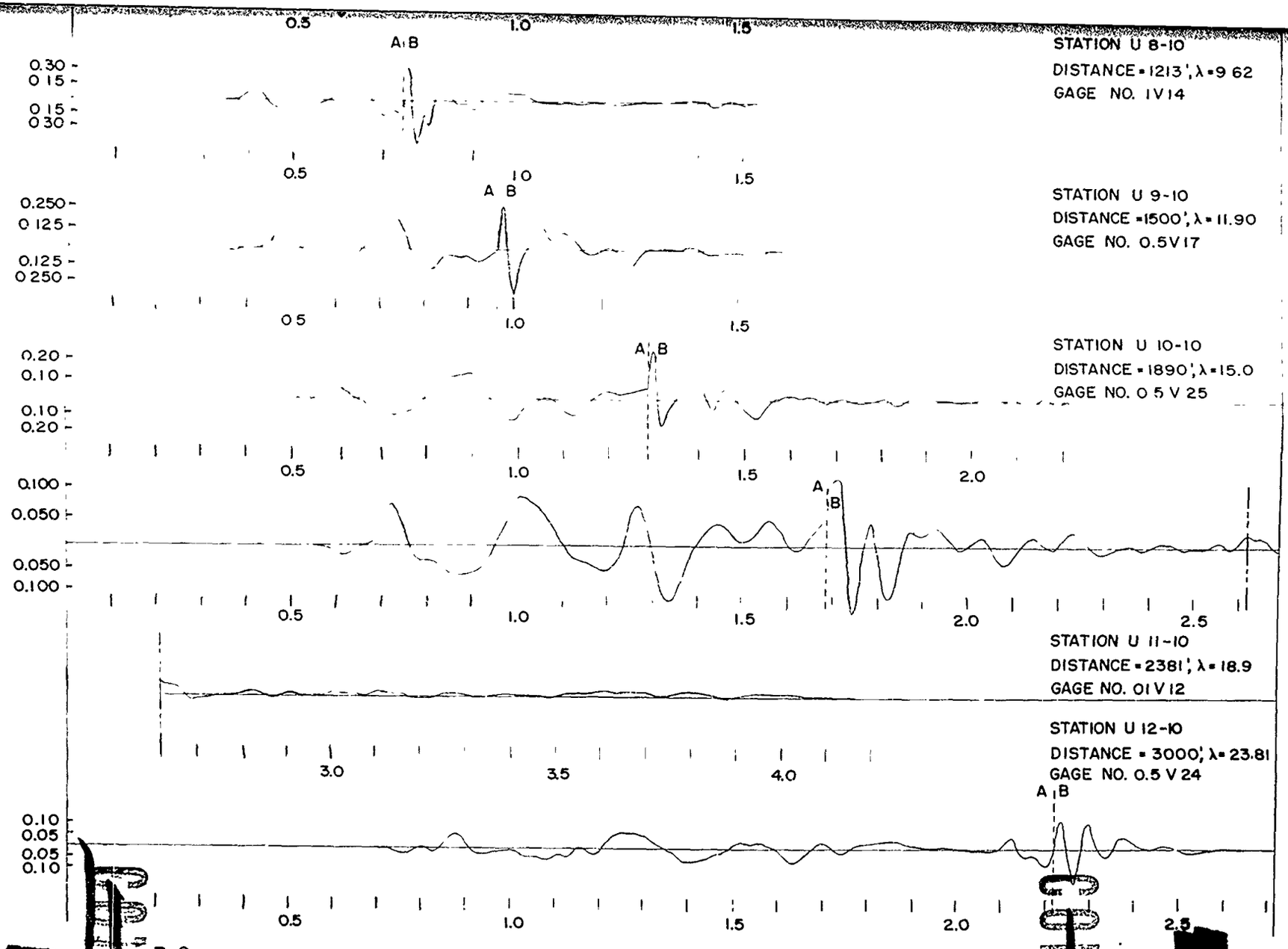


VERTICAL ACCELERATIONS FROM UNDERGROUND SHOT



PROJECT 1.1

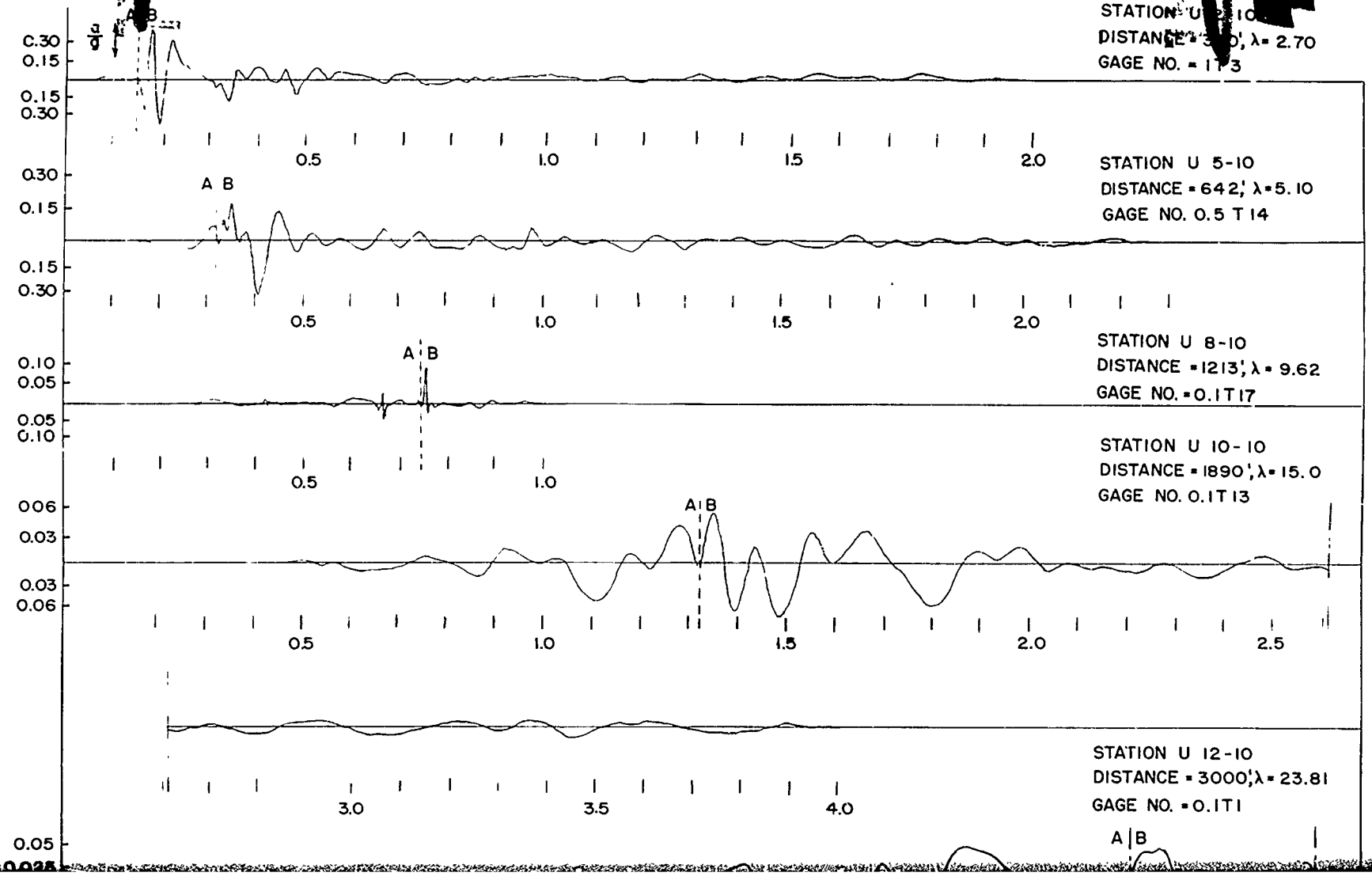
STATION U 2-10
DISTANCE = 300', λ = 2.70
GAGE NO. = 1 T 3
STATION U 5-10
DISTANCE = 642', λ = 5.10
GAGE NO. 0.5 T 14
STATION U 8-10
DISTANCE = 1213', λ = 9.62
GAGE NO. = 0.1 T 17
STATION U 10-10
DISTANCE = 1890', λ = 15.0
GAGE NO. 0.1 T 13
STATION U 12-10
DISTANCE = 3000', λ = 23.81
GAGE NO. = 0.1 T 1
A B
0.5
1.0
1.5
2.0
2.5
3.0
3.5
4.0

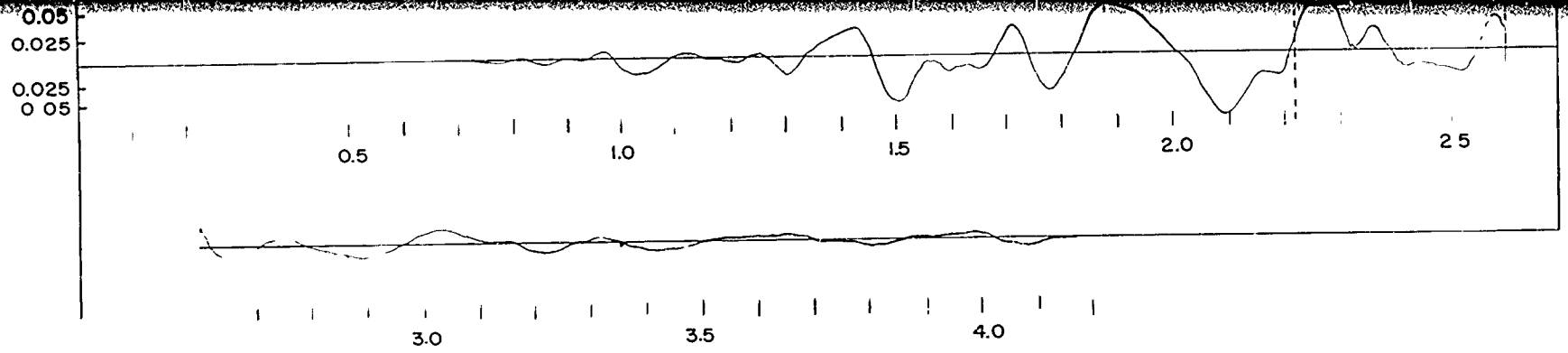


B.10 TRANSVERSE ACCELERATIONS FROM UNDERGROUND SHOT

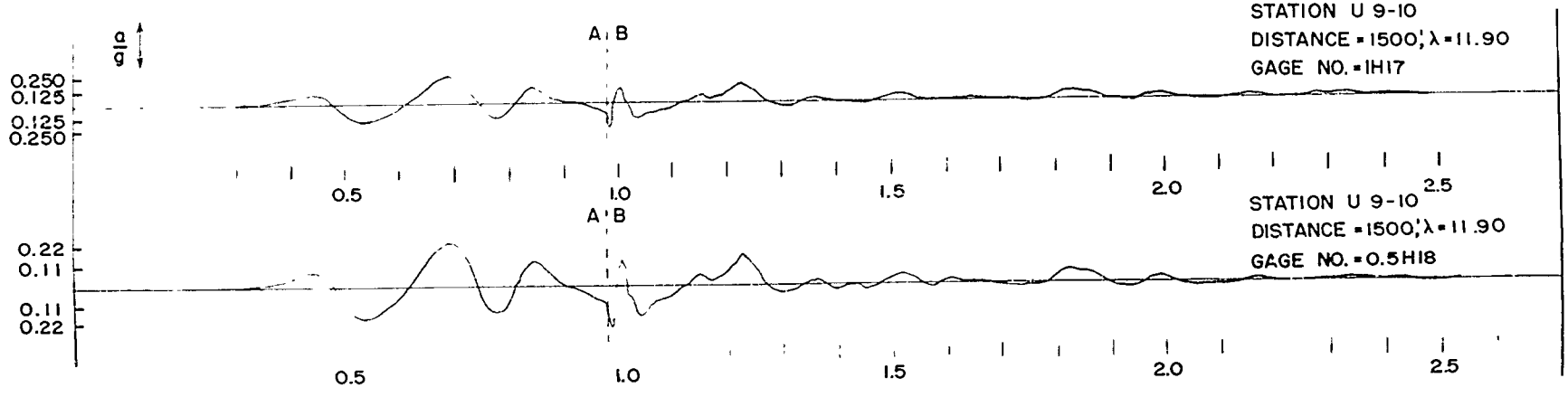


B.11 HORIZONTAL ACCELERATION FROM PRIMARY AND BACKUP GAGES ON UNDERGROUND SHOT

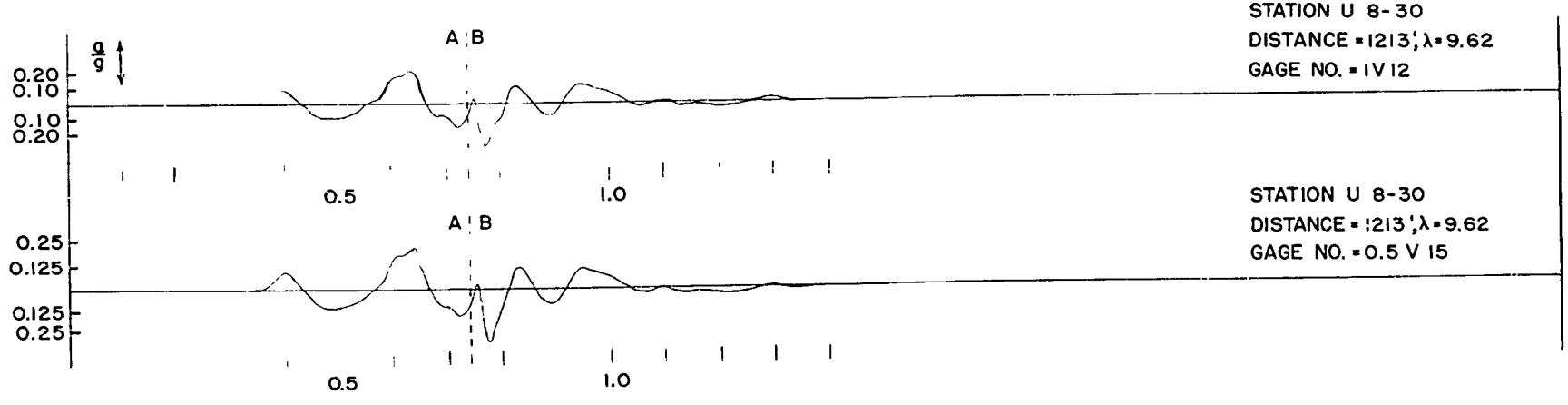

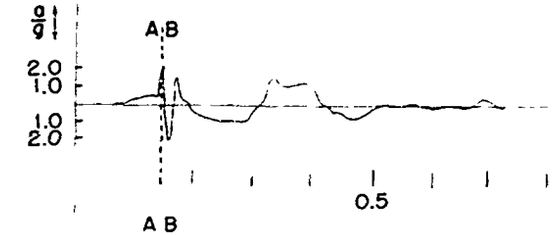


STATION U2-10
DISTANCE = 340', λ = 2.70
GAGE NO. 10H3

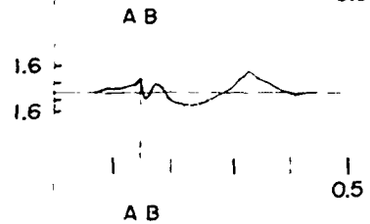


STATION U2-20
DISTANCE = 340', λ = 2.70
GAGE NO. 20H3

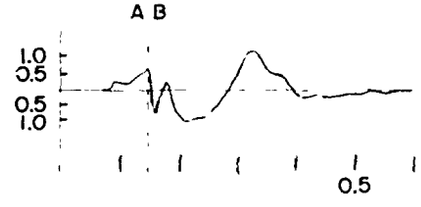


STATION U2-30
DISTANCE = 340', λ = 2.70
GAGE NO. 3H11

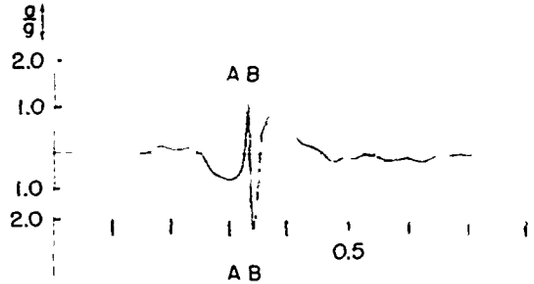


STATION U5-10
DISTANCE = 642', λ = 5.10
GAGE NO. 3H12

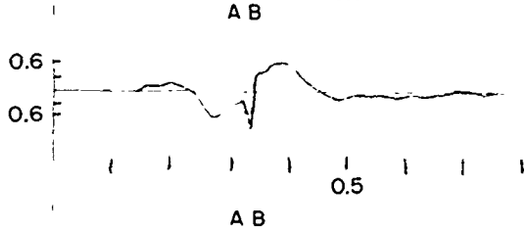


STATION U5-20
DISTANCE = 642', λ = 5.10
GAGE NO. 3H10

STATION U5-30
DISTANCE = 642', λ = 5.10
GAGE NO. 3H15

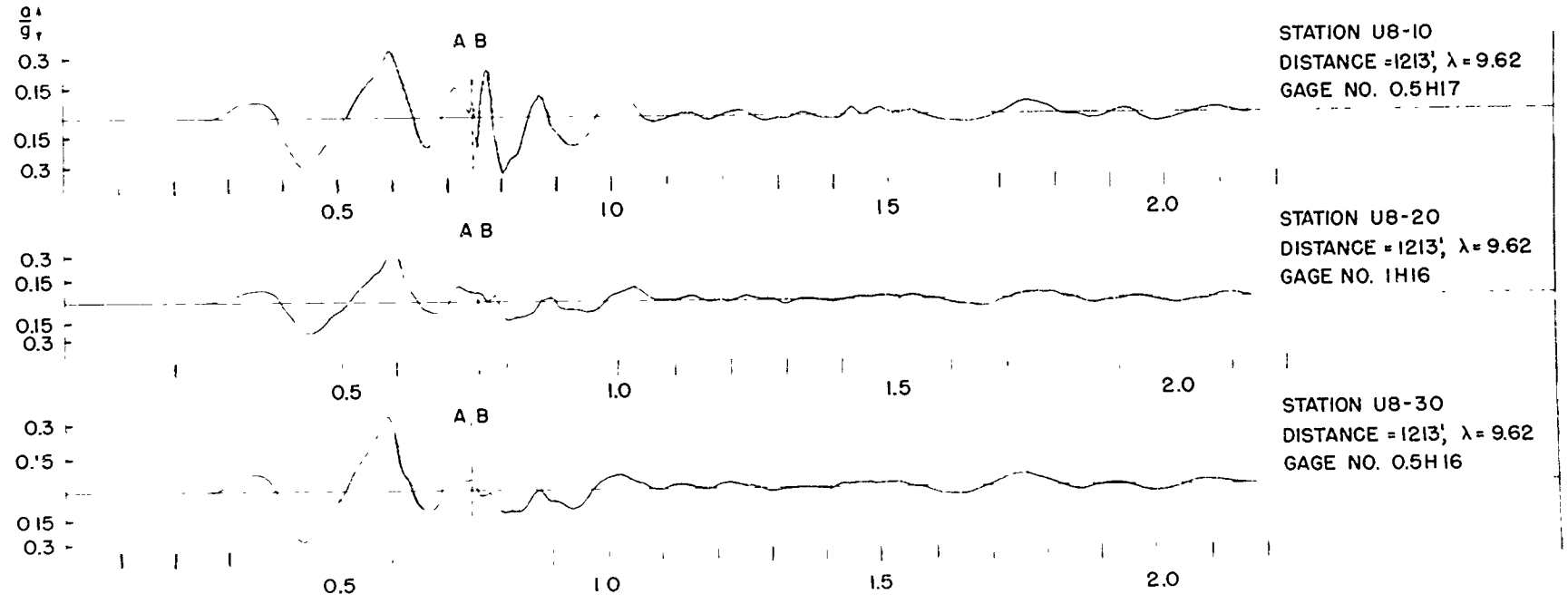
a/g
0.3
0.15
0.15
0.3
A B
0.5
1.0
1.5
2.0
STATION U8-10
DISTANCE = 1213', λ = 9.62
GAGE NO. 0.5H17
STATION U8-20
DISTANCE = 1213', λ = 9.62
GAGE NO. 1H16
STATION U8-30
DISTANCE = 1213', λ = 9.62
GAGE NO. 0.5H16

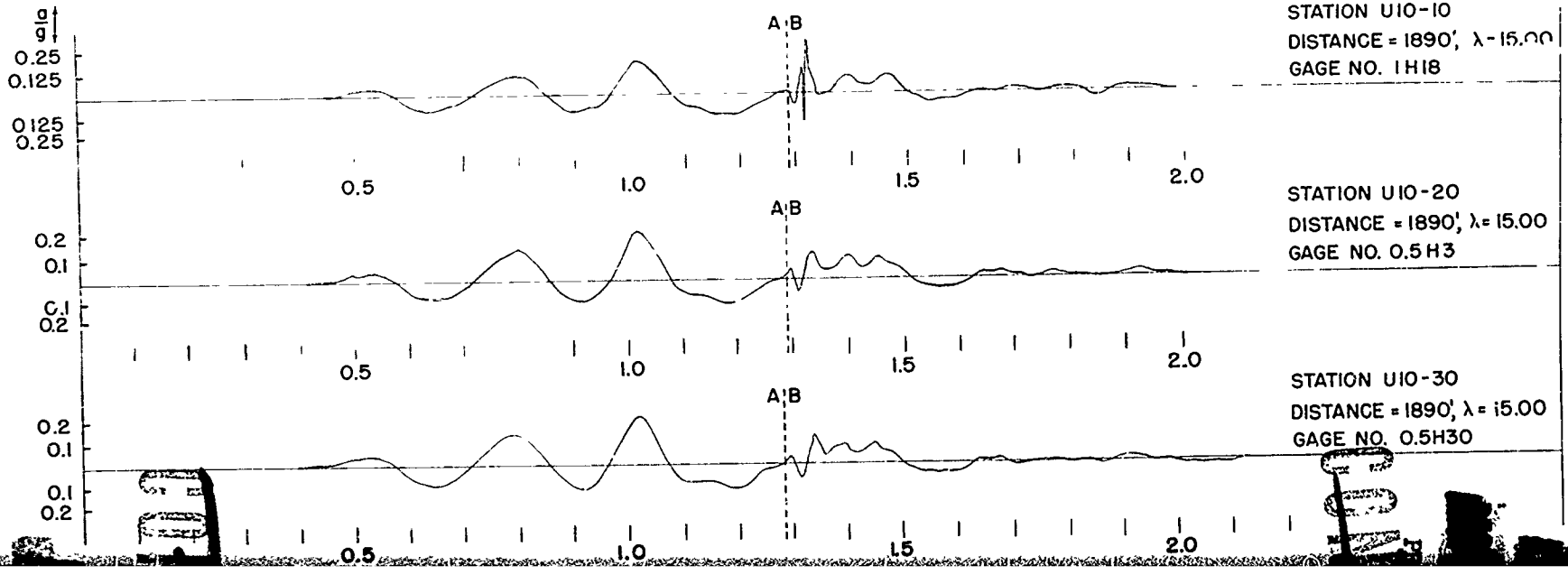
a/g
0.25
0.125
0.125
0.25
0.2
0.1
0.1
0.2
A B
0.5
1.0
1.5
2.0
STATION U10-10
DISTANCE = 1890', λ = 15.00
GAGE NO. 1H18
STATION U10-20
DISTANCE = 1890', λ = 15.00
GAGE NO. 0.5H3
STATION U10-30
DISTANCE = 1890', λ = 15.00
GAGE NO. 0.5H30

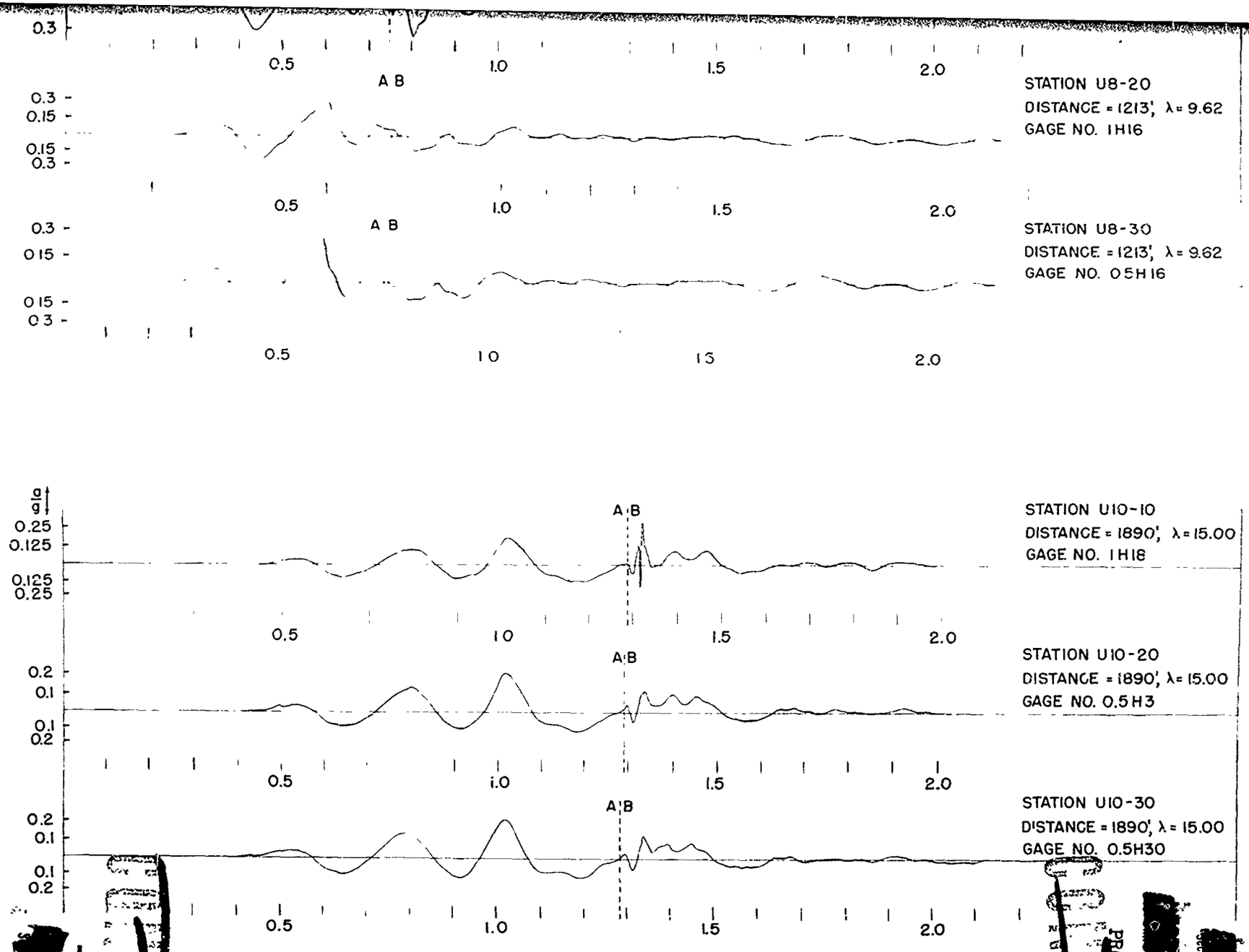


B.13 HORIZONTAL ACCELERATIONS FROM UNDERGROUND SHOT FOR 10, 20, 30 FT DEPTHS

[redacted]

[redacted]

PROJECT 1.1

[redacted]

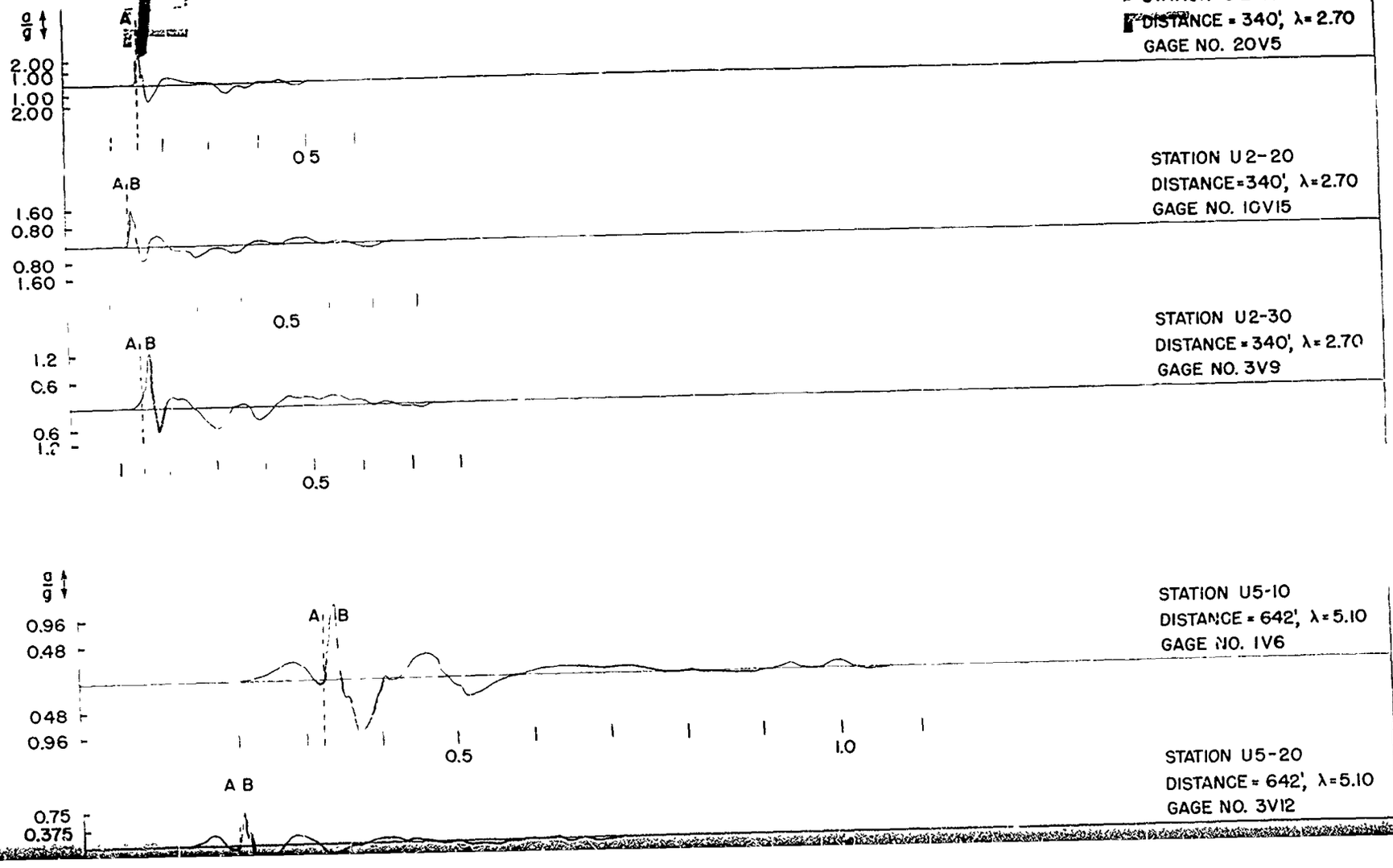

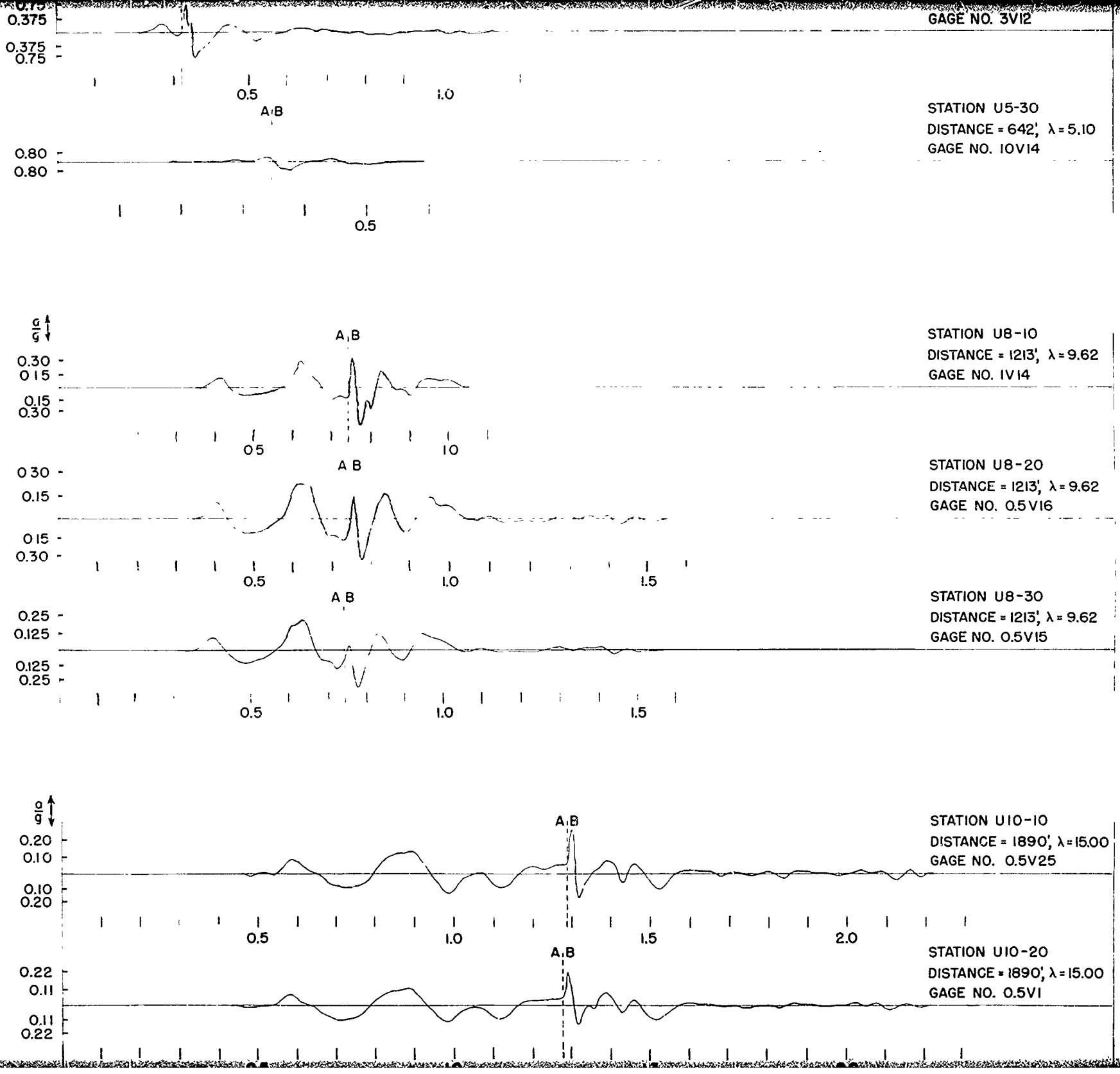
GAGE NO. 3V12
0.375
0.375
0.75
0.5
1.0
A B
STATION U5-30
DISTANCE = 642', λ = 5.10
GAGE NO. 10V14
0.80
0.80
0.5
a/g
A B
STATION U8-10
DISTANCE = 1213', λ = 9.62
GAGE NO. 1V14
0.30
0.15
0.15
0.30
0.5
1.0
A B
STATION U8-20
DISTANCE = 1213', λ = 9.62
GAGE NO. 0.5V16
0.30
0.15
0.15
0.30
0.5
1.0
1.5
A B
STATION U8-30
DISTANCE = 1213', λ = 9.62
GAGE NO. 0.5V15
0.25
0.125
0.125
0.25
0.5
1.0
1.5
a/g
A B
STATION U10-10
DISTANCE = 1890', λ = 15.00
GAGE NO. 0.5V25
0.20
0.10
0.10
0.20
0.5
1.0
1.5
2.0
A B
STATION U10-20
DISTANCE = 1890', λ = 15.00
GAGE NO. 0.5V1
0.22
0.11
0.11
0.22

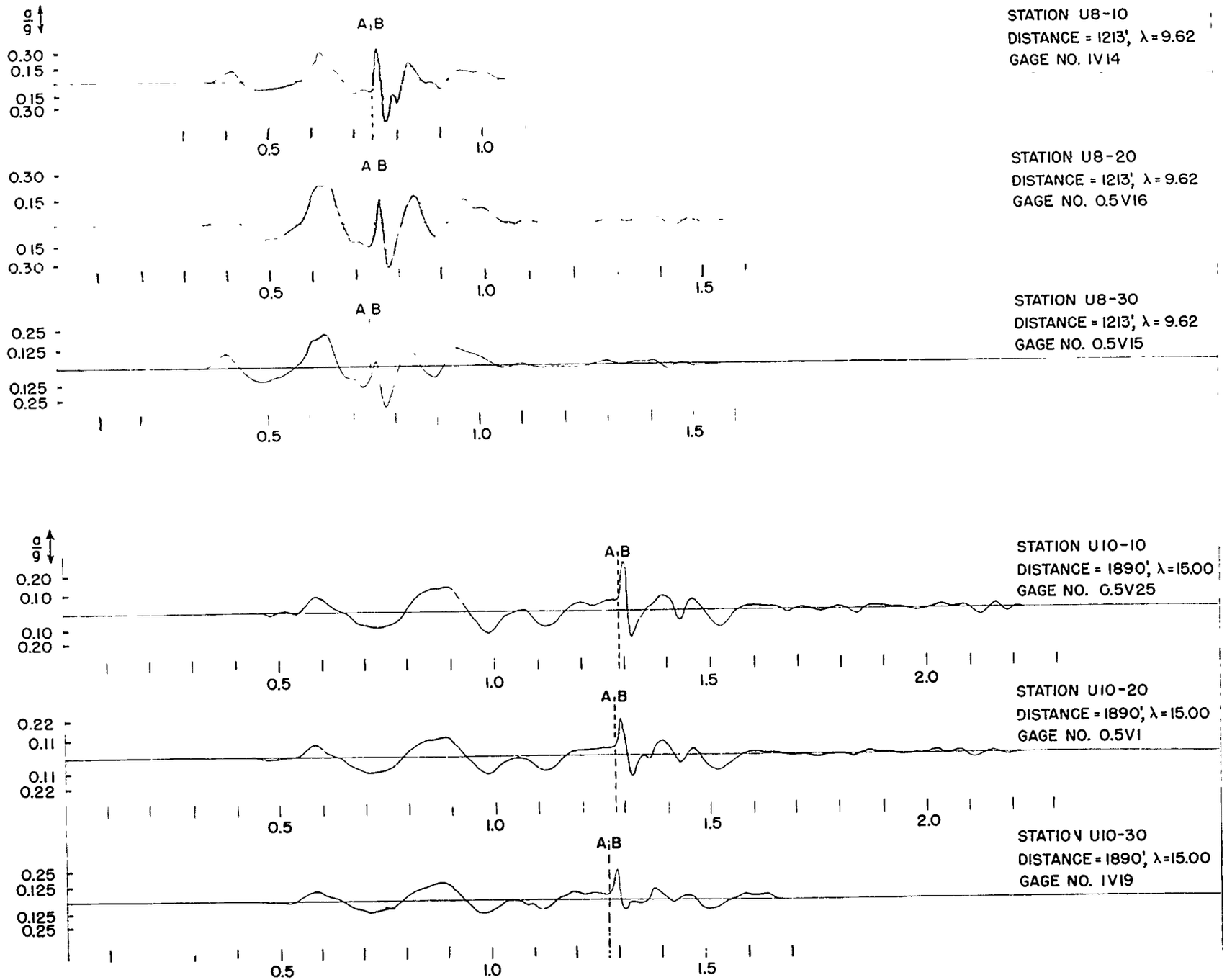


B.14 VERTICAL ACCELERATIONS FROM UNDERGROUND SHOT FOR 10, 20, 30 FT. DEPTHS

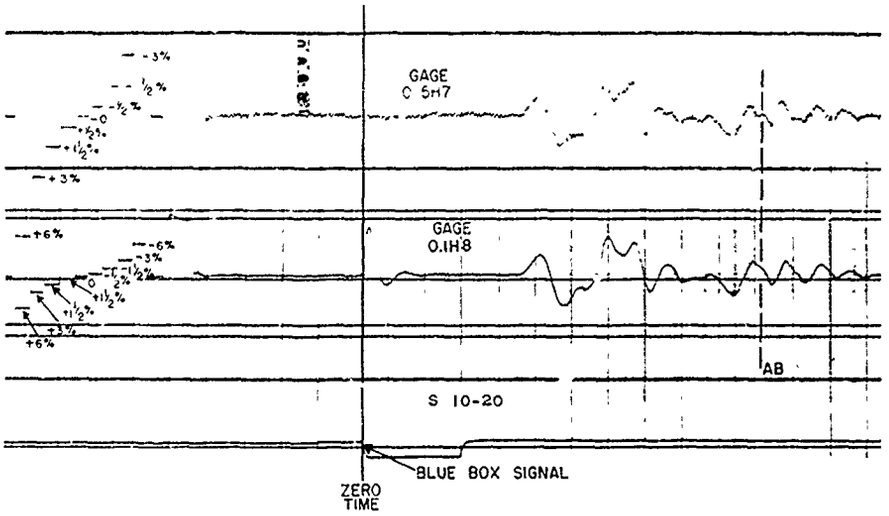


HIGH SIGNAL TO NOISE RATIO

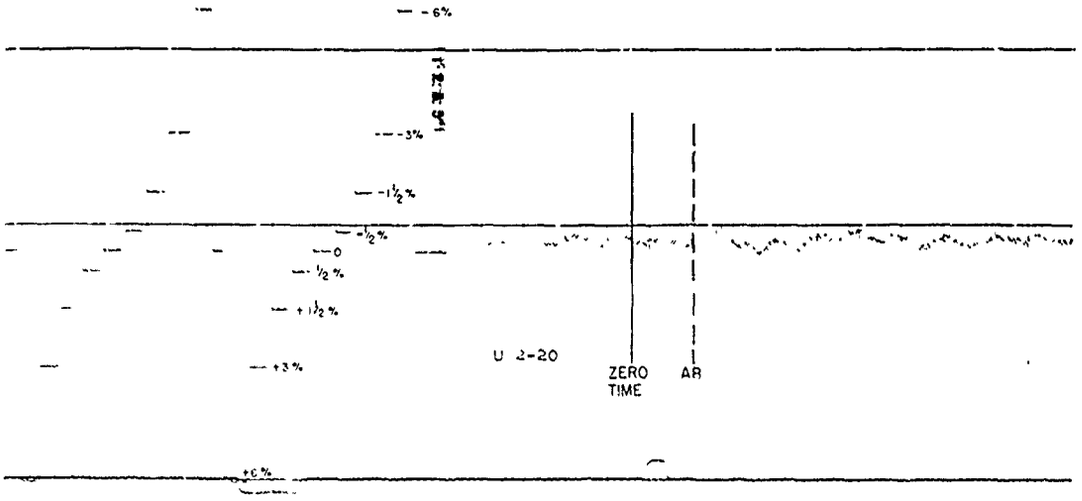


LOW SIGNAL TO NOISE RATIO

**Fig. B.15 Samples of Original Records Showing High and Low Signal to Noise Ratio**

[redacted]

OPERATION JANGLE

PROJECT 1.2a-1

# PEAK AIR BLAST PRESSURES FROM SHOCK VELOCITY MEASUREMENTS ALONG THE GROUND

by

Robert A. Eberhard
Charles N. Kingery
Walter F. Molesky, Lt Col, Sig C

BALLISTIC RESEARCH LABORATORIES
ABERDEEN PROVING GROUND, MARYLAND

[redacted]

# PREFACE

The purpose of this report is to present the peak air blast pressures along the ground calculated from the measurement of the velocity of the air blast wave resulting from underground and surface explosions detonated during Operation JANGLE. Preparation and execution of this project was performed by members of the Explosion Kinetics Branch of the Ballistic Research Laboratories, Aberdeen Proving Ground, Maryland.

Overall guidance and supervision was exercised by Dr. Edward E. Minor, Chief of the Explosion Kinetics Branch, assisted by Nicholas M. Masich, Lt. Col., USAF. The Air Blast Project Chief, Walter F. Molesky, Lt. Col., Signal Corps, was ably assisted by the following personnel in installing the field instrumentation, analyzing the data, and writing this report:

William L. Bowne, Lt USNR

Marvin F. Clarke

Robert A. Eberhard

John S. Fischer, Pfc., Ord Corps

Charles N. Kingery

James A. Mallin, Pvt., Ord Corps

Julius J. Meszaros

John W. Mobarry, Pfc., Ord Corps

James I. Randall

Dr. C. W. Lampson, Chief of the Terminal Ballistic Laboratory, Ballistic Research Laboratories, aided greatly in consulting work.

[redacted]

PROJECT 1.2a-1

CONTENTS


PREFACE . . . . . iii

ABSTRACT. . . . . ix

CHAPTER 1 INTRODUCTION . . . . . 1

1.1 Objectives . . . . . 1
1.2 History of Previous Related Work . . . . . 1
1.3 Basic Theory . . . . . 3
1.3.1 Basic Formulae . . . . . 3
1.3.2 Pressure-Distance Correction . . . . . 4
1.3.3 Correction for Wind Velocity . . . . . 5
1.3.4 Sound Velocity . . . . . 5
1.3.5 The Effect of Humidity . . . . . 7
1.3.6 Errors . . . . . 8
1.3.7 Blast Switch Delay . . . . . 10

CHAPTER 2 EXPERIMENTAL PROCEDURE . . . . . 12

2.1 Field Layout. . . . . 12
2.1.1 General Description of Field Equipment . . . 12
2.1.2 Blast Range Layout . . . . . 13
2.2 Detailed Description of Field Equipment . . . . . 13
2.2.1 Microphone and Blast Switch Equipment . . . 13
2.2.2 Zero Time Equipment. . . . . 18
2.2.3 Direct and Indirect Recording Equipment. . . 18
2.2.4 Microphone Recording Equipment . . . . . 20
2.2.5 Remote Control Equipment . . . . . 20
2.2.6 Meteorological Equipment . . . . . 22
2.3 Reading of Records. . . . . 22
2.3.1 Procedure . . . . . 22

CHAPTER 3 RESULTS AND DISCUSSION . . . . . 25

3.1 HE-1 Shot . . . . . 25
3.1.1 Peak Pressure vs Distance . . . . . 25
3.1.2 Velocity of Sound . . . . . 29
3.1.3 Meteorological Data . . . . . 29
3.2 HE-2 Shot . . . . . 29
3.2.1 Peak Pressure vs Distance . . . . . 29
3.2.2 Velocity of Sound . . . . . 30
3.2.3 Meteorological Data [redacted]




[redacted]

3.3 Surface Shot . . . . . 30
3.3.1 Peak Pressure vs Distance . . . . . 30
3.3.2 Time of Arrival of Blast Wave . . . . . 37
3.3.3 Velocity of Sound . . . . . 37
3.3.4 Meteorological Data . . . . . 41
3.4 Underground Shot . . . . . 41
3.4.1 Peak Pressure vs Distance . . . . . 41
3.4.2 Time of Arrival of Blast Wave . . . . . 44
3.4.3 Velocity of Sound . . . . . 44
3.4.4 Meteorological Data . . . . . 44

CHAPTER 4 CONCLUSIONS AND RECOMMENDATIONS . . . . . 46

4.1 Peak Overpressure vs Reduced Distance . . . . . 46
4.1.1 HE-1, HE-2, and Underground Shots . . . . . 46
4.1.2 Surface Shot . . . . . 46
4.2 Error Evaluation. . . . . 48
4.3 Velocity of Sound . . . . . 48
4.4 Instrumentation . . . . . 48
4.4.1 Trailers . . . . . 48
4.4.2 Blast Switches . . . . . 49
4.4.3 Blast Transducers . . . . . 49
4.4.4 Zero Time . . . . . 49
4.4.5 Recording . . . . . 49

ILLUSTRATIONS

CHAPTER 1 INTRODUCTION

1.1 Pressure vs Blast Switch Delay . . . . . 11

CHAPTER 2 EXPERIMENTAL PROCEDURE

2.1 Block Diagram Blast Arrival Time Measuring Equipment. . . . . 14
2.2 Photograph of Blast Range for Underground Shot . . 15
2.3 Front View of Recording Equipment in Van . . . . . 15
2.4 Rear View of Recording Equipment in Van. . . . . 15
2.5 Blast Range Layout for Shot HE-1 . . . . . 16
2.6 Blast Range Layout for Shot HE-2 . . . . . 16
2.7 Blast Range Layout for Surface Shot. . . . . 16
2.8 Blast Range Layout for Underground Shot. . . . . 16
2.9 Photograph of Velocity Head. . . . . 17
2.10 Circuit Diagram for Blue Box Fiducial Marker . . . 17
2.11 Photograph of Blue Box Fiducial Mark . . . . . 19
2.12 Block Diagram of Direct and Indirect Recording System . . . . . 19
2.13 Circuit Diagram of Direct and Indirect Recording System . . . . . 21
2.14 Block Diagram Blast Transducer Recording System. . 21
2.15 Circuit Diagram Blast Transducer Recording System. 23
2.16 Photograph of Typical Blast Wave Record on 35mm Film . . . . . 24

CHAPTER 3 RESULTS AND DISCUSSION

3.1 Peak Overpressure vs Reduced Distance, HE-1 Shot . 28
3.2 Peak Overpressure vs Reduced Distance, HE-2 Shot . 33
3.3 Peak Overpressure vs Distance, Surface Shot. . . . 38
3.4 Peak Overpressure vs Reduced Distance, Surface Shot . . . . . 39
3.5 Arrival Time vs Distance, Surface Shot . . . . . 40
3.6 Peak Overpressure vs Distance, Underground Shot. . 43
3.7 Peak Overpressure vs Reduced Distance, Underground Shot . . . . . 43
3.8 Peak Overpressure vs Reduced Distance HE-1, HE-2, and Underground Shots. . . . . 47
3.9 Arrival Time vs Distance, Underground Shot . . . . 47

TABLES

CHAPTER 3 RESULTS AND DISCUSSION

3.1 HE-1 Peak Pressure vs λ . . . . . 26
3.2 HE-1 Correction for Switch Delay. . . . . 27
3.3 HE-1 Switch Correction Applied. . . . . 27
3.4 HE-2 Peak Pressure vs λ . . . . . 31
3.5 HE-2 Corrections for Switch Delay . . . . . 32
3.6 HE-2 Switch Correction Applied. . . . . 32
3.7 Peak Pressure vs Reduced Distance, Surface Shot . 35
3.8 Correction for Switch Delay, Surface Shot . . . . 36
3.9 Switch Correction Applied, Surface Shot . . . . . 36
3.10 Blast Arrival Time, Surface Shot . . . . . 40
3.11 Peak Pressure vs Reduced Distance, Underground Shot . . . . . 42
3.12 Blast Arrival Time, Underground Shot. . . . . 45

[redacted]

PROJECT 1.2a-1

## ABSTRACT


The objective of Project 1.2a-1, Program One, Operation JANGLE was to determine the peak air blast pressure along the ground by measurement of the air blast velocity for a surface and an underground nuclear explosion at the Nevada Test Site.

The four explosions with which this report is concerned are as follows:

| Title | Weight | $w^{1/3}$ | Depth of Charge ft | Depth of Charge $\lambda$ |
|---|---|---|---|---|
| HE-1 | 2560 lbs TNT | 13.68 | 1.8 | 0.135 |
| HE-2 | 40,000 lbs TNT | 34.2 | 4.6 | 0.135 |
| Surface Nuclear | 1 KT Equivalent | 126 | -2.5 | -0.024 |
| Underground Nuclear | 1 KT Equivalent | 126 | 17 | 0.135 |

Participation in the preliminary high explosive program, Project 1.2a (9) was limited to HE-1 and HE-2, to correlate use of scaling laws. and to check instrumentation procedures.

Velocities were calculated using pre-determined distances and the measurement of arrival times of the shock wave at those distances. Pressures were calculated from a pressure-velocity equation derived from the Rankine-Hugoniot relations based on the conservation of mass, momentum, and energy across the shock front, and from the ideal gas law for computing the internal energy of a gas.

Anticipated pressures for the nuclear shots were predicted from a series of tests conducted with 1 lb charges at Aberdeen Proving Ground and the results of HE-1 and HE-2.

Equivalent TNT blast tonnages for the nuclear shots as calculated from the velocity measurements were:

Surface Shot $1 \pm .05$ Kilo tons

Underground Shot $1 \pm .26$ Kilo tons

Using the calculated equivalent tonnage, the pressure vs reduced distance curve obtained from the Surface shot coincided with the free air curve, and the Underground curve compared favorably with the curves from HE-1 and HE-2.


[redacted]



[redacted]

# CHAPTER 1

# INTRODUCTION

## 1.1 OBJECTIVES

Operation JANGLE was directed principally for the purpose of determining the effects on structures of ground shock resulting from the detonation of an underground and a near surface nuclear explosion based on an equivalent of 1 KT of TNT. The measurement of the air blast pressures associated with explosions of this type was necessary in order to determine its relative importance in relation to the ground shock effects measured. The main purpose of the work described in this report was to provide peak air blast pressure measurements, along a radial blast line, resulting from underground and surface nuclear explosions.

Secondary objectives of this work were:

(1) To provide arrival times of the air blast waves at the air blast stations set up on radial blast lines.

(2) To determine whether scaling laws for peak air blast pressures derived from conventional explosions could be applied to underground and surface nuclear explosions.

## 1.2 HISTORY OF PREVIOUS RELATED WORK

Determinations of peak air blast pressures from shock velocity measurements are based on the use of the Rankine-Hugoniot relationships which have been used by many investigators in the field of shock wave measurements. Some of these works are reported in the literature of

NDRC Division 2 [1,3] and Ballistic Research Laboratories Reports [2]. The basic theory of the method is described in Section 1.3 of this report.

For accurate peak air blast pressure determinations the velocity method requires that a sharp front, as distinct from adiabatic waves, be generated by the explosion. Pressure determinations of this type have been previously obtained on nuclear explosions detonated in the air on Operations SANDSTONE [4] and GREENHOUSE [5]. From these operations it was found that scaling laws derived from conventional HE explosions could be applied to nuclear explosions detonated at corresponding height above ground. Velocity measurements apply ideally only where a true blast wave exists.

A limited amount of experimental work on air blast measurements resulting from HE charges buried underground has previously been carried out both by the Ballistic Research Laboratories and by the Naval Ordnance Laboratory. This work, based on the use of one pound charges detonated on the surface and underground at shallow depths, indicated that low overpressures were to be expected in the region of interest in the present work.

---

1 R. G. Stoner, "The Pressure-Distance Relationship for TNT, Determined by Measurement of Shock Velocity", NDRC Report A-474 (OSRD-6637)

2 T. D. Carr, M. Scharzchild, and P. Weiss, "An Improved Method for the Measurement of Blast from Bombs", Ballistic Research Laboratories Report No. 336

3 C. W. Tait, and W. D. Kennedy, "Characteristics of Air Blast Gauges II" NDRC Report No. AES-11C

4 G. L. Beyer, J. Petes, and E. J. Culling, "Blast Measurement of Peak Pressure", Scientific Directors Report on Atomic Weapons Test at Eniwetok, Chapter 10.1 Annex 5, Part 2, 1948

5 W. E. Curtis, "Determination of Mach Region Peak Blast Pressures from Shock Velocity Measurements" Operation GREENHOUSE, Annex 1.6, Part III, Section 1

The results of the 320,000 lb HE shot detonated 22 May 1951 at Dugway[6] at a depth of 0.5λ have shown that step-type air blast waves were generated by the explosions which were probably caused by a venting effect due to the deeper charge location. In view of the large scaling factors involved in the use of the data resulting from the 1 lb charges, and the non-ideal type shock waves observed at Dugway, it was decided in the present work to instrument for air blast effects the preliminary 2,560 and 40,000 lb HE shots which were detonated at the Nevada Test Site at charge depths of 0.135λ. It was believed that scaling laws derived from these detonations would be more applicable to the underground nuclear explosions detonated at a corresponding charge depth in the same test area.

## 1.3 BASIC THEORY

### 1.3.1 Basic Formula

A measure of average air blast velocity was taken over various intervals radially along a blast line and converted to peak over-pressure by means of the Rankine-Hugoniot relationship which gives peak over-pressure as a function of velocity. The equation[7,8] follows:

$$\frac{P_s}{P_o} = \frac{2\gamma}{\gamma+1}\left[\frac{U^2}{a_o^2} - 1\right] \qquad (1.3.1)$$

where $P_s$ = excess pressure in shock wave (lb/in$^2$)

$P_o$ = atmospheric pressure ahead of the shock (lb/in$^2$)

---

6 Interim Report "Underground Explosion Tests at Dugway" prepared for Sacramento District Office, Corps of Engineers, by the Stanford Research Institute

7 Part III, Technical Note No. 139, March 1950, Ballistic Research Laboratories, Aberdeen Proving Ground, Maryland

8 Stoner, op. cit.

$U$ = the shock velocity relative to the medium into which it is moving (ft/sec)

$a_o$ = velocity of sound in the medium ahead of the shock (ft/sec)

$\gamma$ = the ratio of specific heat at constant pressure to specific heat at constant volume (1.40 for dry air)

### 1.3.2 Pressure-Distance Correction

The average velocity as obtained by arrival time data is not equal to the instantaneous velocity at the midpoint of the interval because the velocity-distance decay is not linear. The distance correction to determine the point in the interval at which the average velocity is applicable was applied on the HE shots as follows: [9]

$$R_v = R_m \left[ 1 - (n+1) \frac{q^2}{24} \right] \qquad (1.3.2)$$

where $R_v$ = the distance from the charge at which the actual pressure equaled the pressure computed from the average velocity.

$R_m$ = the distance from the charge to the midpoint of the velocity interval.

$n$ = the exponent of the pressure distance law when approximated by a power function $P = AR^{-n}$.

$q = \frac{L}{R_m}$ where L was the interval distance.

This formula applied for pressures less than 17 psi and assumed a relation $P = AR^{-n}$ over the particular interval used in these tests.

---

9 Carr, op. cit.

### 1.3.3 Correction for Wind Velocity

The effect of the wind measured at the recording station was incorporated in the results as another correction in obtaining true air blast velocities. The wind component parallel to the blast line was computed from the meteorological data. This component, depending on direction, was either added or subtracted from the air blast velocity.

If the wind component (V) along the blast line were neglected then the effect of this error would show up as dU where the shock velocity is U. Take the basic equation (1.3.1) where:

$$P_s = \frac{7}{6}\left[\frac{U^2}{a_o^2} - 1\right] P_o$$

Differentiate with respect to U:

$$dP_s = \frac{7}{6} P_o \left[\frac{2U}{a_o^2}\right] dU$$

Then if V = dU, derive the fractional error in pressures $\frac{\Delta P_s}{P_s}$ due to neglecting the wind component as:[10]

$$\frac{\Delta P_s}{P_s} = \frac{7}{3}\frac{P_o}{P_s}\left(\frac{U}{a_o}\right)\left(\frac{V}{a_o}\right) \qquad (1.3.3)$$

### 1.3.4 Sound Velocity

The velocity of sound is given by the equation:

$$a^2 = \frac{\gamma P_o}{\rho} \qquad (1.3.4)$$

---

10 G. K. Frankel, "Apparatus for the Measurement of Air Blast Pressure by Means of Piezoelectric Gauges" NDRC Report No. A-373 OSRD Report No. 6251

which in this case becomes:

$$a_d = \frac{1.4\ P_o}{\rho/g} \qquad (1.3.4)$$

where $a_d$ = velocity of sound in dry air (ft/sec)

$\gamma$ = 1.4, ratio of specific heats in dry air

$P_o$ = atmospheric pressure (lb/ft$^2$)

$g$ = gravity constant 32.2 (ft/sec$^2$)

$\rho$ = density of the air (lb/ft$^3$)

$$\rho = \frac{0.001293H}{(1 + 0.00367\ T)\ 76}\ (\text{gm/cc}) \qquad (1.3.6)$$

H = barometric reading in centimeters of mercury

T = the temperature in degrees Centigrade

This particular determination was used because it was applicable to dry air conditions.

To find the fractional error $\frac{\Delta\ P_s}{P_s}$ due to an error in sound velocity, take the basic equation (1.3.1) where:

$$P_s = \frac{7}{6}\ P_o \left[\frac{U^2}{a_o^{\ 2}} - 1\right]$$

Differentiate with respect to $a_o$:

$$dP_s = -\frac{7}{3}\ P_o \left[\frac{U^2}{a_o^{\ 3}}\right] da_o$$

Considering $da_o$ as the error in sound velocity then:

$$\frac{\Delta\ P_s}{P_s} = -\frac{7}{3}\frac{P_o}{P_s}\left[\frac{U^2}{a_o^{\ 2}}\right]\left[\frac{da_o}{a_o}\right] \qquad (1.3.7)$$

To find the error in sound velocity by the method used, follow a similar procedure:

$$a_o^2 = \frac{\gamma P_o}{\rho} \qquad \frac{da}{a} = -\frac{1}{2}\frac{d\rho}{\rho}$$

$$\rho = \frac{0.001293H}{(1 + 0.00367\ T)\ 76} \qquad \frac{d\rho}{\rho} = \frac{\beta T}{H\beta T}\frac{dT}{T}$$

where $\beta = .00367$

$$\frac{\Delta a}{a} = -\frac{1}{2}\left(\frac{\beta T}{1+\beta T}\right)\frac{\Delta T}{T} \qquad (1.3.8)$$

1.3.5 The Effect of Humidity

Shock pressures obtained by the velocity method depend upon the ratio of specific heats which in turn are dependent upon humidity by the relations:[11]

$$\gamma = \gamma_a\left[1 + \left(\frac{\gamma_a - 1}{\gamma_w - 1}\right)\left(\frac{\gamma_w}{\gamma_a} - 1\right)\frac{P_w}{P_a}\right] \qquad (1.3.9)$$

where $\gamma$ = the ratio of specific heats of air in moist air

$\gamma_a$ = ratio of specific heats of air in dry air

$\gamma_w$ = ratio of specific heats of water vapor

$P_w$ = partial pressure of water vapor

$P_a$ = partial pressure of air

Any change in the ratio of specific heats, $\gamma$, will results in an error in shock pressures as given by the following relation:

$$\frac{\Delta P_s}{P_s} = \frac{1}{\gamma+1}\frac{\gamma}{\gamma} \qquad (1.3.10)$$

11 Ibid.

The effect of humidity on sound velocity is given approximately by:[12]

$$a_o = a_d \left[1 - 0.149 \frac{P_w}{P_a}\right] \qquad (1.3.11)$$

where $P_w$ = partial pressure of water vapor in the air

$P_a$ = partial pressure of air

$P_o$ = atmospheric pressure

$P_w = P_{w'}$ x relative humidity

$P_{w'}$ = vapor pressure of water at saturation at temperature t

$P_a = P_o - P_w$

1.3.6 Errors

Consider the Rankine-Hugoniot equation:

$$P_s = \frac{7}{6} P_o \left[\frac{U^2}{a_o^2} - 1\right]$$

The total fractional error in the peak overpressure due to errors in sound velocity and shock velocity may be obtained by taking the total differential of $P_s$ with respect to its independent variables U and $a_o$. Thus:

$$dP_s = \frac{\partial P_s}{\partial U} dU + \frac{\partial P_s}{\partial P_o} da_o$$

---

12 J. C. Fletcher, W. T. Read, R. G. Stoner, D. K. Weimer, "Final Report on Shock Tube, Piezoelectric Gauges, and Recording Apparatus", NDRC A-356 OSRD-6321, Feb. 1946

where

$$\frac{\partial P_s}{\partial U} = \frac{7P_oU^2}{3a_o^2} \qquad \frac{\partial P_s}{\partial a_o} = -\frac{7}{3}\frac{P_oU^2}{a_o^3}$$

then

$$dP_s = \frac{7}{3}\frac{P_oU^2}{a_o^2}\left[\frac{dU}{U} - \frac{da_o}{a_o}\right]$$

or

$$\frac{\Delta P_s}{P_s} = \left[2 + \frac{7P_o}{3P_s}\right]\left[\frac{\Delta U}{U} - \frac{\Delta a_o}{a_o}\right] \qquad (1.3.12)$$

The shock velocity U was obtained from the interval distance S and the time (t) required for the shock to travel this distance, i.e. $U = \frac{S}{t}$. The error in U due to errors in S and t is found by the same method.

$$dU = \frac{\partial U}{\partial S}\, dS + \frac{\partial U}{\partial t}\, dt$$

$$\frac{\partial U}{\partial S} = \frac{1}{t} \qquad \frac{\partial U}{\partial t} = -\frac{S}{t^2}$$

$$\frac{dU}{U} = \frac{\Delta U}{U} = \left(\frac{\Delta S}{S} - \frac{\Delta t}{t}\right)$$

Substituting in equation (1.3.12) and using equation 1.3.8:

$$\frac{\Delta P_s}{P_s} = \left[2 + \frac{7}{3}\frac{P_o}{P_s}\right]\left[\frac{\Delta S}{S} - \frac{\Delta t}{t} + \frac{\beta T}{2(1+\beta 1)}\frac{\Delta T}{T}\right] \qquad (1.3.13)$$

The maximum error possible would be the absolute value of the fractional errors.

The probable error in the computed over-pressure was found on the following estimated fundamental errors:

| | | |
|---|---|---|
| (1) | Temperature | $1^{\circ}C$ |
| (2) | Relative Humidity | 5% |
| (3) | Barometric Pressure | 0.01 in. Hg. |
| (4) | Wind Velocity | 2 mph |
| (5) | Wind Direction | 10 degrees |
| (6) | Value of $\gamma$ | 0.0005 |
| (7) | Distance between stations | 0.01 ft. |
| (8) | Timing oscillator frequency | 1 cycle in 100,000 cycles |
| (9) | Record reading error | 100 microseconds |

### 1.3.7 Blast Switch Delay

The blast switch which weighs approximately 5 grams and exposes an area of 1.71 square inches is subject to delay in closing. This delay is dependent on shock over-pressure and begins to increase noticeably at pressures below 12 psi. (See Fig. 1.1) It was found that under 5 psi over-pressure the delay is of the order of 1 millisecond with appreciable increase in delay for smaller pressures.

The shock tube used in calibrating the switch delay time was limited in range from 2.5 to 12 psi over-pressure so that the point at which the delay is constant was not obtained. In evaluating the true pressure vs distance curve the pressures at the stations were read from the blast transducer curve, the transducer having no significant delay time. The delay corresponding to the pressure at each station was read from Fig. 1.1 and the successive differences computed. These differences were subtracted from the time intervals between their respective stations, and new pressures computed from the Rankine-Hugoniot formula.

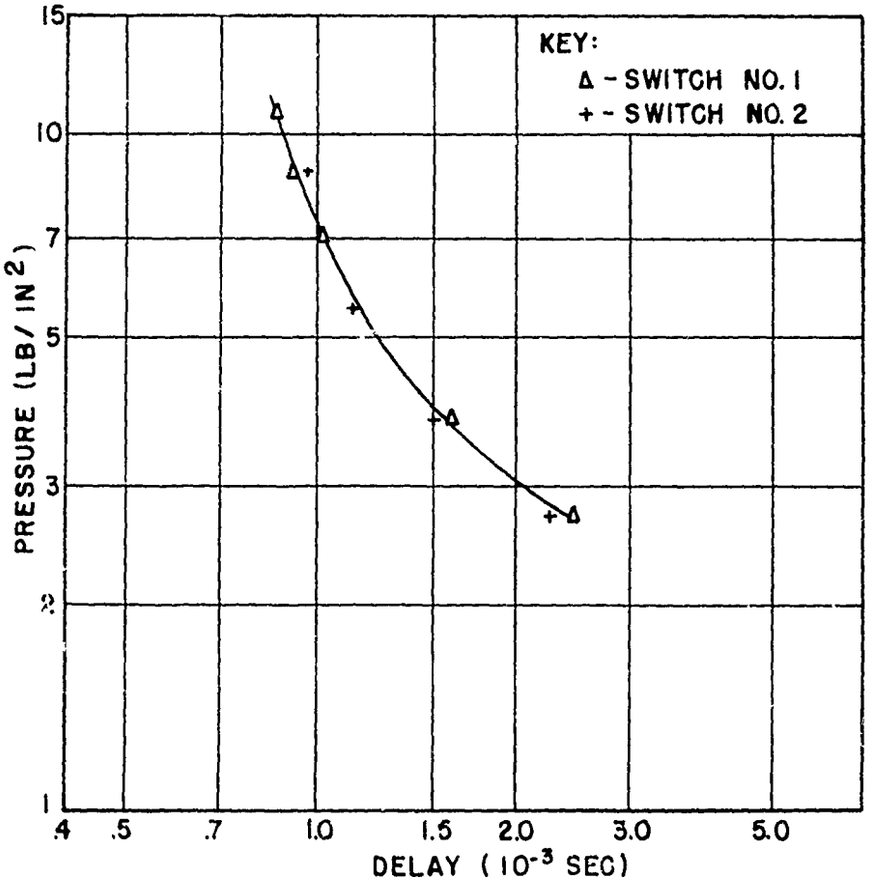


Fig. 1.1 Pressure vs Blast Switch Delay

[redacted]

# CHAPTER 2

## EXPERIMENTAL PROCEDURE

### 2.1 FIELD LAYOUT

#### 2.1.1 General Description of Field Equipment

The instrumentation and the field layout on this operation were similar to that used on Operation GREENHOUSE except for minor modifications. The direct measurement of the velocity of sound along the base and of the wind velocity parallel to the base was omitted since it was felt that meteorological data taken at the blast hut would provide the necessary information to as great a degree of accuracy with less effort.

A block diagram of the equipment used in measuring the arrival time of the blast wave is shown in Fig. 2.1.

Two types of field pick-ups were used to detect the arrival of the blast wave at the blast station - blast switch and blast microphone or transducer. Both types are described in detail in Paragraph 2.2.1. Two different recording systems, direct and indirect, were used with the blast switches. They are described in Paragraph 2.2.3. Two identical blast transducer recording systems were used for detecting air blast arrival times along each blast line and are described in Paragraph 2.2.4.

In both methods, these pick-ups caused a signal pulse to be sent over a two-conductor shielded cable through input circuits to a magnetic tape recorder. These signals were superimposed on a 10kc timing wave which provided a means of calculating the time of transit of the blast wave between blast stations.

Inasmuch as recording equipment was located within a possible radiation danger area all equipment was designed to operate when activated by time signals supplied from a remote control center. Timing signals were required to turn on filament power and to start the recorders. These were provided by Edgerton, Germeshausen, and Grier (EG&G) from the central control station. A zero time pulse was provided by means of a photocell timing signal (Blue Box).

Location of the station nearest ground zero was selected at a point within a few feet of the anticipated radius of the lip of the crater. The distant station was established at a point where a peak pressure of approximately 3 psi was predicted inasmuch as the inherent error in any velocity measuring increases rapidly below pressures of 3 psi.



[redacted]

A photograph of the blast range for the underground shot, is shown in Fig. 2.2; a front view of the recording equipment mounted in the van trailer is shown in Fig. 2.3, a rear view in Fig. 2.4.

### 2.1.2 Blast Range Layout

The velocity heads were mounted 5 feet above the ground on 3 inch diameter pipe for all shots. All lines were situated radially from ground zero except HE-1, which was offset from a radial line by 3 feet. The blast ranges approximated horizontal planes without any significant obstructions to the travel of the blast wave. Six instrument stations were used on HE-1 while nine stations were used on the other three blast lines.

Blast Range Plots are shown as follows:

| | |
|---|---|
| HE-1 | Fig. 2.5 |
| HE-2 | Fig. 2.6 |
| Surface | Fig. 2.7 |
| Underground | Fig. 2.8 |

## 2.2 DETAILED DESCRIPTION OF FIELD EQUIPMENT

### 2.2.1 Microphone and Blast Switch Equipment

The individual field pick-up station consisted of a velocity head mounted on a section of 3 inch pipe cemented into a two foot cube of concrete. The cast aluminum housing called the velocity head, which contained one blast switch and two microphones is illustrated in Fig. 2.9. The velocity head provided the means for mounting the switch and microphones and offered protection against excessive radiation and adverse weather conditions.

The blast microphones, located on each side of the velocity head, were placed side-on to the direction of the blast wave. The bearing surface or paddle of the blast switch was placed face-on to the direction of propagation of the blast wave. The arm of each blast switch protruded through the side of the velocity head through a machined slot. A small permanent magnet mounted on the outside of the housing prevented strong winds from closing the switch prematurely.

The microphones used were diaphragm type headphone receivers, type ANBH-1. The output voltage generated over a range of pressures from 2 psi and 16 psi was between 10 and 23 volts, respectively. The dc resistance was 100 ohms, and the maximum response time for a pressure of 2 psi was approximately 50 microseconds. In series with each microphone was a 1N58 diode to minimize feedback of signals across the phones and in conjunction with a resistance network to decrease any oscillatory effects. One microphone at each station was connected into a parallel circuit which fet into a single recording channel. Since two microphones were used in each velocity head, two separate recording channels were required.

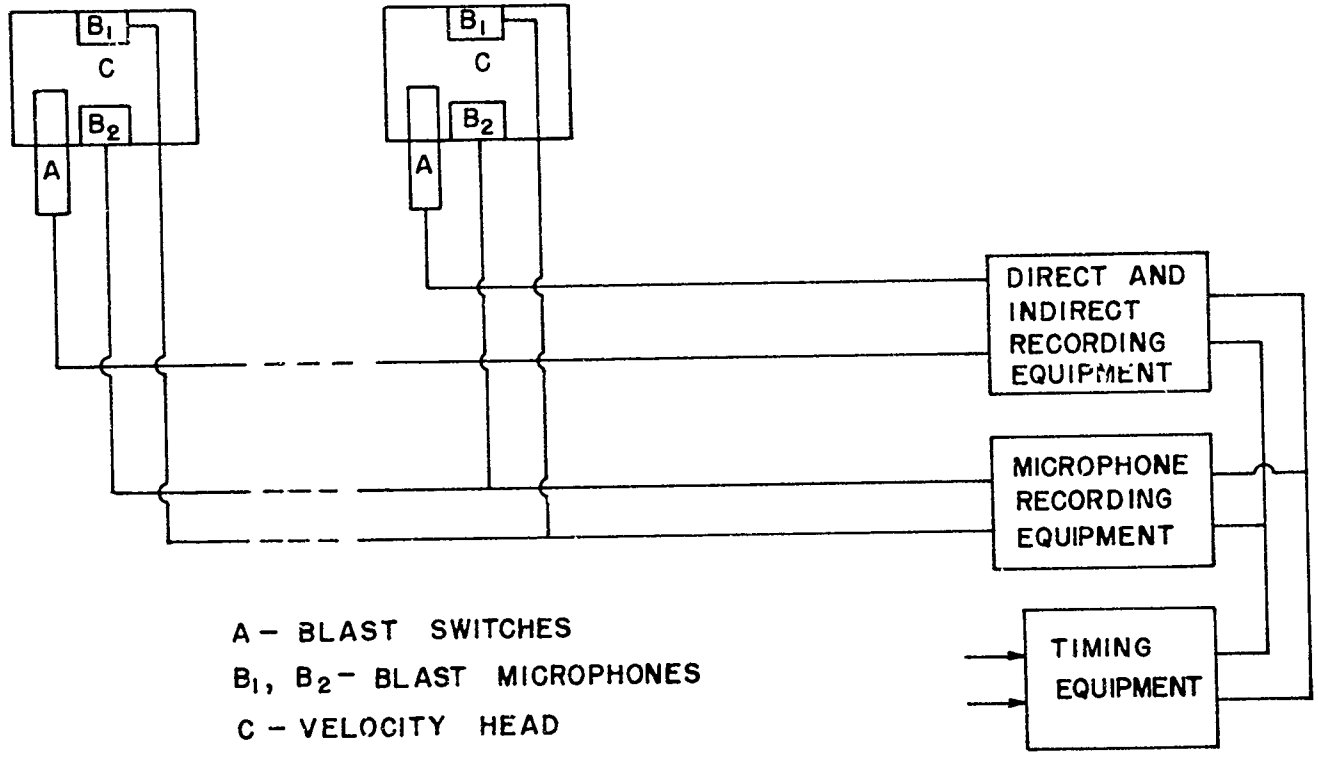


Fig. 2.1 Block Diagram Blast Arrival Time Measuring Equipment

Fig. 2.2 Photograph of Blast Range for Underground Shot

Fig. 2.3 Front View of Recording Equipment in Van

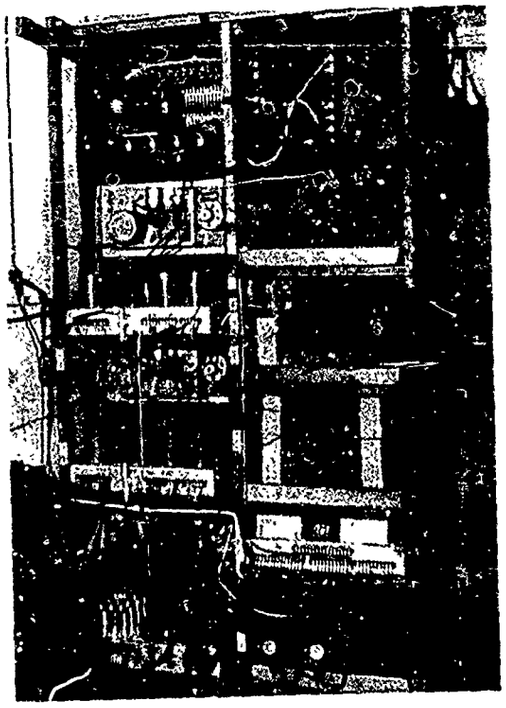

Fig. 2.4 Rear View of Recording Equipment in Van

[redacted]

PROJECT 1.2a-1

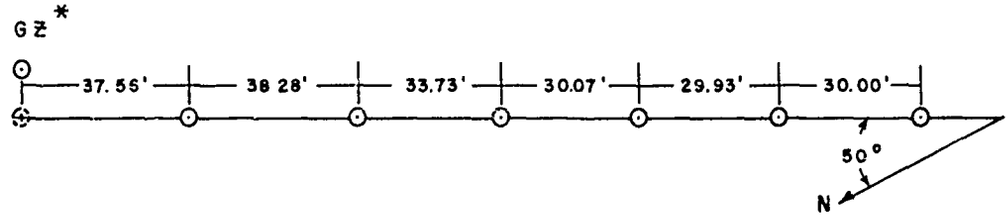


* GROUND ZERO (GZ) OFFSET 3'

Fig. 2.5 Blast Range Layout for Shot HE-1

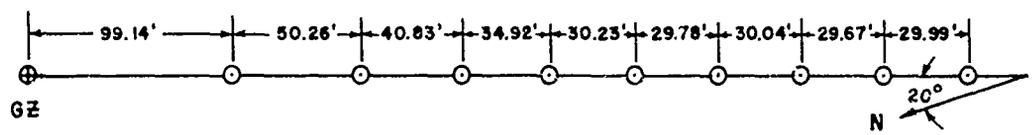


Fig. 2.6 Blast Range Layout for Shot HE-2

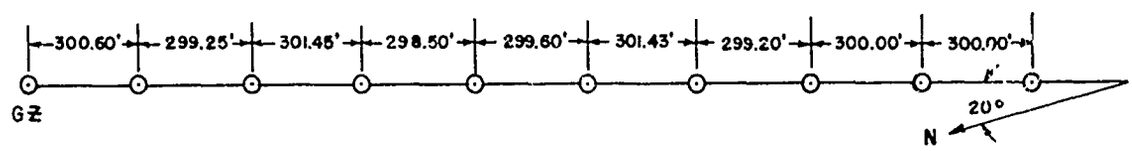


Fig. 2.7 Blast Range Layout for Surface Shot

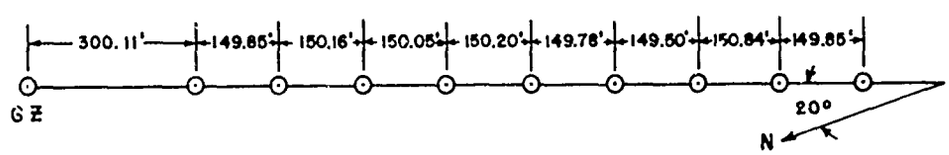


Fig. 2.8 Blast Range Layout for Underground Shot



[redacted]

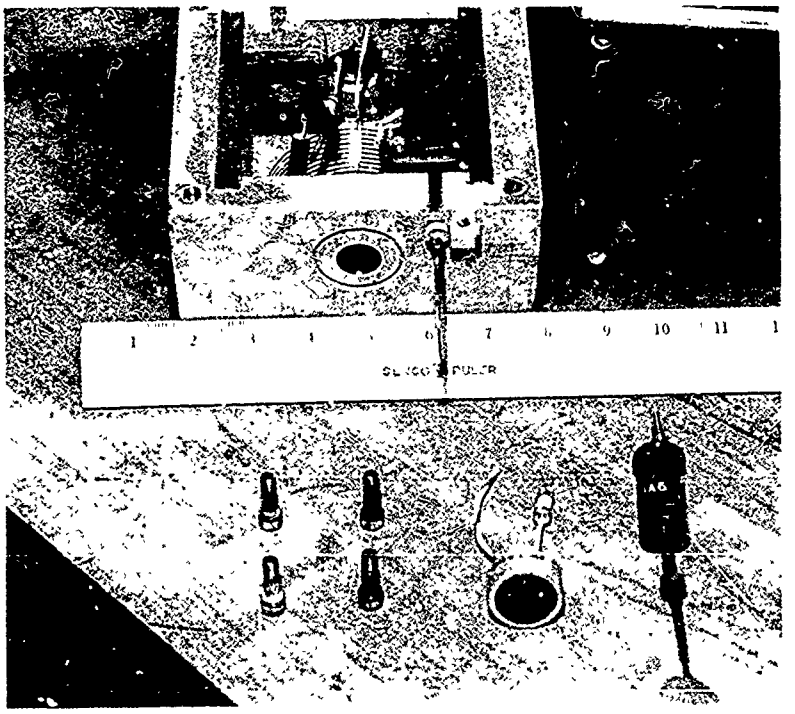

Fig. 2.9 Photograph of Velocity Head

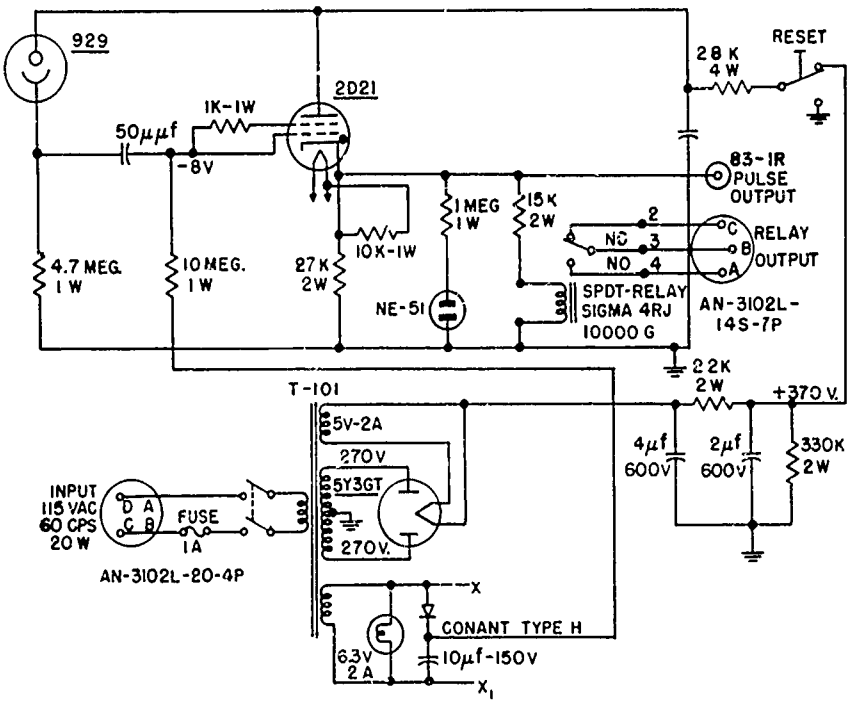


Fig. 2.10 Circuit Diagram of Blue Box Fiducial Marker



[redacted]

[redacted]



General Electric vacuum switches, type FA-6, were used for blast switches. Each switch was connected by a two conductor shielded cable to an individual resistance-capacitance (RC) network at the recording van. The blast wave closed the switch contact, which discharged a condenser and caused a signal pip to be superimposed on the 10 kc timing wave.

### 2.2.2 Zero Time Equipment

In order to provide a common fiducial mark on each channel, a zero time pulse was provided. For the two HE shots, a sensitive relay, operated by the pulse which fired the blasting cap was used to fire the thyratrons which provided "zero" time pulses to the recorders. For the Surface and Underground Shots, a photocell was provided which fired the thyratrons to provide zero pulses to the recorders. The photocell unit (Blue Box) was provided by Edgerton, Germeshausen, and Grier. A circuit diagram of the Blue Box is shown in Fig. 2.10, and a photograph is shown in Fig. 2.11 of a "zero" time pulse.

### 2.2.3 Direct and Indirect Recording Equipment

The direct and indirect recording equipment is essentially two parallel recording channels for the same pulse. A block diagram of the direct and indirect recording equipment is shown in Fig. 2.12. A circuit diagram is shown in Fig. 2.13. A single blast switch is connected to an individual cable which terminates in a resistance-capacitance network. A pulse from this network is superimposed on a 10,000 cycle per second timing signal by means of a resistance bridge. The sensitive element of the tape recorder was inserted in one leg of the bridge and the signal so recorded was called a direct recording. Suitable decoupling was provided so that a single bridge was used with as many as sixteen resistance-capacitance networks.

The indirect recording system is basically identical to the direct system differing only in the addition of a thyratron stage between the RC network and the mixer bridge. A single 10,000 cycle per second oscillator provides timing pulses for both recording channels. The thyratrons insure a single pulse from each switch since one fired, they must be reset manually. They also permit a form of coding by use of alternate positive and negative signals from the thyratrons connected to blast switches at adjacent stations. The signals recorded on the indirect recording channel are cleaner and more easily interpreted than the direct recorded signals, but the possibility of failure to record data by this means is somewhat greater.

[redacted]

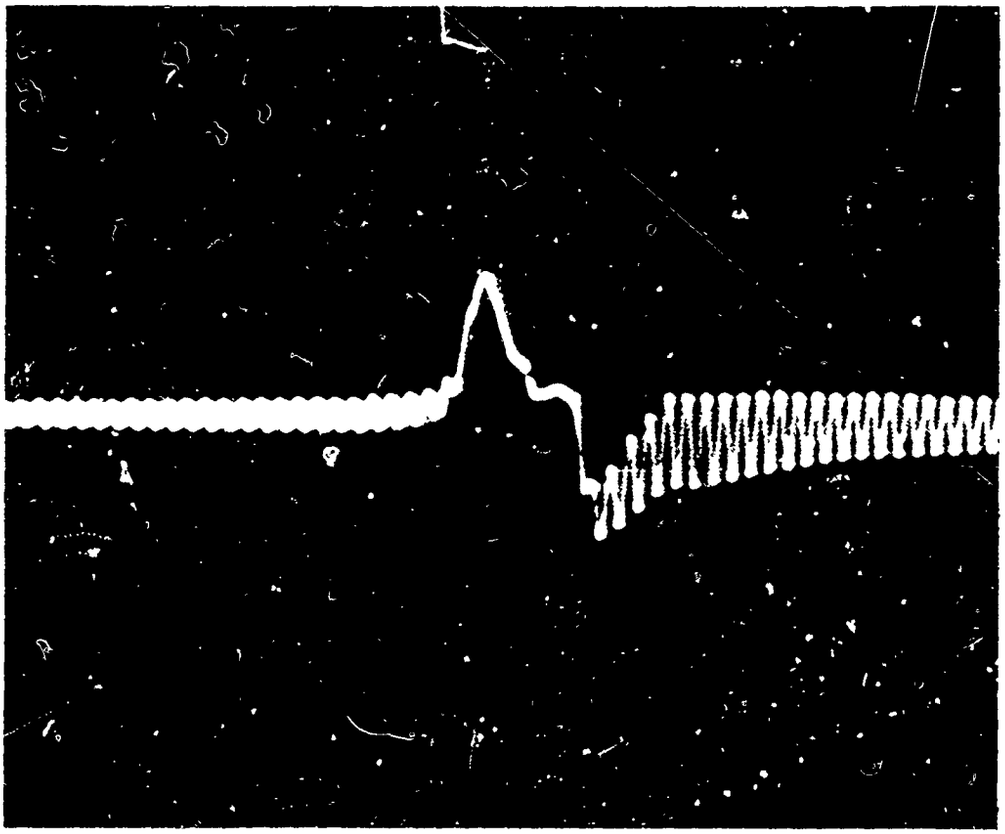

Fig. 2.11 Photograph of Blue Box Fiducial Mark

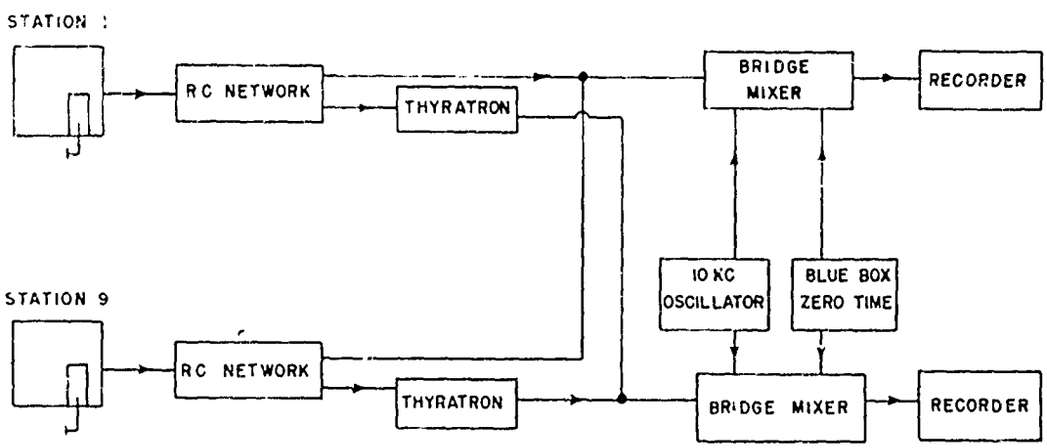


Fig. 2.12 Block Diagram of Direct and Indirect Recording System

[redacted]



The thyratrons in the indirect recording channels were not connected to a plate battery until after the initial radiation had passed. This was accomplished by means of a thyratron which caused a delay fuse to blow. The fuse is a Western Electric 35J fuse which is rated at one-half ampere and has a delay time, as used in this circuit, of two to three milliseconds. When the fuse blows, a spring operated arm moves to connect the plate voltage to the thyratrons. The initiating thyratron is connected to the zero time pulse for operation.

Two thyratrons are also provided to furnish zero time pulses to the direct recording and indirect recording tapes. These thyratrons are activated by the zero time pulse from the Blue Box.

2.2.4 Microphone Recording Equipment

An alternate method of determining the velocity of the air blast wave was obtained through use of the blast microphones. To record the signal from the microphones a two channel system consisting of two amplifiers, two bridge mixers and one 10 KC oscillator was provided. A. block diagram of the complete microphone recording system is shown in Fig. 2.14, a circuit diagram in Fig. 2.15.

One microphone in each blast station was connected to the same two-conductor shielded cable in parallel, which was connected to the input of the amplifier located in the recording trailer. The output of the amplifier was fed directly through the bridge mixer, where it was superimposed on the 10 KC timing wave, then to the recording channel of the tape recorder. A thyratron was provided to furnish a zero time pulse to the recorder when activated by the Blue Box. Two such microphone recording channels were used.

2.2.5 Remote Control Equipment

Due to possible radiation hazards from nuclear shots, all instrumentation was operated unattended. Remote initiation circuits were, therefore, required to turn on the filament power in the electronic circuits of the blast arrival time equipment, and to turn on the tape recorders. These signals were obtained from relays, located in the recording vans, which were supplied, serviced and operated by the EG&G Project. One relay turned on all vacuum tube filaments at -15 minutes, and a second relay turned on the tape recorders at -1 minute.

Four pole double-throw magnetic latch-down relays, activated by the EG&G signals were used to insure positive opeation. In order to release the relays, a manually operated two pole double-throw switch was used to deactivate the latching coil and to activate the unlatching coil. These circuits were self-locking so that once a time signal was received the relays would remain latched until manually reset.



[redacted]

[redacted]

PROJECT 1.2a-1

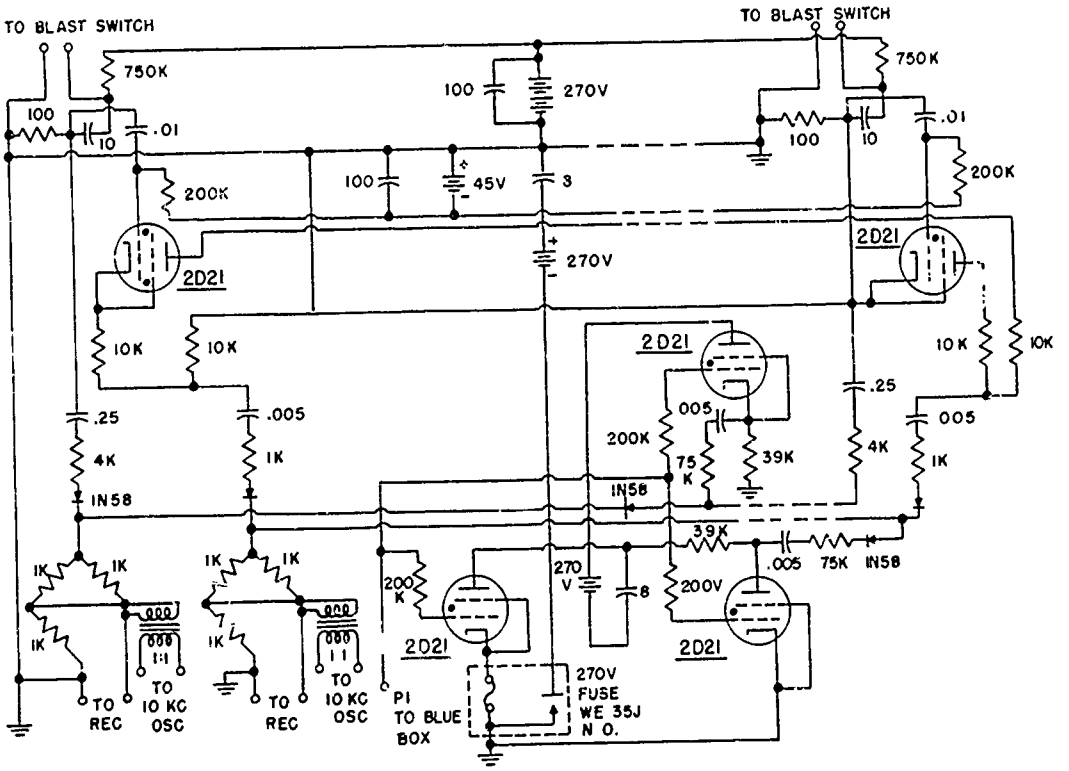


Fig. 2.13 Circuit Diagram of Direct and Indirect Recording System

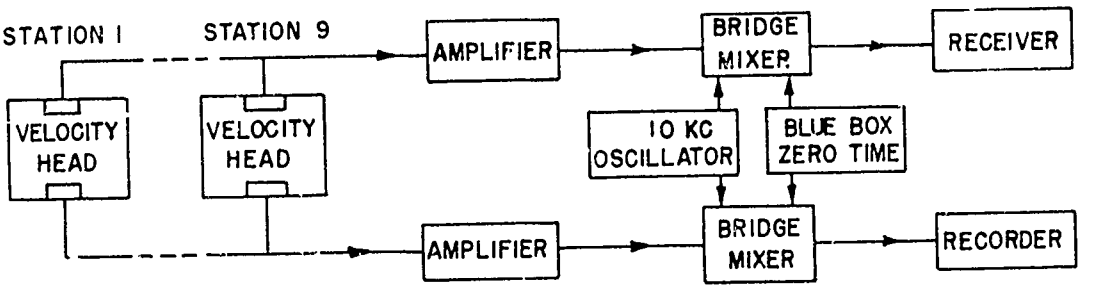


Fig. 2.14 Block Diagram of Blast Transducer Recording System



[redacted]

### 2.2.6 Meteorological Equipment

Meteorological equipment was provided to record the original conditions of the air through which the blast wave would be propagated.

Temperature was recorded to within 1°C by means of a Bendix-Friez Thermograph which was checked against a mercury thermometer.

Atmospheric pressure was recorded by means of a Short and Mason Barograph which was calibrated against a mercury barometer corrected for temperature and accurate to ± 0.01 inches of mercury.

The relative humidity was recorded by means of a Short and Mason Hydrograph which was checked against a sling psychrometer within ± 5 per cent.

The wind speed and direction were recorded by means of a Bendix-Aerovane and an Easterline-Angus recorder. The wind turns a propellor which turns the armature of a generator. The voltage obtained is proportional to the wind velocity. No adequate means of checking this wind velocity was provided, so the manufacturer's values as read from the chart, were used after due care had been taken in zeroing the meter.

The wind direction was recorded by means of a pair of Selsyns. The drive motor was connected to the wind vane and the slave motor actuated a recording pen. Orientation of the wind vane with north was accomplished by means of a compass with alidade after due consideration of the magnetic declination of that particular location. It is thought that the wind direction is accurate to ± 5°.

## 2.3 READING OF RECORDS

### 2.3.1 Procedure

The recordings obtained on the magnetic tape recorders were played back through an amplifier to the horizontal deflection plates of a DuMont 304H Oscilloscope. A General Radio Oscillographic Recording Camera was used to photograph the cathode ray tube of the oscilloscope. Since both sweep and vertical gain of the oscilloscope was turned off, an amplitude change when the record was played back resulted in a horizontal displacement of the bright spot on the cathode ray tube face. The film motion in the camera was at right angles to this horizontal deflection so the resulting film shows a continuous trace of the light spot similar to those shown in Fig. 2.16. The regular waves seen are the 10 kc timing cycles and the irregular pips are those recorded when a blast wave arrived at a blast switch or microphone.

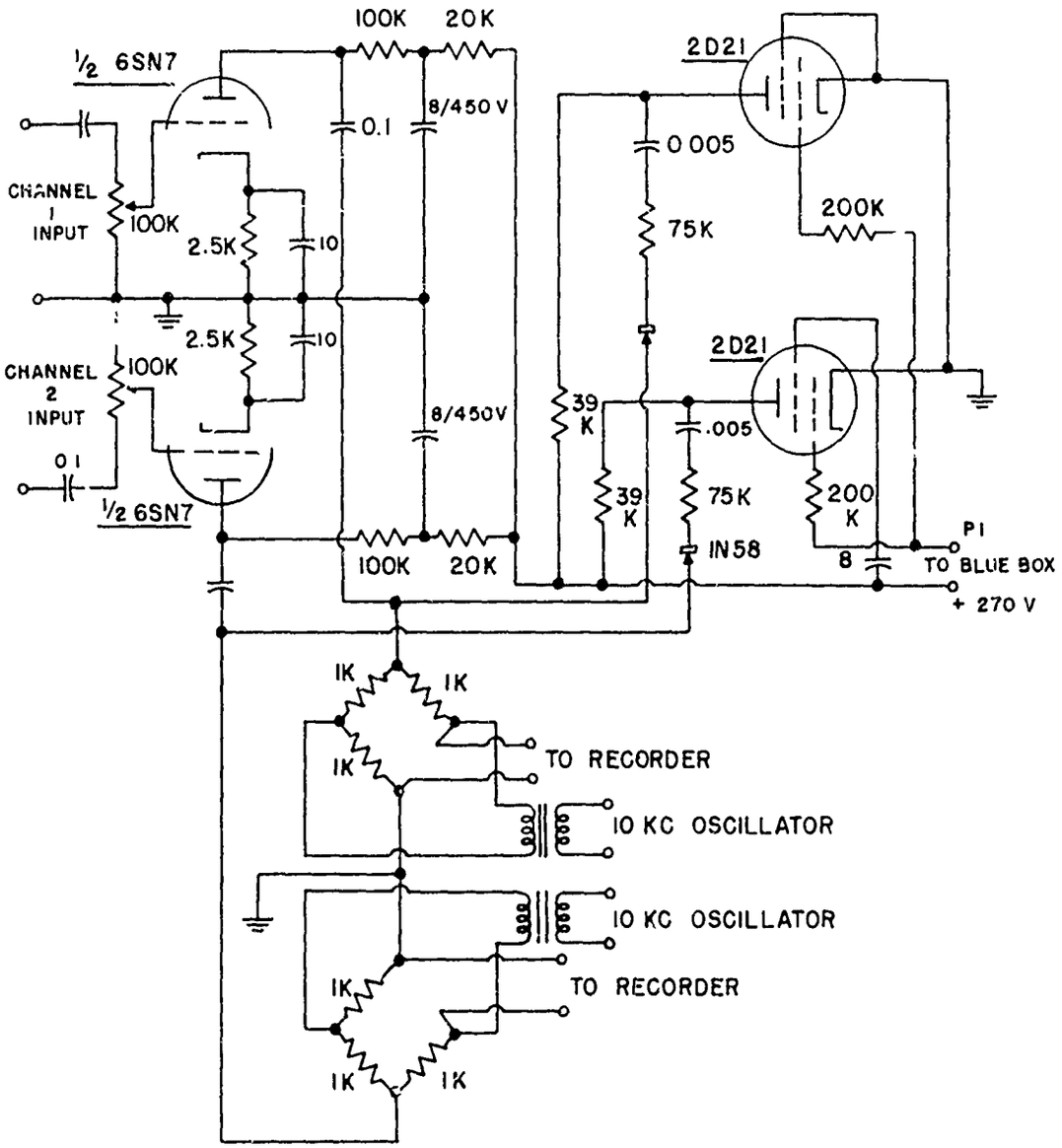


Fig. 2.15 Circuit Diagram of Blast Transducer Recording System

These 35 millimeter films were developed and then enlarged by projection methods to enable an accurate count to be made from one pip to the next.

The records can be read to the closest cycle with ease. The oscillator was considered accurate to one-tenth cycle. The timing pips and the signal pips were recorded simultaneously by the same recorder head on a single tape. Therefore, neither variation in tape speed in recording or playback nor variation in film speed on photographing can effect the accuracy of the measurements as long as the film has sufficient resolving power to show each timing cycle when projected for counting.

The reading of film by this method is laborious but the accuracy obtainable is dependent only on the accuracy with which one can count the individual cycle.

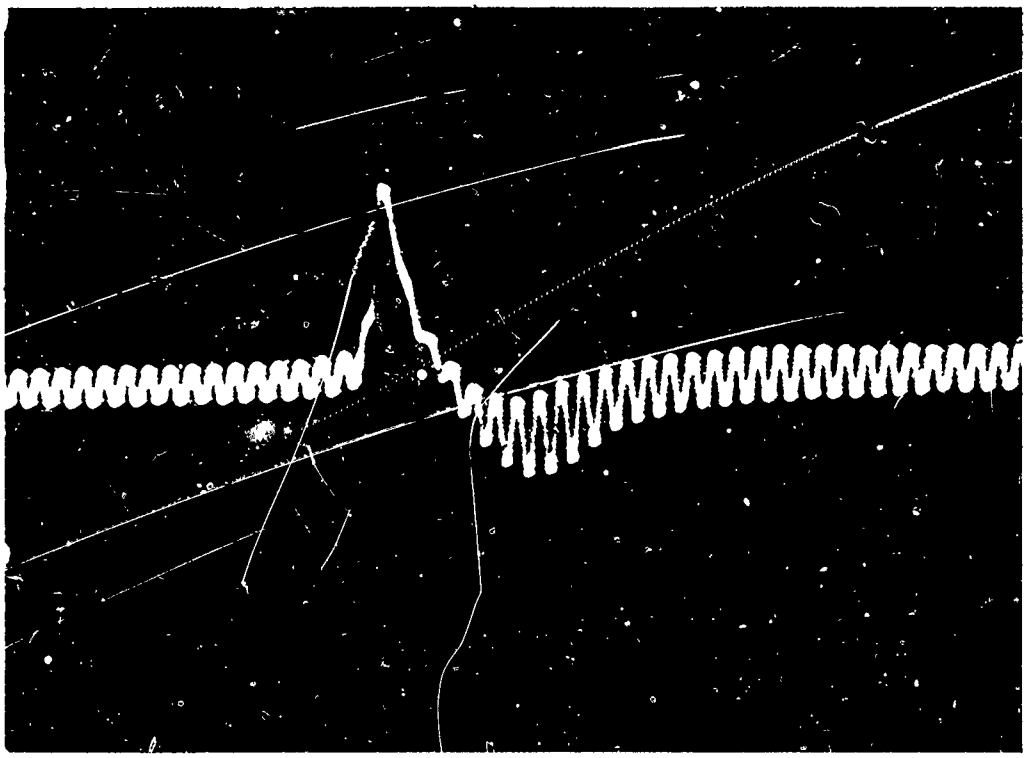

Fig. 2.16 Photograph of Typical Blast Wave Record on 35mm Film

[redacted]

# CHAPTER 3

## RESULTS AND DISCUSSION

### 3.1 HE-1 SHOT

#### 3.1.1 Peak Pressure vs Distance

The peak air blast overpressure vs reduced distance ($\lambda$) values as shown on Fig. 3.1 and Table 3.1 were obtained using the procedure outlined in Section 1.3. The delay corrections, as given in Section 1.3.7, for blast switch closure time were applied in the following manner. The pressure at a particular velocity station was found from the pressure-distance curve plotted from the transducer records. Station distances and pressures are listed in Table 3.2. These pressures were then used to find the delay in the switch closure from Fig. 1.1. The difference in the delay between two stations on the $\Delta$-delay is listed in Table 3.2. The $\Delta$-delay is then subtracted from the transit time of the shock wave over that interval and the pressure is re-determined from the corrected velocity. Corrected pressures are listed in Table 3.3. On Fig. 3.1 are plotted the values from the transducer record listed in Table 3.1 and the Direct and Indirect corrected values from Table 3.3.

A wind velocity component along the blast line of 11 ft/sec was inserted in the calculations. It was in a direction away from ground zero and, therefore, was subtracted from the shock velocity. The effect of the measured relative humidity on sound velocity amounted to less than 1 ft/sec and changed the value of $\lambda$ less than 0.001. Therefore, corrections for relative humidity were neglected in the computations.

The various pick-up and recording devices as described in Section 2.2 produced data points which were in very close agreement. A single curve through all points can be drawn.

The point between consecutive stations, at which the instantaneous velocity is equal to the average velocity, was found using the method of correction discussed in Section 1.3.2.

These distances were then reduced to unit charge weight by dividing by the cube root of the charge weight and listed in Table 3.1 and Table 3.3 as the corrected reduced distances($\lambda$).

The time of arrival of the shock wave at the first station was not measured due to technical difficulties in supplying a zero time signal. Therefore, no arrival time curve is presented for this shot.



[redacted]

TABLE 3.1

HE-1 PEAK OVERPRESSURE VS λ

| Interval | L (ft) | t (sec) | $U = \frac{L}{t}$ | $U_w$ wind corr. | $P_s$ (psi) | $R_m$ (ft) | $\lambda = \frac{R_m}{W^{1/3}}$ | Corrected λ |
|---|---|---|---|---|---|---|---|---|
| Direct | | | | | | | | |
| 1 to 2 | 38.28 | 0.0243 | 1575.3 | 1564.3 | 12.83 | 56.77 | 4.15 | |
| 2 to 3 | 33.73 | 0.02345 | 1438.4 | 1427.4 | 8.19 | 92.85 | 6.77 | |
| 3 to 4 | 30.07 | 0.0223 | 1348.4 | 1337.4 | 5.37 | 124.73 | 9.09 | |
| 4 to 5 | 29.93 | 0.0228 | 1312.7 | 1301.7 | 4.30 | 154.70 | 11.28 | |
| 5 to 6 | 30.00 | 0.0240 | 1250.0 | 1239.0 | 2.50 | 184.66 | 13.48 | |
| Indirect | | | | | | | | |
| 1 to 2 | 38.28 | 0.0243 | 1575.3 | 1564.3 | 12.83 | 56.77 | 4.15 | |
| 2 to 3 | 33.73 | 0.02345 | 1438.4 | 1427.4 | 8.19 | 92.85 | 6.77 | |
| 3 to 4 | 30.07 | 0.0223 | 1348.4 | 1337.4 | 5.37 | 124.73 | 9.09 | |
| 4 to 5 | 29.93 | 0.0228 | 1312.7 | 1301.7 | 4.30 | 154.70 | 11.28 | |
| 5 to 6 | 30.00 | 0.0240 | 1250.0 | 1239.0 | 2.50 | 184.66 | 13.48 | |
| Transducer | | | | | | | | |
| 1 to 2 | 38.28 | 0.0243 | 1575.3 | 1564.3 | 12.83 | 56.77 | 4.15 | 3.89 |
| 2 to 3 | 33.73 | 0.0234 | 1441.4 | 1430.4 | 8.29 | 92.85 | 6.77 | 6.69 |
| 3 to 4 | 30.07 | 0.0220 | 1366.8 | 1355.8 | 5.93 | 124.73 | 9.09 | 9.06 |
| 4 to 5 | 29.93 | 0.0458 | 1308.5 | 1297.5 | 4.18 | 169.70 | 12.39 | 12.34 |
| 5 to 6 | 30.00 | | | | | | | |

[redacted]

TABLE 3.2

HE-1 CORRECTION FOR SWITCH DELAY

| Station Distance (ft) | Reduced Distance ($\lambda$) | $P_s$ at Station (psi) | Switch Delay (Msec.) | $\Delta$-Delay (msec) |
|---|---|---|---|---|
| 37.56 | 2.74 | 21.0 | .72 | .15 |
| 75.97 | 5.55 | 10.0 | .87 | .15 |
| 109.70 | 8.01 | 6.8 | 1.02 | .13 |
| 139.77 | 10.20 | 5.3 | 1.15 | .25 |
| 169.70 | 12.39 | 4.1 | 1.40 | .50 |
| 199.70 | 14.58 | 3.2 | 1.90 | |

TABLE 3.3

HE-1 SWITCH CORRECTION APPLIED

| Interval D & I | L (ft) | t (sec) | t-$\Delta$delay | $U = \frac{L}{t - \Delta \text{ delay}}$ | $U_w$ Wind corr. | $P_s$ (psi) | $R_m$ (ft) | $\lambda = \frac{R_m}{w^{1/3}}$ | Corrected $\lambda$ |
|---|---|---|---|---|---|---|---|---|---|
| 1 to 2 | 38.28 | 0.02430 | 0.02415 | 1585.1 | 1574.1 | 13.18 | 56.77 | 4.15 | 3.89 |
| 2 to 3 | 33.73 | 0.02345 | 0.02330 | 1447.6 | 1436.6 | 8.49 | 92.85 | 6.77 | 6.69 |
| 3 to 4 | 30.07 | 0.02230 | 0.02217 | 1356.3 | 1345.3 | 5.61 | 124.73 | 9.09 | 9.06 |
| 4 to 5 | 29.93 | 0.02280 | 0.02260 | 1324.3 | 1313.3 | 4.65 | 154.70 | 11.28 | 11.26 |
| 5 to 6 | 30.00 | 0.02400 | 0.02350 | 1276.6 | 1265.5 | 3.25 | 184.60 | 13.48 | 13.48 |

[redacted]

[redacted]



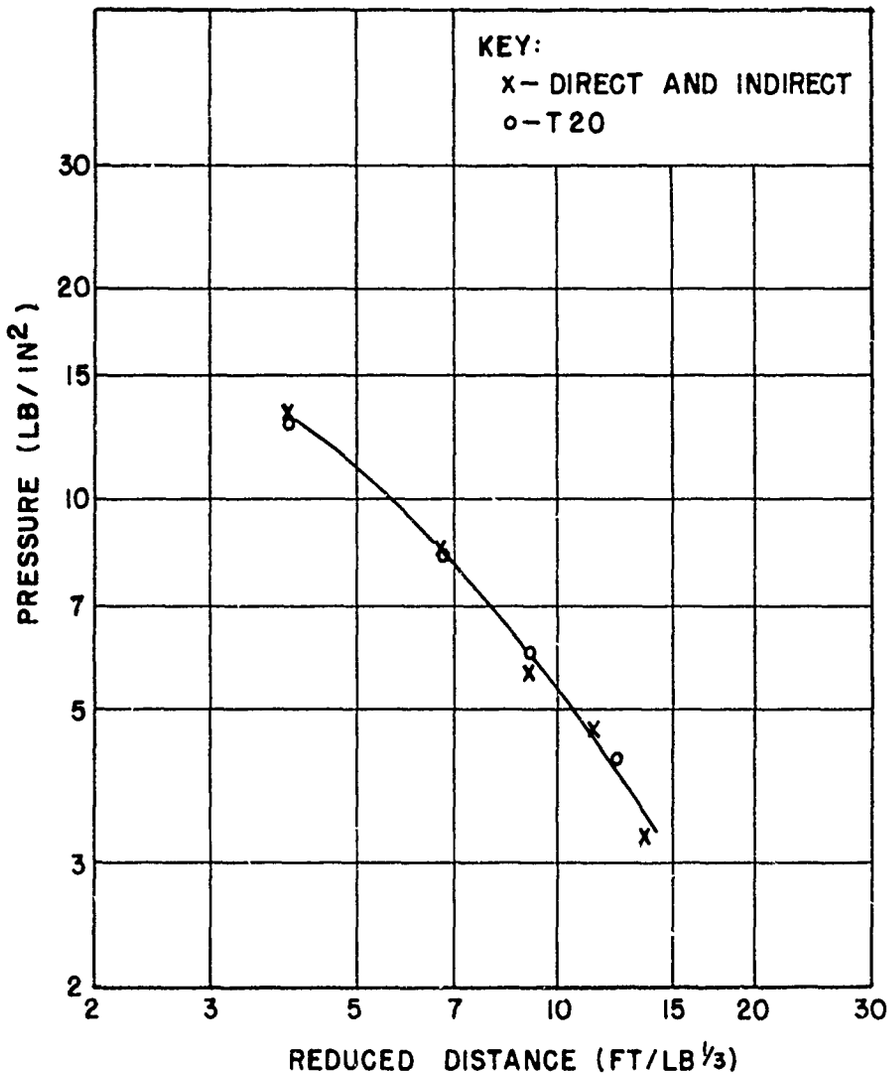


Fig. 3.1 Peak Overpressure vs Reduced Distance, HE-1 Shot

[redacted]

### 3.1.2 Velocity of Sound

The sound velocity was obtained from the meteorological data and the equations indicated in the basic theory, Section 1.3.4. No difficulty was encountered in reading the records from this equipment and the accuracy of all readings was believed to be well within the basic errors of the instruments themselves. The velocity of sound was calculated to be 1147 ft/sec.

### 3.1.3 Meteorological Data

| | |
|---|---|
| Wind velocity | 7.56 MPH N 45°E |
| Blast Line | N 50°E |
| Wind component along blast line | 11 ft/sec |
| Relative humidity | 12% |
| Barometric pressure | 12.77 lbs/in$^2$ |
| Temperature | 86.5°F = 30.28°C |
| $\gamma$ | 1.400 |

## 3.2 HE-2 SHOT

### 3.2.1 Peak Pressure vs Distance

The procedure followed in determining peak air blast pressure vs reduced distance on the HE-2 shot differed from the HE-1 method in only one respect. The wind velocity was less than 2 MPH so the wind component along the blast line was considered negligible. The results obtained using the blast switches were nearly identical to those obtained using earphones. The discrepancy lay in the delay to which the blast switches are subject. This delay was corrected using the method previously described. The interval correction, Section 1.3.2, was applied for determining the point at which the average velocity equaled the instantaneous velocity.

The results are listed in Table 3.4 and the blast switch delay corrections are determined and listed in Table 3.5. These corrections are applied to the Direct and Indirect transit time values and corrected pressures are listed in Table 3.6. The values from the transducer records in Table 3.4 and the corrected values for the Direct and Indirect records as shown in Table 3.6 are plotted on Fig. 3.2.

No zero time signal was available, hence, no air bl[redacted]al time at the first station was recorded.

### 3.2.2 Velocity of Sound

The velocity of sound obtained using the procedure outlined in Section 1.3.4 was found to be 1145 ft/sec. The humidity effected a change of less than one foot per second and was neglected in the computations. The actual value of $\gamma$ differed from 1.4 by less than 0.001 so that 1.4 was used in the calculations.

### 3.2.3 Meteorological Data

| | |
|---|---|
| Wind Velocity | 2 MPH N 196°E |
| Blast Line | N 20°E |
| Wind Component | Neglected in calculations |
| Relative Humidity | 12% |
| Barometric Pressure | 12.77 lbs/in$^2$ |
| Temperature | 86.5°F = 30.28°C |
| $\gamma$ | 1.400 |

## 3.3 SURFACE SHOT

### 3.3.1 Peak Pressure vs Distance

The peak air blast overpressure were determined by the Rankine-Hugoniot formula as stated in Section 1.3.1. Corrections are introduced for wind velocity and relative humidity as related in Section 1.3.5. However, the value of the specific heat ratio $\gamma$ was maintained at 1.400. Although the intervals between stations were comparatively long the blast switch delays were incorporated in the pressure computations. The data obtained from the surface shot is listed in Table 3.7 and the corrections for the blast switch delay are listed in Table 3.8. These corrections were then applied and the corrected pressures are shown in Table 3.9. The values from the transducer records in Table 3.7 and from the Direct records in Table 3.9 are plotted on Fig. 3.4. In no case did the blast switch delay correction exceed 0.004 of the original time between stations.

The pressures vs distance values were first determined using the midpoints between stations (Fig. 3.3). It was found that this curve and a well verified small-charge free-air curve [13] had equal slopes at many different pressure levels. This particular free-air curve was used because it expressed the dependency upon atmospheric pressure, which at the test site was noticeably less than 14.7 lb/sq in. This curve is of the form:

13 Cooney and Sperazza, "Position at Which the Velocity of a Blast Wave Equals the Av[redacted]city over an Interval" BRL Memo Report No. 541.

TABLE 3.4

HE-2 PEAK OVERPRESSURE VS $\gamma$

| Interval | L (ft) | t (sec) | $U = \frac{L}{t}$ | $P_s$ (psi) | $R_m$ (ft) | $\lambda = \frac{R_m}{W^{1/3}}$ | Corrected $\lambda$ |
|---|---|---|---|---|---|---|---|
| Direct | | | | | | | |
| 1 to 2 | 50.26 | 0.0302 | 1664 | 16.62 | 124.27 | 3.63 | |
| 2 to 3 | 40.83 | 0.0258 | 1583 | 13.63 | 169.81 | 4.97 | |
| 3 to 4 | 34.92 | 0.0234 | 1492 | 10.44 | 207.69 | 6.07 | |
| 4 to 5 | 30.23 | 0.0210 | 1440 | 8.71 | 240.27 | 7.03 | |
| 5 to 6 | 29.78 | 0.0216 | 1379 | 6.75 | 270.27 | 7.90 | |
| 6 to 7 | 30.04 | 0.0220 | 1365 | 6.31 | 300.18 | 8.77 | |
| 7 to 8 | 29.67 | 0.0221 | 1343 | 5.63 | 330.03 | 9.65 | |
| 8 to 9 | 29.93 | 0.0231 | 1298 | 4.28 | 359.86 | 10.52 | |
| Indirect | | | | | | | |
| 1 to 2 | 50.26 | 0.0302 | 1664 | 16.62 | 124.27 | 3.63 | |
| 2 to 3 | 40.83 | 0.0258 | 1583 | 13.63 | 169.81 | 4.97 | |
| 3 to 4 | 34.92 | 0.0234 | 1492 | 10.44 | 207.69 | 6.07 | |
| 4 to 5 | 30.23 | 0.0210 | 1440 | 8.71 | 240.27 | 7.03 | |
| 5 to 6 | 29.78 | 0.0216 | 1379 | 6.75 | 270.27 | 7.90 | |
| 6 to 7 | 30.04 | 0.0220 | 1365 | 6.31 | 300.18 | 8.77 | |
| 7 to 8 | 29.67 | 0.0221 | 1343 | 5.63 | 330.03 | 9.65 | |
| 8 to 9 | 29.93 | 0.0230 | 1304 | 4.46 | 359.86 | 10.52 | |
| T - 20 | | | | | | | |
| 1 to 2 | 50.26 | 0.0300 | 1675 | 17.04 | 124.27 | 3.63 | 3.54 |
| 2 to 3 | 40.83 | 0.0256 | 1595 | 14.06 | 169.81 | 4.97 | 4.93 |
| 3 to 4 | 34.92 | 0.0234 | 1492 | 10.44 | 207.69 | 6.07 | 6.05 |
| 4 to 5 | 30.23 | 0.0210 | 1440 | 8.71 | 240.27 | 7.03 | 7.01 |
| 5 to 6 | 29.78 | 0.0212 | 1405 | 7.57 | 270.27 | 7.90 | 7.89 |
| 6 to 7 | 30.04 | 0.0220 | 1365 | 6.31 | 300.18 | 8.77 | 8.77 |
| 7 to 8 | 29.67 | 0.0222 | 1336 | 5.42 | 330.03 | 9.65 | 9.64 |
| 8 to 9 | 29.93 | 0.0227 | 1321 | 4.97 | 359.86 | 10.52 | 10.52 |
| T - 21 | | | | | | | |
| 1 to 2 | 50.26 | 0.0300 | 1675 | 17.04 | 124.27 | 3.63 | 3.54 |
| 2 to 3 | 40.83 | 0.0257 | 1576 | 13.84 | 169.81 | 4.97 | 4.93 |
| 3 to 4 | 34.92 | 0.0235 | 1486 | 10.24 | 207.69 | 6.07 | 6.05 |
| 4 to 5 | 30.23 | 0.0209 | 1433 | 8.90 | 240.27 | 7.03 | 7.01 |
| 5 to 6 | 29.78 | 0.0214 | 1392 | 7.16 | 270.27 | 7.90 | 7.89 |
| 6 to 7 | 30.04 | 0.0219 | 1372 | 6.53 | 300.18 | 8.77 | 8.77 |
| 7 to 8 | 29.67 | 0.0221 | 1343 | 5.63 | 330.03 | 9.65 | 9.64 |
| 8 to 9 | 29.93 | 0.0227 | 1321 | 4.97 | 359.86 | 10.52 | 10.52 |

[redacted]

PROJECT 1.2a-1

TABLE 3.5

HE-2 CORRECTION FOR SWITCH DELAY

| Station Distance (ft) | Reduced Distance ($\lambda$) | $P_s$ at Station (psi) | Switch Delay (Msec.) | $\Delta$ Delay (Msec.) |
|---|---|---|---|---|
| 99.14 | 2.90 | 19.0 | .73 | .03 |
| 149.40 | 4.37 | 15.2 | .76 | .06 |
| 190.23 | 5.56 | 11.8 | .82 | .08 |
| 225.15 | 6.58 | 9.2 | .90 | .05 |
| 255.38 | 7.47 | 8.0 | .95 | .07 |
| 285.16 | 8.34 | 6.9 | 1.02 | .06 |
| 315.20 | 9.22 | 6.0 | 1.08 | .09 |
| 344.87 | 10.08 | 5.4 | 1.17 | .10 |
| 374.86 | 10.96 | 4.65 | 1.27 | |

TABLE 3.6

HE-2 SWITCH CORRECTION APPLIED

| Interval | L (ft) | t (sec) | t-$\Delta$ delay (sec) | $U=\frac{L}{t-\Delta delay}$ | $P_s$ (psi) | $R_m$ (ft) | $\lambda=\frac{R_m}{W^{1/3}}$ | Corrected $\lambda$ |
|---|---|---|---|---|---|---|---|---|
| D & I | | | | | | | | |
| 1 to 2 | 50.26 | 0.0302 | 0.03017 | 1665.9 | 16.70 | 124.27 | 3.63 | 3.54 |
| 2 to 3 | 40.83 | 0.0258 | 0.02574 | 1586 | 13.74 | 169.81 | 4.97 | 4.93 |
| 3 to 4 | 34.92 | 0.0234 | 0.02332 | 1497 | 10.61 | 207.69 | 6.07 | 6.05 |
| 4 to 5 | 30.23 | 0.0210 | 0.02095 | 1443 | 8.81 | 240.27 | 7.03 | 7.01 |
| 5 to 6 | 29.78 | 0.0216 | 0.02153 | 1383 | 6.88 | 270.27 | 7.90 | 7.89 |
| 6 to 7 | 30.04 | 0.0220 | 0.02194 | 1369 | 6.44 | 300.18 | 8.77 | 8.77 |
| 7 to 8 | 29.67 | 0.0221 | 0.02201 | 1348 | 5.79 | 330.03 | 9.65 | 9.64 |
| 8 to 9 | 29.93 | 0.02305 | 0.02295 | 1304 | 4.46 | 359.86 | 10.52 | 10.52 |

[redacted]



[redacted]

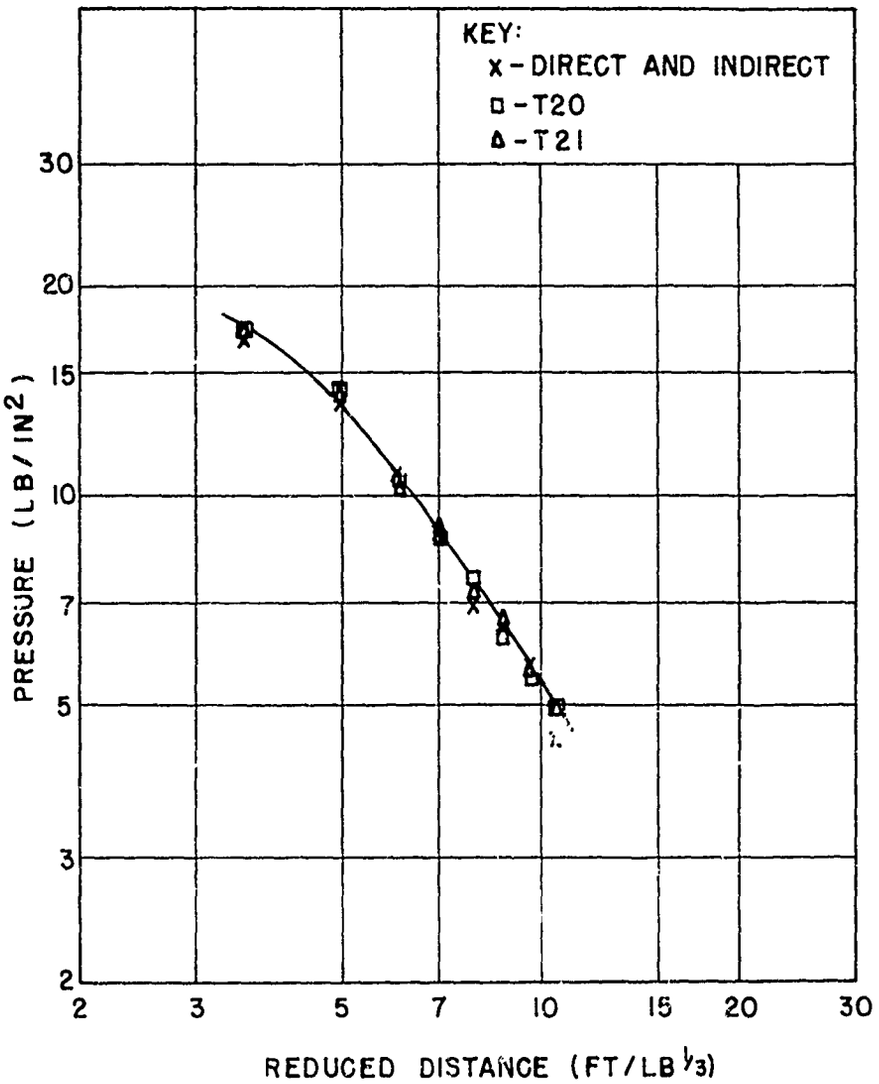


Fig. 3.2 Peak Overpressure vs Reduced Distance, HE-2 Shot

[redacted]



$$P'X = 5.33 + \frac{175}{1 + 0.0383\,X^2} \qquad (3.1)$$

where $\lambda = P_o^{1/3} \dfrac{R}{w^{1/3}}$

$P' = P/P_o$

$P_o$ = atmospheric pressure ($lb/in^2$)

R = distance from the center of charge to the shock front

w = charge weight or equivalent weight

The pressure obtained by the velocity method is considered very reliable at the 10 psi level, the region of greatest general interest. The free-air curve gives a reduced distance of 8.655 at 10 psi overpressure in a region where the atmospheric pressure is 12.78 psi. From Fig. 3.3 a distance of 1075 feet is obtained at 10 psi.

$$\lambda = \frac{R}{w^{1/3}}$$

$$8.655 = 1075/w^{1/3}$$

$$w^{1/3} = 124$$

Thus the equivalent tonnage was assumed to be 1 KT $\pm$ 0.05 KT.

Using this equivalent tonnage the pressure vs reduced distance curve for the surface shot was found to coincide almost exactly with the free-air curve mentioned above (Eq. 3.1) which was derived empirically using small 50/50 pentolite charges (see Fig. 3.4). This was not unexpected since other work done at NOL[15] using small charges indicated that the Mach region disappeared at zero charge weight resulting in a pressure-distance curve which coincided with the normal free-air curve from 5 lbs to 10 lbs.

The corrections for locating the position at which the computed pressure occurred were made in accordance with the pressure-distance formula of Eq. 3.1 as explained in the cited report[14] and not as given in Section 1.3.2. The corrected reduced distance ($\lambda$) values as listed in Tables 3.7 and 3.9 are plotted in Fig. 3.4.

---

14- Ibid. DRL Memo Report No. 541

15- "The behavior of the Shock Wave in Air from Small Underground Explosives" NAVORD 1863



[redacted]

TABLE 3.7

PEAK OVERPRESSURE VS REDUCED DISTANCE, SURFACE SHOT

| Interval | L (ft) | t (sec) | $U = \frac{L}{t}$ | $U_w$ wind corr. | $P_s$ (psi) | $R_m$ (ft) | $\lambda = \frac{R_m}{W^{1/3}}$ | Corrected λ |
|---|---|---|---|---|---|---|---|---|
| Direct | | | | | | | | |
| 0 to 1 | 300.60 | 0.0611 | 4919.8 | 4923.6 | | | | |
| 1 to 2 | 299.25 | 0.1126 | 2657.6 | 2661.4 | 71.33 | 450.23 | 3.57 | |
| 2 to 3 | 301.35 | 0.1635 | 1842.5 | 1846.3 | 26.59 | 750.53 | 5.96 | |
| 3 to 4 | 298.50 | 0.2106 | 1417.3 | 1421.1 | 9.68 | 1050.45 | 8.34 | |
| 4 to 5 | 299.60 | 0.22865 | 1310.3 | 1314.1 | 6.12 | 1349.50 | 10.71 | |
| 5 to 6 | 301.43 | 0.24015 | 1255.1 | 1258.9 | 4.39 | 1650.02 | 13.10 | |
| 6 to 7 | 299.20 | 0.2448 | 1222.2 | 1226.0 | 3.39 | 1950.33 | 15.48 | |
| 7 to 8 | 299.40 | 0.2501 | 1193.8 | 1197.6 | 2.55 | 2249.63 | 17.85 | |
| 8 to 9 | 300.60 | 0.2543 | 1182.1 | 1185.9 | 2.21 | 2549.63 | 20.24 | |
| T - 20 | | | | | | | | |
| 0 to 1 | 300.60 | 0.0611 | 4923.6 | 4923.6 | | | | |
| 1 to 2 | 299.25 | 0.1135 | 2636.5 | 2640.3 | 69.97 | 450.23 | 3.57 | 3.56 |
| 2 to 3 | 301.35 | 0.1624 | 1855.6 | 1859.4 | 27.18 | 750.53 | 5.96 | 5.90 |
| 3 to 4 | 298.50 | 0.2114 | 1412.0 | 1415.8 | 9.50 | 1050.45 | 8.34 | 8.30 |
| 4 to 5 | 299.60 | 0.2271 | 1319.2 | 1323.0 | 6.40 | 1349.50 | 10.71 | 10.69 |
| 5 to 6 | 301.43 | 0.2396 | 1258.0 | 1261.8 | 4.47 | 1650.02 | 13.10 | 13.09 |
| 6 to 7 | 299.20 | 0.2446 | 1223.2 | 1227.0 | 3.42 | 1950.33 | 15.48 | 15.45 |
| 7 to 8 | 299.40 | 0.2501 | 1197.1 | 1200.9 | 2.65 | 2249.63 | 17.85 | 17.82 |
| 8 to 9 | 300.60 | 0.2540 | 1183.4 | 1187.2 | 2.25 | 2549.63 | 20.24 | 20.21 |
| T - 21 | | | | | | | | |
| 0 to 1 | 300.60 | 0.0614 | 4895.8 | 4899.6 | | | | |
| 1 to 2 | 299.25 | 0.1137 | 2631.9 | 2635.7 | 69.67 | 450.23 | 3.57 | 3.56 |
| 2 to 3 | 301.35 | 0.1612 | 1869.4 | 1873.2 | 27.82 | 750.53 | 5.96 | 5.90 |
| 3 to 4 | 298.50 | 0.2095 | 1424.8 | 1428.6 | 9.95 | 1050.45 | 8.34 | 8.30 |
| 4 to 5 | 299.60 | 0.2277 | 1315.8 | 1319.6 | 6.29 | 1349.50 | 10.71 | 10.69 |
| 5 to 6 | 301.43 | 0.2396 | 1258.1 | 1261.9 | 4.48 | 1650.02 | 13.10 | 13.09 |
| 6 to 7 | 299.20 | 0.2446 | 1223.2 | 1227.0 | 3.42 | 1950.33 | 15.48 | 15.45 |
| 7 to 8 | 299.40 | 0.2499 | 1198.1 | 1201.9 | 2.68 | 2249.63 | 17.85 | 17.82 |
| 8 to 9 | 300.60 | 0.2539 | 1183.9 | 1187.7 | 2.27 | 2549.63 | 20.24 | 20.21 |

PROJECT 1.2a-1

TABLE 3.8

CORRECTION FOR SWITCH DELAY, SURFACE SHOT

| Stations Distance (ft) | Reduced Distance (λ) | $P_s$ at Stations (psi) | Switch Delay Msec. | Δ Delay Msec. |
|---|---|---|---|---|
| 300.60 | 2.38 | | | |
| 599.85 | 4.76 | 39.5 | | |
| 901.20 | 7.15 | 14.3 | .78 | |
| 1199.70 | 9.52 | 8.2 | .94 | .16 |
| 1499.30 | 11.90 | 5.2 | 1.15 | .21 |
| 1800.73 | 14.30 | 3.8 | 1.55 | .40 |
| 2099.93 | 16.67 | 3.0 | 2.05 | .50 |
| 2399.33 | 19.04 | 2.5 | 2.80 | .75 |
| 2699.93 | 21.43 | 2.2 | 3.80 | 1.00 |

TABLE 3.9

SWITCH CORRECTION APPLIED, SURFACE SHOT

| Interval | L (ft) | t (sec) | t-Δdelay | $U=\frac{L}{t-\Delta delay}$ | $U_w$ wind corr. | Corrected $P_s$ | Corrected λ |
|---|---|---|---|---|---|---|---|
| S-Direct | | | | | | | |
| 0 to 1 | 300.60 | 0.0611 | 0.0611 | 4919.8 | 4923.6 | | |
| 1 to 2 | 299.25 | 0.1126 | 0.1126 | 2657.6 | 2661.4 | 71.33 | 3.56 |
| 2 to 3 | 301.35 | 0.16355 | 0.16355 | 1842.5 | 1846.3 | 26.59 | 5.90 |
| 3 to 4 | 299.50 | 0.2106 | 0.2104 | 1419. | 1422.8 | 9.74 | 8.30 |
| 4 to 5 | 299.60 | 0.22865 | 0.2284 | 1312. | 1315.8 | 6.17 | 10.69 |
| 5 to 6 | 301.43 | 0.24015 | 0.2397 | 1258. | 1261.8 | 4.47 | 13.09 |
| 6 to 7 | 299.20 | 0.2448 | 0.2443 | 1225. | 1228.8 | 3.47 | 15.45 |
| 7 to 8 | 299.40 | 0.2508 | 0.2501 | 1197. | 1200.8 | 2.65 | 17.82 |
| 8 to 9 | 300.60 | 0.2543 | 0.2533 | 1187. | 1190.8 | 2.36 | 20.21 |

It must be noted that no pressure was calculated for the interval from the charge to the first station since the pressure decay is too rapid in this region to be evaluated by the average velocity method.

The direct recording system yielded the most favorable results of the entire system. The record showed eleven pulses. The first pulse is different in character from all others and is believed to be the zero time pulse. It is possible that the thyratron in the Blue Box fired but only the thyratron which puts a zero pulse on the record fired and not the thyratron which initiates the indirect system. This possibility is advanced since the fuse which is located in the indirect recording circuit did not blow; hence there was no indirect recording.

The second signal or pulse on the record was considered as the one made when the shock wave hit the first station. The third signal pulse that appears on the direct record had an amplitude of the same order of magnitude as the other pulses but does not have all of the same characteristics as the other pulses. Therefore, the fourth signal pip which followed 0.0243 seconds later had been considered as the one caused by the shock wave striking the second station.

To present all data in an unbiased manner, all possibilities were considered. If the third signal pulse is considered correct for arrival time at station No. 2, then the first two pressure levels on Fig. 3.4 would be of different values. The pressure for a ($\lambda$) of 3.57 would be 125.4 lb/sq in. This is much higher than free-air curve estimates which vary from 78 to 85 lb/sq in. Conversely, at $\lambda = 5.90$, the pressure would be 16.5 lb/sq in which is slightly lower than a free-air curve. The reason for the appearance of the third pulse has not been completely explained.

Only one of the blast transducer channels yielded a readable record. This record contained all of the pulses found by the direct system and, in addition, a number of extraneous pulses which complicated the record, rendering it useful only as a back-up system.

### 3.3.2 Time of Arrival of Blast Wave

The first signal appearing on the tape was considered as zero time. The time lapse from the first pip to the second was plotted as the arrival time of the blast wave at the first station. The time between the successive intervals were added and arrival times vs distance are listed in Table 3.10 and plotted in Fig. 3.5.

### 3.3.3 Velocity of Sound

The velocity of sound was determined as outlined in Section 1.3.4. The relative humidity was 42 per cent and the correction as outlined in Section 1.3.5 was applied. This made a difference of [redacted] ft/sec in the velocity of sound which was calculated as [redacted] ft/sec.

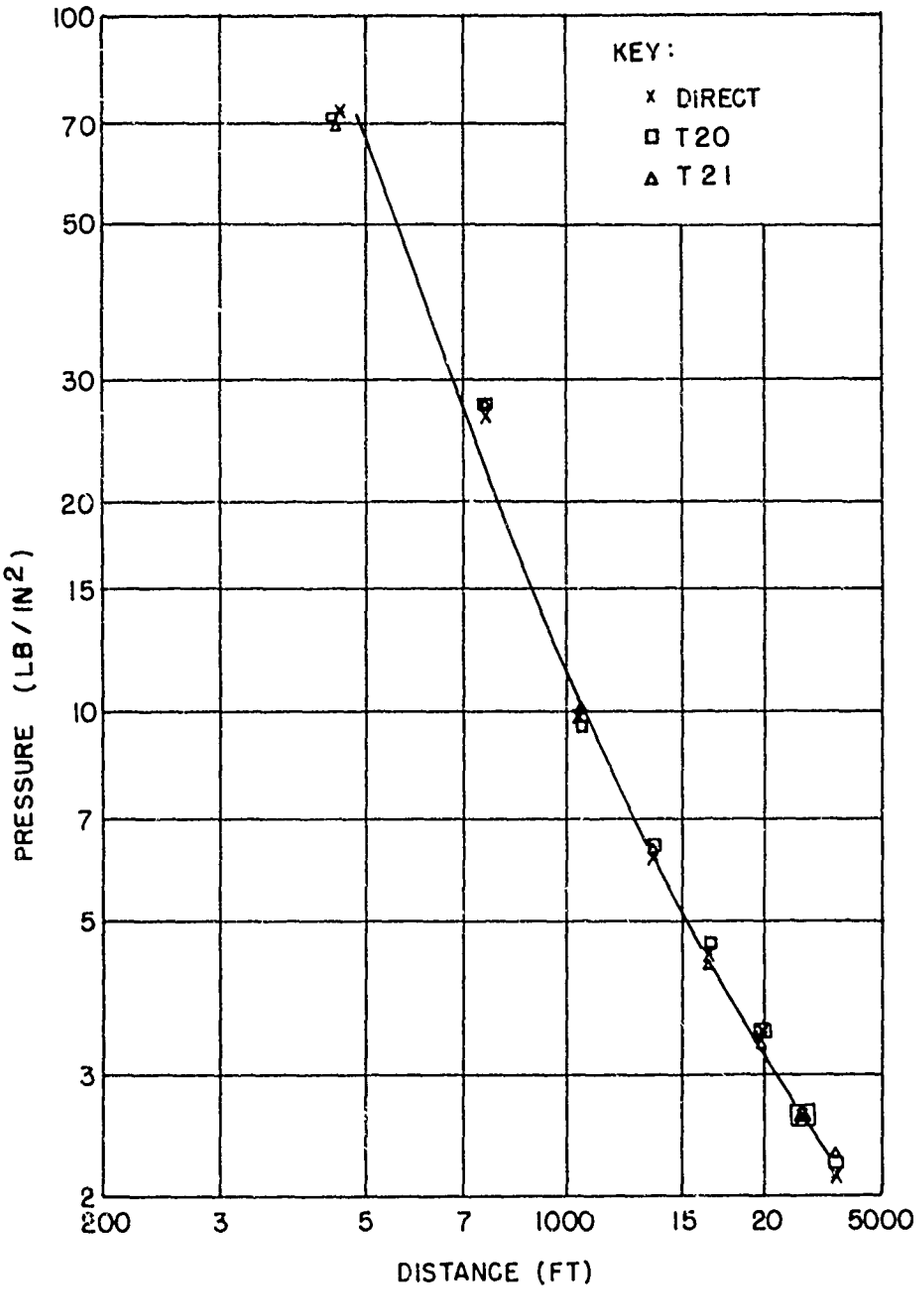


Fig. 3.3 Peak Overpressure vs Distance, Surface Shot

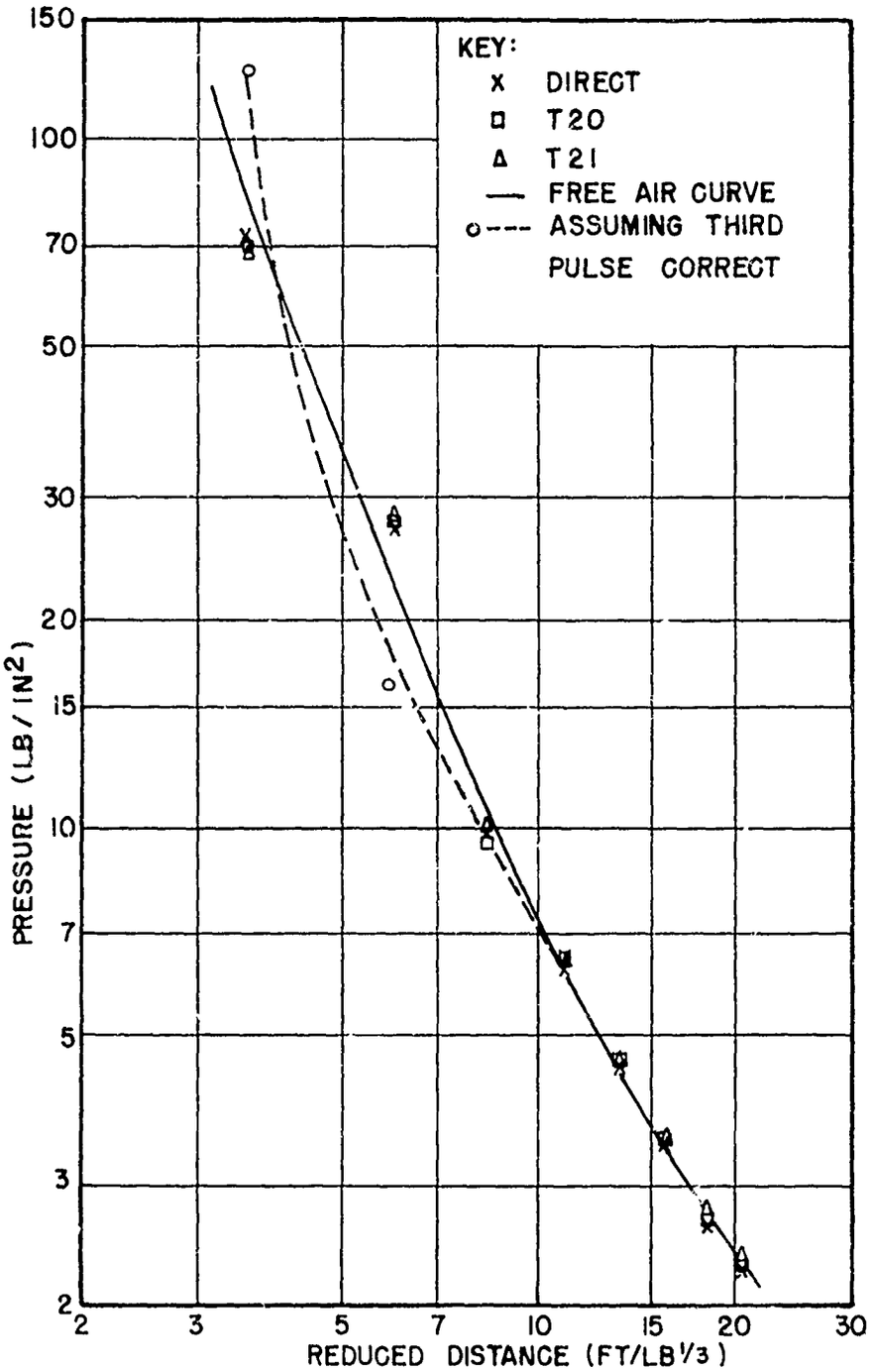


Fig. 3.4 Peak Overpressure vs Reduced Distance, Surface Sh[redacted]

[redacted]

PROJECT 1.2a-1

TABLE 3.10

BLAST ARRIVAL TIME, SURFACE SHOT

| Station | L (ft) | Arrival time blast switch Direct t (sec) | Arrival time transducer T-20 t(sec) | Arrival time Transducer T-21 t (sec) |
|---|---|---|---|---|
| 1 | 300.60 | 0.0611 | 0.0611 | 0.0614 |
| 2 | 599.85 | 0.1737 | 0.1746 | 0.1751 |
| 3 | 901.20 | 0.3372 | 0.3370 | 0.3363 |
| 4 | 1199.70 | 0.5478 | 0.5484 | 0.5458 |
| 5 | 1499.30 | 0.7764 | 0.7755 | 0.7735 |
| 6 | 1800.73 | 1.0165 | 1.0151 | 1.0131 |
| 7 | 2099.93 | 1.2613 | 1.2597 | 1.2577 |
| 8 | 2399.93 | 1.5121 | 1.5098 | 1.5076 |
| 9 | 2699.93 | 1.7664 | 1.7638 | 1.7615 |

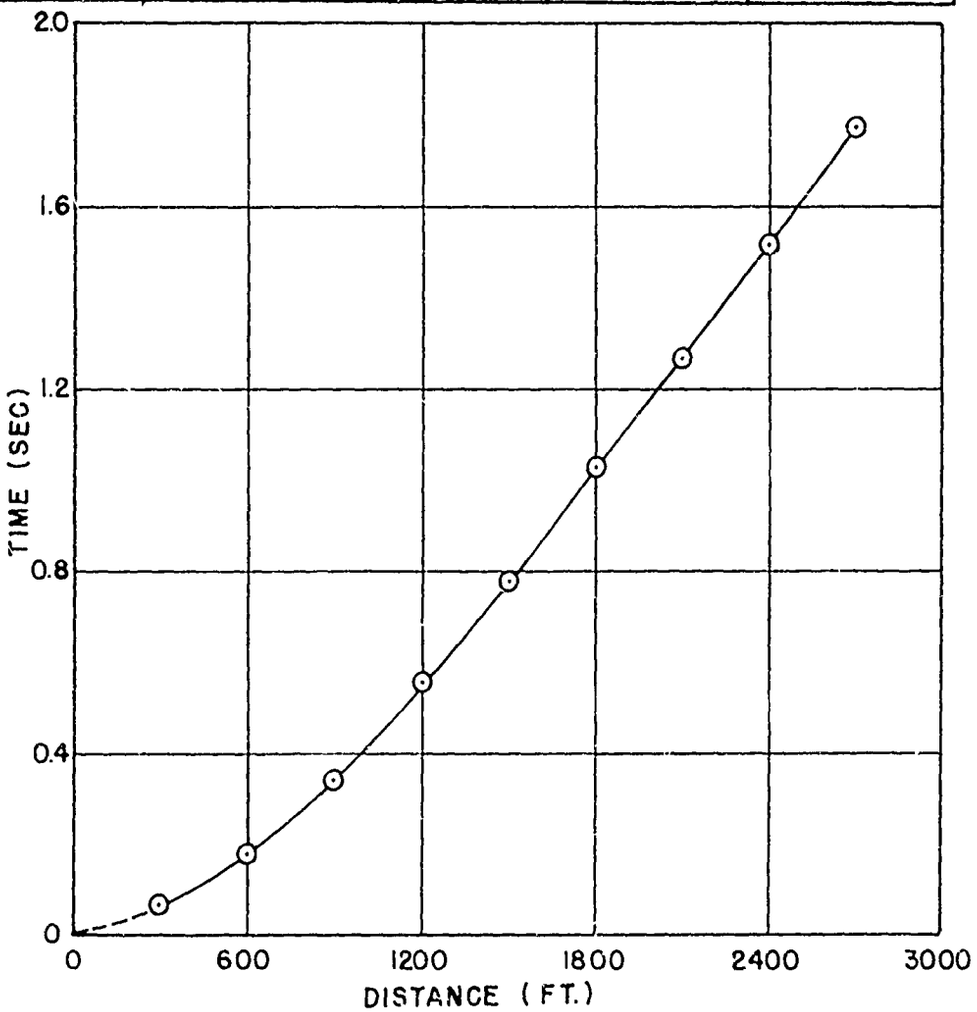


Fig. 3.5 Arrival Time vs Distance, Surface Shot



[redacted]

### 3.3.4 Meteorological Data Surface Shot

| | |
|---|---|
| Wind velocity | 3.5 MPH N 157°E |
| Blast Line | N 20°E |
| Wind component along blast line | + 3.8 ft/sec |
| Temperature | 51°F = 10.6°C |
| Atmospheric pressure | 12.78 lbs/in$^2$ |
| Relative humidity | 42% |
| $\gamma$ | 1.400 |

## 3.4 UNDERGROUND SHOT

### 3.4.1 Peak Pressure vs Distance

Table 3.11 lists data obtained by the two velocity systems employed. The direct blast switch method yielded records whereas the indirect circuit failed to operate due to failure in the thyratron triggering circuit. One blast transducer record contained no 10 kc timing signal but the other blast transducer provided a readable record. The blast transducer record was used only as a back-up for the same reason as on the surface shot as some extraneous pulses were present.

An equivalent tonnage was calculated by the following method. The values of reduced distance which correspond to 10 psi on Shots H-1 and H-2 are 5.5 and 6.4, respectively. The average reduced distance ($\lambda_{av}$) is 5.95. The distance which corresponds to 10 psi on the underground shot is 750 ft. (see Fig. 3.6).

$$\lambda = R/w^{1/3} \qquad 5.95 = 750/w^{1/3} \qquad w^{1/3} = 126$$

Equivalent tonnage = 1 KT $\pm$ .26 KT.

This value of equivalent tonnage yields a curve which agrees with the HE curves fairly well at the other pressures measured (see Fig. 3.8) between $4 \lesssim \lambda \lesssim 14$. For pressure vs reduced distance (see Fig. 3.7).

In contrast to the HE shots which give a curve that is slightly concave downward the underground data exhibits a curve which is slightly concave upward. This difference in curvature is apparently due to a different type venting from nuclear charges.

A wind velocity component of 3.9 ft/sec was added to the average shock velocity. The relative humidity of 45% was used in the sound velocity computations but not in calculation of the specific heat ratio ($\gamma$) where its effect is negligible.

RESTRICTED DATA
ATOMIC ENERGY ACT 1946

TABLE 3.11

PEAK OVERPRESSURE vs REDUCED DISTANCE, UNDERGROUND SHOT

| Interval | L (ft) | t (sec) | $U = \frac{L}{t}$ | $U_w$ wind corr. | $P_s$ (psi) | $R_m$ (ft) | $\lambda = \frac{R_m}{W^{1/3}}$ |
|---|---|---|---|---|---|---|---|
| Direct | | | | | | | |
| 0 to 1 | 300.11 | | | | | | |
| 1 to 2 | 150.16 | 0.0827 | 1811.97 | 1815.9 | 25.72 | 375.04 | 2.98 |
| 2 to 3 | 150.16 | 0.0945 | 1588.99 | 1592.9 | 16.36 | 525.04 | 4.17 |
| 3 to 4 | 150.06 | 0.1026 | 1462.57 | 1466.5 | 11.59 | 675.15 | 5.36 |
| 4 to 5 | 150.20 | 0.1082 | 1388.17 | 1392.1 | 8.97 | 825.27 | 6.55 |
| 5 to 6 | 149.78 | 0.1118 | 1339.71 | 1343.6 | 7.33 | 975.26 | 7.74 |
| 6 to 7 | 149.48 | 0.1142 | 1308.93 | 1312.8 | 6.32 | 1124.89 | 8.93 |
| 7 to 8 | 150.84 | 0.1173 | 1285.93 | 1289.8 | 5.59 | 1275.06 | 10.12 |
| 8 to 9 | 149.86 | 0.1181 | 1268.92 | 1272.8 | 5.05 | 1425.42 | 11.31 |
| Transducer T-21 | | | | | | | |
| 0 to 1 | 300.11 | 0.1119 | | | | | |
| 1 to 2 | 149.85 | 0.0825 | 1816.4 | 1820.3 | 25.92 | 375.04 | 2.98 |
| 2 to 3 | 150.16 | 0.0941 | 1595.7 | 1599.6 | 16.62 | 525.04 | 4.17 |
| 3 to 4 | 150.06 | 0.1026 | 1462.6 | 1466.5 | 11.59 | 675.15 | 5.36 |
| 4 to 5 | 150.20 | 0.1080 | 1390.7 | 1394.6 | 9.05 | 825.27 | 6.55 |
| 5 to 6 | 149.78 | 0.1116 | 1342.1 | 1346.0 | 7.41 | 975.26 | 7.74 |
| 6 to 7 | 149.48 | 0.1139 | 1312.4 | 1316.3 | 6.44 | 1124.89 | 8.93 |
| 7 to 8 | 150.84 | 0.1170 | 1289.2 | 1293.1 | 5.69 | 1275.06 | 10.12 |
| 8 to 9 | 149.86 | 0.1180 | 1270,0 | 1273.9 | 5.09 | 1425.42 | 11.31 |

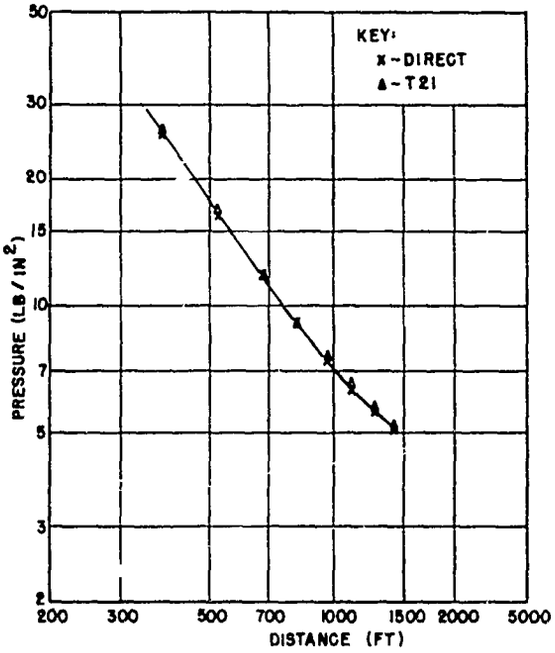


Fig. 3.6 Peak Overpressure vs Distance, Underground Shot

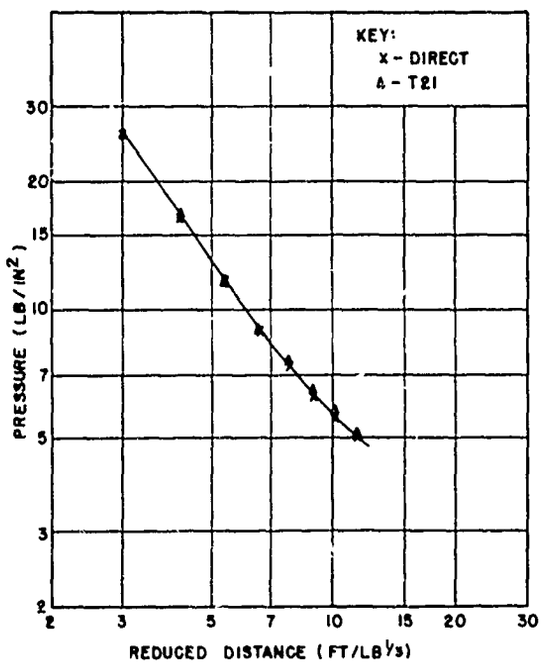


Fig. 3.7 Peak Overpressure vs Reduced Distance, Underground Shot

Since the pressure range was above 5 lbs/in$^2$ the blast switch lag was disregarded. The peak pressure decay between stations was small enough so that the correction described in Section 1.3.2 was not applied to the values of distance from charge to the mid-point between stations.

### 3.4.2 Time of Arrival of Blast Wave

Zero time was recorded only on one blast transducer record. The arrival times vs distance are listed in Table 3.12 and the curve plotted on Fig. 3.9. The reason for the failure of the direct system to record zero time has not been explained. The time of arrival of the blast at the first station as recorded by the transducer was assumed correct for the blast switches also. The following interval times were added to this and listed in Table 3.12. An average of the two systems is plotted in Fig. 3.9.

### 3.4.3 Velocity of Sound

The velocity of sound was calculated by the method outlined in Section 1.3.4. A correction for the relative humidity was applied, since it was 45%, and a difference of -0.9 ft/sec was noted. The velocity of sound after applying the humidity correction was calculated to be 1,100.0 ft/sec.

### 3.4.4 Meteorological Data

| | |
|---|---|
| Wind velocity | 4 MPH S 69°W |
| Blast line | N 20°E |
| Wind component along blast line | + 3.9 ft/sec |
| Temperature | 44.5°F = 6.9°C |
| Atmospheric pressure | 12.78 lbs/in$^2$ |
| Relative humidity | 45% |
| $\gamma$ | 1.400 |

TABLE 3.12

BLAST ARRIVAL TIME, UNDERGROUND SHOT

| Station | Distance (ft) | Arrival time transducer T-21 t (sec) | Arrival time Blast Switch Direct t (sec) | Average t (sec) |
|---|---|---|---|---|
| 1 | 300.11 | 0.1119 | | |
| 2 | 449.96 | 0.1944 | 0.1945 | 0.19445 |
| 3 | 600.12 | 0.2885 | 0.2891 | 0.2888 |
| 4 | 750.17 | 0.3911 | 0.3917 | 0.3914 |
| 5 | 900.37 | 0.4991 | 0.4999 | 0.4995 |
| 6 | 1050.15 | 0.6107 | 0.6117 | 0.6112 |
| 7 | 1199.64 | 0.7245 | 0.7259 | 0.7252 |
| 8 | 1350.49 | 0.8415 | 0.8432 | 0.84235 |
| 9 | 1500.34 | 0.9595 | 0.9613 | 0.9604 |

[redacted]

# CHAPTER 4

## CONCLUSIONS AND RECOMMENDATIONS

### 4.1 PEAK OVERPRESSURE VS REDUCED DISTANCE

#### 4.1.1 HE-1, HE-2, and Underground Shots

In Fig. 3.8, a comparison of pressure vs $\lambda$ for the underground nuclear shot is made with the underground high explosive shot all at a depth (reduced to unit charge weight) of 0.135. The equivalent tonnage was 1 KT $\pm$ 0.26 KT, where $w^{1/3}$ for the underground shot was 126 based on the values found in Section 3.4.1. As can be seen in this figure, there is good agreement from $\lambda = 4$ to 14. If the attenuation of pressure is assumed to be exponential, a curve of the form $P = A\lambda^{-n}$ may be fitted to the points by the method of least squares. In so doing an equation $P = 84.31\lambda^{-1.19}$ was obtained. The pressures at $\lambda = 4$ deviate slightly from the fitted curve. However, there is no reason to believe these points to be erroneous, and it is assumed that the physical size of the charge contribute to this deviation. The conclusion is that between $\lambda = 4$ to 14 the nuclear explosion scales with the TNT explosion when the ($w^{1/3}$) scaling law is applied. There was no evidence of any thermal effects causing a change in the velocity of the shock wave.

#### 4.1.2 Surface Shot

From the nuclear surface shot data it is difficult to draw definite conclusions in regard to scaling with high explosives. There were no preliminary HE surface shots with which to correlate the data. Based on theoretical considerations and data obtained from one pound pentolite spheres, a curve very similar to a free-air curve was expected. In Fig. 3.4, a comparison of pressure vs $\lambda$ for the surface shot is made with a free-air curve. It may be seen that the values of pressure fall within allowable scatter. The equivalent tonnage based on comparison with a free-air curve at 10 psi is 1 KT $\pm$ 0.05 KT. Due to an unexplained spurious signal there is some doubt as to the actual value of the first two pressure levels given in Fig. 3.4. Assuming the spurious signal to be correct, new values have been plotted and a dotted line drawn through them. From the data on hand it is impossible to say which curve is the correct one. There is excellent agreement with the free-air curve at 10 psi and below.

[redacted]



RESTRICTED DATA
[redacted]

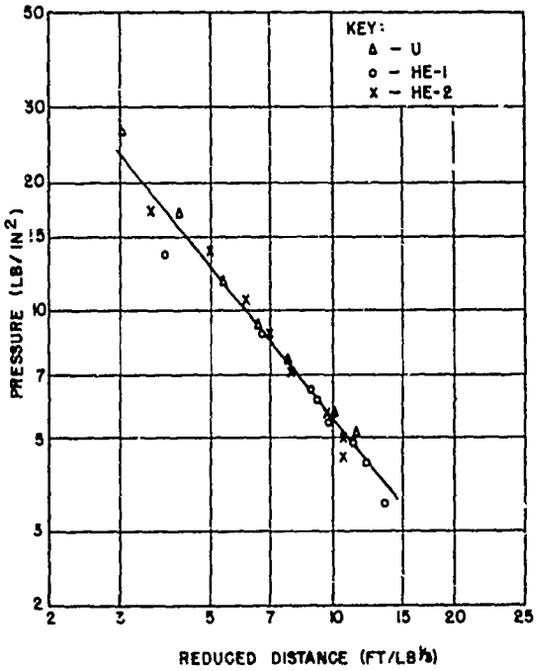


Fig. 3.8 Peak Overpressure vs Reduced Distance, HE-1, HE-2, Underground Shot

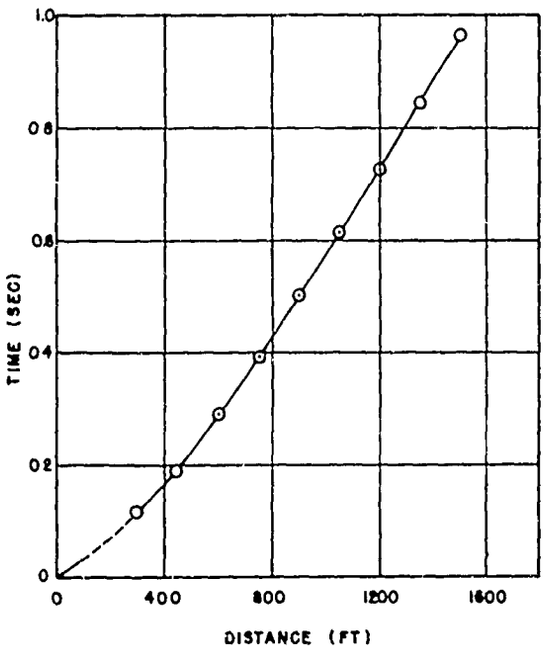


Fig. 3.9 Arrival Time vs Distance, Underground Shot

## 4.2 ERROR EVALUATION

The errors evaluated were purely on the basis of estimated errors in the interval distance, record reading, temperature, and wind velocity.

HE-1 and HE-2 were evaluated together inasmuch as the instrumentation and method of determination of the various factors were practically identical. The surface and underground shots were considered separately. Using the sources of errors listed in Section 1.3.6 and considering the maximum deviation in each case, the fractional errors $\frac{\Delta P_s}{P_s}$ determined from Equation 1.3.13 are listed below:

| Shot | 2.5 psi | 5 psi | 10 psi |
|---|---|---|---|
| HE-1 and HE-2 | .105 | -- | .032 |
| Surface | .065 | -- | .022 |
| Underground | - | .040 | .024 |

## 4.3 VELOCITY OF SOUND

The validity of the velocity of sound determined by meteorological equipment at a position 3,000 feet from the charge and 5,000 feet from the nearest station is somewhat questionable. Firing small charges before the main blast occurs does not solve the problem completely since it does not detect any temperature or wind variations which occur just after the main blast has occurred and before the shock wave arrives at the stations. The ideal set-up involves a system which measures continuously the velocity of sound along the blast line between zero time and the arrival of the blast wave.

## 4.4 INSTRUMENTATION

### 4.4.1 Trailers

For the HE shots a shop truck was equipped with the recording equipment plus tools and miscellaneous parts. This was parked in a revetment which shielded the truck from the blast. The lack of space in the truck was the only major drawback to its use.

On the nuclear shots large air-conditioned van-type trailers were equipped with the magnetic tape recorders, work benches, tools, spare parts, and batteries. The trailers were parked in revetments at 8,000 ft. from ground zero and operations carried on from there. This procedure proved very satisfactory in eliminating damage to electronic equipment due to dust, in providing sufficient work space, and in protection against blast damage.

4.4.2 Blast Switches

In future tests the use of a parallel hook-up for the blast switches might prove valuable in saving large quantities of cable. If the blast switches are to be used in a region of pressure less than 5 psi a delay curve should be obtained for each individual switch in the pressure region for which the switch is intended. This is especially true if the the blast line is to be comparatively short.

Modifying the blast switches so that one and only one pulse could be recorded by each will eliminate any subjective factor in reading the records. This could be accomplished by breaking the circuit as soon as the switch closed and the signal recorded. This would eliminate extraneous pips resulting when poles supporting the gauges are blown down before the shock wave has traversed the entire blast line.

A coding method on the direct blast switch system would help in identifying stations and discovering extraneous signals.

4.4.3 Blast Transducers

The blast transducers seem to be dependable only as a back-up system since any sound other than the shock front produced an extraneous pulse on the record. The short time delay in the transducer response makes them more useful in the low pressure region than blast switches.

4.4.4 Zero Time

The zero time mark on the magnetic tape is necessary for an accurate time of arrival curve. It is recommended that a positive method be used in recording zero time. For future surface or underground shots a pick-up could be placed within or on the surface of the charge. This, of course, is not practical for an air drop.

4.4.5 Recording

In view of the tremendous number of cycles occurring between signal pulses on the record, some means other than manual, should be provided for counting the cycles.

One method of doing this involves marking the record at intervals of 10 and 100 cycles. This might be done at the time of recording or later during the playback of the record. The signal pulse must be necessarily easily distinguished from these marking pulses.

[redacted]

OPERATION JANGLE
Project 1.2a-2

# TRANSIENT GROUND MECHANICAL EFFECTS FROM HE AND NUCLEAR EXPLOSIONS

by


Thomas J. Andrews, Lt Col, USAF

Edward J. Bryant

Paul H. Lorrain

Nicholas M. Masich, Lt Col, USAF


June 1952


Ballistic Research Laboratories
Aberdeen Proving Ground, Maryland


[redacted]

# PREFACE

The primary purpose of the work described in this report was to determine the ground accelerations and ground pressures resulting from nuclear explosions detonated underground and on the surface of the ground at the Nevada Test Site. Personnel of the Explosion Kinetics Branch of the Ballistic Research Laboratories participated in this phase of Program One, Operation JANGLE, under Project 1.2a-2. A preliminary program involving the detonation underground of HE explosives was also conducted at the test site by the same personnel as an aid in predicting the results of the nuclear explosions. This work is also described in this report.

The following personnel participated in Project 1.2a-2 of Operation JANGLE:

Project Officer - Dr. E. E. Minor - Chief, Explosion Kinetics Branch

Deputy Project Officer - N. M. Masich, Lt Col, USAF

Consultant - Dr. C. W. Lampson - Chief, Terminal Ballistic Laboratory

Section Chief - T. J. Andrews, Lt Col, USAF

Ground Shock Section - W. L. Bowne, Lt, USNR
E. J. Bryant
R. A. Eberhard
J. S. Fischer, Pfc., USA
P. H. Lorrain
J. P. McLain, Sgt., USAR
R. E. Reisler

Acknowledgement is made to the personnel of the Naval Ordnance Laboratory (NOL) for their assistance in setting-up appropriate recording equipment required for the ground pressure gauges, and for taking the necessary ground pressure recordings.

SECRET
Security Information

PROJECT 1.2a-2

CONTENTS

PREFACE . . . . . iii

ABSTRACT . . . . . ix

PART I TRANSIENT GROUND ACCELERATIONS . . . . . 1

CHAPTER 1 INTRODUCTION . . . . . 1
1.1 General . . . . . 1
1.2 Objectives . . . . . 1
1.3 Previous Related Work . . . . . 1
1.4 Basic Formulae and Predictions . . . . . 2

CHAPTER 2 EXPERIMENTAL PROCEDURE . . . . . 5
2.1 Description of Accelerometers . . . . . 5
2.2 Accelerometer Mounting and Initiation System . . . 7
2.3 Field Instrumentation . . . . . 7
2.3.1 Blast Range Layout, Surface and Underground Nuclear Shots . . . . . 7
2.3.2 Blast Range Layout, Shot HE-1 . . . . . 10
2.3.3 Blast Range Layout, Shot HE-2 . . . . . 10

CHAPTER 3 TEST RESULTS . . . . . 13
3.1 Surface Nuclear Shot . . . . . 13
3.2 Underground Nuclear Shot . . . . . 13
3.3 Shots HE-1 and HE-2 . . . . . 14
3.4 Discussion of Test Results . . . . . 23

CHAPTER 4 CONCLUSIONS AND RECOMMENDATIONS . . . . . 25
4.1 Conclusions - Ground Accelerations . . . . . 25
4.2 Recommendations . . . . . 26

PART II TRANSIENT GROUND PRESSURES . . . . . 27

CHAPTER 5 INTRODUCTION . . . . . 27
5.1 General . . . . . 27
5.2 Objectives . . . . . 27
5.3 Previous Related Work . . . . . 23
5.4 Basic Formulae and Predictions . . . . . 28

CHAPTER 6 EXPERIMENTAL PROCEDURE . . . . . 31
6.1 Field Layout . . . . . 31
6.1.1 General Description of Gauge . . . . . 31
6.1.2 Blast Range Layout, Surface Shot (Nuclear) . . . . . 31



SECRET
Security Information

RESTRICTED DATA
ATOMIC ENERGY ACT

CONTENTS

6.1.3 Blast Range Layout, Underground Shot (Nuclear) . . . . . 33
6.1.4 Blast Range Layout, HE-2 Shot . . . . . 34
6.2 Detailed Description of Test Equipment . . . . . 34
6.2.1 The Wiancko Ground Pressure Gauge . . . . . 34

CHAPTER 7 TEST RESULTS . . . . . 38
7.1 Surface Shot (Nuclear) . . . . . 38
7.2 Underground Shot (Nuclear) . . . . . 42
7.3 Shot HE-2 (High Explosive) . . . . . 42
7.4 Discussion of Test Results . . . . . 46

CHAPTER 8 CONCLUSIONS AND RECOMMENDATIONS . . . . . 49
8.1 Conclusions - Ground Pressures . . . . . 49
8.2 Recommendations . . . . . 50

ILLUSTRATIONS

CHAPTER 2 EXPERIMENTAL PROCEDURES

2.1 Accelerometer Loaded with Tape . . . . . 6
2.2 Accelerometer Starting Mechanism . . . . . 6
2.3 Playback Equipment . . . . . 8
2.4 Accelerometer Place Gear . . . . . 9
2.5 Place Gear Tripod Assembly . . . . . 9
2.6 Battery Box . . . . . 10

CHAPTER 3 TEST RESULTS

3.1 Maximum Ground Acceleration vs Reduced Distance, Surface Nuclear Shot . . . . . 15
3.2 Maximum Ground Acceleration vs Reduced Distance, Underground Nuclear Shot . . . . . 17
3.3 Maximum Ground Acceleration vs Reduced Distance, Shot HE-1 . . . . . 18
3.4 Maximum Ground Acceleration vs Reduced Distance, Shot HE-2 . . . . . 20
3.5 Predicted and Calculated Maximum Ground Acceleration vs Reduced Distance, Surface Nuclear Shot . 21
3.6 Predicted and Calculated Maximum Ground Acceleration vs Reduced Distance, Underground Nuclear Shot . . . . . 22

CHAPTER 6 EXPERIMENTAL PROCEDURE

6.1 Lateral Trench . . . . . 33
6.2 Wiancko Pressure Gauge (cut-away section) . . . . 37

CHAPTER 7 TEST RESULTS

7.1 Variation of Ground Pressure with Reduced Distance for Surface Nuclear Shot (First Positive Rise, Gauge Depths of 10 ft and 20 ft) . . . . . 40
7.2 Variation of Ground Pressure with Reduced Distance for Surface Nuclear Shot (Maximum Positive Rise excluding Air Blast Effect; Gauge Depths 10 ft and 20 ft) . . . . . 41
7.3 Variation of Ground Pressure with Reduced Distance for Surface Nuclear Shot (Highest Positive Peak Including Air Blast Effect) . . . . . 43
7.4 Variation of Ground Pressure with Reduced Distance for Underground Nuclear Shot (Highest Positive Peak Including Air Blast Effect) . . . . 45
7.5 Variation of Ground Pressures with Reduced Distance for Underground HE-2 Shot . . . . . 47

TABLES

CHAPTER 2 EXPERIMENTAL PROCEDURE
2.1 Gauge Positions, Surface and Underground Nuclear Shots . . . . . 11
2.2 Gauge Positions, Shot HE-1 . . . . . 12
2.3 Gauge Positions, Shot HE-2 . . . . . 12

CHAPTER 3 TEST RESULTS
3.1 Results, Surface Nuclear Shot . . . . . 14
3.2 Results, Underground Nuclear Shot . . . . . 16
3.3 Results, Shot HE-1 . . . . . 16
3.4 Results, Shot HE-2 . . . . . 19

CHAPTER 6 EXPERIMENTAL PROCEDURE
6.1 Blast Range Layout, Surface Shot (Nuclear) . . . 32
6.2 Blast Range Layout, Underground Shot (Nuclear) . 35
6.3 Blast Range Layout, HE-2 (High Explosive) . . . . 36

CHAPTER 7 TEST RESULTS
7.1 Ground Pressure Data, Surface Shot (Nuclear) . . 39
7.2 Ground Pressure Data, Underground Shot (Nuclear) . . . . . 44
7.3 Ground Pressure Data, HE-2 (High Explosive) . . . 46

PROJECT 1.2a-2

ABSTRACT

Ground accelerations and pressures resulting from a surface nuclear detonation at a scaled charge height of 0.024, from an underground nuclear detonation at a scaled burial depth of 0.135, and from two underground HE detonations of different weights at a scaled burial depth of 0.15, were determined as functions of a reduced distance in the present study. The equivalent TNT weight of each nuclear explosive was 1 Kiloton; the weights of the two HE explosives were 2,560 and 40,000 lbs.

The following laws of attenuation of ground acceleration were found applicable to the above explosive materials:

Surface Nuclear Detonation

$$A_V = 22.7\lambda^{-1.8}$$

$$A_H = 65.1\lambda^{-2.2}$$

Underground Nuclear Detonation

$$A_V = 43.8\lambda^{-2.0}$$

$$A_H = 15.9\lambda^{-1.6}$$

Underground HE Detonation (40,000 lbs)

$$A_V = 57.8\lambda^{-1.7}$$

$$A_H = 37.8\lambda^{-1.6}$$

Underground HE Detonation (2,560 lbs)

$$A_V = 81.2\lambda^{-2.0}$$

$$A_H = 96.8\lambda^{-2.1}$$

where $A_V$ = Maximum vertical ground acceleration in g's.

$A_H$ = Maximum horizontal ground acceleration in g's.

$\lambda$ = Reduced distance defined as ratio of horizontal distance from ground zero in feet and cube root of charge weight in pounds of TNT.

The maximum horizontal and vertical ground accelerations were of approximately the same magnitude for each of these detonations. Some correlation between the laws of attenuation of ground acceleration was

found to exist between the underground nuclear detonation and the underground HE detonation of 40,000 lbs.

The present study indicated that air blast pressures had an important effect on the magnitudes of the ground acceleration produced.

The laws of attenuation of ground accelerations previously derived from small charges at greater scale burial depths of gauges in different types of soils were found inapplicable to the nuclear tests reported.

Ground pressure-reduced distance relations were obtained as follows:

Surface Nuclear Detonation

$$p_1\ (10') = 11.87\lambda^{-1.43}$$

$$p_1\ (20') = 12.20\lambda^{-1.17}$$

$$p_2\ (10') = 28.38\lambda^{1.42}$$

$$p_2\ (20') = 33.5\lambda^{-1.2}$$

$$p_3\ (10') = 83.5\lambda^{-1.4}$$

Underground Nuclear Detonation

$$p_3 = 34.59\lambda^{-0.83}$$

Underground HE Detonation

$$p_1\ (5') = 23.9\lambda^{-1.77}$$

$$p_3\ (5') = 10.57\lambda^{-0.54}$$

where $p_1$ = 1st positive pressure rise

$p_2$ = Maximum pressure rise excluding air blast effects

$p_3$ = Maximum pressure rise including air blast effects

$\lambda = r/W^{1/3}$

r = distance from ground zero in feet

W = charge weight in pounds of TNT (1 KT in nuclear shots)

PROJECT 1.2a-2

A comparison of the data from the three shots indicated that ground pressure data from small charges may not be accurately applied to nuclear charges by scaling laws now in use. Maximum ground pressures occuring from the detonation of nuclear charges described in this report were primarily due to air blast effects on the ground surface.

# PART I

## TRANSIENT GROUND ACCELERATIONS

## CHAPTER 1

## INTRODUCTION

### 1.1 GENERAL

During the Fall of 1950, the Armed Forces Special Weapons Project requested the Ballistic Research Laboratories to make measurements of ground shock phenomena resulting from underground nuclear explosions. The Special Weapons Command and the Los Alamos Scientific Laboratory took over this operation early in the summer of 1951 renaming it Operation JANGLE, with field location at the Nevada Test Site.

The Ballistic Research Laboratories made initial studies of the phenomena involved and decided upon the necessary instrumentation during the Winter of 1950. The following Spring, preliminary field tests of the instruments were conducted at Aberdeen Proving Ground.

### 1.2 OBJECTIVE

The main purpose of the present program was to provide back-up measurements of ground acceleration by means of self-recording accelerometers in the event of possible failure of more complicated systems of measurements involving the use of wire transmission of data.

The principal objectives of the program were:

1. To measure the maximum ground acceleration (horizontal and vertical) at various distances from ground zero.

2. To determine from these measurements the laws of attenuation of acceleration vs distance.

3. To determine the degree of correlation between these laws and those derived from HE explosions.

### 1.3 PREVIOUS RELATED WORK

The most complete study of the effects of underground explosions available was that conducted by Division 2 of the National Defense

Research Council (NDRC) during World War II, to determine the effects of underground explosions on model fortifications. Empirical formulae were obtained relating particle acceleration, among other phenomena, in the earth to distance from the charge for various charge sizes, types of soil, and depth of burial of charge and gauges. 1

Further work on ground shock measurements was undertaken by the Stanford Research Institute at Dugway, Utah. 2 Measurements of ground accelerations were made for charge weights up to 320,000 lbs located at shallow charge depths.

## 1.4 BASIC FORMULAE AND PREDICTIONS

Estimates of transient ground acceleration effects to be expected from the various explosions used in the present work were obtained from empirical formulae developed by C. W. Lampson (reference 1). Horizontal and vertical accelerations were estimated for the first shot at the Nevada Test Site (HE-1) by means of such equations for acceleration modified to apply to shallower charge depths. The equation used for prediction of accelerations was:

$$Ag = \frac{0.33k}{\rho W^{1/3}} \left(1400\lambda^{-4} + 3.5\lambda^{-2} + 0.5\lambda^{-1}\right) \times 10^{-5} \qquad (1.1)$$

where Ag = the horizontal or vertical ground acceleration in g's.

k = a constant depending on the soil.

$\rho$ = soil density in slugs per cubic inch.

$\lambda$ = reduced distance defined as the ratio of the horizontal distance from ground zero in feet to the cube root of the charge weight in pounds.

A factor of 0.33 is used in the above equation to take into account the shallower charge depth of $0.135\ W^{1/3}$ used at the Nevada Test Site as compared to a charge depth of $2.1\ W^{1/3}$ used by C. W. Lampson in establishing the basic empirical formula.

---

1 C. W. Lampson, "Final Report on Effects of Underground Explosions", NDRC Report No. A-479 (OSRD-6645)

2 E. B. Doll, Interim Report "Underground Explosions at Dugway", Corp of Engineers, US Army Contract DA-04-167-ENG-379 Stanford Research Institute

The numerical value of the soil constant k may be found approximately from:

$$k = 1/2\ \rho v^2, \tag{1.2}$$

where v = velocity of small amplitude waves in the earth in feet per second.

The dimensions of inches per foot have been assigned to the factor $\frac{1}{2}$ in order to express k in pounds per square inch.

Estimates of the ground acceleration for the nuclear shots were based on the HE results, assuming the acceleration scaled according to the relationship:

$$A_n = \frac{F_n}{F_{HE}} \frac{W_{HE}^{1/3}}{W_n^{1/3}} A_{HE} \tag{1.3}$$

where $A_n$ = horizontal or vertical acceleration in g's, at a given reduced distance, due to a nuclear charge having an equivalent TNT weight of $W_n$ lbs.

$A_{HE}$ = horizontal or vertical acceleration in g's at a reduced distance corresponding to $A_n$, due to an HE charge of weight $W_{HE}$ lbs.

$F_n$ = coupling factor for nuclear charge which depends on burial depth.

$F_{HE}$ = coupling factor for HE charge which depends on its burial depth.

The ratio of the coupling factors for charges having the same scaled burial depth is unity. This ratio was taken to be 0.6 for predicting the effects of the surface nuclear shot with respect to the underground HE shot. Actually, a value of 0.5 was used to allow for more efficient coupling from a nuclear charge having a small volume as compared to an equivalent TNT tonnage having a large volume.

Ground acceleration was also calculated for the nuclear shots based on a knowledge of ground pressures produced by these explosives. This was accomplished by means of the following formula originally derived by C. W. Lampson and modified to include experimentally derived pressure data:

$$A_g = \frac{32x6}{384} \frac{k_o}{\rho W^{1/3}} \lambda^{-n-3}, \tag{1.4}$$

where $A_g$ = ground acceleration in g's at a specified reduced distance where the ground pressure has been determined.

$k_o$ = experimental soil constant derived from ground pressure measurements in pounds per square inch.

$\lambda$ = reduced distance as defined previously.

n = experimental attenuation factor for ground pressure data.

$\rho$ = soil density in slugs per cubic inch.

W = charge weight of explosive in pounds of TNT.

# CHAPTER 2

## EXPERIMENTAL PROCEDURES

### 2.1 DESCRIPTION OF ACCELEROMETERS

For measuring transient groung accelerations it was decided to use a self-recording accelerometer in order to reduce the possibility of failure due to faulty electronics and to make long transmission cables unnecessary. An accelerometer manufactured by Engineering Research Associates (ERA) was believed to possess satisfactory frequency response, recording time, and accuracy, and was selected for use on Operation JANGLE.

Figure 2.1 shots a view of the principle parts of the ERA accelerometer. This gauge consists essentially of a magnetic tape which is moved past seismic elements. The tape has three separate channels, on each of which a 1280 cycle per second signal is recorded. Initially the tape is stored on a drag spool which limits its speed to 4.5 inches per second. When in operation, the tape is pulled past the seismic elements by a spring driven drive spool.

The seismic elements consist of a mass-spring system in which part of the mass is a small permanent magnet. Originally the element is so placed with relation to the tape that the amplitude of the carrier is reduced by one half. When the accelerometer expeciences an acceleration, the distance from the magnet to the tape varies proportionally to the acceleration, thereby varying the amount of the carrier erased. Calibration curves are used to relate the acceleration to the percentage of the carrier erasure.

Natural frequencies of the seismic elements range from 17 cycles per second for the 0.05 g element to 168 cycles per second for the 6 g elements. Damping of the elements was approximately 0.5 of critical. Each accelerometer contains two seismic elements at right angles to each other and a torsion timer to produce a timing signal.

The tape supply spool and the torsion timer are held in position until the desired time of starting by two spring loaded catches which, in turn, are held by a fusible link. To start a recording, a current is passed through the link, causing it to fuse and release the catches. This mechanism is shown in Fig. 2.2.

The playback consists of four units: (1) a mechanical playback unit (turntable), (2) an electronic display unit, (3) an oscillograph record unit, and (4) a power supply. Figure 2.3 shows a photograph of this

DECLASSIFIED

SECRET

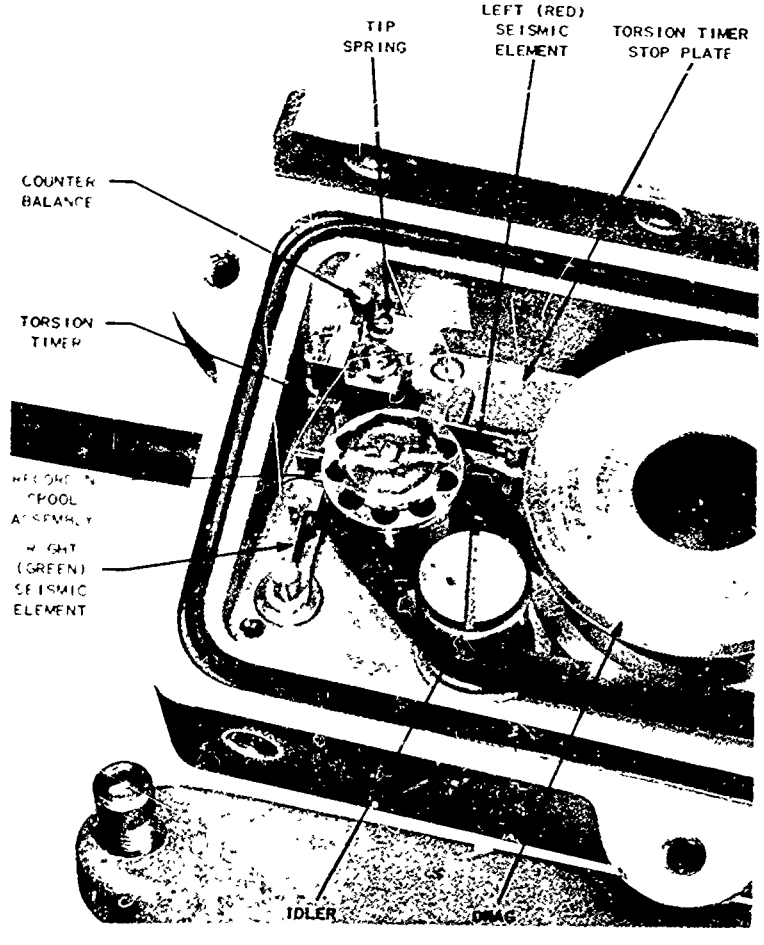


Fig. 2.1 Accelerometer Loaded with Tape

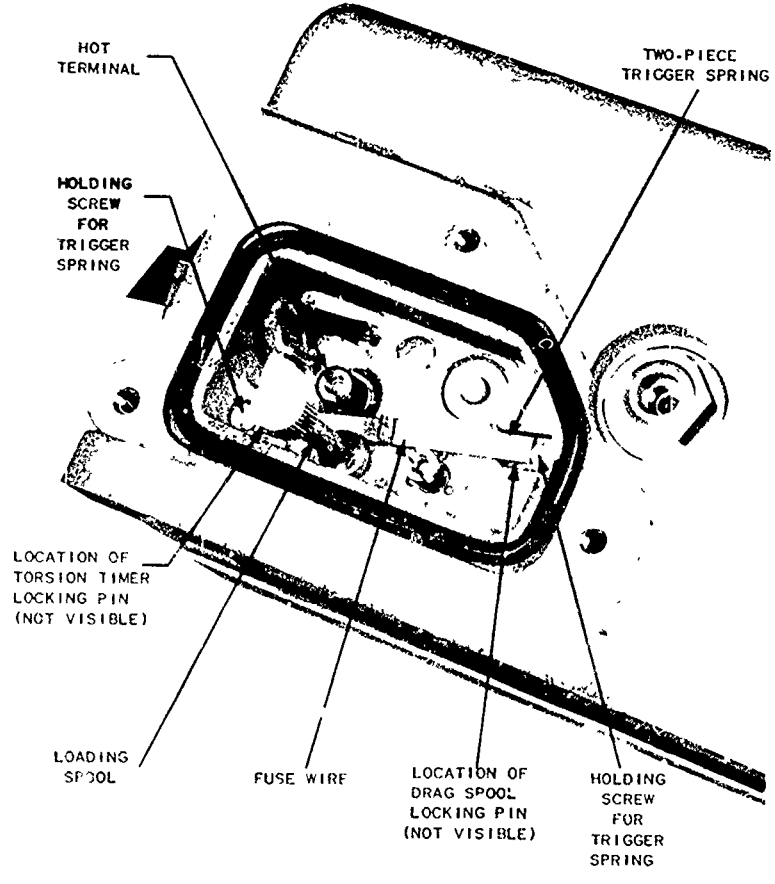


Fig. 2.2 Accelerometer Starting Mechanism



SECRET

DECLASSIFIED

equipment less the oscillograph record unit. This equipment was designed to prepare the tape by recording the carrier signal as well as to play back the recorder acceleration. The recorded signal is played back by the mechanical playback and displayed on a cathode-ray tube screen in the electronic display unit, the necessary triggering and expansion circuits being provided to allow analysis of the record. Due to the use of a long persistence screen, photographic techniques were not necessary for measuring the record, although this was considered desirable in order to provide permanent records of some of the data.

## 2.2 ACCELEROMETER MOUNTING AND INITIATION SYSTEM

For convenience in installing the accelerometers in the ground, they were first mounted in steel capsules. A metal tube was attached to the capsule by means of a bayonet joint, and the capsule and tube suspended in a hole in the ground from a tripod, using a ball-and-socket joint. The gauge was then aligned by using a spirit level and alidade at the upper end of the tube. Each capsule was also equipped with a steel cable which extended to the top of the hole for recovery of the gauges. The mounting equipment is shown in Figs. 2.4 and 2.5.

After the capsules were properly aligned they were secured in place by pouring "Cal-Seal" (a quick setting cement) into the hole until the surface of the cement was approximately flush with the top of the capsule.

Power for melting the fusible link and starting the accelerometers was provided by a 6 volt dry cell located in a box at the top of each hole. This box also contained a relay for connecting the battery to the link at the proper time. This relay was closed at minus 1 second by a signal furnished by the Egerton, Germeshausen, and Greer Project (EG&G). A photograph of the box is shown in Fig. 2.6.

## 2.3 FIELD INSTRUMENTATION

The locations of the accelerometers on the blast ranges for the subject detonations and the ranges of these instruments are tabulated in the tables shown below.

### 2.3.1 Blast Range Layout, Surface and Underground Nuclear Shots

On each of the two nuclear shots, 17 accelerometers were used. These gauges were all placed in holes 10 ft deep at 12 stations along a radial line. Higher range back-up gauges were placed at stations 2, 5, 7, 8 and 10. All gauges were mounted in accordance with the system described in Section 2.2. Distances of the stations from ground zero and other pertinent information for these shots are given in Table 2.1.

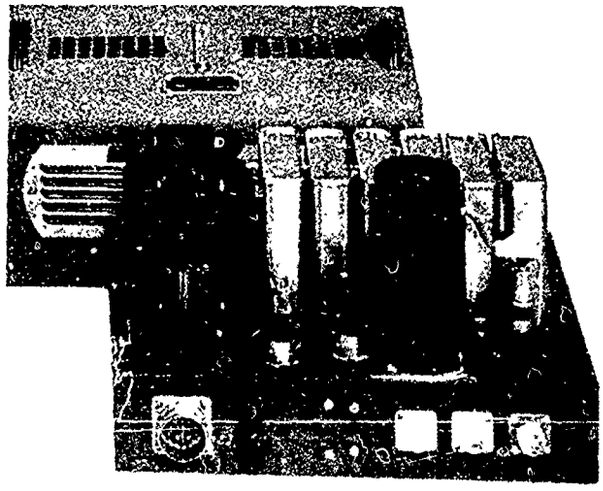

Type 100A1
Power Supply Unit

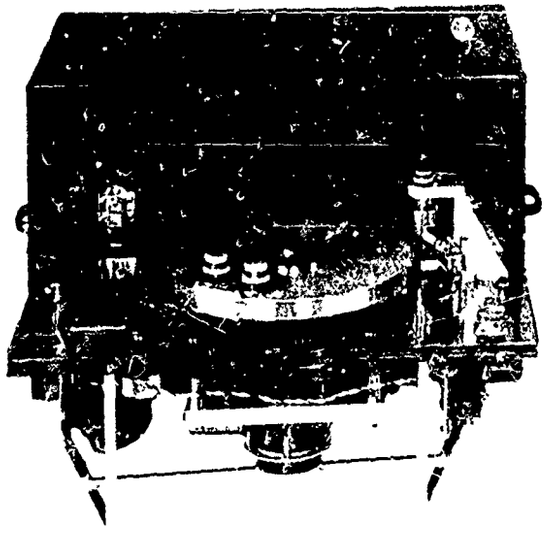

Type 2120A1
Mechanical Playback Unit

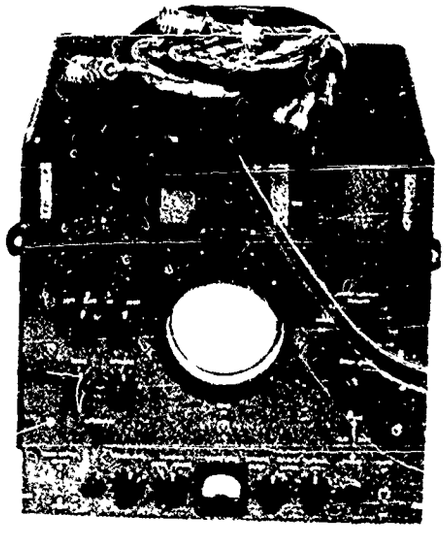

Type 2110A1
Electronic Display Unit

Fig. 2.3. Playback Equipment



RESTRICTED DATA
ATOMIC ENERGY ACT 1946

SECRET
Security Information

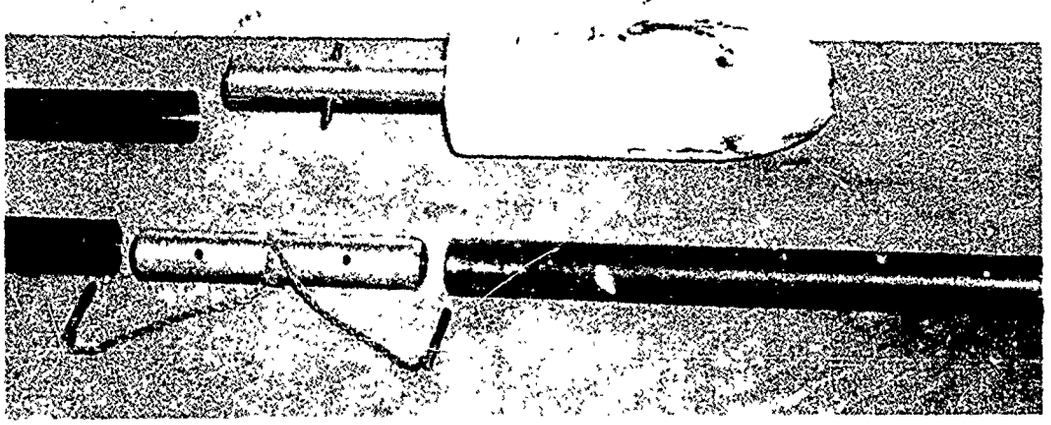

Fig. 2.4. Accelerometer Place Gear

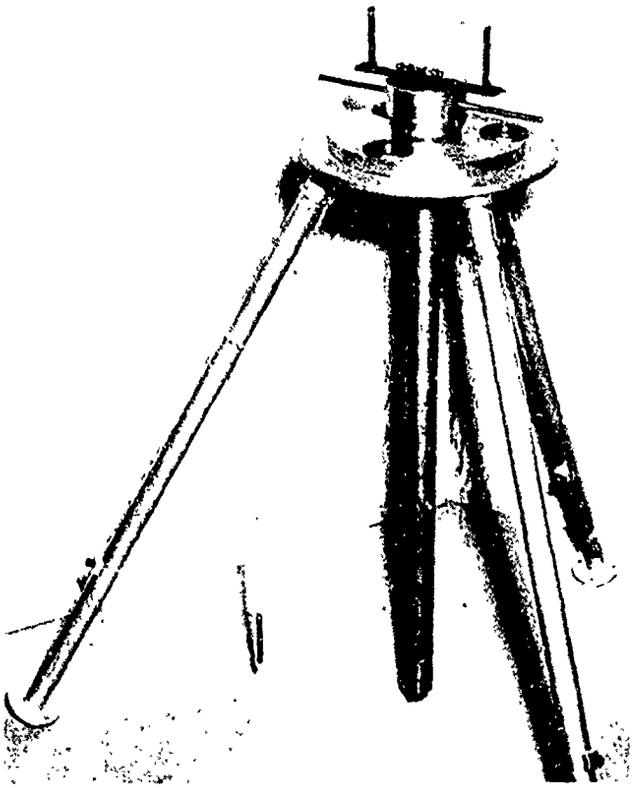

Fig. 2.5. Place Gear Tripod Assembly



[redacted] CO
Security Information

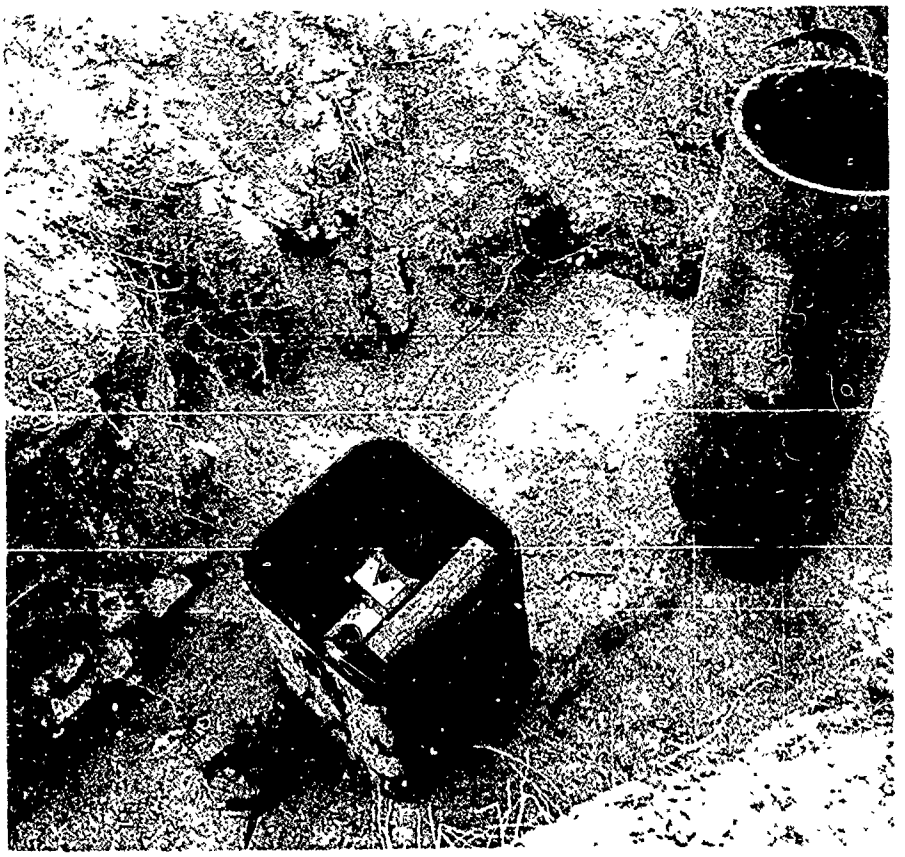

Fig. 2.6. Battery Box

2.3.2 Blast Range Layout, Shot HE-1

Twelve accelerometers were used to instrument shot HE-1 and were distributed along a radial line as shown in Table 2.2. Due to the non-availability of the mounting gear, these gauges were placed in holes 18 inches deep. Four J-bolts were set in "Cal-Seal" in these holes, and the accelerometers were bolted to the J-bolts.

2.3.3. Blast Range Layout, Shot HE-2

Table 2.3 shows the arrangement of ERA gauges for Shot HE-2. Twelve gauges were placed at 9 stations; back-up gauges being placed at stations 4, 5, and 7. The same method of mounting was used for this shot as for the nuclear shots (capsules) except that the gauges were placed in holes only 5 ft deep.



RESTRICTED DATA
ATOMIC ENERGY ACT 1946
SECRET

TABLE 2.1

Gauge Positions, Surface and Underground Nuclear Shots

| Station | Distance (ft) | Reduced Distance (λ) | Gauge Range (g's) |
|---|---|---|---|
| 1 | 275 | 2.18 | 6 |
| 2 | 340 | 2.70 | 3 |
| 2 | 340 | 2.70 | 6 |
| 3 | 420 | 3.34 | 3 |
| 4 | 520 | 4.13 | 2 |
| 5 | 642 | 5.09 | 1 |
| 5 | 642 | 5.09 | 2 |
| 6 | 794 | 6.31 | 0.75 |
| 7 | 982 | 7.80 | 0.5 |
| 7 | 982 | 7.80 | 2 |
| 8 | 1213 | 9.63 | 0.3 |
| 8 | 1213 | 9.63 | 0.5 |
| 9 | 1500 | 11.91 | 0.3 |
| 10 | 1890 | 15.00 | 0.1 |
| 10 | 1890 | 15.00 | 0.3 |
| 11 | 2379 | 18.88 | 0.1 |
| 12 | 3000 | 23.8 | 0.05 |

TABLE 2.2
Gauge Positions, Shot HE-1

| Station | Distance (ft) | Reduced Distance (λ) | Gauge Range (g's) |
|---|---|---|---|
| 1 | 34.22 | 2.49 | 50 |
| 2 | 41.52 | 3.00 | 10 |
| 3 | 58.98 | 4.3 | 2 |
| 3 | 58.98 | 4.3 | 10 |
| 4 | 85.78 | 6.25 | 1 |
| 4 | 85.61 | 6.25 | 2 |
| 5 | 103.03 | 7.5 | 0.5 |
| 5 | 103.03 | 7.5 | 2 |
| 6 | 148.44 | 10.8 | 0.1 |
| 6 | 148.44 | 10.8 | 1 |
| 7 | 262.28 | 18.8 | 0.1 |
| 8 | 378.34 | 27.6 | 0.05 |

TABLE 2.3
Gauge Positions, Shot HE-2

| Station | Distance (ft) | Reduced Distance (λ) | Gauge Range (g's) |
|---|---|---|---|
| 1 | 85.5 | 2.49 | 50 |
| 2 | 102.5 | 3.10 | 10 |
| 3 | 123 | 3.62 | 6 |
| 4 | 178 | 5.2 | 6 |
| 4 | 178 | 5.2 | 10 |
| 5 | 262 | 7.7 | 2 |
| 5 | 262 | 7.7 | 6 |
| 6 | 378 | 11 | 1 |
| 7 | 542 | 16.7 | 0.5 |
| 7 | 542 | 16.7 | 2 |
| 8 | 1025 | 31 | 0.1 |
| 9 | 1350 | 62.4 | 0.05 |

# CHAPTER 3

## TEST RESULTS

### 3.1 SURFACE NUCLEAR SHOT

The data obtained from ERA records for the surface shot (nuclear) (charge height of 42 inches) is shown in Table 3.1. Data were not obtained from all accelerometers because in some cases the acceleration was beyond the range of the instruments, and in others, the accelerometers were inoperative because of faults in the initiation system. The data shown in Table 3.1 refers to maximum accelerations recorded by the gauges, that is, the largest peaks appearing on the records were used to determine acceleration regardless of direction.

These data are also shown in graphical form in Fig. 3.1. The solid lines shown in this figure were determined by using the method of least squares to find the straight line which gave the best fit to the experimental points for each component.

The equations of the lines so determined are:

$$A_v = 22.7\lambda^{-1.8} \tag{3.1}$$

and

$$A_h = 65.1\lambda^{-2.2} \tag{3.2}$$

where $A_v$ = vertical acceleration component (g's).

$A_h$ = horizontal acceleration component (g's).

The value of $W^{1/3}$ was assumed to be 126, based on a TNT equivalent of 1 kiloton.

### 3.2 UNDERGROUND NUCLEAR SHOT

The data obtained for this shot (charge depth of 17 feet) are given in Table 3.2 and the results are shown on graph Fig. 3.2. The equations for the maximum vertical and horizontal accelerations derived by the method of least squares are:

$$A_v = 43.8\lambda^{-2.0} \tag{3.3}$$

$$A_h = 15.9\lambda^{-1.6} \tag{3.4}$$

TABLE 3.1

Results, Surface Nuclear Shot

| Station | Distance (ft) | Reduced Distance (λ) | Maximum Acceleration (g's) Vertical | Horizontal |
|---|---|---|---|---|
| 1 | 275 | 2.18 | 7.8 | |
| 2 | 340 | 2.70 | 7.8 | 5.3 |
| 5 | 642 | 5.09 | .551 | .771 |
| 5 | 642 | 5.09 | 1.61 | 1.86 |
| 6 | 794 | 6.31 | 1.36 | 1.2 |
| 7 | 982 | 7.80 | | .92 |
| 8 | 1213 | 9.63 | | .541 |
| 8 | 1213 | 9.63 | | .994 |
| 9 | 1500 | 11.91 | | .403 |
| 10 | 1890 | 15 | .154 | .093 |
| 10 | 1890 | 15 | .136 | |
| 12 | 3000 | 23.8 | .074 | |

The value of $W^{1/3}$ was assumed to be 126 for this shot, based on a TNT equivalent of 1 kiloton.

## 3.3 SHOTS HE-1 and HE-2

These shots are described in the following table:

| Title | Weight | $W^{1/3}$ | Depth Feet | Depth λ |
|---|---|---|---|---|
| HE-1 | 2,560 lbs of TNT | 13.68 | 2.0 | 0.15 |
| HE-2 | 40,000 lbs of TNT | 34.2 | 5.1 | 0.15 |

The data obtained from these shots were treated in precisely the same way as those for the surface nuclear shot. The data for HE-1 and HE-2 are shown in Tables 3.3 and 3.4 and are illustrated in the graphs shown in Figs. 3.3 and 3.4, respectively. The lines on the graphs were obtained by the method of least squares which yielded the following equations:

HE-1

$$A_v = 8.12\lambda^{-2.0}, \tag{3.5}$$

$$A_h = 96.8\lambda^{-2.1}, \tag{3.6}$$

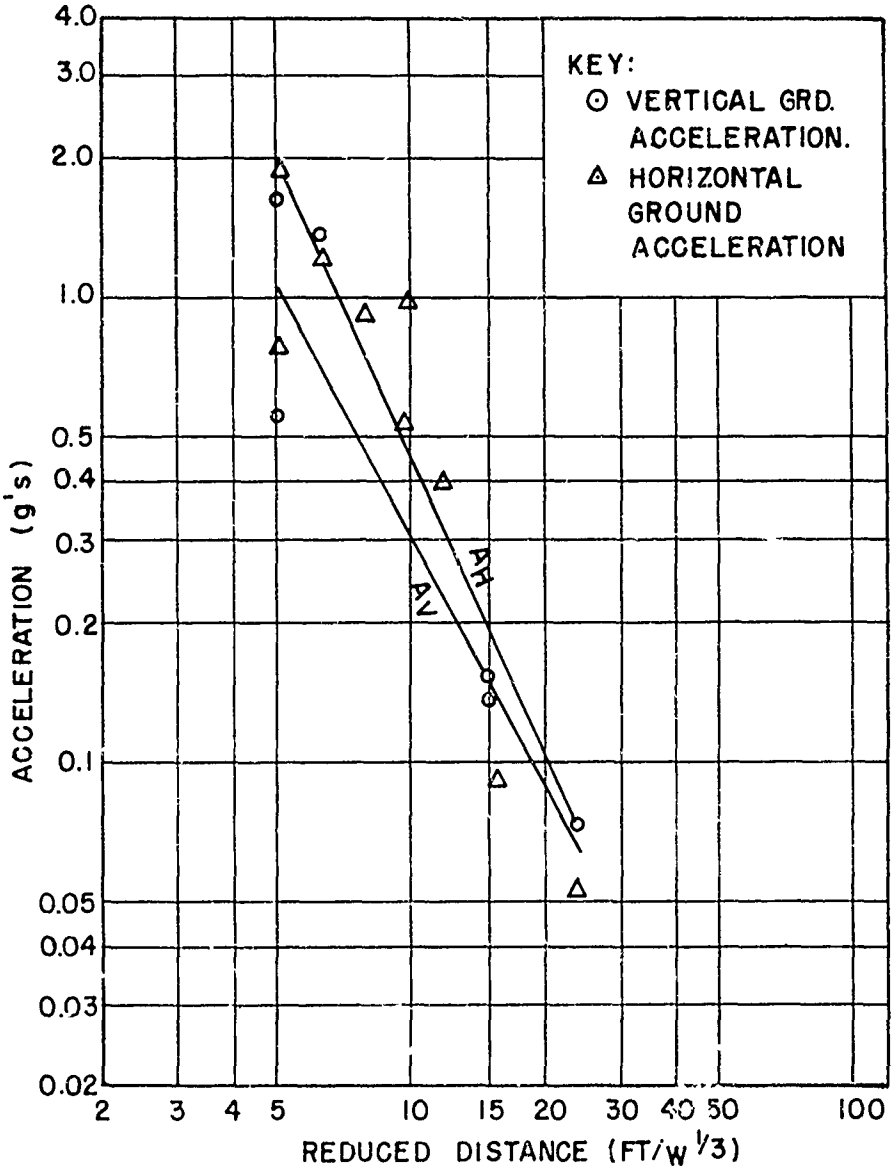


Fig. 3.1. Maximum Ground Acceleration vs Reduced Distance, Surface Nuclear Shot

TABLE 3.2

Results, Underground Nuclear Shots

| Station | Distance (ft) | Reduced Distance (λ) | Maximum Acceleration (g's) Vertical | Horizontal |
|---|---|---|---|---|
| 2 | 340 | 2.70 | 4.13 | 2.49 |
| 3 | 420 | 3.33 | 4.47 | |
| 5 | 642 | 5.1 | | 2.33 |
| 7 | 982 | 7.79 | 1.64 | 0.880 |
| 9 | 1500 | 11.9 | 0.213 | 0.262 |
| 12 | 3000 | 23.81 | 0.07 | 0.077 |

TABLE 3.3

Results, Shot HE-1

| Station | Distance (ft) | Reduced Distance (λ) | Maximum Acceleration (g's) Vertical | Horizontal |
|---|---|---|---|---|
| 2 | 41.52 | 3.0 | 6.6 | 7 |
| 3 | 58.98 | 4.3 | 5 | 5.8 |
| 4 | 85.61 | 6.25 | 3 | 2.92 |
| 5 | 102.65 | 7.5 | 1.55 | 1.13 |
| 6 | 148.25 | 10.8 | 0.92 | |
| 7 | 262.28 | 18.8 | 0.25 | 0.24 |
| 8 | 378.34 | 27.6 | 0.1 | 0.077 |

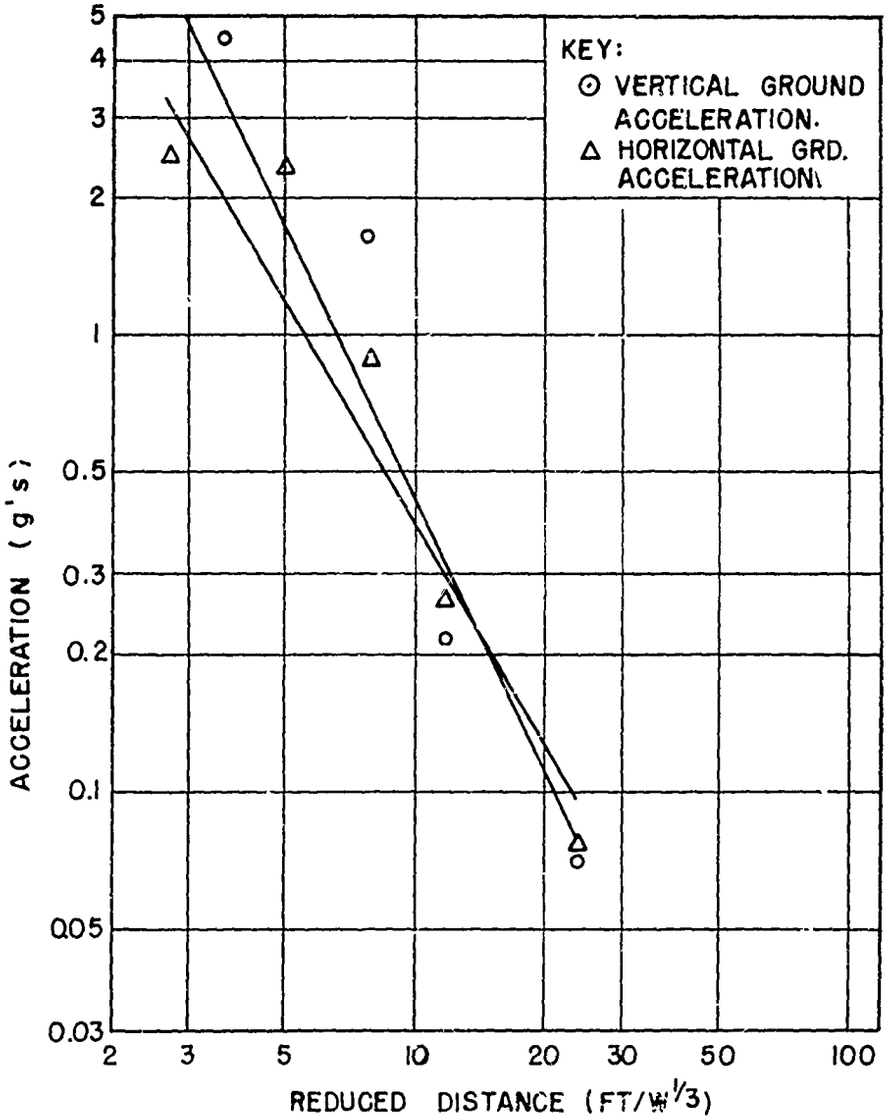


Fig. 3.2. Maximum Ground Acceleration vs Reduced Distance, Underground Nuclear Shot

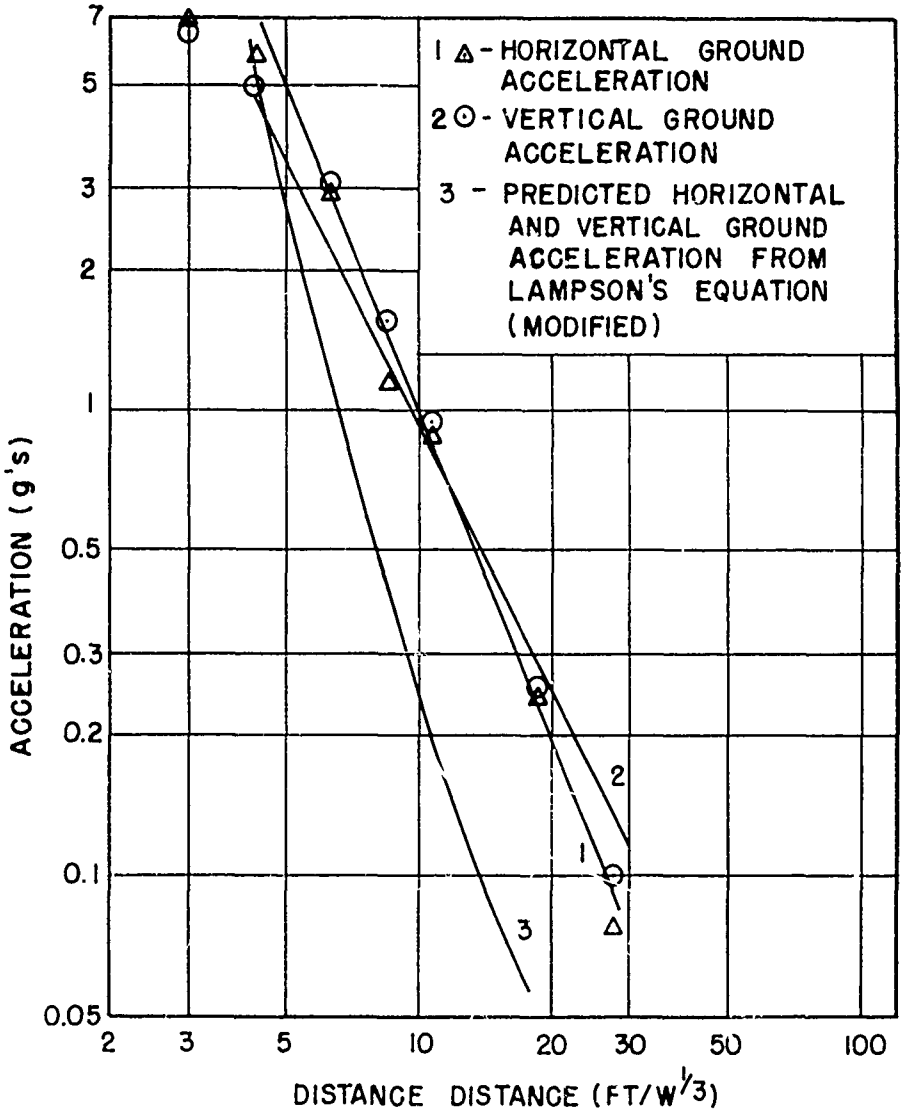


Fig. 3.3. Maximum Ground Acceleration vs Reduced Distance, Shot HE-1

TABLE 3.4
Results, Shot HE-2

| Station | Distance (ft) | Reduced Distance ($\lambda$) | Maximum Acceleration (g's) Vertical | Horizontal |
|---|---|---|---|---|
| 3 | 123 | 3.6 | 5.9 | 3.49 |
| 4 | 178 | 5.2 | 2.44 | 2.07 |
| 5 | 262 | 7.7 | 1.68 | 2.61 |
| 6 | 378 | 11 | | 0.32 |
| 7 | 542 | 16.7 | 1.10 | 1.75 |
| 8 | 1025 | 31 | 0.17 | |
| 9 | 1350 | 39.5 | 0.053 | 0.048 |

HE-2

$$A_v = 57.8\lambda^{-1.7}, \tag{3.7}$$

$$A_h = 37.8\lambda^{-1.6}. \tag{3.8}$$

Figure 3.3 also shows a plot of the predicted horizontal or vertical acceleration for Shot HE-1 based on the following formula:

$$Ag = 1.09\ (1400\lambda^{-4} + 3.5\lambda^{-2} + 0.5\lambda^{-1}). \tag{3.9}$$

In the derivation of this equation, the following values were assumed for the various constants involved:

Seismic velocity $v$ = 3000 feet per second

Soil density $\rho$ = 0.00244 slugs per cubic inch

Cube root of charge
Weight $W^{1/3}$ for HE-1 = 13.64

Predicted values of the horizontal or vertical ground acceleration with respect to reduced distance for the surface and underground nuclear shots are shown in Figs. 3.5 and 3.6, respectively. These predictions were based on the application of scaling laws to Shot HE-2 acceleration data which produced the following equations:

$$A_s = 0.16\ A_2, \tag{3.10}$$

$$A_u = 0.27\ A_2. \tag{3.11}$$

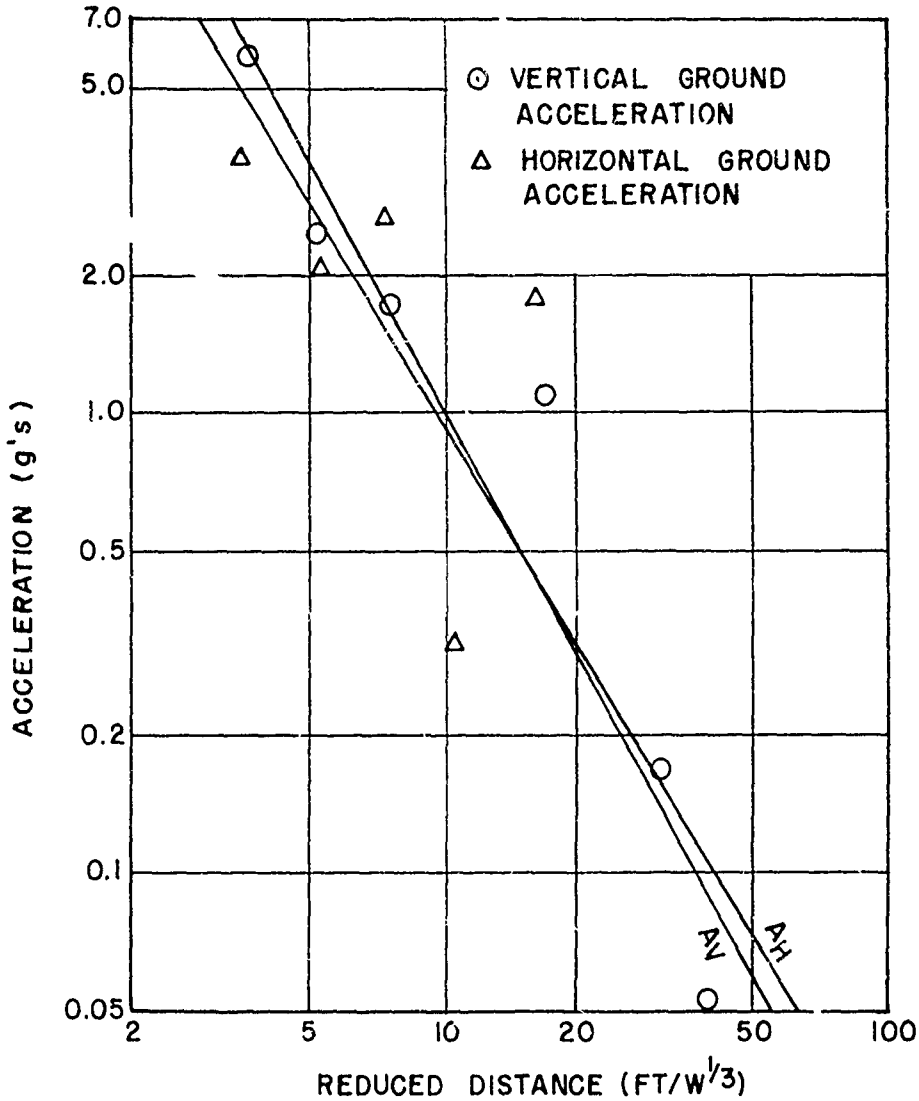


Fig. 3.4. Maximum Ground Acceleration vs Reduced Distance, Shot HE-2

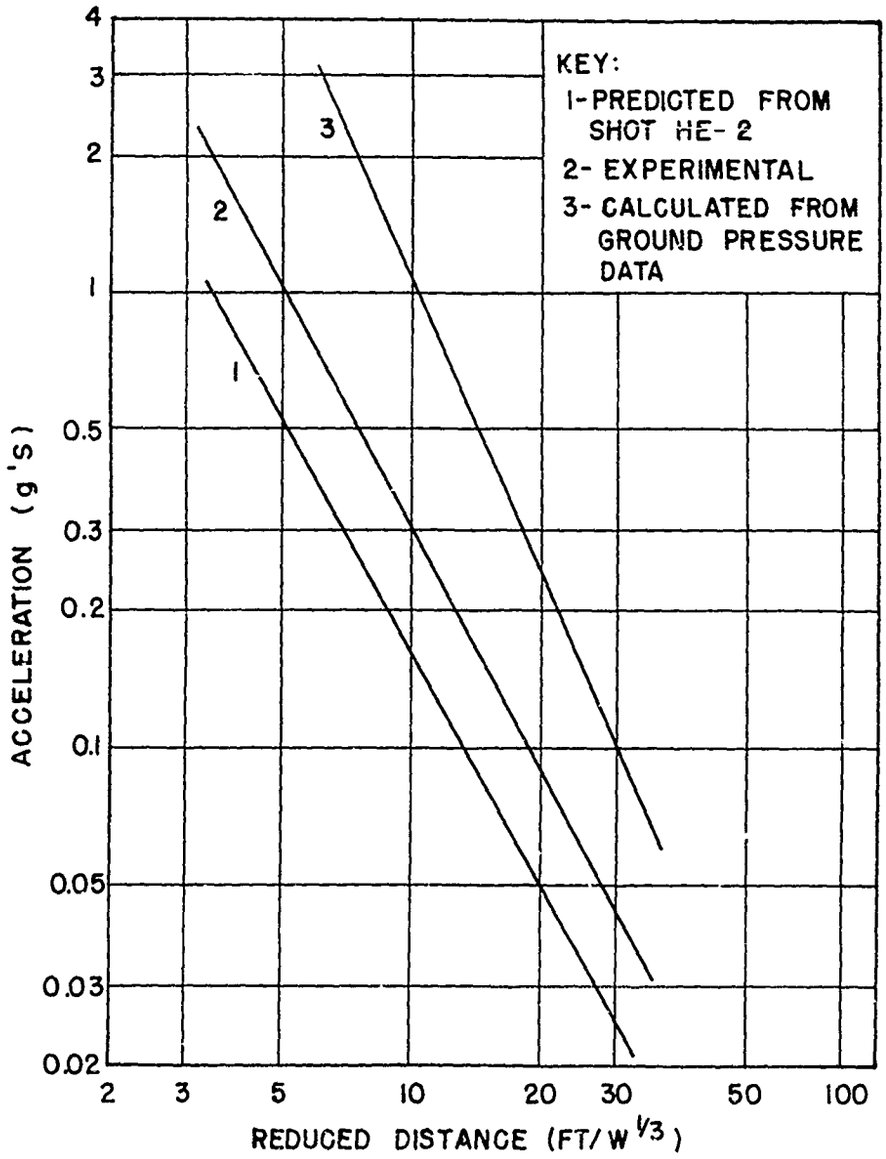


Fig. 3.5. Predicted and Calculated Maximum Ground Acceleration vs Reduced Distance, Surface Nuclear Shot

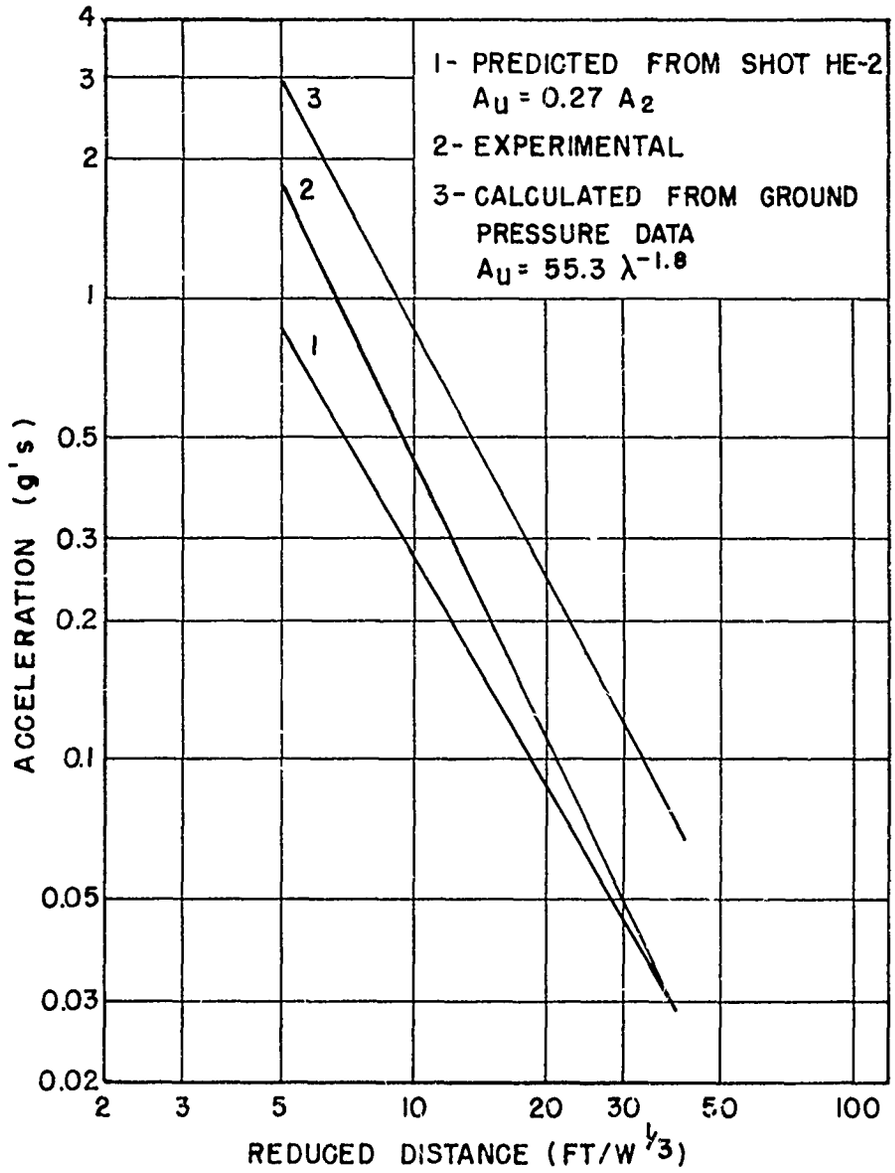


Fig. 3.6. Predicted and Calculated Maximum Ground Acceleration vs Reduced Distance, Underground Nuclear Shot

Calculated values of the horizontal and vertical ground acceleration with respect to reduced distance for the surface and underground nuclear shots, are also shown in Figs. 3.5 and 3.6, respectively. These calculations were based on equations developed from a knowledge of ground pressure data 3 for these shots. These equations are as follows:

$$A_s = 252\lambda^{-2.3}, \tag{3.12}$$

$$A_u = 55.3\lambda^{-1.8}. \tag{3.13}$$

In the above equations, A refers to horizontal or vertical ground acceleration in g units; the subscripts s, u, and 2 refer to the surface nuclear shot, the underground nuclear shot, and Shot HE-2, respectively. The reduced distance is $\lambda$.

## 3.4 DISCUSSION OF TEST RESULTS

The acceleration records obtained on these tests contained several cycles of various magnitudes and frequencies. There was no direct evidence of an induced air blast effect characterized by a short rise in acceleration which was greater than the first observed initial rise as was found to be the case for ground pressure measurements. This may be due to the cushioning effect of the loose earth placed above the accelerometers. Further, as the distance from charge increased, the record, in general became more complicated. This probably indicates that the effect of geological conditions of the earth is increasingly more important as the distance from the charge increases, as might be expected.

Consistently low attenuation factors were obtained for both components of ground acceleration for all the shots observed in the program. These varied in the range from 1.6 to 2.1, and were considerably lower than the attenuation factors expected from experimental data previously derived from small charges in different types of soils; and used with scalewise greater burial depths of gauges and charge. Attenuation factors for air blast pressures for the surface and underground nuclear detonations as determined by the Ballistic Research Laboratories 4 using

---

3 See Part II of this report.

4 W. F. Molesky, R. E. Eberhard, C. N. Kingery, "Peak Air Blast Pressures from Shock Velocity Measurements Along the Ground", Project 1.2a-1 Operation JANGLE.

other instrumentation in this program were 1.7 and 1.2, respectively for pressures less than 20 pounds. From a comparison of attenuation factors, it thus appears that air blast has an important effect on the rate of attenuation of the ground acceleration in these tests. From theoretical considerations, if it is assumed that ground pressure effects only cause acceleration, the attenuation factor for ground acceleration should be greater than that for ground pressure by a factor of 1 under ideal conditions. This is partially verified in the present tests at least for the underground nuclear shot.

Acceleration levels for the underground nuclear shot were somewhat greater than for the surface nuclear shot particularly at a reduced distance of $\lambda = 2$. Higher acceleration levels were obtained for the HE shots for given reduced distances than for the nuclear shots. For a reduced distance of $\lambda = 10$, these were approximately 2 1/2 times greater than for the nuclear shots. This is as expected because of the scaling effect for ground acceleration which is inversely related to the cube root of the charge weight.

The prediction equations for the surface and underground nuclear shots based on the use of HE-2 data showed better agreement with the experimental data than the calculations of ground acceleration based on the use of ground pressure data for these shots. In the former case, the acceleration levels differed by no more than a factor of 2 in the range of $2 < \lambda < 20$ as compared to a factor of approximately 4 using ground pressure data.

# CHAPTER 4

## CONCLUSIONS AND RECOMMENDATIONS

### 4.1 CONCLUSIONS - GROUND ACCELERATIONS

Maximum horizontal and vertical ground acceleration measurements have been obtained for a surface and an underground nuclear detonation, and for underground HE detonations investigated in this program by means of self-recording accelerometers involving the use of magnetic tape. The instruments provided successful back-up acceleration measurements although the data obtained showed a somewhat greater spread in the test results, as compared to those obtained from other accelerometers of superior dynamic range and response set-up in the program using wire data transmission methods.

Simple power laws relating the maximum horizontal and vertical ground acceleration to reduced distance were found to be applicable to the nuclear and HE detonations investigated in the program. Within the limits of experimental error, the rates of attenuation of the maximum horizontal and vertical ground acceleration for these detonations were approximately the same, varying in the range from 1.6 to 2.1. Since the attenuation factors for the peak air blast pressures for these detonations varied from 1.2 to 1.7, the results suggest that air blast pressures had an important effect on the maximum ground acceleration observed on these tests.

The maximum horizontal ground acceleration was of approximately the same magnitude as the maximum vertical ground acceleration respectively for both the nuclear shots and the HE detonations. The ground acceleration levels for the underground nuclear detonation were somewhat greater than for the surface nuclear detonation particularly at small reduced distances. Ground acceleration levels for the underground HE-2 detonation was approximately 2.66 times greater than those obtained for the nuclear underground detonation at a reduced distance of 10. Scaling laws indicate that HE-2 detonation scaled to the underground nuclear, should give a scale factor of 3.7.

Good correlation was found to exist between the laws of attenuation for maximum ground acceleration for the underground nuclear detonation and for the underground HE detonation as evidenced by similar attenuation factors. However, the levels of ground acceleration for these two detonations did not differ in accordance with differences expected from scaling effects involving the weights of the explosives. Poor correlation was found to exist between the prediction equation for the surface nuclear shot based on the underground HE shot, and the experimental

curve of ground acceleration found for the surface nuclear shot. This was probably due to the lack of accurate coupling factors for the two charges having different effective burial depths.

The prediction equations for the surface and underground nuclear detonations based on the use of HE-2 results showed better agreement with the experimental data than the calculations of ground acceleration based on the use of ground pressure data. In the latter case the calculated ground acceleration levels for the nuclear detonations differed from the experimental data by a factor of approximately 4.

The prediction equations derived from small charge detonation in other types of soils and for greater scale burial depths of gauges and charge were found inapplicable to the present experimental data.

## 4.2 RECOMMENDATIONS

To obtain a more thorough understanding of the effects of underground explosions, it appears that more refined measurements under more ideal conditions of testing are necessary. These should be made with the view of determining the effects of geology and air blast pressures on the resulting accelerations, particularly with respect to burial depth of charge and gauges. A small charge program would probably be an effective but difficult beginning study and should yield information which might be more helpful in the interpretation of data from the large nuclear detonations for cases where gauge burial depth is shallow scalewise, i.e.; $0.079\lambda$ and $0.158\lambda$. Such scale depths for small nuclear charges are comparable to normal foundation depths of buildings.

It is believed that efforts should be made at the present time to develop a more satisfactory self-recording accelerometer than that used in the present study. Self-recording accelerometers having satisfactory dynamic range and response would be superior to other systems requiring cables for the transmission of data to remote recording stations because they would be less subject to electromagnetic disturbances from the nuclear explosions.

[redacted] CONFIDENTIAL

PART II

TRANSIENT GROUND PRESSURES

CHAPTER 5

INTRODUCTION

## 5.1 GENERAL

The preparation by the Ballistic Research Laboratories (BRL) for taking measurements of Ground Shock Phenomena resulting from underground nuclear explosions began in the Fall of 1950. This operation was originally called "Project WINDSTORM" by the Armed Forces Special Weapons Project and later changed to Operation JANGLE when the operation was taken over jointly by the Special Weapons Command (SWC) and the Los Alamos Scientific Laboratory (LASL) in the Summer of 1951.

Initial studies of the phenomena involved were made during the Winter and Spring months of 1950-51 to decide upon the necessary instrumentation for this project.

Preliminary high explosive tests were conducted at the Nevada Test Site to determine soil transmission characteristics at this location in order to allow a reasonable prediction of the transient effects to be expected from nuclear explosions. The two HE tests (HE-1 and HE-2) that BRL participated in were fired on 25 August 1951 and 3 September 1951, respectively.

Installation of equipment for the two nuclear tests, (surface and underground) took place during October and November 1951. These detonations took place on 19 and 29 November 1951, respectively.

## 5.2 OBJECTIVE

To measure transient ground pressures as a function of time at various distances from the detonation of a surface and an underground nuclear explosion.

To determine from these measurements, the laws of attenuation of the phenomena through the ground.

To determine the degree of correlation between the pressure-distance relation found and those obtained from HE explosions at comparable depths



[redacted] [redacted] CONFIDENTIAL

in the same type soil, as well as those derived by other agencies for various charge depths and sizes in different types of soil.

## 5.3 PREVIOUS RELATED WORK

One of the most comprehensive studies of transient ground phenomena was conducted by Division 2 of the National Defense Research Committee (NDRC) 1. In the final report of this committee, empirical formulae were derived relating peak ground pressure, impulse, particle velocity, and acceleration as a function of distance, size of charge, depth of charge and gauges, and type of soil. The largest charge used in this program was 2,500 lbs of TNT.

A program conducted by the Corps of Engineers using larger charges, up to 320,000 lbs of TNT, was instrumented in part by Stanford Research Institute (SRI) 2 at Dugway, Utah in May 1951. Transient ground pressures as a function of charge and gauge depth were found to have high attenuation factors as predicted by the empirical formulae established by C. W. Lampson in reference 1 for shallow charges.

## 5.4 BASIC FORMULAE AND PREDICTIONS

Initial predictions for transient ground pressures for the surface shot and the underground shot were based on the formula developed by C. W. Lampson (reference 1). The magnitude of the peak ground pressure is given by the following equations:

$$p = FEk\lambda^{-n}, \tag{5.1}$$

where p = peak pressure in pounds per square inch.

F = a coupling factor dependent on depth of burial of charge.

E = a constant determined by the type of explosive.

k = soil constant having the dimensions of pounds per square inch.

---

1 C. W. Lampson, "Final Report on Effects of Underground Explosions" NDRC Report No. A-479 (OSRD-6645).

2 E. B. Doll, Interim Report "Underground Explosions at Dugway", Corps of Engineers, U. S. Army Contract DA-04-167-ENG-379 Stanford Research Institute, July 1951.

$\lambda$ = reduced distance defined as the ratio of the horizontal distance from ground zero in feet and the cube root of the charge weight in pounds.

n = attenuation factor determined by the depth of charge or gauge.

This equation has been pointed out to be a best fit in the range of reduced distances of $2 < \lambda < 15$, and the general value of the exponent n is 3 except for charge depths or gauge depths less than the critical value of $3/2\ W^{1/3}$. For depths less than this critical value, the exponent approaches the value of 4.

For TNT buried at depths greater than $2\ W^{1/3}$ and with gauges at depths greater than $3/2\ W^{1/3}$, equation (5.1) for peak ground pressure reduces to:

$$p = k\lambda^{-3}, \tag{5.2}$$

In this equation k has been defined as a soil constant related to a modulus of elasticity and is approximated by the following equation:

$$k = 1/2\rho v^2 \tag{5.3}$$

where $\rho$ = density of soil in slugs per cubic inch.

v = seismic velocity in feet per second.

k = soil constant in pounds per square inch.

Equation (5.3) is dimensionally accurate if it is assumed that the factor 1/2 has the dimensions of inches per foot. This has been taken into consideration by C. W. Lampson (reference 1) in the development of the equation from empirical data.

Since the explosions instrumented by this group at the Nevada Test Site were located near the surface ($\lambda c = 0.135$ for the underground shots), an explosive coupling factor of 0.33 (from reference 1) was used in equation 5.2 to predict the pressure. Equation (5.1) then becomes:

$$p = 0.33k\lambda^{-4}, \tag{5.4}$$

The value for k in equation 5.4 was calculated from the information obtained from a report written by the United Geophysical Company, Inc. [3] who have conducted a geophysical survey of the area. This report gives the seismic velocities versus depth, and the values vary as follows:

---

3 United Geophysical Company, Inc., "Seismic Refraction Survey", Navy Contract NOT-26616, Nye County, Nevada.

| Depth | Velocity |
|---|---|
| 0 - 100 ft | 3,000 ft/sec |
| 100 ft - 350 ft | 4,000 - 4,500 ft/sec |
| 350 ft and deeper | 5,000 - 5,500 ft/sec |

The density near the surface is about 90 lbs/cu ft with some layers of cemented caliche of varying thicknesses occuring at various depths. Therefore, the value of k, according to the equation (5.3), is approximately:

$$k = 10{,}400 \text{ psi.}$$

# CHAPTER 6

## EXPERIMENTAL PROCEDURE

### 6.1 FIELD LAYOUT

A description of the ground pressure gauges used in the present work with their location on the various blast ranges is given below. The description of the recording system for these gauges may be found in the report on ground accelerations for Operation JANGLE by the Naval Ordnance Laborat

#### 6.1.1 General Description of Gauges

The primary requirement for measuring transient ground pressure during this operation involved the selection of gauges having characteristics such that they could be used in conjunction with the recording system developed by the Naval Ordnance Laboratory (NOL). A variable inductance gauge manufactured by the Wiancko Engineering Co., Pasadena, California, was found suitable for the purpose. This gauge consists essentially of an "E" coil and a twisted Bourdon tube with a high permeability slug attached to it. A transient pressure change displaces the Bourdon tube and slug, and this causes a change in the inductance of the "E" coil. The "E" coil is the inductance element of a Hartley oscillator, so that a change in inductance causes a change in the frequency of the oscillator which is remotely recorded on a tape recorder. The Wiancko gauge is designed to respond to transient hydrostatic pressures.

#### 6.1.2 Blast Range Layout, Surface Shot (Nuclear)

A total of 24 ground pressure gauges were used for this shot. These gauges were placed in holes of different depths located at 12 stations varying in range from 275 ft to 3,000 ft from ground zero. All holes were approximately 8 ins in diameter and depths were 10 ft, 20 ft, and 30 ft. Table 6.1 lists the locations of the gauges with respect to horizontal distance from ground zero and depth.

A mixture of "Aqua-Gel" (Bentonite clay) and water was used as a coupling medium for the pressure gauges. Proper consistency was obtained by mixing thoroughly 200 pounds of "Aqua-Gel" in 400 gallons of water with a circulatory pump. All holes were completely filled with this mixture and then covered with plywood and approximately 6 ins of earth. The seepage rate of "Aqua-Gel" through the ground was very low, being of the order of 1 ft per day for a 20 ft hole depth. Figure 6.1 is a photograph of a lateral trench at Station 2 showing the ground pressure holes. The steel cylinders shown contain the Hartley oscillators

TABLE 6.1

Blast Range Layout, Surface Shot

| Station No. | Distance (ft) | $\lambda$ $R/W^{1/3}$ | 10' Holes Gauge No. | 10' Holes Gauge Range | 10' Holes Gauge Depth | 20' Holes Gauge No. | 20' Holes Gauge Range | 20' Holes Gauge Depth | 30' Holes Gauge No. | 30' Holes Gauge Range | 30' Holes Gauge Depth |
|---|---|---|---|---|---|---|---|---|---|---|---|
| 1 | 275 | 2.18 | 5523 | 50 | 10' | | | | | | |
| 2 | 340 | 2.70 | 5535 | 25 | 10' | 5524(a) | 50 | 10' | 5527 | 25 | 30' |
| | | | | | | 5531 | 25 | 20' | | | |
| 3 | 420 | 3.34 | 5536 | 15 | 10' | | | | | | |
| 4 | 520 | 4.13 | 5524 | 10 | 10' | | | | | | |
| 5 | 642 | 5.09 | 5553 | 5 | 10' | 5547 | 5 | 20' | 5537(a) | 15 | 10' |
| | | | | | | | | | 5545 | 5 | 30' |
| 6 | 794 | 6.31 | 5569 | 2 | 10' | | | | | | |
| 7 | 982 | 7.80 | 5559 | 2 | 10' | | | | | | |
| 8 | 1213 | 9.63 | 5565 | 2 | 10' | 5550(a) | 5 | 10' | 5557 | 2 | 30' |
| | | | | | | 5548 | 5 | 20' | | | |
| 9 | 1500 | 11.91 | 5561 | 2 | 10' | | | | | | |
| 10 | 1890 | 15.0 | 5560 | 2 | 10' | 5573 | 2 | 20' | 5551(a) | 5 | 10' |
| | | | | | | | | | 5549 | 5 | 30' |
| 11 | 2381 | 18.88 | 5564 | 2 | 10' | | | | | | |
| 12 | 3000 | 23.80 | 5558 | 2 | 10' | | | | | | |

(a) Back-up Gauges

$W = 1$ kT; $W^{1/3} = 126$

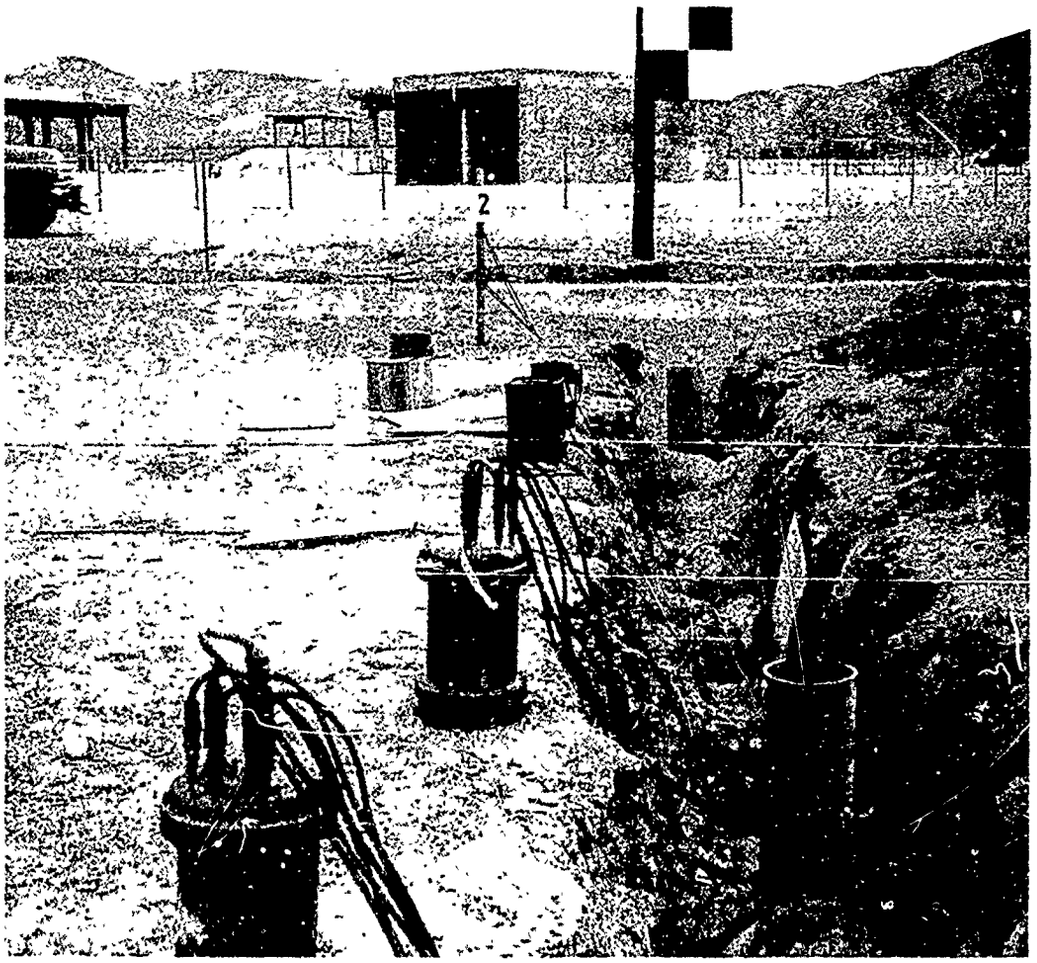


Fig. 6.1 Lateral Trench

to which the pressure gauges were connected by means of shielded cables.

6.1.3 Blast Range Layout for Underground Shot (Nuclear)

Twenty-five pressure gauges were used on the blast range for this shot. The gauges were placed in holes of varying depths located at 13 stations ranging in horizontal distance from 200 ft to 3,000 ft from ground zero. The gauge locations at the various stations are listed in Table 6.2. "Aqua-Gel" was used as the coupling medium previouly described in Paragraph 6.1.1. The holes at stations 3, 6, 9, 12 were covered with sandbags, all the others were left open to air.

### 6.1.4 Blast Range Layout for Shot HE-2 (HIGH EXPLOSIVE)

Seven stations at horizontal distance ranging from 85 to 512 ft, were used for this shot. All gauges were placed in holes 5 ft deep. These holes were filled with "Aqua-Gel" solution of the same consistency as described in Paragraph 6.1.1 and covered with a layer of dirt. Table 6.3 lists the gauge locations

## 6.2 DETAILED DESCRIPTION OF TEST EQUIPMENT

A detailed description of the Wiancko pressure gauge is given in the paragraph below.

### 6.2.1 The Wiancko Pressure Gauges

Figure 6.2 shows a cut-away section of the Wiancko gauge used for this program. The gauge consists of an "E" coil and a twisted Bourdon tube with a high premeability slug attached to its closed end. The "E" coil is housed in the cylindrical steel casing, and the Bourdon tube, which is the pressure sensitive element, is encased in a rubber bag. The gauge is completely filled with oil. The oil serves as a medium to transmit transient pressures, and provides damping. Automatic compensation for external static pressure changes due to the gauge being buried underground is provided for in the instrument. This pressure compensation is accomplished by means of a porous plug which permits a slow movement of oil from outside the Bourdon tube to the inside of the steel casing when a long time pressure differential exists. Since the pressure equalization time is about 10 minutes, transient pressures are measured with negligible error due to the release of pressure through the porous plug.

The "E" coil acts as the inductance element of a Hartley oscillator. An application of a transient pressure to the Bourdon tube, through the oil-filled bag, causes the tube to untwist and move the slug in the air gap of the "E" coil, thus varying the inductance and in turn, resulting in a frequency change of the oscillator. The frequency shift is recorded on a magnetic tape. A calibration curve showing a plot of frequency shift versus pressure is supplied with each gauge. When the frequency shift has been calculated from records, the pressure is obtained directly from the calibration curve by finding the pressure which corresponds to the frequency shift calculated.

The Hartley oscillator is part of a frequency-modulated recording system employed by NOL. Detailed descriptions of the oscillator and the F. M. recording system may be found in a report published by NOL on acceleration measurements for Operation JANGLE.

TABLE 6.2

Blast Range Layout, Underground Shot

| Station No. | Distance (ft) | $\lambda$ $R/W^{1/3}$ | 10' Holes Gauge No. | 10' Holes Gauge Range | 10' Holes Gauge Depth | 20' Holes Gauge No. | 20' Holes Gauge Range | 20' Holes Gauge Depth | 30' Holes Gauge No. | 30' Holes Gauge Range | 30' Holes Gauge Depth |
|---|---|---|---|---|---|---|---|---|---|---|---|
| A | 200 | 1.59 | 5506 | 275 | 10' | | | | | | |
| 1 | 275 | 2.18 | 5518 | 100 | 10' | 5512(a) | 150 | 20' | 5517 | 100 | 30' |
| | | | | | | 5521 | 100 | 20' | | | |
| 2 | 340 | 2.70 | 5519 | 100 | 10' | | | | | | |
| 3(b) | 420 | 3.34 | 5522 | 50 | 10' | | | | | | |
| 4 | 520 | 4.13 | 5528 | 25 | 10' | | | | | | |
| 5 | 642 | 5.09 | 5529 | 25 | 10' | 5534 | 25 | 20' | 5520(a) | 100 | 30' |
| | | | | | | | | | 5525 | 25 | 30' |
| 6(b) | 794 | 6.31 | 5530 | 25 | 10' | | | | | | |
| 7 | 982 | 7.80 | 5533 | 25 | 10' | | | | | | |
| 8 | 1213 | 9.63 | 5543 | 10 | 10' | 5532(a) | 25 | 20' | 5541 | 10 | 30' |
| | | | | | | 5540 | 10 | 20' | | | |
| 9(b) | 1500 | 11.91 | 5539 | 10 | 10' | | | | | | |
| 10 | 1890 | 15.00 | 5552 | 5 | 10' | 5544 | 5 | 20' | 5526(a) | 25 | 30' |
| | | | | | | | | | 5546 | 5 | 30' |
| 11 | 2381 | 18.88 | 5557 | 5 | 10' | | | | | | |
| 12(b) | 3000 | 23.80 | 5562 | 2 | 10' | | | | | | |

(a) Back-up Gauges

(b) Holes covered with sandbags

$W = 1$ kT; $W^{1/3} = 126$





SECRET

RESTRICTED DATA

TABLE 6.3

Blast Range Layout, HE-2

| Station No. | Distance (ft) | $\lambda$ $R/W^{1/3}$ | Gauge No. | Range psi | Depth (ft) |
|---|---|---|---|---|---|
| 1 | 85.5 | 2.5 | 5531 | 25 | 5 |
| 2 | 102.5 | 3.1 | 5543 | 10 | 5 |
| 3 | 123.0 | 3.6 | 5550 | 5 | 5 |
| 3(a) | 123.0 | 3.6 | 5530 | 25 | 5 |
| 4 | 178.0 | 5.2 | 5559 | 2 | 5 |
| 5 | 262.0 | 7.7 | 5562 | 2 | 5 |
| 5(a) | 262.0 | 7.7 | 5542 | 5 | 5 |
| 6 | 378. | 11. | 5565 | 2 | 5 |
| 7 | 512. | 16.7 | 5572 | 2 | 5 |

(a) Back-up Gauges

$W = 40,000$ lbs

$W^{1/3} = 34.2$

Characteristics of the pressure gauge are such that its natural frequency is 75 cycles/second or greater. The inductance of the coil is 130 millihenries and its Q is 5 measured at 1,000 cycles/second. The full scale output of the gauge corresponds to an inductance change of $\pm$ 15%.

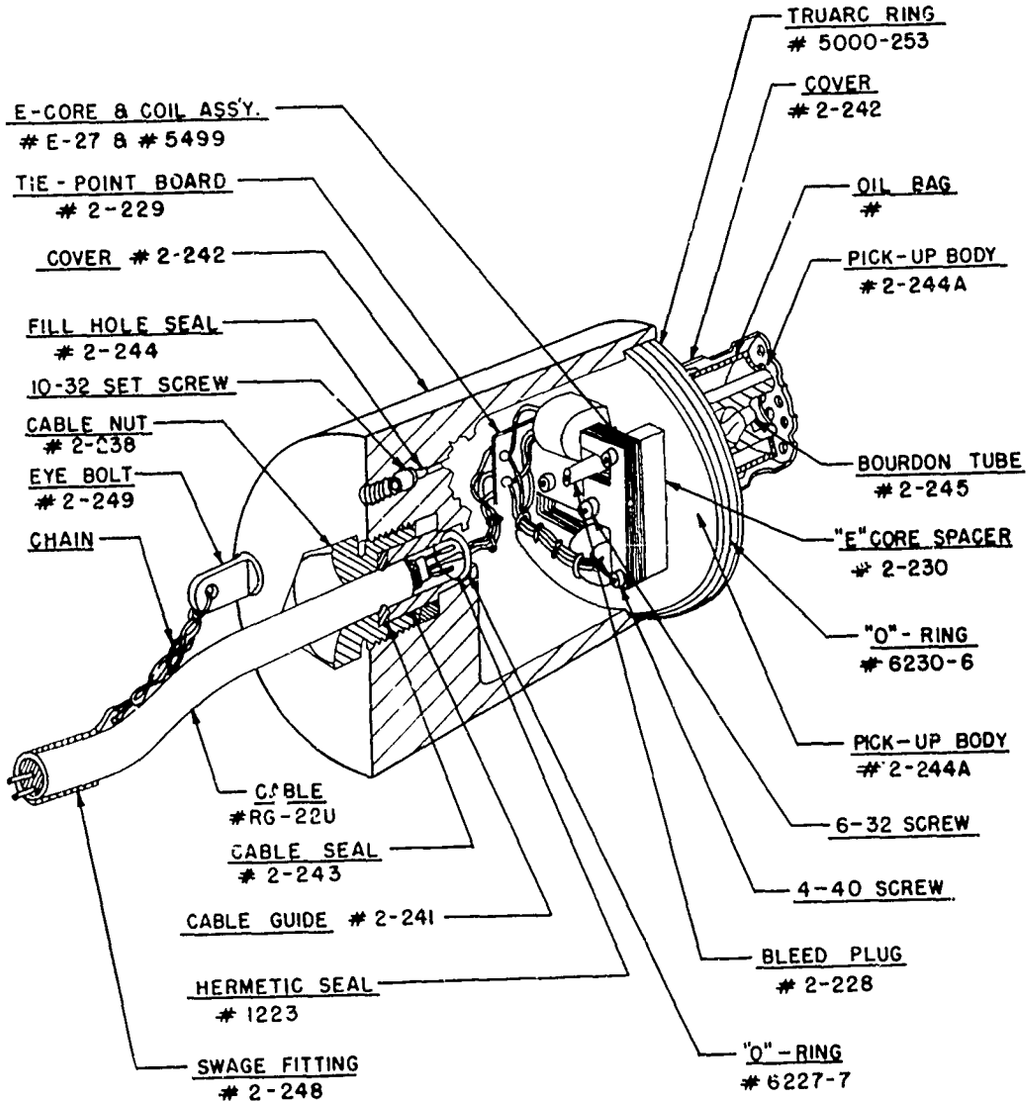


Fig. 6.2. Wiancko Pressure Gauge (Cut-Away Section)

# CHAPTER 7

## TEST RESULTS

### 7.1 SURFACE SHOT (NUCLEAR)

The surface shot was fired at a scaled charge height of $\lambda c = 0.024$ based on 1 kT equivalent TNT charge weight. Table 7.1 presents the ground pressure data as calculated from the pressure records. The information includes the values of three peaks noted on the records, i.e. the first positive rise peak, the maximum positive peak excluding air blast effects, and the maximum positive peak including air blast effects. The latter maximum positive peak is apparently due to a pressure induced into the "Aqua-Gel" by air blast when it arrives at the station. The arrival time for air blast along the surface of the ground was obtained from velocity measurements taken by the air blast section of BRL 4 and plotted on the ground pressure records. The highest peaks on the pressure records occurred just after the arrival of air blast at each station.

Curves have been fitted by the method of least squares to the points, assuming a pressure-distance relation of the form $p = A\lambda^{-n}$.

The points for the 10 ft gauge depths and 20 ft gauge depths of the first positive rise peaks shown in Fig. 7.1 yielded the following equations:

$$p_1 = 11.87\lambda^{-1.43} \text{ - 10 ft gauge depth,} \tag{7.1}$$

$$p_1 = 12.20^{-1.17} \text{ - 20 ft gauge depth.} \tag{7.2}$$

The curves for the maximum positive ground pressure peaks, excluding air blast effects, for the 10 ft gauge depths, and the 20 ft gauge depths are shown in Fig. 7.2. The equations for these points are:

$$p_2 = 28.38\lambda^{-1.42} \text{ - 10 ft gauge depth,} \tag{7.3}$$

$$p_2 = 33.52\lambda^{-1.20} \text{ - 20 ft gauge depth.} \tag{7.4}$$

---

4 W. F. Molesky, R. E. Eberhard, C. N. Kingery, "Peak Air Blast Pressures from Shock Velocity Measurements Along the Ground", Operation JANGLE, Project 1.2a-1.

TABLE 7.1

Ground Pressure Data, Surface Shot

| Station Number and Gauge Depth | $\lambda$ $R/W^{1/3}$ | 1st Rise | | Maximum Positive Excluding Air Blast Effect | | Maximum Ground Pressure Including Air Blast Effect | |
|---|---|---|---|---|---|---|---|
| | | % Frequency Shift | Pressure psi | % Frequency Shift | Pressure psi | % Frequency Shift | Pressure psi |
| 1-10 | 2.18 | .55 | 4.9 | 2.09 | 16.5 | 6.0 | 42.0 |
| 2-10 | 2.70 | | | | | | |
| 2-10(a) | 2.70 | | | | | | |
| 2-20 | 2.70 | .48 | 3.5 | 3.0 | 10.75 | 5.5 | 18.75 |
| 2-30 | 2.70 | | | | | | |
| 3-10 | 3.34 | | | | | | |
| 4-10 | 4.13 | 1.65 | 2.5 | | | | |
| 5-10 | 5.09 | 1.05 | .78 | 2.70 | 1.98 | | |
| 5-10(a) | 5.09 | | | | | | |
| 5-20 | 5.09 | 2.70 | 1.90 | 6.5 | 4.3 | | |
| 5-30 | 5.09 | 2.34 | 1.73 | | | | |
| 6-10 | 6.31 | | | | | | |
| 7-10 | 7.80 | 1.79 | .54 | 2.03 | .61 | | |
| 8-10 | 9.63 | 1.17 | .35 | 2.32 | .67 | | |
| 8-10(a) | 9.63 | .50 | .40 | 1.67 | 1.25 | | |
| 8-20 | 9.63 | 1.40 | 1.05 | 3.07 | 2.26 | 4.2 | 3.0 |
| 8-30 | 9.63 | | | | | 2.5 | 1.82 |
| 9-10 | 11.91 | | | | | | |
| 10-10 | 15.00 | .795 | .24 | 3.0 | .88 | | |
| 10-10(a) | 15.00 | .522 | .40 | 2.09 | 1.63 | | |
| 10-20 | 15.00 | 1.46 | .43 | 4.69 | 1.32 | | |
| 10-30 | 15.00 | | | | | | |
| 11-10 | 18.88 | .493 | .16 | 1.075 | .33 | | |
| 12-10 | 23.80 | | | | | 6.15 | 1.68 |

(a) Back-up Gauges



PROJECT 1.2a-21

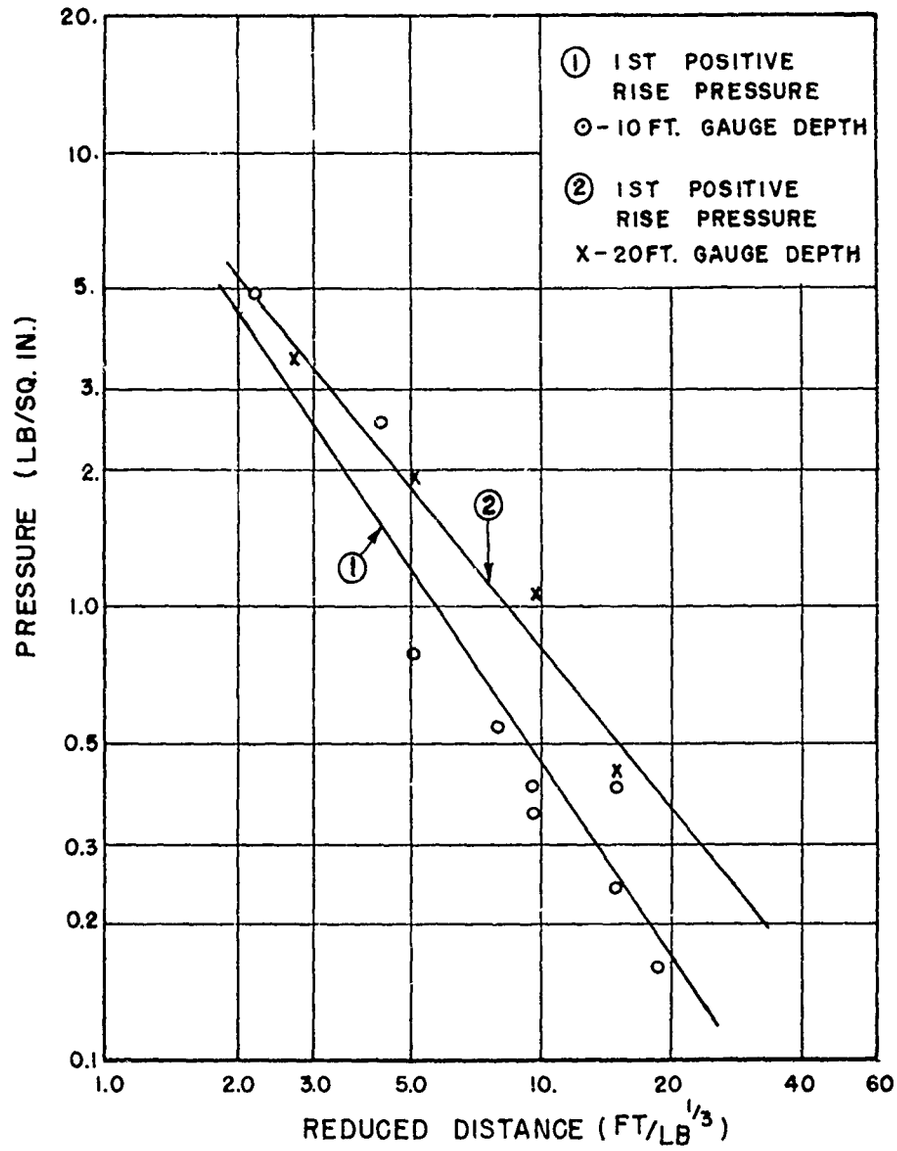


Fig. 7.1. Variation of Ground Pressure with Reduced Distance for Surface Nuclear Shot (First Positive Rise, Gauge Depths 10 ft and 20 ft)

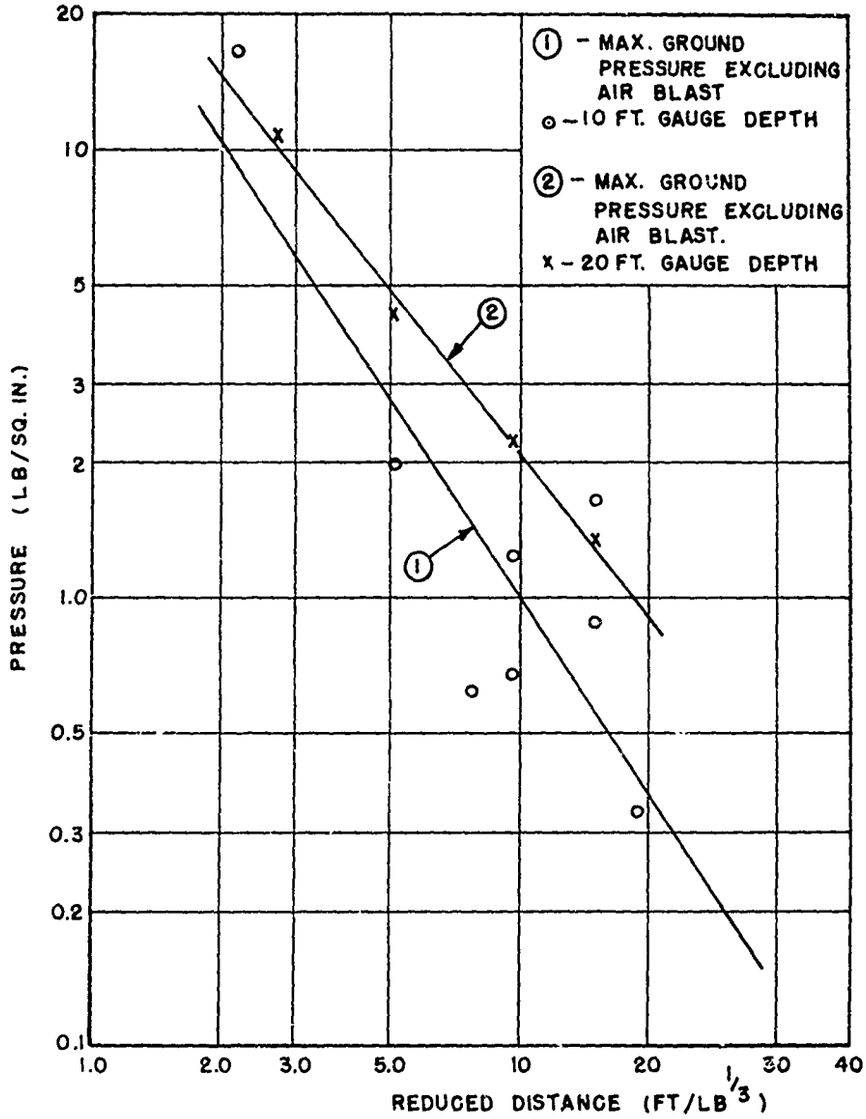


Fig. 7.2 Variation of Ground Pressure with Reduced Distance for Surface Nuclear Shot (Maximum Positive Rise Excluding Air Blast Effect; Gauge Depths 10 ft and 20 ft)

The highest positive maximum peak ground pressure including air blast effects, and air blast pressures along the surface of the ground are shown in Fig. 7.3. The air blast pressure curve was obtained from the velocity measurements taken by BRL (Reference 4) group project 1.2a-1. The equation best fitting the ground pressure curve for this condition is:

$$p_3 = 83.50\lambda^{-1.40}. \tag{7.5}$$

The equation of the corresponding peak air blast pressures as determined by the velocity method mentioned in reference 4 is:

$$p_{AB} = 443.10\lambda^{-1.74}, \tag{7.6}$$

for pressure levels less than 20 psi.

## 7.2 UNDERGROUND SHOT (NUCLEAR)

The depth of the underground shot was 17 feet, equivalent to a scaled charge depth of $\lambda = 0.135$ again based on 1 kT equivalent TNT charge weight. The ground pressure records obtained from this shot were poor as shown by the paucity of data in Table 7.2. There were no curves drawn nor equations obtained for the pressures of the first rise or the maximum positive pressures excluding air blast effects because of insufficient data points obtained. The curve for pressure of maximum positive peaks including air blast effects was fitted by the method of least squares and is shown in Fig. 7.4. The curve may be expressed by the following equation:

$$p_3 = 34.59\lambda^{-.83} \tag{7.7}$$

Together with this curve, a plot of the air blast pressures obtained by the velocity method (reference 4) is shown. The equation for the corresponding peak air blast pressures for this shot is:

$$p_{AB} = 84.31\lambda^{-1.19}. \tag{7.8}$$

## 7.3 HE-2 TEST (HIGH EXPLOSIVE)

The charge weight for this test was 40,000 lbs of TNT and the depth of charge was $\lambda c = 0.135$ similar to the scaled depth of the underground nuclear shot. Table 7.3 shows the ground pressure data, and Fig. 7.5 shows the curves of the first positive rise peaks and the highest maximum positive peaks including air blast effects together with the predicted curve. Analysis of the data by the method of least squares yielded the following equations of best fit:

SECRET
Security Information
CONFIDENTIAL

PROJECT 1.2a-2

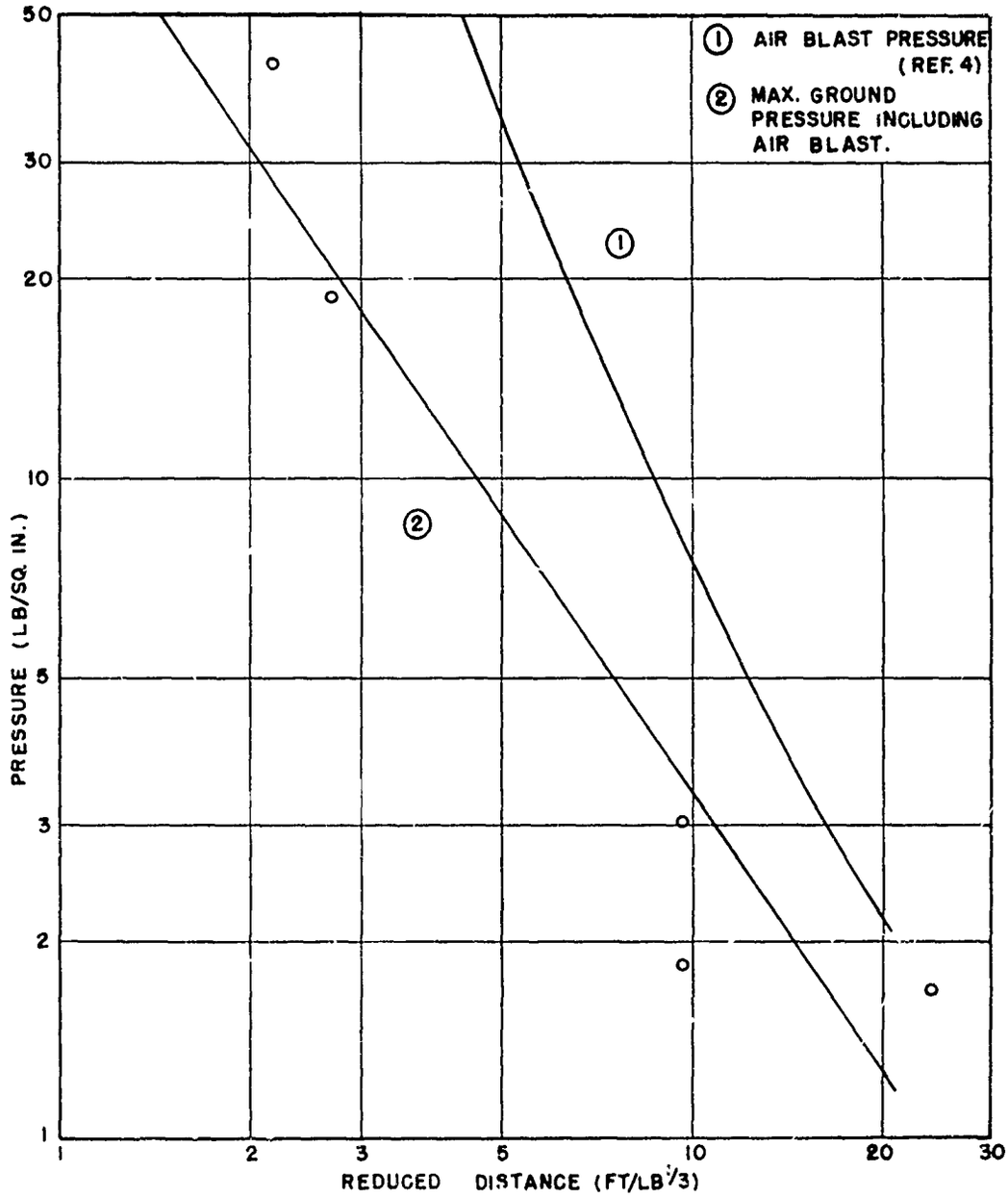


Fig. 7.3. Variation of Ground Pressure with Reduced Distance for Surface Nuclear Shot (Highest Positive Peak Including Air Blast Effect)



SECRET
Security Information
CONFIDENTIAL
RESTRICTED DATA
ATOMIC ENERGY ACT 1946

[redacted]

[redacted]

TABLE 7.2

Ground Pressure Data, Underground Nuclear Shot

| Station Number and Gauge Depth | $\lambda$ $R/W^{1/3}$ | 1st Rise | | Maximum Positive Excluding Air Blast Effect | | Maximum Ground Pressure Including Air Blast Effect | |
|---|---|---|---|---|---|---|---|
| | | % Frequency Shift | Pressure psi | % Frequency Shift | Pressure psi | % Frequency Shift | Pressure psi |
| A-10 | 1.59 | | | | | .354 | 25 |
| 1-10 | 2.18 | | | | | 1.035 | 16 |
| 2-10 | 2.70 | | | | | 1.00 | 15.5 |
| 2-20 | 2.70 | | | | | .328 | 5.00 |
| 2-20(a) | 2.70 | | | | | .333 | 5.83 |
| 2-30 | 2.70 | | | | | .364 | 8.30 |
| 3-10(b) | 3.34 | | | | | .424 | 10.40 |
| 4-10 | 4.13 | | | | | 3.74 | 13.75 |
| 5-10 | 5.09 | | | | | 2.86 | 10.38 |
| 5-20 | 5.09 | | | | | 1.54 | 6.50 |
| 5-30 | 5.09 | | | | | 4.13 | 14.6 |
| 5-30(a) | 5.09 | | | | | 1.52 | 16.5 |
| 6-10(b) | 6.31 | .085 | .44 | | | 1.36 | 5.00 |
| 7-10 | 7.80 | | | .278 | 1.25 | 2.64 | 9.12 |
| 8-10 | 9.63 | .178 | .25 | .286 | .50 | 3.50 | 5.20 |
| 8-20 | 9.63 | .267 | .50 | 1.865 | 2.85 | 4.40 | 6.40 |
| 8-20(a) | 9.63 | | | | | | |
| 8-30 | 9.63 | | | | | | |
| 9-10(b) | 11.91 | .182 | .30 | .694 | 1.00 | 2.49 | 3.60 |
| 10-10 | 15.00 | | | | | | |
| 10-20 | 15.00 | | | | | | |
| 10-30 | 15.00 | .334 | .25 | 3.54 | 2.57 | 5.0 | 3.50 |
| 10-30(a) | 15.00 | | | | | | |
| 11-10 | 18.88 | .177 | .15 | .6 | .475 | 4.45 | 3.10 |
| 12-10(b) | 23.80 | | | | | | |

(a) Back-up Gauges

(b) Holes covered with sandbags



[redacted]

[redacted]

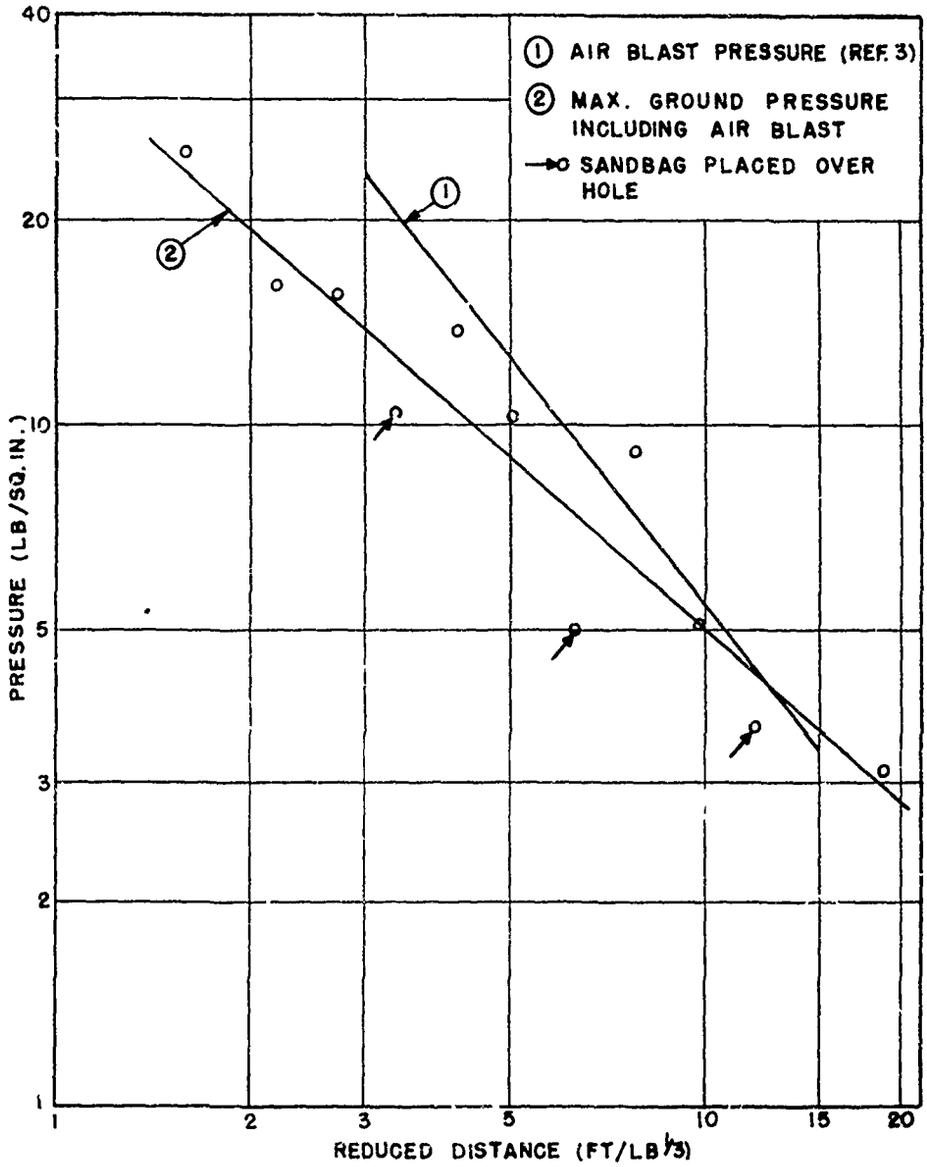


Fig. 7.4. Variation of Ground Pressure with Reduced Distance for Underground Nuclear Shot (Highest Positive Peak Including Air Blast Effect)

TABLE 7.3

HE-2 Pressure Data

| Station No. | $\lambda$ $R/W^{1/3}$ | 1st Rise | | Highest Positive Maximum Including Air Blast Effect | |
|---|---|---|---|---|---|
| | | % Frequency Shift | Pressure psi | % Frequency Shift | Pressure psi |
| 1 | 2.5 | 1.7 | 6.25 | | |
| 2 | 3.1 | 2.6 | 3.9 | 5.6 | 7.8 |
| 3 | 3.6 | 3.25 | 2.35 | 7.3 | 4.9 |
| 3(a) | 3.6 | .7 | 2.55 | 1.65 | 4.5 |
| 4 | 5.2 | 2.35 | .70 | | |
| 5 | 7.7 | .8 | .56 | | |
| 5(a) | 7.7 | 1.55 | .45 | | |
| 6 | 11. | .75 | .22 | 8.75 | 2.16 |
| 7 | 16.7 | .65 | .20 | 11.1 | 3.00 |

$$p_1 = 23.90\lambda^{-1.77}, \tag{7.9}$$

$$p_3 = 10.57\lambda^{-0.54}, \tag{7.10}$$

where $p_1$ = pressure of the first positive rise peaks.

$p_3$ = pressure of the maximum positive peaks including air blast effects.

The equation for the corresponding peak air blast pressures for this shot as determined from the measurements in reference 4 is:

$$p_{AB} = 84.31\lambda^{-1.19}. \tag{7.11}$$

## 7.4 DISCUSSION OF TEST RESULTS

The attenuation factors for all transient ground pressures found for these tests are considerably less than those predicted by the equations of Lampson's OSRD report (reference 1) derived from smaller charges in different types of soils and for deeper gauge burial depths. The attenuation of the maximum positive ground pressure including air blast effects for the surface shot is greater than for the underground shot. This is as it should be, because the attenuation of air blast pressures along the surface of the ground is greater for the surface shot. Other observations of the test results for the surface shot are:

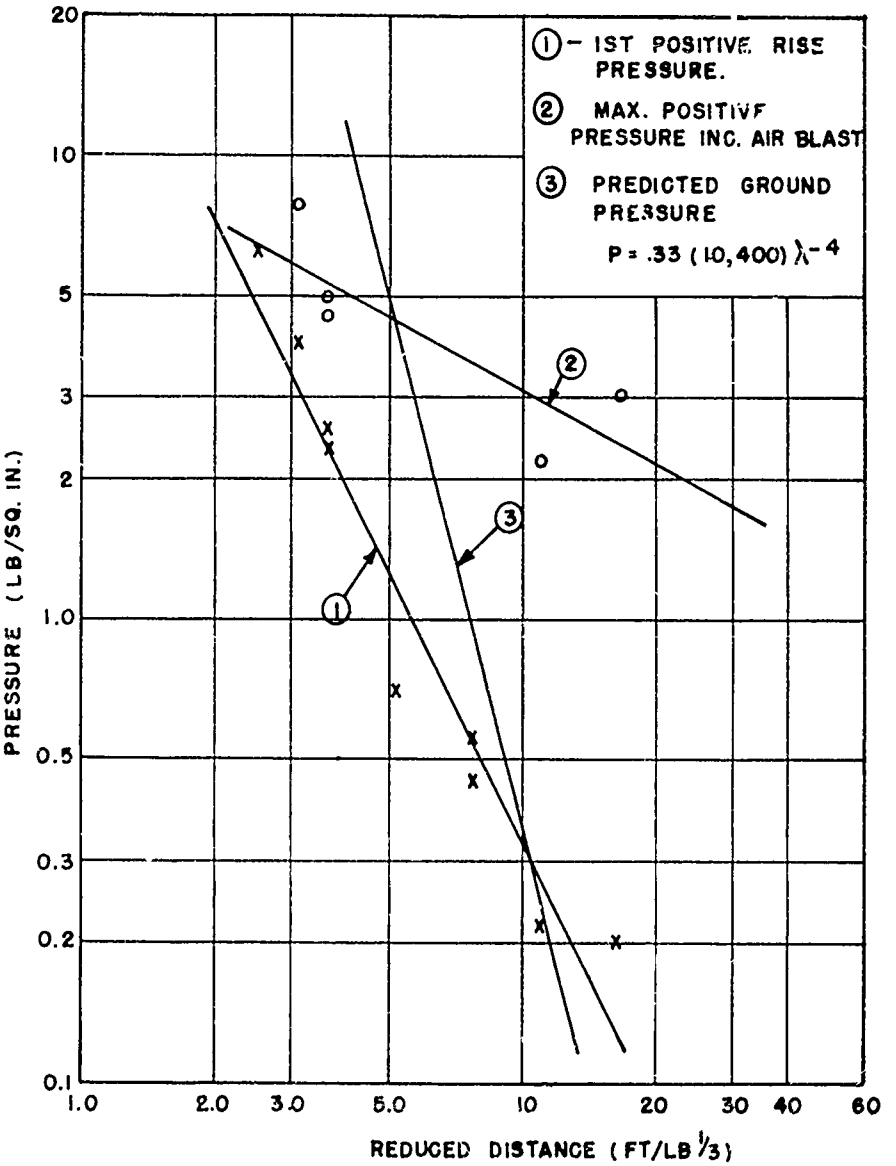


Fig. 7.5 Variation of Ground Pressures with Reduced Distances for Underground HE-2 Shot

1. At the 10 ft gauge depth, the first positive pressure and the maximum pressure excluding air blast effects attenuate at the same rate.

2. At the 20 ft gauge depth, the first positive pressure and the maximum pressure excluding air blast effects also attenuate at the same rate.

3. The first positive pressure and the maximum pressure excluding air blast effects attenuate at a somewhat greater rate for 10 ft gauge depths than at 20 ft gauge depths.

4. The first positive ground pressure peak is less at the 10 ft gauge depth than the first positive ground pressure peak at the 20 ft gauge depth.

5. The maximum ground pressure excluding air blast effects is less at the 10 ft gauge depth than the maximum pressure excluding air blast effects at the 20 ft gauge depth.

6. The maximum pressures including air blast effects are approximately 8 times greater than the first positive pressures and approximately 3 times greater than the maximum pressures excluding air blast effects.

Observations of the test results for the underground shot are:

1. The first rise and maximum ground pressure excluding air blast effect were very small at distances close to zero. These values were so small compared to maximum ground pressure, including air blast effect, that they were not readable on the records. At the farther distances from zero some values were obtained and are indicated in Table 7.2.

2. The curve in Fig. 7.4 indicates that the maximum ground pressures obtained are effectively due to summation of ground pressure transmission through the ground with the coupled air blast effect. The air blast pressures along the surface of the ground are of greater magnitude than the maximum ground pressure including air blast effect. The attenuation of both the air blast curve and the maximum ground pressure including air blast effect are approximately of the same order.

3. Covering the gauge holes with sandbags as done at Stations 3, 6, 9, and 12 for the underground shot, apparently reduces the air blast effect as indicated by the points of Fig. 7.4.

# CHAPTER 8

## CONCLUSIONS AND RECOMMENDATIONS

### 8.1 CONCLUSIONS - GROUND PRESSURES

Ground pressures as a function of time resulting from the detonations of a surface nuclear charge and an underground nuclear charge buried at a depth of 17 feet ($\lambda c = 0.135$) have been measured at various horizontal distances from ground zero along a radial line. Of the many ground pressure peaks observed on the records, 3 have been investigated in detail in the present work. These have been defined as the first positive ground pressure peak, the maximum ground pressure peak excluding air blast effects, and the maximum ground pressure peak including air blast effects. Based on arrival time data, the first two of these ground pressure transients appear to be caused mainly by the transmission of pressure from the source through the ground, whereas the maximum ground pressure including air blast effects appears to be caused mainly by the peak air blast pressure whose effects are coupled through the ground at the time of its arrival at the gauge stations.

The maximum ground pressures including air blast effects were found to be approximately 8 times greater than the first rise positive ground pressure and approximately 3 times greater than the maximum ground pressure less the air blast effects for all the shots investigated in this work. The free air blast pressure along the surface of the ground was greater than all transient ground pressures indicated on the records. The maximum ground pressure including air blast effects for the nuclear surface shot was greater than the similar transient for the underground nuclear shot for close-in distances of approximately $2\lambda$. No definite information was obtained indicating that the ground pressure transients excluding air blast effects were greater for the underground nuclear shot than for the surface nuclear shot for given horizontal distances from ground zero.

Within the limits of experimental error, simple power laws were found applicable in expressing the pressure-reduced distance relations. In general, the attenuation factors for all ground pressure transients were considerably less than those predicted from equations previously derived from small charges in different types of soils and greater scale burial depths. The attenuation factor of the maximum ground pressure including air blast effects was greater for the surface nuclear shot than for the underground nuclear shot. This was in agreement with the fact that the attenuation factor for peak air blast pressures for the surface shot was also greater than the attenuation factor for the underground shot. Within the limits of these tests, the first positive rise ground

pressure transient and the maximum ground pressure excluding air blast effects increased with greater gauge depths.

Poor correlation was found to exist between the ground pressure reduced distance relations obtained for the underground nuclear and HE shots. This was due to a difference in attenuation factors for these shots. Ground pressures at a distance of 2λ did not differ by more than 10 percent. However, at 20λ the ground pressure for the HE shot was approximately 2 times greater than that for the nuclear shot.

The ground pressure-reduced distance relation derived for small HE charges in different types of soils was found inapplicable as an aid in predicting the effects to be expected from nuclear explosions. This was due mainly to the large difference in their attenuation factors and may be attributed to soil characteristics at the Nevada Test Site. It was noted that the soil at this site held much free air which would considerably reduce pressure transients transmitted through the medium.

It should be noted that previous work was based on depths of gauges equal to approximately 3/2 $W^{1/3}$. The phenomena investigated in this report, especially for the nuclear charges, were for gauge depths of 10' and 20' or scale burial depths of 0.079 and 0.158, respectively. Such burial depths, scale wise, are dealing with phenomena near the surface of the ground and is a rather indeterminate region as previously indicated in work by C. W. Lampson, insofar as true ground propagation is concerned.

## 8.2 RECOMMENDATIONS

Since air blast has been found to have an important effect on the ground pressure-reduced distance relations for surface and shallow underground nuclear explosions, and for shallow depths of placement of the gauges corresponding to normal building foundation depths; the present study has indicated a need for the following:

(1) A study of coupling of the gauges to the medium to give a realistic measure of ground pressure.

(2) Improvement of instrumentation for measuring ground pressures to allow measuring all transients on a single record. This may be accomplished by designing a non-linear gauge element which is more sensitive to low pressure levels.

(3) Theoretical investigation of nature of ground pressures for scale wise shallow depths of burial of gauges with a differentiation between so called "hydrostatic" pressures (scalers) as measured by Wiancko gauges and modified Carlson type gauges which introduce an element of directivity (vector) of the pressure impulse. Carlson gauges indicate normally pressures several times those obtained by "hydrostatic" type measurements.

[redacted] CONFIDENTIAL

DISTRIBUTION

| | Copy No. |
|---|---|
| **ARMY ACTIVITIES** | |
| Asst. Chief of Staff, G-1, Department of the Army, Washington 25, D. C. | 1 |
| Asst. Chief of Staff, G-2, Department of the Army, Washington 25, D. C. | 2 |
| Asst. Chief of Staff, G-3, Department of the Army, Washington 25, D. C. | 3- 6 |
| Asst. Chief of Staff, G-4, Department of the Army, Washington 25, D. C. | 7- 11 |
| Chief of Ordnance, Department of the Army, Washington 25, D. C. | 12- 14 |
| Chief Chemical Officer, Temp. Bldg. T-7, Room G-522, Gravelly Point, Va. | 15- 18 |
| Chief of Engineers, Temp. Bldg. T-7, Room G-425, Gravelly Point, Va. | 19- 21 |
| The Quartermaster General, Second and T Sts. SW, Room 1139A, Washington 25, D. C. | 22- 26 |
| Chief of Transportation, Temp. Bldg, T-7, Room G-816, Gravelly Point, Va. | 27- 28 |
| Chief Signal Officer, Department of the Army, Washington 25, D. C. | 29- 31 |
| The Surgeon General, Main Navy Bldg., Room 1651, Washington 25, D. C. | 32- 34 |
| Provost Marshal General, Main Navy Bldg., Room 1065, Washington 25, D. C. | 35- 37 |
| Chief, Army Field Forces, Fort Monroe, Va. | 38- 41 |
| President, Army Field Forces Board No. 1, Fort Bragg, N. C. | 42 |
| President, Army Field Forces Board No. 2, Fort Knox, Ky. | 43 |
| President, Army Field Forces Board No. 3, Fort Benning, Ga. | 44 |
| President, Army Field Forces Board No. 4, Fort Bliss, Tex. | 45 |
| Commandant, The Infantry School, Fort Benning, Ga. | 46- 47 |
| Commandant, The Armored School, Fort Knox, Ky. | 48- 49 |
| President, The Artillery School Board, Fort Sill, Okla. | 50- 51 |
| Commandant, The AA&GM Branch, The Artillery School, Fort Bliss, Tex. | 52- 53 |
| Commandant, Army War College, Carlisle Barracks, Pa. | 54- 55 |
| Commandant, Command and General Staff College, Fort Leavenworth, Kans. | 56- 57 |
| Commandant, Army General School, Fort Riley, Kans. | 58 |



CONFIDENTIAL [redacted]

DISTRIBUTION (Continued)

| | Copy No. |
|---|---|
| Commanding General, First Army, Governor's Island, New York 4, N. Y. | 59- 60 |
| Commanding General, Second Army, Fort George G. Meade, Md. | 61- 62 |
| Commanding General, Third Army, Fort McPherson, Ga. | 63- 64 |
| Commanding General, Fourth Army, Fort Sam Houston, Tex. | 65- 66 |
| Commanding General, Fifth Army, 1660 E. Hyde Park Blvd., Chicago 15, Ill. | 67- 68 |
| Commanding General, Sixth Army, Presidio of San Francisco, Calif. | 69- 70 |
| Commander-in-Chief, European Command, APO 403, c/o Postmaster, New York, N. Y. | 71- 72 |
| Commander-in-Chief, Far East, APO 500, c/o Postmaster, San Francisco, Calif. | 73- 74 |
| Commanding General, U. S. Army, Pacific, APO 958, c/o Postmaster, San Francisco, Calif. | 75- 76 |
| Commanding General, U. S. Army, Caribbean, APO 834, c/o Postmaster, New Orleans, La. | 77- 7[illegible] |
| Commanding General, U. S. Army, Alaska, APO 942, c/o Postmaster, Seattle, Wash. | 79- 8[illegible] |
| Director, Operations Research Office, 6410 Connecticut Ave., Chevy Chase, Md. | 81- 8[illegible] |
| Commanding Officer, Ballistic Research Laboratories, Aberdeen Proving Ground, Aberdeen, Md. | 84- 85 |
| Commanding Officer, Engineer Research and Development Laboratory, Fort Belvoir, Va. | 86- 87 |
| Commanding Officer, Signal Corps Engineering Laboratories, Fort Monmouth, N. J. | 88- 89 |
| Commanding Officer, Evans Signal Laboratory, Belmar, N. J. | 90- 91 |
| Commanding General, Army Chemical Center, Md. ATTN: Chemical and Radiological Laboratory | 92- 93 |

NAVY ACTIVITIES

| | |
|---|---|
| Chief of Naval Operations, Department of the Navy, Washington 25, D. C. ATTN: Op-36 | 94- 95 |
| Chief, Bureau of Ships, Department of the Navy, Washington 25, D C. | 96- 99 |
| Chief, Bureau of Ordnance, Department of the Navy, Washington 25, D. C. | 100 |
| Chief, Bureau of Medicine and Surgery, Department of the Navy, Washington 25, D. C. | 101-102 |
| Chief, Bureau of Aeronautics, Department of the Navy, Washington 25, D. C. | 103-104 |
| Chief, Bureau of Supplies and Accounts, Department of the Navy, Washington 25, D. C. | 105-106 |
| Chief, Bureau of Yards and Docks, Department of the Navy, Washington 25, D. C. | 10[illegible]-109 |

DISTRIBUTION (Continued)

| | Copy No. |
|---|---|
| Chief of Naval Personnel, Department of the Navy, Washington 25, D. C. | 110 |
| Commandant of the Marine Corps, Washington 25, D. C. | 111-113 |
| Commander-in-Chief, U. S. Pacific Fleet, Fleet Post Office, San Francisco, Calif. | 114 |
| Commander-in-Chief, U. S. Atlantic Fleet, Fleet Post Office, New York, N. Y. | 115 |
| President, U. S. Naval War College, Newport, R. I. | 116 |
| Commandant, Marine Corps Schools, Quantico, Va. | 117-118 |
| Chief of Naval Research, Department of the Navy, Washington 25, D. C. | 119-120 |
| Commander, U. S. Naval Ordnance Laboratory, Silver Spring 19, Md. | 121 |
| Commander, U. S. Naval Ordnance Laboratory, Silver Spring 19, Md. ATTN: Aliex | 122 |
| Director, U. S. Naval Research Laboratory, Washington 25, D. C. | 123 |
| Commanding Officer and Director, U. S. Naval Electronics Laboratory, San Diego 52, Calif. | 124 |
| Commanding Officer, U. S. Naval Radiological Defense Laboratory, San Francisco 24, Calif. | 125-128 |
| Commanding Officer and Director, David Taylor Model Basin, Washington 7, D. C. | 129 |
| Commander, Naval Material Laboratory, New York Naval Shipyard, Naval Base, New York 1, N. Y. | 130 |
| Officer-in-Charge, U. S. Naval Civil Engineering Research and Evaluation Laboratory, U. S. Naval Construction Battalion Center, Port Hueneme, Calif. | 131-132 |
| Commanding Officer, U. S. Naval Medical Research Institute, National Naval Medical Center, Bethesda 14, Md. | 133 |
| Commander, U. S. Naval Ordnance Test Station, Inyokern, China Lake, Calif. | 134 |

AIR FORCE ACTIVITIES

| | |
|---|---|
| Assistant for Atomic Energy, Headquarters, United States Air Force, Washington 25, D. C. | 135-136 |
| Director of Operations, Headquarters, United States Air Force, Washington 25, D. C. ATTN: Operations Analysis Division | 137-138 |
| Director of Plans, Headquarters, United States Air Force, Washington 25, D. C. ATTN: AFOPD-P1 | 139 |
| Director of Requirements, Headquarters, United States Air Force, Washington 25, D. C. | 140 |
| Director of Research and Development, Headquarters, United States Air Force, Washington 25, D. C. | 141-142 |
| Director of Intelligence, Headquarters, United States Air Force, Washington 25, D. C. ATTN: Phys. Vul. Branch, Air Targets Division | 143-144 |

DISTRIBUTION (Continued)

| | Copy No. |
|---|---|
| Director of Installations, Headquarters, United States Air Force, Washington 25, D. C. | 145 |
| Asst. for Development Planning, Headquarters, United States Air Force, Washington 25, D. C. | 146 |
| Asst. for Materiel Program Control, Headquarters, United States Air Force, Washington 25, D. C. | 147 |
| The Surgeon General, Headquarters, United States Air Force, Washington 25, D. C. | 148 |
| Commanding General, Strategic Air Command, Offutt Air Force Base, Nebr. | 149-151 |
| Commanding General, Air Research and Development Command, P.O. Box 1395, Baltimore 3, Md. | 152-161 |
| Commanding General, Air Materiel Command, Wright-Patterson Air Force Base, Dayton, Ohio | 162-163 |
| Commanding General, Air Materiel Command, Wright-Patterson Air Force Base, Dayton, Ohio. ATTN: Air Installations Division | 164-165 |
| Commanding General, Tactical Air Command, Langley Air Force Base, Va. | 166-168 |
| Commanding General, Air Defense Command, Ent Air Force Base, Colo. | 169-171 |
| Commanding General, Air Proving Ground, Eglin Air Force Base, Fla. | 172-173 |
| Commanding General, Air Training Command, Scott Air Force Base, Belleville, Ill. | 174-176 |
| Commanding General, Air University, Maxwell Air Force Base, Montgomery, Ala. | 177-179 |
| Commanding General, Special Weapons Center, Kirtland Air Force Base, N. Mex. | 180-182 |
| Commanding General, 1009th Special Weapons Squadron, 1712 G St. NW, Washington 25, D. C. | 183 |
| Commanding General, Wright Air Development Center, Wright-Patterson Air Force Base, Dayton, Ohio | 184-187 |
| Commanding General, Air Force Cambridge Research Center, 230 Albany St., Cambridge 39, Mass. | 188-189 |
| Commanding General, U. S. Air Forces in Europe, APO 633, c/o Postmaster, New York, N. Y. | 190-191 |
| Commanding General, Far East Air Forces, APO 925, c/o Postmaster, San Francisco, Calif. | 192-193 |
| Commanding General, Air Force Missile Center, Patrick Air Force Base, Cocoa, Fla. | 194 |
| Commandant, USAF School of Aviation Medicine, Randolph Air Force Base, Randolph Field, Tex. | 195 |
| Asst. to the Special Asst., Chief of Staff, United States Air Force, Washington 25, D. C. ATTN: David T. Griggs | 196 |
| The RAND Corporation, 1500 Fourth St., Santa Monica, Calif. | 197-198 |

DISTRIBUTION (Continued)

| | Copy No. |
|---|---|
| **AFSWP ACTIVITIES** | |
| Chief, Armed Forces Special Weapons Project, P.O. Box 2610, Washington 13, D. C. | 199-207 |
| Commanding General, Field Command, Armed Forces Special Weapons Project, P.O. Box 5100, Albuquerque, N. Mex. | 208-210 |
| Commanding Officer, Test Command, Armed Forces Special Weapons Project, P.O. Box 5600, Albuquerque, N. Mex. | 211-213 |
| **OTHER ACTIVITIES** | |
| Chairman, Research and Development Board, Department of Defense, Washington 25, D. C. | 214 |
| Director, Weapons System Evaluations Group, Office of the Secretary of Defense, Washington 25, D. C. | 215 |
| Executive Director, Committee on Atomic Energy, Research and Development Board, Department of Defense, Washington 25, D. C. ATTN: David Beckler | 216 |
| Executive Director, Committee on Medical Sciences, Research and Development Board, Department of Defense, Washington 25, D. C. | 217 |
| U. S. Atomic Energy Commission, Classified Document Room, 1901 Constitution Ave., Washington 25, D. C. ATTN: Mrs. J. M. O'Leary | 218-220 |
| Los Alamos Scientific Laboratory, Report Library, P.O. Box 1663, Los Alamos, N. Mex. ATTN: Helen Challenger | 221-223 |
| Sandia Corporation, Classified Document Division, Sandia Base, Albuquerque, N. Mex. ATTN: Wynne K. Cox | 224-243 |



AEC, Oak Ridge, Tenn., A31903